

NASA/CP-2010-215864



International VLBI Service for Geodesy and Astrometry 2010 General Meeting Proceedings

"VLBI2010: From Vision to Reality"

*Dirk Behrend (ed.)
NVI, Inc., Greenbelt, Maryland*

*Karen D. Baver (ed.)
NVI, Inc., Greenbelt, Maryland*

National Aeronautics and
Space Administration

*Goddard Space Flight Center
Greenbelt, MD 20771-0001*

December 2010

Available from:

NASA Center for AeroSpace Information
7115 Standard Drive
Hanover, MD 21076-1320

National Technical Information Service
5285 Port Royal Road
Springfield, VA 22161

Preface

This volume is the proceedings of the sixth General Meeting of the International VLBI Service for Geodesy and Astrometry (IVS), held in Hobart, Tasmania, Australia, February 7–13, 2010. The contents of this volume also appear on the IVS Web site at

<http://ivscc.gsfc.nasa.gov/publications/gm2010>

The sixth General Meeting was held in Hobart, Tasmania, Australia on the Sandy Bay Campus of the University of Tasmania. The meeting was hosted by the University of Tasmania, School of Mathematics and Physics, which supports the IVS Network Station at Hobart and is responsible for managing the AuScope project.

The keynote of the sixth General Meeting was new perspectives of the next generation VLBI system under the theme “VLBI2010: From Vision to Reality”. The vision of the VLBI2010 system is gradually being realized. The unprecedented new capabilities of 1-mm positional accuracy and station velocities of 0.1 mm/yr, continuous observational time series for station positions and Earth orientation parameters, and fast turnaround time from observation to geodetic and astrometric results will foster new science and applications. The goal of the meeting was to provide an interesting and informative program for a wide cross-section of IVS members, including station operators, program managers, and analysts.

On the Tuesday of the General Meeting week an official dedication ceremony of the 12-m AuScope antenna was held at Hobart station. The inauguration was done by the Governor of Tasmania, His Excellency, The Honourable Peter Underwood. The back cover of this volume shows a photo sequence from the construction of the 12-m antenna up to the inauguration event. The front cover shows the “old” 26-m antenna, which has been operating at Mt. Pleasant for many years.

This volume contains the following:

- **The papers presented at the meeting.** There are five major sections of this volume, each corresponding to a meeting session. Poster and oral papers are mixed. This volume includes 88 papers. The overheads of the oral presentations as well as selected poster presentations are available on the Web at

http://ivscc.gsfc.nasa.gov/meetings/gm2010/GM2010_present.html.

All papers were edited by the editors for usage of the English language, form, and minor content-related issues. Poster papers about IVS component status are not included in this volume; they have been published in the 2009 Annual Report, available on the Web.

- **A list of registered participants.**
- **The meeting program.**
- **An author index.**

The April 2010 issue of the IVS Newsletter has a feature article about the meeting. The Newsletter is available at

<http://ivscc.gsfc.nasa.gov/newsletter/issue26.pdf>

Photographs taken during the meeting are available on the Web at

<http://ivscc.gsfc.nasa.gov/meetings/gm2010/#Pictures>

This URL displays a section of the 2010 General Meeting Web page with links to pages of photographs.

Table of Contents

Preface	iii
Session 1. Realization and New Perspectives of VLBI2010	1
<i>Bill Petrachenko</i> : VLBI2010: An Overview	3
<i>Richard Porcas</i> : VLBI2010: The Astro-Geo Connection	8
<i>Brian Corey</i> : Differences Between VLBI2010 and S/X Hardware	18
<i>Arthur Niell and the Broadband Development Team</i> : The NASA VLBI2010 Proof-of-concept Demonstration and Future Plans	23
<i>Gino Tuccari, Walter Alef, Alessandra Bertarini, Salvatore Buttaccio, Giovanni Comoretto, Dave Graham, Alexander Neidhardt, Pier Raffaele Platania, Antonietta Russo, Alan Roy, Michael Wunderlich, Reinhard Zeitlhöfler, Ying Xiang</i> : DBBC VLBI2010	28
<i>Hayo Hase, Ed Himwich, Alexander Neidhardt</i> : Differences Between S/X and VLBI2010 Operation ..	31
<i>Christopher Beaudoin, Arthur Niell</i> : Post-correlation Processing for the VLBI2010 Proof-of-concept System	35
<i>Thomas Hobiger, Moritaka Kimura, Kazuhiro Takefuji, Tomoaki Oyama, Yasuhiro Koyama, Tetsuro Kondo, Tadahiro Gotoh, Jun Amagai</i> : GPU Based Software Correlators - Perspectives for VLBI2010	40
<i>Arnaud Collioud, Patrick Charlot</i> : VLBI2010 Imaging and Structure Corrections	45
<i>Jim Lovell, John Dickey, Sergei Gulyaev, Tim Natusch, Oleg Titov, Steven Tingay</i> : The AuScope Project and Trans-Tasman VLBI	50
<i>Atsutoshi Ishii, Ryuichi Ichikawa, Hiroshi Takiguchi, Kazuhiro Takefuji, Hideki Ujihara, Yasuhiro Koyama, Tetsuro Kondo, Shinobu Kurihara, Yuji Miura, Shigeru Matsuzaka, Daisuke Tanimoto</i> : Current Status of the Development of a Transportable and Compact VLBI System by NICT and GSI	55
<i>Oleg Titov</i> : VLBI2020: From Reality to Vision	60
<i>J. M. Dickey</i> : How and Why to Do VLBI on GPS	65
<i>Vincenza Tornatore, Rüdiger Haas, Guifré Molera, Sergei Pogrebenko</i> : Planning of an Experiment for VLBI Tracking of GNSS Satellites	70
Session 2. Network Stations, Operation Centers, Correlators	75
<i>John Gipson</i> : An Introduction to Sked	77
<i>Cynthia C. Thomas, Dirk Behrend, Daniel S. MacMillan</i> : The Composition of the Master Schedule ..	85

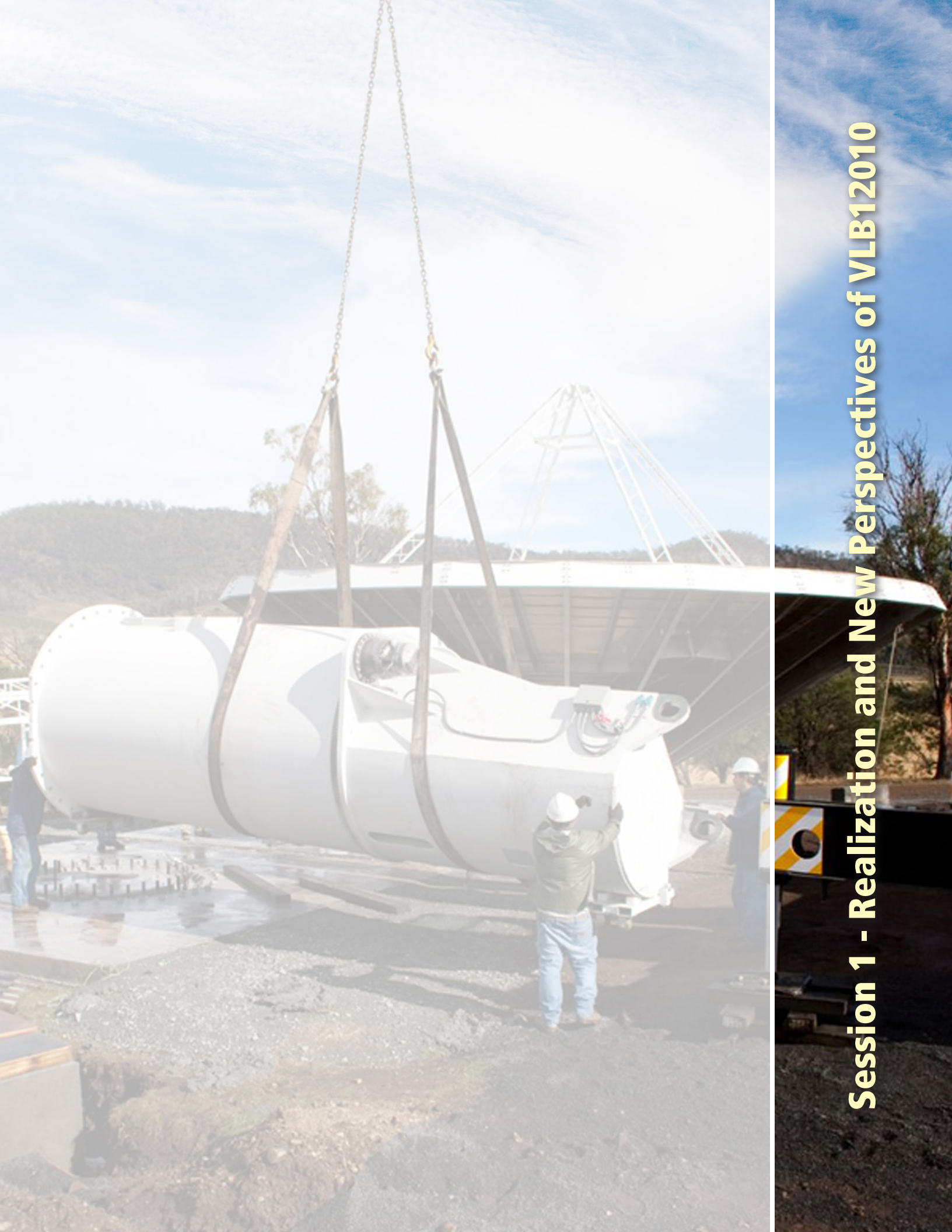
<i>John Gipson, Dirk Behrend, David Gordon, Ed Himwich, Dan MacMillan, Mike Titus, Brian Corey: Coordinating, Scheduling, Processing and Analyzing IYA09</i>	90
<i>Hyunhee Ju, Myungho Kim, Suchul Kim, Jinsik Park, Tetsuro Kondo, Tuhwan Kim, Hongjong Oh, Sangoh Yi: The State and Development Direction of the Geodetic VLBI Station in Korea</i>	95
<i>Jesús Gómez González, Francisco Colomer, José Antonio López Fernández, Marlene C.S. Assis: RAEGE: An Atlantic Network of Geodynamical Fundamental Stations</i>	101
<i>Andrey Finkelstein, Alexander Ipatov, Sergey Smolentsev, Vyacheslav Mardyshev, Leonid Fedotov, Igor Surkis, Dmitriy Ivanov, Iskander Gayazov: The New Generation Russian VLBI Network</i>	106
<i>Line Langkaas, Terje Dahlen, Per Erik Opseth: New Fundamental Station in Ny-Ålesund</i>	111
<i>Sergei Gulyaev, Tim Natusch, David Wilson: Characterization and Calibration of the 12-m Antenna in Warkworth, New Zealand</i>	113
<i>Rüdiger Haas, Sten Bergstrand: COLD MAGICS – Continuous Local Deformation Monitoring of an Arctic Geodetic Fundamental Station</i>	118
<i>Axel Nothnagel, Judith Pietzner, Christian Eling, Claudia Hering: Homologous Deformation of the Efelsberg 100-m Telescope Determined with a Total Station</i>	123
<i>L. Liu, Z. Y. Cheng, J. L. Li: Analysis of the GPS Observations of the Site Survey at Sheshan 25-m Radio Telescope in August 2008</i>	128
<i>Alexander Neidhardt, Michael Lösler, Cornelia Eschelbach, Andreas Schenk: Permanent Monitoring of the Reference Point of the 20m Radio Telescope Wettzell</i>	133
<i>Benno Schmeing, Dirk Behrend, John Gipson, Axel Nothnagel: Proof-of-Concept Studies for a Local Tie Monitoring System</i>	138
<i>Shigeru Matsuzaka, Shinobu Kurihara, Mamoru Sekido, Thomas Hobiger, Rüdiger Haas, Jouko Ritakari, Jan Wagner: Ultra-rapid dUT1 Measurements on Japan-Fennoscandian Baselines – Application to 24-hour Sessions</i>	143
<i>Andrey Finkelstein, Alexander Ipatov, Michael Kaidanovsky, Ilia Bezrukov, Andrey Mikhailov, Alexander Salnikov, Igor Surkis, Elena Skurikhina: The “Quasar” Network Observations in e-VLBI Mode Within the Russian Domestic VLBI Programs</i>	148
<i>Alan Fey, Roopesh Ojha, Dave Boboltz, Nicole Geiger, Kerry Kingham, David Hall, Ralph Gaume, Ken Johnston: Implementation and Testing of VLBI Software Correlation at the USNO</i>	153
<i>Weimin Zheng, Ying Quan, Fengchun Shu, Zhong Chen, Shanshan Chen, Weihua Wang, Guangli Wang: The Software Correlator of the Chinese VLBI Network</i>	157
<i>David Gordon: RDV77 VLBA Hardware/Software Correlator Comparisons</i>	162
<i>Igor Surkis, Alexey Melnikov, Violet Shantyr, Vladimir Zimovsky: The IAA RAS Correlator First Results</i>	167

<i>Guifré Molera Calvés, Jan Wagner, Alexander Neidhardt, Gerhard Kronschnabl, Miguel Pérez Ayúcar, Giuseppe Cimó, Sergei Pogrebenko: First Results of Venus Express Spacecraft Observations with Wettzell</i>	171
<i>Oleg Titov, Dirk Behrend, Fengchun Shu, Dan MacMillan, Alan Fey: CRF Network Simulations for the South</i>	176
<i>Gennady Il'in, Sergey Smolentsev, Roman Sergeev: About the Compatibility of DORIS and VLBI Observations</i>	180
Session 3. VLBI Data Structure, Analysis Strategies and Software	185
<i>John Gipson: IVS Working Group 4: VLBI Data Structures</i>	187
<i>Alan Whitney, Mark Kettenis, Chris Phillips, Mamoru Sekido: VLBI Data Interchange Format (VDIF)</i> 192	
<i>Sergei Bolotin, John M. Gipson, Daniel S. MacMillan: Development of a New VLBI Data Analysis Software</i>	197
<i>Hana Spicakova, Johannes Böhm, Sigrid Böhm, Tobias Nilsson, Andrea Pany, Lucia Plank, Kamil Teke, Harald Schuh: Estimation of Geodetic and Geodynamical Parameters with VieVS</i>	202
<i>Halfdan Pascal Kierulf, Per-Helge Andersen, Sarah Böckmann, Oddgeir Kristiansen: VLBI Analysis with the Multi-technique Software GEOSAT</i>	207
<i>Thomas Hobiger, Tadahiro Gotoh, Toshimichi Otsubo, Toshihiro Kubooka, Mamoru Sekido, Hiroshi Takiguchi, Hiroshi Takeuchi: c5++ - Multi-technique Analysis Software for Next Generation Geodetic Instruments</i>	212
<i>Lucia Plank, Johannes Böhm, Harald Schuh: Comparison Campaign of VLBI Data Analysis Software - First Results</i>	217
<i>Sarah Böckmann, Thomas Artz, Axel Nothnagel: Correlations Between the Contributions of Individual IVS Analysis Centers</i>	222
<i>Dan MacMillan, Despina Pavlis, Frank Lemoine, Douglas Chinn, David Rowlands: VLBI-SLR Combination Solution Using GEODYN</i>	227
<i>Susana García-Espada, Rüdiger Haas, Francisco Colomer: Application of Raytracing through the High Resolution Numerical Weather Model HIRLAM for the Analysis of European VLBI</i>	232
<i>Ryuichi Ichikawa, Thomas Hobiger, Yasuhiro Koyama, Tetsuro Kondo: Atmospheric Delay Reduction Using KARAT for GPS Analysis and Implications for VLBI</i>	237
<i>David Gordon: Use of GPS TEC Maps for Calibrating Single Band VLBI Sessions</i>	242
<i>Sergey Kurdubov, Elena Skurikhina: Antenna Axis Offset Estimation from VLBI</i>	247
<i>Johannes Böhm, Tobias Nilsson, Harald Schuh: Prospects for UT1 Measurements from VLBI Intensive Sessions</i>	251

<i>Karen Baver, John Gipson: Strategies for Improving the IVS-INT01 UT1 Estimates</i>	256
<i>Zinovy Malkin: CPO Prediction: Accuracy Assessment and Impact on UT1 Intensive Results</i>	261
<i>Masachika A. Kijima: Application of Geodetic VLBI Data to Obtaining Long-term Light Curves for Astrophysics</i>	266
Session 4. Interpretation of VLBI Results in Geodesy, Astrometry and Geophysics	271
<i>Chopo Ma: The Second International Celestial Reference Frame (ICRF2)</i>	273
<i>Karine Le Bail, David Gordon: Time-dependent Selection of an Optimal Set of Sources to Define a Stable Celestial Reference Frame</i>	280
<i>C. S. Jacobs, D. S. Bagri, M. J. Britcliffe, J. E. Clark, M. M. Franco, C. Garcia-Miro, C. E. Goodhart, S. Horiuchi, S. T. Lowe, V. E. Moll, R. Navarro, S. P. Rogstad, R. C. Proctor, E. H. Sigman, L. J. Skjerve, M. A. Soriano, O. J. Sovers, B. C. Tucker, D. Wang, L. A. White: X/Ka Celestial Frame Improvements: Vision to Reality</i>	285
<i>Vladimir Zharov, Mikhail Sazhin, Valerian Sementsov, Olga Sazhina: Long-term Variations of the EOP and ICRF2</i>	290
<i>Gerald Engelhardt, Volkmar Thorandt: Long-term Stability of Radio Sources in VLBI Analysis</i>	295
<i>Ed Fomalont, Kenneth Johnston, Alan Fey, Dave Boboltz, Tomoaki Oyama, Mareki Honma: The Position/Structure Stability of Four ICRF2 Sources</i>	300
<i>C. S. Jacobs, M. B. Heflin, G.E. Lanyi, O. J. Sovers, J. A. Steppe: Rotational Alignment Altered by Source Position Correlations</i>	305
<i>Géraldine Bourda, Arnaud Collioud, Patrick Charlot, Richard Porcas, Simon Garrington: Global VLBI Observations of Weak Extragalactic Radio Sources: Imaging Candidates to Align the VLBI and Gaia Frames</i>	310
<i>María Rioja, Richard Dodson: Astrometric “Core-shifts” at the Highest Frequencies</i>	315
<i>Victor L’vov, Zinovy Malkin, Svetlana Tsekmeister: Forthcoming Occultations of Astrometric Radio Sources by Planets</i>	320
<i>Hayley E. Bignall, David L. Jauncey, James E. J. Lovell, Roopesh Ojha, Cormac Reynolds: Finding Extremely Compact Sources Using the ASKAP VAST Survey</i>	325
<i>Younghee Kwak, Tetsuro Kondo, Tadahiro Gotoh, Jun Amagai, Hiroshi Takiguchi, Mamoru Sekido, Ryuichi Ichikawa, Tetsuo Sasao, Jungho Cho, Tuhwan Kim: The First Experiment with VLBI-GPS Hybrid System</i>	330
<i>L. Guo, F.C. Shu, W.M. Zheng, T. Kondo, R. Ichikawa, S. Hasegawa, M. Sekido: Ionospheric Response to the Total Solar Eclipse of 22 July 2009 as Deduced from VLBI and GPS Data</i>	335
<i>Robert Heinkelmann, Christian Schwatke: The Tropospheric Products of the International VLBI Service for Geodesy and Astrometry</i>	340

<i>O. J. Botai, L. Combrinck, V. Sivakumar, H. Schuh, J. Böhm</i> : Extracting Independent Local Oscillatory Geophysical Signals by Geodetic Tropospheric Delay	345
<i>Thomas Artz, Sarah Böckmann, Laura Jensen, Axel Nothnagel, Peter Steigenberger</i> : Reliability and Stability of VLBI-derived Sub-daily EOP Models	355
<i>Ulla Kallio, Markku Poutanen</i> : Simulation of Local Tie Accuracy on VLBI Antennas	360
<i>Carsten Rieck, Rüdiger Haas, Kenneth Jaldehag, Jan Johansson</i> : VLBI and GPS-based Time-transfer Using CONT08 Data	365
Session 5. Progress in Technology Development	371
<i>Alan Whitney, Chester Rusczyk, Jon Romney, Ken Owens</i> : The Mark 5C VLBI Data System	373
<i>Kazuhiro Takefuji, Hiroshi Takeuchi, Masanori Tsutsumi, Yasuhiro Koyama</i> : Next-generation A/D Sampler ADS3000+ for VLBI2010	378
<i>Xiuzhong Zhang, Fengchun Shu, Ying Xiang, Renjie Zhu, Zhijun Xu, Zhong Chen, Weimin Zheng, Jintao Luo, Yajun Wu</i> : VLBI Technology Development at SHAO	383
<i>Renjie Zhu, Xiuzhong Zhang, Wenren Wei, Ying Xiang, Bin Li, Yajun Wu, Fengchun Shu, Jintao Luo, Jinqing Wang, Zhuhe Xue, Rongbin Zhao, Lan Chen</i> : The Progress of CDAS	388
<i>Gino Tuccari, Walter Alef, Alessandra Bertarini, Salvatore Buttaccio, Giovanni Comoretto, Dave Graham, Alexander Neidhardt, Pier Raffaele Platania, Antonietta Russo, Alan Roy, Michael Wunderlich, Reinhard Zeitlhöfler, Ying Xiang</i> : DBBC2 Backend: Status and Development Plan	392
<i>A. Niell, M. Bark, C. Beaudoin, W. Brisken, H. Ben Frej, S. Doeleman, S. Durand, M. Guerra, A. Hinton, M. Luce, R. McWhirter, K. Morris, G. Peck, M. Revnell, A. Rogers, J. Romney, C. Rusczyk, M. Taveniku, R. Walker, A. Whitney</i> : RDBE Development and Progress	396
<i>Leonid Fedotov, Eugeny Nosov, Sergey Grenkov, Dmitry Marshalov</i> : The Digital Data Acquisition System for the Russian VLBI Network of New Generation	400
<i>Se-Jin Oh, Duk-Gyoo Roh, Jae-Hwan Yeom, Hideyuki Kobayashi, Noriyuki Kawaguchi</i> : First Phase Development of Korea-Japan Joint VLBI Correlator and Its Current Progress	405
<i>Mamoru Sekido, Kazuhiro Takefuji, Moritaka Kimura, Thomas Hobiger, Kensuke Kokado, Kentarou Nozawa, Shinobu Kurihara, Takuya Shinno, Fujinobu Takahashi</i> : Development of an e-VLBI Data Transport Software Suite with VDIF	410
<i>Miroslav Pantaleev, Jian Jang, Yogesh Karadikar, Leif Helldner, Benjamin Klein, Rüdiger Haas, Ashraf Zaman, Mojtaba Zamani, Per-Simon Kildal</i> : Cryogenic Integration of the 2–14 GHz Eleven Feed in a Wideband Receiver for VLBI2010	415
<i>Christopher Beaudoin, Per-Simon Kildal, Jian Yang, Miroslav Pantaleev</i> : Development of a Compact Eleven Feed Cryostat for the Patriot 12-m Antenna System	420
<i>Alexander Ipatov, Vyacheslav Mardyshev, Andrey Cherepanov, Vitaly Chernov, Dmitry Diky, Evgeny</i>	

<i>Khvostov, Alexander Yevstigneyev</i> : Radio Telescope Focal Container for the Russian VLBI Network of New Generation	425
<i>Dmitrij Ivanov, Anatolij Maslenikov, Alexander Vytnov</i> : Experiment of Injecting Phase Cal Ahead of the Feed: First Results	429
<i>Bill Petrachenko</i> : The Impact of Radio Frequency Interference (RFI) on VLBI2010	434
<i>Alexander Neidhardt, Martin Ettl, Helge Rottmann, Christian Plötz, Matthias Mühlbauer, Hayo Hase, Walter Alef, Sergio Sobarzo, Cristian Herrera, Ed Himwich</i> : E-control: First Public Release of Remote Control Software for VLBI Telescopes	439
<i>Martin Ettl, Alexander Neidhardt, Matthias Mühlbauer, Christian Plötz, Christopher Beaudoin</i> : The Wettzell System Monitoring Concept and First Realizations	444
<i>Hongjong Oh, Tetsuro Kondo, Jinoo Lee, Tuhwan Kim, Myungho Kim, Suchul Kim, Jinsik Park, Hyunhee Ju</i> : Round-trip System Available to Measure Path Length Variation in Korea VLBI System for Geodesy	449
About the Meeting	455
Registered Participants	457
Program	461
Author Index	475



Session 1 - Realization and New Perspectives of VLB12010

VLBI2010: An Overview

Bill Petrachenko

Natural Resources Canada (NRCan)

e-mail: Bill.Petrachenko@nrcan.gc.ca

Abstract

The first concrete actions toward a next generation system for geodetic VLBI began in 2003 when the IVS initiated Working Group 3 to investigate requirements for a new system. The working group set out ambitious performance goals and sketched out initial recommendations for the system. Starting in 2006, developments continued under the leadership of the VLBI2010 Committee (V2C) in two main areas: Monte Carlo simulators were developed to evaluate proposed system changes according to their impact on IVS final products, and a proof-of-concept effort sponsored by NASA was initiated to develop next generation systems and verify the concepts behind VLBI2010. In 2009, the V2C produced a progress report that summarized the conclusions of the Monte Carlo work and outlined recommendations for the next generation system in terms of systems, analysis, operations, and network configuration. At the time of writing: two complete VLBI2010 signal paths have been completed and data is being produced; a number of VLBI2010 antenna projects are under way; and a VLBI2010 Project Executive Group (V2PEG) has been initiated to provide strategic leadership.

1. Introduction

The current VLBI system was conceived and constructed mostly in the 1960s and 1970s. Aging antennas, increasing radio frequency interference (RFI) problems, obsolete electronics, and high operating costs have made it increasingly difficult to sustain required levels of accuracy, reliability, and timeliness. In September 2003 the IVS, recognizing the limitations of existing VLBI infrastructure and the increasingly demanding requirements of space geodesy, established Working Group 3 (WG3): VLBI2010 to investigate options for modernization [1].

Guided by emerging space geodesy science and operational needs [9] [10], WG3 established challenging goals for the next generation VLBI system:

- 1 mm position and 0.1 mm/year velocity accuracy on global scales,
- continuous measurements for time series of station positions and EOP,
- posting of initial geodetic results less than 24 hours after observations are complete.

In its final report [4], WG3 proposed strategies to move toward the unprecedented 1 mm position accuracy target and broad recommendations for a next generation system based on the use of smaller (~ 12 m) fast-slewing automated antennas.

In order to encourage the realization of the recommendations of WG3, the IVS, in September 2005, established the VLBI2010 Committee (V2C) as a permanent body of the IVS. The V2C takes an integrated view of VLBI and evaluates the effectiveness of proposed system changes based on the degree to which they improve the final products. The V2C work goes hand-in-hand with the gradual establishment of the Global Geodetic Observing System (GGOS) [8] of the International Association of Geodesy (IAG).

2. Monte Carlo Simulators

Making rational design decisions for VLBI2010 requires a realistic understanding of the impacts of new operating modes on final products. To fill this gap, Monte Carlo simulators were developed [3] [5] [11]. The concept of a Monte Carlo simulator involves the generation of several sets (typically 25 for the VLBI2010 studies) of artificial input data, with each set driven by different random numbers. All data sets are then processed as if they were from real sessions, and the ensemble of output products is analyzed statistically to produce estimates of the bias and standard deviation of those products.

The simulators have been used to study the effects of the dominant VLBI random error processes (related to the atmosphere, the reference clocks, and the delay measurement noise) and the benefit of new approaches to reduce them, such as decreasing the source-switching interval and improving analysis and scheduling strategies. Of particular merit is the strategy to reduce the source-switching interval which results in a nearly proportionate improvement in station position accuracy [7]. Regardless of the strategy employed, the simulators confirm that the dominant VLBI error source is the atmosphere.

3. System Considerations

Based on the Monte Carlo studies, high priority is placed on finding strategies for reducing the source-switching interval. This entails decreasing both the on-source time and the time required to slew between sources. From these two somewhat competing goals, recommendations for the VLBI2010 antennas are emerging, e.g., use either a single 12-m diameter antenna with very high slew rates (e.g., $12^\circ/\text{s}$ in azimuth and $4^\circ/\text{s}$ in elevation) (see Figure 1) or a pair of 12-m diameter antennas, each with more moderate slew rates (e.g., $5^\circ/\text{s}$ in azimuth and $1.5^\circ/\text{s}$ in elevation [6]).

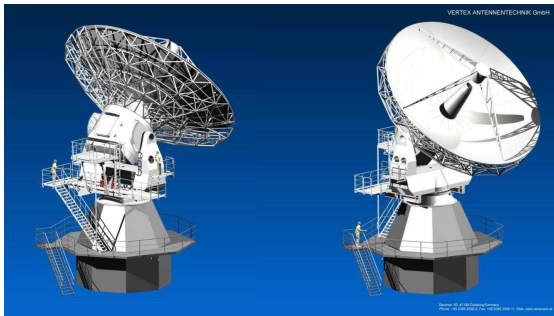


Figure 1. An artist's conception of the VLBI2010 antenna designed by Vertex Antennentechnik GmbH. A pair of these fully VLBI2010 compliant antennas is being installed at the Geodetic Observatory Wettzell in Germany.

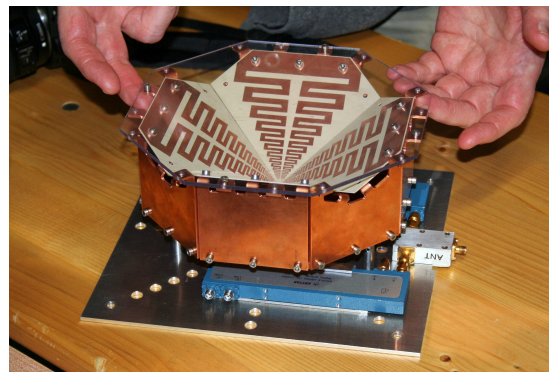


Figure 2. Prototype of a broadband 2-14 GHz "Eleven" feed for VLBI2010. The feed is being developed at Chalmers University of Technology in Sweden.

In order to shorten the on-source observing time, a new approach is being developed in which several widely spaced frequency bands are used to unambiguously resolve the interferometer phase.

The new observable is being referred to as the broadband delay (bbd). To do this, a four-band system is recommended that uses a broadband feed to span the entire frequency range from 2 to 14 GHz (see Figure 2). In order to be able to detect an adequate number of radio sources, a total instantaneous data rate as high as 32 Gbps and a sustained data storage or transmission rate of 8 Gbps are necessary. The system development effort for VLBI2010 involves nearly a complete reworking of the current S/X system. Since the bbd technique is new and untested, NASA is funding a proof-of-concept development effort to verify that it works and to gain experience with the new VLBI2010 systems.

It is also recognized that reducing systematic errors plays a critical role in improving VLBI accuracy. For minimizing electronic biases, updated calibration systems and processes are being developed. For errors due to source structure, the application of corrections based on images derived directly from the VLBI2010 observations is under study. For antenna deformations, conventional surveying techniques continue to be refined, while the use of a small reference antenna for generating deformation models and establishing site ties is also under consideration [2].

4. Network Considerations

It is recommended that a globally distributed network of at least 16 VLBI2010 antennas observe every day to determine Earth Orientation Parameters (EOP), and that other antennas be added as needed for the maintenance of the International Celestial Reference Frame (ICRF) and the International Terrestrial Reference Frame (ITRF). A subset of antennas with access to high-speed fiber networks is also required to enable daily delivery of initial IVS products in less than 24 hours. For the observation of faint radio sources for densification of the ICRF, at least four large radio telescopes per hemisphere are also recommended. High priority is placed on increasing the number of stations in the southern hemisphere.

5. Operational Considerations

In order to increase reliability and to reduce the cost of operations, enhanced automation will be introduced both at the stations and in the analysis process. Stations will be monitored centrally to ensure compatible operating modes, to update schedules as required, and to notify station staff when problems occur.

Since IVS products must be delivered without interruption, a transition period to VLBI2010 operations is required in which there will be a mix of antennas with current and next-generation receiving systems. For this period a compatibility mode of operation has been identified. To preserve continuity in particular with respect to the strength of stable long-term time series of station positions, baseline lengths, and troposphere parameters, among other things, several existing radio telescopes are expected to continue VLBI observations for many years to come.

6. Status at the Beginning of 2010

Sponsored by NASA, full progenitor VLBI2010 signal paths have been implemented on two antennas, the 18-m antenna at the Haystack Observatory in Westford, Massachusetts, and the 5-m MV-3 antenna at the NASA Goddard Space Flight Center (GSFC) in Maryland, a baseline of 597 km. With the new systems, fringes are now routinely detected. As an example, in Figures 3 and

4, phase delays are displayed from a seven minute scan of 4C39.25 taken on day 314 of 2009. In Figure 3 the scan is broken down into 10-s segments, each with an SNR of about 28. Integer cycles of phase are resolved independently for each 10-s segment using the bbd technique. There are no apparent phase resolution errors. Rms delay scatter is a few ps relative to a 30-ps p-p systematic signal. In Figure 4, when the segments are reduced to 8-s each, SNR becomes about 24 and two of the segments can be seen to have phase resolution errors. This implies that, for this system, phase resolution with about 2-sigma confidence can be achieved at an SNR of about 25. This is a very encouraging first step. When the proof-of-concept system is brought to full VLBI2010 compliance (i.e., an increase of bandwidth from 512 to 1024 GHz per band, and an increase in frequency range from 3.5-8.5 GHz to 2.2-14 GHz), it has been calculated that phase resolution with 4- to 5-sigma confidence can be achieved at the VLBI2010 target SNR of 15 to 20.

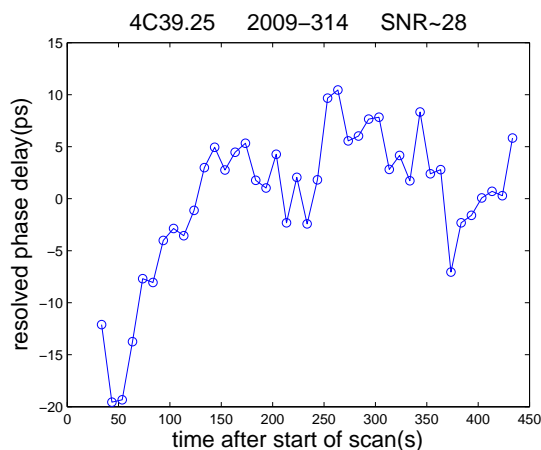


Figure 3. Phase delays for a 450-s scan of 4C39.25 taken on day 314 of 2009. The scan is divided into 10-s segments, each with an SNR of about 28. Cycles of phase were resolved independently for each segment using the bbd technique.

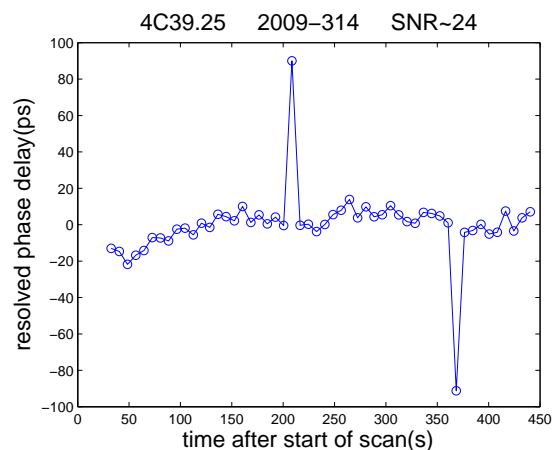


Figure 4. Phase delays for a 450-s scan of 4C39.25 taken on day 314 of 2009. The scan is divided into 8-s segments, each with an SNR of about 24. Cycles of phase were resolved independently for each segment using the bbd technique.

Worldwide, about ten VLBI2010 antennas have been funded and are currently in various stages of implementation. New antennas are coming up in Australia, Korea, New Zealand, Germany, Spain, Portugal, and the USA. The IVS has been approached by several other countries regarding VLBI2010, and a number of proposals for new sites are in various stages of preparation and approval.

Beyond the NASA development effort, organizations in other countries are involved in system developments potentially applicable to VLBI2010. These include Australia, China, Finland, Germany, Italy, Japan, Norway, Sweden, and possibly others.

The VLBI2010 concept also needs strategic and political support to be realized. In March 2009 a small VLBI2010 Project Executive Group (V2PEG) was established to move to the next level of defining development and deployment schedules and soliciting contributions.

7. Acknowledgements

The work on the definition, design, and prototyping of VLBI2010 was supported by many IVS members and components. All of them are gratefully acknowledged. I would also like to acknowledge specific writing contributions from D. Behrend, B.E. Corey, A.E. Niell, and H. Schuh.

References

- [1] Behrend D., Böhm J., Charlot P., Clark T., Corey B., Gipson J., Haas R., Koyama Y., MacMillan D., Malkin Z., Niell A., Nilsson T., Petrachenko B., Rogers A., Tuccari G. (2009). Recent Progress in the VLBI2010 Development. In: *Observing our Changing Earth*, ed. by M. Sideris, IAG Symposia, Vol. 133, pp. 833-840.
- [2] Ichikawa, R., Ishii A., Takiguchi H., Kuboki H., Kimura M., Nakajima J., Koyama Y., Kondo T., Machida M., Kurihara S., Kokado K., Matsuzaka S. (2008). Development of a Compact VLBI System for Providing over 10-km Baseline Calibration. In: *“Measuring the Future”, Proceedings of the Fifth IVS General Meeting*, ed. by A. Finkelstein and D. Behrend, Nauka, St. Petersburg, ISBN 978-5-02-025332-2, pp. 400-404.
- [3] MacMillan D. (2008). Simulation Analysis of the Geodetic Performance of Networks of VLBI Stations. In: *“Measuring the Future”, Proceedings of the Fifth IVS General Meeting*, ed. by A. Finkelstein and D. Behrend, Nauka, St. Petersburg, ISBN 978-5-02-025332-2, pp. 416-420.
- [4] Niell A., Whitney A., Petrachenko B., Schlüter W., Vandenberg N., Hase H., Koyama Y., Ma C., Schuh H., Tuccari G. (2006). VLBI2010: Current and future requirements of geodetic VLBI systems. In: *International VLBI Service for Geodesy and Astrometry 2005 Annual Report*, ed. by D. Behrend and K. Baver, NASA/TP-2006-214136, pp. 13-40.
- [5] Nilsson T., Haas R. (2008). Modelling Tropospheric Delays with Atmospheric Turbulence Models. In: *“Measuring the Future”, Proceedings of the Fifth IVS General Meeting*, ed. by A. Finkelstein and D. Behrend, Nauka, St. Petersburg, ISBN 978-5-02-025332-2, pp. 361-370.
- [6] Petrachenko B., Böhm J., MacMillan D., Pany A., Searle A., Wresnik J. (2008). VLBI2010 Antenna Slew Rate Study. In: *“Measuring the Future”, Proceedings of the Fifth IVS General Meeting*, ed. by A. Finkelstein and D. Behrend, Nauka, St. Petersburg, ISBN 978-5-02-025332-2 pp. 410-415.
- [7] Petrachenko B., Niell A., Behrend D., Corey B., Böhm J., Charlot P., Collioud A., Gipson J., Haas R., Hobiger T., Koyama Y., MacMillan D., Malkin Z., Nilsson T., Pany A., Tuccari G., Whitney A., Wresnik J. (2009). Design Aspects of the VLBI2010 System - Progress Report of the VLBI2010 Committee, NASA/TM-2009-214180, 58 pp.
- [8] Plag H-P., Gross, R., Rothacher, M. (2009), Global Geodetic Observing System for Geohazards and Global Change. *Geosciences, BRGM’s journal for a sustainable Earth*, **9**, 96-103.
- [9] Plag H-P., Pearlman M. (Eds.) (2009). Global Geodetic Observing System Meeting the Requirements of a Global Society on a Changing Planet in 2020, *Springer-Verlag*, ISBN 978-3-642-02686-7, doi: 10.1007/978-3-642-02687-4
- [10] Schuh H., Charlot P., Hase H., Himwich E., Kingham K., Klatt C., Ma C., Malkin Z., Niell A., Nothnagel A., Schlüter W., Takashima K., Vandenberg N. (2002). IVS Working Group 2 for Product Specification and Observing Programs. In: *International VLBI Service for Geodesy and Astrometry 2001 Annual Report*, ed. by N. Vandenberg and K. Baver, NASA/TP-2002-21000181, pp. 13-45.
- [11] Wresnik J., Böhm J., Pany A., Schuh H. (2008). VLBI2010 simulations at IGG Vienna. In: *“Measuring the Future”, Proceedings of the Fifth IVS General Meeting*, ed. by A. Finkelstein and D. Behrend, Nauka, St. Petersburg, ISBN 978-5-02-025332-2, pp. 421-426.

VLBI2010: The Astro-Geo Connection

Richard Porcas

Max-Planck-Institut für Radioastronomie, Bonn, Germany

e-mail: porcas@mpifr-bonn.mpg.de

Abstract

VLBI2010 holds out promise for greatly increased precision in measuring geodetic and Earth rotation parameters. As a by-product there will be a wealth of interesting new astronomical data. At the same time, astronomical knowledge may be needed to disentangle the astronomical and geodetic contributions to the measured delays—and phases. This presentation explores this astro-geo “link”.

1. New Astrophysics with VLBI2010

Under the watchword VLBI2010 the geodetic VLBI community is planning a major upgrade, including new telescopes, instrumentation and procedures, in order to make a dramatic improvement in the precision of IVS products. The goals are 1 mm (3 ps) station position accuracy, 0.1 mm/year velocity accuracy, with continuous observing and initial results available within 24 h.

Such precision implies (and requires) global source positions with $\sim 30 \mu\text{as}$ accuracy and stabilities of $\sim 3 \mu\text{as}/\text{year}$. The radio sources observed in IVS programs are all Active Galactic Nuclei (AGN) at high redshifts, constituting some of the most distant objects known in the Universe, and are used to define a fundamental inertial frame. Precise astrometric measurements will thus allow a number of basic properties of the Universe as a whole to be investigated with hitherto unprecedented precision. These could include:

- Micro-arcsecond instability of the celestial reference frame (micro-lensing by visible Galactic stars—Sazhin et al. 1998)
- Mass-energy of cosmological gravitational wave background (limits from quasar proper-motion upper-limits—Gwinn et al. 1997)
- Anisotropic Hubble expansion of the Universe? (redshift-dependence of proper-motions—Titov 2009)

The ESA space mission GAIA (Lindgren et al. 2007) will measure the optical positions of many AGN with precisions as good as $24 \mu\text{as}$ for bright (16 m) objects. IVS and GAIA astrometry, taken together, will determine a very precise alignment of the radio and optical reference frames, and hence permit a detailed investigation of displacements between the optical and radio emission regions.

2. AGN Astrophysics

Astronomers have used VLBI to study AGN astrophysics for 40 years. The radio emission from quasars and BL Lac objects (“blazars”) is believed to be due to the synchrotron process, and arises from the collimated, relativistic ($\Gamma = 5\text{--}20$) outflow of plasma jets from a central region whose

physics is dominated by the presence of a central, massive black hole. The 1-sided appearance is due to relativistic Doppler boosting. The bright, compact feature (the “core”) at the inner end of the visible jet provides an apparently obvious positional reference point. Optical emission may arise from either an accretion disk surrounding the black hole, or from the jet, or both (Fig. 1).

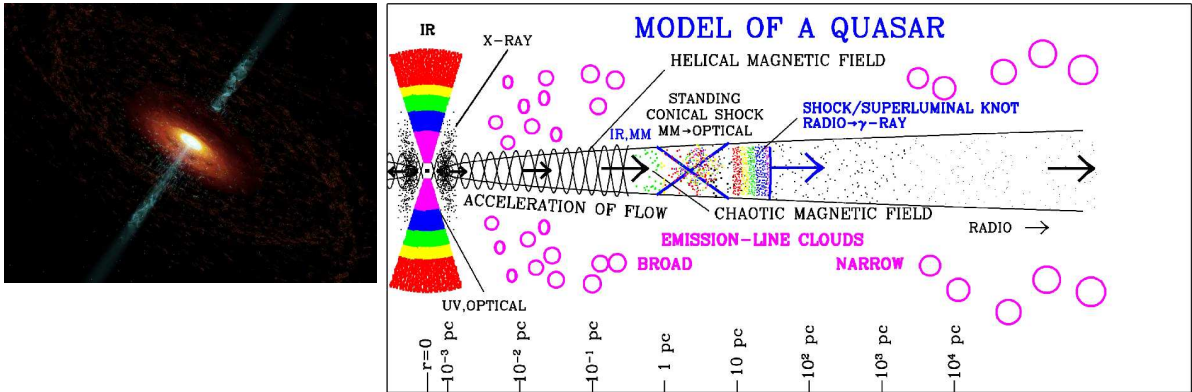


Figure 1. Left: An AGN (courtesy W. Steffen, Cosmovation). Right: An AGN (courtesy Alan Marscher).

VLBI imaging of AGN is vigorously carried out by the astronomical community. For example, the MOJAVE program (Lister et al. 2009) uses the VLBA (10 antennas) at 15 GHz to monitor structural variability in 135 sources, observing 25 sources each month. Observations comprise typically ten 5-minute observations per source with 45 baselines, yielding ~ 450 visibility measurements, with spacings between observing epochs tailored to known source activity. Imaging, using closure-phase relations, provides maps down to ~ 0.5 mas resolution and *internal* component separations and proper motions already with accuracies of $\sim 30 \mu\text{as}$ and $\sim 3 \mu\text{as}/\text{year}$, respectively—comparable to the *global* precision which will be reached by VLBI2010 (see Figs. 2 and 3).

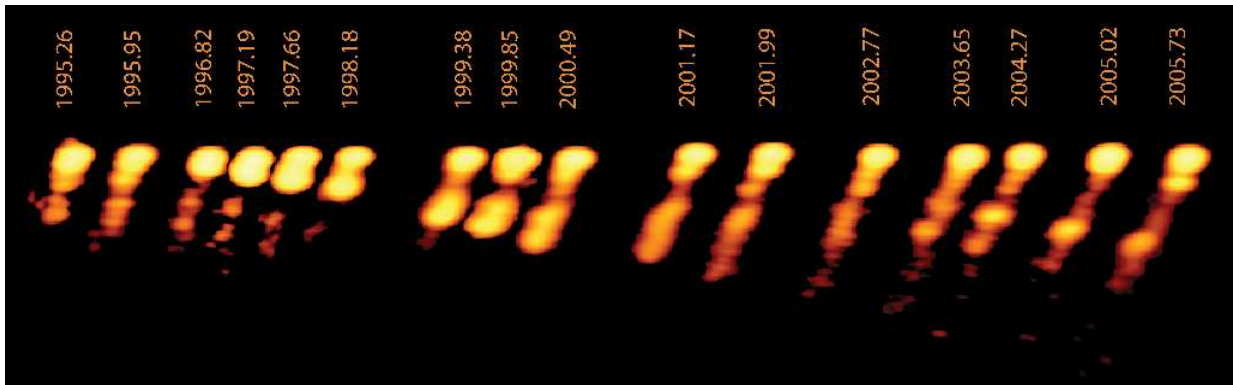


Figure 2. Seyfert Galaxy 3C 111 (redshift 0.0485) from VLBA 2 cm MOJAVE observations 1995–2005. Beam 0.5×1.0 mas. Extent (2005.73) ~ 11 mas. From Kadler et al. 2008 (courtesy Christian Fromm).

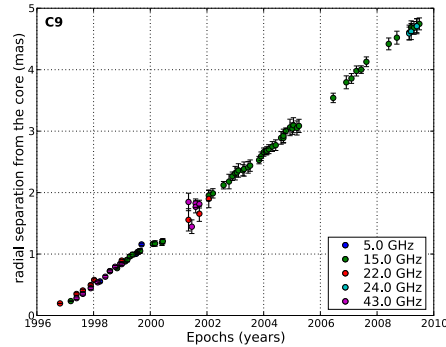


Figure 3. Outward motion of jet component C9 in 3C 345 (courtesy Frank Schinzel).

There is a long tradition of astronomers using the IVS data base to supplement their own observations of structural variations (see Fig. 4 for an ancient example). However, the use of sub-netting for geodetic runs greatly decreases the astronomical yield. Currently ~ 230 sources are used for IVS S- and X-band observations. As an example, the R1409 run observed 60 sources in a total of 1092 observations. Only 48 of these sources had any closure phases (≥ 3 antennas), only 36 had four or more antennas, and there were only nine sources with 100 or more visibility measurements.

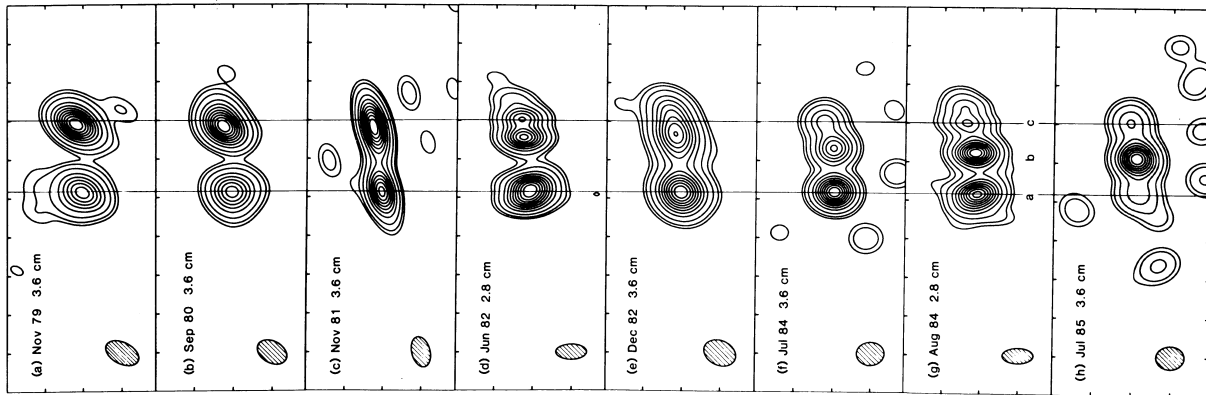


Figure 4. X-band images of quasar 4C 39.25 (redshift 0.699), mostly from the NASA Crustal Dynamics Program, 1979–1985 (Shaffer et al. 1987).

3. VLBI2010 and AGN Properties

Implementation of the VLBI2010 goals will require a considerable change in IVS observing methodology. No doubt the process will proceed via a gradual transition but it is worth considering the final situation and the method elements required to get there, as I understand (or do not understand) them:

- A network of ~ 30 fast-slewing, 12 m-class antennas
- Broadband group delays derived from four wide frequency bands from 2–14 GHz (or broadband “phase delays” $(\phi_{\text{tot}}(\nu)/(2\pi\nu))$ derived from the (ambiguity-resolved) total phase, ϕ_{tot})
- Dual polarization observing (and full polarization correlating?)
- Rapid source changes every 15–30 s (between how many sources?)
- Continuous 24 h observing (and correlating? real-time VLBI?)
- Accounting for thermal and gravitational deflections of antennas
- Accounting for electronic drifts and avoiding RF interference
- **Accounting for radio source structure**

An astronomer hoping to raid the VLBI2010 data base might then expect some fantastic material—from daily monitoring of (230?) sources in four frequency bands in dual polarization with 30 antennas. Some exciting uses could be:

- Monitoring jet component outflows
- Spectral and polarization evolution of jet components
- Component flux-density variations on daily and intra-day timescales. (Note the variability on an *hourly* timescale of the geodetic favourite B 1156+295; see Savolainen & Kovalev 2008.)
- Short timescale positional variations of the “core”

It is here, however, that the contrasting interests of the geodetic and astronomical VLBI communities become apparent. Sources for IVS observations would ideally be non-variable, achromatic points; such sources would in general, however, be of only marginal interest for astrophysical VLBI studies. To the extent that no sources are likely to fulfill such idealized IVS requirements, **astronomers and geodesists will need to work closely together** to meet the VLBI2010 goals. In the remaining sections of this contribution the effects of some of the properties of real astronomical sources on VLBI2010 methodology are considered.

4. Source Strength and Spectrum

Synchrotron sources are sometimes referred to as either “steep” or “flat” spectrum objects. However, VLBI2010 will use a wide frequency range (2–14 GHz) which spans a factor of 7 and account will need to be taken of the flux-density in all four bands. Suitable sources will need to be above the detection threshold of an IVS observation in each of the four bands; and the whole spectrum will need to be monitored continuously since variability can occur in all the bands. Fig. 5 shows an example of a typical synchrotron source spectrum.

5. Source Structure

All synchrotron sources have a finite angular size (otherwise they would have infinite brightness temperature), that is, **all sources have structure**. A further complication is that AGN source structures are highly asymmetric, vary with time and are, in general, different at different

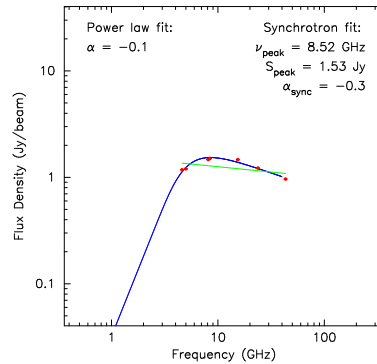


Figure 5. Radio spectrum of the synchrotron source 0827+243. The straight (green) line is a single power-law fit to the points; the (blue) curve is the fit of a synchrotron spectrum (courtesy Kirill Sokolovsky).

frequencies. And, of course, the resolution of VLBI observations will vary by a factor of 7 over the range of VLBI2010 observing frequencies. It is useful here to distinguish two distinct regimes in which the effects of source structure can be considered:

Visible Structure: Here the extent of the detected emission is greater than the observing beamwidth¹. Such structure can be recognized by imaging high-resolution VLBI observations.

Invisible Structure: Here the extent of the detected emission is less than the observing beamwidth. You do not see it—but it is there.

5.1. Effects of Visible Structure

The effects of visible source structure on VLBI delay measurements have been discussed by Charlot (1990). In general the delays (and phases) do not correspond to a unique point within the structure for all baselines; the delays do not “close”. Thus a geodetic solution where sources are treated as points will have a large “structural delay noise” contribution to the residuals.

The current IVS approach is to classify sources based on the expected magnitude of the structure delay, τ_{str} , using the “structure index” (Fey & Charlot 1997 & 2000) and to observe only those sources where the effect should be small at both X- and S-band. Adopting this methodology for VLBI2010 will require selecting sources with suitably low structure index at all four frequency bands. To remove systematic errors down to 1 mm (3 ps), only a structure index of 1 ($\tau_{\text{str}} < 3$ ps) will be permissible. Both these requirements will thus limit the number of sources which can be used. (See also further restrictions mentioned in Section 5.2.) Note that because source structures can vary, so too can their structure index; their structures must thus be monitored. The VLBI2010 observations themselves can be used to monitor visible source structure, in order to determine a current structure index. The observing schedule must be constructed to permit reasonable imaging—and maybe geodesists will be convinced that global fringe-fitting (Schwab & Cotton 1983) is useful in this context. In any case, geodesists must learn to love their sources as much as their antennas, and keep updating a source data base for planning observations. Perhaps observations of a source should be rejected if subsequent imaging reveals too great a structure index.

¹A measure of the angular resolution in VLBI images, ~ 0.4 of the fringe spacing on the longest baseline

The other approach, which is rarely used in practice (but see Petrov 2007), is to calculate structural delay corrections for each baseline, based on an image of the source structure and a reference point within it. Currently there appears to be little return from this laborious effort, presumably because tropospheric delay noise is comparable to, or greater than, structural delay terms. However, it is hoped that VLBI2010 observations, with their rapid source changes, will reduce this tropospheric component considerably, making source structure corrections worthwhile. Will VLBI2010 data be sufficient to determine structural corrections? Imaging will require scans with large enough sub-arrays (e.g., ≥ 5 telescopes) to provide sufficient closure phase relations.

As a diversion I would like to suggest a (possibly crazy) idea. Structural delay terms arise when there is a rapid change of structure phase, ϕ_{str} , with frequency, ν , and can be sensitive, for example, to the relative flux density and separation of beating sub-components (see Charlott 1991). This corresponds to a rapid change of ϕ_{str} with resolution coordinates u, v . When imaging, interferometer visibility data is traditionally assigned to a (u, v) grid before Fourier transformation to the image plane, with a cell size determined by the expected image size and the sampling theorem. This is sufficient only when the visibility plane is fully sampled—which in the case of geodetic VLBI data it certainly is not. Can we construct a more faithful image by using a much finer-scale (u, v) sampling, with no averaging of the data in either time or frequency, which preserves rapid ϕ_{str} gradients? Perhaps such a procedure could result in more precise relative flux densities, for example, and this in turn could lead to more robust structure delay estimates. Again, global fringe-fitting would be the key algorithm in this process by forcing a separation of geometric and structural terms.

An important point to note is that source structures can change dramatically over the factor of 7 range of frequencies of VLBI2010. Often they are larger at lower frequencies (because steep-spectrum extended jet features become more dominant) and this may counteract the moderating influence of larger beamwidths. A more serious issue arises from the VLBI2010 goal of using broadband group delays (or even “phase delays”) by phase interpolation between frequency bands. With the present IVS observing scheme, source structure delay corrections should, in principle, be made at both S- and X-band. However, S-band is only used as an “auxiliary” band for correcting the X-band ionospheric delay, and any contaminating S-band structural delay term, $\tau_{\text{str}}^{\text{S}}$, is “diluted” by a factor $(8.4/2.3)^2$. VLBI2010 analysis will require accurate interpolation of the phases *between* the four frequency bands, simultaneously solving for the dispersive ionospheric path. Thus source structure *phase* corrections, evaluated with respect to a suitable reference point, will be necessary in all four bands. Even for the case of the VLBI2010 fall-back plan, when group delays are determined from only the upper three frequency bands around K_u -band, such corrections will be necessary in these bands.

5.2. Effects of Invisible Structure

When the extent of a source is less than the interferometer beamwidth, the delay and phase response corresponds closely to that of a point source at the position of the radio brightness centroid. For present IVS observations the typical source position accuracies of $250 \mu\text{as}$ correspond to $\sim 1/3$ of the X-band beam. VLBI2010 observations will enter a new regime where the required source position accuracies are \sim **1/30 of the beam**. Variations of the invisible structure will thus result in a significantly variable source position. Structural variations in the low redshift source 3C 111 were shown in Fig. 2. Fig. 6 shows the structure at a single epoch and, bottom left, the

beam, and the same image reduced in size to correspond to a redshift of 0.6. Clearly, the visible structural variations would lead to an instability of the centroid position if the source were at that redshift.

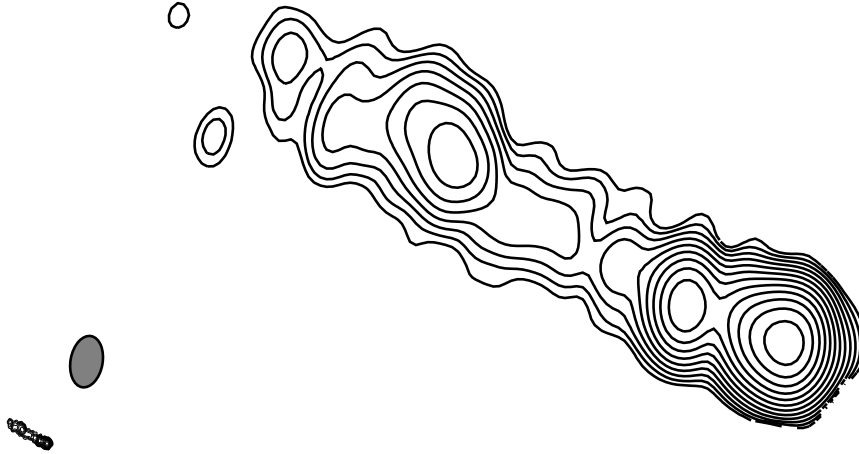


Figure 6. Source 3C 111 (redshift 0.048) at epoch 2005.73. The image at the extreme bottom left is as it would appear at a redshift of 0.6. The beamwidth is 0.9×0.5 mas at PA -10° ; the overall source extent of 11 mas becomes 0.9 mas (courtesy Christian Fromm).

A possible remedy to ameliorate the effect of variable centroid positions is to use the fact that most mas-scale source structures are highly *linear* and that the position instability is likely to be along the jet direction. This direction is roughly stable for most sources, leading to a more stable component of position in the direction transverse to the jet. One could thus consider giving low weights to data from baselines oriented close to the (known) inner jet direction, and high weights from baselines transverse to it. Observations could even be planned to avoid jet directions. Such a scheme is not unprecedented in IVS analysis (see Elevation-Dependent Weighting, Malkin 2008). The idea of assuming component motions to be along inner jet directions has been used by Rioja & Porcas (2000) to decompose the measured relative motions between the quasars 1028+528A,B.

5.3. Frequency-dependent Centroids and Core-shifts

Centroid positions will, in general, also be frequency-dependent, arising either from the effect of frequency-dependent beamwidths (see Rioja, *these proceedings*), or from real, frequency-dependent source structures, or from both (see, e.g. Porcas & Rioja 1997). These position changes must be taken into account when determining VLBI2010 broadband group delays and “phase delays” or the correct phase interpolation between the four frequency bands may not be made.

It has long been known from both measurements and theory that the bright, compact “core” feature seen at the end of jets has a frequency-dependent position—the “core-shift”. This arises from the frequency-dependent opacity of synchrotron radiation, which results in a gradual shift of the peak of radio emissivity away from the “jet base” at lower frequencies (see Fig. 7). Kovalev et al. (2008a) have investigated the prevalence of core-shifts in a sample of 29 sources for which a secondary (presumed achromatic) feature in the jet could be used as a reference point. They found a typical (sample median) shift of $440 \mu\text{as}$ between S- and X-band core positions, which clearly

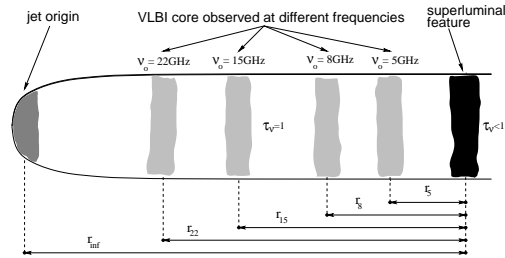


Figure 7. Frequency-dependent synchrotron opacity in jets (Lobanov 1998).

cannot be ignored at VLBI2010 levels of precision. The radio emission from synchrotron jets has been modeled, with predictions of core-shifts from the jet base, $\Delta \mathbf{x}$, varying as a power-law with wavelength ($\Delta \mathbf{x}(\lambda) \propto \lambda^\beta$) or, re-writing:

$$\Delta \mathbf{x}(\nu) = \Delta \mathbf{x}_{\text{ref}} (\nu/\nu_{\text{ref}})^{-\beta}$$

where $\Delta \mathbf{x}_{\text{ref}}$ is the core-shift at a reference frequency ν_{ref} , $\beta = 1/k_r$ and k_r is determined by the physical conditions in the jet (Lobanov 1998). For equipartition of energy in particles and magnetic field, $k_r = 1$ and $\beta = 1$, and $\Delta \mathbf{x}_{\text{ref}} \propto (\text{luminosity})^{2/3}$ (Blandford & Königl 1979). Examples of measured core-shifts are given in Fig. 8.

The consequences of core-shifts on the use of group delays for global astrometry have been investigated by Porcas (2009). A “chromatic” core position introduces an additional interferometer phase term as a function of frequency, equivalent to a “dispersive” path (see Fig. 9). This is also true if the “core” is used as the reference point for visible structure corrections (see Section 5.1). In general, group delays measure a “reduced” core-shift from the jet base, $\Delta \mathbf{x}_{\text{group}}(\nu)$ of

$$\Delta \mathbf{x}_{\text{group}}(\nu) = (1 - \beta)\Delta \mathbf{x}(\nu)$$

Curiously, for the astrophysically significant case of $\beta = 1$, group delays measure **no** core-shift at all *at any frequency* because the phase term is a *constant over all frequencies*. They do, however, measure the position of the jet base. Note that “X-band positions” listed for the ICRF sources and the VLBA Calibrator Survey (VCS) also refer to this point, and not to the position of the

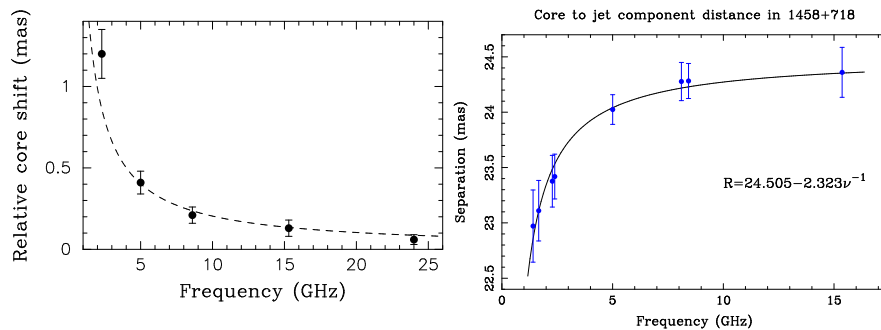


Figure 8. Left: Frequency dependence of the core position of 0850+581 measured relative to its position at 43 GHz. The curve represents the best fit for the function $r_c \propto \nu^{-1/k_r}$, where $k_r = 1.1 \pm 0.1$ (from Kovalev et al. 2008b). Right: Frequency dependence of the distance between the position of the core of 1458+718 (3C 309.1) and the centroid position of a reference feature in the jet. The curve fitted to the data is for the pure synchrotron self-absorption case with $k_r = 1$ (from Kovalev et al. 2008c).

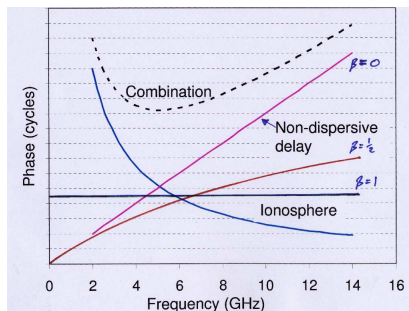


Figure 9. Modified “Petrachenko” plot showing dispersive phase for core-shifts with $\beta = 0.5$ and $\beta = 1$ (adapted from Petrachenko 2009).

X–band core, which is offset by (typically) $\sim 170 \mu\text{as}$ (corresponding to the median S–X shift of $440 \mu\text{as}$). These jet base positions are much closer to the central AGN black holes (which **are**, unfortunately, black!) and may even be more stable than “core” positions.

For VLBI2010 it will be necessary for the dispersive contributions to the broadband group delays and “phase delays” of both the ionospheric paths *and* core-shifts to be estimated and removed. Whereas the ionospheric contribution must be estimated for every scan, it can be hoped that a 3-parameter description of the core-shift (β , and the magnitude and position–angle of $\Delta\mathbf{x}_{\text{ref}}$) for each source may be stable for months or years, and can be stored (and updated) in a source database. This would, of course, be a valuable resource for astrophysical studies. (An inferior scheme would be to avoid observations with baselines along jet directions—see Section 5.2.) Hobiger et al. (2009) have investigated how ionospheric and *discrete* core-shift contributions affect the integer phase ambiguity estimates when interpolating the phase between the four separate frequency bands. However, it seems unlikely that the *continuous* nature of the core-shift phase contribution, both within and between the bands, will make this phase interpolation more difficult.

A special case occurs when $\beta=1$, where the effect of the core-shift is a *frequency-independent* phase offset, ϕ_{cs} . For the typical core-shift value at X–band of $170 \mu\text{as}$, ϕ_{cs} can reach values up to $\sim 50^\circ$ on long baselines such as Westford to Wettzell, when oriented parallel to the core-shift direction. When $\beta=1$ the core-shift has *no* effect on the estimate of VLBI2010 broadband group delays, which are derived from phase differences and phase gradients only (Petrachenko 2009). Source positions derived from this analysis (after removal of the ionospheric delay contribution) refer to the position of the jet base at all frequencies. However, ϕ_{cs} *does* make a contribution to the total phase, ϕ_{tot} , and hence must be accounted for when using VLBI2010 broadband “phase-delays”. Petrachenko (2009) has outlined a procedure whereby the unknown integer cycles of phase, $n(\nu)$, (where $\phi_{\text{tot}}(\nu) = \phi(\nu) + 2\pi n(\nu)$) can be deduced from group delays by successively refining estimates of the non-dispersive delay, τ , and the ionospheric path, K . This method assumes that any constant phase terms (e.g., instrumental phases) have been accounted for. The core-shift phase, ϕ_{cs} , is such a term, however, which cannot be estimated from a single scan. Thus determination of the $n(\nu)$ for each broadband “phase delay” will require either prior knowledge of $\Delta\mathbf{x}_{\text{ref}}$ or it must be estimated *simultaneously* with the $n(\nu)$ from a number of scans. Note that source positions derived from “phase delays” will refer to the position of the core at the frequency for which the total phase is estimated if ϕ_{cs} is included as part of the “phase delay”, but to the jet base if it is removed.

6. Acknowledgements

I thank Bill Petrachenko and Arthur Niell for interesting discussions on the topic of VLBI2010, Walter Alef for thoughtful comments on the manuscript, and Christian Fromm for providing images of 3C 111. This presentation has made use of data from the MOJAVE database that is maintained by the MOJAVE team (Lister et al. 2009).

References

- [1] Blandford, R.D. & Königl, A. 1979, *ApJ* 232, 34–48
- [2] Charlot, P. 1990, *AJ* 99, 1309–1326
- [3] Charlot, P. 1991, *Proc. IAU Coll. 131*, ed. Cornwell & Perley, *ASP Conf. Series* 19, 302–306
- [4] Gwinn, C.R., Eubanks, T.M., Pyne, T., Birkinshaw, M. & Matsakis, D.N. 1997, *ApJ* 485, 87–91
- [5] Fey, A.L. & Charlot, P. 1997, *ApJ Sup.* 111, 95–142
- [6] Fey, A.L. & Charlot, P. 2000, *ApJ Sup.* 128, 17–83
- [7] Hobiger, T., Sekido, M., Koyama, Y. & Kondo, T. 2009, *Adv. Sp. Res.* 43, 187–192
- [8] Kadler, M., Ros, E., Perucho, M. et al. 2008, *ApJ* 680, 867–884
- [9] Kovalev, Y.Y., Lobanov, A.P., Pushkarev, A.B. & Zensus, J.A. 2008a, *A&A* 330, 759–768
- [10] Kovalev, Y.Y., Lobanov, A.P. & Pushkarev, A.B. 2008b, *MmSAI* 79, 1153–1156
- [11] Kovalev, Y.Y., Pushkarev, A.B., Lobanov, A.P. & Sokolovsky, K.V. 2008c, *Proc. 9th EVN Symposium*, POS 7, 1–6
- [12] Lindegren, L., Babusiaux, C., Bailer-Jones, C. et al. 2007, *Proc. IAU Symp.* 248, ed. Jin et al., Cambridge UP, 217–223
- [13] Lister, M.L., Aller, H.D., Aller, M.F. et al. 2009, *AJ* 137, 3718–3729
- [14] Lobanov, A.P. 1998, *A&A* 330, 79–89
- [15] Malkin, Z. 2008, *Proc. 5th IVS GM*, ed. Finkelstein & Behrend, Saint Petersburg, 178–182
- [16] Petrachenko, B. 2009, “Broadband Delay Tutorial”, *FRFF Workshop*, Wetzell.
http://www.wetzell.ifag.de/veranstaltungen/vlbi/frff2009/Part2/01-Bill_bbd2.pdf
- [17] Petrov, L. 2007, *Proc. 18th Working Meeting on European VLBI for Geodesy & Astrometry*, ed. Böhm et al., TU Wien, 141–146
- [18] Porcas, R.W. 2009, *A&A* 505, L1–L4
- [19] Porcas, R.W. & Rioja, M.J. 1997, *Proc. 12th Working Meeting on European VLBI for Geodesy & Astrometry*, ed. Pettersen, Statens Kartverk Geodesidivisjonen, Honefoss, 133–143
- [20] Rioja, M.J. & Porcas, R.W. 2000, *A&A* 355, 552–563
- [21] Savolainen, T. & Kovalev, Y.Y. 2008, *A&A* 489, L33–L36
- [22] Sazhin, M.V., Zharov, V.E., Volynkin, A.V. & Kalinina, T.A. 1998, *MNRAS* 300, 287–291
- [23] Schwab, F.R. & Cotton, W.D. 1983, *AJ* 88, 688–694
- [24] Shaffer, D.B., Marscher, A.P., Marcaide, J. & Romney, J.D. 1987, *ApJ* 314, L1–L5
- [25] Titov, O. 2009, *Proc. 19th Working Meeting on European VLBI for Geodesy & Astrometry*, ed. Bourda et al., Université Bordeaux, 14–19

Differences Between VLBI2010 and S/X Hardware

Brian Corey

MIT Haystack Observatory

e-mail: bec@haystack.mit.edu

Abstract

While the overall architecture is similar for the station hardware in current S/X systems and in the VLBI2010 systems under development, various functions are implemented differently. Some of these differences, and the reasons behind them, are described here.

1. Scope

This paper compares various aspects of the station hardware in S/X-band geodetic VLBI systems and in forthcoming VLBI2010 systems. Components in the signal path from the antenna feed down to the data formatter are treated. Outside the scope of this paper are the antenna structure itself, the data formatter and recorder, the time and frequency standard, and ancillary equipment (e.g., meteorological instruments). The discussion here of VLBI2010 is biased toward the hardware under development for the NASA proof-of-concept system. Other groups are investigating alternative approaches, some of which are described in other papers in these proceedings.

2. Drivers Behind Design Decisions

Table 1 summarizes the most important characteristics of the S/X and VLBI2010 systems as they relate to the hardware design. For VLBI2010, it is assumed that the primary observable is the so-called “broadband delay,” which is described in [4].

Table 1. Some S/X and VLBI2010 Characteristics

	S/X	VLBI2010
<i>No. polarizations</i>	1	2
<i>No. observing bands</i>	2	4
<i>Bandwidth per band</i>	~200 MHz / ~800 MHz	1 GHz ¹
<i>Center frequencies of bands</i>	~2.3 GHz / ~8.6 GHz	Tunable over 2–14 GHz
<i>Total recorded data rate</i>	128–512 Mbps	32 Gbps ¹
<i>Delay precision per observation</i>	10–30 ps	~4 ps

Compared with S/X, VLBI2010 will record more bandwidth over a wider frequency span and will therefore “see” more RFI. In order to avoid RFI, the frequency locations of the four VLBI2010 bands must be adjustable, possibly from session to session. This wider frequency range and band tunability are the primary drivers behind many of the differences in hardware design.

¹The bandwidth and data rate of the NASA proof-of-concept system are half these values.

3. Antenna Feed

S/X feeds are designed to receive circularly polarized (CP) radio waves, not linearly polarized (LP). The primary advantage of CP feeds is related to the fact that the relative orientation of the two feeds on a VLBI baseline changes as a source is tracked across the sky, for all antenna mount types besides equatorial. For LP feeds, this change in orientation causes each parallel- or cross-hands fringe amplitude to vary with time, and in some cases can cause the amplitude to pass through a null. In contrast, for CP feeds the amplitude is independent of feed orientation.

Constructing a CP feed with low loss and good polarization purity is relatively straightforward for a fractional bandwidth of order 10%, as for S/X, but it is difficult for bandwidths exceeding an octave. Almost all wideband feeds that have been, or are being, developed (e.g., the Eleven feed [3]) and could be used in VLBI2010 are intrinsically LP. There are at least three options for creating CP signals from two orthogonal LP signals:

- Add a wideband quadrature hybrid after the feed to create circular from the two linears.
- After the sampler, create circular from the two linears in the digital domain [1].
- Record both LP signals at each station; after correlating all LP parallel- and cross-hands, create CP visibilities from the four LP cross-products.

The choice among these options (and others) has yet to be made for VLBI2010.

4. Low-noise Amplifier

The essential features and performance of an S/X and VLBI2010 low-noise amplifier (LNA) are similar: multi-stage, cryogenically cooled, transistor amplifiers with 30–40 dB gain and 5–20 K noise temperature. Unlike the S/X case, however, where only one LNA is required per polarization/band, the design of some VLBI2010-suitable feeds (e.g., [3]) entails the use of two, and perhaps even four, LNAs per polarization, with their outputs combined in one or three hybrids.

The wider bandwidth of the VLBI2010 system makes it more likely that RFI will fall within the LNA frequency range. Even if the RFI falls outside the frequency range of the recorded data, it can degrade the data SNR if it is strong enough to saturate the LNA or the post-LNA electronics. The electronics must therefore have sufficient output power capability to withstand any in- or out-of-band RFI without saturating. Notch filters could be employed to attenuate severe, fixed-frequency RFI, but it may not be possible to insert them ahead of the LNA.

5. Frequency Downconversion

For both S/X and VLBI2010, downconversion from the sky frequency to the frequency of the recordings is normally done in two steps: first from the sky frequency (RF) to an intermediate frequency (IF) somewhere in the range 100–2000 MHz, and then from IF to baseband, which extends from DC to <50 MHz.

5.1. Downconversion from RF to IF

Figure 1 illustrates two downconversion techniques used at cm wavelengths. The upper one is common in S/X systems, where the RF frequency band of interest never changes. The IF output

from the mixer is the same as the RF input except shifted down in frequency by the local oscillator (LO) signal. In the absence of any filtering ahead of the mixer, RF signals at two frequencies can appear at the same IF output frequency: one at $RF1 = LO + IF$ (the upper sideband = USB) and another at $RF2 = LO - IF$ (the lower sideband = LSB). The “image rejection” filter in the RF path ensures that the output signal comes from just one input sideband and is not contaminated by the “image” frequency sideband.

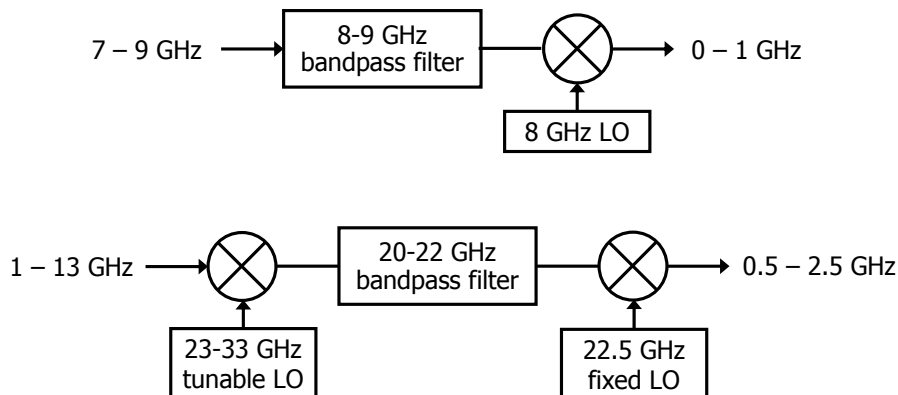


Figure 1. Simplified block diagrams of two types of single-sideband frequency downconverters. *Top*: Fixed-frequency downconverter, in which the 8–9 GHz input is translated down to 0–1 GHz, and all other input frequencies are blocked. *Bottom*: Tunable up/down converter [6], in which the 2-GHz-wide portion of the input spectrum that is translated down to 0.5–2.5 GHz varies with the first LO frequency. The input frequency corresponding to the output center frequency of 1.5 GHz is (1st LO – 21 GHz).

The above technique is impractical for VLBI2010, since the RF observing bands must be adjustable, and high-quality filters that are tunable over 2–14 GHz do not exist. An alternative scheme, which has been implemented in the NASA proof-of-concept test-bed, is the so-called up/down converter (UDC) illustrated in the lower part of Figure 1. Here the downconversion is carried out in two steps, first raising the frequency by mixing the input signal with a high-frequency LO, and then dropping the frequency to IF by mixing with a fixed-frequency LO. A bandpass filter between the two mixers provides image rejection. By changing the first LO frequency, the input RF frequency that appears at a given output frequency can be changed.

A potential future candidate for a tunable VLBI2010 RF-to-IF downconverter is an image-rejection, or single-sideband (SSB), mixer. Such a mixer employs two mixers driven by a common LO and phasing techniques among the signals to generate separate outputs for the input upper and lower sidebands, without the need of a filter. As with the UDC, the output can be tuned to different input frequencies by varying the LO frequency. It has not yet proven possible to build an SSB mixer operating over the wide VLBI2010 bandwidth with acceptable image rejection (of order 50 dB). But recent developments [2] in mixed analog/digital circuit design demonstrate that such an SSB mixer might be feasible in the near future. An advantage of an SSB mixer is that it does not use high-frequency (>20 GHz) components, which tend to be costly and less phase-stable.

Four downconverters per polarization are required to support the four-band observations of VLBI2010. Considerations of size, maintenance, and thermal control, among others, argue for

placing the downconverters in the control room, rather than on the antenna, where they are located in nearly all (but not all) S/X receivers. The VLBI2010 RF signals will be brought down over optical fiber, instead of the coaxial cable used in most (but not all!) S/X systems.²

5.2. Downconversion from IF to Baseband

Until recent years, all S/X systems used analog baseband converters (BBCs) to downconvert from IF to baseband. In each BBC, an SSB mixer provides separate USB and LSB outputs. The multiple frequency channels per band needed for bandwidth synthesis are realized by multiple BBCs, each with a different LO frequency.

In principle, VLBI2010 could also use analog BBCs, but digital back-ends (DBEs) provide an alternative that is far more flexible, electrically stable in phase and gain magnitude, and affordable. DBEs under development at several institutions are described in papers in these proceedings. DBE firmware comes in two flavors:

- Digital downconverter (DDC or DBBC): Each DDC functions like an analog BBC, with a tunable LO to downconvert two IF sidebands on either side of the LO to baseband. As in analog systems, multiple DDCs are needed to provide the multiple baseband channels for bandwidth synthesis.
- Polyphase filterbank (PFB): A PFB splits the input into 2^N equal-width frequency channels, which are in effect all downconverted simultaneously to baseband on separate outputs. The input-to-output frequency mapping is much less flexible in a PFB than in a DDC, but that loss of flexibility ought not to be a significant limitation for VLBI2010.

An obvious difference between analog BBCs and DBEs is that signal sampling/digitization occurs after the BBC but before the DBE. With analog baseband bandwidths generally ≤ 16 MHz, the sample clock need run no faster than 32 MSps. In VLBI2010, however, the analog bandwidth defined by the anti-alias filter at the sampler input will be 1024 MHz, and the sample clock must run at 2048 MSps. (As noted in Table 1, the bandwidth and clock rate in the proof-of-concept system are half as large.)

6. Phase Calibration

A phase calibration system enables corrections for temporal variations in: (1) relative LO phases between BBCs within a band, (2) relative LO phases between bands, and (3) phase/delay drifts in RF or IF cables or electronics. The first type of correction is critical for S/X geodesy but is unnecessary with the super-stable, digital-equivalent LOs of a (properly functioning!) DBE. On the other hand, the second is important for VLBI2010 but is irrelevant to S/X unless the phase delay observable is being used. Even aside from the third factor, it is thus apparent that phase calibration is needed for both S/X and VLBI2010.

Compared with an S/X calibration system, a VLBI2010 system must operate to a somewhat higher frequency (~ 14 GHz vs. ~ 9 GHz). A lower temperature sensitivity is also desirable, to help meet the more stringent VLBI2010 performance goals. A new calibrator design [5], which has been adopted for the NASA proof-of-concept system, generates the calibration pulses with a high-speed

²An early exception on both counts was the c.1995 Green Bank 20-meter receiver, which transmitted the S/X RF signals over optical fiber from the antenna to the control room, where the downconversion took place.

comparator and digital logic gate, rather than with a tunnel diode as in older S/X designs. The temperature sensitivity of <1 ps/ $^{\circ}$ C is better by an order of magnitude over S/X.

A potential problem for any VLBI2010 calibration system is overload in the RF analog electronics when the pulse is “on”. For the X-band portion of an S/X system with a bandwidth of ~ 1 GHz and a pulse repetition rate of 1 MHz, the peak pulse power is typically ~ 10 dB stronger than the system thermal noise. The pulse/noise power ratio scales with bandwidth, so that in the 12-GHz VLBI2010 bandwidth, the pulse will be ~ 20 dB above the system noise, and amplifiers may be in danger of saturating. A method adopted in the proof-of-concept system to reduce this danger is to attenuate the pulses, while at the same time increasing the pulse rate from 1 to 5 MHz. The increase in rate has two effects: it reduces the number of tones in the frequency domain, from one every 1 MHz to one every 5 MHz, and it increases the amplitude of each of the remaining tones by a factor of five. By balancing this amplitude increase against the decrease from the pulse attenuation, the strength of the tones can be maintained at a level high enough to ensure satisfactory phase measurement precision and immunity from spurious signal contamination.

The pulses should be injected into the receiver as close as possible to the point where the microwaves enter the receiver. In S/X receivers this is normally done in a directional coupler between the feed and LNA. This method may not be practical in VLBI2010 receivers because of the nature of the wideband feeds. Instead, injection for each polarization may occur after the LNAs and combiners. Alternatively, pulses could be radiated into the feed from a small antenna mounted on the main antenna structure. Multipath is a potential problem with this approach.

Most S/X systems include a cable measurement system for measuring variations in the electrical length of the cable (coax or optical) carrying the reference signal to the pulse generator. Use of cables with low sensitivity of delay to temperature and mechanical stress may make a cable measurement system unnecessary in VLBI2010, but this issue requires further study.

7. Acknowledgments

I have benefited from conversations with all members of the “broadband development team,” including especially Bill Petrachenko, Chris Beaudoin, Arthur Niell, Alan Rogers, and Tom Clark.

References

- [1] Das, K., A. L. Roy, R. Keller, G. Tuccari, Conversion from Linear to Circular Polarization in FPGA, *Astron. Astrophys.*, **509**, A23, 2010.
- [2] Morgan, M. A., J. R. Fisher, Experiments with Calibrated Digital Sideband-Separating Downconversion, *Publ. Astron. Soc. Pacific*, **122**, 326–335, 2010.
- [3] Pantaleev, M., et al., Cryogenic Integration of the 2–14 GHz Eleven Feed in Wideband Receiver for VLBI2010, these proceedings, 2010.
- [4] Petrachenko, B., et al., Design Aspects of the VLBI2010 System: Progress Report of the IVS VLBI2010 Committee, In: *International VLBI Service for Geodesy and Astrometry 2008 Annual Report*, NASA/TP–2009-214183, D. Behrend and K. D. Baver (eds.), 13–67, 2009.
- [5] Rogers, A. E. E., Tests of New “Digital” Phase Calibrator, Haystack BBDev Memo #023, available at http://www.haystack.mit.edu/geo/vlbi_td/BBDev/023.pdf, 2010.
- [6] Rogers, A. E. E., Updown Converter Notes, Haystack Mark 5 Memo #070, available at http://www.haystack.mit.edu/tech/vlbi/mark5/mark5_memos/070.pdf, 2010.

The NASA VLBI2010 Proof-of-concept Demonstration and Future Plans

Arthur Niell and the Broadband Development Team

MIT Haystack Observatory

e-mail: aen@haystack.mit.edu

Abstract

The next generation geodetic VLBI instrument is being developed with a goal of 1 mm position uncertainty in twenty-four hours. We have implemented a proof-of-concept system for a possible VLBI2010 signal chain, from feed through recorder, on the Westford (Massachusetts, USA) 18-m and MV-3 (Maryland, USA) 5-m antennas. Data have been obtained in four 512 MHz bands spanning the range 3.5 to 11 GHz to investigate the sensitivity and phase delay capability of the system. Using a new phase cal design, the phases have been aligned across four bands spanning 2 GHz with an RMS deviation of approximately eight degrees. Several components of the system will be improved for the prototype version of VLBI2010, including the feed, digital backend, and recorder, and these will be installed on a 12-m antenna that has been purchased and is ready for installation at the Goddard Space Flight Center outside of Washington, D.C., USA, site of the MV-3 antenna.

1. Proof-of-concept System

Recognizing that spatial and temporal fluctuations in the atmosphere delay are a major component of the error in position determination, the VLBI2010 Committee carried out a large number of simulations to arrive at design goals for the next generation geodetic VLBI antenna system [1]. A primary goal is the implementation of fast slewing antennas that attain high delay precision per observation. Taking into account existing and anticipated data recording capabilities, these translate to an antenna diameter of 12 m or larger and delay precision of approximately 4 psec. With funding from NASA's Earth Surface and Interior Focus Area, a proof-of-concept (PofC) project was initiated to demonstrate that the VLBI2010 concept is attainable.

Obtaining good sensitivity from relatively small antennas in a short time requires a large data acquisition rate. By spreading the data acquisition over four bands spanning 2-14 GHz instead of the two bands used by the current geodetic VLBI systems at S-band and X-band, enough phase precision is expected to be obtained to estimate both the phase delay and the dispersive phase deviation due to the ionosphere for each scan.

Of course the large total bandwidth increases the probability that radio frequency interference (RFI) will lie within the observed frequency range of the feed and receiver. Thus the band selection has been made tunable by using four separate UpDown Converters (UDC), one for each band. In addition to offering some RFI avoidance capability, the flexibility is important to be able to accommodate placing bands at S and X for compatibility with legacy antennas that are not able to upgrade, while having the option to use a higher minimum frequency to avoid RFI when only stations with the VLBI2010 broadband capability are participating.

The large instantaneously available bandwidth of the PofC front-end is made possible with the ETS-Lindren 3164-05 dual linearly-polarized broadband antenna. While this antenna has neither

a frequency-independent beam size nor phase center, it was commercially available at the initiation of the project and was affordable. A new feed is under development with the desired properties.

Thus the solution for obtaining enough sensitivity and delay precision from fast, and therefore likely to be small, antennas is a dual polarization, wideband feed followed by four independent local oscillators and digital backends, recording at 2 Gbps on four Mark 5B+ recorders (Figure 1a). In order to increase the sensitivity, the feed and low noise amplifiers are cooled to 20 K. Phase and noise calibration signals are injected immediately following the feed. A new phase cal generator was designed and implemented to replace the obsolete S/X phase cal [2]. The amplified RF signals for each polarization are brought down on fiber optic cable to the control room where the signals are split, down-converted [3], digitized, and recorded. All of the control room electronics are contained in a single rack (Figure 1b).

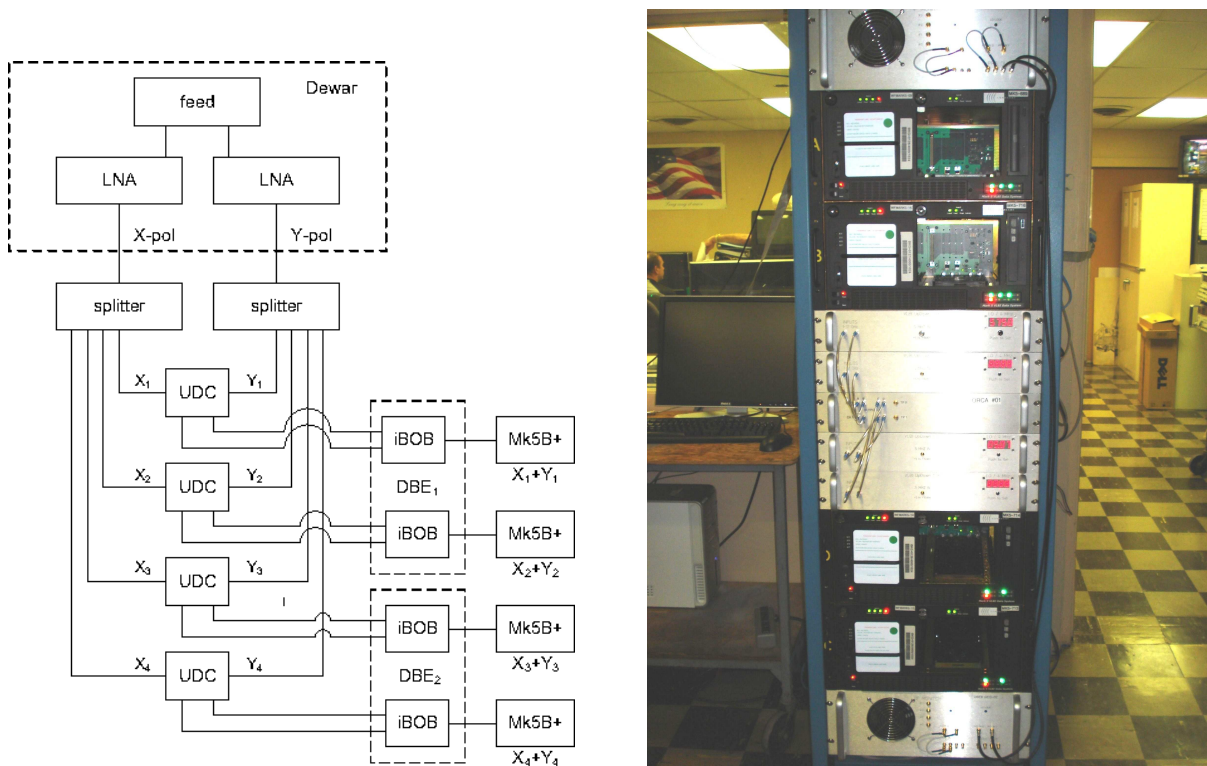


Figure 1. a) Configuration for the VLBI2010 system: LNA – low noise amplifiers; UDC – UpDown Converter (flexible local oscillator); iBOB/DBE – digital back end; Mk5B+ – high speed (2 gigabits per second) digital recorder; X and Y – two orthogonal components of linear polarization. b) Rack at Westford containing all of the VLBI2010 proof-of-concept backend equipment.

The PofC systems were installed on the Westford (Massachusetts, USA) 18-meter antenna and the MV-3 5-meter antenna at Goddard Geophysical and Astrophysical Observatory (Maryland, USA). Figure 2 shows the Dewar mounted on MV-3.

The optimum focus setting for Westford was determined by varying the distance of the Dewar from the vertex of the antenna for successive VLBI scans. The optimum focus is frequency dependent, and there appears to be a dependence on polarization at the higher frequencies. We expect these effects to be significantly reduced with the next generation of feed.



Figure 2. MV-3 5-m antenna at GGAO with the VLBI2010 proof-of-concept Dewar mounted at the Cassegrain focus.

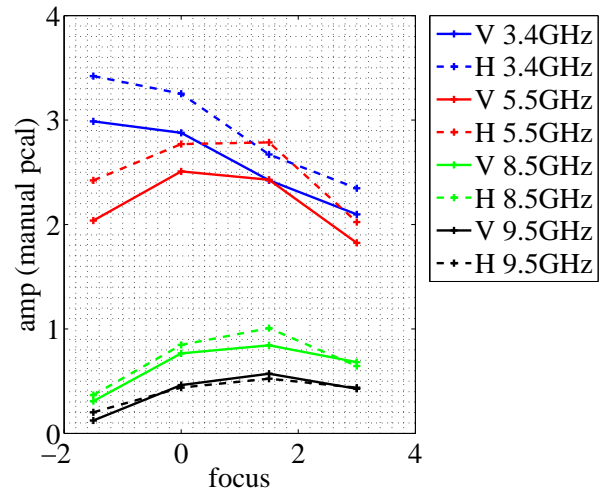


Figure 3. Amplitude as a function of focal distance for the Westford antenna. Frequency increases from top to bottom at focus = 0.

2. Results

The fundamental observable for the VLBI2010 system is planned to be the ambiguity-resolved phase delay. The quadratic phase term due primarily to the differential ionosphere will be estimated simultaneously with the phase delay. However, with two independent polarizations there are two estimates of the delay. These two estimates should differ only by a constant amount due to the uncalibrated electrical path lengths preceding the phase cal injection at each site, i.e., through the feed and coax to the injection points.

Several observations have been conducted to study various aspects of the broadband system and the associated delay observables. Firstly, observations of the source 4C39.25, which transits north of MV-3 and south of Westford, were conducted because of the large change in parallactic angle. This observation demonstrated the expected amplitude variation for the change in differential parallactic angle. The cross-correlation amplitudes for VV (called LL for historical reasons) and for HV (RL) are shown in Figure 4. The variations agree at least qualitatively with the expected characteristics.

Secondly, a pair of sources, 3C273 and 3C279, was observed alternately ten minutes at a time to see what changes might occur due to antenna movement. For the latter pair it is expected that there will be some common atmosphere delay variation that will cancel on differencing, although the sources are too far apart and the scans too long for very accurate differencing.

Lastly, an independent 10 minute 6.4–8.4 GHz observation of 4C39.25 was also conducted. The results of this observation show that the RMS of the fringe phases after phase cal correction is approximately 8° , which corresponds to a group delay uncertainty of ~ 10 psec. (See Beaudoin and Niell, this volume, for figure.)

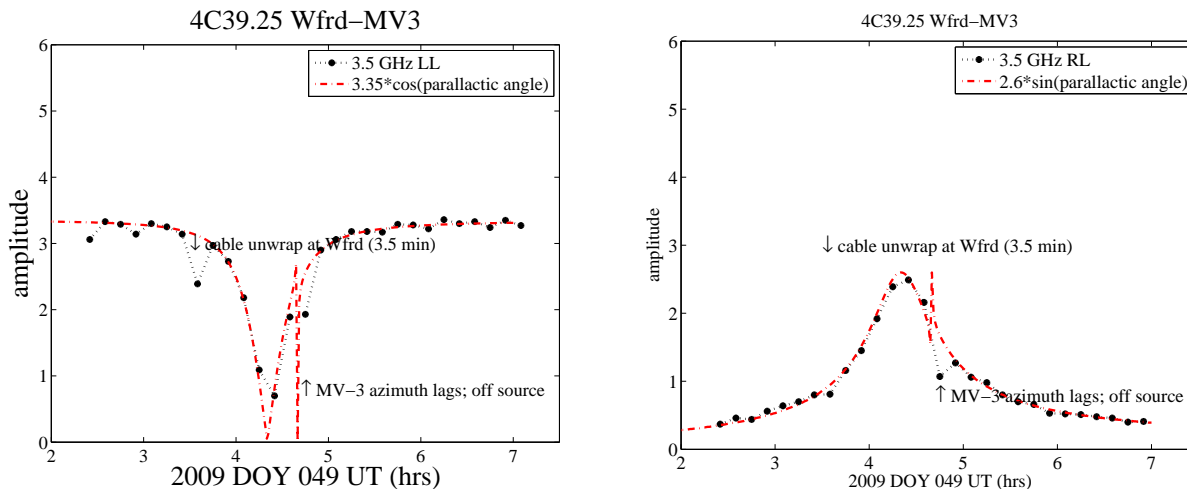


Figure 4. Cross-correlation amplitudes for LL (VV) and RL (HV) polarizations for 3.5 - 4 GHz band. The amplitude of the fitted curve is estimated from the data, not from any a priori system calibration and source information. Parallactic angle refers to the difference of the parallactic angles.

3. Next Steps

The PofC demonstration has taken much longer than anticipated, but finally there is a data set to work with to investigate the best way to derive the phase delay observable. Although not discussed here, the post-correlation analysis program fourfit has been enhanced to fit all four bands of one polarization with an ionosphere term, in preparation for estimating the ionosphere contribution along with the other scan observables.

Many improvements are in progress for the prototype system. The most significant is the construction of a 12-m antenna to replace MV-3 at GGAO. The phase cal unit will be installed in a temperature control box. The iBOB and Mark 5B+ combination will be replaced by the RDBE and Mark 5C. The quadridge feed will be replaced by the Eleven feed. All of these will improve either the sensitivity or the delay measurement precision and accuracy.

4. Acknowledgments

The broadband demonstration system is funded by the NASA Earth Surface and Interior Focus Area through the efforts of John LaBrecque, Chopo Ma, and Herb Frey.

Important contributions were made by all participants of the Broadband Development Team: Bruce Whittier, Mike Titus, Jason SooHoo, Dan Smythe, Alan Rogers, Jay Redmond, Mike Poirier, Arthur Niell, Chuck Kodak, Alan Hinton, Ed Himwich, Skip Gordon, Mark Evangelista, Irv Diegel, Brian Corey, Tom Clark, and Chris Beaudoin.

In addition, the system could not have been put together without the work of Sandy Weinreb and Hamdi Mani of Caltech, whose design of the Dewar, feed, and LNAs has been copied directly. Beyond that they generously provided advice as we constructed the front ends. We also want to thank Dan MacMillan, Peter Bolis, Don Sousa, and Dave Fields for their help.

References

1. Beaudoin, C., Niell, A., Post-Correlation Processing for the VLBI2010 Proof-of-Concept System, this volume.
2. Petrachenko, B., et al., Design Aspects of the VLBI2010 System: Progress Report of the IVS VLBI2010 Committee, In: International VLBI Service for Geodesy and Astrometry 2008 Annual Report, NASA/TP-2009-214183, D. Behrend and K. D. Baver (eds.), 13-67, 2009.
3. Rogers, A. E. E., Tests of New “Digital” Phase Calibrator, Haystack BBDev Memo #023, available at http://www.haystack.mit.edu/geo/vlbi_td/BBDev/023.pdf, 2010.
4. Rogers, A. E. E., Updown Converter Notes, Haystack Mark 5 Memo #070, available at http://www.haystack.mit.edu/tech/vlbi/mark5/mark5_memos/070.pdf, 2010.

DBBC VLBI2010

*Gino Tuccari*¹, *Walter Alef*², *Alessandra Bertarini*³, *Salvatore Buttaccio*¹,
*Giovanni Comoretto*⁴, *Dave Graham*², *Alexander Neidhardt*⁵, *Pier Raffaele Platania*¹,
*Antonietta Russo*⁴, *Alan Roy*², *Michael Wunderlich*², *Reinhard Zeitlhöfner*⁶,
*Ying Xiang*⁷

¹) *Istituto di Radioastronomia – INAF*

²) *Max-Planck-Institut für Radioastronomie Bonn*

³) *Institut für Geodäsie und Geoinformation, Universität Bonn*

⁴) *Osservatorio di Arcetri – INAF*

⁵) *FESG München*

⁶) *BKG Wettzell*

⁷) *Shanghai Astronomical Observatory – CAS*

Contact author: *Gino Tuccari*, e-mail: g.tuccari@ira.inaf.it

Abstract

The DBBC2 backend system has been adapted for supporting the VLBI2010 demands. The system architecture for this application is presented.

1. Introduction

The VLBI2010 geodetic world is rapidly evolving, and a better delay estimation will be obtained using a collection of strategies including a much different antenna-receiver-backend system. Wider portions of band will be used, extracted from a very wide sky frequency range.

A pretty different backend is required, which is able to handle a higher data rate and has enough capability to down-convert a larger number of wide bandwidth channels in appropriate mode for correlation.

The DBBC system is modular in hardware and firmware, allowing it to realize an architecture able to include everything necessary to support the new VLBI2010 observational needs. The system in this implementation was named DBBC2010.

2. Architecture

A number of eight bands coming from the receiver represent the information input to the DBBC2010 backend. These are portions of band, 500 or 1000 MHz wide, down-converted with analog methods from a receiver able to observe between 2 and 15 GHz. So the first important difference with respect to a standard DBBC2 is the number of IFs the system needs to support: an increase from four to eight.

It was felt important that the total space for supporting the entire functionality would not be modified and so simple mechanical solutions have been required to handle the doubled number of input IFs.

The four Conditioning Modules have been then mechanically modified in order to handle two UNICA3 boards in the same space. Additionally a development is underway in order to reduce the filter size in the board and integrate all the amplification functionalities. As a result of all of this, eight input bands are conditioned and available internally to the system for further processing.

Twice the number of IFs requires twice the number of sampling boards. There are two possibilities, or to be more precise, three. The width of instantaneous bands can be selected between 512 MHz and 1024 MHz, but it was also introduced the possibility to handle 2048 MHz wide pieces of band, adopting the ADB3 sampling module. Such module is a stack of two ADB2 boards with an accompanying element, to make the sampling boards able to operate interleaved with a 2048 MHz clock. Nyquist input bands possible are 10–2048 MHz and 2048–3500 MHz. The output of such module is an aggregate of eight data busses to be sent in the standard HSI bus to the processing boards.

In order to have eight ADB sampling boards operating, it needs to have a doubled number of sampling clocks and related high resolution 1PPS signals, all of this operating at 1024 or 2048 MHz. This was realized with the new CAT2 board, where in a single PCB all the functionalities are present to generate clock and timing for the entire system, driven by the internal DBBC PC set.

At this point we have internally available a number of eight IFs in digital representation, ready to be introduced in the processing boards for the fixed band (FT) down-conversion. The difference is that we have twice the number of bands to handle now. Again we have more options to consider. A number of Core2 boards could be adopted to process the block of eight IFs, but if we need a much more efficient and cheaper method, the Core3 could be considered for this massive data handling.

The Core3 board is an evolution of the present Core2 processing board. It is mainly devoted to very high demanding processing capabilities. It is planned to be used as digital preprocessor for L2C polarization conversion and in applications like a very-high-number-of-channels spectrometer. For the VLBI2010 FT configurations with 1 or 2 GHz input bandwidth it looks like a very appropriate choice. In the DBBC2010 architecture it needs to have between two and four Core3 boards for processing all the eight IFs, depending on the instantaneously selected input bandwidth, as we have seen ranging between 512 and 2048 MHz. The Core3 hardware has been fully defined, and it is expected to have the boards available and tested before the end of 2010.

After the digital down-conversion we have a pretty high number of channels to handle. Let's have a look at how they aggregate. The clock accompanying the data is 64 MHz, and each 512 MHz is divided into 15 channels 32 MHz wide. This means we still have several possible conditions depending on the input bandwidth of our eight IFs. If we consider 8 x 512 MHz, there are 8 times 15 channels, while if we consider 8 x 1024 MHz, there are 8 times 31 channels to be transferred to an appropriate number of recorders. The Core3 board has a dedicated output channel able to feed the FILA10G network board directly, without having to transit from any VSI connection. This means that a number of FILA10G boards can be selected considering that a single FILA10G can support two Mark 5C recorders.

3. Conclusions

What was described here is the adaptation of a standard DBBC system to the VLBI2010 needs, with the implementation architecture named DBBC2010. It is evident that the modular structure

can easily accommodate such an observational mode, while it grows in data rate capacity. The number of IFs is well selected from the start, the input bandwidth with consequent increase of data rate demand can be selected and in case of need increased, so as the number of connections to Mark 5C units considering the total data rate to be obtained. Burst mode operation is possible even with the use of piggy-back memory modules, available in both Core2 and Core3 boards.

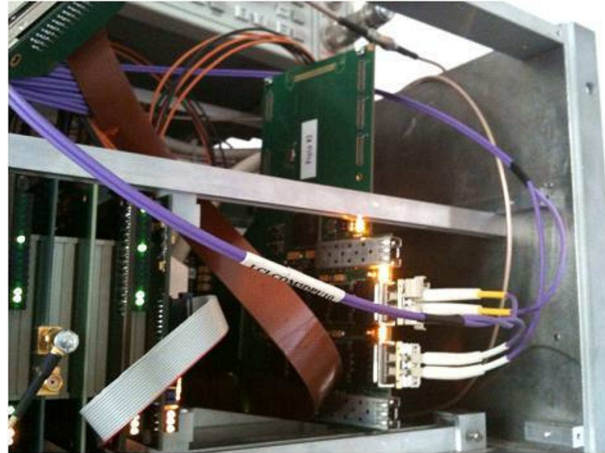


Figure 1. FILA10G board in the DBBC system.



Figure 2. GLAPPER (glass to copper) prototype board to connect a DBBC with a Mark 5C.

Differences Between S/X and VLBI2010 Operation

Hayo Hase ¹, Ed Himwich ², Alexander Neidhardt ³

¹) *BKG, Geodetic Observatory Wettzell*

²) *NVI Inc./NASA Goddard Space Flight Center*

³) *Forschungseinrichtung Satellitengeodäsie, TU München, Geodetic Observatory Wettzell*

Contact author: Hayo Hase, e-mail: hayo.hase@bkg.bund.de

Abstract

The intended VLBI2010 operation has some significant differences to the current S/X operation. The presentation focuses on the problem of extending the operation of a global VLBI network to continuous operation within the frame of the same given amount of human resources. Remote control operation is a suitable solution to minimize operational expenses. The implementation of remote control operation requires more site specific information. A concept of a distributed-centralized remote control of the operation and its implications is presented.

1. Present and Future Operation

The present IVS network operation is based on regular *24h* observation sessions, which are conducted by different networks with five or more stations, and on daily *1h* observation sessions with smaller networks up to three stations. The VLBI2010 idea proposes to replace the different sessions by a continuously observing (24/7) VLBI network, in which stations are permanently participating or are joining a couple of sessions per week. For the first case, the permanent observation, a new VLBI2010 radio telescope concept was developed, the so-called Twin-Telescope Wettzell. Having two identical radio telescopes at one site makes it possible to observe even if one of the telescopes stops for maintenance [1].

The increase of radio telescope usage time for geodetic VLBI requires not only increased availability of the radio telescope itself, but also of operators controlling the increased number of observing hours per station. Due to the fact that human labor cannot be increased at many IVS sites, a new strategy of network control instead of individual station control of VLBI operation needs to be implemented.

Considering the fact that VLBI observations will occur around the clock, it is possible to take advantage of the different daylight zones throughout the observation period for the network control operation (see Fig. 1). In this case, individual night shifts, which are difficult for the human body and therefore more expensive, may be saved at stations. The saved labor hour volume becomes available for a redistribution of network control shifts during the entire week. Therefore it will become in general possible to introduce continuous 24/7 operation into the future VLBI2010 observation scheme, without creating a big burden on the staff situation at each observatory.

The requirements for a network operation of a global VLBI network are:

- **reliable radio telescopes.** It is necessary that radio telescopes and the VLBI hardware may work unattended for 24 hours. This implies that a robust VLBI system is available at each of the VLBI2010 sites and that more sensors (video and acoustic), which will control the operation remotely, will be installed and become part of the operational system.

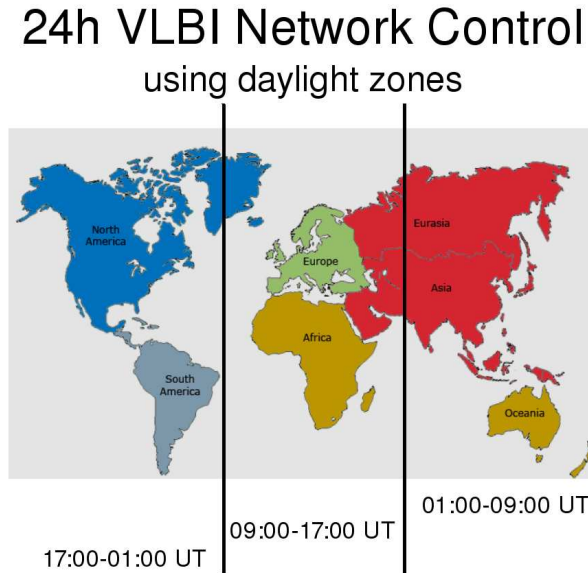


Figure 1. World map showing three daylight zones with proposed time slots for network control enabling continuous VLBI2010 observation.

- **reliable remote control software.** For remote control operation, safety issues and full Field System operation must be covered by the used software. This addresses standardization as much as possible for the radio telescope control as well for the station interface in general. Finally the remote control software must be robust against power failures and contain the information of an emergency hotline in case of a local failure which cannot be recovered remotely. A first attempt towards this goal is the e-control development at the Geodetic Observatory Wettzell, which allows radio telescopes to be controlled remotely [2]
- **reliable communication links between the control station and radio telescopes.** The Internet of today is fairly robust and could be the underlying technology to receive the necessary remote information about the status of the controlled instruments. Smart software developments must consider the minimization of the number of transmitted bytes from/to a remote controlled station. This is because the control of n radio telescopes requires n -times the bandwidth to the network controller of intercontinental distances with sometimes small bandwidth available.

2. Comparison Between Station Control vs. Network Control of an 8-Station Network

The current operation is labor intensive. Tab. 1 compares the number of staff needed with individual station control (current) versus network control (future VLBI2010). A usual VLBI operation shift is set to 8h. In an 8-station network, covering the entire week with continuous VLBI operations requires 168 ($=3 \times 7 \times 8$) shifts of 8h each for individual station control. Realizing the same amount of observation with network control creates the need for 21 ($=3 \times 7$) shifts for the network control itself. This control is done by one of the network stations and is handed over around the globe from daylight zone to daylight zone. In addition we request that once per

day each remote station is visited once during daylight to do local data carrier exchange work and local checking at each remotely operated station—adding 49 (=7x7) shifts. In total 70 shifts, instead of 168 shifts, need to be considered. These numbers can be translated to the number of staff needed at each site to do the VLBI operation. In the 24/7 continuous observation mode, six staff per station are needed with individual station control versus three staff per station with network control. (The number of staff considers five working days per week, a minimum of 12h pause between labor shifts, and vacations according to western European labor laws.)

The conclusion of this calculation is that only with network control can the ambitious goal of continuous 24/7 operation be reached with the available operator staff at many stations of the IVS network.

Table 1. Individual station control vs. network control of an 8-station network (24/7).

Number of	station control	network control
operators per 8h shift	8	1
shifts per week	168	70
staff needed	48	24
staff needed/station	6	3

3. Network Control

Once network control becomes available the question arises of where the network control should be located. There are two extreme positions, which are both valid:

- **decentralized network control by stations.** This requires perhaps some investments at radio telescope stations so that they can host the network control for regular daylight zone shifts in a globally shared manner. This way of operation will not lead to a cut in the existing staff at the sites, as the staff will be needed for both maintenance and operation. Past experience has shown that a minimum number of experienced staff is a necessity for providing a certain quality and quantity of data. The shared network operation with passing the network control through the daylight zones keeps the importance of each individual station and staff alive and strengthens the VLBI spirit. The shared and distributed network control is robust against failures of one controller as it can be passed easily to another station.
- **centralized network control by one center.** This control center could be located at one of the correlators or at the IVS Coordinating Center. If the network control is not shared among the participating network stations, it will become difficult to keep the importance of VLBI within the individual institutions alive.

Therefore it is concluded that the ownership of remote control shall be shared among the contributing network stations and perhaps further IVS components. From the perspective of most network stations, only the option of being sometimes in the position to control the entire network will enable the access to be remotely controlled. For the implementation of VLBI2010 operation in the future VLBI2010 network, the development of at least three network control centers, one in each daylight zone, will be the minimum to avoid costly night-shifts.

References

- [1] Hase, H., R. Dassing, G. Kronschnabl, W. Schlüter, W. Schwarz, R. Kilger, P. Lauber, A. Neidhardt, K. Pausch, W. Göldi, Twin Telescope Wettzell - a VLBI2010 Radio Telescope Project, In: *Measuring the Future, Proceedings of the Fifth IVS General Meeting, St. Petersburg, Nauka, 2008*, A. Finkelstein and Dirk Behrend (eds.), 109–113, 2008.
- [2] Neidhardt, A., Ettl, M., Zeitlhöfler, R., Plötz, C., Mühlbauer, M., Dassing, R., Hase, H., Sobarzo, S., Herrera, C., Alef, W., Rottmann, H., Himwich, E., A concept for remote control of VLBI-telescopes and first experiences at Wettzell, In: *Proceedings of the 19th Working Meeting on European VLBI for Geodesy and Astrometry, Bourda, G., Charlot, P., Collioud, A. (eds.), 136–140, 2009.*

Post-correlation Processing for the VLBI2010 Proof-of-concept System

Christopher Beaudoin, Arthur Niell

MIT Haystack Observatory

Contact author: Christopher Beaudoin, e-mail: cbeaudoin@haystack.mit.edu

Abstract

For the past three years, the MIT Haystack Observatory and the broadband team have been developing a proof-of-concept broadband geodetic VLBI microwave (2-12 GHz) receiver. Also on-going at Haystack is the development of post-correlation processing needed to extract the geodetic observables. Using this processing, the first fully-phase-calibrated geodetic fringes have been produced from observations conducted with the proof-of-concept system. The results we present show that the phase-calibrated phase residuals from four 512 MHz bands spanning 2 GHz have an RMS phase variation of 8° which corresponds to a delay uncertainty of 12 ps.

1. Raw Fringe Phasor Model

This development begins by assuming that one has at their disposal the normalized correlation coefficients for each frequency channel (whether represented in the cross-power frequency or lag domain) for each single correlator accumulation period (AP). The raw fringe phasor $\Phi_r(f)$ is then defined as the phase of the cross-power spectrum produced from the correlator output data and is assumed to be the product of the fringe phasor $\Phi_g(f)$ due to the residual geodetic delay and the hardware (phase cal) phasor $\Phi_{pc}(f)$, where f is the sky frequency. Furthermore, since amplitudes are currently not incorporated in the phase cal processing, the magnitude of all phasors considered in this note are arbitrarily set to unity.

The hardware-related phase is given by the phase calibration phasor $\Phi_{pc}(f)$ which represents the arithmetic difference between the phase cal phases obtained at each station. $\Phi_{pc}(f)$ is also sampled every $f = 5n$ MHz, where n is the rail harmonic number. In the context of this note, $\Phi_{pc}(f)$ will be modeled as a piecewise-linear phasor function composed of as many pieces as there are frequency channels as indicated in Figure 1. It is important to note that $\Phi_{pc}(f)$ is not simply the difference of the phase cal phases obtained directly from the correlator, since the pcal phases are sampled every 5 MHz and the fringe phases in each frequency channel, generally, are sampled at a different rate. Additional processing (interpolation) is needed to obtain $\Phi_{pc}(f)$ from the correlator pcal phases. This is discussed in the section on phase calibration fitting.

In regards to the phase due to the residual geodetic delay, systematic errors such as those introduced by clock drift and ionosphere delay are neglected here to place emphasis on the phase calibration processing needed to connect the raw fringe phases across several receiver bands. The residual geodetic fringe phasor (i.e., the error-free fringe phase), represented by the function $\Phi_g(f)$, is assumed to be linear in frequency since the aforementioned errors are ignored; estimation of $\Phi_g(f)$ from knowledge of $\Phi_r(f)$ and $\Phi_{pc}(f)$ is the goal of the correlator post-processing described in this paper. $\Phi_g(f)$ can be formally written as:

$$\Phi_g(f) = e^{2\pi f\tau_g} \tag{1}$$

where τ_g is the residual time delay (between the two stations) to the geodetic model. Under this development the raw fringe phase is assumed to be the product of the geodetic and phase cal phasors:

$$\Phi_r(f) = \Phi_g(f)\Phi_{pc}(f) \quad (2)$$

Figure 1 displays a graphical example of the phases $\Phi_r(f)$, $\Phi_{pc}(f)$, and $\Phi_g(f)$ for the current receiver architecture (eight 32 MHz channels per band and four 512 MHz bands) and band-to-band spacings Δf_1 through Δf_3 .

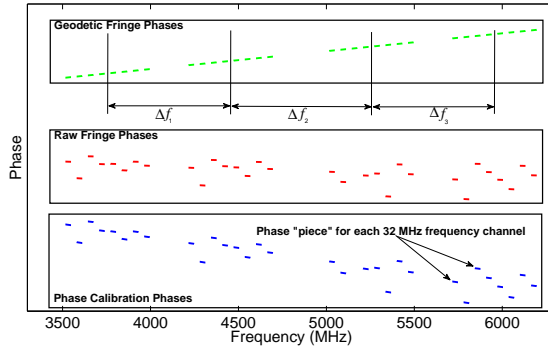


Figure 1. Graphical representation of geodetic fringe, raw fringe, and phase calibration phases.

2. Phase Calibration Phase Fitting - Derivation of $\Phi_{pc}(F)$

As mentioned previously, the phase cal tones are injected in the front-end of the receiver at frequencies which are multiples of 5 MHz whereas the frequencies at which the raw fringe phases are sampled, in general, are different. As a result, the phase cal data provided by the correlator must be fit to a model (linear in this case) in order that the phase calibration phases can be evaluated at the same sky frequencies as the raw fringe phases. The following model is used to describe the phase cal phasor provided by the correlator:

$$\Phi_{pc}^m(f) \Big|_{f=nf_r} = e^{2\pi n f_r \tau_{pc}^m + \phi_{pc}^m} \quad (3)$$

$\Phi_{pc}^m(f)$ describes the phase cal model for the m th frequency channel as a function of tone index n ; in this model $\Phi_{pc}^m(f)$ represents the arithmetic difference of the phase cal phases (as provided by the correlator) between the two stations for the given channel. In equation (3), f_r is the rail frequency spacing (5 MHz) and τ_{pc}^m and ϕ_{pc}^m are the phase cal delay and phase, respectively, for the m th channel; f and therefore n are bounded by the frequencies of the channel from which the phase calibration tones were extracted. Given the samples of $\Phi_{pc}^m(f)$, the task is to estimate τ_{pc}^m and ϕ_{pc}^m which, by inspection of equation (3), can be accomplished by applying a discrete Fourier transform (DFT) to $\Phi_{pc}^m(f)$. The DFT makes no assumptions about the frequency locations of the tones in any given channel, so there is no restriction on the tone selection. After τ_{pc}^m and ϕ_{pc}^m have been estimated, the interpolated pcal phasor $\Phi_{pc}^{mi}(f)$ can be expressed using the same linear model in equation (3) by simply substituting for the tone frequency nf_r the sky frequency

f corresponding to that at which the raw fringe phasor is evaluated:

$$\Phi_{pc}^{mi}(f) = e^{2\pi f\tau_{pc}^m + \phi_{pc}^m} \quad (4)$$

The complete phase calibration phasor (assuming there is no overlap of the frequency channels) is just the sum of the interpolated pcal phasors for each frequency channel:

$$\Phi_{pc}(f) = \sum_m \Phi_{pc}^{mi}(f) \quad (5)$$

3. Phase Calibration Correction of Raw Fringe Phases

The raw fringe phasor $\Phi_r(f)$ and phase calibration phasor $\Phi_{pc}(f)$ are produced by the correlator after each accumulation period (AP); therefore, $\Phi_r^m(f)$ can be corrected for each AP independently (this is the so-called AP-by-AP pcal mode). The benefit of the AP-by-AP mode is that hardware drift over extended scan periods is removed. Equation (2) indicates that the residual geodetic phasor can be obtained by simply multiplying the raw fringe phasor by the complex conjugate of the phase calibration phasor:

$$\Phi_g(f) = \Phi_r(f)\Phi_{pc}^*(f) \quad (6)$$

For the polyphase filter implementation of the frequency channelization currently implemented in the digital backend, the sky frequency f can be decomposed into a summation of the LO frequencies of the channels and the cross-power frequency relative to the channel LO frequency. Formally put:

$$f \equiv f_{LO}^m - k\Delta f_{cpf} \quad (7)$$

where f_{LO}^m is the LO frequency of channel m , f_{cpf} is the cross-power frequency sample interval, k is the cross-power frequency index (i.e., $0,1,2,\dots,N_{sc}-1$), and N_{sc} is the number of cross-power spectral samples in a single 32 MHz frequency channel. Equation (6) can now be rewritten using equations (4-5,7) to provide a more detailed formulation of the method used to correct the raw fringe phases and obtain the residual geodetic phases:

$$\Phi_g(f) = \Phi_r(f) \sum_m e^{-j2\pi f_{LO}^m \tau_{pc}^m} e^{j2\pi k \Delta f_{cpf} \tau_{pc}^m} e^{-j\phi_{pc}^m} \quad (8)$$

4. Broadband Phase Calibration Processing of Experiment 3296

Since the goal of the broadband phase calibration processing is to remove the hardware-related delay and phase from the raw fringe phasor, broadband fringe tests have been conducted on the Westford-GGAO baseline to demonstrate the performance of this processing. The broadband system possesses the flexibility to change the inter-band spacings Δ_{f1} through Δ_{f3} (depicted in Figure 1) with 400 kHz precision. In fact, the inter-band spacings can be set identically to zero which provides a quite useful diagnostic for validating the broadband phase calibration processing as outlined in this note. In this so-called ‘‘overlapping bands’’ configuration, all four bands observe an identical set of frequency channels, and the residual geodetic fringe phasors for each band (fringe fit independently) are expected to be identical if the receiver is truly front-end noise limited. In practice, the residual geodetic fringe phasors must be coherently averaged over all APs in the integration period in order to detect the interference fringes. Table 1 displays the raw

Table 1. Raw singleband/multiband delays, fringe rate, and phase results from fringe fitting.

	A	B	C	D
Singleband Delay (ns)	-2.334	1.374	-10.086	-4.063
Multiband Delay (ns)	-1.970	1.768	6.011	-3.635
Fringe Rate (mHz)	1.522	2.216	2.016	2.043
Fringe Phase ($^{\circ}$)	-157.7	-91.5	55.6	-72.2

Table 2. Phase-calibrated singleband/multiband delays, fringe rate, and phase results from fringe fitting.

	A	B	C	D
Singleband Delay (ns)	-0.503	0.180	-0.223	-0.241
Multiband Delay (ns)	0.076	0.069	0.083	0.092
Fringe Rate (mHz)	1.578	1.576	1.586	1.588
Fringe Phase ($^{\circ}$)	-144.5	-142.5	-144.6	-143.6

singleband/multiband delays, fringe rate, and phase for HH polarization obtained from an observation conducted on Day258 at 1403UT year 2009 (Haystack Exp: 3296) coherently averaged over the entire 10 minute scan. In this experiment, all four bands observed 6408.4-6888.4 MHz. The raw fringe phasors processed without the broadband phase calibration method are given in Table 1 and the calibrated counterparts of those parameters are given in Table 2. The uncertainties associated with the singleband/multiband delay, fringe rate, and phase are 0.2 ns, 0.013 ns, 0.011 mHz, and 1.4° , respectively. Comparison of Tables 1 and 2 demonstrates that the phase calibration processing is performing nearly as expected since the calibrated results for all four bands are in such good agreement; the minor discrepancies are under investigation.

During this same experiment, data were also collected such that the four bands spanned a total contiguous bandwidth of 2 GHz (6.4–8.4 GHz). Differences in cable lengths and local oscillator phases in the hardware comprising each frequency band introduce a hardware-related component to the raw residual fringe phase shown in Figure 2a. The discontinuities in Figure 2a appear at the spectral boundaries of adjacent frequency bands as a result of these hardware-related components. The raw data were phase calibrated using the technique described above, and the resultant calibrated fringe phases are shown in Figure 2b. As is obvious in comparing Figure 2a to 2b, the discontinuities are suppressed in the calibrated geodetic fringe phases. The resultant rms phase noise is 8.5° , which translates to a delay uncertainty of 12 ps across the 2 GHz of contiguous bandwidth. This delay uncertainty will be reduced by observing larger spanned bandwidths and this is one of the explicit goals of VLBI2010.

5. Conclusions and Future Plans

In order to remove the hardware-related phase and delay components from the raw fringe phasors, a new phase calibration correction algorithm has been developed. This processing was shown to reconcile the band-to-band delay and fringe rate differences when all four bands observed the identical set of sky frequencies, thus demonstrating the algorithm’s ability to remove the

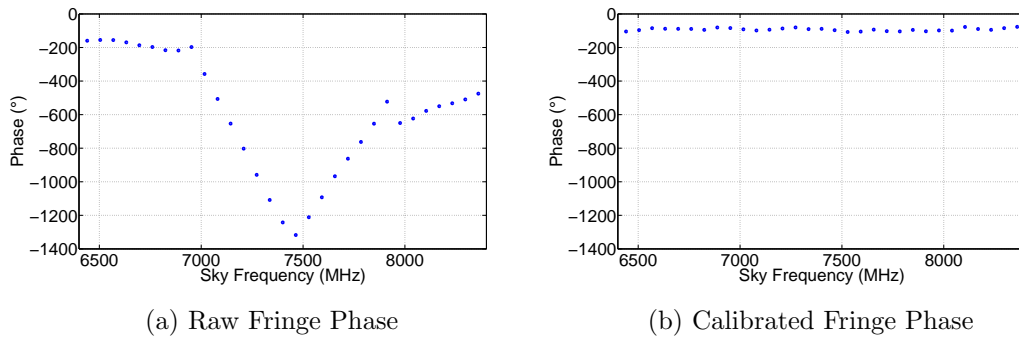


Figure 2. Raw and Calibrated Residual Fringe Phase vs. Sky Frequency

hardware-related components of the aforementioned delay/rate parameters. Though the observable parameters are fairly consistent, Table 2 demonstrates that there are post-correction differences between the bands. Observation of such discrepancies suggests that additional independent noise is added to the signal recorded in each frequency band after the 2-12 GHz microwave signal received by the front-end is equally split into each of the four frequency bands (signal chain [1] pp. 35). A signal chain cascade analysis indicates that the noise contributed by the analog components in each frequency band is negligible. The noise contributed by the digital backend (DBE) (i.e., ADC, fixed point math quantization errors), however, is not currently a quantity that can be measured directly. As such, there may be significant noise contribution by the DBE of which we are unaware. This situation will be rectified with the introduction of the next-generation DBE, at which point a full signal chain (analog/digital) noise budget can be developed to assess the expected uncertainties in the band-to-band post-correction residuals.

The phase calibration correction algorithm was also shown to align the raw fringe phases across a total bandwidth of 2 GHz, which resulted in a delay uncertainty of 12 ps. In order to reduce the delay precision of the geodetic observables, future observations will be conducted which span bandwidths greater than 2 GHz. In observing these wider bandwidths the ionosphere is expected to introduce a dispersive (non-linear) behavior in the fringe phase function (e.g., Figure 2b) which will require modification of the fringe fitting routine from a linear model to one that is dispersive. Finally, the results reported in this paper were for the linear HH polarization only. Developments of the fringe fitting algorithm will also need to incorporate all four polarization components (HH, HV, VH, and VV) into the geodetic fringe fitting process in order to further enhance the SNR and realize the goals of VLBI2010 [1].

6. Acknowledgements

This development of the processing algorithm described in this work is the result of many discussions with Brian Corey and Bill Petrachenko. Many thanks to them for their contributions.

References

- [1] B. Petrachenko, et. al., “Design Aspects of the VLBI2010 System,” International VLBI Service for Geodesy and Astrometry Annual Report 2008, NASA/TP-2009-214183, pp.13-66, July 2009

GPU Based Software Correlators - Perspectives for VLBI2010

Thomas Hobiger¹, Moritaka Kimura¹, Kazuhiro Takefuji¹, Tomoaki Oyama²,
Yasuhiro Koyama¹, Tetsuro Kondo¹, Tadahiro Gotoh¹, Jun Amagai¹

¹) *Space-Time Standards Group, National Institute of Information and Communications Technology*

²) *National Astronomical Observatory of Japan*

Contact author: Thomas Hobiger, e-mail: hobiger@nict.go.jp

Abstract

Caused by historical separation and driven by the requirements of the PC gaming industry, Graphics Processing Units (GPUs) have evolved to massive parallel processing systems which entered the area of non-graphic related applications. Although a single processing core on the GPU is much slower and provides less functionality than its counterpart on the CPU, the huge number of these small processing entities outperforms the classical processors when the application can be parallelized. Thus, in recent years various radio astronomical projects have started to make use of this technology either to realize the correlator on this platform or to establish the post-processing pipeline with GPUs. Therefore, the feasibility of GPUs as a choice for a VLBI correlator is being investigated, including pros and cons of this technology. Additionally, a GPU based software correlator will be reviewed with respect to energy consumption/GFlop/sec and cost/GFlop/sec.

1. Introduction

Graphics Processing Units (GPUs) have been undergoing tremendous development in recent years, in order to reduce the burden on the central processing unit (CPU) and enable ultra-fast computation of complex scenarios and output the results on the PC's display. As many of the underlying mathematical algorithms can be parallelized, GPUs have been equipped with hundreds of simple computing cores which can be programmed to solve these equations and output the results to the video buffer.

1.1. CPU vs. GPU

Unlike the CPU, which is equipped with a relatively large cache, GPUs work with smaller cache sizes, assigned to each processing core. Although also the arithmetical units are less sophisticated than those on the CPU, the large number of these cores, which are available for parallel processing, yields a significant speed-up of various applications [4].

1.2. General Purpose GPU - GPGPU

Soon after the first powerful graphics cards entered the market, scientists started to get interested in porting their (parallel) computing problems on the GPU, based on OpenGL. NVIDIA was the first company who provided a sophisticated C-like programming environment named "Computing Unified Device Architecture (CUDA)", and other vendors started to work on similar programming environments for their products. Moreover, as for instance CUDA came with a set of libraries (e.g., FFTs and BLAS) and tools (debuggers and profilers), coding became as simple

as writing a C-program, and the number of scientific and technical applications which run on a graphics card has grown rapidly and is expected to increase in the future as well. Additionally, the new OpenCL standard, which realizes a multi-platform programming language, is expected to overcome the problem that code is currently only usable for a certain device.

2. GPUs for VLBI

GPUs have been used successfully within the Murchinson Widefield Array post-processing pipeline [3], and tests, which utilize the graphics cards as a software correlator, were made as well [5]. Harris et al. [1] have shown that GPUs can help to speed-up signal convolution, and NICT has developed a GPS software receiver running on a single off-the-shelf graphics card [2].

2.1. Benchmarking the GPU Concerning the Possibility as an FX Correlator

In order to reveal the potential of the GPU as a co-processor on which a software correlator could run, we start with benchmarking an off-the-shelf graphics card (specifications listed in Table 1). As it turned out very soon that an XF-type correlator does not perform well on a parallel architecture, we will focus only on the FX-type implementation of the software correlator. Thereby, we can assume that for each FX engine

$$10 \cdot N \cdot \log_2(N) + 6 \cdot N \tag{1}$$

floating point operations are being carried out to compute the cross-spectrum of two signals with length N . Thus, measuring the time taken on the GPU for calling such an FX engine in different configurations allows one to draw conclusions on the performance of the GPU. Figure 1 depicts the FX performance in Gflops for different FFT sizes as well as varying configurations of how these engines are called on the graphics card. As expected, the parallel computing power of the graphics card cannot be used when the FX engines are called serially, yielding more than 10 GFlops only for FFT sizes larger than 4096. When the FX engines are called in parallel, one can start taking advantage of the GPU and achieve more than 100 GFlops for FFT sizes larger than 256. Since the amount of shared memory on the GPU is restricted to a few kilobytes per thread, performances saturate as soon as this limit is reached.

Table 1. Specifications of the NVIDIA GTX 280 card used for the benchmark test.

Processor Cores	240
Processor Clock	1296 MHz
Memory	1 GB GDDR3
Price	~ 300 \$
Power consumption	200 W

2.2. Data-transfer CPU ↔ GPU

In order to make sure that neither the data-transfer from the CPU memory to the GPU nor the way back turns out to be a severe bottleneck, tests were carried out to determine the transfer

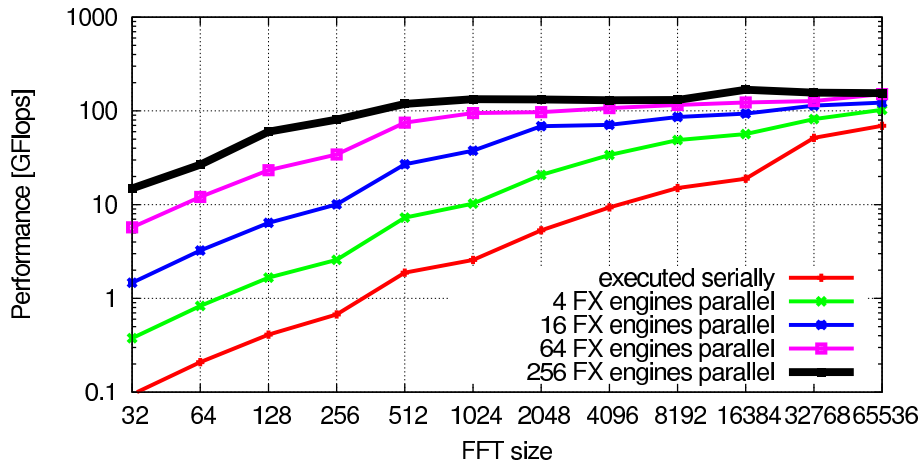


Figure 1. FX performance on the GPU.

rates. Figure 2 summarizes the results obtained for different data sizes. For small blocks of data (i.e., from 1 KB to 100 KB) moderate transfer rates are observed, which have the potential to slow down any application. But as the FX engines of a VLBI correlator are expected to be fed with rather large amounts of data, one can be sure that data sizes larger than 1 MB will be used. Thus, for such data sizes, more than 5 GB/sec can be achieved in both directions, which appears to be fast enough to not be a severe bottleneck of the correlator. Moreover, modern graphics cards recently even support asynchronous data-transfer, which allows running the code while data is transferred to/from the device.

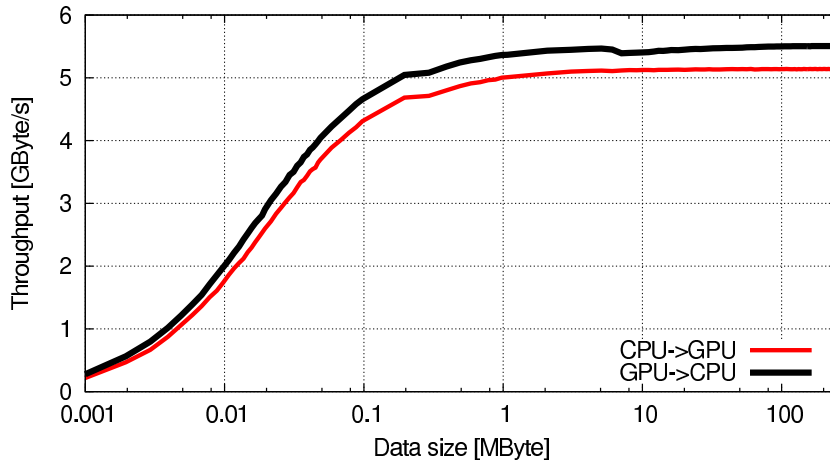


Figure 2. Data transfer rates to/from the GPU.

3. Implementing the Correlator

Based on two off-the-shelf graphics cards (NVIDIA GTX295) for a price of less than 800 US\$ a complete software correlator was implemented. The correlator carries out the following tasks:

1. data-transfer from the CPU to the GPU,
2. unpacking of the data,
3. fringe stopping,
4. FFT,
5. delay tracking,
6. correlation and integration.

All modules are implemented on the GPU, which is expected to be a little bit slower as compared to the tests with the FX engine only (prior section). Test runs with recorded data (1024 Msps, 2 bits) were made in single- (i.e., auto-correlation) and multi-station mode. The results, showing the performance in Msps, are displayed in Figure 3. Thereby, it turns out that four stations (six baselines) can be correlated in real-time, when a sampling rate of 1 Gsps is chosen. Moreover, eight stations with a sampling rate of 500 Msps can be processed as well in real-time, when slightly larger FFT sizes are selected.

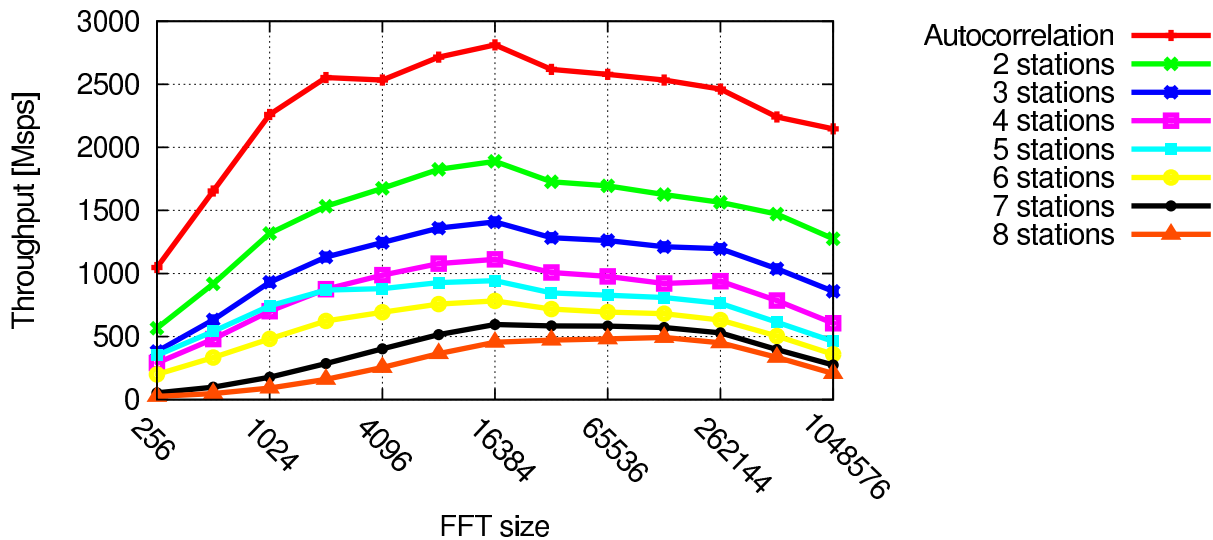


Figure 3. Data transfer rates to/from the GPU.

4. Summary

Graphics processing units seem to be an alternative to CPU-based software correlators. Considering that vendors provide simple programming environments, there appears to be no real hurdle in using these devices. Table 2 compares the graphics cards described in Section 2.1 w.r.t. to a modern CPU. Additionally, data-transfer, as discussed in Section 2.2, should not be a severe restriction for the usage of graphic cards as VLBI correlators.

Table 2. Comparison of the GPU w.r.t. a CPU.

	GPU	CPU (3.6 GHz Pentium 4)
Perf.	~ 200 Gflops (unoptimized)	12 Gflops (based on best FFTW score)
Cost	~ 0.5 Gflops/\$	~ 0.1 Gflops/\$
Energy	~ 0.8 Gflops/Watt	~ 0.2 Gflops/Watt

5. Outlook

The next generation of GPUs, which will have twice as many computing cores as current devices, will enter the market in April 2010. Moreover, the new cards will have larger shared memory blocks as well as L2 cache, which will help to improve the speed of the FFTs and other highly parallel operations. Thus, given that the developmental progress of GPUs continues to be faster than those of the CPU, the graphics card appears to be a really strong competitor for the realization of a software correlator, running on off-the-shelf components.

Acknowledgements

Parts of this work were supported by a Grant-in-Aid for scientific research (KAKENHI, No. 24241043) from the Japan Society for the Promotion of Science (JSPS).

References

- [1] Harris, C., K. Haines, L. Staveley-Smith, GPU accelerated radio astronomy signal convolution. *Exp Astron*, 22, 1-2,129–141, 2008.
- [2] Hobiger, T., T. Gotoh, J. Amagai, Y. Koyama, T. Kondo, A GPU based real-time GPS software receiver, *GPS Solutions*, 14, 2, 207–216, 2010.
- [3] Ord, S., L. Greenhill, R. Wayth, D. Mitchell, K. Dale, H. Pfister, R. Edgar, GPUs for data processing in the MWA, ADASS XVIII, ASP Conference Series, 411, 127-130, 2009.
- [4] Nguyen, H., GPU Gems 3: programming techniques for high-performance graphics and general-purpose computation, Addison-Wesley Professional, 2007.
- [5] Wayth, R.B., L. Greenhill, F. Briggs. A GPU-based Real-time Software Correlation System for the Murchison Widefield Array Prototype, *Publications of the Astronomical Society of the Pacific*, 121, 857-865, 2009.

VLBI2010 Imaging and Structure Corrections

Arnaud Collioud, Patrick Charlot

Laboratoire d’Astrophysique de Bordeaux, Université de Bordeaux, CNRS, UMR 5804

Contact author: Arnaud Collioud, e-mail: collioud@obs.u-bordeaux1.fr

Abstract

Simulations show that the next generation VLBI system is generally well suited for imaging extragalactic radio sources. In addition to revealing the morphology of the sources, simulated VLBI2010 images may also be used to generate structure correction maps, which characterize the impact of source structure on the VLBI measurements. By comparing structure corrections for a set of simulated images based on Monte-Carlo generated visibilities with theoretical structure corrections derived from the model, we assess the accuracy of VLBI2010 structure corrections. In the most favorable case (32-station network, source at declination $+40^\circ$), statistics demonstrate that the structure corrections obtained from simulated images are statistically close to the theoretical model ones, which seems very promising for the VLBI2010 system.

1. Introduction

In the forthcoming years, the successor of the current geodetic VLBI system—the VLBI2010 system—is expected to become operational. This new system is based on 12m-class fast-moving antennas associated with broadband recording systems, as prescribed by the VLBI2010 Committee [1]. Significant progress in the determination of IVS products is anticipated with this new system, such as the improvement of the International Celestial Reference Frame (ICRF) source positions.

The ICRF sources, as most of the extragalactic radio sources, are generally not point-like on VLBI scales [2]. The source structure introduces an additional unmodeled delay, called “structural delay” or “structure correction”, to the group delay measurements. This structural delay has a direct impact on the source position accuracy derived from VLBI observations. The magnitude of this delay is related to the complexity of the structure, ranging from a few picoseconds for compact structures to tens of picoseconds for more extended structures, as shown in Figure 1. Moreover, the source structure, and hence the structural delay, may evolve in time, which requires monitoring the sources over time.

Until now, efforts were put into the selection of sources with minimal structure. This method was used for example to select the defining sources of the ICRF2, adopted by the IAU General Assembly in August 2009 [3]. On the other hand, the additional structural delay, as a systematic effect, may be removed from the group delay measurements if source structure is known, which should lead to an improvement of the final source positions. In the future, it is anticipated that such structure corrections may be routinely determined and applied with the new VLBI2010 system.

Studying the accuracy of the structure corrections achievable with the VLBI2010 system based on simulated images is a prerequisite in order to reach this goal. In this paper, we first summarize the imaging capabilities of the VLBI2010 system. The simulated images are then used to infer structure corrections, the accuracy of which may be estimated by comparison with theoretical structure corrections derived from the model. Results of this estimation are discussed in Section 3.

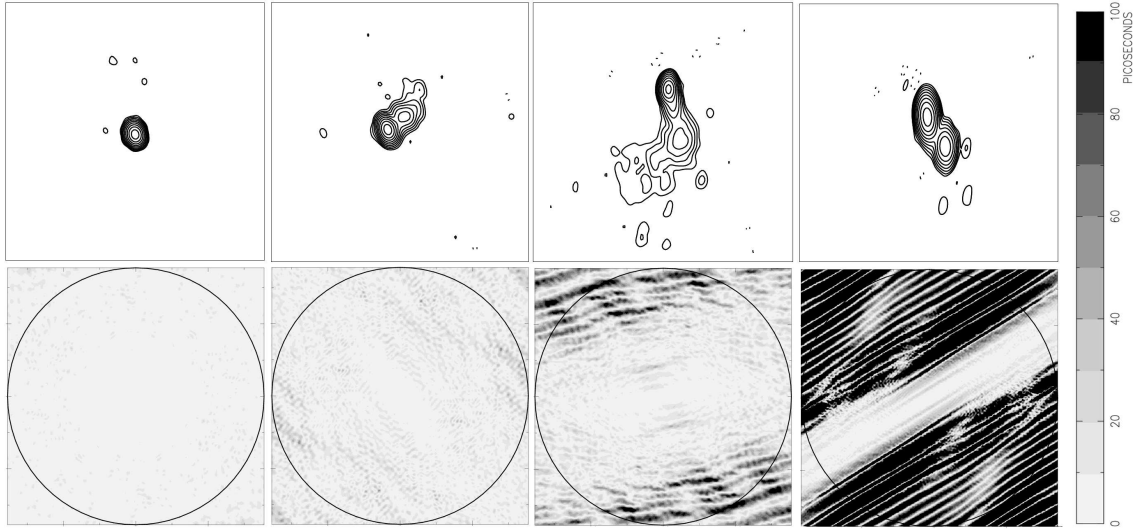


Figure 1. VLBI images and structure correction maps showing the magnitude of the structural delay for a sample of sources with different structure complexity. The scale of the structure corrections is given on the right-hand side of the panel. The four VLBI images and corresponding structure correction maps are excerpted from the Bordeaux VLBI Image Database (<http://www.obs.u-bordeaux1.fr/BVID>).

2. Simulation of VLBI2010 Images

Imaging capabilities of the VLBI2010 system have been studied thanks to a dedicated processing pipeline that generates VLBI images using VLBI2010 test schedules with different network configurations and observing strategies. In this study, simulations are carried out using the traditional S/X frequency setup. Details about the pipeline and initial results obtained in the case of high SNR sources were presented in [4]. Since then, additional simulations have been carried out for weaker sources (40 mJy) assuming a typical noise level equivalent to an SNR of 20 [1].

The simulations demonstrated that the VLBI2010 schedules lead to a better coverage of the u - v plane compared to the current geodetic sessions due to the increase of the number of observations per session and the better station distribution on the Earth. Simulated images are found to be high-quality, with a dynamic range ranging from 1:200 to 1:1000, depending on the configuration. Simulations also show that the standard hypothetical 16-station network is generally well suited to producing high-quality images. However, it is to be noticed that extended structures for sources at low declination are not well reconstructed with only 16 stations due to the lack of short baselines in the southern hemisphere [4]. Additional simulations demonstrate that the addition of two stations at carefully selected locations in the southern hemisphere could help fill the central hole in the u - v plane and hence mitigate this image reconstruction problem of the 16-station network. The resulting image quality clearly improves, giving simulated images at southern declinations a quality comparable to that of northern sources when such two stations are added [1].

3. Structure Corrections

In addition to revealing the morphology of the sources, simulated VLBI2010 images may be used to generate structure correction maps. These represent the effects of source structure on the delay observable as a function of interferometer resolution. Additionally, structure correction maps serve as a basis for calculating structure indices, which characterize the astrometric suitability of the sources [2].

In order to assess the accuracy of the structural corrections derived from VLBI2010 images, a sample of 25 similar VLBI2010 images was generated as described in Section 2. These images were produced from the same input source model (presented in [4]) but using a different input noise level in each simulation (as obtained by a Monte Carlo method). An additional image was generated from a simulation without additive noise. Structure correction maps were then derived from all such images and were compared with the theoretical structure correction map calculated from the “true” source model, thereby allowing us to estimate the accuracy of the corrections.

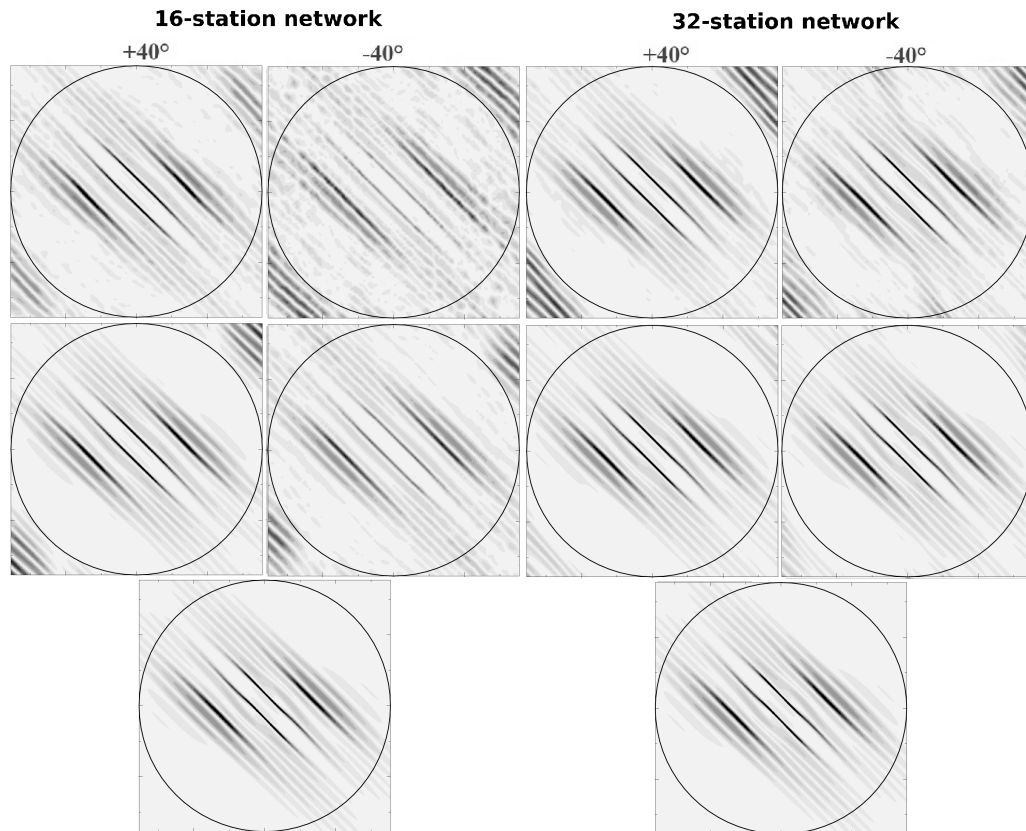


Figure 2. Structure correction maps derived from simulated VLBI2010 images for 16- and 32-station networks (left and right panels, respectively) and for two identical sources placed at declination $+40^\circ$ and -40° , respectively. The upper (middle) panels show the results obtained with (without) additive noise, while the lower panels show the results obtained for the theoretical model. The scale of the structure corrections is the same as the one used in Figure 1.

By examining these structure correction maps (Figure 2, above), it appears that the noise level is larger (compared to the theoretical structure correction map) when the structure is not fully reconstructed, as for the 16-station network and a source at declination -40° . In the case of the 32-station network, the structure corrections resulting from the simulated images are closer to the theoretical structure corrections.

Statistics may be calculated using the median correction from these maps. For example, the study of the difference between the mean of the median corrections and the theoretical model correction helps us to understand the systematic error due to imperfect u-v coverage. Additionally, the study of the RMS of the median corrections provides indications on the impact of the noise on the simulations. See Figure 3 for a graphical representation of these errors in the case of the sample source at declination $+40^\circ$. In this case, the difference between the mean of the median corrections and the theoretical model correction is 2.2 ps with the 16-station network, and only 0.5 ps with the 32-station network. The corresponding RMS values are 0.5 and 0.4 ps, respectively.

These statistics were calculated for several network configurations and source declinations. The results are shown in Figure 3. In the most favorable case (source at declination $+40^\circ$ and 32-station network), the corrections obtained from the simulated images are statistically very close to the theoretical model corrections, which seems very promising for implementing such corrections in future VLBI2010 operations.

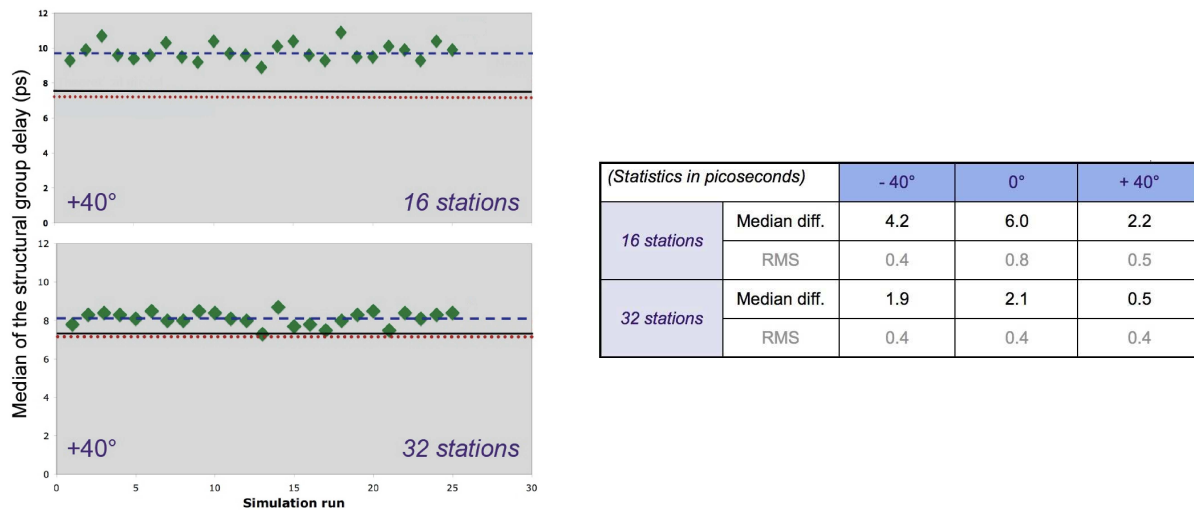


Figure 3. Left: Plot of the median structural delay in picoseconds (green diamond) for each simulation run when the sample source is placed at declination $+40^\circ$. The mean of the distribution is plotted as a blue (dashed) line while the median correction for the theoretical model is plotted as a black continuous line. Additionally, the median correction for the simulation obtained without additive noise is plotted as a red (dotted) line. Right: Differences between the mean of the distribution and the median correction for the theoretical model, and RMS of the corrections around the mean of the distribution for several configurations of network and source declination.

4. Conclusion

Previous studies showed that the VLBI2010 system is well adapted to produce high-quality images of extragalactic radio sources. In addition, such studies highlighted that 32-station networks should be preferred over 16-station networks since the latter fails to reconstruct extended structures for sources at low declination.

In this paper, we calculated statistics on structure corrections for a set of simulated images based on Monte-Carlo generated visibilities and for theoretical structure corrections derived from the model. These statistics demonstrated once again that 32-station networks are recommended to obtain structure corrections statistically close to the theoretical model ones.

Future prospects include studying such statistics not for the whole u-v plane as done here, but for the individual u-v points actually observed during hypothetical VLBI2010 sessions. It will also be important to extend this study in the context of the broadband system, noting that some difficulties may arise, such as the change of structure with frequency or the position dependency of the source core with frequency (known as “core-shift”).

References

- [1] Petrachenko, W.T., Niell, A.E.E., Behrend, D., Corey, B.E., Boehm, J., Charlot, P., Collioud, A., Gipson, J.M., Haas, R., Hobiger, T., Koyama, Y., MacMillan, D.S., Malkin, Z., Nilsson, T., Pany, A., Tuccari, G., Whitney, A., Wresnik, J., Design Aspects of the VLBI2010 System. Progress Report of the IVS VLBI2010 Committee, NASA/TM-2009-214180, 2009.
- [2] Fey, A., Charlot, P., *ApJS*, 128, 17, 2000.
- [3] IERS/IVS Working Group, The Second Realization of the International Celestial Reference Frame by Very Long Baseline Interferometry, IERS Technical Note No. 35, 2009.
- [4] Collioud, A., Charlot, P., Proceedings of the Fifth IVS General Meeting, ed. by A. Finkelstein and D. Behrend, 433–438, 2008 .

The AuScope Project and Trans-Tasman VLBI

*Jim Lovell*¹, *John Dickey*¹, *Sergei Gulyaev*², *Tim Natusch*², *Oleg Titov*³,
*Steven Tingay*⁴

¹⁾ *University of Tasmania*

²⁾ *Auckland University of Technology*

³⁾ *Geoscience Australia*

⁴⁾ *International Centre for Radio Astronomy Research - Curtin University of Technology*

Contact author: *Jim Lovell*, e-mail: jim.lovell@utas.edu.au

Abstract

Three 12-meter radio telescopes are being built in Australia (the AuScope project) and one in New Zealand. These facilities will be fully-equipped for undertaking S and X-band geodetic VLBI observations and correlation will take place on a software correlator (part of the AuScope project). All sites are equipped with permanent GPS receivers to provide co-location of several space geodetic techniques. The following scientific tasks of geodesy and astrometry are considered.

1. Improvement and densification of the International Celestial Reference Frame in the southern hemisphere;
2. Improvement of the International Terrestrial Reference Frame in the region;
3. Measurement of intraplate deformation of the Australian tectonic plate.

1. AuScope Project

In 2007 the National Cooperative Research Infrastructure Strategy (NCRIS) initiated program 5.13, “Structure and Evolution of the Australian Continent”, which is funded by the Department of Innovation, Industry, Science and Research and managed by AuScope Ltd. (www.auscope.org.au). A major component of this project is the establishment of a national geospatial framework to provide an integrated spatial positioning system spanning the whole continent (Figure 1). Total federal funding for this undertaking is AUD\$ 15.8 M, together with AUD\$ 21 M from Universities, State Governments, and Geoscience Australia. The infrastructure includes:

- three 12-meter radio telescopes and a software correlator
- about 100 GNSS receivers
- upgrade of existing SLR facilities
- an absolute gravimeter and three tidal gravimeters
- improved computing facilities

As part of this effort, the University of Tasmania (UTAS) is constructing three new radio telescopes, located near Hobart, Yarragadee (Western Australia), and Katherine (Northern Territory). UTAS is responsible for construction and operation of three new VLBI sites. The software correlator is being developed at Curtin University of Technology. In a coordinated international effort in New Zealand, Auckland University of Technology (AUT) has purchased a similar radio telescope, now completed and in the commissioning phase.

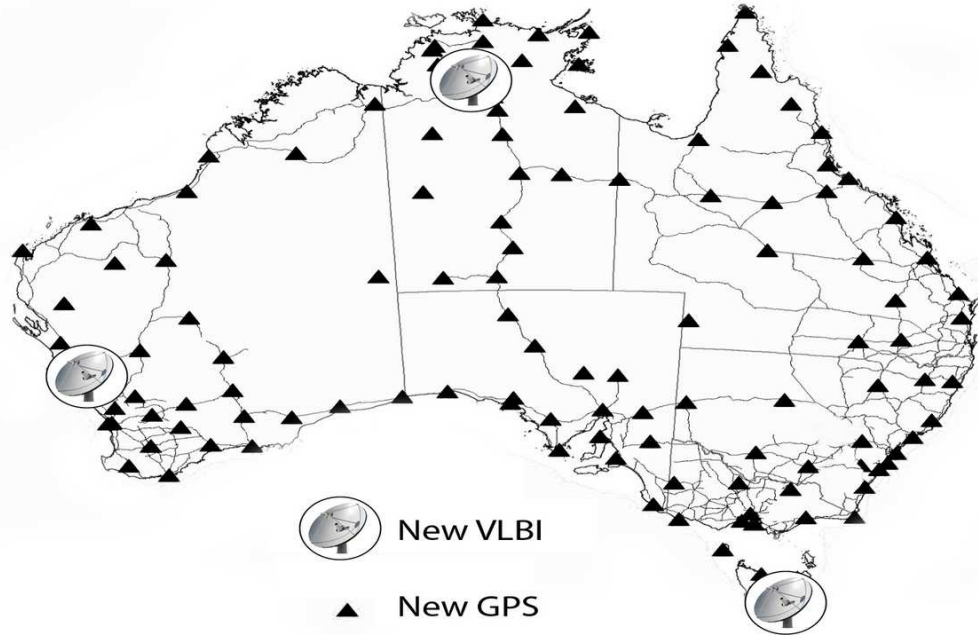


Figure 1. The geographical distribution of VLBI and GPS infrastructure for AuScope. New VLBI stations will be established at Yarragadee (WA), Katherine (NT), and Hobart (Tas) with co-located GPS receivers. An additional ~ 100 GPS receivers will be distributed across the continent.

These new telescopes will double the number of IVS stations in the Southern Hemisphere. They will allow the extension of astrometric VLBI solutions to radio sources south of declination -40° , an area of the sky that has been severely under-sampled by the existing array because so few telescopes are available in the South. The AuScope antennas will observe for 180 days per year, increasing the number of geodetic VLBI observations in Australia by a factor of nine. The AuScope and AUT telescopes closely follow the IVS VLBI2010 specification for the next generation of telescopes for geodesy [3] or provide an upgrade path to meet the specification where it is not currently possible to do so.

1.1. AuScope VLBI Observatories

Each AuScope VLBI observatory is equipped with a 12.1 m diameter antenna designed and constructed by COBHAM Satcom, Patriot Products division. The characteristics are: 0.3 mm of surface precision (RMS), fast slewing rates (5 deg/s in azimuth and 1.25 deg/s in elevation), and acceleration (1.3 deg/s/s).

All three sites will be equipped with dual polarization S and X-band feeds from COBHAM with room temperature receivers, developed at UTAS by Prof. Peter McCulloch. The receiver systems cover 2.2 to 2.4 GHz at S-band and 8.1 to 9.1 GHz at X-band. System Equivalent Flux Densities (SEFDs) are expected to be 2900 Jy at S-band and 3500 Jy at X-band. Data digitization and formatting will be managed by the Digital Base Band Converter (DBBC) system from HAT-Lab, and data will be recorded using the Conduant Mark 5B+ system. Each site will be equipped with VCH-1005A Hydrogen maser time and frequency standards from Vremya-CH.

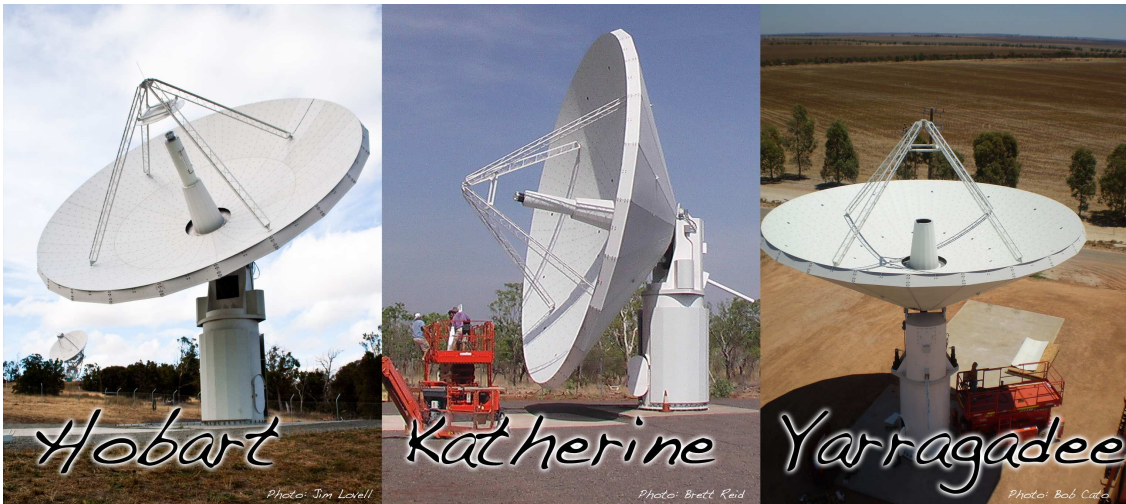


Figure 2. The three AuScope VLBI sites as of March 2010 (photos by Jim Lovell, Brett Reid, and Bob Cato).

At time of writing (April 2010) the Hobart antenna is installed and initial end-to-end testing of the system is under way. Interferometric fringes between the 12 m and 26 m antennas have been detected. Once the hardware and software for Hobart have been completed and tested, duplicate systems for the other sites will be built and tested at Hobart prior to deployment. At Yarragadee, the antenna is in the final stages of acceptance testing, and acceptance tests will take place in Katherine next.

1.2. Software DiFX Correlator

The software correlator facility is being developed by Curtin University of Technology. It is an implementation of the DiFX correlator, described in Deller et al. (2007) [1]. The DiFX correlator has been used extensively for radio astronomy and is starting to make a global impact in the geodetic community. DiFX has been compared to the trusted geodetic correlator at MPIfR in Bonn and shown to be capable for geodesy [5]. Other comparisons between DiFX and the USNO correlator show a very high degree of agreement [2], as do comparisons between DiFX and the VLBA correlator [4].

At Curtin University of Technology the software correlator is installed on a 20 node Beowulf cluster, each node containing two quad-core Intel processors, 8 GB of RAM, at least 2 TB of disk space per node, and interconnects using 1 Gbps ethernet. In addition, mass storage is provided by five Apple Xraid chassis, each capable of holding 9 TB in raid5 configuration. Three Mark 5B+ VLBI playback units are integrated into the cluster, for compatibility with the AuScope recording systems. The cluster has a 10 Gbps connection to the iVEC petabyte store, for additional storage and staging of large volumes of data.

The correlator is capable of e-VLBI observations and if high capacity network connections are made available to the AuScope antennas in the future, real-time correlation and extraction of geodetic parameters will be possible.

1.3. AuScope Operations

As the AuScope antennas come on line in 2010 they will participate in more and more geodetic observations, building to a rate of 180 days per antenna per year. Of these, approximately 100 days will be dedicated to existing IVS programs while the remainder will focus on scientific goals with a southern-hemisphere emphasis and include other IVS observatories in the region when available:

- Astrometry of the reference radio sources in the southern hemisphere, especially, with declination south of -40 degrees
- Underpinning of the International Terrestrial Reference Frame
- Measurement of local tectonic motion, for instance, intraplate deformation across the Australian tectonic plate

2. Project of Auckland University of Technology

The IVS VLBI2010 Progress Report [3] outlines a number of strategies to improve the long-term accuracy of geodetic VLBI with an eye to achieving 1 mm precision on baselines. Among these strategies are: “to increase the number of antennas and improve their geographic distribution” and “to increase the number of observations per unit of time”. These IVS strategies can best be addressed through construction of new small (~ 12 m), fast-slewing automated antennas in areas that are under-represented (Southern Hemisphere) or lack (e.g., New Zealand) geodetic VLBI stations.

Developing this approach, AUT University has invested US\$1m in a geodetic VLBI system, consisting of a fast-slewing automated 12-m antenna, hydrogen maser clock, receiving and digital backend systems, and a 1 Gbps network connectivity.

Like the AuScope antennas, the AUT radio telescope is equipped with the coaxial dual band (S and X) dual polarization (circular left/right) feed horn, which was specifically developed by COBHAM. An S/X receiver has been constructed with the help of Peter McCulloch and the University of Tasmania. A Symmetricom Active Hydrogen Maser MHM-2010 (75001-114) with 5 MHz, 10 MHz, 100 MHz, and 1 pps (pulse per second) outputs and a 1 pps sync facility is installed. A digital base band converter (DBBC) developed at the Italian Institute of Radio Astronomy is expected to be installed in May 2010. The AUT VLBI receiving system uses the Mark 5B+ data recorder developed at MIT Haystack Observatory. Both S and X receivers have been installed and preliminary figures for SEFD are around 4000 Jy, a figure that is higher than expected. Investigations in collaboration with the manufacturer are underway, and several areas have been identified in which improvements can be made. Modifications to the feed design, which will be applied to the AuScope and AUT antennas in 2010, are expected to yield SEFDs of 2900 Jy at S-band and 3500 Jy at X-band.

In November 2008 a new GNSS station (WARK) was built at the AUT radio telescope site. It is a part of the New Zealand GNSS network “PositioNZ”. An accurate tie is established between the radio telescope antenna and the GNSS station.

The New Zealand 12-m antenna is scheduled to start participating in regular IVS VLBI sessions from the middle of 2010.

Being a research tool for astronomy and geodesy, the antenna is also used in a new educational program in astronomy started in 2009 at AUT’s School of Computing and Mathematical Sciences—an Astronomy Major in the framework of the Bachelor of Mathematical Sciences degree. It is

envisaged that both undergraduate and postgraduate students will use the radio telescope in their research projects and as a teaching resource in the courses taught at AUT such as Astrophysics, Radio Astronomy, Practical Astrophysics, Space Geodesy, and others.

References

- [1] Deller, A., Tingay, S., Bailes, M., West, C. DiFX: A Software Correlator for Very Long Baseline Interferometry Using Multiprocessor Computing Environments”, *PASP*, 119, 318, 2007
- [2] Ojha, R., Boboltz, D. & Fey, A. 2008, *IVS Newsletter*, 22, 7
- [3] Petrachenko, B. et al., Design Aspects of the VLBI2010 System. Progress Report of the IVS VLBI2010 Committee. NASA/TM-2009-214180, June 2009.
- [4] Petrov., L. et al Precise geodesy with the Very Long Baseline Array *Journal of Geodesy* 83, 859, 2009
- [5] Tingay, S., W. Alef, D. Graham, A. Deller Geodetic VLBI Correlation in Software *Journal of Geodesy* 83, 1061, 2009

Current Status of the Development of a Transportable and Compact VLBI System by NICT and GSI

Atsutoshi Ishii¹, Ryuichi Ichikawa², Hiroshi Takiguchi², Kazuhiro Takefuji², Hideki Ujihara², Yasuhiro Koyama², Tetsuro Kondo², Shinobu Kurihara³, Yuji Miura³, Shigeru Matsuzaka³, Daisuke Tanimoto⁴

¹⁾ AES, Co.,Ltd.(assistant researcher for GSI) / NICT, Japan

²⁾ NICT, Japan

³⁾ Geospatial Information Authority of Japan (former Geographical Survey Institute, GSI)

⁴⁾ AES, Co.,Ltd.

Contact author: Atsutoshi Ishii, e-mail: a.ishii@aes.co.jp

Abstract

MARBLE (Multiple Antenna Radio-interferometer for Baseline Length Evaluation) is under development by NICT and GSI. The main part of MARBLE is a transportable VLBI system with a compact antenna. The aim of this system is to provide precise baseline length over about ~10 km for calibrating baselines. The calibration baselines are used to check and validate surveying instruments such as GPS receiver and EDM (Electro-optical Distance Meter). It is necessary to examine the calibration baselines regularly to keep the quality of the validation. The VLBI technique can examine and evaluate the calibration baselines.

On the other hand, the following roles are expected of a compact VLBI antenna in the VLBI2010 project. In order to achieve the challenging measurement precision of VLBI2010, it is well known that it is necessary to deal with the problem of thermal and gravitational deformation of the antenna. One promising approach may be connected-element interferometry between a compact antenna and a VLBI2010 antenna. By measuring repeatedly the baseline between the small stable antenna and the VLBI2010 antenna, the deformation of the primary antenna can be measured and the thermal and gravitational models of the primary antenna will be able to be constructed.

We made two prototypes of a transportable and compact VLBI system from 2007 to 2009. We performed VLBI experiments using these prototypes and got a baseline length between the two prototypes. The formal error of the measured baseline length was 2.7 mm. We expect that the baseline length error will be reduced by using a high-speed A/D sampler.

1. Introduction

We are developing a transportable and compact VLBI system. One of the purposes of the development is to measure accurately the baseline length of about 10 km. The Geospatial Information Authority of Japan (former Geographical Survey Institute, GSI) has a calibration baseline of 10 km to calibrate and validate surveying instruments for public purposes. These surveying instruments are GPS receiver and EDM (Electro-optical Distance Meter). To keep the quality of the calibration, the calibration baseline has to be examined regularly. However, the calibration baseline has been examined only by GPS up to now. Since this approach does not account for possible systematic errors, the examination by an independent technique is required. The VLBI technique can give an independent measurement of the calibration baseline in order to determine the systematic errors.

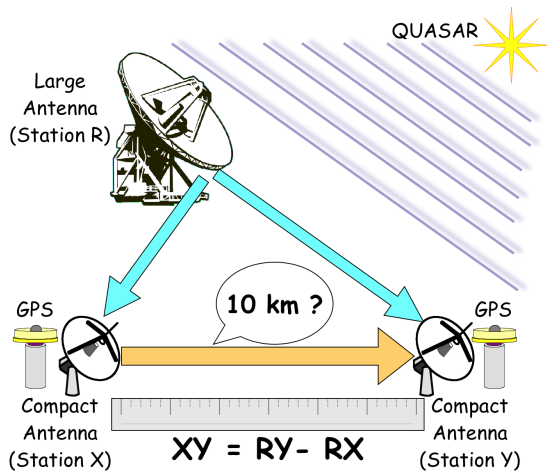


Figure 1. Measurement concept of MARBLE (Multiple Antenna Radio interferometer for Baseline Length Evaluation).

To achieve our goal, we made the following ideas. The geodetic VLBI system consists of a pair of compact VLBI stations with small antennas and a reference VLBI station with a large aperture antenna (Figure 1). The two small VLBI antennas are placed about 10 km apart. We can obtain the time delay between the small antennas by the time delays between the large antenna and each small antenna, even if we do not obtain the delay time between the small antennas directly. The baseline length of 10 km can be estimated by means of the indirect time delay. One of the advantages of this concept is not to have to get the time delay between the small antennas. Another advantage is that the comparison between the VLBI measurement and the GPS measurement is easy, because we only compare the reference point of a small VLBI antenna with the reference point of the GPS antenna. We do not need to compare the reference point of a large VLBI antenna with the GPS reference point. We call this idea ‘**M**ultiple **A**ntenna **R**adio-interferometer for **B**aseline **L**ength **E**valuation (MARBLE)’.

2. Compact VLBI System

The compact VLBI system is the core equipment of the MARBLE system as explained in the previous section. To perform measurements at several calibration baselines in Japan, one of the important requirements for the VLBI system is transportability. We made two prototypes of transportable and compact VLBI systems from 2007 to 2009. The VLBI systems consist of a small aperture antenna with drive unit of Az/EI-mount type (Figure 2), a receiver on ambient temperature, the K5 VLBI system [1, 2], and a frequency standard, among other parts. In the following, we describe details of the prototypes.

2.1. Small Antenna and Mount

The type of antenna is a front-fed paraboloid. The diameters of the reflectors are 1.65 m and 1.5 m for the first and second prototype respectively. The two reflectors have the same F/D of 0.45. At the focal point of the reflector, a wide-band feed (Quad-ridge horn antenna [3]) is placed. At the back of the feed, there is a front-end receiver with wide-band LNAs which can amplify up to 11 GHz. The front-end receiver also plays the roles of polarizer and frequency discriminator. At present, the receiver is only for S and X bands [4]. However, by replacing RF filters and other RF components, it will be able to receive the frequency bands from 2 to 11 GHz.

The antenna and mount can be disassembled into many parts avoiding the need for heavy machinery. This feature is for transportability. For an easy comparison of the VLBI measurement

with the GPS measurement, the antenna has the following features: The compact VLBI antenna can host a GPS antenna on top of the El drive-unit, on top of the Az drive-unit, and on top of the base pillar. The antenna can also mount a target mirror for surveying at the azimuth-elevation intersection point which is the reference point of the geodetic VLBI measurement.

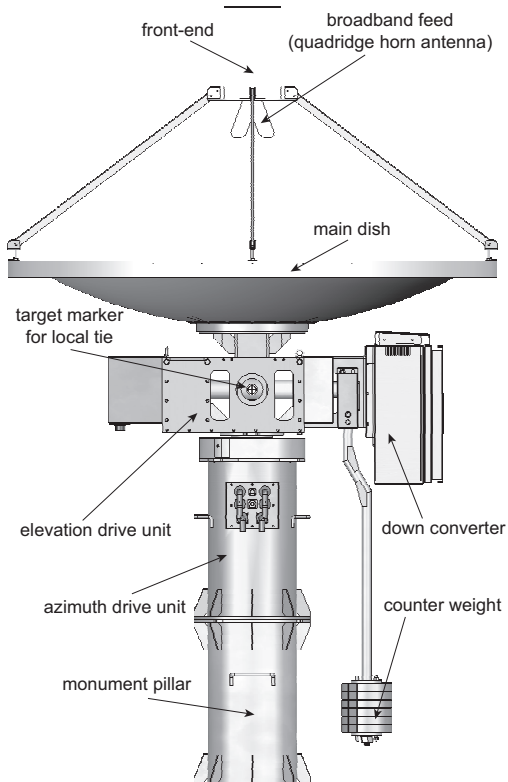


Figure 2. Schematic image of the antenna of the MARBLE system.

2.3. Applications

This compact and transportable VLBI system can be applied to various observations. For instance, it can be used for a comparison of VLBI time and frequency [8]. Only one VLBI station with a large antenna is needed for this purpose. By bringing a compact VLBI station with small antenna, time and frequency comparison is possible anywhere.

In the VLBI2010 project, it is expected that the compact VLBI station with small antenna can be used for gravity and thermal deformation model construction of a large VLBI antenna [9]. By repeating geodetic VLBI measurements using a large antenna and a small stable antenna placed near the large antenna, we will be able to model the deformation of the large antenna.

2.2. Frequency Standards

Transportability is required for the frequency standard of the compact VLBI system as well as the antenna. However, a conventional hydrogen maser frequency standard is unsuitable for transportation.

The frequency standard that we are going to use is a laser-pumped Cs gas-cell frequency standard (hereafter, we call it ‘Cs gas-cell oscillator’) [5]. The size and weight of the oscillator is roughly equal to a desktop PC. Its stability lies between that of a hydrogen maser frequency standard and a Cs beam type frequency standard. It is good enough to keep coherence for VLBI observation at the frequency of 8 GHz. Moreover, we confirmed the Cs-gas cell oscillator on geodetic VLBI using the Koganei 11-m antenna and the Kashima 34-m antenna [6].

Another option for the frequency standard system is the radio frequency transfer using optical fiber [7]. The development purpose of this system is a comparison of optical frequency standards which have much higher frequency stability than that of conventional microwave frequency standards. Therefore, this system can transmit the radio frequency from the hydrogen maser oscillator without degradation of stability. The only disadvantage of the system is that it requires dark fibers.

3. Performance Tests of the Prototypes

To test the performance of the prototypes, we installed the first prototype near the Kashima 34-m antenna in NICT in December 2008 and the second prototype near the Tsukuba VLBI station (32-m antenna) at GSI in October 2009. Before setting up the second prototype, we performed general geodetic VLBI experiment of 24 hours using the first prototype. In the experiment, we also used the Tsukuba VLBI station and the Kashima 11-m station. The hydrogen maser oscillators were used as frequency standards at each station, the observed bands were S and X band, and the total recording data rate was 512 Mbps in the experiment. As a result of the experiment, we successfully obtained fringes over the 24 hours and could estimate the baseline length between the Kashima 11-m station and the first prototype to about 200 m (Table 1). The formal error of the measured baseline length was 2.4 mm.

After installation of the second prototype, we carried out another VLBI experiment of 24 hours using the two prototypes and the Tsukuba VLBI station. The frequency standards, observed band, and the total recording rate were the same as in the previous experiment. We could estimate the baseline length between the two prototypes to be about 54 km (Table 1). The formal error of the estimated baseline length was 2.7 mm. However, in this experiment, there were many outliers of several tens of nsec in the delay residuals. We could not find the origin of the failure, but we expect that the cause is the failure of bandwidth synthesis. Since the influence was large in S band, we did not include the time delays from S band in the analysis. Though there was such a problem, the baseline length could be measured by using the two prototypes. This result is evidence that these prototypes are usable for geodetic VLBI. Moreover, there is room for making the observation data rate higher. The higher observation data rate will bring a smaller measurement error for the baseline length.

Table 1. Results of experiments using the MARBLE system(s).

date	baseline	WRMS	baseline	formal error* ¹		
		residual (psec)	length* ¹ (mm)	u-d	e-w	n-s
2009. 6.25	R* ² -B* ³	58	193845.7 ± 2.4	6.2	2.7	3.5
2009.12.24	B* ³ -C* ⁴	18	54184878.6 ± 2.7	19.5	2.7	2.6

*1 The errors represent 1 sigma of the formal errors.

*2 R : Kashima 11-m station

*3 B : first prototype of MARBLE

*4 C : second prototype of MARBLE

4. Conclusion and Outlook

We made two prototypes of a compact and transportable VLBI system. We performed geodetic VLBI experiments using these prototypes. The formal errors of the baseline length estimation are about 2 to 3 mm. From the result, we confirm that these prototypes can be used on geodetic VLBI. There is room for improvement of the error of the measurement. If we identify the cause, and it is possible to solve it, the measurement error will be decreased. On the other hand, now the

higher speed A/D sampler (ADS3000+) is available [10]. The measurement error will be decreased by using ADS3000+ also. To obtain a higher measurement precision than the current precision, we continue the development. We plan to make another prototype. We will review the antenna design and the receiver design, and we will make a more sensitive VLBI station.

This compact and transportable VLBI system can be applied to various observations. We are also planning to apply our prototype to time and frequency comparison experiments in 2010.

Acknowledgments

We wish to express our gratitude to Teruaki Orikasa, Yoshiyuki Fujino, Jun Amagai, Mamoru Sekido, Eiji Kawai, Moritaka Kimura, and Junichi Nakajima of NICT for a lot of advice for this research. We are very grateful for cooperation in the experiments by Hiromitsu Kuboki, Masanori Tsutsumi and Shingo Hasegawa of NICT. Part of this work was supported by a Grant-in-Aid for scientific research (KAKENHI, No.212410043). We used CALC/SOLVE made by GSFC for VLBI analysis.

References

- [1] Koyama, Y., T. Kondo, H. Osaki, A. Whitney, and K. Dudevoir, Rapid turnaround EOP measurements by VLBI over the Internet, Proceedings of the IAGG02 Symposium in the 23rd IUGG General Assembly, Sapporo Japan, July, 2003.
- [2] Kondo, T., Y. Koyama, R. Ichikawa, M. Sekido, E. Kawai, and M. Kimura, Development of the K5/VSSP System, *J. Geod. Soc. Japan*, Vol.54, No 4, pp. 233-248, 2008.
- [3] Rodriguez, Vincent., A Multi-octave Open-boundary Quad-ridge Horn Antenna for Use in the S- to Ku-band, *Microwave Journal*, 49, 84-92, 2006.
- [4] Ichikawa, R., A. Ishii, T. Takiguchi, Y. Koyama, T. Kondo, K. Kokado, S. Kurihara, and S. Matsuzaka, Present Status and Outlook of Compact VLBI System Development for Providing over 10 km Baseline Calibration, *IVS TDC-News*, No. 30, pp. 22-25, 2009.
- [5] Ohuchi, Y., H. Suga, M. Fujita, T. Suzuki, M. Uchino, K. Takahei, M. Tsuda, and Y. Saburi, A HIGH-STABILITY LASER-PUMPED Cs GAS-CELL FREQUENCY STANDARD, *Proc. IEEE/EIA International Frequency Control Symp.*, pp.651-655, 2000.
- [6] Ishii, A., R. Ichikawa, H. Takiguchi, H. Kuboki, M. Sekido, Y. Koyama, and Y. Ohuchi, Evaluation of a Laser-pumped Cs Gas-cell Frequency Standard on Geodetic VLBI, *Journal of the Geodetic Society of Japan*, Vol. 54, No. 4, pp.259-268, 2008.
- [7] Kumagai, M., M. Fujieda, S. Nagano, and M. Hosokawa, Stable radio frequency transfer in 114 km urban optical fiber link, *OPTICS LETTERS*, Vol. 34, No. 19, October 1, 2009.
- [8] Takiguchi, H., Y. Koyama, R. Ichikawa, T. Gotoh, A. Ishii, and T. Hobiger, Comparison Study of VLBI and GPS Carrier Phase Frequency Transfer -Part- II, *IVS TDC-News*, No. 30, pp. 26-29, 2009.
- [9] Petrachenko, B., A. Niell, D. Behrend, B. Corey, J. Bohm, P. Charlot, A. Collioud, J. Gipson, R. Haas, T. Hobiger, Y. Koyama, D. MacMillan, Z. Malkin, T. Nilsson, A. Pany, G. Tuccari, A. Whitney, J. Wresnik, Design Aspects of the VLBI2010 System, Progress Report of the IVS VLBI2010 Committee, NASA/TM-2009-214180, June, 2009.
- [10] Takefuji, K., Y. Koyama, and H. Takeuchi, First Fringe Detection with Next-Generation A/D Sampler ADS3000+, *IVS TDC-News*, No. 30, pp. 17-21, 2009.

VLBI2020: From Reality to Vision

Oleg Titov

Geoscience Australia

e-mail: oleg.titov@ga.gov.au

Abstract

The individual apparent motions of distant radio sources are believed to be caused by the effect of intrinsic structure variations of the active galactic nuclei (AGN). However, some cosmological models of the expanded Universe predict that systematic astrometric proper motions of distant quasars do not vanish as the radial distance from the observer to the quasar grows. These systematic effects can even increase with the distance, making it possible to measure them with high-precision astrometric techniques like VLBI. The Galactocentric acceleration of the Solar System barycenter may cause a secular aberration drift with a magnitude of $4 \mu\text{as}/\text{yr}$. The Solar System motion relative to the cosmic microwave background produces an additional dipole effect, proportional to red shift. We analyzed geodetic VLBI data spanning from 1979 until 2009 to estimate the vector spherical harmonics in the expansion of the vector field of the proper motion of 687 radio sources. The dipole and quadrupole vector spherical harmonics were estimated with an accuracy of $1\text{--}5 \mu\text{as}/\text{yr}$. We have shown that over the next decade the geodetic VLBI may approach the level of accuracy on which the cosmological models of the Universe could be tested. Hence, it is important to organize a dedicated observational program to increase the number of measured proper motions to 3000.

1. Introduction

Technological development over the last decade has led to an increase in the precision of geodetic VLBI data. This increased precision has allowed a detailed study of the stability of the International Celestial Reference Frame (ICRF). Table 1 shows a statistical comparison of the two ICRF catalogs, ICRF1 [1] and ICRF2 [2].

Table 1. Statistical comparison of the ICRF1 and ICRF2 catalogs.

	ICRF1	ICRF2
Year	1995	2009
Number of defining sources	212	295
Formal error (μas)	60	7
Inflated error (μas)	250	41

The International Celestial Reference System (ICRS) is based on several assumptions and definitions from the early 1990s. Hence, the improvement in accuracy of the ICRF realization has highlighted some previously unknown problems. For instance, the proper motions of reference radio sources are assumed to be negligible, and only the apparent motion due to a change of the intrinsic structure is considered as measurable. This assumption opens a way to impose no-net-rotation (NNR) constraints to fix the fundamental ICRS axes. Indeed, the individual apparent motions reach several hundred $\mu\text{as}/\text{yr}$ and may result in a ‘spurious’ rotation of the ICRF. However,

they are not correlated for all sources around the sky. Therefore, the problem comes down to the appropriate deselection of the radio sources with large individual proper motions.

A detailed statistical analysis of the reference radio source individual motions is highly desirable. The proper motion of reference radio sources, caused by some physical reasons, have a smaller magnitude, but they are highly correlated over the sky. Therefore, their impact on the ICRF stability and accuracy could also be significant. Once the fundamental axes of the ICRS are tied with the position of defining radio sources, a systematic effect, if it exists, causes instability of these axes. As a result, orthogonality of the reference axes may be lost. Some authors, therefore, warned that the basic assumptions should be verified on a regular basis [3] to be sure that they are consistent with the current observational results.

2. Possible Reasons for a Non-zero Proper Motion

There are several reasons which could cause systematic effects in proper motion.

1. Secular aberration drift which appears due to the galactocentric acceleration of the Solar System. This results in a dipole systematic effect in the proper motions of all radio sources irrelevant to distance. Vectors of all source motions are streamed towards the Galactic center with a theoretical magnitude of 4-5 $\mu\text{as/yr}$ [4], [5], [6], [7], [8], [9].

2. Anisotropic expansion of the Universe. In the Friedman-Robertson-Walker-Lemetre (FRLW) model the expansion of the Universe is isotropic, and the systematic proper motions are zero. Any deviation from the isotropy will result in a quadrupole systematic effect described by electric-type second degree vector spherical harmonics [10], [11].

3. Primordial gravitational waves. This results in a variation of the metric at the early stage of the Universe expansion. The systematic is described by electric- and magnetic-type second degree vector spherical harmonics. These systematic proper motions could increase with distance (red shift) [5], [10], [12].

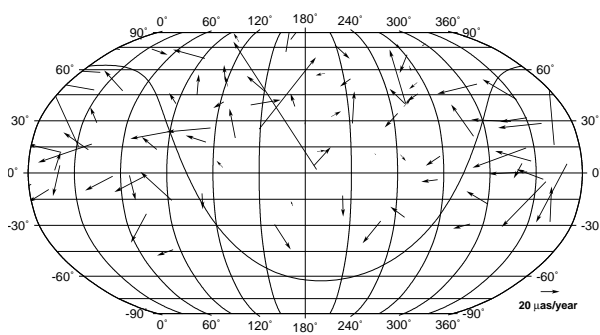
4. Instantaneous velocity of the Solar System with respect to the cosmic microwave background (CMB) [13]. The rectilinear velocity of the barycenter (about 380 km/sec) causes another dipole effect depending on the distance to the sources. While for most of the quasars this effect is small ($\leq 1 \mu\text{as/yr}$), it might be large for close galaxies (up to 14 $\mu\text{as/yr}$ for M81) [14].

3. Data Analysis

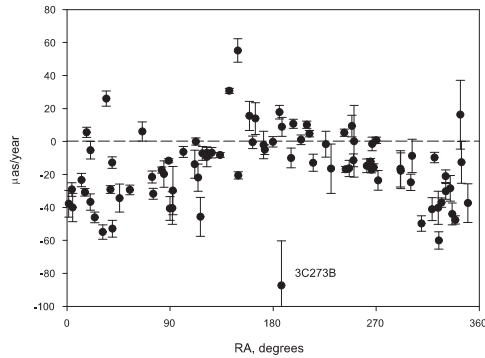
Figure 1a shows the vector field of the individual proper motions for the 86 most observed radio sources, and Figure 1b shows the proper motion component $\mu_\alpha \cos \delta$ as a function of right ascension. Two systematic effects were found. The first was the non-zero mean proper motion indicating a net rotation of the radio sources. The second was a cosine-like signal leading to a dipole systematic. In spite of the fact that most of the frequently observed radio sources are astrometrically unstable, the only obvious outlier is the quasar 3C273B. This demonstrates that the risk of ‘spurious’ rotation of the fundamental reference system induced by apparent motion of an individual astrometrically unstable radio source [17], [18], [19], [20] is overestimated.

A more rigorous analysis was completed using the proper motions of 687 radio sources observed in at least three epochs, and having at least three group delays in each epoch. It was found that 42 of the 687 sources were outliers, and they were removed from the final solution.

The second solution is based on the radio sources with a smaller number of observations;



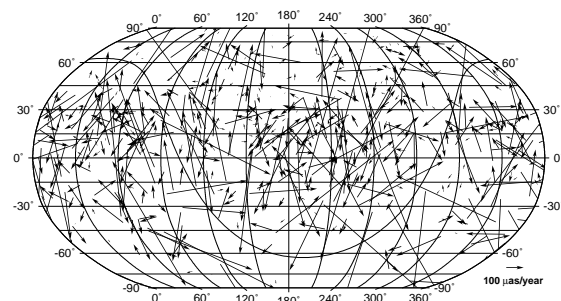
a) Individual proper motions on sky map.



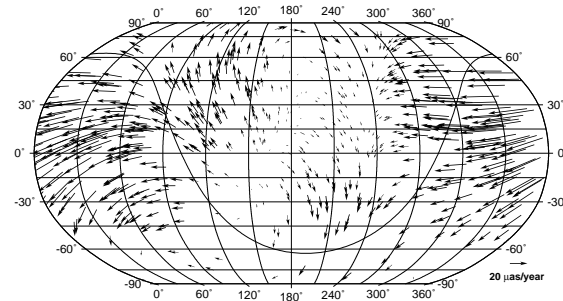
b) Proper motion component $\mu_\alpha \cos \delta$ as a function of right ascension.

Figure 1. Proper motions of 86 radio sources measured in ≥ 200 sessions with ≥ 15 group delays in each session.

therefore, the pattern of the individual proper motion in Figure 2 is noisier than in Figure 1, and the scale of the plot was increased to $100 \mu\text{as}/\text{yr}$. For this reason, the systematic effect is not as clear as in Figure 1. Nonetheless, due to an increase of the total number of proper motions and better coverage across the celestial sphere, the parameter estimates for this new solution are more robust. The estimate of the dipole component has a magnitude of $13.5 \pm 1.3 \mu\text{as}/\text{yr}$, and the total magnitude of the second degree vector spherical harmonics is about $10 \pm 2 \mu\text{as}/\text{yr}$.



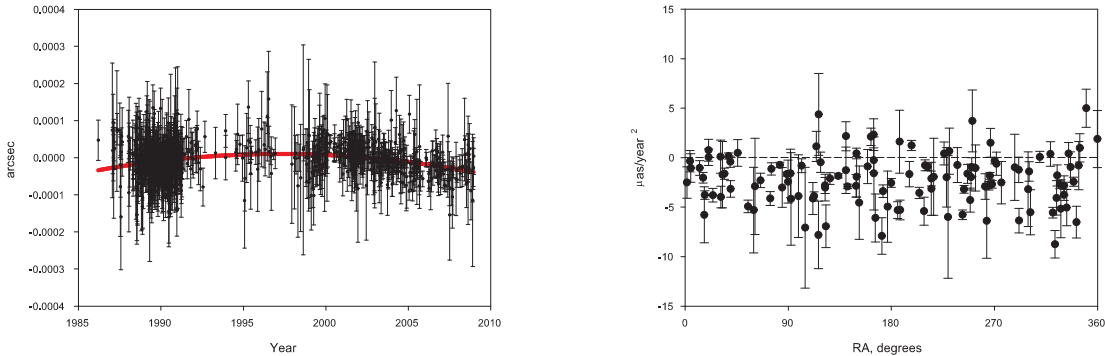
a) Individual proper motions on sky map.



b) Systematic of first and second order.

Figure 2. Individual motion and resultant systematic of 645 radio sources measured in ≥ 3 sessions with ≥ 3 group delays in each session.

Figure 3a shows the quadratic trend of the time series of right ascension of radio source 2121+053 with $A_\alpha \cos \delta = -5.5 \pm 0.6 \mu\text{as}/\text{yr}^2$. Figure 3b shows the proper ‘acceleration’ component $A_\alpha \cos \delta$ for the 86 most observed radio sources as a function of right ascension. The mean value of the effect is equal to $-2.2 \mu\text{as}/\text{yr}^2$. We have no obvious explanation for this effect.



a) Time series of 2121+053 right ascension; quadratic trend of $-5.5 \pm 0.6 \mu\text{as}/\text{yr}^2$ is shown. b) Proper ‘acceleration’ component $A_\alpha \cos \delta$ as a function of right ascension.

Figure 3. Proper ‘acceleration’ $A_\alpha \cos \delta$ for source 2121+053 and for the 86 radio sources measured in ≥ 200 sessions with ≥ 15 group delays in each session.

4. Conclusion

About 3000 radio sources have been observed by VLBI in the geodetic and astrometric programs. Unfortunately, most of the radio sources were observed in one or two epochs only. Therefore, reliable proper motions can only be estimated for about 700 radio sources. This paper has shown that the apparent motions of individual radio sources are not random on the sky, and some interesting systematics are detected at the accuracy level of $10 \mu\text{as}/\text{yr}$. More signals will be expected, if the standard error of the estimates reduces to $0.1 \mu\text{as}/\text{yr}$ for the dipole effect. All the discussed systematic effects will be estimated with a higher accuracy if the remaining 2300 sources are observed several times by 2020. We believe that scheduling each of the 2300 sources in three to four sessions (with four to five scans for each session) for the next 10 years will allow an increased accuracy of the estimated systematic effects. If this program is realized, the geodetic VLBI will approach the level of accuracy required to test the cosmological models of the Universe.

References

- [1] Ma, C., E. F. Arias, T. M. Eubanks, et al., The International Celestial Reference Frame as realised by Very Long Baseline Interferometry, *AJ* 116, 516–546, 1998.
- [2] Fey, A., D. Gordon, and C. Jacobs (eds.), The second realization of the International Celestial Reference Frame by Very Long Baseline Interferometry, *IERS Technical Notes* 35, 2009.

- [3] Walters, H. G., O. J. Sovers, *Astrometry of Fundamental Catalogues*, Springer-Verlag, 2000.
- [4] Bastian, U., Direct detection of the Sun's Galactocentric acceleration, In Proc of the RGO-ESA Workshop Future Possibilities for Astrometry in Space (ESA SP-379), Perryman, M. A. C, and F. Van Leeuwen (eds.), 1995.
- [5] Gwinn, C. R., T. M. Eubanks, T. Pyne, et al., Quasar proper motions and low-frequency gravitational waves, *ApJ* 485, 87–91, 1997.
- [6] Sovers, O. J., J. L. Fanelow, C. S. Jacobs, *Astrometry and geodesy with radio interferometry: experiments, models, results*, *Rev. Mod. Phys.* 70, 1393–1454, 1998.
- [7] Kovalevsky, J., Aberration in proper motions, *AA* 404, 743–747, 2003.
- [8] Klioner, S., A practical relativistic model of microarcsecond astrometry in space, *AJ* 125, 1580–1597, 2003.
- [9] Kopeikin, S. M., V. V. Makarov, *Astrometric effects of secular aberration*, *AJ* 131, 1471–1478, 2006.
- [10] Kristian, J., R. K. Sachs, *Observations in cosmology*, *ApJ* 143, 379–399, 1966.
- [11] Titov, O., Systematic effect in the radio source proper motion. In Proc of the 19th European VLBI for Geodesy and Astrometry Working Meeting, Bourda, G., P. Charlot and A. Collioud (eds.), 2009.
- [12] Pyne, T., C. R. Gwinn, M. Birkinshaw, et al., *Gravitational Radiation and Very Long Baseline Interferometry*, *ApJ* 465, 566–577, 1996.
- [13] Kardashev, S., *Cosmological proper motion*, *Sov. Astronomy*, 30(5), 501–504, 1986.
- [14] Eubanks, M., *Astrometric cosmology using radio interferometry*, *Bull. of the AAS*, 23, 1465, 1998.
- [15] MacMillan, D. S., *Quasar apparent proper motions observed by geodetic VLBI networks*. In *Future Directions in High Resolution Astronomy, The 10th Anniversary of the VLBA* Romney, J. D. and M. J. Reid (eds.), 2005.
- [16] Titov, O., Z. Malkin, *Effect of asymmetry of the radio source distribution on the apparent motion kinematic analysis*, *AA* 506, 1477–1485, 2009.
- [17] Charlot, P., *Radio source structure in astrometric and geodetic Very Long Baseline Interferometry*, *AJ* 99, 1309–1326, 1990.
- [18] Feissel-Vernier, M., *Selecting stable extragalactic compact radio sources from the permanent astro-geodetic VLBI program*, *AA* 403, 105–110, 2003.
- [19] Titov, O., *Construction of a celestial coordinate reference frame from VLBI data*, *Astron. Rep.* 48, 941–948, 2004.
- [20] MacMillan, D., C. Ma, *Radio source instability in VLBI analysis*, *JoG* 81, 443–453, 2007.

How and Why to Do VLBI on GPS

J. M. Dickey

University of Tasmania

e-mail: john.dickey@utas.edu.au

Abstract

In order to establish the position of the center of mass of the Earth in the International Celestial Reference Frame, observations of the Global Positioning Satellite (GPS) constellation using the IVS network are important. With a good frame-tie between the coordinates of the IVS telescopes and nearby GPS receivers, plus a common local oscillator reference signal, it should be possible to observe and record simultaneously signals from the astrometric calibration sources and the GPS satellites. The standard IVS solution would give the atmospheric delay and clock offsets to use in analysis of the GPS data. Correlation of the GPS signals would then give accurate orbital parameters of the satellites **in the ICRF reference frame**, i.e., relative to the positions of the astrometric sources. This is particularly needed to determine motion of the center of mass of the earth along the rotation axis.

1. Background

Methods of observing the Global Positioning System (GPS) satellites with the International Very Long Baseline Interferometry Service for Geodesy and Astrometry (IVS) telescopes have been discussed for more than a decade (Hase 1999 [9], Petrachenko et al. 2004 [12]). The motivation is to measure the orbits of the GPS spacecraft in near-real-time with high precision **directly in the reference frame** defined by the extragalactic radio sources, i.e., the International Celestial Reference Frame (ICRF, Ma 2008 [11], Boboltz et al. 2010 [5]). The challenge of extending the ICRF to the International Terrestrial Reference Frame (ITRF) involves combining data from other sources such as Satellite Laser Ranging (SLR), the Gravity Recovery and Climate Experiment (GRACE), the Doppler Orbitography and Radiopositioning Integrated by Satellite (DORIS) systems, and measurements using GPS receivers themselves (e.g., Argus et al. 2010 [2], Tregoning et al. 2009 [14]).

A particularly important issue is the motion of the Earth's center of mass (CE). A discrepancy between the ITRF2000 and ITRF2005 suggests that the mass distribution of the Earth is changing in such a way that the CE is moving northward at a rate of 1.8 mm yr^{-1} (Altamimi et al. 2007 [1], Tregoning and Watson 2009 [15]). If this motion were real it would raise problems with other precision measurements such as sea level rise and glacial isostatic adjustment (e.g., Beckley et al. 2007 [4]). The problem is the reference frames themselves. While SLR, GRACE, and DORIS are ultra-sensitive to the Earth's gravitational field, the IVS solutions for the Earth Orientation Parameters (EOPs) are sensitive only to the rotation of the Earth's surface. The frame-tie between the ICRF and the satellite orbits (measured in the ITRF) introduces uncertainty in the CE position at the level of millimeters. This frame-tie could be simplified by correlating the GPS signals along with those from the ICRF-defining quasars as part of the IVS operation.

The CE position could be a sensitive measure of the global average of glacial melting, given the asymmetry of the latitudinal distribution of land and sea between the Northern and Southern Hemispheres. Melting of sea ice has no impact on the CE, but melting of ice caps such as those in

Greenland and Antarctica leads to a redistribution of the mass as the melt water adjusts to follow an equipotential. This glacial melting contributes to sea level rise, and so it has been studied quantitatively (Bahr et al. 2007 [3] and references therein); the mass of ice whose melting gives a rise in the mean sea level of 1 mm is $m_i = 3.3 \cdot 10^{14}$ kg (Dyrugerov and Meier 2005 [7] figure 5 ff). Comparing this to the total Earth mass gives a prediction for the motion of the CE along the axis of rotation of \dot{z} :

$$\dot{z} = -R_{\oplus} \left(\frac{f m_i}{2 M_{\oplus}} \right) \left(\frac{\dot{s}}{\text{mm yr}^{-1}} \right) \simeq -0.4 \text{ mm yr}^{-1}$$

where R_{\oplus} and M_{\oplus} are the Earth radius and mass, and f is a dimensionless number between -1 and +1 given by the mass-weighted mean of the sine of the latitude where the ice melts. Assuming that $f \sim 1$ gives the value of -0.4 mm yr⁻¹ above, with the minus indicating southward motion because most glacial melting is (for now) in the Northern Hemisphere. More accurate measurement of the motion of the CE would be a valuable addition to our knowledge of the effects of global warming (Dickey et al. 2002 [6]). This could be accomplished by determining the orbital parameters of the GPS satellites directly from measurements coupled with routine IVS observations. Combining the two would circumvent the need for a series of techniques, each based on a different observable, to establish the CE together with the ITRF itself. The main advantage of combining IVS and GPS satellite orbit measurement is not improved precision in the measurements, although that might be possible, but rather the direct measurement of satellite orbits relative to the ICRF calibrators.

2. IVS Techniques

The simplest approach (method 1) to measuring GPS signals with the IVS array is to use the radio telescopes themselves to record the GPS signals, and then to correlate these signals to determine the delay on each baseline and hence the position of each satellite as a function of time. The radio telescope beams are narrow, so that the satellites are observed one at a time, and their approximate positions must be tracked using an ephemeris. The main disadvantage of this method is that the GPS signals are in the 1500-1600 MHz and 1200-1300 MHz ranges, which are well below the S-band (2100-2400 MHz) frequencies of the IVS receivers. Thus new, wideband receivers would have to be built for all the network telescopes, in order to accommodate observations of both GPS and the standard IVS calibration sources together.

A more ambitious but ultimately simpler method (method 2, illustrated in Figure 1) is to use a standard, geodetic-quality GPS antenna and receiver near each IVS telescope, using local oscillators locked to the same station clock for the GPS and IVS receivers and simultaneously recording the receiver outputs on separate channels on the same media. A precise frame-tie or survey of the relative positions of the two antennas is also needed. The GPS antennas are nearly omni-directional and so they receive the signals from all satellites that are above the horizon. Correlating the outputs from the GPS receivers should give multiple delay peaks on each baseline, one for each spacecraft. With three or more baselines the positions of all the satellites can be fixed, and their orbital parameters determined from the position vs. time over an extended observation. Note that it is the carrier signal that gives the correlation peak and hence provides the relative delay on each baseline; there is no need to decode the information carried in the modulation of the carrier as for normal GPS operation.

The main advantage of the second method is that the radio telescopes simultaneously carry out normal IVS observing, so that the correlation and position solutions from the ICRF sources

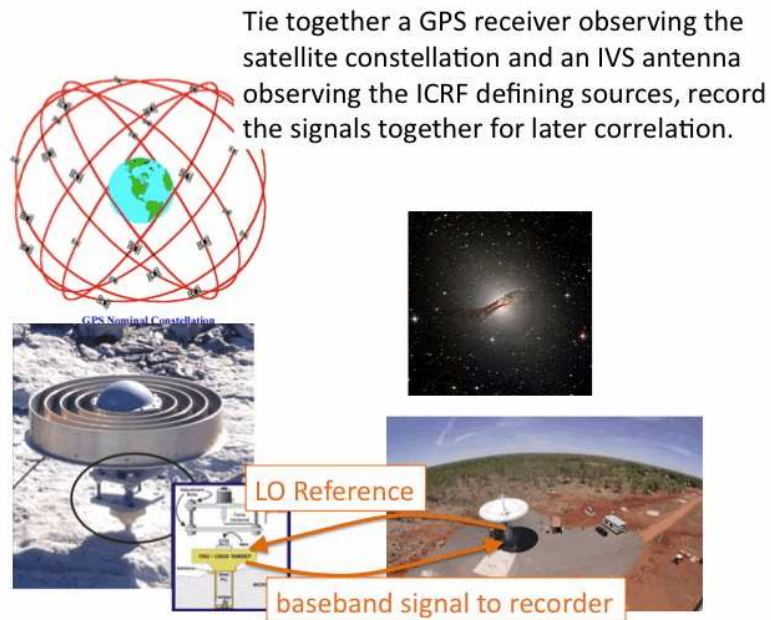


Figure 1. An illustration of the second method for combining observations of the GPS signals with the IVS calibrators. The advantages of recording signals from two antennas simultaneously at each station outweigh the difficulties of measuring the offset between the two, both in position and in the LO/RF round-trip delay.

provide clock offsets, EOPs, and atmospheric delays at all times during the observation. These results can be extended to the frequency of the GPS to predict values for the propagation delay through the neutral and ionized components of the atmosphere. Determination of the clock offsets effectively puts the GPS satellite positions in the reference frame of the astronomical sources. This accomplishes the frame-tie that allows the CE to be **directly measured in the ICRF** with a single technique. Other satellite measurement techniques could still improve the precision of the measured CE position, but the fundamental reference frame of the measurement would become the ICRF rather than the ITRF. This avoids problems with the registration (offset) of one reference frame relative to the other.

3. Applications

Evidence of the need for better long-term monitoring of the GPS orbital elements in the ICRF frame comes from comparison of time series of terrestrial reference positions using GPS and GRACE. Figure 2 from Tregoning and Watson (2009 [15]) shows the time series and resulting power spectrum of a reference point near Darwin, NT. There is strong vertical motion with an annual period resulting from seasonal groundwater variation. Unfortunately, determination of this variation, and hence of the groundwater supply in the region, is confused by another effect with a similar period, the synodic period of the GPS constellation or draconitic period, 351.4 days. The GRACE and GPS positions agree well except for periods between 0.5 and 1.5 years in the vertical direction as seen in Figure 2. This problem could be alleviated by independent measurement of the

What's the point?

- Frame tie the ICRF with the GPS orbits
- Monitor GPS satellite motion (like SLR)
- Establish the Earth center of mass position in the ITRF

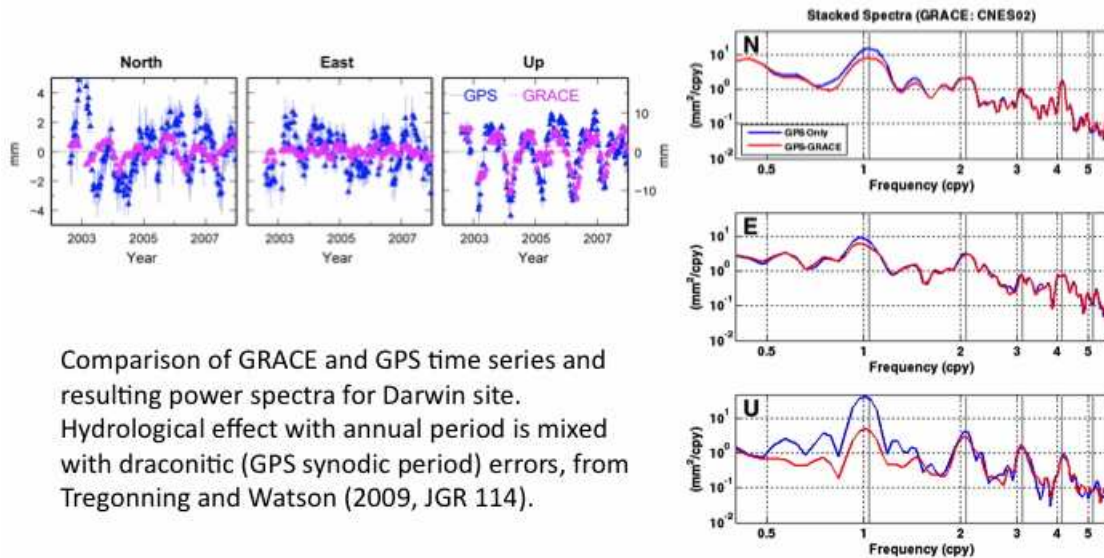


Figure 2. An illustration of the current problem with GPS orbital elements. At the draconitic period of the GPS satellites, i.e. the synodic period of the constellation as a whole, there is a significant discrepancy between position measurements using GRACE and those using GPS. The figures are taken from Tregonning and Watson (2009) [15], who studied time series of positions for a geodetic reference site near Darwin, NT.

GPS satellite positions in the ICRF, that could be provided by the extension of the IVS technique described here.

4. Conclusions

The modest proposal of this contribution is that IVS operations in the future should include recording of one or more bands in the 1.5 GHz range collected from a GPS receiver near the main radio astronomy antenna. The GPS receiver should have its local oscillator phase-locked to the station clock. As a preliminary experiment, three antennas could be equipped in this way for test observations. As an ultimate goal, the GPS signal from each satellite could be decoded to predict the delay expected on each baseline, to save time in the correlation step. Two very important steps toward the operation described here are the pioneering studies by Tornatore and Haas (2010 [13]) and Kwak et al. (2010 [10]) described in this volume.

5. Acknowledgements

I am grateful to Paul Tregoning, Christopher Watson, Richard Coleman, and Jim Lovell for suggesting and explaining this topic to me.

References

- [1] Altamimi, Z., Sillard, P., and Boucher, C., 2002b, *J. Geophys. Res.*, 107(B10), 2214, doi:10.1029/2001JB000561.
- [2] Argus, D.F., Gordon, R.G., Heflin, M.B., Ma, C., et al. 2010, *Geophys. Journal International* 180, 913-960.
- [3] Bahr, D.B., Dyurgerov, M., Meier, M.F., 2009 *Geophysical Research Letters*, 36, CiteID L03501.
- [4] Beckley B. D., F. G. Lemoine, S. B. Luthcke, R. D. Ray, N. P. Zelensky, 2007, *Geophys. Res. Lett.*, 34, L14608, doi:10.1029/2007GL030002.
- [5] Boboltz, D.A., Gaume, R.A., Fey, A.L., Ma, C., Gordon, D., IERS/IVS Working Group on ICRF2, 2010, AAS Meeting 215 no. 469.06, BAAS 41, 512.
- [6] Dickey, J.O., Marcus, S.L., de Viron, O., and Fukumori, I., 2002 American Geophysical Union abstract U72A-0013.
- [7] Dyurgerov, M.B. and Meier, M.F., 2005, *Glaciers and the Changing Earth System: A 2004 Snapshot*, INSTAAR, Occasional Paper No. 58, (University of Colorado at Boulder: Boulder), ISSN 0069-6145.
- [8] Fey, A.L., Ma, C., Arias, E.F., Charlot, P., Feissel-Vernier, M., et al., 2004, *A.J.* 127, 3587.
- [9] Hase, H., 1999, *Proceedings of the 13th Working Meeting on European VLBI for Geodesy and Astrometry*, pp. 273-277.
- [10] Kwak, Y., Kondo, T., Gotoh, T., Amagai, J., Takiguchi, H., et al., 2010, *Proceedings of the Sixth General Meeting of the IVS*, in press (this volume).
- [11] Ma, C. 2008, *Proceedings of IAU Symposium* 248, p. 337.
- [12] Petrachenko, W. et al. 2004, *IVS 2004 General Meeting Proceedings*, ed. N.R. Vandenberg and K.D. Bavar, NASA/CP-2004-212255, 2004.
- [13] Tornatore, V. and Haas, R., 2010, *Proceedings of the Sixth General Meeting of the IVS*, in press (this volume).
- [14] Tregoning, P., Ramillien, G., McQueen, H., and Zwartz, D., 2009, *J. Geophys. Res.*, 114, B06406, doi:10.1029/2008JB006161.
- [15] Tregoning, P. and Watson, C.S., 2009, *J. Geophys. Res.*, Vol. 114, No. B9, B09403, doi:10.1029/2009JB006344.

Planning of an Experiment for VLBI Tracking of GNSS Satellites

Vincenza Tornatore ¹, Rüdiger Haas ², Guifré Molera ³, Sergei Pogrebenko ⁴

¹) *DIAR, Politecnico di Milano*

²) *Chalmers University of Technology, Department of Radio and Space Science*

³) *Aalto University School of Science and Technology, Metsähovi Radio Observatory*

⁴) *Joint Institute for VLBI in Europe*

Contact author: Vincenza Tornatore, e-mail: `vincenza.tornatore@polimi.it`

Abstract

As a preparation for future possible orbit determination of GNSS satellites by VLBI observations an initial three-station experiment was planned and performed in January 2009. The goal was to get first experience and to verify the feasibility of using the method for accurate satellite tracking. GNSS orbits related to a satellite constellation can be expressed in the Terrestrial Reference Frame. A comparison with orbit results that might be obtained by VLBI can give valuable information on how the GNSS reference frame and the VLBI reference frame are linked. We present GNSS transmitter specifications and experimental results of the observations of some GLONASS satellites together with evaluations for the expected signal strengths at telescopes. The satellite flux densities detected on the Earth's surface are very high. The narrow bandwidth of the GNSS signal partly compensates for potential problems at the receiving stations, and signal attenuation is necessary. Attempts to correlate recorded data have been performed with different software.

1. Introduction

Several possibilities are known to track high orbiting satellites using the VLBI technique. VLBI geodetic observations by radio telescope networks [11] demonstrated the feasibility of using the method for accurate tracking of the communications satellite TACSAT and for geodesy already in 1972.

Phase referencing observations with respect to the background radio sources is often used today for Deep Spacecraft navigation [8], [10]. However phase referencing observations show differences of the propagation media for the sources at infinity and the near-Earth satellites. Such differences need to be studied in more detail.

The use of dedicated emitters directly installed on GNSS satellites sending signals to Earth radio telescopes is also a promising method for orbitography. An early proposal [3] foresaw the installing of additional transmitters on a GPS satellite and using the signal for interferometric techniques with fairly simple ground equipment. The project was called Miniature Interferometer Terminal for Earth Surveying (MITES), but it was never built in the proposed way, the system was only privately built to prove the concept by D. Steinbrecher and C. Counselman. Anyway, many of today's algorithms for GPS carrier phase measurements can be tracked back to this development [13]. A slight different principle has been recently proposed [5], [7]. According to this method GPS data are acquired with a modified receiver and then recorded with VLBI equipment.

At present two projects aboard multitechnique satellites are carried out by JPL and GFZ. GRASP (Geodetic Reference Antenna in Space) a mission to enhance the Terrestrial Reference Frame is developed at JPL [2] and MicroGEM, a small LEO satellite that can, among other things,

receive GNSS signals, can be tracked with SLR, and can send artificial VLBI signals [18], is under development at GFZ Potsdam.

In this paper we present some observations that we performed in a geodetic VLBI mode to receive the signals of GLONASS satellites.

2. Goals and Characteristics of the Experiment

An initial three-VLBI-station experiment was planned to track the same satellite in geodetic VLBI mode. We chose GLONASS satellites since the frequencies of emitted signals were observable by the L-band receivers of the three involved European stations Medicina, Noto, and Onsala. Several tests were performed during 2009 with the goal to develop and test the scheduling for different satellites, to verify satellite tracking at different azimuth and elevation, to test possible necessary signal attenuation, and to verify correlation detection. GLONASS carrier signals in L1 band are in the interval 1602.56 MHz and 1615.50 MHz. On L1 a C/A code of 1.022 MHz bandwidth and a P code of 10.220 MHz are superimposed. The effectively isotropic radiated power (EIRP) is on the order of 26 dBW, and considering the distance from the Earth of about 19,000 km, the calculated receiving temperature for Medicina and Noto is 1.5×10^6 K.

We performed tests at 1 MHz and 10 MHz bandwidth using an artificial signal with the same power as the GNSS satellites. The receiver could still work in the linear area without reaching saturation. At Onsala, a 20 dB attenuation was necessary during these tests with artificial signals.

The four satellites PR02, PR03, PR17, and PR18 were simultaneously visible at Medicina, Noto, and Onsala on January 21, 2009 from 08:00 UT to 12:00 UT. Observations were performed using the standard Mark IV VLBI data acquisition rack for Onsala and Medicina, and a VLBA rack for Noto. Two channels (VCs) of 8 MHz bandwidth (upper, 1 RHCP, 1 LHCP) were selected at all the stations. Individual signal attenuation was used at the stations. The formatted data were recorded with Mark 5A equipment, and phasecal was used. The telescopes were positioned stepwise with 20 seconds updates to follow the satellites. The recording scans had a length of 10 seconds, so 5 seconds were left to point the antenna to the new satellite position. After the satellite tracking, a one-minute-long observation was carried out on Cygnus A using the same setup, but with different attenuation at the stations.

3. Results and Future Developments

Signal spectra have been recorded individually at all three stations, both for LHCP and RHCP, see for example the case for Onsala in Figure 1. In general the power level was quite different for RHCP and LHCP. For example, at Onsala the RHCP signal was 20 dB stronger than the LHCP signal. This is consistent with the LHCP component originating at the satellite since the GLONASS signal is specified to have RHCP stronger than LHCP by 16 dB [6]. The difference of 20 dB versus 16 dB might originate from possible imperfections in the VLBI feed, for example insufficient polarization isolation. The LHCP channel might have picked up some RHCP signal.

Later, when the calibrator Cygnus A was observed, it was necessary to reduce the additional attenuation again. It was necessary to reduce attenuation by 19 dB / 16 dB (RHCP / LHCP) at Noto, 29 dB / 10 dB (RHCP / LHCP) at Medicina, and 27 dB / 5 dB (RHCP / LHCP) at Onsala. This gives an impression on how much stronger the satellite signals are than signals from natural radio sources.

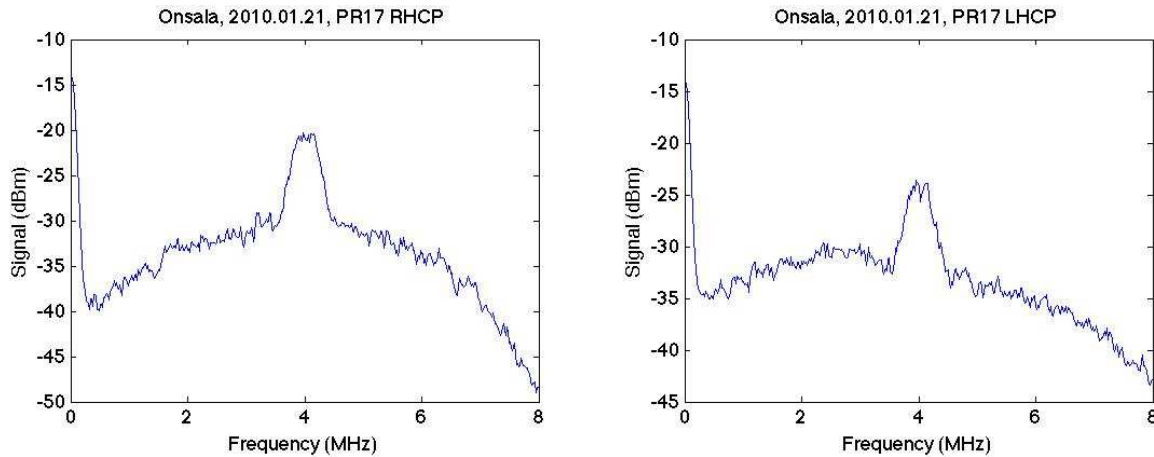


Figure 1. Spectra of the LHCP and RHCP signals of PR17 GLONASS satellite observed at Onsala.

The spectrometer graph from Medicina, see Figure 2 (left), clearly shows the 10 seconds acquisition and the time intervals where no acquisition is made. Signal power fluctuations are therefore present. At some epochs the signal fluctuations were very large, for example at Medicina in Figure 2 (right), and similar effects were observed for Onsala and Noto, too. The reason of these strong fluctuations still needs to be investigated.

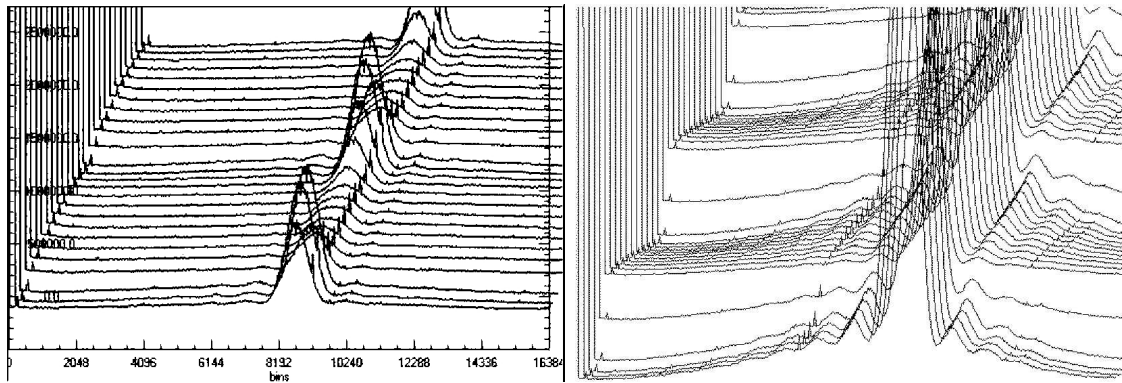


Figure 2. Temporal evolution of spectra for GLONASS satellites PR17 (left) and PR03 (right) observed at Medicina. In a right-hand-coordinate system the X-axis shows frequency, the Y-axis time, and the Z-axis signal strength in arbitrary units. These spectra cannot be compared directly to the ones observed at Onsala shown in Figure 1. Strong variations in signal strength become clearly visible.

Attempts to correlate the recorded data have been performed with the DiFX software correlator [4] and the Space Navigation Signal correlator at JIVE and Metsähovi, SWspec and SCtracker software [14]. Unfortunately, it turned out that there was a recording problem at Noto and that the VC center frequencies had been chosen slightly differently at Medicina and Onsala. Thus, the cross-correlation attempts were not successful. However, auto-correlation of the Medicina data and the Onsala data worked fine. Figure 3 shows autocorrelation results for both LHCP and RHCP

data of one of the observed GLONASS satellites at Medicina and Onsala.

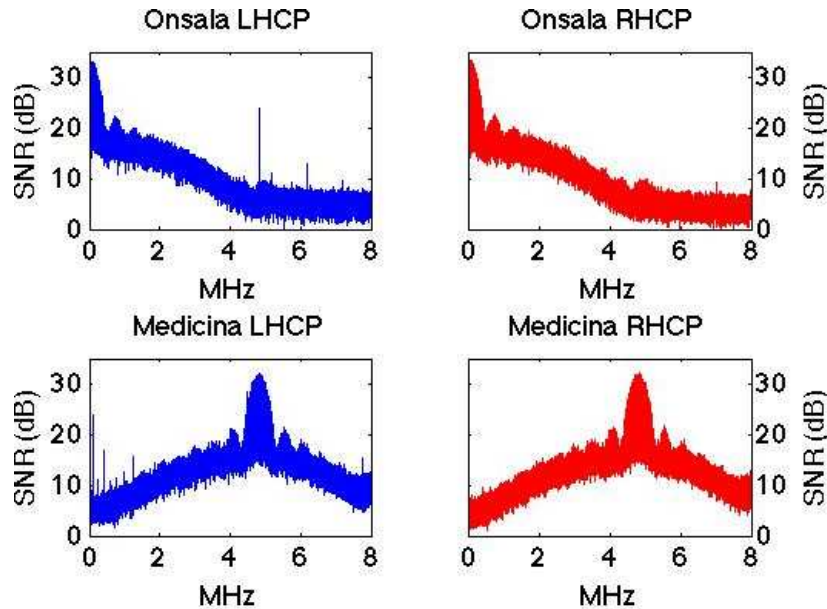


Figure 3. Autocorrelation spectra of the LHCP and RHCP signals of one GLONASS satellite observed at Onsala and Medicina.

Our experiment shows that it is in principle possible to track GNSS satellites directly with VLBI telescopes. To achieve successful correlation a number of aspects has to be revisited, e.g. the setup of the data acquisition system. A simplification of satellite tracking by an inclusion of the SatTrack-module for the FS in the next official FS-release is desirable. We plan to perform simulations to improve the routines and to perform new experiments and new observations.

VLBI tracking of GNSS satellites might have an impact on GNSS orbitography. This is in particular interesting since there are new systems in development, e.g. Galileo and Compass. A direct comparison of orbits derived from GNSS themselves, SLR and VLBI can support orbit calculations. For the future, artificial VLBI beacons on LEO satellites could support VLBI phase calibration.

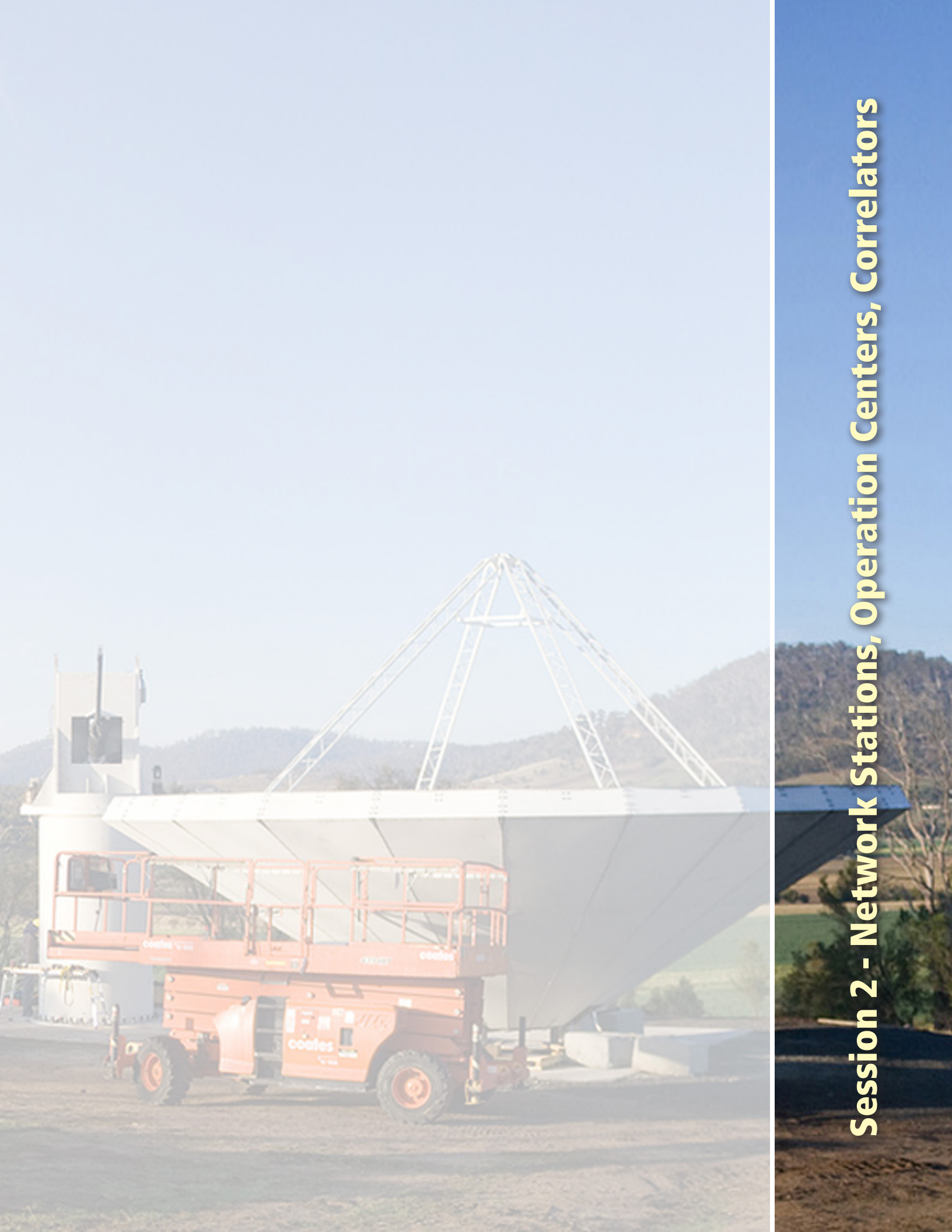
4. Acknowledgements

This work is based on observations with the Medicina and Noto radiotelescopes operated by INAF, Istituto di Radioastronomia, Italy and Onsala operated by Swedish National Facility for Radio Astronomy, Sweden. We thank the personnel at the VLBI stations of Medicina, Noto, and Onsala for supporting our experiment. We thank Simon Casey at Onsala Space Observatory for his help with the DiFX software correlator and Brian Corey for helpful discussions.

References

- [1] Altamimi Z., Collilieux X., Legrand J., Garayt B. & Boucher C. (2007) ITRF2005: A new release of the International Terrestrial Reference Frame based on time series of station positions and Earth

- Orientation Parameters. *J. Geophys. Res.*, **112**, B09401, doi:10.1029/2007JB004949.
- [2] Bar-Sever Y., Haines B., Wu S., Lemoine F., Willis P. (2009) The Geodetic Reference Antenna in Space (GRASP) Mission Concept. EGU meeting in Vienna 2009
- [3] Counselman C., Shapiro I.I. (1979) Miniature Interferometer terminals for earth surveying. *Bull. Geod.*, **53(2)**, 139–163.
- [4] Deller A.T., Tingay M., Bailes M., West C. (2007) DiFX: A Software correlator for very Long Baseline Interferometry using Multiprocessor Computing Environments. *The Astr. Soc. of the Pacific*, **119**: 318–336, 2007
- [5] Dickey J. (2010), How and Why to do VLBI on GPS, Proceedings of the Sixth General Meeting of the IVS, in press (this volume)
- [6] ICD, 1998. ICD, GLONASS Interface Control Document 4.0 (1998), Coordinational Scientific Information Center of Russian Space Forces, Moscow, Russia (1998) www.gnss.umaine.edu/PDF-files/glonass.pdf
- [7] Kwak Y., Kondo T., Gotoh T., Amagai J.2, Takiguchi H., Sekido M., Ichikawa R., Sasao T., Cho J., Kim T. (2010) The first experiment with VLBI-GPS hybrid system, Proceedings of the Sixth General Meeting of the IVS, in press (this volume)
- [8] Lebreton J.P., Gurvits L.I. et al., An overview of the descent and landing of the Huygens probe on Titan(2005) *Nature* **438**, 758-764
- [9] Moya Espinosa M. & Haas R. (2007) SATTRACK – A Satellite Tracking Module for the VLBI Field System. In: *Proc. 18th European VLBI for Geodesy and Astrometry Working Meeting*, edited by J. Böhm, A. Pany, and H. Schuh, Geowissenschaftliche Mitteilungen, Schriftenreihe der Studienrichtung Vermessung und Geoinformation, Technische Universität Wien, **79**, 53–58.
- [10] Pogrebenko S.V., Gurvits L.I.(2008) Planetary Radio Interferometer and Doppler Experiments with Europa-Jupiter mission, Presentation at Europa-Jupiter International Science Workshop, 22-23 April 2008, Frascati, Italy
- [11] Preston R.A., Ergas R. , Hinteregger H.F., Knight C.A., Robertson D.S, Shapiro I.I., Whitney A.R., Rogers A.E.E., & Clark T.A. Interferometric Observations of an Artificial Satellite. *Science*, 27 October 1972, Vol. 178. no. 4059, 407–409, DOI: 10.1126/science.178.4059.407A
- [12] Sekido, M. & T. Fukushima (2006) A VLBI Model for a Radio Source at Finite Distance. *J. Geod.*, **80**, 137–149.
- [13] Seeber G. (2003) *Satellite Geodesy*, 2nd Edition de Gruyter
- [14] Software spectrometer and SpaceCraft tracking instructions. <http://www.metsahovi.fi/en/vlbi/spec/index>.
- [15] Thaller D., Krügel M., Rothacher M., Tesmer V., Schmid R. & Angermann D. (2007) Combined Earth orientation parameters based on homogeneous and continuous VLBI and GPS data. *J. Geod.*, **81**, 529–541.
- [16] Tornatore V., Tuccari G. & Wei E. (2008) First considerations on the feasibility of GNSS observations by the VLBI technique. In: IVS 2008 General Meeting Proceedings “Measuring the Future”, edited by A. Finkelstein and D. Behrend, 439-444.
- [17] Tornatore V., Haas R. (2009) Considerations on the observation of GNSS-signals with the VLBI2010 system. In: *19th European VLBI for Geodesy and Astrometry (EVGA) Working Meeting*, Bordeaux 24-25 March 2009, edited by G. Bourda, P. Charlot, A. Collioud, 151–155.
- [18] Wickert J., Schmidt T., Beyerle G., Heise S., Stosius R. (2009) Radio occultation at GFZ Potsdam: Current status and future prospects. COSMIC workshop 2009



Session 2 - Network Stations, Operation Centers, Correlators

An Introduction to Sked

John Gipson

NVI, Inc., Code 698, NASA Goddard Space Flight Center, Greenbelt, MD, 20771

e-mail: john.m.gipson@nasa.gov

Abstract

In this note I give an overview of the VLBI scheduling software *sked*. I describe some of the algorithms used in automatic scheduling and some *sked* commands which have been introduced at users' requests. I also give a "cookbook" for generating some schedules.

1. Introduction

In this note I give an introduction to the VLBI scheduling software *sked*¹ widely used to schedule geodetic VLBI sessions. Nancy Vandenberg began writing *sked* as a graduate student in 1978. *Sked* has grown and evolved over time, becoming ever more sophisticated. Some highlights are summarized in Table 1. Vandenberg maintained *sked* until I took over this function in 2002.

Sked reads and writes *.skd* files which are special ASCII files that contain a complete description of the session, the schedule, and additional information used in scheduling the session. To schedule the session, *sked* needs to model many aspects of the VLBI system. The *.skd* file contains sufficient information to do so including:

1. Stations: Position, antenna slew rates and accelerations, horizon masks.
2. Equipment: Rack, recorder, recording options.
3. Source: Position, flux model.
4. Frequency setup: Number of channels, frequencies, bandwidths, 1 or 2 bit recording.

Sked can be run in either manual or automatic mode, or as a mixture of the two. Manual mode gives the user complete control over the schedule: for each scan they can specify the source, stations, start-time, and duration. Manual mode was used to schedule all sessions during the first decade of VLBI. However, as the number of stations and sources in sessions increased, it became increasingly cumbersome to schedule them manually. Currently a typical R1 session has 7 stations, 60 sources, and 1000 scans. Assuming it takes the scheduler only one minute to schedule a scan (which is actually quite optimistic) it would take almost two eight-hour days to schedule an R1.

Automatic scheduling was introduced in the early 1990s. The initial algorithm used covariance optimization—the user specified a set of parameters they were interested in estimating, and *sked* built up the schedule, scan-by-scan. At each step it would generate a set of trial scans and would choose the scan that, after being added to the schedule, would reduce the RMS sum of the formal errors of the parameters being optimized by the greatest amount. Although this approach seems reasonable, it led to schedules that looked strange to human eyes, and hence this approach

¹*Sked* should not be confused with the similar sounding *sched* used to schedule VLBI astronomy sessions and maintained by Craig Walker of NRAO.

Table 1. *Sked* History Highlights.

1978	Basic program created by Nancy Vandenberg. Command line input. Manual selection of scans. Catalogs for sources, stations, equipment.
1981	Automatic calculation of antenna motion and tape handling.
1988	Automatic selection of observations (Autosked). Optimization by strict covariance.
1992	Evaluation of schedules using SOLVE simulations. Creation of pseudo-databases to evaluate formal errors.
1993	Autosked merged into standard version. “Strange” schedules caused autosked not to be used.
1995	Beginning of rule-based schedules.
1996	Mark IV/VLBA recording mode support added. Last time <i>sked</i> documentation updated.
1997	Support for VEX files. Y2K fixes. New Java-based catalog interface. (Too slow, so generally not used.) S2 and K4 support.
2002	John Gipson takes over development/maintenance. Fill-in mode. Best-N Source Selection.
2004	Linux port by Alexey Melnikov. Beginning of death of HP- <i>sked</i> . Astrometric option: Specify min, max observing targets for set of sources.
2005	Full support of Disk-based recording: Mark 5A, Mark 5B, K5.
2006	Downtime: Ability to specify when an antenna is unavailable.
2007	Resurrection of covariance optimization. Found and fixed various bugs in algorithms. Still not used routinely. By-product: <i>sked</i> can predict formal errors internally.
2008	Master command: Read session setup from master file. Check session against master file.
2009	Station limit raised from 32 to 64, and made parameter.
2010	Update documentation. Begin process of removing obsolete code for handling tapes.
2011	Make VEX native format.

was ultimately abandoned. Subsequently Vandenberg developed an alternative rule-based system based on a set of criteria about what constitutes good and bad schedules. For example, generally speaking, you do not want to observe the same source twice in a row. This leads to a rule saying ‘do not observe a source if it has been observed in the last X minutes,’ where X is user settable.

Quite often, different criteria of goodness are in conflict. On the one hand you want schedules that have good sky distribution—that is, that sample as much of the sky as possible in a short period of time. This can lead to schedules where the antennas spend a lot of time slewing from one source to another. On the other hand, you want to maximize the number of observations, which means you want to reduce slewing time.

In the next section we give an overview of the general algorithm currently used in automatic scheduling. This is followed by a review of a few useful *sked* commands. Lastly we give a cookbook example of scheduling a typical R1 session.

2. Overview of Automatic Scheduling

In automatic mode the scheduler instructs *sked* to generate a schedule until some end time, and new scans are added to the schedule, scan-by-scan, until the finish of the last scan is past the end time. This process is illustrated schematically in Figure 1 and described in more detail below.



Figure 1. Schematic illustration of automatic scheduling.

1. *Sked* calculates the source visibility table (a table which indicates which stations can see each source). This is used to generate the universe of possible scans.
2. The *major options*, together with SNR targets, determine which of the scans are actually generated and kept for further consideration.
3. *Sked* does an initial ranking by either covariance or sky coverage. The best $X\%$ are kept.
4. The *minor options* are used to assign a score to each scan based on several criteria.
5. The scan with the highest score is scheduled.
6. This process is repeated until there is no more time.

2.1. Major Options

Major options determine which scans are generated and kept for later consideration. Many of the *major options* (top of Table 2) describe properties a scan must (or must not) have to be kept

for further consideration. In this sense they are hurdles, because a scan is rejected if it fails to pass any of them. The remaining *major options* (bottom of Table 2) determine scan generation in other ways. For example, the third stage in automatic mode is to perform an initial ranking of the scans and keep the top $X\%$. How this ranking is done, and the percentage kept, is controlled by *SkyCov* and *Best*.

Table 2. Major Options.

Hurdles	
Option	Brief Description.
AllBlGood	Yes: All baselines must meet SNR targets. No: At least 1/2 of the baselines for each station must meet SNR targets.
MinAngle	Minimum angular distance (degrees) between scans.
MinBetween	Minimum time (minutes) between observations of the same source.
MinSunDist	Minimum angular distance of a source from the sun.
MaxSlewTime	Maximum allowable slew time of an antenna to source
MinSubNetSize	Smallest Subnet to schedule.
Other Major Options	
SkyCov	Yes: Do initial ranking by sky coverage. No: Do initial ranking by covariance.
Best	% of scans kept for further consideration.
NumSubNet	Number of subnets to schedule simultaneously.
FillIn	Yes: Try to schedule additional observations using ‘idle’ antennas. No: Wait until all antennas become idle before scheduling.
FillMinTime	Minimum time (seconds) an antenna must be idle before it can be used.
FillMinSub	Minimum subnet size to schedule in FillIn mode.
FillBest	% of scans to keep for further consideration.

2.2. Minor Options

Minor options are a set of 13 criteria used to evaluate scans. Unlike the *major options*, where a scan must satisfy all of the criteria or it is rejected, a scan can be selected if it does well on some but not all of the criteria. Each of the *minor options* corresponds to a possible positive aspect of a scan. For example, all things being equal, a scan with more observations is better than one with fewer. The *minor option* that instructs *sked* to prefer scans with more observations is *NumObs*. The scheduler can select which options to use and how much weight to assign to them. A typical schedule will use 3–6 options. For each scan, *sked* calculates a score for each of the options in effect. The total score for the scan is the weighted sum of the sub-scores, and the scan with the highest total score is scheduled.

3. Some Useful *Sked* Commands

Sked currently has 76 commands, and in this brief note it is impossible to touch on more than a few. Many of the more recent commands originate from user feedback, and in this section I will

Table 3. Minor Options.

Option	Preferentially select scans with/that:
Astro	Astrometric sources that don't meet targets.
BegScan	Begin soon after previous scan ends.
EndScan	End soon after previous scan ends.
LowDec	With low dec sources.
NumLoEl	Low elevation sources.
NumRiseSet	Sources rising or setting.
NumObs	More observations.
SkyCov	Better sky coverage.
SrcEvn	More even distribution of observations/source.
SrcWt	Involving certain sources.
StatEven	More even distribution of observations/stations.
StatWt	Involving certain stations.
StatIdle	Sources that are idle.
TimeVar	Minimize variance of end times by station.

briefly describe three of these.

3.1. Master Command

Although it is possible to design a schedule ‘from scratch’—that is, starting from nothing—most schedules are based on previous schedules. Figure 2 is a schematic illustration of how this works, and the steps involved in this process are summarized below.

1. Start with a similar schedule file and copy it, e.g., `cp r1412.skd r1414.skd`.
2. Open the file using *sked*.
3. Delete all observations.
4. Change the session code inside the schedule file.
5. Change the start and stop times of the session. This is usually done using information from the master file.
6. Change the stations. This is usually done using information from the master file.
7. If necessary, select a new frequency sequence.
8. Set the SNR targets.
9. Select the sources.
10. Generate the schedule.
11. Review and modify schedule if necessary.

Many of these steps are prone to error, the most frequent being wrong start and stop times or wrong stations. These can prevent the schedule from being run at all. To make scheduling easier, I introduced the *master* command. This command has two modes:

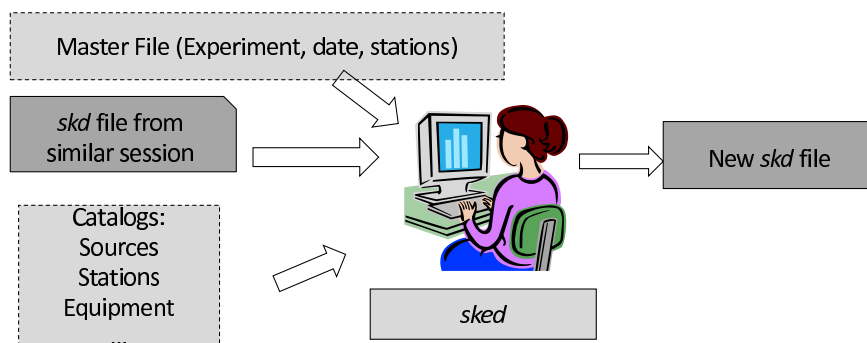


Figure 2. Writing a new schedule.

1. *Master check* compares the schedule against the master file, using the session code contained in the schedule, and issues a warning message if it finds any discrepancies in the station list or the start and stop times.
2. *Master get* initializes the schedule file using information from the master file. The session code in the schedule file serves as a key. *Sked* sets the start and stop times and the station list. It deletes all observations. If the SNRs of the original session were uniform by band, *sked* sets the SNRs. If not, it issues a warning message. The frequency sequence is left untouched.

At NASA Goddard we always use *master get* to initialize schedules. I encourage other centers to do so, not only because it makes it easier for the scheduler, but also because it reduces the possibility of error. Before being posted on the data center, all schedules are checked for consistency with the master schedule using *master check*.

3.2. Downtime Command

Frequently a station is unavailable for some part of the session. The most common reason is that it is participating in an Intensive session. Previously this situation was handled by the scheduler who would do the following:

1. Generate a schedule using all stations until some station(s) became unavailable.
2. Change the subnet to remove these station(s) from the network.
3. Continue generating until these station(s) again become available.
4. Change the subnet to include the stations that were unavailable.
5. Continue generating until the end of the schedule or another station becomes unavailable.

None of these steps is particularly difficult. However, they are all prone to error. To simplify the process of generating a schedule when some stations are unavailable for part of it, I introduced the *downtime* command. Using the *downtime* command the scheduler specifies an interval when a station or subnet is unavailable ('down'), and *sked* will automatically ignore these stations during this interval.

Sked employs the following algorithm in *downtime*. After *sked* generates a preliminary scan it checks to see if a station is down during the scan. If so, it rejects it from further consideration. A station is down (see Figure 3) when:

1. The end of the scan occurs while the station is down.
2. The beginning of the scan occurs while the station is down.
3. The station is down during the scan.

Originally only the first two tests were done. These were sufficient if the station was down for a long interval, for example, during an Intensive. In January of 2010 a scheduler tried to use a *downtime* of less than 3 minutes, and an unanticipated situation occurred. *Sked* generated a trial scan which started before *downtime* began, and ended after *downtime* ended, and hence it passed the first two tests. The user did not know why *downtime* failed—only that it failed. When the cause of failure was investigated and found, the *downtime* algorithm was modified to include criterion 3.

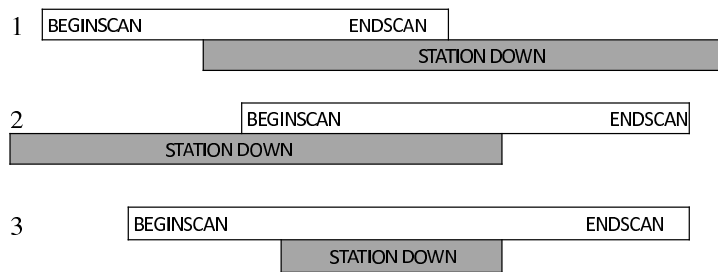


Figure 3. Scans which are invalid because of *downtime*.

3.3. Fill-in Mode

By default *sked* waits until all stations are free before scheduling a new scan. This can lead to periods of time in the schedule when many stations are idle, waiting for the rest of the stations to become free. I introduced Fill-In mode to reduce the amount of idle time.

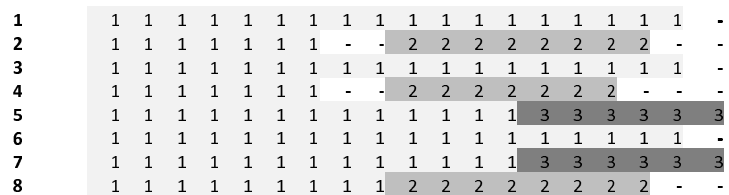


Figure 4. Using Fill-In Mode to reduce idle time.

Recall that which scans are considered for scheduling is governed by the major options. *Sked* will only attempt to schedule scans during idle time if *Fillin* is set to *Yes* and there are at least *FillMinSub* stations which are idle for at least *FillMinTime*. If successful, it repeats the process until either the amount of idle time or the number of idle stations drops below their threshold values. A typical result is displayed in Figure 4. The original scan involves all of the stations. Following this, *sked* schedules an additional scan using stations 2, 4, and 8, and then one more scan using stations 5 and 7.

4. Cookbook Example for Generating a Schedule

In this section we present a recipe for generating an R1 schedule (see Table 4). This same procedure, with obvious changes, can be adapted to generating other schedules. For most routine sessions the entire time required to generate a schedule is around ten minutes or less. Prior to the introduction of many of the labor-saving commands in *sked* it could easily take hours or days to generate a simple schedule.

Table 4. Scheduling an R1 Schedule.

#	Command line	Brief description
1	<i>linux_prompt</i> > cp r1412.skd r1413.skd	Copy an old schedule.
2	<i>linux_prompt</i> > sked r1413.skd	Open schedule in <i>sked</i> . <i>Sked</i> displays lots of information about the schedule.
3	? param exper r1413	Change internal session code. Required to use master command.
4	? master get	Initialize schedule based on master file.
5	? SNR _ X 20	Set X band SNR to 20. May not be required.
6	? SNR _ S 15	Set S band to 15. May not be required.
7	? Best 60	Get the best 60 sources for current network.
8	? Auto _ end	Generate the schedule until the end time.
9	? summ _ _ _ li	Do a summary listing of the schedule to review.
10	? Wr	Write the schedule to disk.
11	? Quit	Quit.

5. Conclusions

Sked continues to grow and mature with VLBI. Some of the changes in *sked* are driven by changes in equipment. Many changes are driven by user requests to make *sked* easier to use and less error prone. At Goddard we use *sked* to generate all of our VLBI schedules. I welcome all suggestions from users on improving *sked*. I give especially high priority to fixing bugs.

The Composition of the Master Schedule

Cynthia C. Thomas, Dirk Behrend, Daniel S. MacMillan

NVI, Inc./NASA Goddard Space Flight Center

Contact author: Cynthia C. Thomas, e-mail: Cynthia.C.Thomas@nasa.gov

Abstract

Over a period of about four months, the IVS Coordinating Center (IVSCC) each year composes the Master Schedule for the IVS observing program of the next calendar year. The process begins in early July when the IVSCC contacts the IVS Network Stations to request information about available station time as well as holiday and maintenance schedules for the upcoming year. Going through various planning stages and a review process with the IVS Observing Program Committee (OPC), the final version of the Master Schedule is posted by early November. We describe the general steps of the composition and illustrate them with the example of the planning for the Master Schedule of the 2010 observing year.

1. Introduction

One of the major tasks of the IVS Coordinating Center (IVSCC) is the creation and maintenance of the yearly observing plan—the Master Schedule. The Master Schedule is the central tool for coordinating and optimizing the usage of available resources such as station observing time, correlator time, and recording media. Given the importance of the observing plan, the Master Schedule is prepared for an entire calendar year well in advance of the start of the year. The IVSCC commences work for a new Master Schedule in early July of the preceding year by sending a request to the IVS Network Stations for their available station time as well as for their holiday and maintenance schedules. Furthermore, a request is sent to the IVS Correlators for their loading potential. After going through several planning phases and a review process with the IVS Observing Program Committee (OPC), the final version is made available on the IVS Web site by early November. However, the Master Schedule continues to require maintenance, because updates during the year need to be made for stations going “down”, for additional or canceled sessions, or for correlator changes.

2. Master Schedule Creation Process

The IVS observing program follows the overall structure as outlined in the general guidelines of the IVS Working Group 2 report. It consists of several series of 24-hour observing sessions and daily 1-hour Intensive sessions. The program is planned by the OPC, coordinated by the IVSCC, and executed by the Network Stations, Operations Centers, and Correlators. The result of the observing program is data held in the Data Centers, which is then available for analysis.

The general steps involved in creating the Master Schedule for a new observing year are illustrated in Figure 1. The IVSCC contacts each station about their availability for the upcoming observing year and each correlator about how much data they can process. The acquired information is used to formulate the Station Usage Chart and the Correlator Projection Report. The

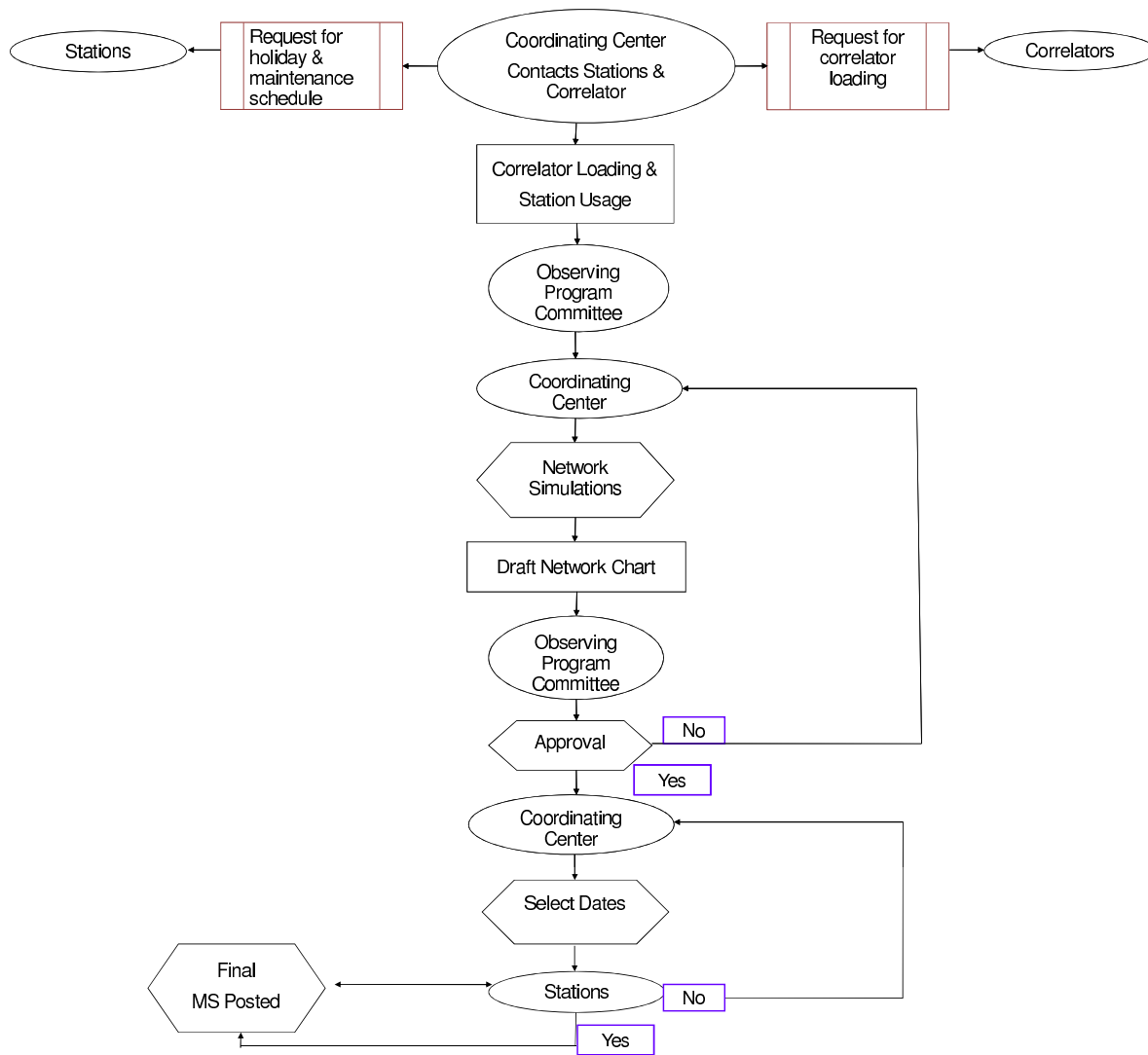


Figure 1. Flowchart showing the general steps of how the master schedule is created.

Station Usage Chart (Figure 2) displays each station’s availability for the upcoming year and the number of times each station will participate in various session types. The Correlator Projection Report (Figure 3) displays which sessions will be processed at each correlator, the number of sessions processed at each correlator, and the estimated processing factor for each session. After the report and the chart are produced, the information is presented to the OPC for review. At that time the IVSCC asks the members of the OPC for any additions or changes for the next observing year. Any suggested additions or changes are taken into consideration when formulating the next year’s observing schedule.

The IVSCC organizes the available station time into the various networks. Then simulations are done for the IVS-R1 and IVS-R4 networks to ensure that the EOP guidelines are met. The simulation results along with the various networks are incorporated into the Draft Networks Chart

3. Validation of Simulations

In order to ensure that the simulations for the IVS-R1 and IVS-R4 networks are representative of the actual results (or to properly scale the simulated EOP formal error estimates), for both the IVS-R1 and IVS-R4 series, a recent session is selected to compare simulated and actual EOP formal errors. In the example at hand the simulated EOP formal errors are too optimistic by about 10–20% for both sessions. For a more reliable statement with respect to the simulation results, we investigated the IVS-R1 and IVS-R4 sessions of the observing year 2009, for which we have simulated and actual results available. We selected only those IVS-R1 and IVS-R4 sessions that were observed, correlated, and analyzed with the fully scheduled network. We found that only eight IVS-R1 and fourteen IVS-R4 sessions fulfilled this requirement, because there were several stations that could not observe in their scheduled sessions and because some sessions had other problems which resulted in ‘incomplete’ data compared with the simulated data. Figure 5 displays the averaged values of the simulated vs. actual EOP formal errors from the selected 2009 sessions.

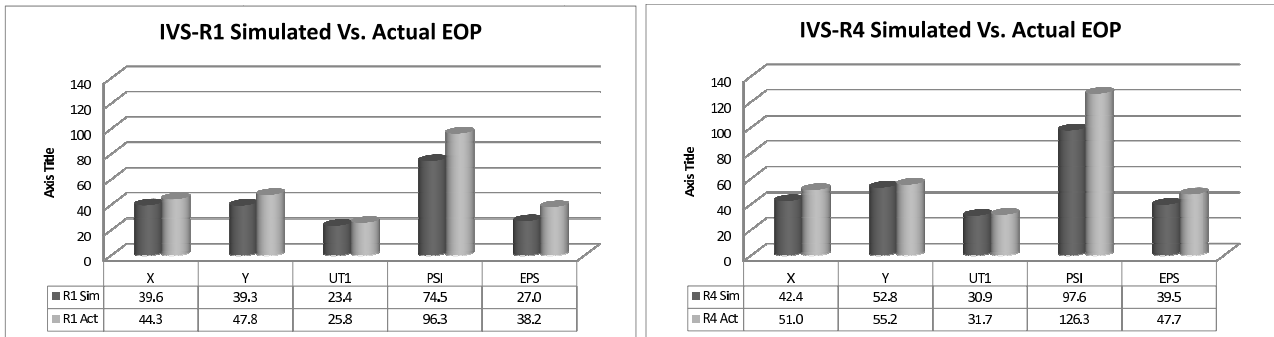


Figure 5. Averaged values of simulated and actual EOP formal errors from selected IVS-R1 (left) and IVS-R4 (right) sessions of the year 2009.

The results basically confirm the findings from the single session analysis: the simulation results are too optimistic by 10–20%. It can be seen that the simulated UT1 formal errors are very close to the actual values.

4. Conclusion

It takes about four months for the IVSCC to create the final version of the Master Schedule for a new observing year. The schedule composition accounts for the available resources of station time, correlator time, and media. The IVSCC gathers information from the stations and the correlators to create the schedule. The OPC and IVSCC work together to optimize network choices by generating test schedules and performing simulations. After the “final version” of the Master Schedule is posted, modifications continue to be made on an as-needed basis (sometimes even before the observing year starts) because of changes in the availability of resources; e.g., because a station has to change its availability for the year due to funding and/or personnel issues, because equipment failure requires a station to be “down” for a specific period, or because unscheduled maintenance becomes necessary at a station. Information about the IVS observing program can be found at <http://ivscc.gsfc.nasa.gov/program/>.

Coordinating, Scheduling, Processing and Analyzing IYA09

*John Gipson*¹, *Dirk Behrend*¹, *David Gordon*¹, *Ed Himwich*¹, *Dan MacMillan*¹,
*Mike Titus*², *Brian Corey*²

¹⁾ *NVI, Inc./NASA Goddard Space Flight Center*

²⁾ *MIT Haystack Observatory*

Contact author: *John Gipson*, e-mail: john.gipson@nasa.gov

Abstract

The IVS scheduled a special astrometric VLBI session for the International Year of Astronomy 2009 (IYA09) commemorating 400 years of optical astronomy and 40 years of VLBI. The IYA09 session is the most ambitious geodetic session to date in terms of network size, number of sources, and number of observations. We describe the process of designing, coordinating, scheduling, pre-session station checkout, correlating, and analyzing this session.

1. Introduction

To commemorate 400 years of optical telescopic observing, the International Astronomical Union (IAU) and UNESCO initiated the International Year of Astronomy 2009. Since the year 2009 also marked the 40th anniversary of geodetic VLBI, the 30th anniversary of regular S/X observing, and the 10th anniversary of the IVS, the IVS decided to schedule for 18 November 2009—as an activity for IYA09—the most ambitious astrometric VLBI session to date: a global network able to observe most of the celestial sphere with the largest number of stations possible.

A Task Force was formed that determined the key goals for the IYA09 session (see Table 1). The IVS Observing Program Committee (OPC) then initiated the realization of this very large astrometry session in collaboration with various groups and individuals. The Coordinating Center (CC) assumed the task of coordinating the session, the Goddard VLBI Group of preparing the schedule, the Goddard and Haystack groups of performing station checkout and troubleshooting, the Haystack Observatory of correlating the session, and the Goddard group of performing the preliminary analysis.

Table 1. Key goals of the IYA09 session of the IVS.

Scientific Goals	Strengthen ICRF2 by observing as many sources (243 out of 295) as possible in a single session. Measure arc-lengths between observed sources.
Outreach Goals	Press releases through IYA2009 (IAU), IVS, and other organizations. News coverage in regional and national media. Open doors at stations.
Ancillary Goals	Celebrate 40 years of geodetic and astrometric VLBI. Demonstrate capability of handling large networks. Tie stations into global frame.

2. Designing the Session

The Coordinating Center sent out a call for participation to which twenty-five stations responded positively. Following feasibility discussions with the VLBA, the CC submitted a ‘Target of Opportunity’ proposal to the VLBA which was accepted; the total number of stations thus increased to thirty-five (cf. Figure 1 and Table 2).

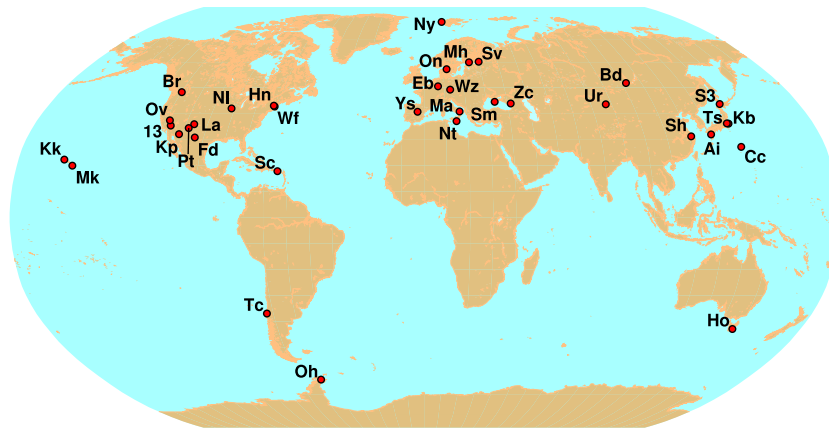


Figure 1. Geographical distribution of the 35 stations that agreed to participate in IYA09.

Apart from securing station and correlator resources, the availability of recording media also needed to be evaluated. First, the session involved many more stations than a typical IVS session. Secondly, because the correlator would have to make many passes (~ 20), the recording media would be tied up for many months while being processed. After numerous discussions media resources were identified for this session; however, a constraint was put on the maximum amount of data recordable at the stations.

Table 2. List of stations that agreed to participate in IYA09. (K5 translated to Mark 5B at Haystack.)

IVS	Mark 5A	HOBART26, KOKEE, MATERA, NOTO, NYALES20, ONSALA60, OHIGGINS, SESHAN25, SVETLOE, TIGOCONC, URUMQI, WETTZEHL, ZELENCHK
	Mark 5B	BADARY, CRIMEA, WESTFORD, YEBES40M
	K5 to Mark 5B	KASHIM34, TSUKUB32
GARNET	K5 to Mark 5B	AIRA, CHICHI10, SINTOTU3
DSN	Mark 5A	DSS13
EVN	Mark 5A	EFLSBERG, METSAHOV
VLBA	Mark 5A	BR-VLBA, FD-VLBA, HN-VLBA, KP-VLBA, LA-VLBA, NL-VLBA, PIETOWN, MK-VLBA, OV-VLBA, SC-VLBA

After looking at several possibilities, we settled on the standard 8-channel RDV mode. This has four X-band and four S-band channels; each channel is 8 MHz wide and uses two-bit sampling. The total data rate is 256 Mbps. The primary argument in favor was the participation of the VLBA, and because many stations had experience with this mode. We also considered a mixed

mode, where the VLBA would observe eight channels, and other stations fourteen. This would have had greater sensitivity for the non-VLBA stations, but it was ruled out because of insufficient media.

Eight stations could not observe in standard RDV mode but instead used a modification of it. In particular, AIRA, CHICHI10, CRIMEA, and SINTOTU3 had 4-MHz-wide channels; at AIRA, CHICHI10, CRIMEA, METSAHOV, NOTO, SINTOTU3, and URUMQI only two of the four X-band channels lay within the receiver passband; and DSS13 had only two S-band and two X-band channels. Furthermore, although CRIMEA could observe in full RDV mode, it had no AGC, and the power levels were increased for better 2-bit recording.

3. Scheduling

With 35 stations, IYA09 was by far the largest network ever scheduled, breaking the previous record of 23 stations. In order to schedule it, the maximum number of stations in *sked* was increased from 32 to 64. In the process of scheduling IYA09, we found and fixed many bugs related to the large number of stations.

The source list was the 295 defining sources in ICRF2. A design goal was to observe as many of these sources as possible. To reliably schedule these sources we needed good flux models. For most of the sources we used flux models generated from IVS data. For some of the sources we put in flux models obtained externally. For two of the sources we assumed fluxes of 0.25 mJy in both bands over all baselines.

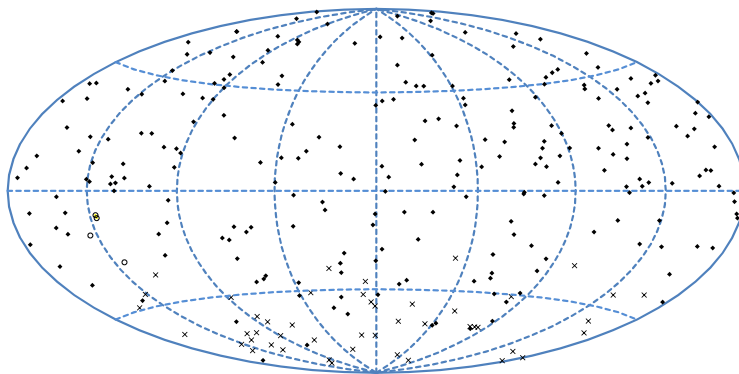


Figure 2. The 295 ICRF2 defining sources. Circles indicate sources too close to the sun to be observed. X's indicate southern sources that were not observed.

Goddard generated a reference schedule with ‘plain vanilla’ *sked* settings. This schedule had about 45,000 observations. Unfortunately, about 80 sources were observed sparsely or not at all. Four sources were too close to the sun to be observed. Most of the remaining sources were in the far south. We used the astrometric mode of *sked* to try to increase the number of observations of these southern sources. In astrometric mode the scheduler assigns observing targets for some set of sources, and *sked* will preferentially select scans involving these sources until they meet their targets. In spite of these efforts, many of the sources in the far south were not observed. Further investigation showed that it was impossible to meet the SNR targets on these sources because of the small size of two of the three southern stations.

4. Pre-session Station Checkout

Goddard and Haystack spent considerable time prior to the session to ensure that all stations would perform well. Special attention was paid to the Japanese GARNET stations. These stations had a maximum sampling of 8 Mbps (in contrast to the 16 Mbps of the other stations), so “data doubling” had to be used to make it possible to correlate the data. This reduced the sensitivity of these stations beyond that, due to the narrow bandwidth (4 MHz) they used. A fringe test was done prior to IYA09 to make sure that this would work. It was planned that all of the Japanese stations would be e-transferred to Haystack and translated from K5 to Mark 5B format. T. Kondo of NICT wrote the translation software. This was a new data-path, and it was exercised and debugged prior to IYA09. Goddard generated snap files for eight of the stations, because their field software was too old to support the number of stations in the schedule.

5. Correlation

The number of playback units determines the number of passes required to correlate the data. As a simple example, consider a 9-station session with four playback units. This session will have 36 baselines. With four playback units you can correlate six baselines at one pass. Naïvely you could do the correlation in six passes (i.e., 36 baselines with 6 baselines per pass). However, it is impossible to have all the passes independent. Inevitably some baselines will be correlated in more than one pass, which increases the number of required passes to eight (see Table 3).

Table 3. Correlating nine stations with four playback units.

Pass	1	2	3	4	5	6	7	8	9	New Bl	Old Bl	# NewBl
1	X	X	X	X						12, 13, 14, 23, 24, 34	–	6
2				X	X	X	X			45, 46, 47, 56, 57, 58	–	6
3	X						X	X	X	17, 18, 19, 78, 79, 89	–	6
4		X			X	X			X	25, 26, 29, 59, 69	56	5
5			X	X				X	X	38, 39, 48, 49	34, 89	4
6	X		X		X	X				15, 16, 35, 46	13, 56	4
7		X	X				X	X		27, 28, 37	23, 38, 89	3
8					X	X		X		58, 68	56	2

Two stations were not correlated. SVETLOE did not participate in IYA09 because of hardware problems. Haystack discovered problems with one of the X-band channels of DSS13. Since the data would be unusable for analysis, DSS13 was dropped.

Haystack had seven Mark 5A playback units and four Mark 5B units. Originally Haystack hoped to increase the number of playback units temporarily. Unfortunately they discovered that one of the programs limited the number of playback units to eleven.

The Japanese data was recorded on K5 disks and then e-transferred to Haystack. It would have been possible to translate the K5 data into either Mark 5A or Mark 5B format. It was translated to Mark 5B format to minimize the number of Mark 5A units.

The final correlation involved 33 stations: 24 Mark 5A stations and 9 Mark 5B stations. The total number of stations suitable for correlation in IYA09 was 33, with a total of 528 baselines. The

minimum number of passes required to correlate this is 17, which is constrained by the number of recording units of each type and the number of playback units. The actual number of passes made was 22. This was higher than required because the first seven passes were constructed to gain as much station and baseline coverage as possible, and not to minimize the total number of passes. Prior to the IVS 2010 General Meeting, Haystack sent Goddard a preliminary version of the database containing 29 stations, 240 sources, and 14,500 observations.

During correlation Haystack identified many limits in the processing software which had to be increased to handle IYA09. For example, the *tgen* and *a2t* programs were limited to handling 16 stations. The *HOPS* processing system had a file limit of 100,000 files which was increased to 300,000. *Corrman* and *aedit* were also modified.

Some correlator hardware related quirks had to be worked around as well. Two correlator station units exhibited byte-slip-type behavior in some data paths, requiring swapping headstack inputs to avoid the problems. One hardware path through the correlator board had to be avoided. This path had never been exercised prior to 11-station IYA09 scans.

6. Preliminary Analysis

Goddard analyzed the preliminary IYA09 database before the IVS General Meeting. The preliminary solution used 26 stations, 168 baselines, and 12,826 observations. The *Solve* postfit residual was 20.8 psec.

Table 4. Comparison of IAY09 with other IVS sessions.

Kind	#/yr	Typical	Date	# Stats	# Srcs	# Scans	# Obs
Int	200	I09240	2009-08-24	2	11	26	26
R1	52	R1397	2009-09-29	8	60	687	4,376
Euro	6	Euro97	2009-05-25	9	53	288	6,473
RDV	6	RDV77	2009-10-07	15	94	791	22,044
As scheduled		IYA09	2009-11-18	35	243	721	37,236
In database		IYA09	2009-11-18	32	239	658	28,920

The final database was made after the IVS meeting. Of the 33 stations, TIGOCONC had only 66 observations on seven baselines, and most were of very low SNR. Therefore, TIGOCONC was removed from the final database, leaving only 32 stations, which was the nominal limit of *Solve*. However, during analysis, it was found that many *Solve* routines actually had lower limits. These cases were corrected, and the *Solve* analysis was completed. The final database used 26,696 observations of 237 sources on 455 baselines. The *Solve* postfit residual was 22.5 psec.

7. Conclusions

The IYA09 session is the most ambitious VLBI session scheduled to date. It has posed, and continues to pose, challenges to all aspects of data analysis and dataflow. It is a useful precursor to VLBI2010 data.

The State and Development Direction of the Geodetic VLBI Station in Korea

Hyunhee Ju¹, Myungho Kim¹, Suchul Kim¹, Jinsik Park¹, Tetsuro Kondo²,
Tuhwan Kim³, Hongjong Oh³, Sangoh Yi³

¹⁾ *National Geographic Information Institute*

²⁾ *Ajou University and National Institute of Information and Communications Technology*

³⁾ *Ajou University*

Contact author: *Hyunhee Ju*, e-mail: `hee919@korea.kr`

Abstract

A permanent geodetic VLBI station with a 22-m diameter antenna will be newly constructed in Korea by the National Geographic Information Institute (NGII) under the project Korea VLBI system for Geodesy (KVG) that aims at maintaining the Korean geodetic datum accurately on the International Terrestrial Reference Frame (ITRF).

KVG can receive 2, 8, 22, and 43 GHz bands simultaneously in order to conduct geodetic and astronomical VLBI observations with Korea astronomical VLBI stations along with geodetic observations with IVS stations. This simultaneous four-band receiving capability is a unique feature of the KVG system. The KVG has started officially in October 2008. A new geodetic VLBI station will be constructed at Sejong city (about 120 km south of Seoul and about 20 km north-northwest of Daejeon) and construction of all systems will be completed in 2011.

1. Introduction

This paper describes the state of the geodetic VLBI station project in Korea which is carried out by the National Geographic Information Institute (NGII). We focus on the overall status rather than give technical explanations. Firstly, we give information about NGII such as vision and main mission. Secondly, the state of the Korea VLBI system for Geodesy (KVG) is explained. Finally, we talk about the development direction and future plans.

2. Korean Geodetic Datum

2.1. About NGII

This section gives an introduction to NGII. NGII is tasked with establishing surveying standards and implementing surveying policies in Korea. More specifically, NGII's tasks are to:

- maintain the national control points,
- produce a national base map,
- construct a national geo-spatial database,
- publish the geographic book and land survey results,
- operate geographical names committee,
- develop surveying and GIS technology, and

- strengthen the relationship with overseas organizations.

NGII consists of six divisions under the President. These divisions are Planning & Policy, General Service, Geodesy, Geospatial Imagery Information & Photogrammetry, Geographic Information, and National Land Information Survey division, employing a total of 103 civil servants. The directors in each division work with high technology equipment for geodesy, photogrammetry, cartography, and print and computerized management systems. Figure 1 shows an organizational chart of NGII.

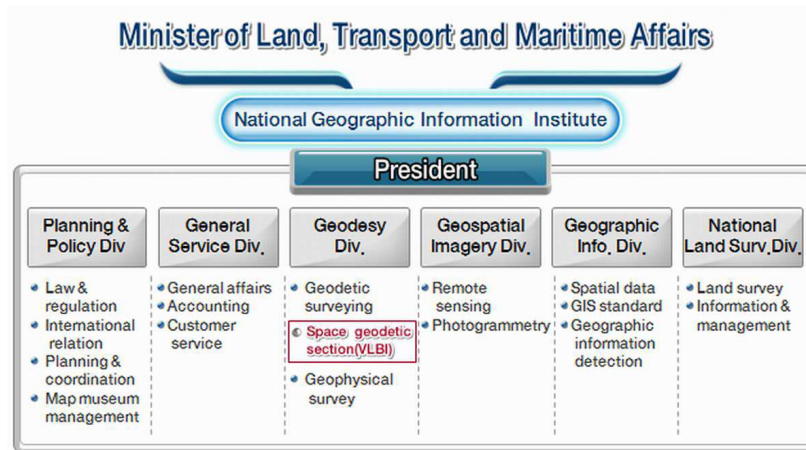


Figure 1. Organization of NGII

2.2. History of the Korean Geodetic Datum

A locally defined datum was used as Korean Geodetic Datum until 2002. It was realized through Bessel coordinates by carrying out astronomical surveys from 1981 to 1985. As the geodetic reference system of Korea was changed to geocentric in 2003, the Korean geodetic datum was redetermined accurately based on GPS and VLBI measurements. To maintain a Korean geodetic reference network, NGII has maintained 68 GPS stations continuously observing since 2000, 16,400 triangulation points, and 7,000 BMs, and it provided and published accurate coordinates and heights.

3. The State of the Korea VLBI System for Geodesy

3.1. Overview of the KVG Project

The first Korean VLBI experiment was done between NGII (National Geographic Information Institute, Korea) and GSI (Geographical Survey Institute, Japan) in 1995 using a 3.8-m mobile antenna at the Korean end. Step by step, the KVG project was proceeding. After that, the Korea VLBI system for Geodesy (KVG) started officially in October 2008. Construction of all systems will be completed in 2011.

Ajou University, High Gain Antenna Co., Ltd, and GigaLane Co., Ltd, are involved in a domestic collaboration in the project. NICT (National Institute of Information and Communications

Technology) and GSI participate as international partners. Figure 2 shows an overview of the KVG project.

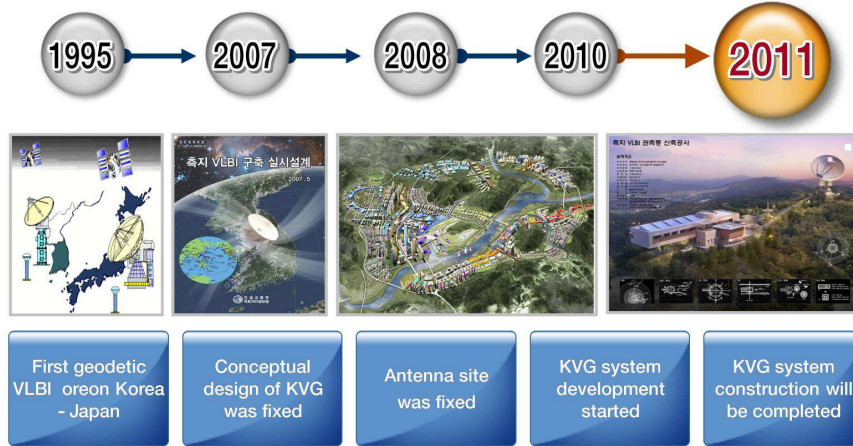


Figure 2. Overview of the KVG project.

3.2. Antenna Site

A new geodetic VLBI station for the KVG project will be constructed at Sejong city, which is located about 120 km south of Seoul and about 20 km north-northwest of Daejeon. Three VLBI antennas at Seoul, Ulsan, and Jeju are for a radio astronomical project, which is called KVN. Sejong is located within the triangle formed by the KVN stations. Figure 3 shows the location of the KVG antenna and the KVN antenna sites.

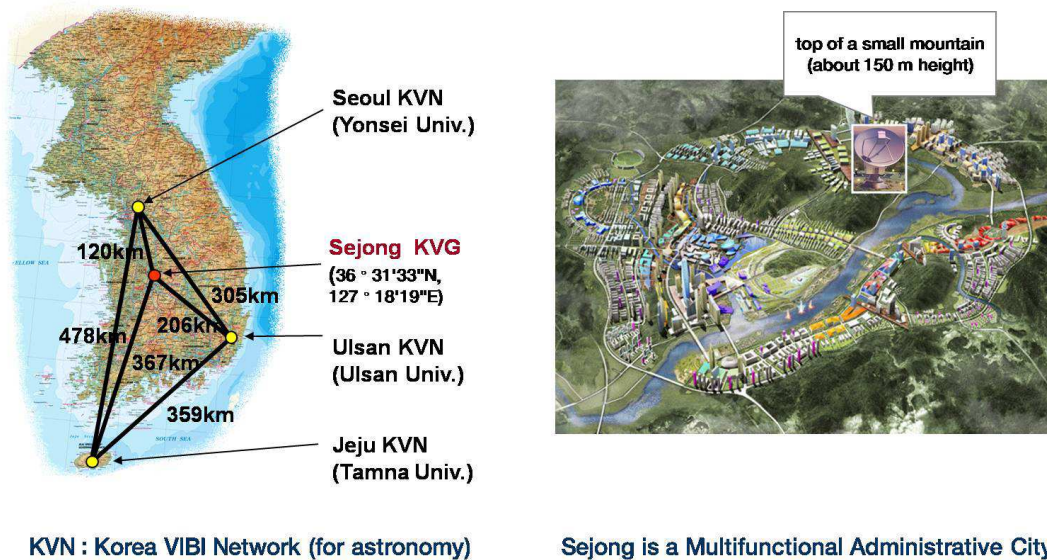


Figure 3. Location of the KVG system.

Figure 4 shows a bird's eye view of the KVG antenna site.



Figure 4. Bird's eye view of the KVG site.

3.3. System Outline

Construction of the antenna is carried out by High Gain Antenna Co., Ltd. This company also built part of the antennas of the KVN project in a domestic collaboration. The type of the antenna is Cassegrain. The KVG antenna will look similar to the KVN antennas after completion.

The receiver is designed to be able to receive 2, 8, 22, and 43 GHz bands simultaneously. This choice was made in order to be able to carry out geodetic VLBI observations with the current geodetic VLBI stations equipped with 2/8 GHz receivers and also with the KVN stations that will be equipped with 22/43 GHz receivers in the future. This is an outstanding feature of the KVG system, distinguishing it from other geodetic VLBI stations. Figure 5 summarizes the specifications of the KVG system. The unique features of the KVG system and its optics are shown in Figure 6.

The development of the backend system progressed in close cooperation with NICT. The backend system consists of two parts. The down converter, phase-calibration-signal generation system, and E/O transmission system will be installed in the antenna cabin. The IF selector, PC-based formatter and recorder, frequency standard, and software correlator will be installed in the observation building. The color of the equipment indicates a progress schedule.

The 22 and 43 GHz receiver systems, as well as the K5/VSSP32 and S/X down converter, are shown in Figure 7. Figure 8 shows a block diagram of the backend system.

4. Conclusions

The Korea VLBI system for Geodesy (KVG) has officially started in October 2008. Construction of all systems will be completed in 2011. We believe that the KVG system will play an important role for the Korea Geodetic Datum. Furthermore, we hope to become an IVS Network Station, and we look forward to exchanging information with IVS partners.

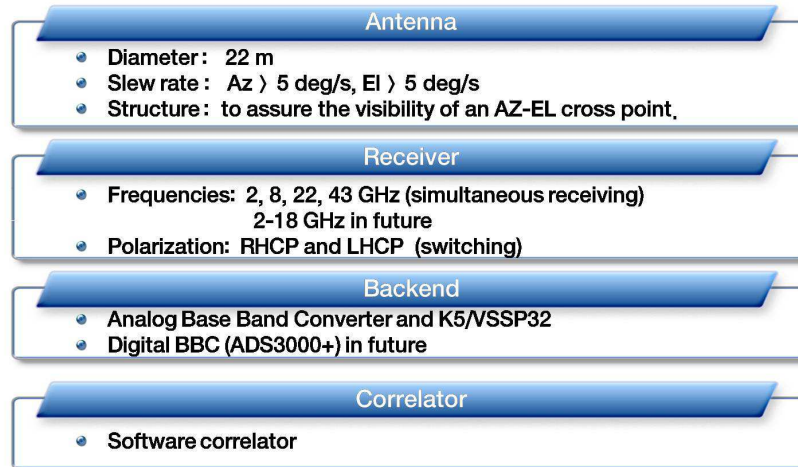


Figure 5. Specifications of the KVG system.

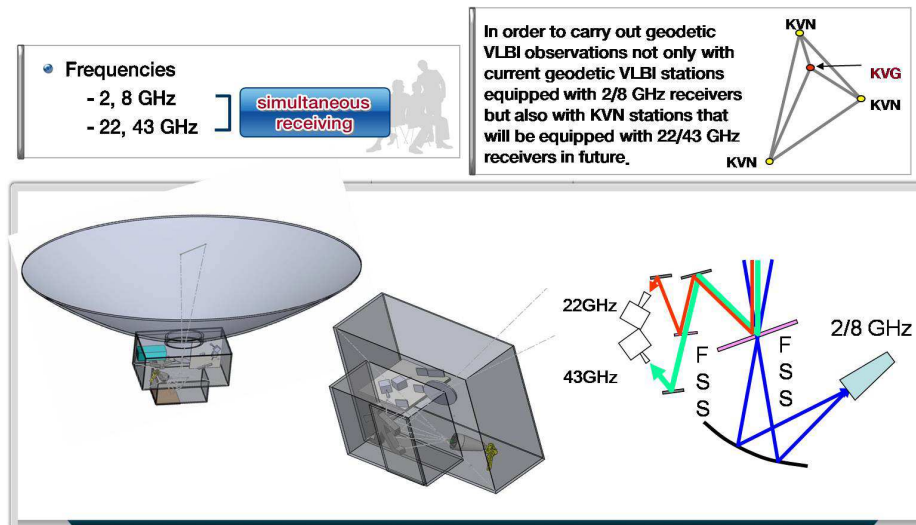


Figure 6. Unique features of the KVG system and KVG optics.



Figure 7. The 22 and 43 GHz receiver systems (left) and the K5/VSSP32 and S/X down converter (right).

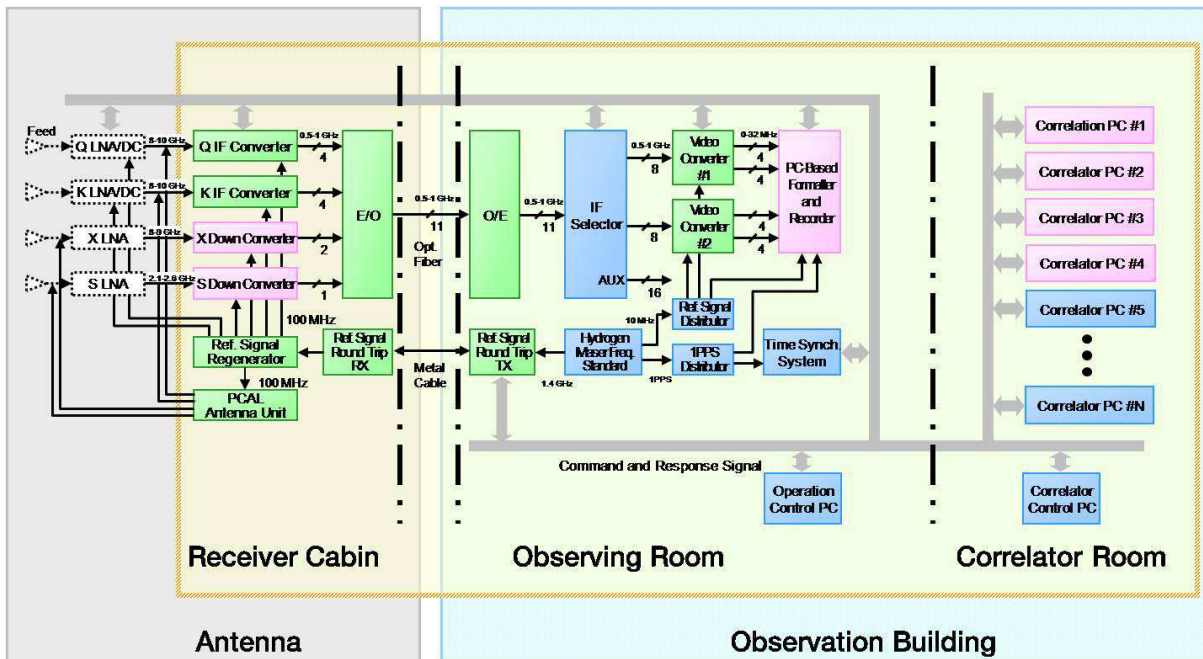


Figure 8. Block diagram of the backend system.

RAEGE: An Atlantic Network of Geodynamical Fundamental Stations

Jesús Gómez González¹, Francisco Colomer¹, José Antonio López Fernández¹,
Marlene C.S. Assis²

¹) *National Geographical Institute (IGN)*

²) *Secretaria Regional da Ciência, Tecnologia e Equipamentos (SRCTE) in Açores*

Contact author: Jesús Gómez González, e-mail: jggonzalez@fomento.es

Abstract

Project RAEGE (*Red Atlántica de Estaciones Geodinámicas y Espaciales*) intends to set up a Spanish-Portuguese network of four Geodetic Fundamental Stations in Yebes (1), Canary Islands (1), and Açores Islands (2), as part of the developments needed for the IVS VLBI2010 scenario. It is envisaged that each Geodetic Fundamental Station will be equipped with one radio telescope of VLBI2010 specifications (at least 12-m diameter, fast slewing speed, but also able to operate up to 40 GHz), one gravimeter, one permanent GNSS station, and, at least at the Yebes site, one SLR facility.

The National Geographical Institute of Spain (IGN) has experience in VLBI, having been a member of the European VLBI Network since 1993 and being one of the founding institutions of the Joint Institute for VLBI in Europe (JIVE), and it has been participating in geodetic VLBI campaigns with the 14-m radio telescope in Yebes since 1995. A new 40-m radio telescope has been built and was recently put into operation. It regularly participates in IVS sessions. There is infrastructure available for the new stations at Yebes and the Canary Islands. An agreement between IGN, the Portuguese Geographical Institute (IGP), and the Regional Government of the Açores ensures that the RAEGE project can become a reality by 2013.

1. Introduction

The International Association of Geodesy (IAG) is establishing a Global Geodetic Observing System (GGOS) [1] for a complete and continuous monitoring of the Earth. The International VLBI Service for Geodesy and Astrometry (IVS) provides products to IAG, in particular to the global reference frames through the station positions for plate tectonics (ITRF), coordinates of celestial objects (ICRF), and Earth pole position plus length of day (EOP).

In order to increase the precision of the products by an order of magnitude and to provide fast turnaround of initial geodetic results, upgrades to the current IVS infrastructures and data processing and analysis are needed. The project to coordinate these upgrades is known as VLBI2010 [2], born from the IVS Working Group #3 [3]. RAEGE is the Spanish-Portuguese contribution to the new VLBI2010 scenario.

2. The Stations

RAEGE [4] will consist of the construction and operation of four new Fundamental Geodetic Stations, where several geodetic techniques will be co-located. Two stations will be placed in Spain: one in Yebes (Guadalajara) and one on the Canary Islands. The other two stations will be placed in Portugal, on the Açores Islands: one on Santa María and one on Flores (see Fig. 1). The exact location of the last three stations is still to be decided.

At the Yebes station, the National Geographical Institute of Spain (IGN) already operates an observatory with two radio telescopes equipped with VLBI instrumentation (a 14-m antenna and a new 40-m antenna; as a member of the IVS and the European VLBI Network). It also operates the reference receiver of the GPS network in Spain (IGS YEBE). Recently a gravimeter pavilion was built, which may hold up to seven instruments operating simultaneously.

At Canary Islands, IGN operates a geodetic station on Tenerife island. However, conditions suggest consideration of better placements on Gran Canaria (at or close to Maspalomas, where the Spanish INTA operates a satellite tracking station) or on Lanzarote. Studies will be conducted in 2010 to decide the exact placement of this RAEGE station.

Through cooperation between IGN and the Regional Government of the Açores, two RAEGE stations will be placed there on different islands. The best choice is Santa María, on the African tectonic plate, and Flores, on the American plate. These stations could be operated remotely from a control center on the main Açores island of San Miguel. Measurements of local RFI and meteorological conditions will be performed in order to select the most convenient location for these RAEGE stations.

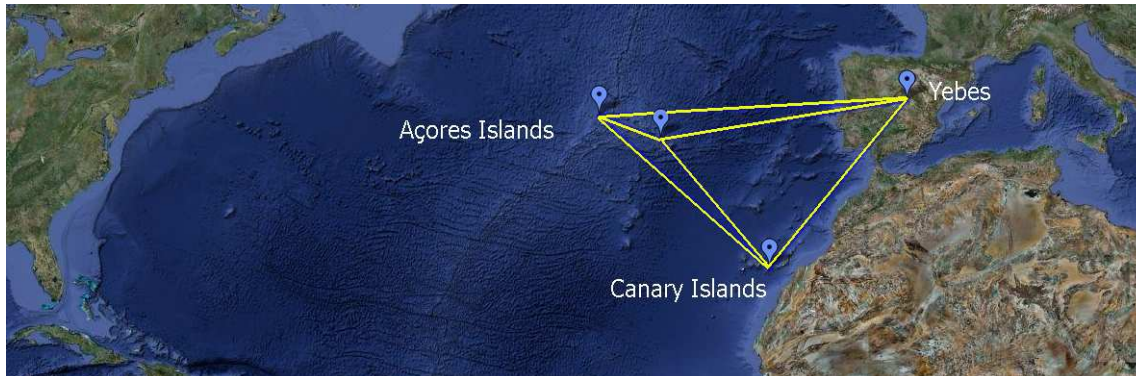


Figure 1. Location of the four RAEGE stations.

3. RAEGE Instrumentation

A goal of RAEGE is to build a new antenna of VLBI2010 specifications in Yebes, for which studies have been conducted following the expertise of similar systems such as the Twin Telescope Wettzell (TTW) project already under construction. The new antenna should have a > 12 -m diameter, be capable of operating up to 40 GHz, and have very fast slew rates ($12^\circ/\text{sec}$ in azimuth) for better determination of atmospheric effects.

The call for tenders for the construction of the antennas was set in May 2010. Two well known companies offered to build the instruments: Vertex (who is building the Twin Telescope Wettzell project) and MT Mechatronics GmbH (who built the Yebes 40-m radiotelescope).

These new radio telescopes will be initially equipped with current state-of-the-art receivers of the S and X frequency bands (2 and 8 GHz), which will be replaced by wideband receivers of the VLBI2010 bands (2 to 14 GHz) when available. Moreover, all equipment needed for VLBI observations (e.g., H-maser, meteorological station) will be provided.

All stations will be equipped with a permanent GNSS receiver (already in operation at Yebes).



Figure 2. Aerial view of the Yebes station, showing the existing and new RAEGE facilities.

All stations will be equipped with a gravimeter. Two such systems are already available at IGN (absolute gravimeters FG5 and A10); one new superconducting gravimeter has been purchased and will be installed at Yebes in May 2010.

Finally, at least at the Yebes station (see Fig. 2), a Satellite Laser Ranging (SLR) telescope will be installed at a new control building under design.

Table 1. RAEGE stations instrumentation.

Station	VLBI RT	GNSS	Gravimeter	SLR
Yebes	X	X	X	X
Canaries	X	X	X	
Sta María	X	X	X	
Flores	X	X	X	

4. Deployment of RAEGE

The call to bid on the RAEGE antennas is open, and the contract for the construction of the first three antennas will be signed in June 2010.

Meanwhile, Yebes and other potential sites on the Canary and Açores Islands are being monitored for the presence of radio frequency interferences (RFI) and meteorological conditions. Some preliminary results are shown in Figs. 3, 4, and 5.

Initial infrastructure work has started in Yebes. Soil trial pit excavations are being made to select the optimum location of the new RAEGE antenna at the observatory premises.

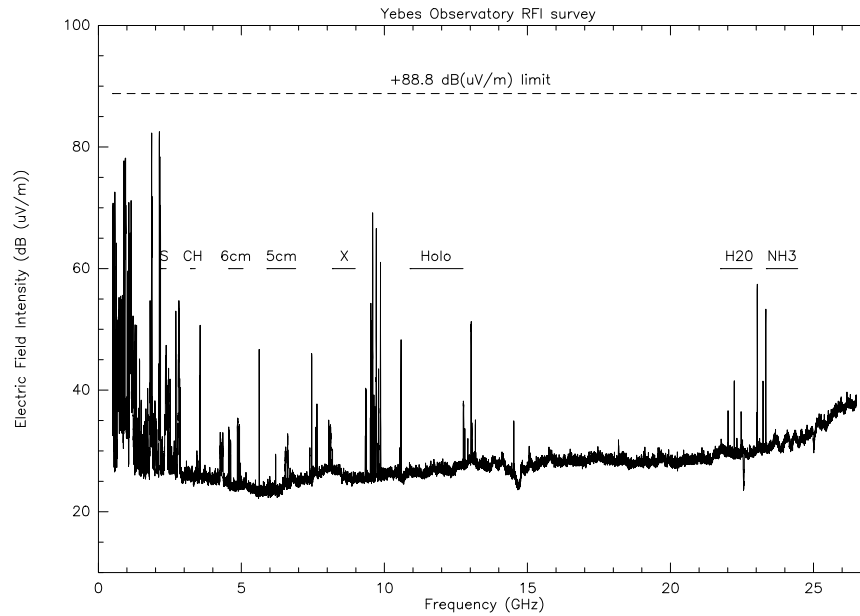


Figure 3. Current radio frequency interference (RFI) status at Yebes (Spain) in the 0 – 26 GHz band.

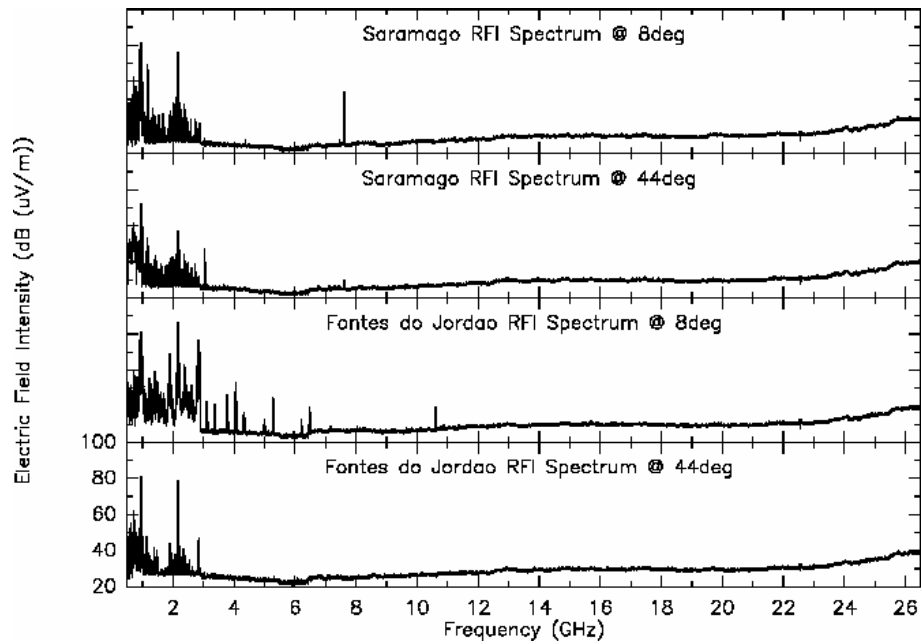


Figure 4. Radio frequency interference status at two sites on the Açores island of Santa María, much cleaner than that in Yebes.

References

- [1] The Global Geodetic Observing System (GGOS) of the International Association of Geodesy. <http://www.iag-ggos.org/>

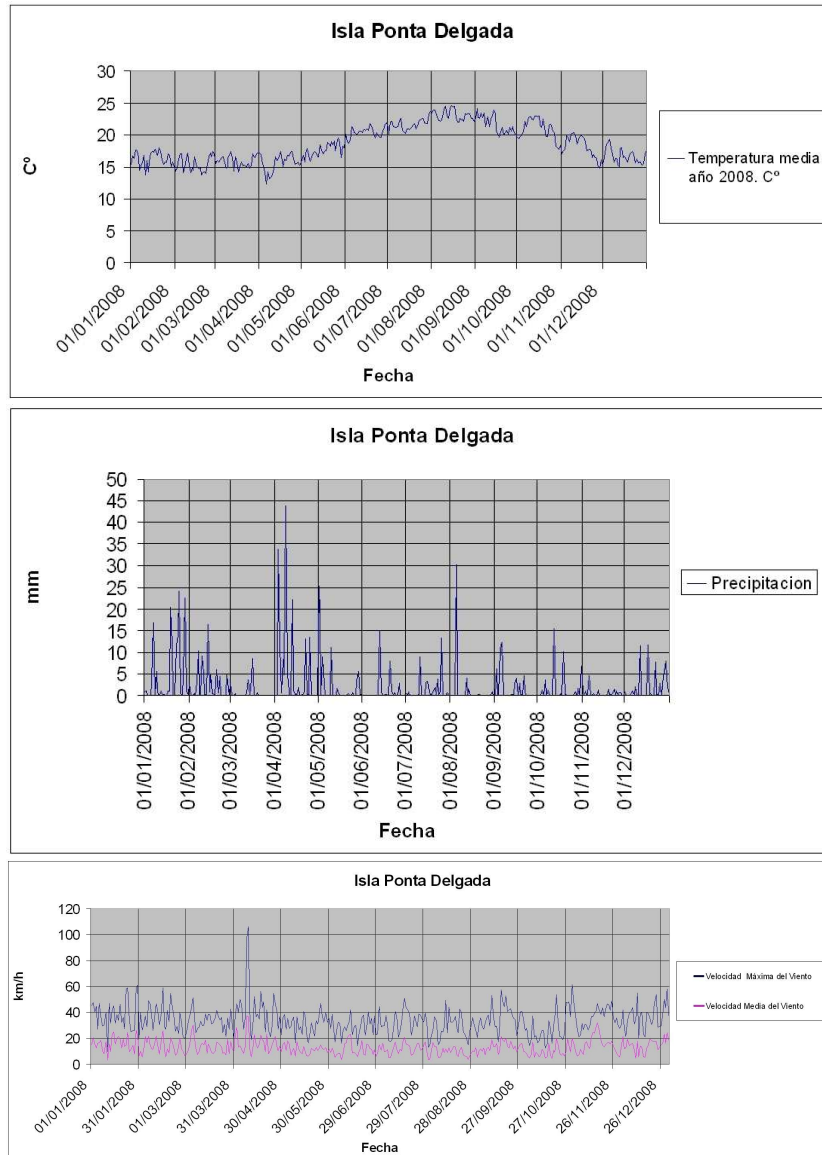


Figure 5. Meteorological conditions (temperature, precipitation and wind velocity) near one Açores RAEGE station.

- [2] Petrachenko, B., Niell, A., Behrend D., et al. Design Aspects of the VLBI2010 System. Progress Report of the IVS VLBI2010 Committee. Report NASA/TM-2009-214180. <ftp://ivscc.gsfc.nasa.gov/pub/misc/V2C/TM-2009-214180.pdf>
- [3] IVS Working Group #3 on VLBI2010. <http://ivscc.gsfc.nasa.gov/about/wg/wg3/index.html>
- [4] Red Atlántica de Estaciones Geodinámicas y Espaciales (RAEGE project) <http://www.raege.net>

The New Generation Russian VLBI Network

*Andrey Finkelstein, Alexander Ipatov, Sergey Smolentsev, Vyacheslav Mardyshkin,
Leonid Fedotov, Igor Surkis, Dmitriy Ivanov, Iskander Gayazov*

Institute of Applied Astronomy, Russian Academy of Sciences

Contact author: Alexander Ipatov, e-mail: ipatov@ipa.nw.ru

Abstract

This paper deals with a new project of the Russian VLBI Network dedicated for Universal Time determinations in quasi on-line mode. The basic principles of the network design and location of antennas are explained. Variants of constructing receiving devices, digital data acquisition system, and phase calibration system are specially considered. The frequency ranges and expected values of noise temperature are given.

1. Introduction

Since 2006 the radio astronomical observatories of the VLBI Network “Quasar” have actively participated in both international and national programs of observations. In 2008–2009 essential upgrade and development of the “Quasar” Network was performed including replacement of gear and pointing system electronics, modernization of frequency and time keeping system, replacement of data acquisition and data recording systems [1]. All observatories were linked by optical fiber lines, providing operational determinations of Universal Time from 1-hour sessions in e-VLBI mode. In 2010–2011 further modernization of the Network “Quasar” will include co-location of radio telescopes with “Sazhen-TM” SLR system and combined GPS/GLONASS/Galileo receivers at the observatories.

Further development of the GLONASS navigation system puts forward higher requirements to its fundamental segment particularly in maintenance of celestial and earth fixed coordinate systems and in monitoring the Earth orientation parameters in real time mode. Moreover, the Russian VLBI Network gives the unique possibility for quasi on-line determinations of Universal Time for supporting GLONASS. According to these requirements the design of a new generation Russian VLBI Network has been initiated.

2. Design Principles

The following principles are assumed as a basis of the new generation Russian VLBI Network:

- The network should have maximum longitudinal separation of sites for precise determination of Universal Time;
- Equipment of observatories should be compatible with the VLBI2010 system and that of the “Quasar” Network;
- Infrastructure of new observatories should be similar to the one of the “Quasar” Network.

The supposed geometry of the new VLBI Network is presented in Figure 1. The largest baseline of the new VLBI Network is more than 1.5 times larger than that of the “Quasar” Network. All the sites have good infrastructure, optical fiber communication lines, and comparatively good radio

climate with low level of radio interference. The specific features of a radio telescope of the new Network will be described below.



Figure 1. Proposed location of sites of the new generation Russian VLBI Network.

3. Front-end

Typical configuration of a VLBI site includes an antenna equipped with receivers for 2–14 GHz band. The reception of radio signals should be fulfilled not in the whole range 2–14 GHz, but in several sub-bands (Figure 2). Such a solution arises from the requirement to have two circular polarizations in S/X bands and to avoid an interference at different radio frequencies. A block-diagram of the new receiver is shown in Figure 3.

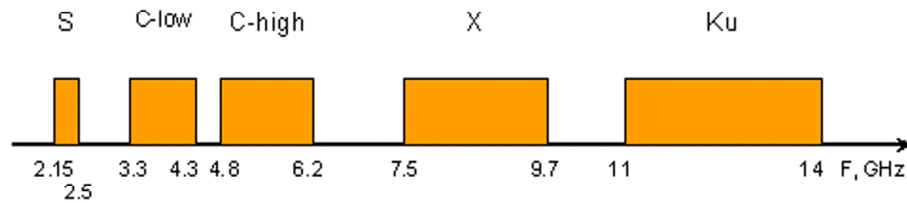


Figure 2. Working frequency bands for the new generation Russian VLBI Network.

The output signals from receivers should be processed by digital signal processing (DSP) units, recorded to disk modules and transmitted through optical fiber lines.

It is suggested to use relatively lightweight 12-meter antennas with fast slew rates. We are considering the options of either constructing such an antenna in Russia or purchasing an existing communication antenna.

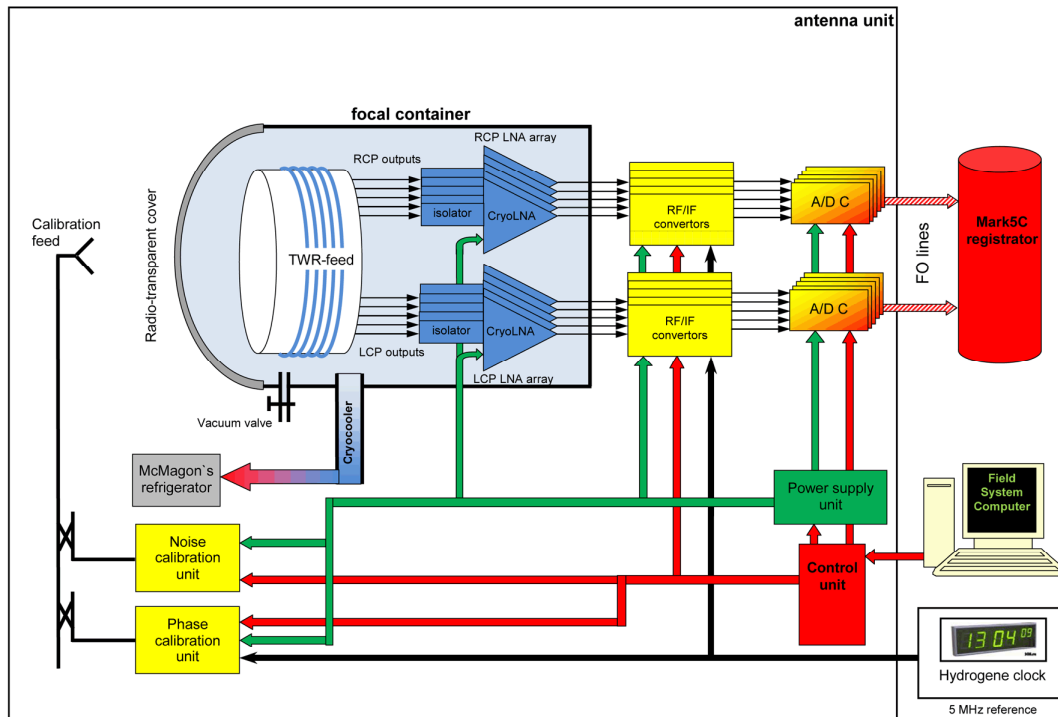


Figure 3. Block diagram of radio telescope for the new generation Russian VLBI Network.

An assembly of receiver and feed will be placed in the primary focus of the antenna. It is considered to use a circular travelling-wave-resonator (TWR) antenna as a feed. The TWR antenna should be cooled by a cryogenic system to 20 K level, and the heat shield to 80 K level. The low noise amplifiers should be cooled down to 20 K, and their gain should be about 30 dB. The total system noise temperature is expected to be 16–20 K (Table 1).

Table 1. The expected system noise temperature.

Band	System Noise Temperature
S	16 K
C-low	16 K
C-high	17 K
X	18 K
Ku	20 K

4. Digital DAS

The new generation digital data acquisition system (DAS) consists of a 10-channel RF/IF down converter and four identical DSP units (Figure 4). The RF/IF down converter transforms the input signal spectrum from a multi-band TWR antenna of the radio telescope (C, X, S, and

Ku bands) to IF range of 1–2 GHz. Eight out of the ten channels of the RF/IF down converter can be tuned in the wide frequency range of 3–14 GHz. There is no down conversion in the remaining two channels intended for S-band because it can be directly digitized by analog digital converter (ADC), but the signal is amplified and filtered. Each DSP unit can be connected to the outputs of RF/IF down converter through IF switch. Each channel of the DAS requires one Mark 5C. As the DAS is located on the antenna, the signal is transmitted to the control room by an optical fiber line in digital form.

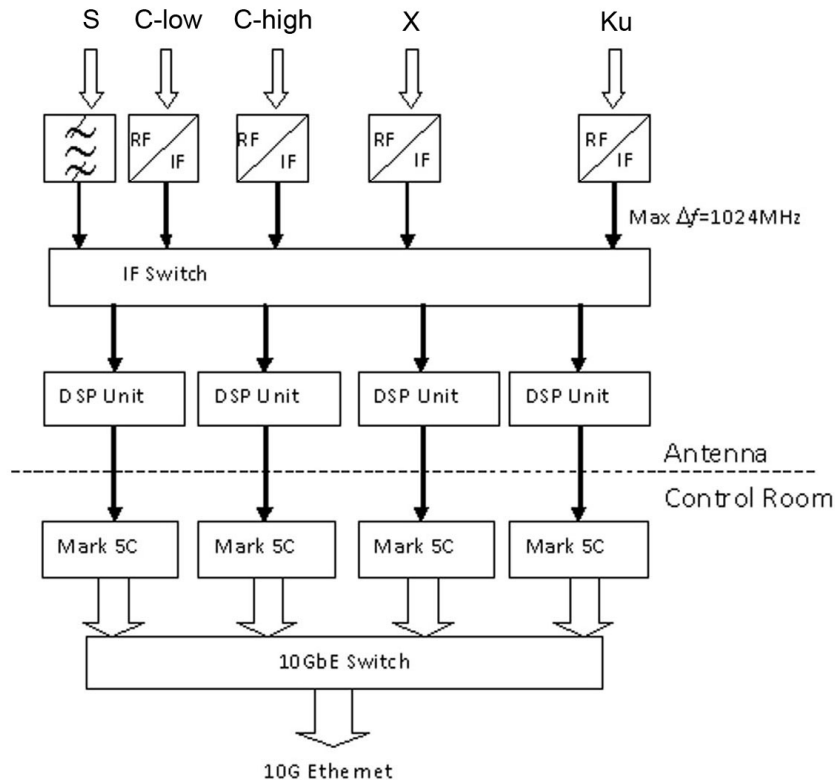


Figure 4. The Digital Data Acquisition System for the new generation Russian VLBI Network.

The DSP unit is the basis of the DAS and contains: ADC, field programmed gate array (FPGA), clock oscillator, demultiplexer of the ADC output signal, flash RAM to store FPGA firmware, microcontroller, and optical transmitters.

It will be implemented as a single multilayer printed circuit board (PCB).

The FPGA is the basis of the DSP unit. It performs the measurement of an RMS level of the input signal, 2-bit quantization of output signals, generation of a test vector to check a transmission line and data recording system, formatting the output data in accordance with a data recording system interface and sending them to the optical transmitters.

The prototype of the DSP unit was made to check the basic principles. It consists of evaluation boards of the 10-bits ADC (AT84AS008-EB) and FPGA XC5VFX70T (ML507).

The tests of the prototype provided an opportunity to implement the digital DAS with modern electronic components.

5. Phase Calibration

A phase calibration system is under development. The main purpose of the phase calibration system is to monitor the instrumental delay of receiver and data acquisition equipments. A special pulse generator is suggested to be used as the main component of the phase calibration system. A spectrally pure 5 MHz signal is transmitted by cable to the receiver, where it is converted to a 1 MHz signal which makes a charge-storage diode to generate pulses of very short (≈ 30 ps) duration (Figure 5).

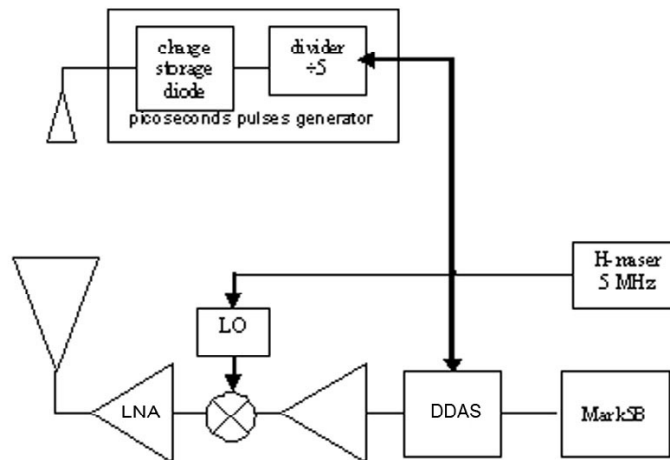


Figure 5. The phase calibration system for the new VLBI Network.

The possibility of locating the phase calibration injection point ahead of the horn is studied. Phase calibration impulses are radiated from a special broadband feed fixed on one of the legs supporting the focal box. To meet the requirement of a distant radiation zone the feed is to be placed at a point far away from a mirror. The key advantage of such a system is that the horn and all the following devices are included into the phase calibration loop.

The prototype of a transverse electromagnetic (TEM) horn with TEM double-ridged transition for 2–14 GHz frequency has already been made at IAA RAS and is being tested now. The prototype parameters measured prove the possibility of using this feed for phase calibration.

Coaxial cables connecting the H-maser and the pulse generator are selected taking into account the low temperature coefficient and mechanical stress sensitivities. For the LMR type cable the temperature coefficient is about 10 ppm/K. If 10 meters of this cable are exposed to significant temperature fluctuations, its stability should be under 0.3 ps/K. Typical cable length change with a 360° wrap on 4 inch radius is under 1 ps. So, in this case a cable measurement system is not required.

References

- [1] Finkelstein A., Ipatov A., Smolentsev S., The Network “Quasar”: 2008–2011, Proc. 5th IVS General Meeting, 39–46, 2008.

New Fundamental Station in Ny-Ålesund

Line Langkaas, Terje Dahlen, Per Erik Opseth

Norwegian Mapping Authority (NMA)

Contact author: Per Erik Opseth, e-mail: Per.Erik.Opseth@statkart.no

Abstract

The Norwegian Mapping Authority's (NMA) geodetic observatory has been operating in Ny-Ålesund since 1994. To adapt to the VLBI2010 standard and extend our activity to also integrate SLR, NMA is in the process of funding a new fundamental station. Handling more Intensive observations in real time requires a fiber optic cable to Ny-Ålesund. The Norwegian Mapping Authority is currently applying for project funding of 26 million euros.

1. About the Project

The site in Ny-Ålesund is currently equipped with an old and slow-moving VLBI antenna, a superconducting gravimeter, GNSS receivers, a tide gauge, and DORIS equipment. An upgrade of the site in Ny-Ålesund will add a twin telescope and an SLR system in addition to the existing techniques.

The existing observatory is located very close to the runway at Ny-Ålesund airport and is already a challenge due to aviation safety. Also a future development of the airport might affect our activity. Therefore, we have proposed to move the observatory about 1 km away, to the “Knudsen Ridge”. In Ny-Ålesund we have radio silence to a large degree, which is of great benefit for VLBI. This is one of the key reasons for staying in Ny-Ålesund rather than moving to Longyearbyen, which has far better infrastructure. The project plans include preparation for the installation of an automatic stability control system of the antennas.

2. Challenges

The development of a new feed has to be completed; we need to make sure this is finished in due time. Continuous operation (24 hours a day, 365 days a year) is a challenge for NMA when it comes to manning the station in Ny-Ålesund. For NMA, it is important to establish a system for remote control within the IVS network. NMA appreciates the support we have received from the IVS network, and we are depending on this cooperation to be able to go through with the project. Complete radio silence (only selected frequencies today) might be possible to achieve in Ny-Ålesund if this is of great importance for the VLBI community, but this will reduce options for other scientists in the area.

3. Project Plan

The Norwegian Mapping Authority is in the process of funding the project, and support from the “geodetic community” is necessary to raise the funds. An application was submitted to the Ministry of Environment in December 2009. Additional clarification will be carried out during the

first half of 2010 with respect to environmental impact assessment, air traffic, and ground stability. A decision on the funding to be appropriated for 2011 is expected in autumn 2010. In case of a positive feedback on funds for 2011 we will have a project kick off during winter 2010/11 with tender invitations and other activities. The project period is expected to be 2011-20.



Figure 1. Ny-Ålesund geodetic observatory.

Characterization and Calibration of the 12-m Antenna in Warkworth, New Zealand

Sergei Gulyaev, Tim Natusch, David Wilson

Auckland University of Technology

Contact author: Sergei Gulyaev, e-mail: sergei.gulyaev@aut.ac.nz

Abstract

The New Zealand 12-m antenna is scheduled to start participating in regular IVS VLBI sessions from the middle of 2010. Characterization procedures and results of calibration of the New Zealand 12-m radio telescope are presented, including the main reflector surface accuracy measurement, pointing model creation, and the system equivalent flux density (SEFD) determination in both S and X bands. Important issues of network connectivity, co-located geodetic systems, and the use of the antenna in education are also discussed.

1. Antenna Location

The New Zealand 12-m VLBI radio telescope is located some 60 km north of the city of Auckland, near the township of Warkworth. A preliminary survey has been conducted to find the precise coordinates of the invariant point of the antenna (the intersection of the azimuth and elevation axes). They are [1]:

$$\begin{aligned}\text{Latitude} &= 36^\circ 26' 05.3375'' \text{ S} \\ \text{Longitude} &= 174^\circ 39' 47.6988'' \text{ E}\end{aligned}$$

or using geocentric coordinates:

$$\begin{aligned}X &= -5115327.28 \text{ m} \\ Y &= 477844.04 \text{ m} \\ Z &= -3767196.04 \text{ m}.\end{aligned}$$

The coordinates are given in terms of ITRF2000 at the epoch of the survey (March 2010). The survey was conducted in close collaboration with the New Zealand Geological and Nuclear Science Research Institute (GNS Science) and the Land Information New Zealand (LINZ). Real-time kinematic GPS was used in order to survey several points on the rim of the main reflector for the series of positions in azimuth and elevation. Coordinates were calculated with respect to GPS station “WARK” — one of the “PositioNZ” network stations established in November 2008 at the radio telescope site. The accuracy of the axes intersection point, with respect to WARK is estimated to be within 0.1 m.

New Zealand’s traditional role in contributing to the global reference frame determination is through its GNSS “PositioNZ” network operated by LINZ in a partnership with GNS Science. The PositioNZ network [2] consists of thirty-three GNSS continuously operating reference stations (CORS) in mainland New Zealand, plus one station on Chatham Island (400 km east of

Christchurch) and three in Antarctica. Data from several of these sites are forwarded to the International GNSS Service (IGS) where they are incorporated into solutions used to determine GNSS satellite orbit and global reference frame determinations. The GNSS station at the radio telescope site (WARK) is one of them.

The accuracy of the radio telescope invariant point coordinates will be subsequently refined with the use of a variety of survey techniques. With this purpose, four geodetic monuments have been built in the vicinity of the antenna (15–20 m from its pedestal).

2. Technical Characteristics, Equipment and Network Connectivity

The 12-m antenna was manufactured by Patriot Antenna Systems Inc. in Albion, Michigan, USA. The antenna specifications are provided in [3].

The radio telescope is equipped with a coaxial dual band (S and X) dual polarization (circular left/right) feed horn, which was specifically developed by Patriot Antennas. An S/X receiver has been constructed with the help of Peter McCulloch and the University of Tasmania. A Symmetricon Active Hydrogen Maser MHM-2010 (75001-114) with 5MHz, 10MHz, 100MHz, 1pps (pulse per second) outputs and a 1pps sync facility is installed. A digital base band converter (DBBC) developed at the Italian Institute of Radio Astronomy is expected to be installed in May 2010. The AUT VLBI receiving system uses a Mark 5B+ data recorder developed at MIT Haystack Observatory.

Both S and X receivers have been installed and preliminary figures for SEFD are around 4000 Jy, a figure that is higher than expected. Investigations in collaboration with the manufacturer are underway and several areas in which improvements can be made have been identified.

With wide-spread development of e-VLBI, the issue of broadband network connectivity becomes essential for both existing and emerging radio astronomical facilities. Internationally, New Zealand's major broadband supplier is Southern Cross Cables Ltd — a commercial organization, which owns and operates the cable connecting New Zealand with Australia in the West and with the US in the North-East direction. This is a multi-wavelength cable with the capacity of up to 2 Tbps. Locally, the regional advanced network operating in New Zealand is KAREN (Kiwi Advanced Research and Education Network), which provides a 10 Gbps connectivity between New Zealand's educational and research institutions. The establishment of a KAREN GigaPoP at the 12-m radio telescope site in Warkworth is currently in progress.

3. Surface Accuracy

Photogrammetric measurements of the antenna surface were performed by Kevin Sinclair and Bob Cato from Patriot Antenna Systems (Cobham SATCOM). Figure 1 shows contours for the deviation of the real surface from the theoretical (shaped) surface. The absolute values of deviation reach a maximum of 0.5 mm, with an $rms = 0.4$ mm, which is somewhat higher than the expected rms according to the manufacturer's initial specification of $0.012'' = 0.3$ mm. No noticeable change in rms with the elevation angle was detected. Holographic measurements of the dish are planned in the near future.

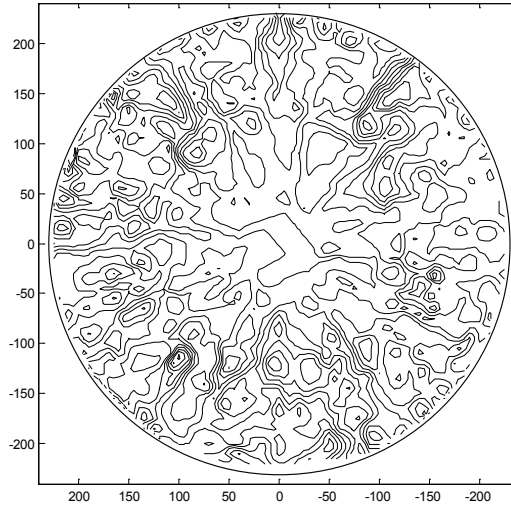


Figure 1. Contour map showing the deviation of the measured main reflector surface from the theoretical one. Ten contours are used in the range from -0.5 to 0.5 mm. X and Y axes are in inches.

4. Pointing Map

The AUT radio telescope has an azimuth-elevation mount. For engineering reasons, there always exists a difference dA and dE between the desired and actual azimuth, A , and elevation, E , positions. The aim of the pointing map is the minimization of the errors dA and dE for the observable hemisphere. The true angle for the horizontal component of this mis-pointing is the so-called cross-elevation $dXE = dA \cos E$. The telescope control system is capable of pointing corrections, which are calculated by the control system as follows

$$dXE = \theta_1 + \theta_2 \cos E + \theta_3 \sin E + \theta_4 \sin E \cos A + \theta_5 \sin E \sin A \quad (1)$$

$$dE = -\theta_4 \sin A + \theta_5 \cos A + \theta_7 + \theta_8 \cos E + \theta_9 \cot E \quad (2)$$

Here the nine regressed coefficients, θ_1 to θ_9 , used in (1) and (2), correspond to different physical offsets and errors in the vertical (elevation) and horizontal (cross-elevation) positions as described in Table 1.

Note that θ_4 and θ_5 coefficients are used in both dXE and dE expressions. The parameter θ_6 is not used in this approximation, but is retained to correct for gravitational bending proportional to $\sin E$ in possible future applications.

Mathematically, the problem of finding nine coefficients from nine or more observations can be solved using the method of least squares. In this case the regression problem is linear, despite the duplication of the parameters. The MATLAB code given in Listing 1 provides the solution in terms of pointing coefficients and the *rms* for both dXE and dE . Note that the algorithm concatenates the two Vandemonde matrices associated with equations (1) and (2), but never forms the possibly ill-conditioned normal equations in order to solve for the unknown parameters.

Table 1. The physical interpretation and subsequently regressed values of the parameters used in Equations (1) and (2).

	<i>Description</i>	<i>value</i>
θ_1	Azimuth collimation error	0.1218
θ_2	Azimuth encoder offset	-0.4861
θ_3	Elevation axis skew angle	-0.0576
θ_4	Inclination of the azimuth axis in the N-S direction	0.1266
θ_5	Inclination of the azimuth axis in the E-W direction	-0.0254
θ_6	Not used in this model	—
θ_7	Elevation encoder offset	0.5119
θ_8	Gravitational deformation of radio telescope	0.0586
θ_9	Residual refraction coefficient	-0.0173

Listing 1. MATLAB code for fitting parameters to (1) and (2).

```

1 % Define the models to be fitted
dXE = @(p,A,E) p(1) + p(2)*cos(E) + p(3)*sin(E) + p(4)*sin(E).*cos(A) + ...
    p(5)*sin(E).*sin(A); % Eqn. (1)
dE = @(p,A,E) -p(4)*sin(A) + p(5)*cos(A) + p(6) + p(7)*cos(E)+p(8)*cot(E);
    % Eqn. (2) with numbering change
6
% Data Input
B = xlsread('D:\data.xls'); % read Excel file with observational data
A = B(:,1); % Column 1: Azimuth in rad
E = B(:,2); % Column 2: Elevation in rad
11 dAz = B(:,3); % Column 3: measured error in cross-elevation in degrees
dEl = B(:,4); % Column 4: measured error in elevation in degrees

% Set up the Data matrix
N = length(dAz); % # of observations
16 y = [dAz; dEl];
Va = [ones(N,1), cos(E), sin(E), sin(E).*cos(A), sin(E).*sin(A), zeros(N,3)];
Vb = zeros(N,8);
Vb(:,[4:8]) = [-sin(A), cos(A), ones(N,1), cos(E), cot(E)];
V = [Va; Vb];
21
% Pointing map correction coefficients -- same units as dAz and dEl (deg).
pfit = V\y % Do the Least-squares fit

dAfit_error = norm(dXE(pfit,A,E) - dAz)/sqrt(N) % Compare fits
26 dEfit_error = norm(dE(pfit,A,E) - dEl)/sqrt(N) % RMS, 1 sigma

```

Several bright and compact radio sources were observed both in S and X bands in both polarizations (RCP and LCP). With the Matlab code from Listing 1, we processed the observational data, which consisted of 19 measured positions on the sky in S-band and 25 positions in X-band. As the result, the regressed pointing coefficients were determined for the X-band (Table 1).

The error (*rms*) of this solution is pretty small: 0.03° for both azimuth and elevation. No detectable offsets between the X-band RCP and X-band LCP were found. However, we detected

a noticeable elevation offset (squint) of the S-band beams relative to the X-band beam position. The measured elevation offsets are:

$$(\text{S-band RCP}) - (\text{X-band}) = -0.15^\circ \quad \text{and} \quad (\text{S-band LCP}) - (\text{X-band}) = 0.07^\circ .$$

5. Conclusion

The IVS VLBI2010 Progress Report [4] outlines a number of strategies to improve the long-term accuracy of geodetic VLBI with an eye to achieving 1-mm long-term accuracy on baselines. Among these strategies are: “to increase the number of antennas and improve their geographic distribution” and “to increase the number of observations per unit of time”. These IVS strategies can best be addressed through construction of new small (~ 12 m), fast-slewing automated antennas in areas that are under-represented (Southern Hemisphere) or lack (e.g., New Zealand) geodetic VLBI stations. Developing this approach, AUT University has invested US\$1m in a geodetic VLBI system, consisting of a fast-slewing automated 12-m antenna, hydrogen maser clock, digital receiving and digital backend systems, and a 1 Gbps network connectivity.

In November 2008, a new GNSS station (WARK) was built at the AUT radio telescope site. It is part of the New Zealand GNSS network “PositionZ”. An accurate tie is established between the radio telescope antenna and GNSS station.

The New Zealand 12-m antenna is scheduled to start participating in regular IVS VLBI sessions in the middle of 2010.

Being a research tool for astronomy and geodesy, the antenna will be used in a new educational program in astronomy which was started in 2009 at AUT’s School of Computing and Mathematical Sciences — an Astronomy Major in the framework of the Bachelor of Mathematical Sciences degree. It is envisaged that both undergraduate and postgraduate students will use the radio telescope in their research projects and as a teaching resource in the courses taught at AUT such as Astrophysics, Radio Astronomy, Practical Astrophysics, Space Geodesy, and others.

6. Acknowledgements

We are grateful to Lewis Woodburn (AUT), Peter McCulloch (University of Tasmania), Mark Godwin, Peter Shield, Kevin Sinclair and Bob Cato from Cobham SATCOM (Patriot Antenna Systems), Neville Palmer and John Beavan from GNS Science, as well as David Collett and Graeme Blick from LINZ.

References

- [1] Palmer, N. et al., Report on the Warkworth Radio Telescope Local Tie Survey. (In preparation.)
- [2] www.linz.govt.nz/positioNZ
- [3] Gulyaev, S., T. Natusch, New Zealand 12-m VLBI Station for Geodesy and Astronomy. In: International VLBI Service for Geodesy and Astrometry 2008 Annual Report, NASA/TP-2009-214183, D. Behrend and K. D. Baver (eds.), 68–73, 2009.
- [4] Petrachenko, B. et al., Design Aspects of the VLBI2010 System. Progress Report of the IVS VLBI2010 Committee. NASA/TM-2009-214180, June 2009.

COLD MAGICS – Continuous Local Deformation Monitoring of an Arctic Geodetic Fundamental Station

Rüdiger Haas ¹, Sten Bergstrand ²

¹) *Chalmers University of Technology, Department of Radio and Space Science*

²) *SP Technical Research Institute of Sweden, Mätteknik*

Contact author: Rüdiger Haas, e-mail: rudiger.haas@chalmers.se

Abstract

We describe the experience gained in a project to continuously monitor the local tie at the Geodetic Observatory Ny-Ålesund. A PC-controlled robotic total station was used to monitor survey prisms that were attached to survey pillars of the local network and the monuments used for geodetic VLBI and GNSS measurements. The monitoring lasted for seven days and had a temporal resolution of six minutes. The raw angle and distance measurements show clear sinusoidal signatures with a daily period, most strongly for a four-day period with 24 hours of sunshine. The derived topocentric coordinates of the survey prisms attached to the GNSS monument and the VLBI radio telescope act as approximation for the local tie. We detect clear signatures at the mm-level. With the current approach we cannot distinguish between real motion of the prisms and potential thermal influences on the instrument used for the observations. However, the project shows that continuous local tie monitoring is feasible today and in the future can and should be used for all geodetic co-location stations.

1. Introduction

The Global Geodetic Observing System (GGOS) [1] aims at a combination and integration of observations and results of various geodetic techniques. An important ingredient for the GGOS are geodetic co-location stations, often called Geodetic Fundamental Stations, that host equipment for several geodetic techniques. The local geodetic relations between the techniques' reference points, usually called "local ties", have to be known accurately in the spatial and temporal domain. The goal is up-to-date local ties with sub-mm accuracy and full variance-covariance information.

Usually local tie surveys are performed every couple of years only. This is mainly due to the fact that a local tie survey is a difficult and time consuming engineering task (e.g., [2], [3]). Often these surveys are a combination of direction and distance measurements with tachymeters, and height differences from spirit levelling. Some deficiencies of this approach are:

Inconsistency: Different survey campaigns and survey teams do not agree on the results. Did something really change or is it an effect of method, operator or instrumentation?

Insufficiency: The temporal sampling is too low. So, if something really changed, when exactly did it change? And what about possible periodic changes?

Interpretation: Depending on the size of the local network, the local systems are not necessarily truly cartesian systems that can be transformed easily to a global cartesian system.

One possible answer to the above listed deficiencies is the idea of continuous cartesian connections (CCC) [4], i.e., continuous local tie monitoring that is operated in an automatic mode and uses angular and distance measurements independently of the geoid's curvature. We tested this idea in the summer of 2009 at the Geodetic Observatory Ny-Ålesund on Svalbard.

2. The Geodetic Observatory Ny-Ålesund

The Geodetic Observatory Ny-Ålesund is a very important co-location station due to its northern location at 79° N. The station hosts a radio telescope for geodetic VLBI, several monuments for GNSS observations, and a superconducting gravimeter, and there is also a tide gauge and a DORIS station within 2 km distance.

Figure 1 shows an aerial photo of the station. The VLBI telescope and GNSS monuments and some of the survey pillars of the local survey network are depicted.



Figure 1. Aerial picture of the Geodetic Observatory Ny-Ålesund on Svalbard. The VLBI telescope and GNSS monuments and some of the survey pillars of the local survey network are depicted.

3. Method

We used a PC-controlled robotic total station (Leica TM30) (Fig. 2a) to measure distances and angles to 14 retro-reflecting prisms (Leica GPR112). Six prisms were attached to the survey pillars P91, P92, P94, P95, P96, and P97 (e.g., Fig. 2b). Another six prisms were attached with strong magnets to the structure of the radio telescope. Prisms T1-T5 were mounted directly on the non-moving telescope tower (Fig. 2c), while prism T6 was mounted on a moving part of the telescope. One prism was attached to the GNSS monument NYAL (Fig. 2d) which is a 5 m high steel truss mast on a concrete block foundation. Another prism was mounted close to the tide gauge in the harbor.

The total station was placed on survey pillar P93 (Fig. 2a) that had the best visibility to a large number of other survey pillars, the radio telescope, and the GNSS monument. The total station

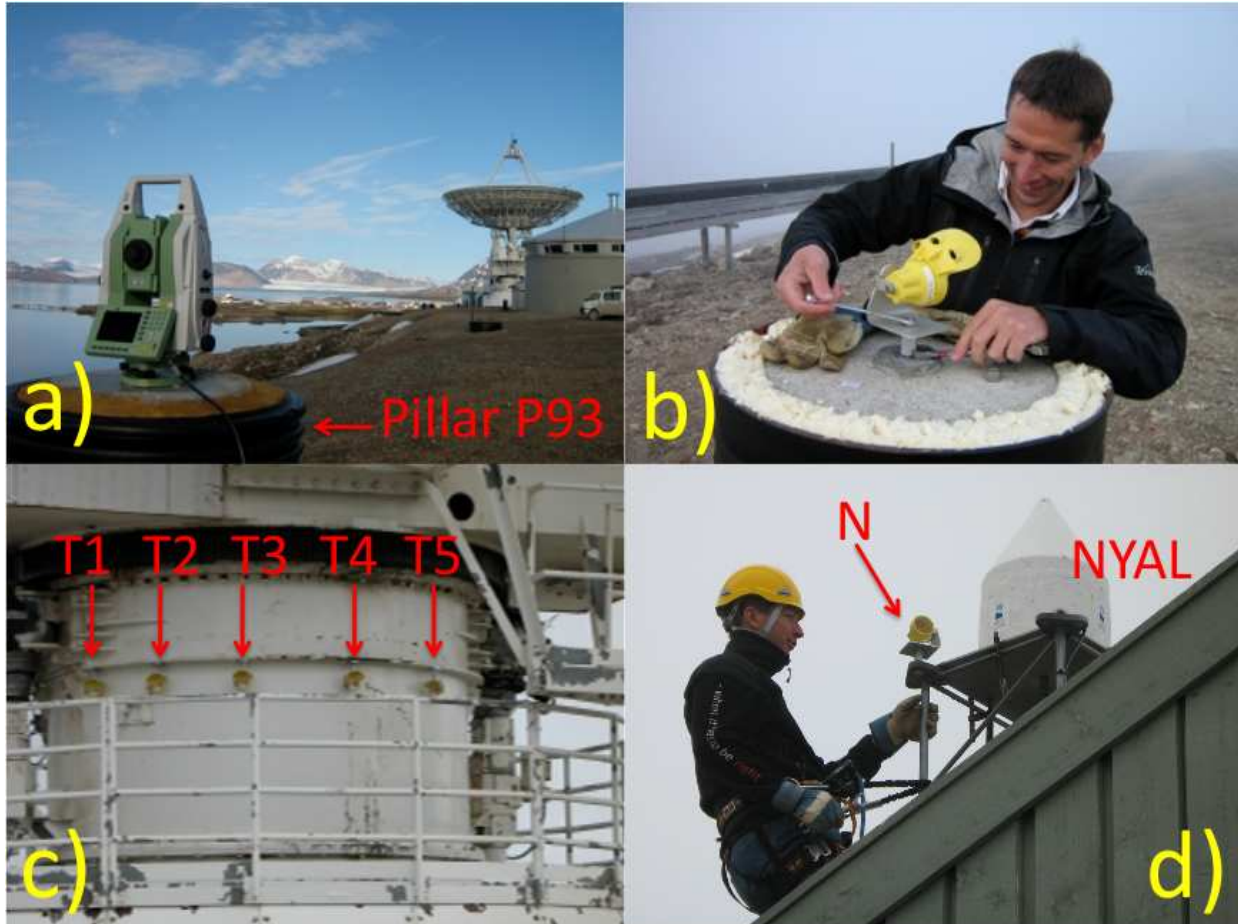


Figure 2. The measurement setup: (a) The total station on pillar P93; (b) One of the retro-reflecting prisms mounted on one of the survey pillars; (c) Five prisms mounted with strong magnets on the tower of the radio telescope; (d) The prism mounted on the GNSS monument NYAL.

was controlled and operated using software (Leica GeoMos). A temperature and air pressure sensor was connected to the data acquisition system in order to correct the distance measurements for refractive index variations.

4. Results

The total station performed measurements in two faces (angles and distances) and automatic target recognition (ATR) to all 14 prisms with a repetition cycle every 6 minutes. The instrument specifications with the used prisms are 0.30 mgon and 1 mm + 1 ppm for angular and distance measurements, respectively. In parallel, meteorological data were recorded at the total station every 1 minute. In this operation mode measurements were performed continuously for 7 days.

The measurements are shown in Fig. 3. Mean values of each time series are subtracted, and the series are offset with respect to each other to improve the readability of the plots. A common

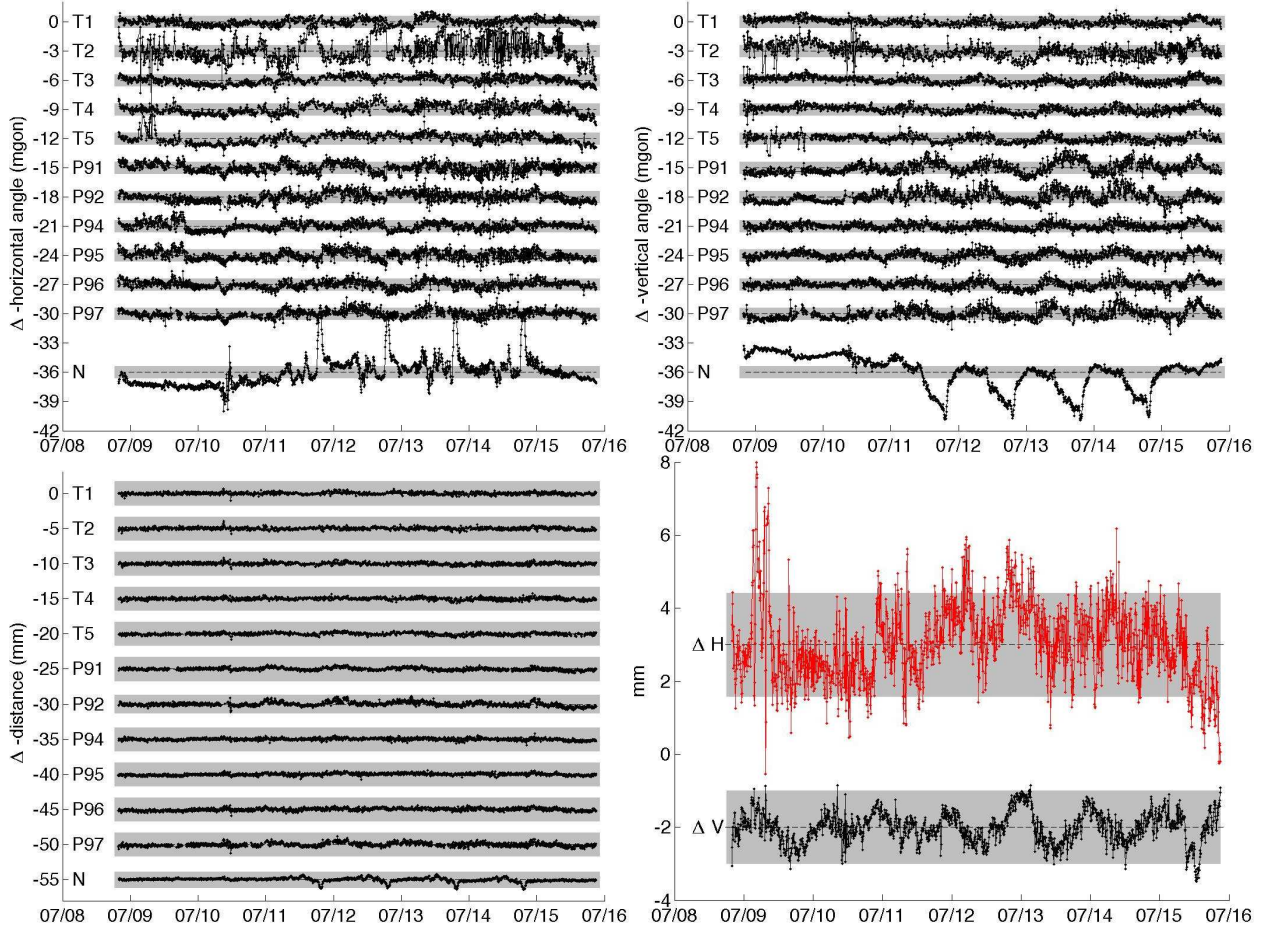


Figure 3. Measurements of horizontal angles (upper left), vertical angles (upper right), and distances (lower left). Mean values of each time series are subtracted and offsets introduced to improve readability. The gray background gives the 2-sigma uncertainties according to the instrument specifications. The horizontal and vertical distance between the prism N at the GNSS monument NYAL and the fitted center of the tower of the radio telescope are shown in the lower right picture. Mean values are subtracted and the gray background gives the expected uncertainties (1-sigma).

horizontal angle drift, possibly related to an unfortunate but necessary use of shims when fastening the total station's tribrach, has been removed.

The grey background of each time series shows the expected 2-sigma uncertainty according to the instrument specifications. It becomes clear that in particular several of the angle measurements show sinusoidal signatures that are larger than the expected 2-sigma uncertainties based on the instrument specifications. The prism N that was attached to the GNSS monument NYAL shows very large variations of horizontal and vertical angles.

The measurements show in general diurnal signatures for many prisms, most clearly during July 11-15. During these four days we experienced 100 hours of consecutive sunshine, confirmed by solar radiation observations with a strong sinusoidal signature of a 24-hour period [5].

In the next step we used the angle and distance measurements for every epoch to determine

coordinates in a local system by polar point determination. Then we fitted circles to the horizontal positions of prisms T1-T5 for every epoch and calculated the mean vertical position. These coordinates can to some extent be regarded as representing the center of the tower of the radio telescope. Thus, the geometric relation between the center of the radio telescope tower and the prism at the GNSS monument are regarded as an approximation for the local tie between the IVS and IGS monuments. Variations of this geometric relation are shown in the lower right graph in Fig. 3. Daily signatures are visible in the coordinate differences, both for the horizontal (upper series) and vertical components (lower series). The uncertainty band is dominated by the distance measurements.

5. Conclusions and Outlook

We monitored the local network at Ny-Ålesund continuously for 7 days using an automated observation strategy.

The diurnal signatures seen in our raw measurements are often larger than the expected measurement uncertainties. In particular the angular measurements have signatures that are larger than 2-sigma. Measurements to the prism (N) attached on the GNSS monument NYAL (5 m steel truss mast) show the strongest signatures.

Topocentric coordinates for the observed prism were determined every epoch by simple polar point determination. We identify diurnal signatures at the mm-level in the coordinate differences between the VLBI telescope and the GNSS monument. At this point we cannot distinguish if this apparent coordinate variation is real local deformation due to thermal effects or due to thermal influences on the instrument used for the observations, since we lack redundant observations. However, the concept of continuous monitoring of local ties appears to work fine. Future continuous monitoring projects should thus use several total stations for redundancy purposes and include a dense network of meteorological sensors.

6. Acknowledgements

We acknowledge support by the European Centre for Arctic Environmental Research (ARC-FAC). We thank for their support Line Langkaas, Ole Bjørn Årdal, and Carl Petter Nielsen from Statens Kartverk Norge, and Hans Borg and Christer Thunell from Leica Geosystems Sweden.

References

- [1] Rummel R., Rothacher M., Beutler G.. (2005) Integrated Global Geodetic Observing System (IGGOS) – science rationale. *Journal of Geodynamics*, **40**, 357–362.
- [2] Sarti P., Sillard P., Vittuari L.. (2004) Surveying co-located space-geodetic instruments for ITRF computation. *Journal of Geodesy*, **78**, 210–222, doi:10.1007/s00190-004-0387-0.
- [3] Haas R., Eschelbach C. (2005) The 2002 Local Tie at the Onsala Space Observatory. In: *Proc. IERS Workshop on site co-location*, B. Richter, W. Schwegmann and W. R. Dick (eds.), IERS Technical Note, **33**, Verlag des Bundesamts für Kartographie und Geodäsie, 55–63.
- [4] Haas R., Bergstrand S. (2010) Continuous Cartesian Connections at Geodetic Fundamental Stations. in preparation.
- [5] Debatin S. (2009) Alfred Wegener Institut, Potsdam, personal communication.

Homologous Deformation of the Effelsberg 100-m Telescope Determined with a Total Station

Axel Nothnagel, Judith Pietzner, Christian Eling, Claudia Hering

Institute of Geodesy and Geoinformation, University of Bonn

Contact author: Axel Nothnagel, e-mail: nothnagel@uni-bonn.de

Abstract

Due to gravitation the main reflector of the Effelsberg 100-m telescope of the Max Planck Institute for Radio Astronomy is deformed whenever it is tilted from zenith to arbitrary elevation angles. However, the resulting shape always is a paraboloid again, though with different parameters, a phenomenon which is called homologous deformation. In summer 2008, we have carried out measurements with a total station to determine the magnitude of these deformations in order to evaluate existing assumptions provided by the manufacturer from the telescope's design phase. The measurements are based on a newly developed approach with a Leica TCRP 1201 total station mounted head down near the subreflector. Mini-retro-reflectors are placed at various locations on the paraboloid itself and on the subreflector support structure. The results indicate that the measurement setup is suitable for the purpose and provides the information needed for a determination of elevation dependent delay corrections. The focal length changes only by about 8 mm when the telescope is tilted from 90° to 7.5° elevation angle.

1. Motivation and Constraints

The 100-m radio telescope of the Max Planck Institute for Radio Astronomy (Fig. 1) was completed in 1972 and is mainly used with feed horns and receivers in secondary focus employing a Gregorian subreflector. For certain frequencies, prime focus operation is maintained with relocatable receiver boxes installed in an opening of the subreflector. The main parabolic reflector is designed for homologous deformation. When tilted to non-zenith elevations, this design permits the paraboloid to deform but guides the deformation to end up as a paraboloid again, though with different parameters. For this purpose, the subreflector support structure with its four legs is completely disconnected from the main reflector (Fig. 4). As a consequence of the homologous deformation, the focal length and, thus, the focal point are elevation dependent. To maintain optimal gain of the telescope, the secondary reflector or the receiver box in prime focus are shifted to compensate for the gravitational displacements. The elevation-dependent model for these shifts has originally been provided by the manufacturer of the telescope and since then has been updated by empirical gain optimization models from test measurements.

In summer 2008, a geodetic survey was carried out to validate the empirical model and to evaluate the deformations for VLBI delay corrections. For these measurements the paraboloid is represented by 16 mini-retro-reflectors mounted in groups of four reflectors each along four meridians (Figures 2 and 5). Ideally, the local coordinates of these reflectors are determined from a single invariant position of a total station outside of the telescope. However, when the telescope is pointing to higher elevations, not all the reflectors are visible simultaneously from anywhere on the ground or adjacent hilltops. The only way around this limitation is that the total station is placed within the movable part of the dish. So, we mounted the instrument head-down close to

the subreflector and controlled it with a cable link to a PC. The operator had to sit in the focus cabin of the telescope and trigger the measurement program for all reflectors with automatic target recognition for each elevation position. The paraboloid was sampled in seven different elevation positions (90° , 75° , 60° , 45° , 30° , 15° , and 7.5°).



Figure 1. Effelsberg 100-m telescope with primary focus cabin at the top.

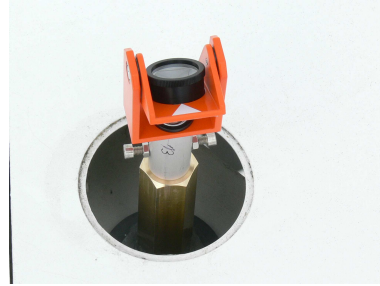


Figure 2. Retro-reflector on paraboloid surface.

The mounting of the instrument near the subreflector had the disadvantage that the position and orientation of the instrument was subject to the displacements and distortions of the prime focus cabin and the subreflector. For this reason, no relationship of the estimated paraboloids existed between the positions when the telescope pointed at different elevations. To link the independent systems related only to the orientation of the axes of the total stations, four more reflectors were observed which were mounted as low as possible on the four subreflector support legs (Fig. 4). A first assumption was that these four points could serve as invariant points for all elevation positions.



Figure 3. Leica TCRP 1201, mounted top-down.

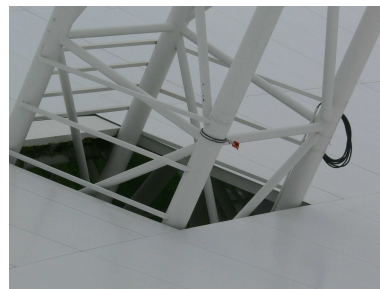


Figure 4. Retro-reflector on support leg.

2. Data Reduction

2.1. Instrument Location and Orientation

When computing the positions of all reflectors relative to the (arbitrary) axes of the total station, it was of course immediately obvious that none of the reflector points maintained its position when tilting the telescope in elevation because the instrument itself was not only displaced but also tilted by about a quarter of a degree. What was unexpected, however, was the fact that

the distances between the four points assumed as invariant changed significantly. When tilting the telescope from 90° to 7.5° elevation, the distances changed continuously and monotonically to a maximum of 18 mm (Fig. 6). The reason for these distance changes is a bending of the subreflector support legs which depends on various factors, in particular on what geometrical position each individual beam has w.r.t. the gravitation vector and in what directions the gravitational force is actually acting. When the telescope, for example, is in a 60° elevation position, the lower leg is almost upright with the consequence that the bending force is eliminated while the upper leg is inclined by about 30° and, thus, subject to a bending force which is close to 90% of the gravitational force (Fig. 7). The reflectors near the bottom ends of the legs are, however, only affected by a small fraction of the bending.

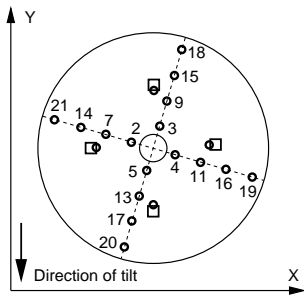


Figure 5. \circ = Positions of reflectors, \square = Intersections of subreflector support legs.

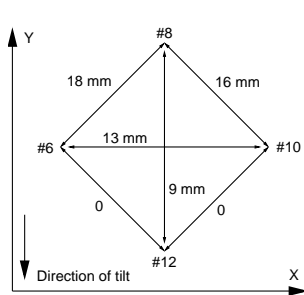


Figure 6. Differences in distances between foot points of subreflector support legs when tilting from 90° to 7.5° elevation.

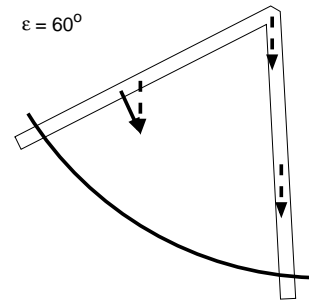


Figure 7. Gravitational force (dashed vector) and bending force (solid vector) acting on upper and lower support legs.

To end up with quasi-invariant reference points at the bottom parts of the subreflector support legs, we developed a simple gravitational model for each of the four legs. Since we are only interested in the movements of the reflectors close to the bottom ends of the support legs, the model can assume simple beams which are joint at the free end (at the prime focus cabin) and supporting each other. Thus, the main deformation is in the middle of the beams with a greatly reduced effect at the bottom of the legs.

With the corrections for the bending applied, the positions of the reflectors could be considered as invariant to the tilting of the telescope. The quality of the model can best be characterized by the resulting residuals of the distance determinations from the measurements (Fig. 8).

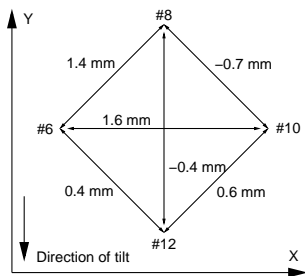


Figure 8. Residual differences in distances between foot points when tilting from 90° to 7.5° elevation.

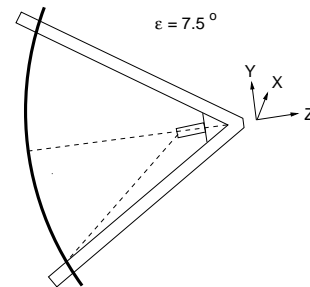


Figure 9. Sketch of telescope at 7.5° elevation with axis definition.

Now, having established invariant points, the position and orientation of the total station or rather its displacement from the initial position at 90° elevation was determined from a 6-parameter similarity transformation. As expected, the largest displacement of the instrument occurred in the direction tangential to the main reflector and the subreflector. This effect is most obvious when the telescope points at 7.5° elevation and the weight of the prime focus cabin and of the subreflector pull the whole construction down. In our local coordinate system, this axis is the y-axis, while the x-axis is perpendicular (parallel to the elevation axis, Fig. 9). This movement, which is tangential to the incoming radiation, reaches 47 mm at 7.5° elevation (Fig. 10). In the radial direction with the z-axis towards the observed object, the maximum displacement of 5 mm towards the main reflector is surprisingly small (Fig. 11). The graph does not appear as smooth as that of the Δy component; this, however, originates from a slight deviation of the measurement at 45° elevation together with the scale which is only 1/10 of the other component.

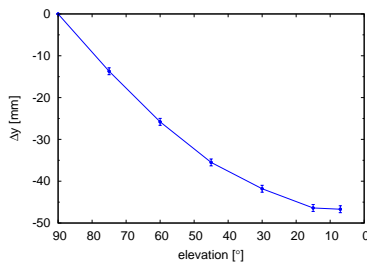


Figure 10. Displacement of instrument in y direction vs. elevation.

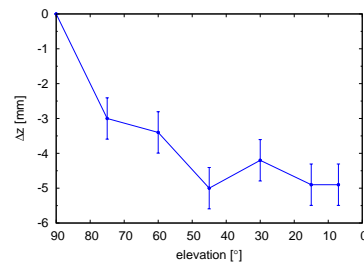


Figure 11. Displacement of instrument in z direction vs. elevation.

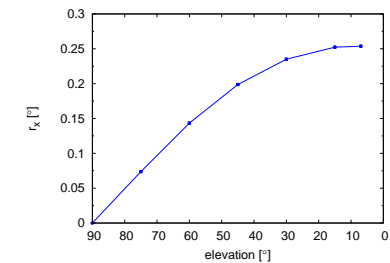


Figure 12. Rotation of instrument about x-axis.

The last effect is a tilt of the instrument about the x-axis of at maximum 0.25° . This is a clockwise rotation towards $-y$ resulting in the head of the total station being pulled down. Here, 0.25° is equivalent to 1.1 mm displacement of the instrument's intersection of axes. This is a very small effect and is assumed to be a consequence of the deformation of the whole prime focus cabin and support leg structure. However, due to the long lever arm of more than 35 m, this rotation shifts the apparent positions of the points on the main reflector by about 15 cm.

2.2. Reflectors on the Paraboloid

The flexibility of the main reflector is an important design element of the Effelsberg 100-m radio telescope, being the basis for homologous deformation at all elevation angles. Having determined the position and orientation of the total station in each elevation step through simple six-parameter similarity transformations, the positions of the subreflectors on the main paraboloid can now be determined applying the respective transformation parameters to these positions as well. When the telescope is tilted from 90° elevation angle downwards the reflectors are displaced in the y and z direction in a monotonous way confirming the high quality of the measurements (Figures 13 and 14). Here, reflector #20 is displaced as much as 50 mm in y direction and 41 mm in z direction when the 7.5° elevation position is reached.

Looking at the results for the 7.5° elevation angle tilt in a 2D representation (Fig. 15), it can be seen that the upper part of the paraboloid is folded inwards (#15 by 57 mm). Unfortunately the very top reflector (#18) was not visible any more at 7.5° elevation due to obstruction by the

subreflector support leg. Towards the vertex, the magnitude of the folding naturally decreases changing direction at the bottom part with reflector # 20 pulled down by as much as 66 mm.

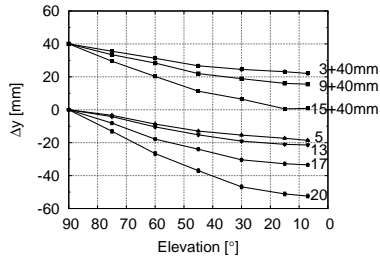


Figure 13. Displacement of reflectors in y direction. Points 3, 9 and 15 (see Fig. 5) are offset by +40 mm for better readability.

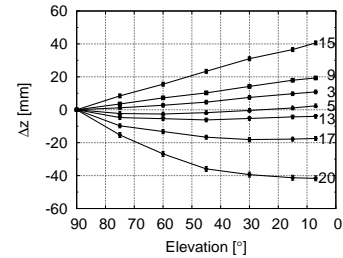


Figure 14. Displacement of reflectors in z direction.

2.3. Focal Length Results

A first result of the project is the estimate of the focal lengths of the telescope in the individual elevation angle positions. This quantity is invariant to any transformations which are necessary for a determination of the shift of other parameters, e.g., of the vertex. Taking into account the formal errors, the focal lengths of the 75° and 60° positions are hardly changed while down to 7.5° elevation, it is shortened by 13 mm. For such a large telescope, this result is surprisingly small. However, together with an upward movement of the vertex of about 7 mm, the results agree well with an empirical model for a gain adjustment through focus/subreflector movements. These results indicate that the earlier steps have been carried out correctly, and the approach looks very promising for further steps of data analysis.

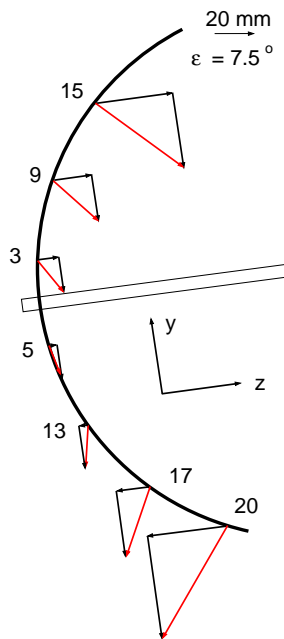


Figure 15. Folding of main paraboloid along the 10° meridian at 7.5° elevation. The top reflector is missing due to visibility problems.

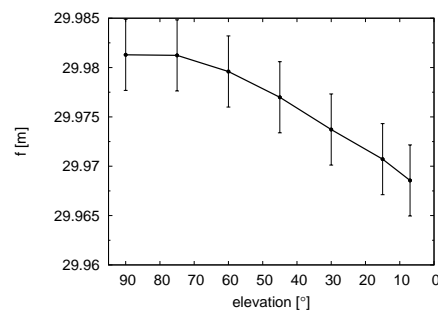


Figure 16. Focal length estimates w.r.t. elevation angle of telescope.

Acknowledgements. We are grateful to the staff of the Max Planck Institute for Radio Astronomy at Effelsberg for their efforts to make these measurements possible. In particular, we should mention Klaus Bruns, who did not hesitate to mount our reflectors at the edge of the paraboloid, which required some really acrobatic exercises.

Analysis of the GPS Observations of the Site Survey at Sheshan 25-m Radio Telescope in August 2008

L. Liu, Z. Y. Cheng, J. L. Li

Shanghai Astronomical Observatory, CAS

Contact author: L. Liu, e-mail: liuli@shao.ac.cn

Abstract

The processing of the GPS observations of the site survey at Sheshan 25-m radio telescope in August 2008 is reported. Because each session in this survey is only about six hours, not allowing the subdaily high frequency variations in the station coordinates to be reasonably smoothed, and because there are serious cycle slips in the observations and a large volume of data would be rejected during the software automatic adjustment of slips, the ordinary solution settings of GAMIT needed to be adjusted by loosening the constraints in the *a priori* coordinates to 10 m, adopting the “quick” mode in the solution iteration, and combining Cview manual operation with GAMIT automatic fixing of cycle slips. The resulting coordinates of the local control polygon in ITRF2005 are then compared with conventional geodetic results. Due to large rotations and translations in the two sets of coordinates (geocentric versus quasi-topocentric), the seven transformation parameters cannot be solved for directly. With various trial solutions it is shown that with a partial pre-removal of the large parameters, high precision transformation parameters can be obtained with post-fit residuals at the millimeter level. This analysis is necessary to prepare the follow-on site and transformation survey of the VLBI and SLR telescopes at Sheshan.

1. Introduction

The reference point of a station may change due to maintenance of equipment, replacement of devices, earthquakes, or various other reasons, which may lead to uncertainties in the study of geophysical phenomena or the position determination of targets. Therefore, it has been proposed to conduct site surveys at the reference stations of the ITRF once or twice per year and to conduct additional surveys when there are fundamental repairs of the station or when unexpected events occur that necessitate the monitoring and tracing of possible changes of the reference point. Local surveys at co-location sites are especially proposed to determine the three-dimensional (3D) coordinate difference vector of reference points, which can be used as a constraint in the combination analysis of terrestrial reference frames and in the analysis of possible systematic errors between various space geodetic techniques.

The VLBI, SLR, and GPS techniques have been co-located at Sheshan station of Shanghai Astronomical Observatory for more than a decade; but Sheshan has lacked for many years any high precision local tie parameters. In 2001, the International Earth Rotation and Reference Systems Service (IERS) reported that the local tie parameters between VLBI and SLR at Sheshan were in error in the three components by 2.4, 1.3, and 1.9 cm, respectively [1]. In November 2003 the IERS organized an international expert team to survey at Sheshan [2]. The SLR equipment however was moved to its present new location in 2005, and in 2007 the VLBI antenna underwent track foundation repair and wheel bearing replacement. Therefore the tie parameters at Sheshan needed to be re-determined; this includes a survey of the SLR telescope and the 25-m VLBI antenna as well as a transformation survey between the two sites.

The 25-m radio antenna at Sheshan has an alt-azimuth mount; the vertical axis is firmly connected to the foundation. The reference point usually is considered to be the intersection of the vertical axis with the plane containing the horizontal axis. If the two axes do not intersect, then the distance between the two axes is the axis offset, which will cause systematic errors at different orientations of the antenna. To do a local survey of the antenna is to determine the 3D geocentric coordinates of the reference point, plus a possible axis offset. Such a survey is an important part of the work to get the local tie parameters among the co-located space geodetic techniques at Sheshan.

In order to monitor a possible change of the reference point of a station in ITRF, the coordinates of the reference point in the local control polygon is usually determined by a conventional geodetic survey, the ITRF coordinates of the control points in the polygon are usually determined by a GPS survey, and through coordinate transformation between the local and ITRF coordinates of the control polygon, the coordinates of the reference point in the ITRF are obtained. So the precision of the local tie parameters is closely related to the reduction precision of the GPS observations and the precision of the transformation parameters between the GPS measurements and the conventional geodetic measurements. In this report the GPS observations of the August 2008 site survey at the Sheshan 25-m antenna are processed, and the transformation parameters to the conventional geodetic measurements are determined. This constitutes a necessary preparation for the follow-on site survey and local tie survey of VLBI and SLR at Sheshan.

2. The GPS Survey of the Local Control Polygon and Data Analysis

The local control polygon (LCP) for the survey of the Sheshan 25-m antenna is shown in Figure 1. Points 1 through 5 are reinforced concrete pillars with a stainless steel plate on top bearing a forced centering screw; the design is according to reference [3]. The reference points of the pillars are on the upper surface of the plate and in the center of the screw. All the points are directly visible from each other, except for the view between points 2 and 3 which is obstructed by the antenna control room. In Figure 1 the relative location of the IGS fiducial station, SHAO, is labeled by “GPS”. Equal precision GPS surveys were performed on all baselines between points 1 through 5 using Topcon Legend-C receivers at a sampling interval of 5 s, cut-off elevation angle of 10° , and using static processing mode. Each session lasted about six hours, and there are 12 sessions in total.

2.1. GPS Data Processing

Currently the most commonly used processing softwares for GPS observations include GAMIT, Bernese, and GIPSY. With precise satellite ephemerides and precisely known coordinates of the reference stations, the determination precision for a baseline is up to 10^{-9} by GAMIT, which has open source code and can be modified by users. Since we used single frequency GPS receivers in our survey, SHAO, which is less than 150 m from the local control points, can be taken as the reference station with precisely known coordinates in ITRF. With double difference solution mode in GAMIT the effects of error sources such as the satellite orbit uncertainty, clock bias, and ionosphere and troposphere delays on the solution can be mitigated.

The ordinary settings for processing GPS observations in GAMIT are to apply strong constraints to the *a priori* coordinates of the reference station, for instance 5 mm in the horizontal

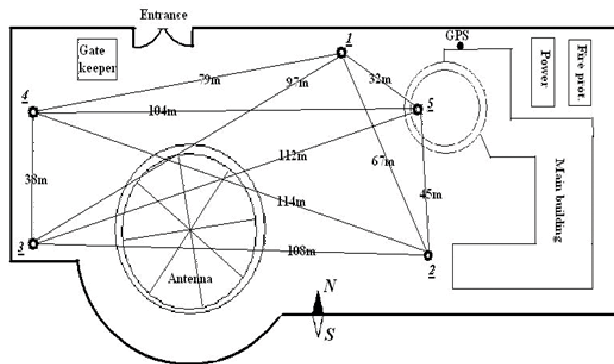


Figure 1. The local control polygon at the site of the Sheshan 25-m antenna.

direction and 5 cm in the vertical, as well as automatic correction of cycle slips and solution iteration. We take session 2008.237X as an example, which includes points 1, 4, and SHAO in Figure 1. From Table 1 it is clear that with the ordinary settings of GAMIT there are only about several hundreds of double difference observations, which are rather below the ordinary data level of several thousands collected within six hours by three stations of very short baselines. The formal errors of the baseline vectors are too large, up to one meter, so the solution is unsuccessful. A similar situation occurs when processing other sessions in this survey with the ordinary settings of GAMIT. For some cases the formal errors of baseline vectors are relatively small but the postfit normalized root mean square (*nrms*) of residuals is too large, which also indicates an unsuccessful solution. In a closer look, we found that there are too many cycle slips in the GPS observations of the survey. The automatic correction of cycle clips by GAMIT usually causes the whole path of a satellite to be deleted. In this report some adjustment to the ordinary solution settings of GAMIT are adopted as follows.

- Taking into account that each session is only about 6 hours, which is inadequate to smooth out the subdaily high frequency variations due to solid earth tide, ocean loading, and so on. If strong constraints were applied to the coordinates of the reference station SHAO, the high frequency variations would seriously affect the determination precision of the unknowns. Concerning the ultra-short baselines of about 100 m in length in our survey, the variation of coordinates of the two ends of the baseline caused by tidal effects could be treated as synchronous and in the same direction. So in our analysis a loose constraint of 10 m is applied to the *a priori* coordinates of all the stations, and the baseline solution mode is adopted.
- During the data processing with GAMIT, the data files of orbit and station coordinates (L and T file) are updated, and the “Quick” iteration mode is adopted. The ambiguity is not solved for in order to avoid deleting too much data. After the quick intermediate solution, the interactive editing software Cview is used to manually repair cycle clips until the data series becomes smoothed.
- The batch file is modified to let GAMIT read the data file (C file) resulting from the manual repair of the cycle slips and perform the follow-on automatic correction of the slips and

solution iterations.

- The previous two steps are repeated until the observation series becomes smooth and the postfit residuals are normally distributed.

Comparing the results of the adjusted and ordinary settings of GAMIT, Table 1 shows that after the adjustment the number of double difference observations has significantly increased and is on a relatively reasonable level. The *nrms* is usually taken as a checking standard for the quality of a single-session solution, whose value is theoretically 1 and is 0.25 by experience. After the adjustment to the solution settings all the resulting *nrms* of the baseline vectors of the GPS survey sessions are smaller than 0.5, and the formal errors of the baseline vectors are on the millimeter level. So the adjustment to GAMIT ordinary solution settings is effective.

Table 1. A comparison between the ordinary and adjusted settings of GAMIT.

Baseline	ordinary	adjusted
1.4	79.6089±0.0040 m	79.6081±0.0017 m
1.SHAO	36.3658±0.6393 m	36.6668±0.0019 m
4.SHAO	113.6863±0.6508 m	114.0645±0.0021 m
Observations	525	3916
Prefit <i>nrms</i>	89.99	44.34
postfit <i>nrms</i>	0.19	0.22

2.2. The Coordinates of the Control Polygon in the ITRF2005 System

Since the GPS survey of the polygon only lasted about five days, the variations of the coordinates of control points in the polygon due to plate motion could be neglected on the millimeter level; the mean epoch of the survey is adopted as the reference epoch, which is MJD54702.5. At this epoch the coordinates and velocities of SHAO in the ITRF2005 frame are theoretically deduced and taken as reference. Then those of the polygon deduced from the solutions of baseline vectors from GAMIT are taken as *a priori* values of unknowns. Through spatial error compensation software `GPS_net` [4], the results are shown in Table 2, from which it is clear that the coordinate precision of all the points in the polygon is better than 2 mm.

Table 2. The coordinates of the control points in ITRF2005.

Station	X/m	Y/m	Z/m	$\delta X/m$	$\delta Y/m$	$\delta Z/m$
1	2831698.7023	4675677.0289	3275367.9915	0.0018	0.0018	0.0018
2	2831741.6347	4675686.7828	3275317.0931	0.0018	0.0018	0.0018
3	2831649.2418	4675743.1305	3275316.8390	0.0018	0.0018	0.0018
4	2831638.7847	4675726.2489	3275349.9700	0.0018	0.0018	0.0018
5	2831729.4385	4675675.8735	3275359.0483	0.0019	0.0019	0.0019

2.3. Transformation Between GPS and Conventional Geodetic Surveys

A conventional geodetic survey to the LCP was completed by total stations. Point 1 was taken as the origin of the local frame and point 2 as the reference direction ($y = 0$). The local frame is right-handed, and the coordinates of all control points resulted from a 3D error compensation of the conventional geodetic observations [5]. In order to determine the transformation relationship from the local frame to the GPS survey and to check the GPS data processing, a seven-parameter transformation was solved for. The local frame is a quasi-topocentric one at point 1 (SEU), while that in Table 2 is a geocentric right-handed frame, so there are a large translation in the magnitude of the Earth's radius and a large orientation difference, which possibly obstruct the high precision determination of the transformation parameters. Various trial solutions are performed to solve for the seven transformation parameters with a dynamic range for the *a priori* values of unknowns from 0.01 to 1000. Tests show that it is helpful to partly remove the large translations and rotations before the parameter fitting. The postfit residuals are less than 5 mm, and the seven parameters are as follows.

$$\vec{T} = \begin{bmatrix} -2831698.701 \pm 0.0011 \\ 4675677.029 \pm 0.0012 \\ 3275367.989 \pm 0.0011 \end{bmatrix} m, \quad D = (-6.70 \pm 1.50) \times 10^{-5}, \quad \vec{R} = \begin{bmatrix} 55291.1 \pm 6.1 \\ -67161.1 \pm 4.7 \\ -62009.9 \pm 3.5 \end{bmatrix} as$$

3. Conclusions

The GPS observations in the site survey at the Sheshan 25-m antenna in 2008 were processed with GAMIT, Cview, and GPS_net. Due to serious cycle slips in the GPS observations, some adjustments are adopted to the ordinary solution settings of GAMIT. In the determination of the seven transformation parameters from the conventional geodetic survey to the GPS survey, because large rotations and large translations may leave unfavorable effects on the parameters, several trial solutions are made and compared, which show that a pre-treatment of the large rotations and translations is necessary in order to precisely determine the parameters. The analysis in this report is a necessary preparation for the follow-on site survey and local tie survey of VLBI and SLR at Sheshan.

References

- [1] Altamimi, Z, IERS Message No. 7, IERS ITRS Product Center, Institut Geographique National, 2001.
- [2] Garayt, B., S. Kaloustian, J. Long et al., Sheshan Co-location Survey, Report and Results, Service de Geodesie et de Nivellement, German: Direction de la Production, 2005.
- [3] Zang, D. Y., The Manufacture of Forced Centering Device for Precise Engineering Survey, Bulletin of Surveying and Mapping, Vol. 10, pp. 46–48, 2006.
- [4] Xiong F. W., Zhu W. Y., Zhang H. P., et al., Precise Determination of the new SLR Station of Shanghai Observatory, Progress in Astronomy, Vol. 25, Issue 2, pp. 177–183, 2007.
- [5] Li, J. L., S. B. Qiao, L. Liu. The application of coordinate transformation into the data reduction of site survey at the Sheshan 25-m radio telescope, Science of Surveying and Mapping, Vol. 35, Issue 2, pp. 69–71, 2010.

Permanent Monitoring of the Reference Point of the 20m Radio Telescope Wettzell

Alexander Neidhardt ¹, Michael Lösler ², Cornelia Eschelbach ², Andreas Schenk ²

¹) *Forschungseinrichtung Satellitengeodäsie, TU München, Geodätisches Observatorium Wettzell*

²) *Karlsruher Institut für Technologie (KIT), Geodätisches Institut, Universität Karlsruhe*

Contact author: Alexander Neidhardt, e-mail: neidhardt@fs.wettzell.de

Abstract

To achieve the goals of the VLBI2010 project and the Global Geodetic Observing System (GGOS), an automated monitoring of the reference points of the various geodetic space techniques, including Very Long Baseline Interferometry (VLBI), is desirable. The resulting permanent monitoring of the local-tie vectors at co-location stations is essential to obtain the sub-millimeter level in the combinations. For this reason a monitoring system was installed at the Geodetic Observatory Wettzell by the Geodetic Institute of the University of Karlsruhe (GIK) to observe the 20m VLBI radio telescope from May to August 2009. A specially developed software from GIK collected data from automated total station measurements, meteorological sensors, and sensors in the telescope monument (e.g., Invar cable data). A real-time visualization directly offered a live view of the measurements during the regular observation operations. Additional scintillometer measurements allowed refraction corrections during the post-processing. This project is one of the first feasibility studies aimed at determining significant deformations of the VLBI antenna due to, for instance, changes in temperature.

1. Introduction

The combination of different reference frames is only possible when the positions of the co-located systems for the different space techniques are well known [1]. The determination of position and orientation between the reference points of the space geodetic instruments is done by highly precise and regularly made local surveys. But in general these measurements are just snapshots that neglect variations over time such as temperature changes over the course of a day or a year. Indeed there is a correction model for height differences for VLBI antennas due to temperature changes (see [9] and [7]); however, changes in position are not yet considered. Therefore a permanent monitoring concept was realized at the 20m radio telescope of the Geodetic Observatory Wettzell to evaluate the movements of the reference point over a period of three months in the summer of 2009 [5]. It also shows a possible realization of a permanent monitoring system for the determination of the local-ties with sub-millimeter accuracy, as required by the Global Geodetic Observing System (GGOS, see [8]).

2. The Used Monitoring Concept HEIMDALL

In order to realize a permanent monitoring system for the geometric reference point of the radio telescope at the Geodetic Observatory Wettzell in Germany, the special software HEIMDALL was developed at the Geodetic Institute of the University of Karlsruhe (GIK), Germany. The acronym of the mostly Java software HEIMDALL stands for “High-End Interface for Monitoring and spatial Data Analysis using L2-Norm” and is also the name of the god of protection in old northern

European mythologies. The myth says that the god can see with the same high quality during the day and night and that he can hear the grass growing [2]. In Wettzell, HEIMDALL was installed on a laptop connected to several sensors (see Fig. 1). The main instrument was a programmable total station (Leica TCA2003) with an accuracy for distances of 1mm+1ppm and for angles of 0.15mgon. For the EDM corrections of the distances, a meteorological data logger of the type MSR145W was used. In addition, readings from the four permanently installed temperature sensors in the telescope tower, strain measurements along the azimuth axis, and telescope angles in azimuth and elevation were recorded. All collected data were saved in a MySQL database from which dynamic services offered a Web presentation of the measuring processes. For refraction corrections during post-processing, a parallelly installed scintillometer provided momentum flux and heat flux data, which were used to determine temperature gradients using the Monin-Obukhov-Similarity-Theory [4].

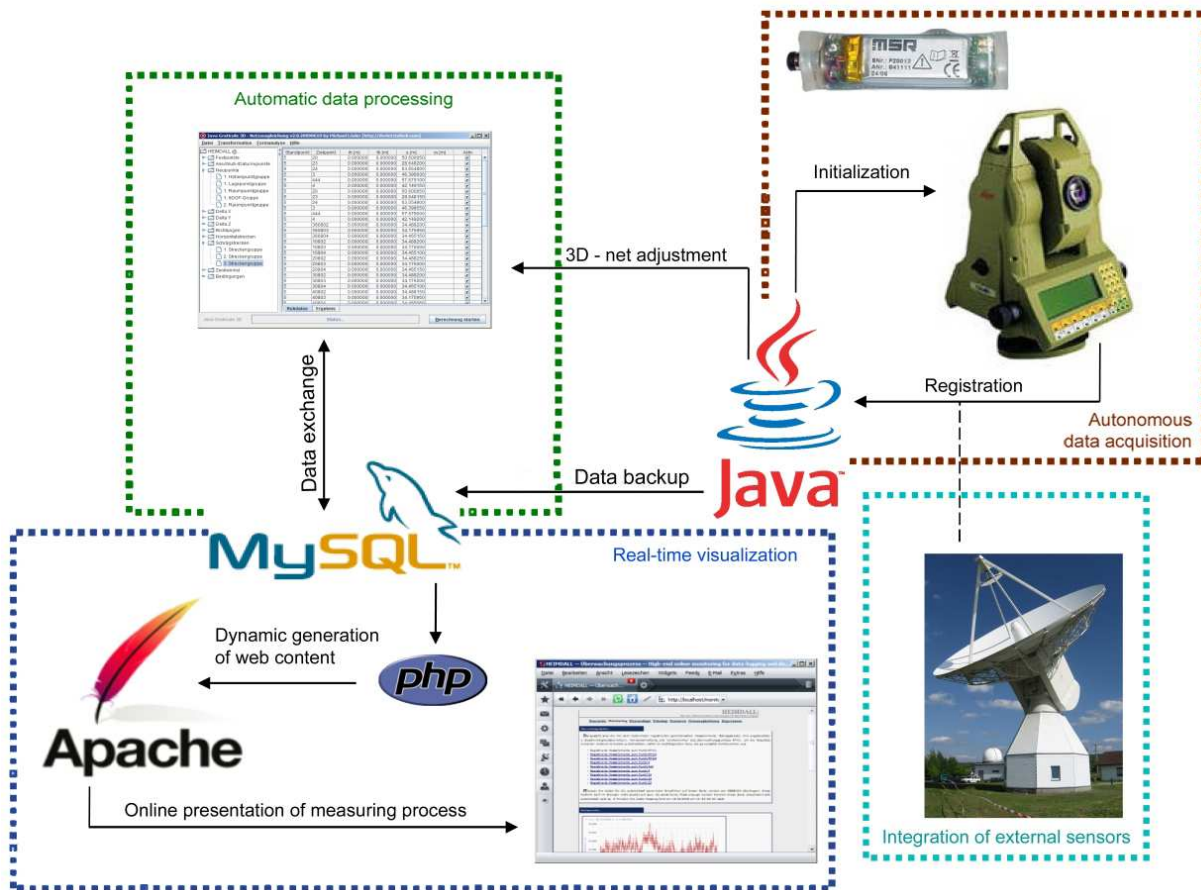


Figure 1. Scheme of the used monitoring system HEIMDALL.

3. The Observing Concept

The observation time was three months total, from mid-May to mid-August 2009. As the geometric reference point, which is the intersection of the azimuth and elevation axes, is not directly accessible, very small, externally mounted reflectors on the outside of the elevation cabin were installed. With this rigid setup, variations of the reference point can be derived indirectly. The whole net was observed in 15-minute intervals. Seven points of the local surveying net in the area of the observatory offered the stable geometry to observe the five object points on the telescope (see Fig. 2). For a later 3D-adjustment, the tipping axis and reflector heights of the network points were classically identified. To offer the possibility of refraction corrections, a scintillometer was installed permanently during the whole project. The correction is done during the post-processing. A gradient of $1^{\circ}\text{C}/\text{m}$ can cause an apparent uplift of 0.8 mm over a distance of 40 m [3]. This variation can be corrected by the setup. But the derived temperature gradients are used at overall zenith angles, which reduces the effectiveness of this method. The setup was completed by parallelly operated dedicated measurements of declinations with a leveling instrument and distances with a laser tracker.

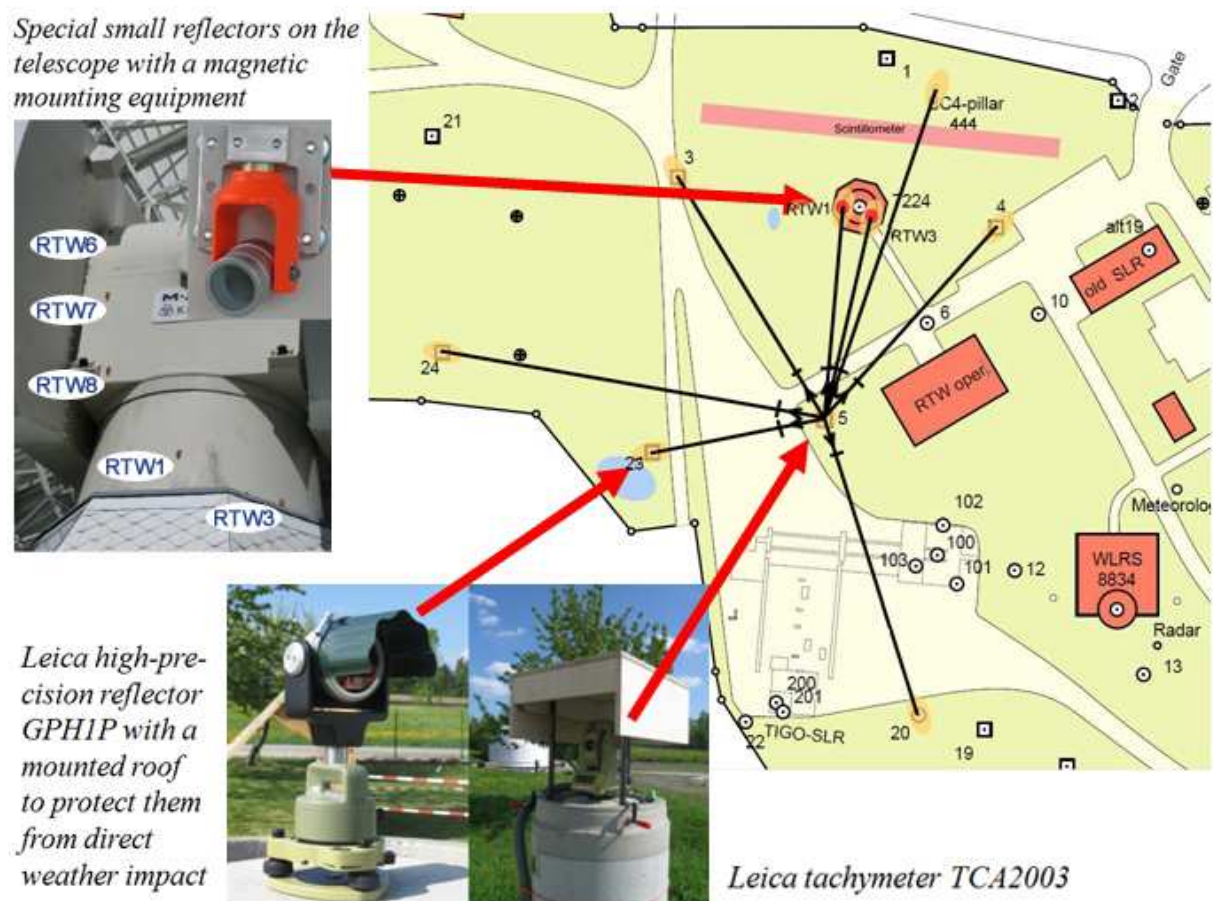


Figure 2. Monitoring network, total station, and reflectors.

4. The Analysis and Results

Changes of the reference point were investigated under different load situations, induced by different elevation positions, using a high-precision tiltmeter “Nivel210”. For these experiments the antenna was moved to ten defined positions in elevation for each of twelve different azimuth angles. At each azimuth position the tilts were registered during the up and down path of the elevation. Additionally the whole experiment was repeated with the tiltmeter at different height positions in the telescope tower. The recorded data show significant deformations depending on the elevation position. This indicates that the reference point changes its position by 0.05 mm between an elevation of 0° and 90° .

Using the adjusted data from the total station measurements, a daily, periodic variation for positions could be derived, which is superposed by a long-term trend. A Fourier analysis allowed the creation of a model for the transfer of the results from the cabin surface to the internally located reference point. It showed that the reference point moves in both axes by about 0.2 mm over a period of one day (see Fig. 3). For a reliable statement about the annual trend a longer observation campaign would be needed.

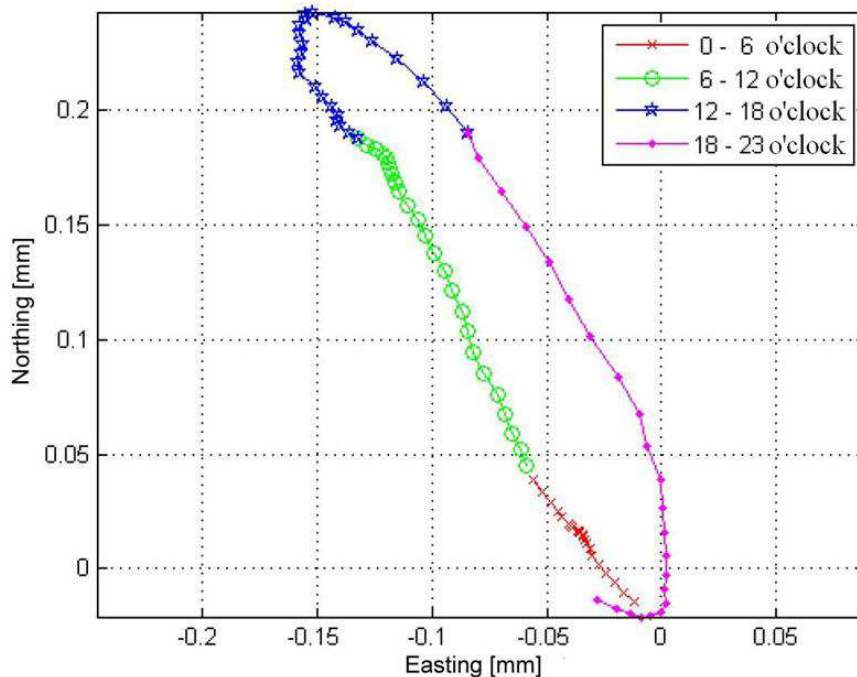


Figure 3. Estimated daily variation of the reference point position.

The permanent measurements at the Geodetic Observatory Wettzell showed that changes in position could be detected for load changes and insolation (temperature changes). Concerning the maximum variations allowed by GGOS of about 0.1 mm [8], the results become more and more relevant. Similar to the used height correction, the usage of derived mapping functions could possibly increase the reliability of VLBI results. Therefore future research on that point is strongly recommended.

5. Conclusion

A major requirement for the telescopes of the VLBI2010 project is a permanent monitoring of relevant system parameters [6]. With HEIMDALL a proof-of-concept test for a possible reference point monitoring system was shown¹. The derived time series showed an impressive stability of the reference point of the 20m radio telescope Wettzell. But to evaluate also the long-term stability, longer lasting monitoring series should be conducted.

References

- [1] Altamimi, Z., Collilieux, X., Legrand, J., Garayt, B., Boucher, C., ITRF2005: A new release of the International Terrestrial Reference Frame based on time series of station positions and Earth Orientation Parameters, *J. Geophys. Res.*, 112, 1–19, 2007.
- [2] Golther, W., *Handbuch der Germanischen Mythologie*, Marix Verlag GmbH, 2004.
- [3] Eschelbach, C., Störanfälligkeit geodätischer Präzisionsmessungen durch lokale Temperaturschwankungen, In: *Beiträge zum 15. Internationalen Ingenieurvermessungskurs*, F. Brunner (ed.), 169–180, 2007.
- [4] Eschelbach, C., Refraktionskorrekturbestimmung durch Modellierung des Impuls- und Wärmeflusses in der Rauigkeitsschicht, Bayer. Akademie d. Wissenschaften, DGK, Reihe C, 635, 2009.
- [5] Loesler, M., Eschelbach, C., Schenk, A., Neidhardt, A., Permanentüberwachung des 20 m VLBI-Radioteleskops an der Fundamentalstation in Wettzell, *ZfV*, 1, 40–48, 2010.
- [6] Niell, A., Whitney, A., Petrachenko, B., Schlüter, W., Vandenberg, N., Hase, H., Koyama, Y., Ma, C., Schuh, H., Tuccari, G., VLBI2010: Current and Future Requirements for Geodetic VLBI Systems, In: *IVS Annual Report 2005*, NASA, D. Behrend and K. Baver (eds.), 13–40, 2006.
- [7] Nothnagel, A., Conventions on thermal expansion modelling of radio telescopes for geodetic and astrometric VLBI, *J. Geod.*, 83, 787–792, 2009.
- [8] Rothacher, M., Beutler, G., Bosch, W., Donnellan, A., Gross, R., Hinderer, J., Ma, C., Pearlman, M., Plag, H.-P., Richter, B., Ries, J., Schuh, H., Seitz, F., Shum, C.K., Smith, D.; Thomas, M., Velacogna, E., Wahr, J., Willis, P., Woodworth, P., The future Global Geodetic Observing System (GGOS), In: *The Global Geodetic Observing System. Meeting the Requirements of a Global Society on a Changing Planet in 2020*, Springer-Verlag, H.-P. Plag and M. Pearlman (eds.), 2009.
- [9] Wresnik, J., Haas, R., Boehm, J., Schuh, H., Modeling thermal deformation of VLBI antennas with a new temperature model, *J. Geod.*, 81, 423–431, 2007.

¹Acknowledgments

We thank the Bundesamt für Kartographie und Geodäsie Wettzell for supporting this project. We are especially thankful for the manual control and maintenance of the equipment during the whole project period by Swetlana Mähler.

Proof-of-Concept Studies for a Local Tie Monitoring System

*Benno Schmeing*¹, *Dirk Behrend*², *John Gipson*², *Axel Nothnagel*¹

¹) *University of Bonn*

²) *NVI, Inc./NASA Goddard Space Flight Center*

Contact author: *Dirk Behrend*, e-mail: Dirk.Behrend@nasa.gov

Abstract

We present preliminary results of proof-of-concept studies for an automatic monitoring system of local site ties. The system is based on the usage of robotic total stations. A set of tests were performed with a Leica TCA2003 total station on the local network of Goddard's Geophysical and Astronomical Observatory (GGAO) and the 5-m VLBI antenna at this site. Both the TCA2003 and the VLBI antenna are controlled from a Matlab-coded control program. Running specific observational programs, data were collected that indicate that the reference point of the VLBI antenna can be automatically determined with an accuracy of 1 mm or better.

1. Introduction

Monitoring the local ties between different techniques at co-located sites is an important task for the Global Geodetic Observing System (GGOS). In order to be able to combine the various space geodetic techniques, local site ties need to be known with high accuracy. Since the GGOS accuracy goal is 1 mm (and 0.1 mm/yr), the tie needs to be known at least at this level of accuracy, probably better. Hence, it is necessary to monitor the position and the stability of the invariant reference point (IVP) of the different techniques and to determine the local ties between them. To date, this task has been done by manual measurements, which are costly in terms of time and manpower. The surveys need to be repeated on a regular basis (e.g., semi-annually or annually).

In this paper we address the prospects of an automatic monitoring system to replace manual measurements. The system is based on robotic total stations. These instruments constitute a proven technology that is capable of providing the required high accuracy at a relatively low cost. A demonstration system was set up at the Goddard Geophysical and Astronomical Observatory (GGAO) for the 5-m Very Long Baseline Interferometry (VLBI) antenna there.

2. Location and Equipment

The local site at GGAO features the four geodetic techniques of VLBI, GPS, Satellite Laser Ranging (SLR), and Doppler Orbitography and Radio-positioning Integrated by Satellite (DORIS). The different sensors are connected by a local geodetic network consisting of several survey monuments. Figure 1 shows the 5-m VLBI antenna (MV-3) at GGAO and the local surveying network in its vicinity.

The survey equipment for the proof-of-concept studies were based on a robotic total station Leica TCA2003 and a Trimble 606 360°-mini-prism, which was mounted on the VLBI antenna. Unlike standard prisms, the 360°-mini-prism does not need to be oriented towards the total station. However, as the 360°-mini-prism consists of seven individual prisms arranged in a full circle, the

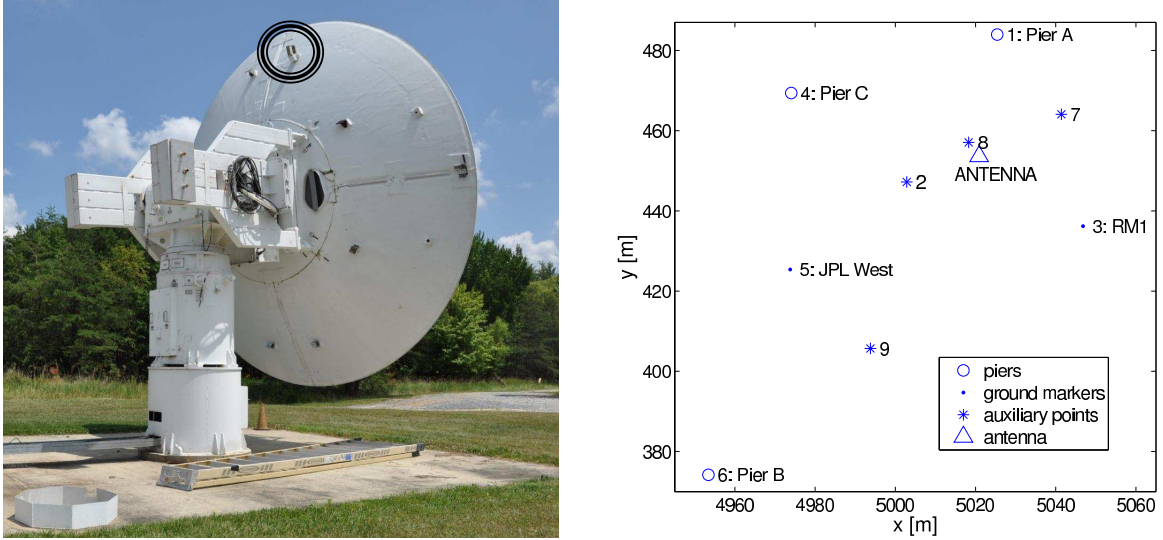


Figure 1. (left) The 5-m VLBI antenna (MV-3) at Goddard Geophysical and Astronomical Observatory (GGAO). The black circles indicate the location where the 360°-mini-prism was mounted. (right) The local surveying network around GGAO’s 5-m VLBI telescope.

mini-prism’s reference point may change depending on its orientation with respect to the instrument. Hence, the mini-prism requires a correction which is dependent on the angle of incidence. In a calibration survey the mini-prism was rotated around its vertical axis in small steps, and the total station measured changes in the reference point. A correction is then determined based on the orientation of the mini-prism with respect to the “zero reference direction” (marked by a white arrow). Figure 2 shows the distance variations when rotating the 360°-mini-prism. The effect of the seven individual prisms within the mini-prism is clearly discernible.

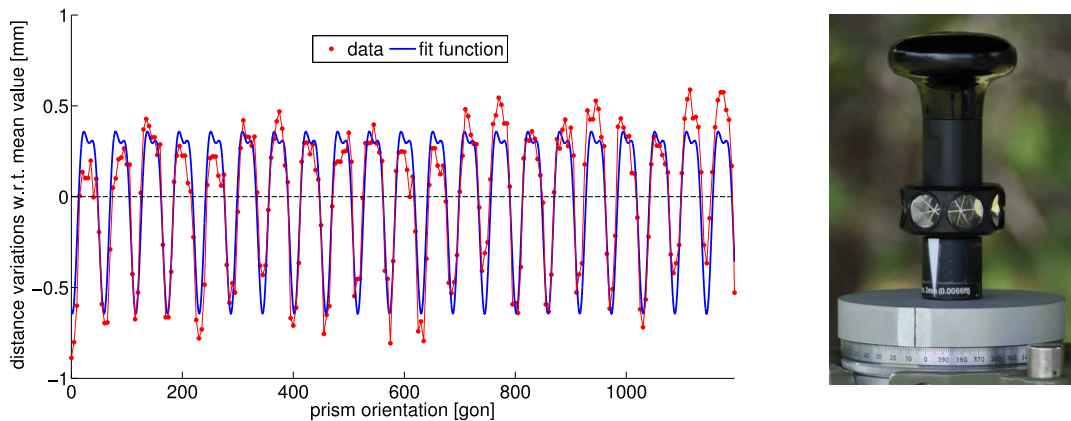


Figure 2. Results of the calibration of the 360°-mini-prism. A double *cos* base function was fitted to the real data. Depicted are three full circles (1200 gon).

Since the calibration can be done only for angles of incidence orthogonal to the vertical axis of

the mini-prism, a limit is put on the degrees of freedom for the movement of the VLBI antenna for each instrument position. The VLBI antenna can only be moved such that the 360°-mini-prism mounted on the antenna describes motion paths with the line-of-sight always being orthogonal to the mini-prism's vertical axis.

3. Simulations and Preliminary Results

The literature basically describes two techniques for the determination of the invariant point (IVP) of a VLBI telescope. The conventional surveying approach involves circle fitting for the positions of markers mounted on the telescope structure as the antenna moves (e.g., Dawson et al. 2007). The survey procedure has to ensure that the markers trace a reasonable portion of a circle in space. The center points of the circles coincide with the IVP. A newer approach, suggested by Lösler (2008), moves away from the geometrical constraints towards a “transformation approach”, where the transformation parameters from an antenna-fixed coordinate system to a local network coordinate system describe the antenna characteristics. This has the advantage that not only the IVP but also other VLBI antenna parameters can be estimated together with their formal errors in a combined solution strategy.

The observation equation of the transformation approach can be written as (Lösler 2008)

$$\begin{bmatrix} x \\ y \\ z \end{bmatrix} = \begin{bmatrix} x_{IVP} \\ y_{IVP} \\ z_{IVP} \end{bmatrix} + R_x(\beta) \cdot R_y(\alpha) \cdot R_z(A + O_A) \cdot R_y(\gamma) \cdot \left(\begin{bmatrix} 0 \\ ecc \\ 0 \end{bmatrix} + R_x(E + O_E) \cdot \begin{bmatrix} a \\ b \\ 0 \end{bmatrix} \right)$$

where the observations are the marker positions x, y, z in the local network system as determined by the total station and the VLBI antenna positions A, E (azimuth and elevation) as given by the VLBI Field System which controls its movements. The unknown parameters are the invariant point $x_{IVP}, y_{IVP}, z_{IVP}$ of the VLBI antenna, the axis offset ecc (eccentricity), the marker positions a, b in the telescope-fixed system, axes non-orthogonality corrections α, β , and an inclination correction γ . In addition, there are two orientation unknowns O_A, O_E . The parameters can be solved for using a least-squares adjustment.

Figure 3 shows the schematics of the planned measurement and analysis procedure. From previous measurements the coordinates and covariances of the local network are known in the local system. From one or several standpoints, measurements (horizontal and vertical angles, slant distances) are taken to orientate the total station into the local system and then to determine positions of the marker on the VLBI antenna in the same system. Using the transformation approach the antenna parameters can then be solved for.

Both the data capturing in the field and the subsequent analysis of the data in the office can be done in an automated fashion. The Leica TCA2003 and the VLBI antenna MV-3 can be controlled from a Matlab-coded control program, which can run predetermined observational sequences. An adjustment program based on the transformation approach was also coded in Matlab.

In order to test the software suite and to check if the target accuracy is attainable, simulations were done using the existing network geometry at GGAO. In a first step, the expected precision of the coordinates of the local geodetic network in the local system was determined. For the total station, an angle accuracy of 0.45 mgon ($= 1.5''$) and a distance accuracy of 1 mm \pm 1 ppm were assumed. Using full sets of measurements between all points of the local network, the analysis package PANDA estimated standard deviations of about 0.2–0.3 mm for the horizontal and of

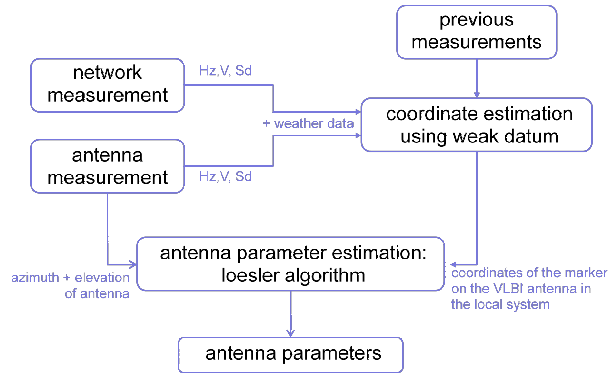


Figure 3. Data flow of the planned measurement and analysis procedure.

about 0.1–0.2 mm for the vertical components.

Using the coordinates and standard deviations previously obtained, measurements from several instrument standpoints to the marker mounted on the telescope were simulated and analyzed. Based on a chosen observation sequence, true measurement values were computed. These values were modified by adding noise based on the instrument and network point accuracies. Then the antenna parameters were estimated using the modified observations and compared to the true values. For each instrument standpoint, the simulated observing schedules had around 60 different azimuth and elevation positions for the VLBI antenna. Table 1 shows the results when using a single instrument standpoint only and when using four instrument standpoints in a combined solution. The formal errors are at the sub-mm level clearly fulfilling the 1-mm target. The line-of-sight dominance visible in the single standpoint solution (in the direction of the x_{IVP} component) vanishes in the combined solution.

Table 1. Simulation results for a single instrument standpoint (left) and for a combined solution using four instrument standpoints (right). The error estimates stem from 200 simulation runs. The true error is the difference between the known parameter value and the estimated value. Listed are the mean values from the 200 repetitions, where the true error is averaged over the absolute values.

<i>Instrument standpoint: 4</i>			<i>Instrument standpoints: 1,3,4,5</i>		
Parameter	True error	Formal error	Parameter	True error	Formal error
x_{IVP}	0.15 mm	0.18 mm	x_{IVP}	0.04 mm	0.05 mm
y_{IVP}	0.08 mm	0.10 mm	y_{IVP}	0.04 mm	0.05 mm
z_{IVP}	0.14 mm	0.17 mm	z_{IVP}	0.06 mm	0.08 mm
axis offset	0.13 mm	0.16 mm	axis offset	0.06 mm	0.08 mm

Following the successful simulation results, a local network measurement campaign was observed on 13 August 2009 and a first set of VLBI antenna observations from four standpoints on 2 September 2009. The analysis of the local network campaign, however, revealed anomalies in the measured data. A comparison of direction measurements between faces I and II showed differences in the range of -25 to 15 mgon, which is significantly higher than the instrument accuracy. We have been unable to identify the reason. Further, a network analysis with PANDA only

yielded consistent results after deleting about 15% of the observations. Such a high outlier rate is not expected given the quality of the total station. These inconsistencies need to be investigated further.

For a preliminary check of the VLBI antenna observations, only approximate coordinates were used for the network points, and each instrument standpoint was considered independently. Thus, we determined four different sets of antenna parameters in slightly different reference frames. It is, however, possible to compare reference frame independent parameters such as the axis offset. Table 2 compiles the four results for the axis offset and its standard deviation.

Table 2. Axis offset parameter and its standard deviation as obtained from four independent determinations.

Standpoint	ecc	σ_{ecc}
#1	0.19 mm	0.23 mm
#3	0.20 mm	0.18 mm
#4	0.15 mm	0.18 mm
#5	0.12 mm	0.18 mm

The independent determinations of the axis offset are consistent within their error estimates. The formal errors are only slightly worse than in the simulation. The formal errors for the IVP coordinates are worse by a factor of 2–3 but can still be considered satisfactory.

4. Conclusions and Future Work

As a first step towards an automatic monitoring system for local site ties using robotic total stations, an automatic measurement procedure was developed. Both the total station and the VLBI antenna can be controlled from a Matlab-coded control program. Running specific observational programs, data was collected that indicate that the reference point of the VLBI antenna can be automatically determined with an accuracy of 1 mm or better. However, anomalies in the combination of the results from different standpoints of the total station require further investigation.

In addition to finding the reason for the data inconsistencies, future work will include the verification of results (e.g., repetition of measurements), improvement of the marker and mounting (e.g., replacement of 360° prism with a reflective target sphere, mounting the marker at different positions on the VLBI antenna structure), and applying the approach to the SLR systems at GGAO.

References

- [1] Dawson, J., et al., Indirect approach to invariant point determination for SLR and VLBI systems: an assessment, *Journal of Geodesy*, Vol. 81, 6–8, 433–441, 2007.
- [2] Lösler, M., Reference point determination with a new mathematical model at the 20 m VLBI radio telescope in Wettzell, *Journal of Applied Geodesy*, 233–238, 2008.

Ultra-rapid dUT1 Measurements on Japan-Fennoscandian Baselines – Application to 24-hour Sessions

Shigeru Matsuzaka¹, Shinobu Kurihara¹, Mamoru Sekido², Thomas Hobiger²,
Rüdiger Haas³, Jouko Ritakari⁴, Jan Wagner⁴

¹⁾ *Geospatial Information Authority of Japan (GSI), formerly Geographical Survey Institute*

²⁾ *National Institute of Information and Communications Technology (NICT), Japan*

³⁾ *Chalmers University of Technology*

⁴⁾ *Helsinki University of Technology*

Contact author: Shigeru Matsuzaka, e-mail: shigeru@gsi.go.jp

Abstract

GSI, NICT, OSO, and MRO have been engaged in Ultra-rapid dUT1 experiments since 2007 aiming at the technological possibility of real-time dUT1 results using the e-VLBI technique. We have already successfully determined dUT1 in less than four minutes after the end of an experimental Intensive session in 2008, and at present we routinely get the results within 30 minutes for regular Intensives. In 2009 we applied the technique to 24-hour sessions and continuously obtained dUT1 values by processing and analyzing Tsukuba–Onsala data in near real-time. It showed a detailed behavior of UT1 variations, which could be very valuable for scientific study as well as for precise prediction of UT1-UTC.

1. Introduction

In 2008, GSI, NICT, Onsala Space Observatory (OSO), and Metsähovi Radio Observatory (MRO) achieved almost real-time UT1 measurements by utilizing fast network connection, software correlator and automatic analysis, and in particular obtained dUT1 in less than four minutes after the session on the Tsukuba–Onsala baseline in February 2008 [1]. In our continuing efforts we applied the method to regular 24-hour VLBI sessions to obtain a series of UT1 values for the whole experiment. We report here the outline of our experiments and the results.

2. Ultra-rapid Intensives

After the success of ultra-rapid measurement in the experimental Intensive sessions, we have arranged to apply it to regular Intensive sessions. As of early 2010, the INT2 sessions, which observe the baseline Tsukuba–Wettzell, are routinely executed as ultra-rapid sessions. Table 1 shows the status as of February 2010 of the Intensive sessions in terms of data-transfer and latency of results.

3. Ultra-rapid 24-hour Sessions

In applying our method to 24-hour experiments, we chose the sessions in which both Tsukuba and Onsala were participating. Figure 1 is a schematic diagram of 24-hour ultra-rapid data processing. Basically the same set-up as for the Intensives [2] was adapted; only, some modifications of data handling scripts and analysis strategy were done.

Table 1. Present Status (February 2010) of IVS Intensive Sessions.

Session	Data transfer	Latency	Stations	Correlator
INT1	Physical shipment	3-5 days	Kooke Wettzell	Washington
INT2	Network Quasi real-time	30 minutes	Tsukuba Wettzell	Tsukuba
INT3	Network Post observation	Few hours	Tsukuba Wettzell Ny-Ålesund	Bonn

The observed data (common to both Onsala and Tsukuba) from Onsala are e-transferred in real-time to GSI at Tsukuba. The Onsala data are converted in near real-time from Mark 5 to K5 format and correlated, and a VLBI database is created. Analysis is executed once 35 good scans have been accumulated in the database, and dUT1 is estimated automatically. The process is repeated so that the analysis is always on the latest 35 scans with each new scan in and the oldest one out. Each result is e-mailed to relevant addresses.

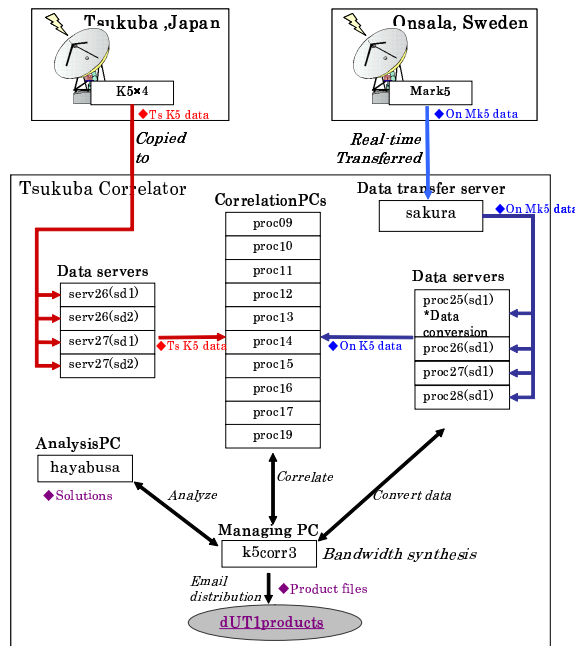


Figure 1. Data transfer and processing for a 24-hour session.

4. Experiments and Results

We conducted six experiments from June 2009 through early 2010. Figure 2 shows the ultra-rapid results from three sessions (R1409, RD0910, and R1413) plotted with USNO finals. The

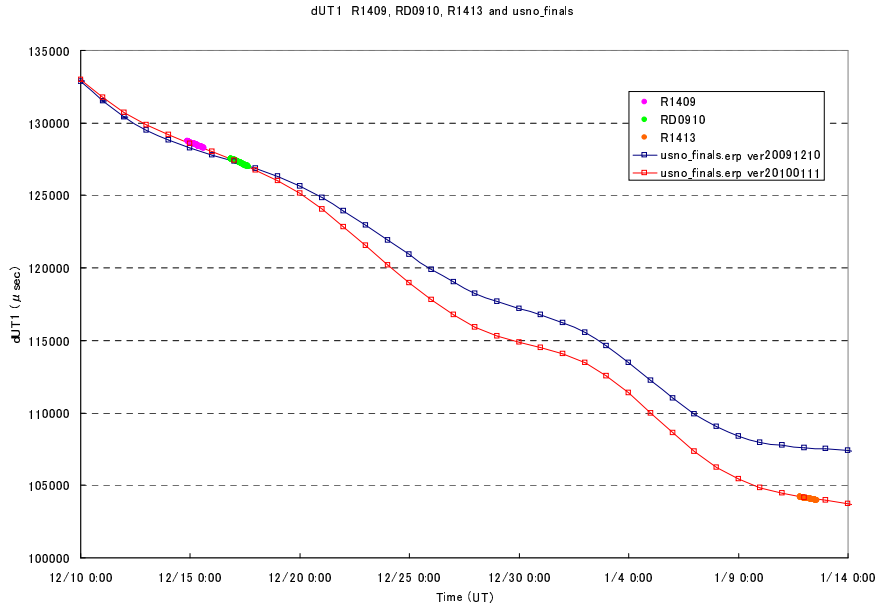


Figure 2. Ultra-rapid results, December 10 – January 14, comparison with USNO finals.

dUT1 results follow well the curve of USNO final values at 20100111.

As an example, for the R1413 session (Jan. 11–12), we e-transferred and processed the following data:

of channels: S:6, X(USB):8, X(LSB):2

Sampling rate: 16 Mbps/ch, 256 Mbps in total

of scans: Tsukuba: 514, Onsala: 425 (common to both: 194)

In this session, the processing started about nine hours after the start, and in the latter half of the experiment we could catch up with the observation and get dUT1s within 20 minutes after the latest scan with formal errors of $\sim 10 \mu\text{s}$ (Figures 4 and 5).

As predicted dUT1 values tend to diverge from the actual final values in as short as a day, ultra-rapid results could put constraints to improve the prediction (see Figures 3–5). These figures also suggest that our results successfully captured the details of short-term variations of dUT1 around the averaged final values. From a scientific point-of-view, sub-daily, continuous dUT1 values offer valuable data for the study of earth rotation and dynamics.

5. Conclusions and Future Prospects

We successfully demonstrated continuous, near real-time dUT1 measurements for 24 hour sessions. If we expanded our network to include north-south baselines, it would enable a real-time determination of polar motion parameters, and one of the goals of VLBI2010—continuous EOP determination—would be well within our reach using current technologies.

For scientific studies, the short-term variation of dUT1 would be a very valuable piece of information in the study of earth dynamics. For practical purposes, the prediction of dUT1 can

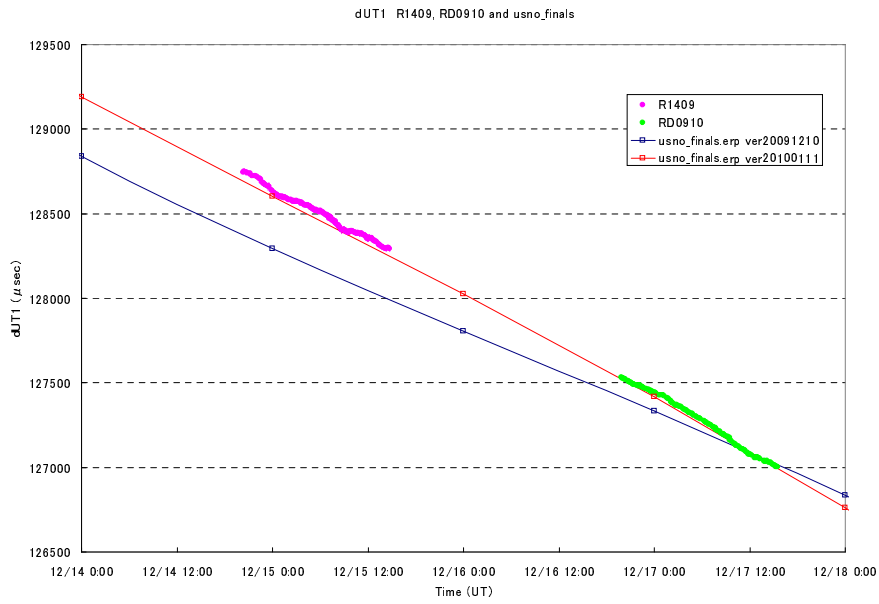


Figure 3. Detailed view of Figure 2 for December 14–18.

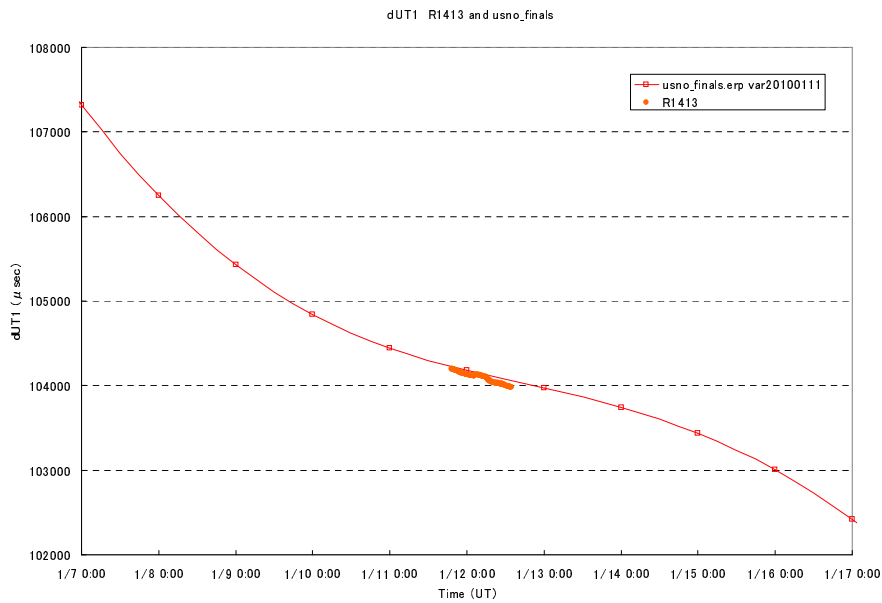


Figure 4. Ultra-rapid results, January 11–12.

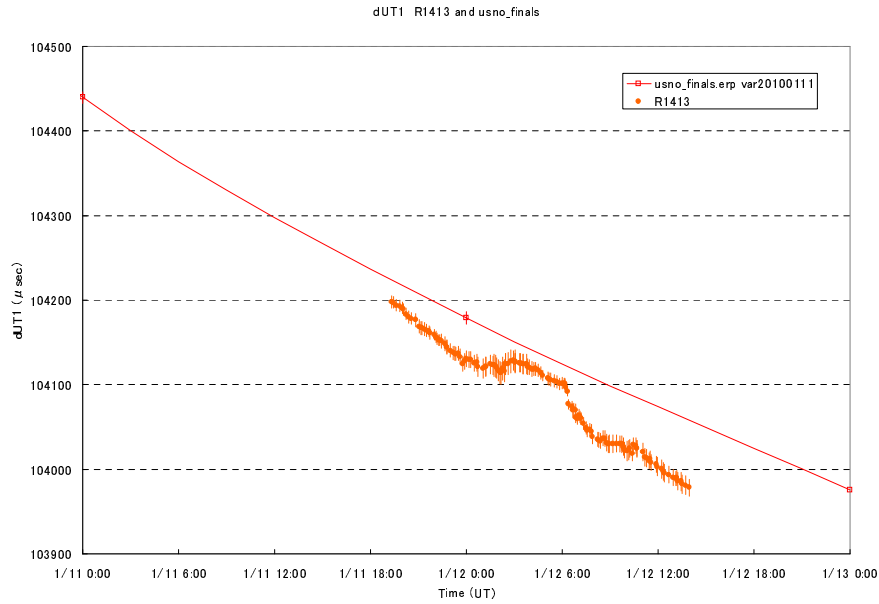


Figure 5. Detailed view of Figure 4 for January 11–12.

be improved with the consideration of continuous values.

References

- [1] Matsuzaka, S., H. Shigematsu, S. Kurihara, M. Machida, K. Kokado, D. Tanimoto, Ultra Rapid UT1 Experiment with e-VLBI, In: *Measuring the Future, Proceedings of the Fifth IVS General Meeting*, A. Finkelstein and D. Behrend (eds.), 68–71, 2008.
- [2] Koyama, Y., M. Sekido, T. Hobiger, H. Takiguchi, T. Kondo, Developments of Automated Data Processing System for Ultra Rapid dUT1 e-VLBI Sessions, In: *Measuring the Future, Proceedings of the Fifth IVS General Meeting*, A. Finkelstein and D. Behrend (eds.), 405–409, 2008.

The “Quasar” Network Observations in e-VLBI Mode Within the Russian Domestic VLBI Programs

*Andrey Finkelstein, Alexander Ipatov, Michael Kaidanovsky, Ilia Bezrukov,
Andrey Mikhailov, Alexander Salnikov, Igor Surkis, Elena Skurikhina*

Institute of Applied Astronomy of RAS

Contact author: Alexander Salnikov, e-mail: ais@ipa.nw.ru

Abstract

The purpose of the Russian VLBI “Quasar” Network is to carry out astrometrical and geodynamical investigations. Since 2006 purely domestic observational programs with data processing at the IAA correlator have been carried out. To maintain these geodynamical programs e-VLBI technology is being developed and tested. This paper describes the IAA activity of developing a real-time VLBI system using high-speed digital communication links.

1. Introduction

At this point, all observatories of the “Quasar” Network are equipped with UNIX servers for data buffering. The observatories have “last mile” communication channels plus Internet connection at a rate of 100 Mbps. Some experiments have been made for transmission of Intensive VLBI session data from Svetloe, Badary, and Zelenchukskaya observatories to the Institute of Applied Astronomy of the Russian Academy of Sciences (IAA) Control and Processing Center. Intensive session data of ~ 40 Gbytes have been transmitted at 50 Mbps rate over shared networks using the Tsunami-UDP protocol in near real-time e-VLBI mode.

To date, 22 Intensive sessions have been transmitted from the Zelenchukskaya and Badary observatories and two Intensive sessions from the Svetloe and Badary observatories to the IAA Control and Processing Center. The transmitted data were processed at the IAA Analysis Center to obtain corrections to UT1. The values of the UT1 corrections obtained from all sessions are in the 1–160 μ s range with an RMS deviation of about 61 μ s.

2. Detailed Status

Institute of Applied Astronomy (IAA) of the Russian Academy of Sciences performs regular observations on the “Quasar” Network (Figure 1) within international and domestic programs. There are two types of VLBI domestic observational sessions: the 24-hour Ru-E series for EOP determination and the 1-hour Ru-U sessions for UT1 evaluation in near real-time mode. Both series are carried out four times per month. All observatories are equipped with Mark 5B recording terminals. The observations are correlated at the IAA Control and Processing Center in Saint Petersburg.

At present all observatories of the VLBI “Quasar” Network are linked by optical fiber lines (Figure 2) to provide both e-VLBI data transfer and real-time remote monitoring of site equipment. The data rate available for both the “last mile” channels and the overall end-to-end Internet

communication is about 100 Mbps. All observatories of the “Quasar” Network are equipped with UNIX servers for additional data buffering.

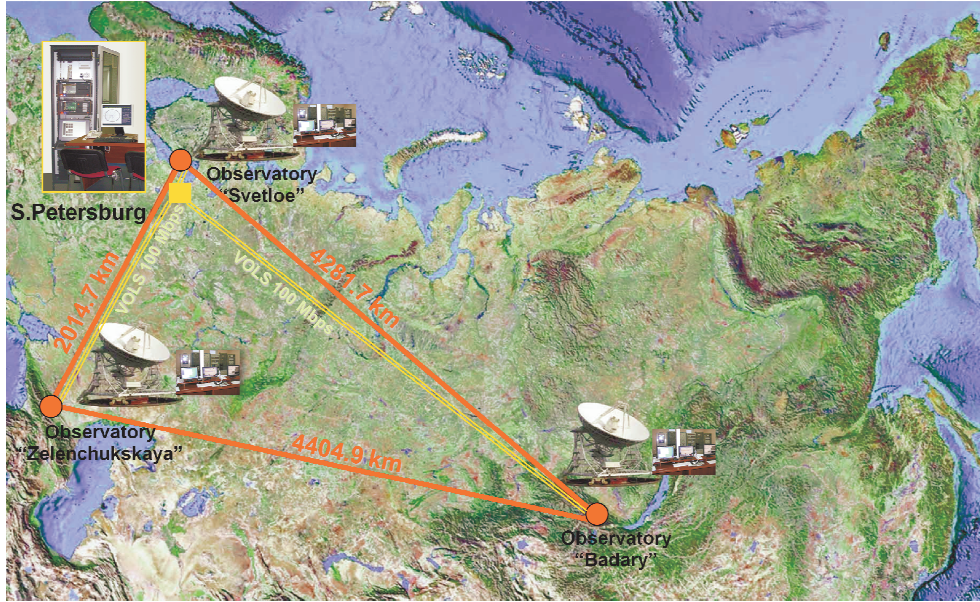


Figure 1. VLBI “Quasar” Network.

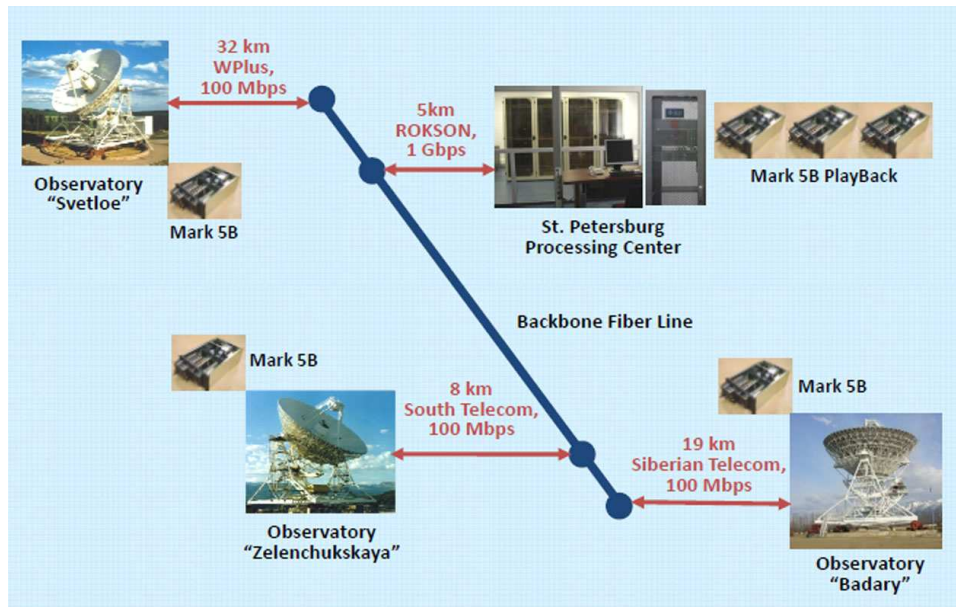


Figure 2. Optical Fiber Lines.

Regular observational sessions for UT1 determination in e-VLBI mode within “Quasar” Network on baselines Svetloe–Badary and Zelenchukskaya–Badary have been carried out since 2009.

The scheme for the data transfer is presented in Figure 3. The data copying from the Mark 5B recorder is performed in breaks between scans while the antenna is slewing to the next source. The “disk2net” function of the Mark 5B software is used for this purpose. Typical 1-hour sessions recorded at 256 Mbps rate contain 20–22 scans with a total data size of about 40 GB. A session may be transmitted at 40–50 Mbps rate over shared networks using the Tsunami-UDP protocol.

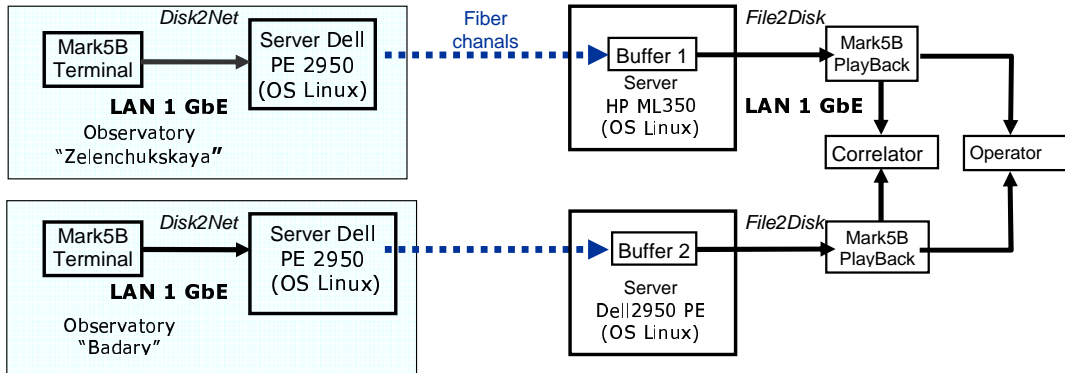


Figure 3. Block scheme of data transmission within e-VLBI mode with buffering: Mark 5B, LAN, Buffering Server, Internet, Buffering Server, LAN, Mark 5B, Correlator. Network testing was realized with iperf (end-to-end).

Time diagrams of single scan transmission via the Internet are presented in Figures 4, 5, and 6.

To date, 22 e-VLBI Intensive sessions have been transmitted from the Zelenchukskaya and Badary observatories and two sessions from the Svetloe and Badary observatories to the IAA Control and Processing Center. These sessions were processed at the IAA Analysis Center to obtain corrections to UT1. The values of the UT1 corrections obtained from all sessions are in the 1–160 μ s range with an RMS deviation of about 61 μ s.

The differences between the UT1 values obtained from all real-time IAA Ru-U sessions and those of the EOP 05 C04 series are given in Figure 7.

The results achieved show the possibility of successful periodic e-VLBI observations via shared Internet channels from all observatories of the “Quasar” Network.

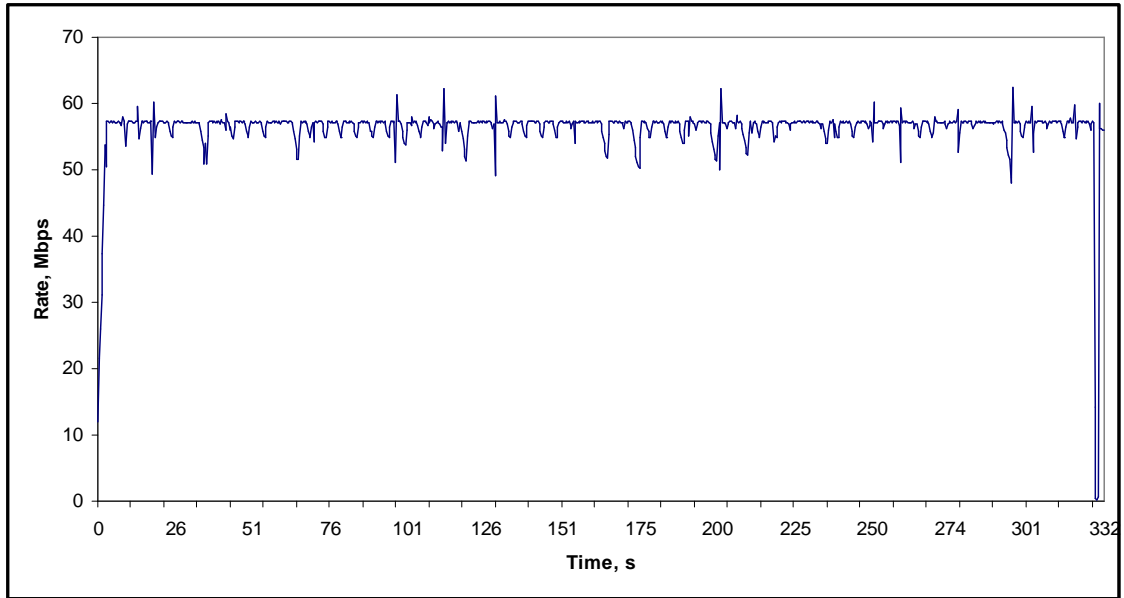


Figure 4. Time diagram of single scan transmission through ISP “South Telecom” at a rate of 100 Mbps from the Zelenchukskaya Observatory to the IAA Control and Processing Center in St. Petersburg. Rate 50 Mbps. Scan size 2 Gbytes. Tsunami-UDP protocol.

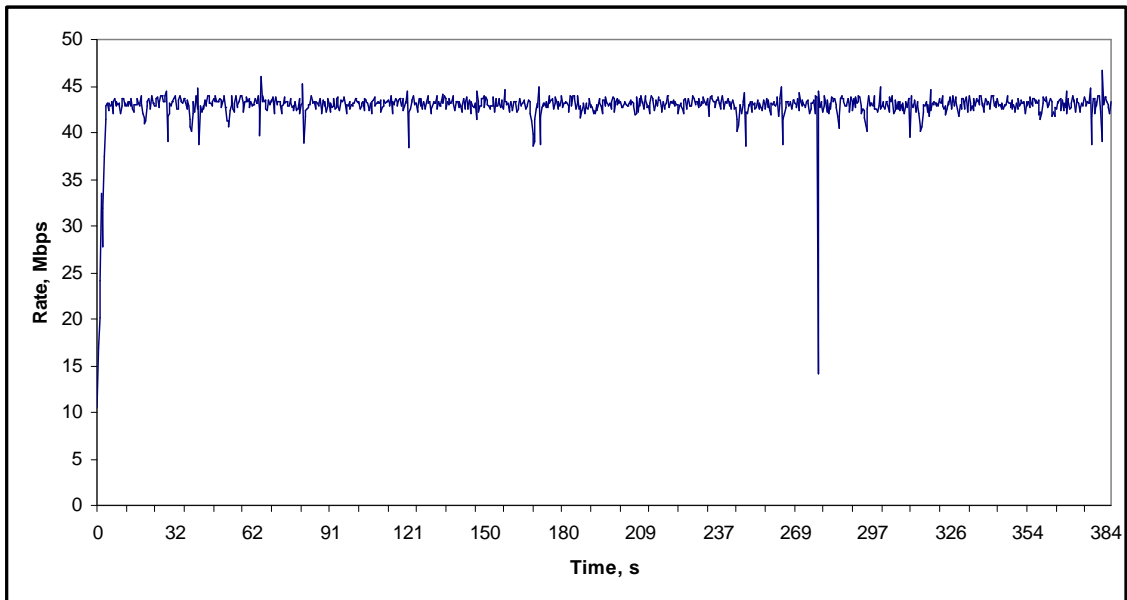


Figure 5. Time diagram of single scan transmission through ISP “Siberian Telecom” at a rate of 100 Mbps from the Badary Observatory to the IAA Control and Processing Center in St. Petersburg. Rate 40 Mbps. Scan size 2 Gbytes. Tsunami-UDP protocol.

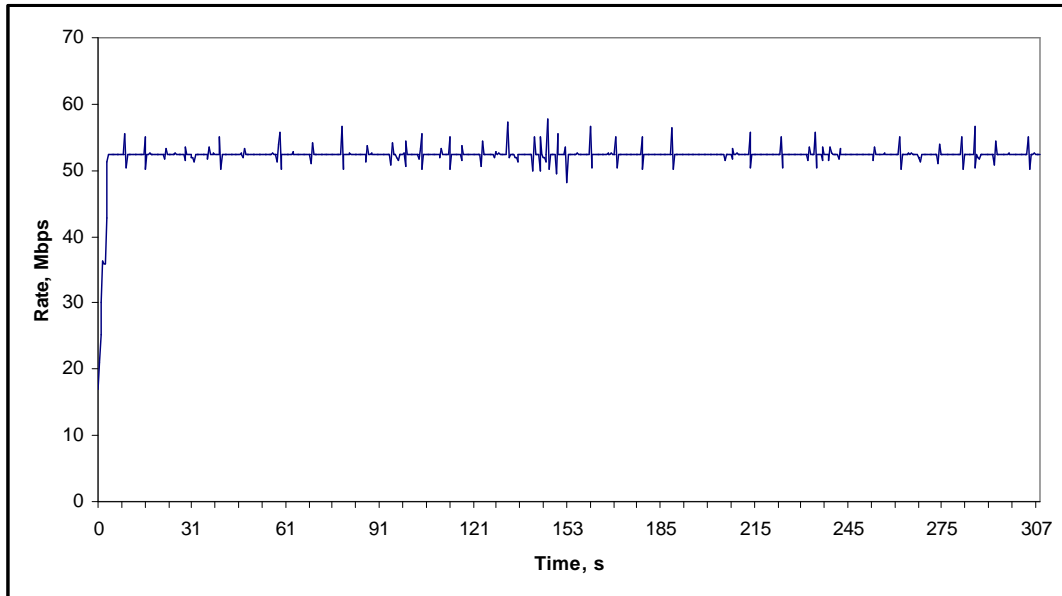


Figure 6. Time diagram of single scan transmission through ISP “WebPlus” (100 Mbps) from Svetloe Observatory to the IAA Control and Processing Center St. Petersburg. Rate 50 Mbps. Scan size 2 Gbytes. Tsunami-UDP protocol.

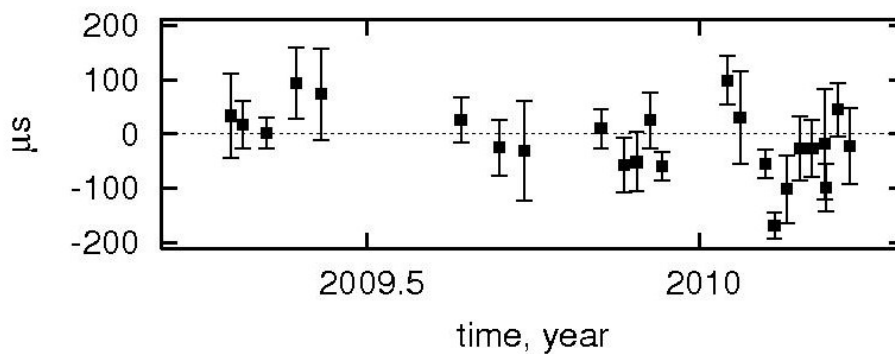


Figure 7. $UT1(IAA) - UT1(EOP\ 05\ C04)$ for 24 e-VLBI sessions.

Implementation and Testing of VLBI Software Correlation at the USNO

Alan Fey¹, Roopesh Ojha², Dave Boboltz¹, Nicole Geiger¹, Kerry Kingham¹,
David Hall¹, Ralph Gaume¹, Ken Johnston¹

¹) *U.S. Naval Observatory*

²) *NVI, Inc./U.S. Naval Observatory*

Contact author: Alan Fey, e-mail: afey@usno.navy.mil

Abstract

The Washington Correlator (WACO) at the U.S. Naval Observatory (USNO) is a dedicated VLBI processor based on dedicated hardware of ASIC design. The WACO is currently over 10 years old and is nearing the end of its expected lifetime. Plans for implementation and testing of software correlation at the USNO are currently being considered. The VLBI correlation process is, by its very nature, well suited to a parallelized computing environment. Commercial off-the-shelf computer hardware has advanced in processing power to the point where software correlation is now both economically and technologically feasible. The advantages of software correlation are manifold but include flexibility, scalability, and easy adaptability to changing environments and requirements. We discuss our experience with and plans for use of software correlation at USNO with emphasis on the use of the DiFX software correlator.

1. VLBI at USNO

The U.S. Naval Observatory (USNO) operates the Washington Correlator (WACO) in cooperation with the National Aeronautics and Space Administration (NASA). See § 2 for further details.

USNO supports and operates the International Earth Rotation and Reference Systems Service (IERS) Rapid Service/Prediction Center. The center is the product center of the IERS responsible for providing Earth Orientation Parameters (EOP) on a rapid turnaround basis. This service is primarily intended for real-time users and others needing the highest quality EOP information sooner than is available in the IERS final series (Bulletin B) published by the IERS Earth Orientation Center, which is based at the Observatoire de Paris.

USNO supports and operates an International VLBI Service for Geodesy and Astrometry (IVS) Associate Analysis Center. The primary services provided by the Analysis Center are the analysis of diurnal experiments, the production of periodic global Terrestrial Reference Frame (TRF) and Celestial Reference Frame (CRF) solutions, and the submission to the IVS of Intensive (EOP-I) and session-based (EOP-S) Earth orientation parameters based on USNO global TRF solutions. The USNO VLBI Analysis Center is responsible for the timely analysis of the IVS-R4 experiments, with the resulting databases submitted within 24 hours of correlation for dissemination by the IVS. Analysis Center personnel maintain the necessary software required to continue these services to the IVS including periodic maintenance updates of the Goddard Space Flight Center (GSFC) CALC/SOLVE software package. In addition to operational VLBI analysis, Analysis Center personnel are actively engaged in research related to future reference frames, e-VLBI, and software correlation.

USNO supports and operates an IVS Special Associate Analysis Center for Source Structure. The charter of the Analysis Center is to provide products directly related to the IVS determination of the “definition and maintenance of the celestial reference frame.” These include, primarily, radio frequency images of ICRF sources, intrinsic structure models derived from the radio images, and an assessment of the astrometric quality of the ICRF sources based on their intrinsic structure.

2. The Washington Correlator

The Washington Correlator (WACO) is a Mark IV VLBI correlator designed and constructed by the MIT Haystack Observatory. The WACO is operated and maintained by the Earth Orientation Department of the USNO, in close cooperation with the VLBI Group of NASA’s Space Geodesy Program. The WACO is located in Washington, D.C. on the grounds of the Observatory.

The WACO work load consists of processing five two-station 1-hour Intensive (INT1) experiments per week, one three-station Intensive (INT3) every two weeks, one multi-station 24-hour R4 experiment per week, one to two multi-station 24-hour R1 experiments per year, one to two multi-station T2 experiments per year, approximately 12 CRF experiments per year, and various other miscellaneous experiments (e.g., CONT, APSG, R&D).

3. Why a Software Correlator

The advent of more powerful computers and network connectivity has brought along the possibility of performing the correlation of VLBI data on a distributed network of commercial off-the-shelf (COTS) computers in a purely software-based mode—a so-called software correlator. COTS computer hardware has advanced in processing power to the point where software correlation is now both economically and technologically feasible.

The advantages of software correlation are manyfold but include flexibility, scalability, and easy adaptability to changing environments and requirements. A software correlator can be implemented with COTS personal computers with as few or as many CPUs as required for the job. Software correlators are robust w.r.t. failure of individual CPUs, the software is easily adaptable to changing requirements, and there can be multiple instances at geographically different locations for back-up and continuity of operations (CoOp).

4. The DiFX Software Correlator

The DiFX software correlator was developed at Swinburne University in Australia [1]. It was designed to run in a cluster computing environment. Parallel processing is fully enabled. DiFX supports VLBA, Mark 5, K5, and various other input data formats. Geometric model calculation is done using the GSFC CALC software. DiFX currently outputs data in a proprietary format which can easily be converted to FITS-IDI format.

5. Current Setup at USNO

During the 2009 calendar year, USNO personnel began implementation and testing of the DiFX software correlator. USNO currently has a small cluster of five multi-core machines on which the software correlator is implemented. The heterogeneous cluster of off-the-shelf personal computers

consists of one dual Quad-Core Xeon (8 CPUs) and four Core 2 duo (eight CPUs) machines running a 32-bit Linux operating system with 2 TB of hard drive storage and Gigabit ethernet links. Post-correlation calibration is currently being performed within the Astronomical Image Processing System (AIPS) and the database production and analysis within CALC/SOLVE.

6. Preliminary Results

Figure 1 shows values of UT1–UTC compared to IERS C04-05 from a dedicated series of 2-hour “pseudo-Intensive” experiments obtained using two radio telescopes (located at Mauna Kea, HI and St. Croix, VI) of the Very Long Baseline Array (VLBA) which is operated by the National Radio Astronomy Observatory (NRAO). The data were correlated at USNO using the DiFX software correlator and subsequently processed using AIPS and CALC/SOLVE. As can be seen in Figure 1 the agreement with the operational EOPI and EOPS series is quite good. Additional testing of DiFX for USNO operational use is currently underway.

7. Future Plans

The preliminary timeline (listed with decision dates) for software correlator implementation at USNO is as follows:

- Preliminary design review - October 2010
- Critical design review - July 2011
 - Design finalized / procure hardware
- Side-by-side operation with WACO - October 2011
 - Daily comparison of results for ≈ 1 year
 - Checking for robustness
 - Checking for reliability
 - Additional software development as required
- Software correlator operations - October 2012

References

- [1] Deller, A. T., Tingay, S. J., Bailes, M., & West, C., DiFX: A Software Correlator for Very Long Baseline Interferometry Using Multiprocessor Computing Environments, PASP, Volume 119, Issue 853, pp. 318-336, 2007.

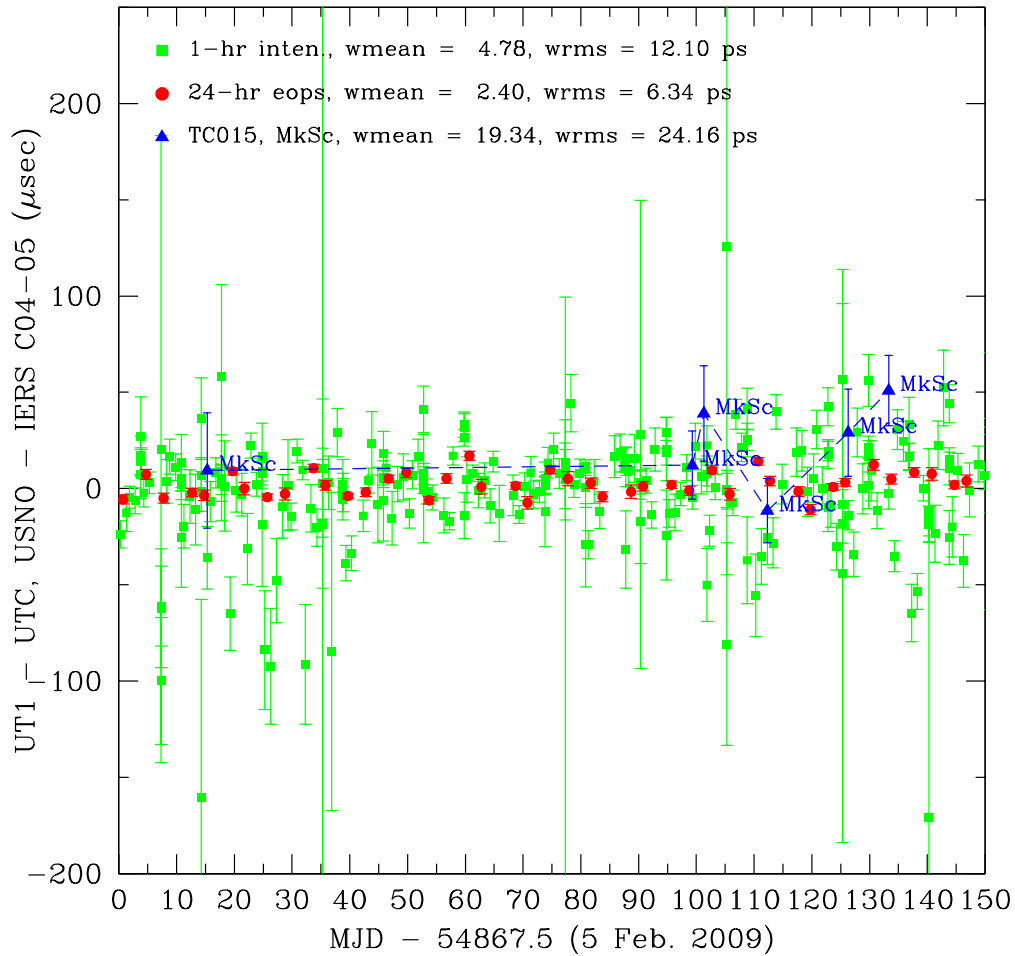


Figure 1. USNO time series of UT1–UTC compared to IERS C04-05. The green squares represent the EOPI series from the IVS 1-hour Intensive experiments, the red circles represent the EOPS series from the IVS 24-hour R1/R4 experiments, and the blue triangles represent values from a dedicated series of 2-hour “pseudo-Intensive” experiments obtained using two radio telescopes (Mauna Kea, HI and St. Croix, VI) of the VLBA.

The Software Correlator of the Chinese VLBI Network

Weimin Zheng, Ying Quan, Fengchun Shu, Zhong Chen, Shanshan Chen, Weihua Wang,
Guangli Wang

VLBI Department, Shanghai Astronomical Observatory, CAS, P.R.China

Contact author: Weimin Zheng, e-mail: zhwm@shao.ac.cn

Abstract

The software correlator of the Chinese VLBI Network (CVN) has played an irreplaceable role in the CVN routine data processing, e.g., in the Chinese lunar exploration project. This correlator will be upgraded to process geodetic and astronomical observation data. In the future, with several new stations joining the network, CVN will carry out crustal movement observations, quick UT1 measurements, astrophysical observations, and deep space exploration activities. For the geodetic or astronomical observations, we need a wide-band 10-station correlator. For spacecraft tracking, a real-time and highly reliable correlator is essential. To meet the scientific and navigation requirements of CVN, two parallel software correlators in the multiprocessor environments are under development. A high speed, 10-station prototype correlator using the mixed Pthreads and MPI (Message Passing Interface) parallel algorithm on a computer cluster platform is being developed. Another real-time software correlator for spacecraft tracking adopts the thread-parallel technology, and it runs on the SMP (Symmetric Multiple Processor) servers. Both correlators have the characteristic of flexible structure and scalability.

1. Introduction

At present, the Chinese VLBI network (CVN) consists of four stations (Shanghai, Yunnan, Urumqi, and Beijing) and one data processing center at Shanghai Astronomical Observatory (Figure 1). CVN has successfully been used in the Chinese lunar exploration project (Chang'E) to track the CE-1 lunar probe. It will join the subsequent Chinese lunar and Martian exploration projects. Besides the deep space exploration activities, CVN will take more geodetic and astrophysical observations. For example, under the framework of the Chinese National Key Scientific Infrastructure Project 'Crustal Movement Observation Network of China' (CMONC), the CVN upgrade plan was approved in 2007. The purpose is to provide the primary fiducial points by performing geodetic VLBI observations monthly using the CVN antennas. Another project for rapid UT1 measurement on the Shanghai-Urumqi baseline was also approved last year. So far, the CVN pulsar observation is also under way [1, 2, 3].

The CVN Data Center now contains a 4-station software correlator and a hardware correlator. The software correlator has played an irreplaceable role in the CE-1 routine data processing. However, both correlators are specifically designed for the Chang'E project and do not meet the scientific data processing demands. After the CE-1 mission, we started upgrading the software correlator. It gradually obtained the geodetic and astrophysical data processing abilities. It was also used in all kinds of experiments, like the pulsar observations and the digital baseband converter test experiments.

In the future, several new domestic antennas, including the new Shanghai 65-m antenna, will join in the CVN observations. Considering the possibility of using some Russian and Japanese

antennas, we can expand CVN to a local area VLBI network. In this VLBI network, the total antenna number will increase to 8–10, and the longest baseline will extend from 3000 km to 7000 km (Figure 2). The expanded CVN is a multi-purpose VLBI network for geodesy, astronomy, and deep space explorations. It can be seen that a new CVN data processing center with a powerful correlator is badly needed. The software correlator is a good choice for such a medium-scale VLBI data center.

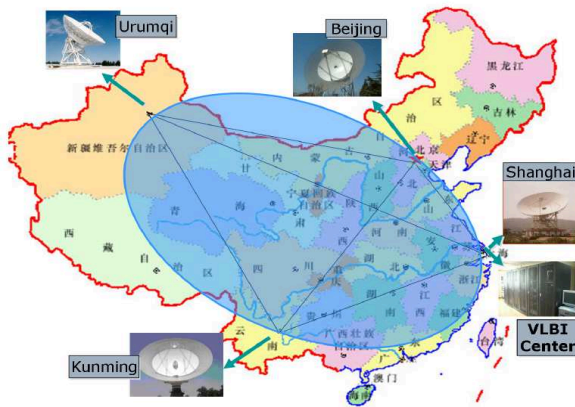


Figure 1. Current CVN stations and data center.

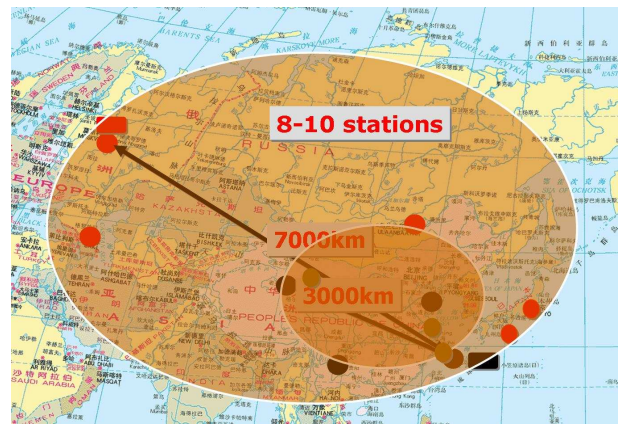


Figure 2. Extended CVN station map.

The requirements on the CVN correlator for science and deep space navigation are different (Table 1). In general, there may be 2–10 stations in geodesy and astronomy observations. For example, we plan to use the Shanghai–Urumqi baseline to perform rapid UT1 measurements. But in astrophysical observations, 5–10 stations are needed to achieve good UV coverage. For tracking the first Chinese Martian deep space probe YH-1, we hope to organize 4–8 Chinese and Russian stations. Similarly, the data speed for geodesy and astrophysics is higher than 1 Gbps/station. But for most deep space applications, the observation data speed is less than 128 Mbps/station. However, the data turnover time and reliability requirement of the navigation observation is much higher than that of scientific observation. For deep space probe navigation, sometimes the total data latency of the VLBI system should be less than 1 minute and the correlator must have real time data processing ability. The special functions like the Differential of One-way Range (DOR) and rapid spacecraft fringe search are essential for some navigation missions. As far as the correlator output data format is concerned, the FITS-IDI and NGS format will be the standard format for geodetic and astrophysical observations; while for navigation, the correlator will use the special CVN format.

To meet the different requirements of CVN observations, we are developing two kinds of software correlators. One is for spacecraft navigation; it adopts the Pthreads parallelization method and uses the Symmetric Multi Processing (SMP) server as the computation platform. The other correlator is for geodesy and astrophysics applications; it adopts the Message Passing Interface (MPI) programming and uses the SMP cluster as the platform. Since the GPU (Graphic Processing Unit) is powerful for data-parallel processing, it can be used as a computation accelerator in both software correlators.

Table 1. New CVN correlator requirements and realization.

Applications	Geodesy/Astronomy	Navigation
Station	2–10	4–8
Processing speed/station	>1 Gbps	16–128 Mbps
Data transport	Disk VLBI, e-VLBI	Real time VLBI, Disk VLBI
Output format	FITS-IDI, NGS	CVN
Special function	none	Rapid fringe search, DOR
Parallel computing	MPI + Pthreads	Pthreads
Hardware Platform	SMP server + GPU	SMP cluster + GPU

2. SMP Software Correlator

The SMP software correlator consists of the correlation module, the data preprocessing module, the satellite fringe search, and the PCAL abstraction module. It uses Pthreads to realize the parallel correlation on any SMP server with x86 family CPUs. It has special functions like the rapid spacecraft fringe search and delay model reconstruction and full Phase Calibration (PCAL) signal detection. First designed for the Chang'E project and as the main VLBI correlator in the CE-1 mission, the SMP software correlator played an irreplaceable role in the CE-1 data processing. In the critical flying mission, there were 36 observations (336.55 hours). All of them were processed by this software correlator. In the long-term in-orbit operation mission, there were in total 120 observations (607.39 hours), and 434.02 hours of them were processed by the software correlator. Especially in the case of several real-time CE-1 maneuver tracking observations, only the software correlator produced the correct results [1].

After the CE-1 mission, the performance improvement of this correlator is still being worked on. Now the SMP software correlator has been upgraded from 4-station to 10-station capability and can output FITS-IDI or NGS format data, besides the CVN format data. Further, the correlator data latency can be less than 1 minute now.

Table 2. Specifications of SMP software correlator.

Architecture	FX
Station number	1–10
IF number	1–16
Frequency channel	32–65536/IF
Input data format	Mark 5A, Mark 5B
Output data format	CVN
Sampling	1-bit, 2-bit
Fringe search	2–4 stations
Correlation speed/station	128 Mbps, 4 stations, 2-bit
Data turnover	< 1 minute
PCAL detection	Yes

Up to now, this correlator has been used in all kinds of experiments. We used the software correlator to get the preliminary image of pulsar B0329+54 last July (Figure 3). This is the first CVN VLBI image. From 2007 to 2009, CVN carried out several Mars Express (MEX) experiments. The SMP software correlator processed all the observation data (Figure 4). For the eclipse of the Sun on 22 July 2009, a China-Japan joint experiment was conducted to measure the Total Electron Content (TEC) by VLBI and GPS observations. In the CVN data center, it was still the software correlator that correlated the VLBI data. The result is under comparison with that of NICT [1, 2, 3].

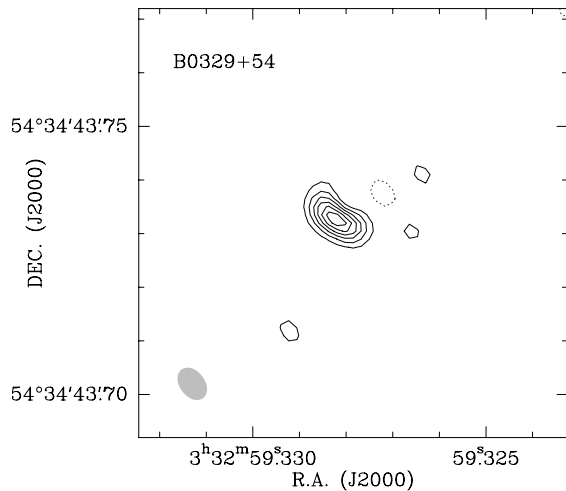


Figure 3. Preliminary image of PSR B0329+54.

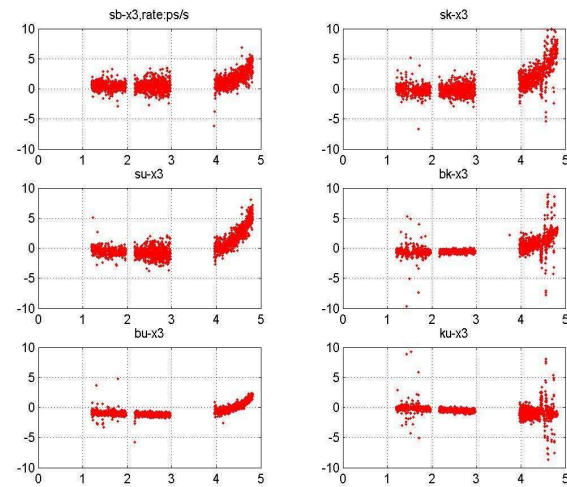


Figure 4. VLBI delay/rate of Mars Express.

3. High Speed SMP Cluster Software Correlator

Although the performance of an SMP server is becoming more powerful, the speed of the correlator on a single SMP server is still strongly restricted. To meet the wide bandwidth scientific VLBI observations, the high speed software correlator can work on the fast High Performance Computing (HPC) cluster. As the hardware platforms of the high speed prototype software correlator, two sets of blade clusters have been installed at the CVN Data Center (Figure 5). One is a 6-node cluster with 48 CPU cores, and there is a 10 Gigabit Ethernet (10GE) connection between each computation node. Another one is a 16-node cluster with 128 CPU cores, using InfiniBand (IB) for data communication. A 10-station prototype software correlation is under development. We will use the prototype correlator to compare the performance difference on the two blade clusters.

Figure 6 shows the structure of the prototype highspeed software correlator. This correlator will read the VEX file and the SKD file in the astrophysical or geodetic observation. The Pulsar binning function will be added later. The output data format is the standard FITS-IDI or NGS. On 6 January 2009, the prototype correlator conducted the first CVN 2-station high speed e-VLBI (256 Mbps/station) experiment on the baseline Shanghai–Urumqi.



Figure 5. Blade cluster.

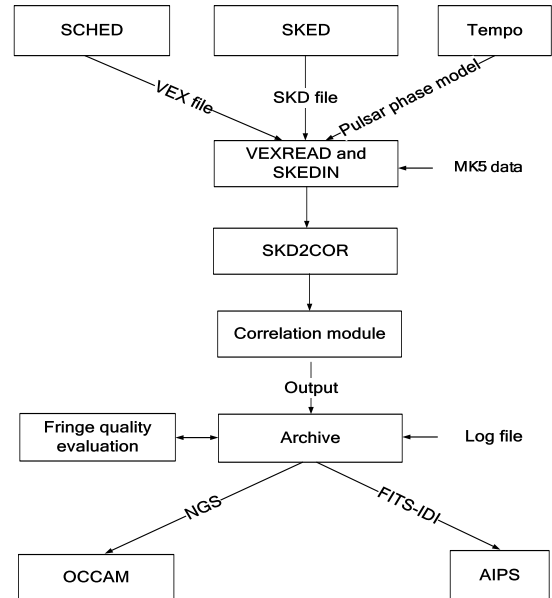


Figure 6. Highspeed software correlator structure.

4. Plans for 2010

In 2010, with the operation of the CMONC Project, a geodesy and astrophysics oriented software will come into operation. We will also utilize the CVN for rapid dUT1 measurements and rapid e-VLBI imaging experiments. A Graphics Processing Unit (GPU) test bench will be used to study the software correlator of CPU + GPU structure.

5. Acknowledgements

The authors gratefully appreciate the support of the National Natural Science Foundation of China General Program (No.10878021), the state 863 High Tech R&D program (2008AA12A209), and the e-science application project of Chinese Academy of Sciences.

References

- [1] Zheng Weimin, Luo Wuchao, CVN Software Correlator Development and Applications in Chinese Lunar Exploration Mission, In: Measuring the future, Proceedings of the fifth IVS general meeting, Nauka, 124-128, 2008.
- [2] Zheng Weimin, Shu Fengchun, Luo Wuchao, Yu Yun, Wang Weihua, Current status of Chinese VLBI network software correlator, Proceedings of the 19th European VLBI for Geodesy and Astrometry Working Meeting, 84-86, 2009.
- [3] Guo Li, Zheng Xingwu, Zhang Bo, Wang Weihua, Zheng Weimin, et al., New determination of the position of the pulsar B0329+54 with Chinese VLBI network, Science in China Series G, accepted, 2010.

RDV77 VLBA Hardware/Software Correlator Comparisons

David Gordon

NVI, Inc./NASA Goddard Space Flight Center

e-mail: David.Gordon-1@nasa.gov

Abstract

Results of a hardware vs. software correlation of the RDV77 session are presented. Group delays are found to agree (WRMS differences) at an average level of 4.2 psec and with a noise floor of ~ 2.5 psec. These RDV77 comparisons agree well with several previous correlator comparison studies.

1. Correlation at the VLBA

The VLBA hardware correlator has now been replaced with the VLBA-DiFX [1] software correlator. This is the VLBA's implementation of the Distributed F/X (DiFX) software correlator, written by Adam Deller [2] and first used at Swinburne University in Australia. The GSFC VLBI group agreed to do a hardware/software (HW/SW) correlator comparison using RDV77 to help validate the software correlator's implementation for geodetic and astrometric sessions. This paper presents results of that comparison.

The RDV77 session ran on October 7-8, 2009. It used the ten VLBA¹ antennas plus the Mark IV antennas at Hobart, Kokee, Ny-Ålesund, Tsukuba, and Wettzell. It was correlated on both the VLBA hardware correlator and the new VLBA-DiFX software correlator in Socorro in November 2009. RDV77 also used 2-bit sampling for the first time in an RDV.

2. Differences Between the Two Correlations

There were some minor differences between the two correlations, which could add noise to the comparisons. Different site and source *a priori*s were used; therefore the correlator models differed. This should not matter though, since we are comparing total observables. Also, the integration times were slightly different, 4.00 seconds for the SW correlator and 4.063232 seconds for the HW correlator, so scan start and stop times, and scan durations will differ. The HW correlator takes longer to sync up and will correlate all data on disk, so the user must flag off-source times. The SW correlator correlates only when the antennas are on-source.

3. The Two Geodetic Solutions

Both versions were processed using AIPS in a similar manner to obtain the group delay and rate observables. Measured phase cal offsets were applied at the VLBA sites. Manual phase offsets were determined using the same scans in the two versions and applied at all sites. Flagging times

¹The VLBA is a facility of the National Radio Astronomy Observatory (NRAO) which is operated by Associated Universities Inc., under cooperative agreement with the National Science Foundation.

(when the antennas were off-source) were applied to both sets. The data was fringed in AIPS and the resultant observations were given identical time tags in the two versions.

The two versions were analyzed using Calc/Solve. Below are the solution statistics. There were 22,044 scheduled observations. Problems at Tsukuba (five hours lost due to a typhoon) and MK-VLBA (four hours lost due to an azimuth ACU failure) are the main reasons for the lower total number of observations. The SW version has fewer total observations, but it uses ~ 1500 more observations in the Solve solution.

	HW	SW
Number total observations:	21595	20938
Number usable observations:	18127	19386
Number used observations:	17019	18541
Number obs. not used:	4576	2397
Solve fit (psec):	32.55	33.93

4. Group Delay and Rate Comparisons

Group delays were differenced for each baseline, then a weighted average value was subtracted out, and a weighted RMS was then computed. Observation pairs were excluded if one or both were not used in the solutions. Also excluded were pairs in which one SNR was much smaller than the other (discussed later). Plotted in Figures 1 and 2 are the WRMS total delay differences versus baseline length for the X-band and the S-band data. A similar plot is shown for the X-band delay rates (Figure 3).

Group delays show a clear baseline length dependence. X-band WRMS differences vary from a minimum of ~ 2.5 psec (~ 0.75 mm) for the KP-VLBA/OV-VLBA baseline, up to ~ 32 psec for Hobart/Ny-Ålesund. The overall WRMS delay difference for all good matches in 104 baselines is 4.22 psec at X-band. The plots are coded by the type of baseline. VLBA/VLBA baselines show the smallest WRMS differences due to their generally higher SNRs and lower formal errors.

In Figure 4 are plotted X-band group delay signal-to-noise ratios (SNRs) versus group delay differences for individual observations. These show, as expected, a clear dependence on SNRs. Delay differences quickly drop to minimal values as the SNR increases.

5. SNR Comparisons

Some large outliers were found in the delay comparisons. These were found to be mostly due to pairs in which one of the SNRs (and fringe coherence coefficients) was considerably smaller than the other, but the integration times were approximately the same. Most of these are cases where the HW version SNR is much less than the SW version. This indicates some problem in the processing, possibly in the setting of flagging times, which is critical for the HW version but not the SW version. The normal database editing eliminated most of these points from the HW version Solve solution, which essentially explains the difference in the number of observations used in the two solutions.

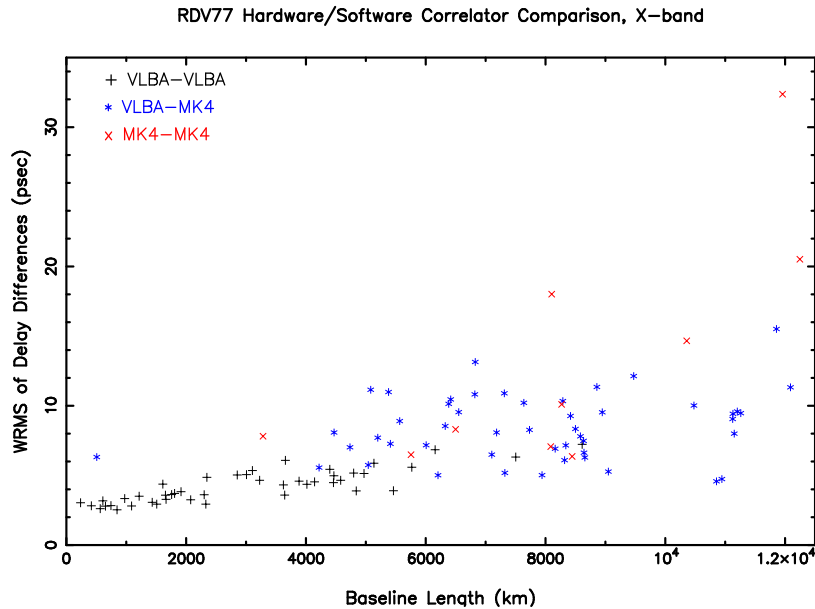


Figure 1. X-band WRMS group delay differences vs. baseline length.

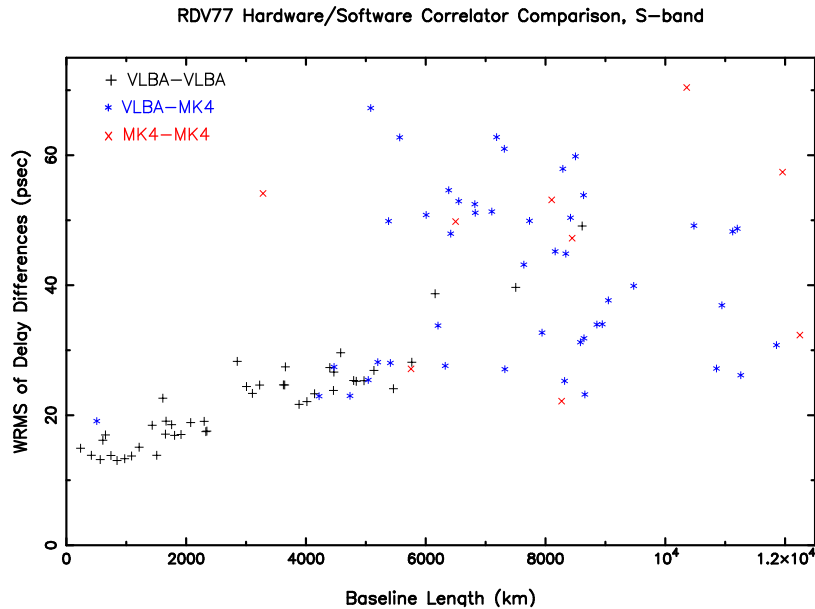


Figure 2. S-band WRMS group delay differences vs. baseline length.

6. Comparison to Earlier Correlator Comparisons

A few earlier geodetic/astrometric correlator comparisons have been made. Nothnagel et al. [3] compared Mark III vs. Mark IV and repeated Mark IV vs. Mark IV correlations. Gordon [4] and Petrov et al. [5] compared 8 stations of RDV22 correlated at the VLBA and on the Mark IV correlator at Haystack Observatory. The editing criteria for these other comparisons differed,

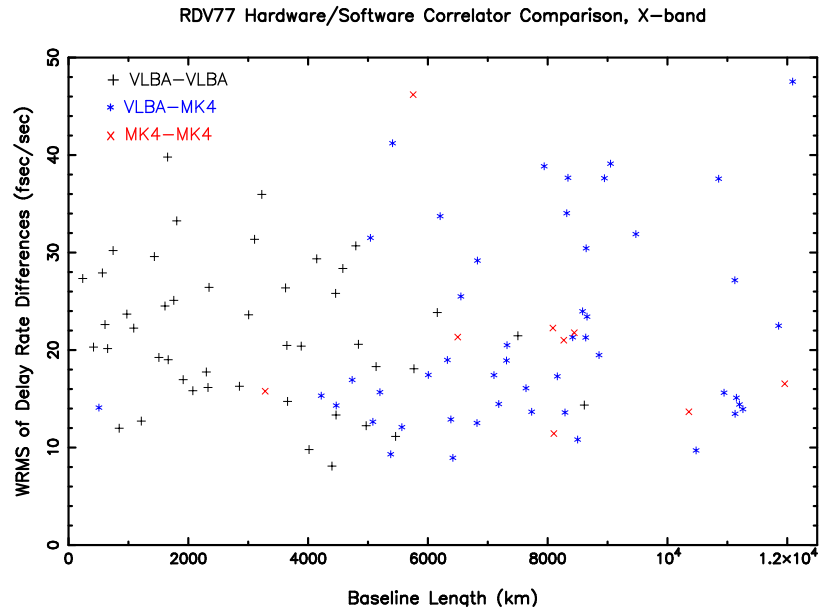


Figure 3. X-band WRMS delay rate differences vs. baseline length.

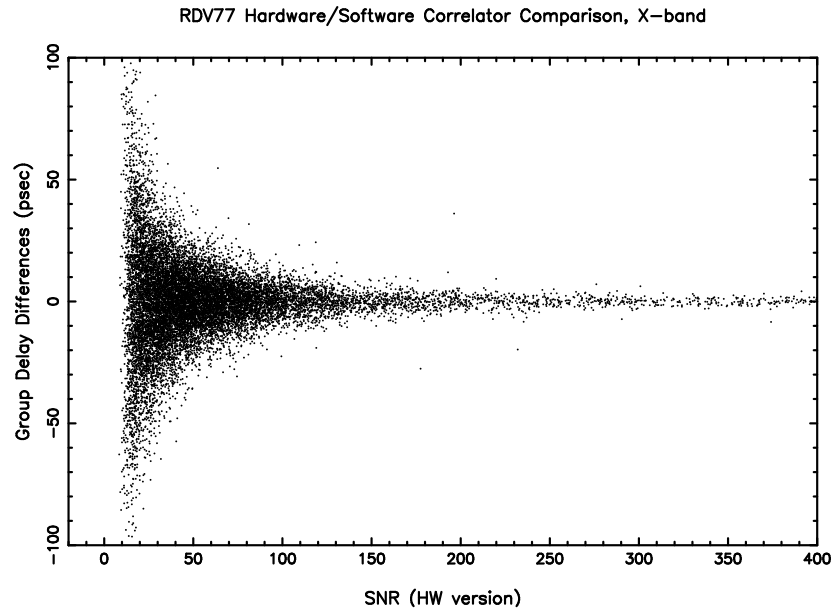


Figure 4. Distribution of individual group delay differences vs. SNRs.

but all are in general agreement. In Figure 5 are plotted the WRMS group delay differences from those other studies along with the results of this study for X-band.

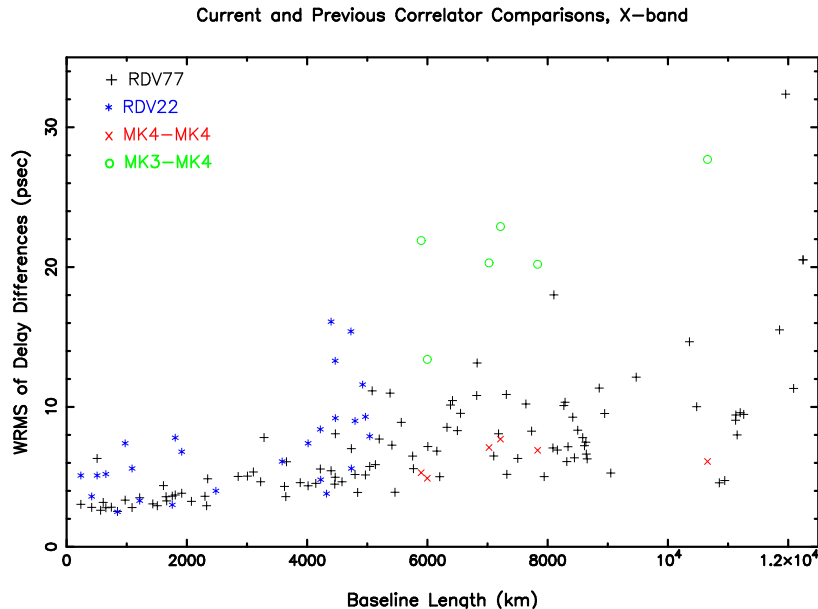


Figure 5. Group delay WRMS differences from this comparison and from earlier correlator comparison studies.

7. Conclusions

Weighted RMS delay differences per baseline at X band show a noise floor of ~ 2.5 psec, or ~ 0.75 mm of light travel time, and an average value of ~ 4.2 psec (~ 1.25 mm) over all baselines. The comparisons shown here compare very well to previous correlator comparisons. With its greater data yield, we believe this indicates that the new VLBA software correlator performs at least as well as the older hardware correlator. This gives us confidence that the switchover to the software correlator will have no adverse effect on future RDV or other VLBA astrometry/geodesy sessions.

References

- [1] Brisken, W., VLBA Sensitivity Upgrade MEMO 23, A Guide to Software Correlation Using NRAO-DiFX Version 1.1, 2008, <http://www.vlba.nrao.edu/memos/sensi/sensimemo23.pdf>.
- [2] Deller, A.T., S.J. Tingay, M. Bailes, and C. West, DiFX: A software correlator for very long baseline interferometry using multi-processor computing environments, *PASP*, **119**, 318, 2007.
- [3] Nothnagel, A., O. Bromorzki, J. Campbell, A. Muskens, H. Rottmann, I. Rottmann, “Comparison of the Output of Repeated Mark III and Mark IV Correlation Results”, in *IVS 2002 General Meeting Proceedings*, NASA/CP-2002-210002, N.R. Vandenberg and K.D. Baver (eds.), 107-111, 2002.
- [4] Gordon, D., “RDV Analysis and Mark IV/VLBA Comparison Results”, in *IVS 2002 General Meeting Proceedings*, NASA/CP-2002-210002, N.R. Vandenberg and K.D. Baver (eds.), 277-281, 2002.
- [5] Petrov, L., D. Gordon, J. Gipson, D. MacMillan, C. Ma, E. Fomalont, R.C. Walker, and C. Carabajal, *Precise Geodesy with the Very Long Baseline Array*, *J. Geodesy*, **83**, 859-876, 2009.

The IAA RAS Correlator First Results

Igor Surkis, Alexey Melnikov, Violet Shantyr, Vladimir Zimovsky

Institute of Applied Astronomy of RAS

Contact author: Igor Surkis, e-mail: surkis@ipa.rssi.ru

Abstract

In 2009 the national Russian VLBI observations were processed by the new correlator ARC (Astrometric Radiointerferometric Correlator). The ARC is a VSI-H correlator and equipped with Mark 5B playback terminals. During 2009 ARC was used to process a series of VLBI sessions, observed on stations Svetloe, Zelenchukskaya, and Badary. NGS files were formed, and EOP parameters were obtained by IAA RAS Analysis Center. The accuracies of the pole coordinates and UT1-UTC were 1–2 mas and 0.07–0.1 ms, respectively.

Using ARC (Astrometric Radiointerferometric Correlator) the national Russian VLBI observations were processed starting from February 2009. ARC is a 6-station, 15-baseline correlator. It is able to process up to 16 frequency channels on each baseline, 240 channels total. The correlator accesses two-bit VLBI signals with 32 MHz maximal clock frequency. The maximal data rate from each station is 1 Gbps. The correlator requires VSI-H input VLBI signals, and it is equipped with Mark 5B playback terminals.

The ARC hardware consists of Mark 5B playback terminals, a system for signal distribution and synchronization, and correlator base modules.

Figure 1 shows the correlator base module. This FPGA-technology device performs all of the hardware data processing. The module enables processing of 16 single-baseline frequency channels — all data of one baseline of a typical geodetic VLBI observation.

The base module is a Compact PCI 6U front plug-in board. Up to three base modules are placed into the Compact PCI 6U crate. The crate is controlled by a computer board. The modules receive commands and model parameters from the computer board CPU and send calculated correlation data through the crate's PCI bus. The base module contains 16 correlation units which are single-baseline, single-channel XF correlators for calculating 64 complex lags and picking phase-cal tones. Each correlation unit consists of two FPGA chips and two RAM chips. The data processing algorithms are implemented as FPGA programs. The six-station, 15-baseline ARC contains 15 base modules to process 240 frequency channels simultaneously. Base modules are mounted into five Compact PCI 6U crates.

The purpose of the system of signal distribution and synchronization is the distribution of signals from the Mark 5B terminals to the base modules, so that each module receives signals from two Mark 5B. The system also generates and sends synchronization signals DPSCLOCK and DPS1PPS to the Mark 5B terminals. The system consists of the set of boards based on FPGA technology and connecting cables. The boards are mounted into two Compact PCI 6U crates.

ARC is shown in Figure 2. All of the ARC hardware parts are mounted in four racks. The two central racks contain five crates with base modules. The six Mark 5B devices are mounted into two flank racks. These racks also consist of two Compact PCI 6U crates with signal distribution and synchronization system.

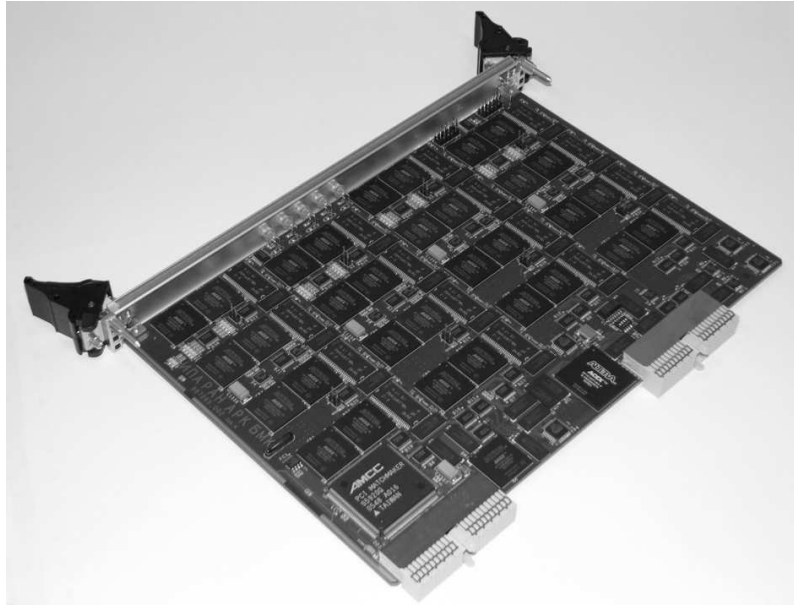


Figure 1. Correlator base module.



Figure 2. The 6-station ARC correlator.

The correlator hardware control is performed by the desktop computer, which is connected to the crates by the correlator local network. The ARC software is the distributed system between the control computer and crates. The software runs under GNU/Linux and has a GUI.

The ARC in minimal 2-station assembly was mounted at the end of 2008. In July 2009 ARC was

expanded to 3-station configuration. The full-scale 6-station correlator was complete in October 2009.

Using ARC the national Russian VLBI observations were processed starting from February 2009. There are two geodetic programs which were performed by Svetloe, Zelenchukskaya and Badary observatories during 2009. The first is the Ru-E observational program aimed at EOP determination. It is a 24-hour session with the three-station network. The observing mode includes 16 MHz VC's bandwidth and one-bit sampling with total bit rate of 512 Mbit/s per station. The second program Ru-U is intended to estimate UT1-UTC. It was started with two hours of observation time and has now become a 1-hour session. The observing mode includes 8 MHz VC's bandwidth and one-bit sampling with total bit rate of 256 Mbit/s per station. One hour sessions are transferred to the correlator in e-VLBI mode.

The group delays in the X and S bands were calculated as a result of the correlator processing, and NGS card files were created. 24 Ru-E and 26 Ru-U sessions were observed and correlated. Using these NGS files the IAA RAS Analysis Center calculated EOPs and UT1-UTC.

Figure 3 shows the differences between IERS 05 C04 and results of IAA RAS EOP determination, calculated from Ru-E observation program. In Figure 4 the differences between UT1-UTC IERS 05 C04 and results of IAA RAS EOP determination, calculated from Ru-U observation program are shown.

As seen from the figures, the accuracy of the dX and dY estimates and the X and Y estimates are close to 1 and 2 mas, respectively. Accuracies of UT1-UTC estimates are within the range of 0.05–0.07 ms for 24-hour sessions and 0.07–0.10 ms for 1-hour sessions.

The closure relation for group delays on baselines Barary–Svetloe, Svetloe–Zelenchk, and Zelenchk–Badary enable the checking of the correlator accuracy, which is 60–70 ps at the present time.

Work on improving the correlator internal algorithms has started now, and we are planning to achieve the Mark IV correlator precision soon.

References

- [1] I. Surkis, A. Bogdanov, A. Fateev, A. Melnikov, V. Shantyr, V. Zimovsky, IAA Correlator Center, In: International VLBI Service for Geodesy and Astrometry 2007 Annual report, NASA/TP-2008-214162, D. Behrend and K. D. Baver (eds.), 143–147, 2008.
- [2] I. Surkis, A. Fateev, A. Melnikov, V. Mishin, V. Shantyr, V. Zimovsky, IAA Correlator Center, In: International VLBI Service for Geodesy and Astrometry 2008 Annual report, NASA/TP-2009-214183, D. Behrend and K. D. Baver (eds.), 209–211, 2009.
- [3] I. Surkis, V. Zimovsky, A. Melnikov, V. Shantyr, A. Fateev, A. Bogdanov, The IAA RAS 6-station VLBI Correlator. In: Measuring The Future, Proceedings of the Fifth General Meeting of the International VLBI Service for Geodesy and Astrometry. Saint Petersburg, 124–128, Nauka, 2008.

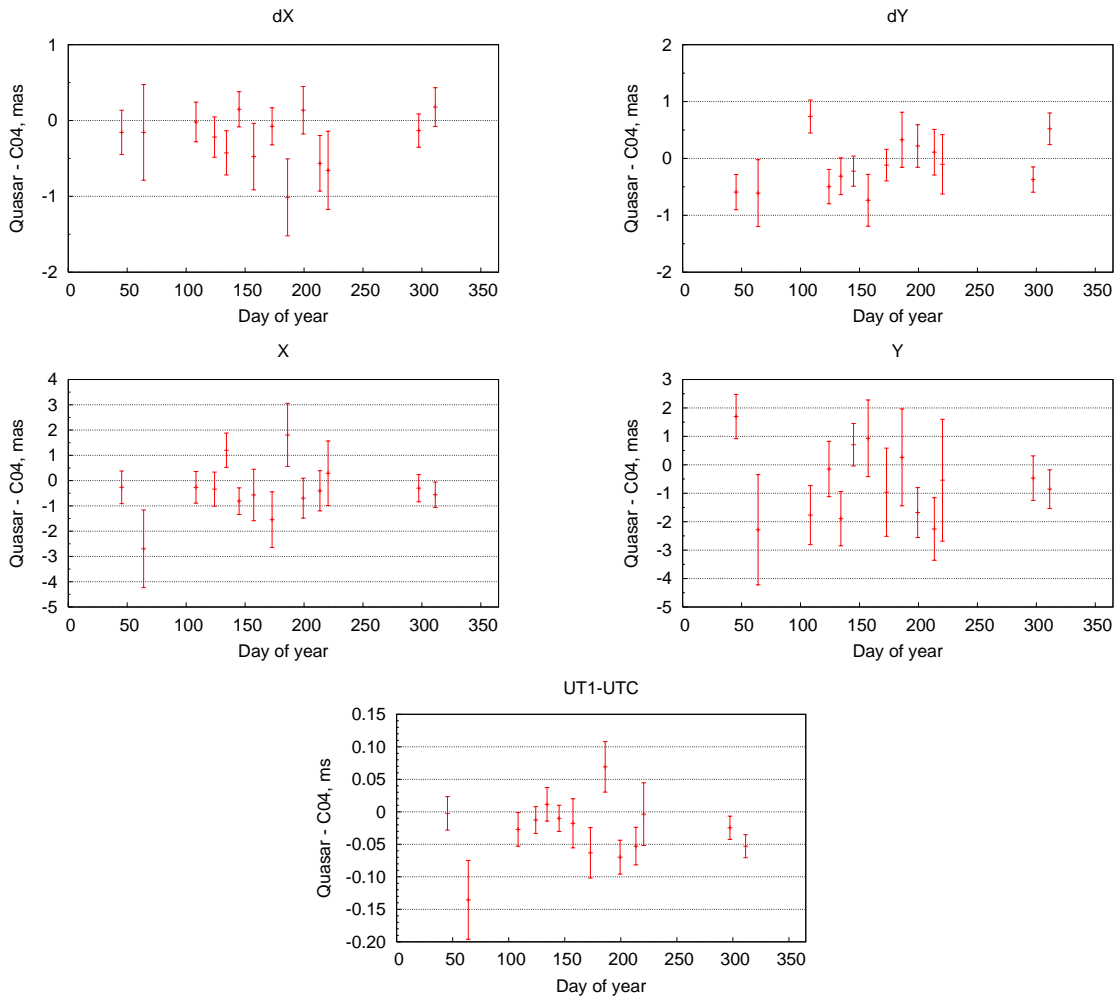


Figure 3. Difference between EOP C04 and results of IAA RAS EOP determination, calculated from 24-hour 3-station Ru-E observation program.

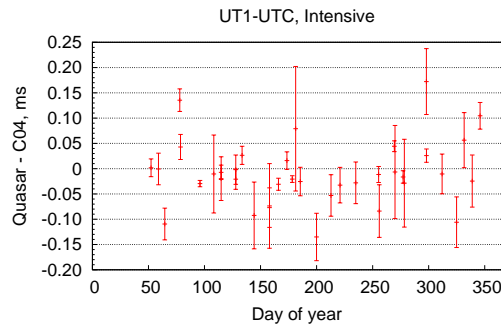


Figure 4. Difference between UT1-UTC C04 and results of IAA RAS EOP determination, calculated from 1-hour 2-station Ru-U observation program.

First Results of Venus Express Spacecraft Observations with Wettzell

Guifré Molera Calvés¹, Jan Wagner¹, Alexander Neidhardt², Gerhard Kronschnabl³, Miguel Pérez Ayúcar⁴, Giuseppe Cimó⁵, Sergei Pogrebenko⁵

¹⁾ *Aalto University Metsähovi Radio Observatory*

²⁾ *FESG/TUM, Wettzell*

³⁾ *BKG, Wettzell*

⁴⁾ *ESA-ESAC, Madrid*

⁵⁾ *Joint Institute for VLBI Europe, Dwingeloo*

Contact author: Guifré Molera Calvés, e-mail: gofrito@kurp.hut.fi

Abstract

The ESA Venus Express spacecraft was observed at X-band with the Wettzell radio telescope in October-December 2009 in the framework of an assessment study of the possible contribution of the European VLBI Network to the upcoming ESA deep space missions. A major goal of these observations was to develop and test the scheduling, data capture, transfer, processing, and analysis pipeline. Recorded data were transferred from Wettzell to Metsähovi for processing, and the processed data were sent from Metsähovi to JIVE for analysis. A turnover time of 24 hours from observations to analysis results was achieved. The high dynamic range of the detections allowed us to achieve a milliHz level of spectral resolution accuracy and to extract the phase of the spacecraft signal carrier line. Several physical parameters can be determined from these observational results with more observational data collected. Among other important results, the measured phase fluctuations of the carrier line at different time scales can be used to determine the influence of the solar wind plasma density fluctuations on the accuracy of the astrometric VLBI observations.

1. Introduction

The ESA Venus Express spacecraft (VEX S/C) radio transmission signals are an interesting target for exercising new science support methods usable in prospective ESA planetary probe and deep space missions. Spacecraft observations, detections, processing and analysis technology are based on the heritage of our team involved in the VLBI support of the VEGA and Huygens missions [1, 2, 3]. During a campaign in 2008-09, a number of European VLBI Network telescopes joined trial observations of VEX in the framework of the PRIDE (Planetary Radio Interferometry and Doppler Experiments). This paper describes the analysis methods, introduces the software developed for handling the analysis flow, and presents the most recent detections we achieved during a single-dish VEX observation performed at Wettzell. The high dynamic range of our phase detections—with a typical SNR of several thousands in 1 Hz or several millions in 1 mHz as achieved in observations with Metsähovi, Wettzell, Yebes, Medicina, Matera, and Noto stations in coordination with ESA Space Astronomy Centre (ESAC), and ESTRACK station Cebreros, Spain—allows to extract and analyze the phase of the S/C carrier line from many different physical perspectives, among which the S/C orbitography and propagation effects are the first in line. In particular we show how the phase-time of the S/C signals was applied to detect interplanetary

plasma scintillation on a novel frequency band (X-band) and present the results of the 2009.11.6 Wetzell observation.

2. Theory

2.1. Spacecraft Detection

The technique employed in our observations enables us to obtain the spectra of the S/C radio signal, to determine the apparent topocentric frequency of the S/C signal carrier line and accompanying “ranging” tones with sub-mHz accuracy, and to determine the phases of these tones with respect to the phase of the Earth-based station’s H-maser clock. Further on, the phases can be calibrated on a baseline basis using a VLBI multi-station phase referencing technique.

2.2. Interplanetary Plasma Effects

Interplanetary scintillation (IPS) originates from the diffraction of radio waves by fluctuations within the solar wind. Measurements of IPS have been conducted during many years to probe the solar wind throughout the inner heliosphere. The phase variations by the density fluctuations scatter the signal and cause the fluctuation in received power and phase. [Density variations and turbulence in the plasma scatter the S/C signal and cause fluctuations in received power and phase.] Large variations ($\gg 1$ radian) introduced across the wave front are known as “strong” scattering. When the variations are small ($\ll 1$ radian) the scattered waves add constructively to generate much larger fluctuations in the signal received, known as “weak” scattering. The standard measurement of the level of IPS is the scintillation index m . This is the ratio of the rms variation in the strength of the source signal due to IPS and the average strength of the signal [4, 5]. It should be noted that, especially at higher frequencies, the scintillation index depends on the source angular size and structure. In this respect, the spacecraft, an almost ideal point source, provides a good opportunity. Although its emitting power is subject to internal power variations which depend on the transmitting data content, the phase of its carrier line is a stable quantity because it is locked to a high precision atomic clock at the communication station. We note that the phase variations in this case are the results of a two-way propagation: from the communication station to the spacecraft and back to the observing station.

3. Methods: Data Processing and Analysis

The VEX observations at Wetzell started on 2009.11.16 using the standard VLBI Mark IV data acquisition rack with four 8 or 16 MHz channels and 2-bit Nyquist sampling for aggregate data rates of 128 or 256 Mbps. The Mark-IV-formatted data were recorded with Mark 5A and PCEVN disk systems. Immediately at the end of the observational run, files were electronically transferred through the Internet with Tsunami UDP to the Metsähovi Radio Observatory (MRO) for processing. Data were processed with the high-performance, ultra-high spectral resolution spectrometer-correlator software under development at MRO. Processing tasks ran in two iterations between MRO and JIVE, with the JIVE analysis software involved in the iterative loop.

With our current facilities the full processing cycle takes 5-10 times longer than the observational time, but we are constantly improving it.

3.1. Spacecraft Detection

Initial detection of tones was performed using the high-resolution spectrometer software developed at MRO (SWSpec). A Python PyQt4 GUI allows fast reconfiguration for new processing jobs. SWSpec supports several input file formats such as the (still common) VLBA and Mark IV magnetic tape formats on Mark 5A and PCEVN and the more modern Mark 5B and VDIF formats. In addition, it can handle various “raw” multi-channel, multi-bit formats. A SWSpec pass extracts one selected raw data channel and performs accurate windowed-overlapped discrete Fourier transforms and spectrum time integration. All parameters are fully adjustable. The S/C processing of 8 or 16 MHz baseband used 3.2M DFT points and cosine-squared windowing. Figure 1 shows the S/C Doppler detection with the Wettzell antenna, and Figure 2 the resulting spectrum (after Doppler model removed) with a spectral resolution of 0.9 mHz.

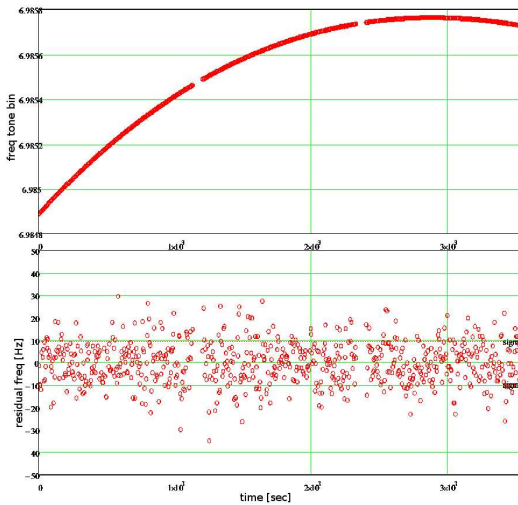


Figure 1. Top graph: Frequency detections of the VEX carrier signal at 8.412 GHz on 2009.11.16. Peak frequency spread is 8.7 kHz over 1 hour. Bottom graph: Post-fit stochastic residual exhibiting an RMS of only 9 mHz at 5s sampling.

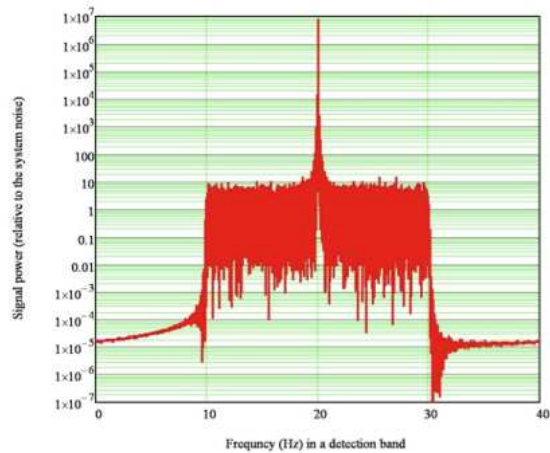


Figure 2. The resulting spectrum of the S/C carrier line in a zoom band after the Doppler correction. Spectral resolution at 0.9 mHz.

3.2. Tone Tracking, Filtering and Phase Detection

The output spectra of SWSpec are processed using MathCAD and Matlab scripts developed at JIVE. They extract S/C tone frequencies (detected by visual inspection) from the series of integrated spectra. A 4 to 7 order phase stopping polynomial is fitted to the S/C carrier line frequency detections using a weighted Least Mean Squares (LMS) method with weight coefficients depending on SNR and RFI considerations. The resulting polynomial coefficients are used as input to the next processing steps: narrow band adaptive filtering and Phase-Lock-Loop (PLL).

The spacecraft tone tracking software (SCTracker) developed at MRO accepts the original raw input data files, a list of S/C tone frequencies (relative to carrier), and the stopping polynomial coefficients for the carrier tone. A double-precision polynomial evaluation is applied for stopping tone phases. Adaptive filtering extracts and filters stopped tones down to a several kHz wide

bandwidth using a 2nd order WOLA (Window-Overlap-Add) DFT-based algorithm of the Hilbert transform approximation. The time-domain sample sequence of every extracted and filtered tone is written as an output data set for further post-processing using digital PLL software at JIVE. The residual phase in a stopped band is determined with respect to a set of subsequent frequency/phase polynomials applied for phase stopping. Depending on the SNR of the carrier line and individual tones, the final bandwidth of phase detections can range from several kHz to several mHz. In the case of VEX carrier line, this bandwidth is in the range of 10-100 Hz. Figure 3 illustrates the carrier line residual (after Doppler correction) phase variation.

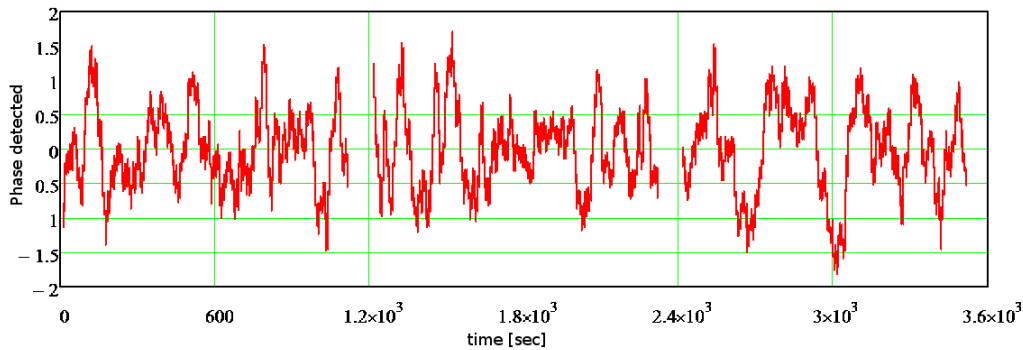


Figure 3. Narrow band phase detections after PLL tone tracking and band filtering of the S/C carrier line.

3.3. Scintillation Analysis

The post-processing analysis of the spacecraft tracking data enables us to study several parameters of the S/C signal with milliHz accuracy, among which the phase fluctuations of the S/C carrier line can be used for characterization of the Interplanetary Plasma (IP) density fluctuations along the signal propagation line at different spatial and temporal scales and at different solar elongations. These fluctuations are well represented by a near-Kolmogorov [6] spectrum. From our VEX measurements we retrieved such essential parameters as the phase scintillation index and bandwidth of scintillations and their dependence on the solar elongation, distance to the target, position of the source in the solar system and the solar activity index. Multi-station observations can distinguish the up- and down-link plasma contributions, because they will observe the S/C through different Fresnel channels. Figure 4 shows the spectral power density of the slow fluctuation phase turbulence below 10 Hz. The S/C carrier line phase scintillations measurements are complementary to the classical power scintillation measurements of signals from the natural radio sources and are crucial for the optimization of the design characteristics of PRIDE.

4. Conclusion

The first results are encouraging, although more test and development observations are needed before obtaining physically significant results. The initial study focused more on the measurement techniques and data analysis. But the physical interpretation of the results is a task that we wish to continue in upcoming studies when more observational data is collected.

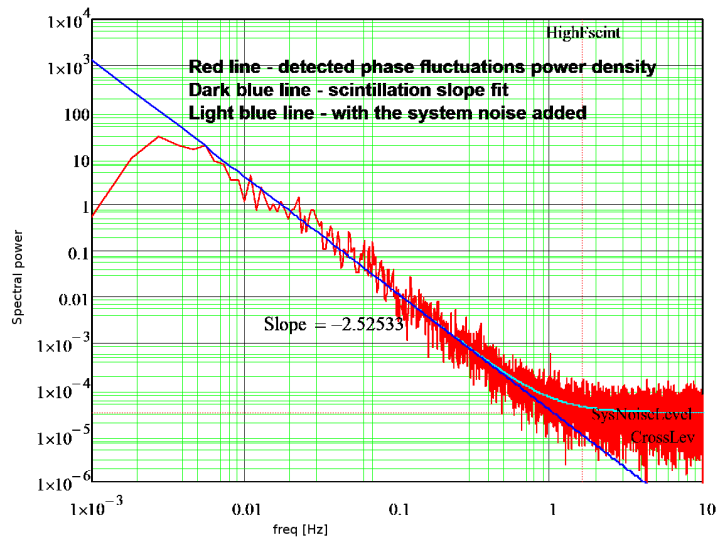


Figure 4. Spectral power density of slow fluctuation phase turbulence below 10 Hz. Note the high dynamic range of 10^6 .

5. Acknowledgements

We are thankful to several members of the VLBI radio astronomy, space science, and technology communities. In particular we thank Ed Himwich, Ari Mujunen, Jouko Ritakari, Giuseppe Maccaferri, Stelio Montebugnoli, Salvatore Pluchino, Francesco Schilliro, Giuseppe Colucci, Giuseppe Bianco, Cristiano Cosmovici, Pablo de Vicente, and Leonid Petrov for their contributions to the ongoing work.

References

- [1] Sagdeev, R.Z., et al. (1992), “Differential VLBI Measurements of the Venus Atmosphere Dynamics by Balloons: VEGA Project”, *Astron. Astrophys.* 254, 387
- [2] Pogrebenko, S.V., et al. (2004), “VLBI tracking of the Huygens probe in the atmosphere of Titan, in *Planetary Probe Atmospheric Entry and Descent Trajectory Analysis and Science*”, ed. A. Wilson, ESA SP-544, 197–204
- [3] Lebreton, J.P., et al. (2005), “An overview of the descent and landing of the Huygens probe on Titan”. *Nature* 438, 758-764.
- [4] Hewish, A., Scott, P.F., and Wills, D. (1964), “Interplanetary Scintillation of Small Diameter Radio Sources”. *Nature* 203: 1214-1217.
- [5] Fallows, R.A., Williams, P.J. and Breen, A.R. (2002), “EISCAT measurements of solar wind velocity and the associated level of interplanetary scintillation”, *Ann. Geophys.* 20: 1279-1289.
- [6] Kolmogorov, A.N.(1941) “The local structure of turbulence in incompressible viscous fluid for very large Reynolds numbers”. *Proceedings of the USSR Academy of Sciences* 30: 299-303 (Russian), translated into English in *Proceedings of the Royal Society of London, Series A: Mathematical and Physical Sciences* 434, 9-13 (1991).

CRF Network Simulations for the South

Oleg Titov ¹, Dirk Behrend ², Fengchun Shu ³, Dan MacMillan ², Alan Fey ⁴

¹) *Geoscience Australia*

²) *NVI, Inc./NASA Goddard Space Flight Center*

³) *Shanghai Astronomical Observatory*

⁴) *U.S. Naval Observatory*

Contact author: Oleg Titov, e-mail: oleg.titov@ga.gov.au

Abstract

In order to monitor and improve the CRF in both the Southern Hemisphere and along the ecliptic, we perform various simulations using station networks based mostly on the Australian AuScope network, New Zealand’s Warkworth antenna, and several Chinese antennas. The effect of other stations such as HartRAO and Kokee Park to enhance the East-West baseline coverage is also considered. It is anticipated that the simulation results will help IVS to decide on the composition of the CRF sessions of the IVS to be run from 2011 onward.

1. Introduction

A deficit of observations of radio sources in the Southern Hemisphere makes development of a program dedicated to exploiting the new Australian and New Zealand radio telescopes a priority. These fast slewing antennas bring the benefit of quickly producing a large number of observations, but due to their small size (12 meters), the number of available sources is limited. We considered different network configurations consisting either of these new antennas alone or these antennas complemented by existing larger diameter antennas. We show that these networks can process a sufficient number of radio sources with a flux density of 1 Jy or more to meet desired astrometric goals. Special attention was devoted to the Australian–Chinese network.

Table 1. Network configurations used in the simulations.

Number	Network
1 \equiv core	Hobart12, Katherine, Yarragadee, Warkworth
2	core + Parkes + Seshan25
3	core + Urumqi + Seshan25
4	core + Hartrao
5	core + Hartrao + Kokee
6	core + Fortaleza + Kokee
7	core + Fortaleza + Kokee + Hartrao
8	core + Fortaleza+ Kokee + Hartrao + Seshan25 + Urumqi
9	core + Seshan25 + Urumqi + Kunming
10	core + Parkes + Kokee + Hartrao + Seshan25 + Urumqi + Kunming

2. Solution Statistics

We used two source selection scenarios. For the first scenario, the SKED program was used to select objects from a list of 120 strong radio sources (flux density ≥ 1 Jy in S/X-bands), almost all of them located in the Southern Hemisphere. For the second scenario, 159 radio sources around the ecliptic zone were added to the list of 120 sources. Figures 1–3 show the number of sources, scans, and group delays scheduled in the ten networks using both source selection scenarios. Due to different network configurations SKED selected different numbers of sources for the simulated 24-hour sessions. For a regional network, comprised of the 12-meter Australian and New Zealand facilities only, the number of sources is 20, whereas for the largest network (No. 10) the number of sources is about 180 (Figure 1). The number of scans varies from 100 to 500 (Figure 2), and the number of group delays varies from 350 to 1000–1500 (Figure 3).

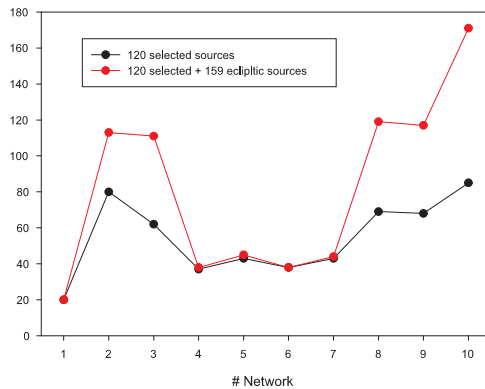


Figure 1. Number of sources scheduled for the two source selection scenarios.

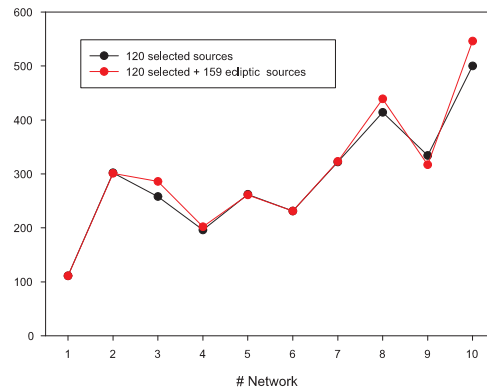


Figure 2. Number of scans scheduled for the two source selection scenarios.

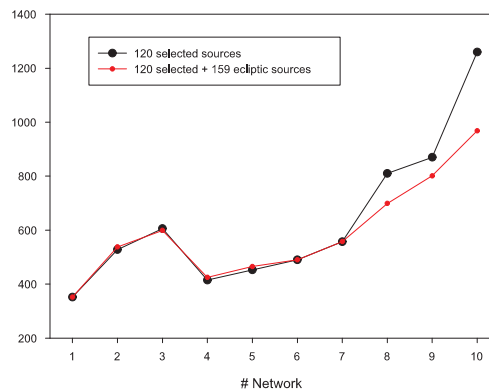


Figure 3. Number of group delays scheduled for the two source selection scenarios.

These statistics show that even the small regional network of four 12-meter antennas produces a sufficient number of observations to fulfill the astrometric goals. The addition of HartRAO,

Fortaleza, and Kokee (networks 4, 5, and 6) does not change these numbers dramatically. The addition of the Chinese stations Seshan25, Urumqi, and Kunming in different combinations (networks 2, 3, 8, and 9) looks more promising. Our results show that the final network (No. 10) with ten antennas is the best option; however, this network is unlikely to be realized on a regular basis.

Simulations for a third scenario using the list of the 295 ICRF2 defining radio sources [1] have also been examined. These sources are more evenly distributed across the sky, so the number of scheduled sources varies from 84 to 200 for the different network configurations.

3. Positional Accuracy

The core network of four 12-meter dishes produces a reasonable accuracy for the 20 selected radio sources. Figure 4a shows that for this schedule the formal standard deviations lie within a range of 1–5 mas. The results for the second scenario (including ecliptic sources) are similar (Figure 4b).

The standard deviations of individual radio sources in the ICRF2 scenario lie within a range of 5–200 mas. Many more sources were scheduled (89) with many observed only one or two times, which results in large formal errors. In Figure 4c we plotted only the 19 sources observed at least 5 times. Alternatively, scheduling 14 ICRF2 defining sources astrometrically yielded formal errors of 2–5 mas.

Simulations for network No. 10 for all three cases are more similar. For the full group of 120 Southern Hemisphere sources the standard deviations are within the range of 1–3 mas, with some values up to 10 mas (Figure 4d). The other two scenarios provide more radio sources to be scheduled; consequently, more formal errors exceed 3 mas (Figures 4e and 4f). Nonetheless, the number of sources with standard deviations within a range of 1–3 mas is still adequate for accurate astrometry.

4. Conclusions

We can use the AuScope/New Zealand network of four VLBI sites for a program of astrometry of strong radio sources in the Southern Hemisphere. In conjunction with the facilities from the wider Asia-Pacific region, the network could be used to densify the reference radio sources along the ecliptic zone. Further improvement of the technical specifications of the 12-meter antennas, such as the reduction of SEFD values, will make the observational astrometric programs significantly more flexible.

5. Acknowledgments

This paper has been published with permission of the Chief Executive Officer of Geoscience Australia.

References

- [1] Fey, A., D. Gordon, and C. Jacobs (eds.), The second realization of the International Celestial Reference Frame by Very Long Baseline Interferometry, IERS Technical Notes 35, 2009.

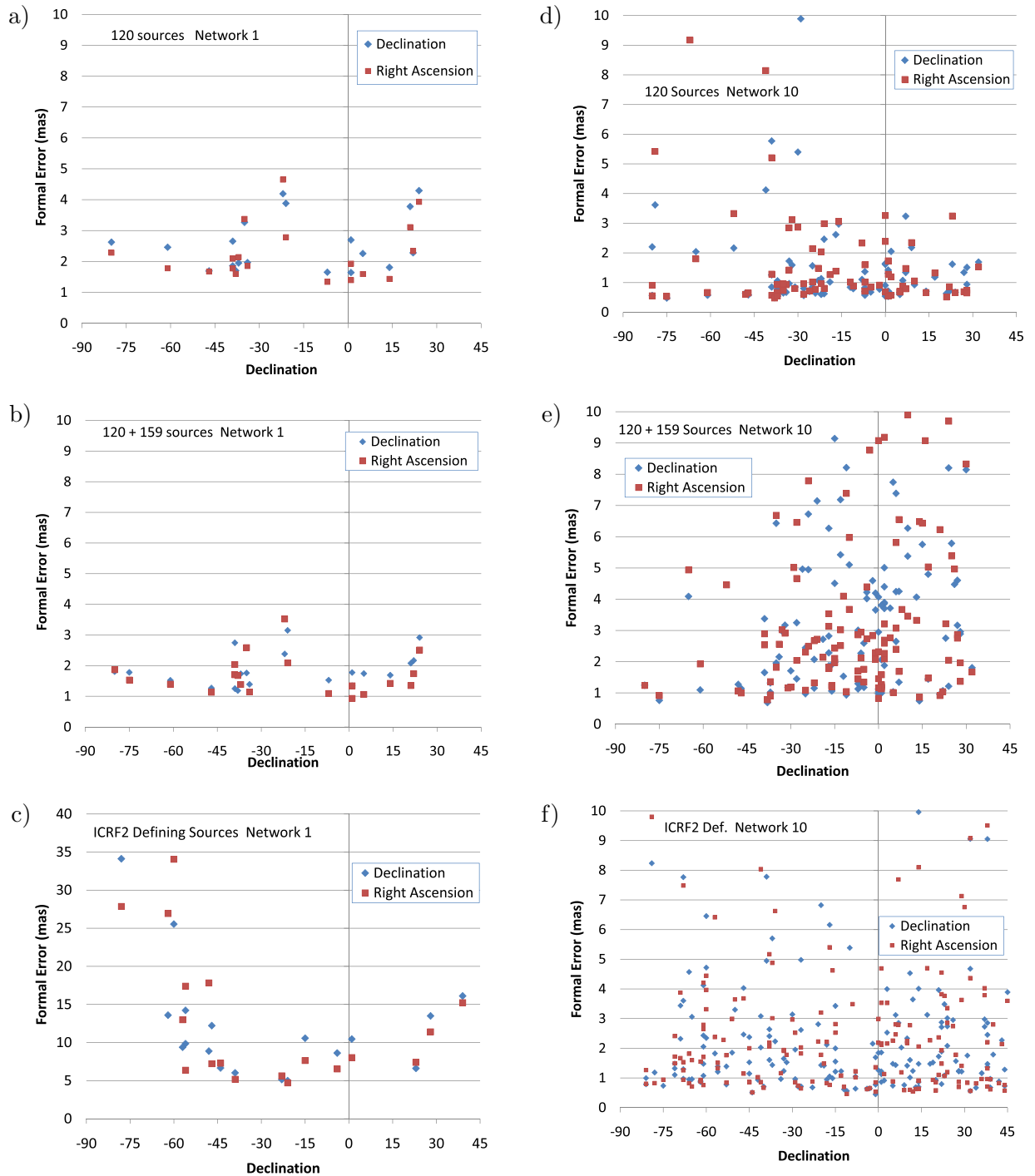


Figure 4. (left) Formal errors obtained in the simulations with the core network (network No. 1) for the source lists of a) 120 sources, b) 120 + 159 sources, and c) the ICRF2 defining sources. (right) Formal errors obtained in the simulations with the network No. 10 for the source lists of d) 120 sources, e) 120 + 159 sources, and f) the ICRF2 defining sources.

About the Compatibility of DORIS and VLBI Observations

Gennady Il'in, Sergey Smolentsev, Roman Sergeev

Institute of Applied Astronomy of RAS

Contact author: Gennady Il'in, e-mail: igen@ipa.rssi.ru

Abstract

We investigated the compatibility of the DORIS and VLBI observations at Badary Observatory. The DORIS beacon stands at 100-m distance from the main radio telescope dish and transmits signals on two frequencies: 2036.25 MHz and 401.25 MHz. The latter frequency is modulated to send messages containing an ID number, timing information, data from the meteorological sensors, and engineering data (e.g., power). Both frequencies affect the *S/X* band radio telescope receivers. The parameters of the DORIS signals were measured at the outputs of the *S/X* band intermediate frequency amplifier. It was found that: (1) The level of RFI, produced by the DORIS beacon, practically corresponds to the level of the system (antenna plus receiver) noise signal and does not overload the *S/X* band receivers. (2) The DORIS 401.25 MHz signal is out of the frequency bands recorded during standard VLBI sessions. As a result, RFI from DORIS does not affect VLBI observations. This conclusion was confirmed after data correlations of actual VLBI observations that were conducted with the DORIS beacon turned on/off.

The Badary DORIS station ground-beacon is equipped with a Starec 52291 type antenna. This antenna was installed on 11.08.2004 (for details, see the logfile at <http://ids.cls.fr/documents/doris/stations/log/archive/BADB200812.LOG>).



Figure 1. Badary's DORIS Starec-type antenna and RT-32 radio telescope. View from control block.

The DORIS beacon stands on the cover of a control block, at a distance of about 100 m from the main radio telescope dish and transmits signals on two frequencies: $f_1 = 2036.25$ MHz and $f_2 = 401.25$ MHz. The latter frequency is modulated to send messages containing an ID number, timing information, data from the meteorological sensors, and engineering data (e.g., power). Signals f_1 and f_2 are classified as “NONE” and “15K0G1D”, according to the recommendation ITU-R SM.1138. Thus we can observe narrowband signals in spectrograms, obtained with a GW Instek GSP-827 Spectrum Analyzer: signal f_1 as a sine signal spectrum and signal f_2 as a 15 kHz bandwidth one.

The Effective Isotropically Radiated Power (EIRP) values of the signals emitted on the f_1 and f_2 frequencies are 16.4 dB and 13.8 dB. Both of these strong signals affect the S/X band radio telescope receivers. In this paper we present results of DORIS and VLBI compatibility investigation.

The DORIS f_1 signal can affect the S band receiver, because the input frequencies of the receiver are 2.15–2.50 GHz and the LO is 2.02 GHz. As a result, the f_1 signal is attenuated and then converted to the intermediate frequencies (IF), producing radio frequency interference (RFI) at 16.25 MHz — near the lower end of the receiver IF bandwidth of 110–480 MHz.

The parameters of the DORIS RFI signals were measured for both S/X band receivers with a GW Instek GSP-827 Spectrum Analyzer. All measurements were taken at the outputs of more than 150 m coaxial phase stable lines, inside the control room, where the receiver IF signals are converted to the video frequencies (see Table 1) and registered.

Table 1. Video converter frequencies for R1 and R4 VLBI sessions, bandwidth 8 Hz, S/X band receivers.

Channel	Sky freq, MHz	LO freq, MHz	Video, MHz	Channel	Sky freq, MHz	LO freq, MHz	Video, MHz
01	2225.99	2020.00	205.99	04	2295.99	2020.00	275.99
02	2245.99	2020.00	225.99	05	2345.99	2020.00	325.99
03	2265.99	2020.00	245.99	06	2365.99	2020.00	345.99
01	8212.99	8080.00	132.99	05	8732.99	8080.00	652.99
02	8252.99	8080.00	172.99	06	8852.99	8080.00	772.99
03	8352.99	8080.00	272.99	07	8912.99	8080.00	832.99
04	8512.99	8080.00	432.99	08	8932.99	8080.00	852.99

The output signal spectrum of the S band receiver is presented in Figure 2. The RFI from the DORIS f_1 signal is marked by red letters. The level of RFI, produced by the f_1 signal (-93 dBm), is significantly lower than the level of the system (antenna plus receiver) noise signal of -75 dBm and does not influence the VLBI observations. For correct identification of RFI, the same spectrum is presented in Figure 3, when the DORIS beacon is turned off.

The DORIS f_2 signal is applied directly to the S/X band receivers’ IF tract, and the long distance coaxial line probably serves as an antenna. The DORIS f_2 signal is effectively attenuated, practically to the receiver system noise signal level, as can be seen in Figures 4 and 5. The same spectrograms were obtained for the X band receiver.

Because of the small level and bandwidth (15 kHz) this signal can not significantly influence the VLBI observations at S/X bands. According to Table 1, the DORIS f_2 signal is outside of the

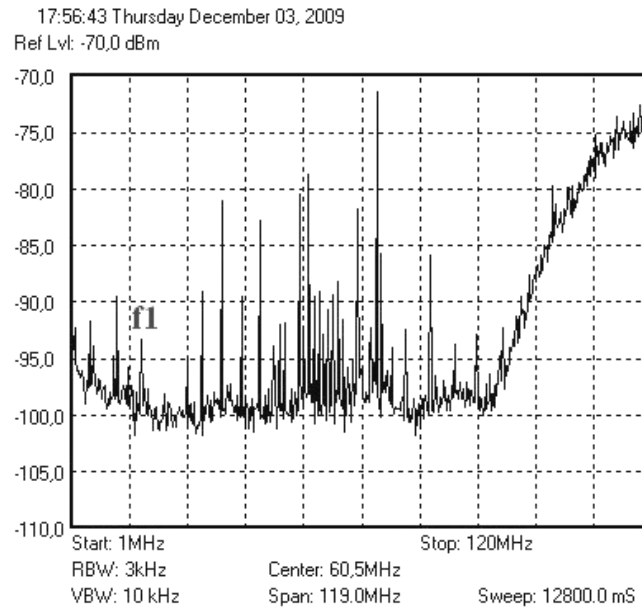


Figure 2. Output signal of the *S* band receiver with the DORIS beacon turned on.

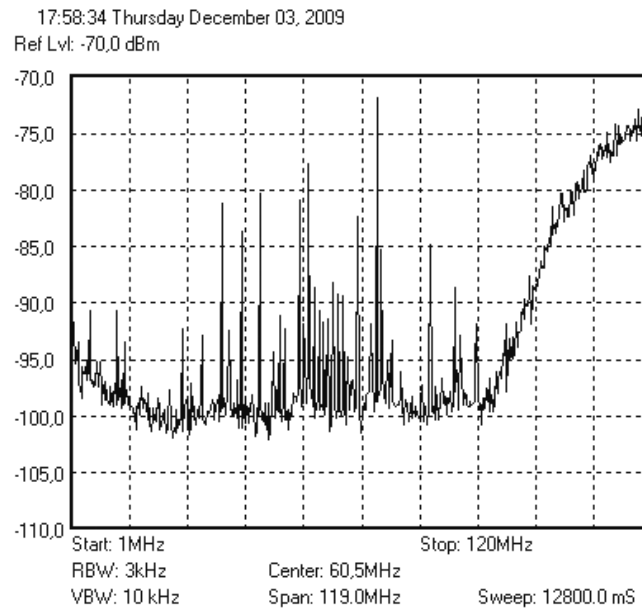


Figure 3. Output signal of the *S* band receiver with the DORIS beacon turned off.

frequency bands recorded during standard VLBI R1 and R4 sessions.

In summary, RFI from the DORIS beacon does not affect standard VLBI observations. This conclusion was confirmed after data correlation of actual VLBI observations that were conducted with the DORIS beacon turned on/off.

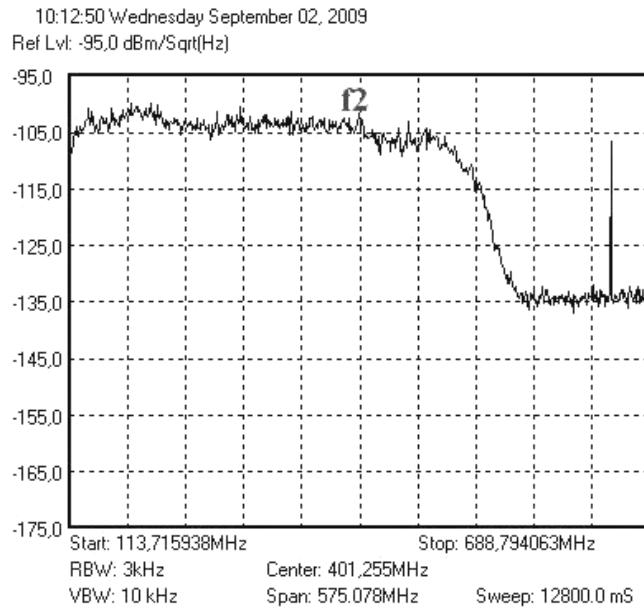


Figure 4. *S* band receiver output signal spectrum with small f_2 RFI (DORIS – turned on).

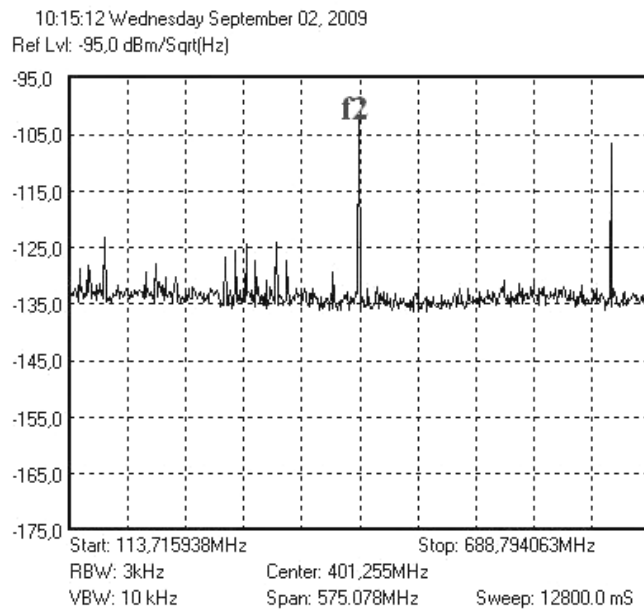


Figure 5. *S* band receiver output signal spectrum with f_2 RFI (DORIS – turned off).

The DORIS beacon f_1 signal must be carefully filtered when a wide-band receiver is used—as is planned for the VLBI2010 system. In this case the DORIS–VLBI compatibility will be a real problem!



Session 3 - VLBI Data Structure, Analysis Strategies and Software

IVS Working Group 4: VLBI Data Structures

John Gipson

NVI, Inc., Code 698, NASA Goddard Space Flight Center, Greenbelt, MD, 20771

e-mail: john.m.gipson@nasa.gov

Abstract

In 2007 the IVS Directing Board established IVS Working Group 4 on VLBI Data Structures. This note discusses the current VLBI data format, goals for a new format, the history and formation of the Working Group, and a timeline for the development of a new VLBI data format.

1. Introduction

At the 15 September 2007 IVS Directing Board meeting I proposed establishing a “Working Group on VLBI Data Structures”. The thrust of the presentation was that, although the VLBI database system has served us very well these last 30 years, it is time for a new data structure that is more modern, flexible, and extensible. This proposal was unanimously accepted, and the board established IVS Working Group 4. Quoting from the IVS Web site [1]: *“The Working Group will examine the data structure currently used in VLBI data processing and investigate what data structure is likely to be needed in the future. It will design a data structure that meets current and anticipated requirements for individual VLBI sessions including a cataloging, archiving, and distribution system. Further, it will prepare the transition capability through conversion of the current data structure as well as cataloging and archiving softwares to the new system.”*

Any change to the VLBI data format affects everyone in the VLBI community. Therefore, it is important that the working group have representatives from a broad cross-section of the IVS community. Table 1 lists the current members of WG4 together with their affiliation or function. The initial membership was arrived at in consultation with the IVS Directing Board. While we wanted to ensure that all points of view were represented we also wanted to make sure that the size did not make WG4 unwieldy. The current composition and size

Table 1. Membership in Working Group 4.

Chair	John Gipson
Analysis Coordinator	Axel Nothnagel
Haystack/Correlator Representative	Roger Cappallo
GSFC/Calc/Solve	David Gordon
JPL/Modest	Chris Jacobs Ojars Sovers
Occam	Oleg Titov Volker Tesmer
TU Vienna	Johannes Böhm
IAA	Sergey Kurdobov
Steelbreeze	Sergei Bolotin
Observatoire de Paris/PIVEX	Anne-Marie Gontier
NICT	Thomas Hobiger Hiroshi Takiguchi

of WG4 is a reasonable compromise between these two goals. My initial request for participation in WG4 was enthusiastic: everyone I contacted agreed to participate with the exception of an individual who declined because of retirement.

2. History of Working Group 4

WG4 held its first meeting at the 2008 IVS General Meeting in St. Petersburg, Russia. This meeting was open to the general IVS community. Roughly 25 scientists attended: ten WG4 members and fifteen others. This meeting was held after a long day of proceedings. The number of participants and the lively discussion that ensued is strong evidence of the interest in this subject. A set of design goals, displayed in Table 2, emerged from this discussion. In some sense the design goals imply a combination and extension of the current VLBI databases, the information contained on the IVS session Web-pages, and much more information [2].

During the next year the working group communicated via email and telecon and discussed how to meet the goals that emerged from the St. Petersburg meeting. A consensus began to emerge about how to achieve most of these goals.

Table 2. Key goals of the new format.

Goal	Description
Provenance	Users should be able to determine the origin of the data and what was done to it.
Compactness	The data structure should minimize redundancy and the storage format should emphasize compactness.
Speed	Commonly used data should be able to be retrieved quickly.
Platform/OS/ Language Support	Data should be accessible by programs written in different languages, running on a variety of computers and operating systems.
Extensible	It should be easy to add new data types.
Open	Data should be accessible without the need of proprietary software.
Decoupled	Different types of data should be separate from each other.
Multiple data levels	Data should be available at different levels of abstraction. For example, most users are interested only in the delay and rate observables. Specialists may be interested in correlator output.
Completeness	All VLBI data required to process (and understand) a VLBI session from start to finish should be available: schedule files, email, log-files, correlator output, and final ‘database’.
Web Accessible	All data should be available via the Web.

The next face-to-face meeting of WG4 was held at the 2009 European VLBI Meeting in Bordeaux, France. This meeting was also open to the IVS community. At this meeting a proposal was put forward to split the data contained in the current Mark III databases into smaller files which are organized by a special ASCII file called a wrapper. I summarized some of the characteristics and advantages of this approach. Overall the reaction was positive.

In the summer of 2009 we worked on elaborating these ideas, and in July a draft proposal was circulated to Working Group 4 members. Concurrently I began a partial implementation of these ideas and wrote software to convert a subset of the data in a Mark III database into the new format. This particular subset included all data in NGS cards and a little more. The subset was chosen because many VLBI analysis packages including Occam, Steelbreeze, and VieVS use NGS cards as input. In August 2009 we made available, via anonymous ftp, three VLBI sessions in the

new format: an Intensive, an R1, and an RDV.

In the fall of 2010, Andrea Pany of the Technical University of Vienna developed an interface to VieVS working with the draft proposal. During this process the definition of a few of the data items needed to be clarified, which emphasizes the importance of working with the data hands on. At NASA's Goddard Space Flight Center, Sergei Bolotin interfaced a variant of this format to Steelbreeze. Steelbreeze uses its own proprietary format, and one motivation for interfacing to the new format was to see if there was a performance penalty associated with using the new format. Bolotin found a performance penalty of $40 \mu s/\text{observation}^1$. There are currently $\simeq 6$ million VLBI observations, which translates into an extra 6 minutes to process all of the VLBI data—a modest price to pay for the many advantages the new format brings.

3. Overview of New Organization

In a paper of this size it is impossible to completely describe the new organization and format. Instead, I will briefly describe three of the key components: 1) modularization; 2) storing data in NetCDF files; and 3) using wrapper files to organize the data.

3.1. Modularization

A solution to many of the design goals of Table 3 is to modularize the data, that is to break up the data associated with a session into smaller pieces. These smaller pieces are organized by ‘type’; e.g., group delay observable, met-data, editing criteria, station names, and station positions. In many, though not all, cases, each ‘type’ corresponds to a Mark III database L-code. Different data types are stored in different files, with generally only one or a few closely related data types in each file. For example, it might be convenient to store all of the met-data for a station together in a file. However, there is no compelling reason to store the met-data together with pointing information. Splitting the data in this way has numerous advantages, some of which are outlined below. The first three directly address the design goals. The remaining are other advantages not originally specified, but are consequences of this design decision.

1. **Separable.** Users can retrieve only that part of the data in which they are interested.
2. **Extensible.** As new data types become used, for example, source maps, they can be easily added without having to rewrite the whole scheme. All you need to do is specify a new data type and the file format.
3. **Decoupled.** Different kinds of data are separated from each other. Observables are separated from models. Data that won't change is separated from data that might change.
4. **Flexible.** Since different data is kept in different files, it is easy to add new data types.
5. **Partial Data Update.** Instead of updating the entire database, as is currently done, you only need to update that part of the data that has changed.²

Data will also be organized by ‘scope’, that is how broadly applicable it is: Does it hold for the entire session, for a particular scan, for a particular scan and station, or for a particular observation. The current Mark III database is observation oriented: all data required to process a

¹No effort was made to optimize the interface. With optimization this figure should be less.

²This is done by making a new version of the relevant file, keeping the old one intact.

given observation is stored once for each observation. This results in tremendous redundancy for some data. For example, in an N -station scan, each station will participate in $N - 1$ observations. Station met-data, which is the same for all observations in a scan, is stored once for each observation instead of once per scan. This results in an $(N - 1)$ -fold redundancy. Organizing data by scope allows you to reduce redundancy.

3.2. Organizing Data by Wrappers

The main disadvantage of breaking up the VLBI data into many smaller files is that you need some way of organizing the files. This is where the concept of a wrapper comes in. A wrapper is an ASCII file that contains pointers to VLBI files associated with a session. VLBI analysis software parses this file and reads in the appropriate data. As new data types are added, or as data is updated, new versions of the wrapper can be generated. The wrapper concept is illustrated schematically in Figure 1. The wrapper can serve several different purposes:

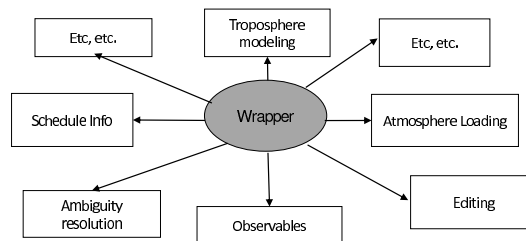


Figure 1. Wrappers organize the data.

1. The wrapper can be used by analysis programs to specify what data to use.
2. The wrapper allows analysts to experiment with ‘what if’ scenarios, for example, to use another analysts editing criteria which is stored in a file. All you need to do is to obtain the editing file and modify the wrapper to point to it.
3. Because of the general structure of the wrapper, different analysis packages can use different wrappers that point to different subsets of the VLBI data.
4. The wrapper is a convenient means of signaling to the IVS data center what information is required. In this scenario, a user writes a wrapper with pointers to the relevant files and sends it to the IVS data center. The data center packages the data in tar-file and makes it available. (Since all data is available via FTP this is a convenience.)

3.3. NetCDF as Default Storage Format

Working Group 4 reviewed a variety of data storage formats including NetCDF, HCDF, CDF, and FITS. In some sense, all of these formats are equivalent—there exist utilities to convert from one format to another. Ultimately we decided to use NetCDF, because it has a large user community and because several members of the Working Group have experience with using NetCDF. At its most abstract, NetCDF is a means of storing arrays in files. The arrays can be of different sizes and shapes, and contain different kinds of data—strings, integer, real, double, etc. Most VLBI data used in analysis is some kind of array. From this point of view

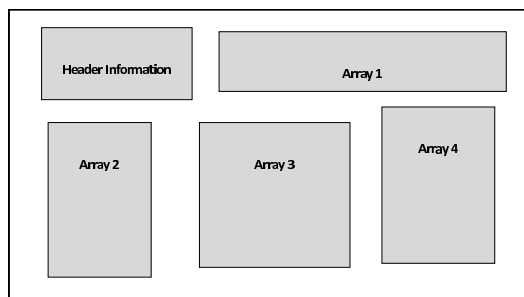


Figure 2. A NetCDF file is a container for arrays.

using NetCDF is a natural choice. These files can contain history entries which aid in provenance. Storing data in NetCDF format has the following advantages:

1. **Platform/OS/Language Support.** NetCDF has interface libraries to all commonly used computer languages running on a variety of platforms and operating systems.
2. **Speed.** NetCDF is designed to access data fast.
3. **Compactness.** The data is stored in binary format, and the overhead is low. A NetCDF file is much smaller than an ASCII file storing the same information.
4. **Open.** NetCDF is an open standard, and software to read/write NetCDF files is freely available.
5. **Transportability.** NetCDF files use the same internal format regardless of the machine architecture. Access to the files is transparent. For example, the interface libraries take care of automatically converting from big-endian to little-endian.
6. **Large User Community.** Because of the large user community, there are many tools developed to work with NetCDF files.

4. Next Steps

The immediate next step is for various VLBI software developers to develop interfaces to the new format. It is likely that this will lead to further refinement.

- VieVS already has an interface to the new format.
- At Goddard we plan on interfacing solve to the new format in the fall of 2010. Initially the new format will be a replacement for solve superfiles and will be used in global solutions. Gradually we will modify *calc/solve* to use the new format at earlier stages of analysis.
- Oleg Titov (private communication) plans on developing an interface to Occam in the winter of 2010 or the spring of 2011.

Beginning in the spring of 2011 we will make a subset of the data in the current Mark III databases available in the new format. This subset will include all data currently in the NGS cards as well as all data required for *calc/solve* analysis. The size of this subset will expand through 2011 until by the end of the year all of the data that is currently in the Mark III database format will be available in the new format. We will also work on gathering correlator output files and making these available on the IVS data center.

In March 2011, there will be an open meeting of IVS Working Group 4 at the European VLBI meeting. This will provide another opportunity for the VLBI community to provide further feedback and for fine-tuning the specifications if they are required. Working Group 4 will also work on its final report, which will be presented to the IVS Directing Board. We anticipate that the last meeting of WG4 will be at the 2012 General Meeting, at which point it will dissolve.

References

- [1] <http://ivscc.gsfc.nasa.gov/about/wg/wg4/index.html>
- [2] Gipson, J., IVS Working Group 4 on VLBI Data Structures, The 5th IVS General Meeting Proceedings, 2008, p. 143-152.

VLBI Data Interchange Format (VDIF)

Alan Whitney¹, Mark Kettenis², Chris Phillips³, Mamoru Sekido⁴

¹) *MIT Haystack Observatory*

²) *Joint Institute for VLBI in Europe*

³) *Australia Telescope National Facility, CSIRO*

⁴) *National Institute of Information & Communications Technology*

Contact author: Alan Whitney, e-mail: arw@haystack.mit.edu

Abstract

One important outcome of the 7th International e-VLBI Workshop in Shanghai in June 2008 was the creation of a task force to study and recommend a universal VLBI data format that is suitable for both on-the-wire e-VLBI data transfer, as well as direct disk storage. This task force, called the VLBI Data Interchange Format (VDIF) Task Force, is the first part of a two-part effort, the second of which will address standardization of e-VLBI data-transmission-protocols. The formation of the VDIF Task Force was prompted particularly by increased e-VLBI activity and the difficulties encountered when data arrive at a correlator in different formats from various instruments in various parts of the world. The task force created a streaming packetized data format that may be used for real-time and non-real-time e-VLBI, as well as direct disk storage. The data may contain multiple channels of time-sampled data with an arbitrary number of channels, arbitrary #bits/sample up to 32, and ‘real’ or ‘complex’ data; data rates in excess of 100 Gbps are supported. Each data packet is completely self-identifying via a short header, and data may be decoded without reference to any external information. The VDIF task force has completed its work, and the VDIF standard was ratified at the 2009 e-VLBI workshop in Madrid.

1. Introduction

The VLBI Standard Interface (VSI) specifications, developed in the early 2000s and designated VSI-H and VSI-S, are aimed primarily at recording and playback systems, and specify standards for a hardware/electrical VLBI data interface and a software control interface, respectively. These VSI specifications intentionally do not address the format of the transported data.

In recent years, a number of new VLBI data-acquisition and capture systems have appeared, along with increasing need to interchange data on a global scale, including real-time and near-real-time transfer via high-speed network, as well as by standard disk-file transfer. These types of data transfers have been increasingly plagued by the lack of an internationally agreed data format, often requiring ad hoc format conversions that require both programming effort and computing/storage resources. Recognizing this problem, a so-called VSI-E (‘E’ for ‘e-VLBI’) specification, based on standard RTP/RTCP network protocol, was first proposed and implemented in 2003-2004, which specified both data formats and data-transport mechanisms for real-time e-VLBI data transfer. Although VSI-E was comprehensive, it was never formally ratified by the larger VLBI community. Its adoption was further hampered by its complexity, and it has been largely abandoned.

The VLBI Data Interface Specification (VDIF) has a somewhat different goal from VSI-E, specifying only a standardized transport-independent VLBI data-interchange format that is suitable for all types of VLBI data transfer, including real-time and near-real-time e-VLBI, as well as disk-file

storage. The VDIF specification, unlike VSI-E, explicitly makes no attempt to define an on-the-wire data-transport protocol, which is expected to be the subject of a subsequent specification document. The combination of VDIF, along with this follow-on data-transport-protocol specification, will, when completed, essentially constitute a replacement for VSI-E. And although the VDIF specification makes no mention of data-transport protocol, it has been developed with an awareness of expected methods of data transport, including network transport using various standard protocols, as well as physical or electronic transport of standard disk files.

2. VDIF Task Force

The 7th International e-VLBI Workshop, held 14-17 June 2008 in Shanghai, China, included panel and group discussions specifically targeting the subject of creating an international data-format standard. Those discussions led to the creation of a small, broadly-based international task force (subsequently known as the VDIF Task Force) to study the problem and make recommendations to the larger VLBI community.

3. Basic VDIF Structure

The discussions at the Shanghai meeting supported the concept of a ‘framed’ data-stream format consisting of a stream of “Data Frames,” each containing a short self-identifying Data Frame Header, followed by a Data Array (containing the actual samples). A similar format is already used by several current and proposed disk-based recording systems.

Accordingly, the VDIF specification is based upon a basic self-identifying Data Frame, which carries a time segment of time-sampled data from one or more frequency sub-bands. The length of a Data Frame may be chosen by the user to best match the chosen transport protocol; for example, in the case of real-time network transfer, a VDIF Data Frame length would normally be chosen so that exactly one Data Frame is carried by each on-the-wire packet. It is important to emphasize that the VDIF Data Frame is fundamentally transport-protocol independent, so that exactly the same set of Data Frames can represent VLBI data through a network transfer or be stored to a physical disk file.

In some cases, an entire set of sampled frequency sub-bands (or ‘channels’) may be carried in each Data Frame. In other cases, a single Data Frame may carry data from only a single data sub-band (channel) from among a set of many, in which case a logically parallel set of Data Frames is needed to represent the entire data set. In the VDIF concept, each time-series of Data Frames from the

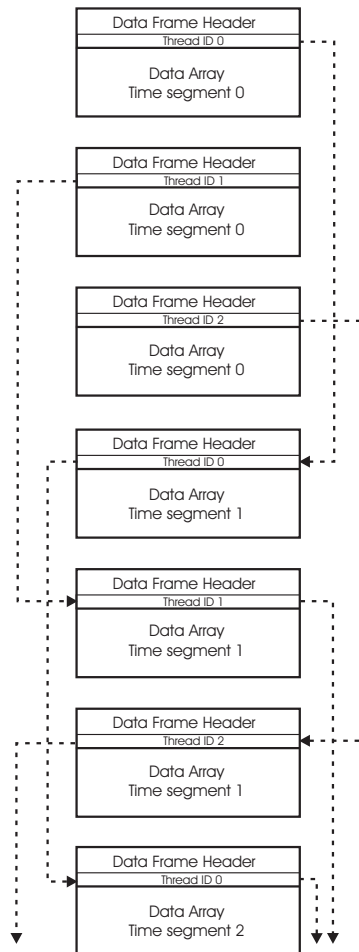


Figure 1. Illustration of Data Threads within a Data Stream.

same set of sub-bands(s) is known as a ‘Data Thread,’ where each of the Data Frames within the Data Thread is identified by a ‘Thread ID’ embedded in the Data Frame Header. For actual transmission over a serial-data network, or for storage on a disk file, the set of Data Threads that comprise the data set are merged into a single serial ‘Data Stream’. Figure 1 shows a schematic example of a Data Stream comprised of three Data Threads. The collection of Data Threads from the beginning to the end of a particular observation, typically lasting seconds to minutes, is known as a Data Segment.

In normal usage, it is expected that two types of Data Streams will predominate: 1) a Data Stream consisting of a single Data Thread carrying multi-channel Data Frames or 2) a Data Stream consisting of multiple single-channel Data Threads, although mixing of single-channel and multi-channel Data Threads is not prohibited.

4. VDIF Attributes

The following considerations guided the creation of the VDIF specification:

1. The data in each Data Stream must be decodable using only information embedded within its constituent Data Frames.
2. A Data Thread may be discontinuous in time at the resolution of a Data Frame (e.g., transmit/capture Data Frames only during the active part of a pulsar period).
3. Each Data Frame may carry single-bit or multiple-bit samples up to 32 bits/sample.
4. Up to a maximum of 1024 Data Threads, each with a unique Thread ID, may be included in a single Data Stream.
5. A minimum of data manipulation should be necessary to move data between various data-transmission techniques (e.g., disk file or real-time transfer).
6. Data rates up to at least ~ 100 Gbps should be supported.
7. The data overhead (e.g., embedded auxiliary information required to meet the VDIF requirements) must be as low as practical.
8. Observations over leap seconds and year boundaries must be transparently supported.
9. The VDIF data format must be compatible, in as natural a way as possible, with all expected data-transport methods (e.g., network transfer, file transfer).
10. Some limited amount of auxiliary user-defined data should be allowed in the Data Stream.
11. Within certain defined limits, out-of-time-order data within a Data Thread should be accommodated.

5. Data Frame Rules

The following rules govern each VDIF Data Frame within a given Data Thread:

Each Data Frame contains a Data Frame Header followed by a Data Array.

1. All Data Frames must have the same Data Frame Header length, Data Array length, #channels, #bits/sample, and Station ID.
2. If a Data Frame contains data from multiple channels, the same time-tag must apply across channels.
3. If a Data Frame contains multiple channels, all channels must be sampled with the same number of bits/sample.
4. Each Data Array contains sample data from one or more channels with format (Section 9) and encoding (Section 10) specified by VDIF.
5. The Data Frame length (including Data Frame header) for each Data Thread must meet the following criteria:
 - (a) Must be a multiple of 8 bytes (for maximum compatibility with various computer-memory-address schemes and disk-addressing algorithms).

- (b) Must be chosen so that an integer number of complete Data Frames are created in a continuous data flow of exactly one-second duration.
- 6. Data Frame #0 of each one-second period must contain, as its first sample, the data taken on a second tick of UTC; note that, in the case of time-discontinuous data, Data Frame #0 may not always be present.

These rules are intended to cover both ‘on-the-wire’ e-VLBI data formats as well as disk-file formats. For ‘on-the-wire’ real-time e-VLBI, it is expected that each transmitted non-fragmented packet will contain a single VDIF Data Frame as its data payload, in which case the Data Frame length is normally restricted to the range ~64–9000 bytes. These restrictions do not apply to disk-file data format, for which the Data Frame length is limited (by the number of bits available to specify the Data Frame length) to 2^{27} bytes (~134 MBytes).

6. Data Frame Header

Each VDIF Data Frame carries a Data Frame Header as shown in Figure 2, which may be either 16 or 32 bytes in length, depending on whether the Extended User Data words are included.

	Byte 3		Byte 2		Byte 1		Byte 0	
	Bit 31 (MSB)						Bit 0 (LSB)	
Word 0	I ₁	L ₁	Seconds from reference epoch ₃₀					
Word 1	Un-assigned ₂		Ref Epoch ₆		Data Frame # within second ₂₄			
Word 2	V ₃		log ₂ (#chns) ₅		Data Frame length (units of 8 bytes) ₂₄			
Word 3	C ₁	bits/sample-1 ₅		Thread ID ₁₀		Station ID ₁₆		
Word 4	EDV ₈			Extended User Data ₂₄				
Word 5	Extended User Data ₃₂							
Word 6	Extended User Data ₃₂							
Word 7	Extended User Data ₃₂							

Figure 2. VDIF Data Frame Header format; subscripts are field lengths in bits; byte #s indicate relative byte address within 32-bit word (little endian format).

7. Byte Ordering

Byte ordering of both the Data Frame Header and Data Frame is little-endian (Intel x86 order) based on 32-bit words, which is consistent with most existing disk-based systems and software-based correlators.

8. Data Frame Ordering

Data coming from a single data source (e.g., a single dBBC or DBE) will normally be transmitted in strict time order. If directly connected to a local recording device, the recorded data

will almost certainly be recorded in exactly the same order. However, Data Frames transmitted through a switch or over a network are not guaranteed to arrive in order.

The VDIF specification does not mandate strict Data Frame ordering within a Data Thread, but a best effort should be made to do so. Some correlation equipment, particularly older types, may be sensitive to Data Frame order, in which case the requirements of Data Frame ordering will be dictated by the correlation equipment. Modern software correlators are generally rather tolerant of minor Data Frame re-ordering of the type that might occur.

9. Data Array Formats

VDIF specifies the format of a Data Array based solely on the #channels and #bits/sample specified in the corresponding Data Frame Header. Since these two pieces of information are contained in each Data Frame Header, the samples in each Data Frame may be decoded with no external information.

The number of channels that can be accommodated in a multi-channel Data Array are limited to 2^n , but it is expected that most users will prefer to use a single-channel Data Array. The use of multiple single-channel Data Threads allows the user to transmit an arbitrary number of channels, as well as being a more compatible format for the evolving generation of software correlators. Any number of bits/sample from 1 to 32 are supported, though the Data Array may contain some pad bits for certain values of bits/sample. Samples may either be ‘real’ or may occur in ‘complex pairs’, such as are sometimes used in standard digital-signal-processing algorithms.

10. Sample Representation

VDIF-encoded data samples are represented by the desired number of bits in a fixed-point ‘offset binary sequence’, beginning with all 0’s for the most-negative sampled value to all 1’s for the most-positive sampled value. For example, 2-bit/sample coding is (in order from most negative to most positive) 00, 01, 10, 11. This coding is compatible with existing Mark 5B, K5, and LBADR disk-based VLBI data systems, though bit-ordering may be different in some cases.

11. Summary

The VDIF specification is one more piece of the on-going effort to achieve global standardization of VLBI interfaces and formats. All of these efforts are intended to ease the interchange of hardware, software, and data among the world’s VLBI practitioners to improve VLBI efficiency and result in higher quality data. The VDIF draft specification, with minor modifications, was formally approved by the participants of the 8th International VLBI Workshop held in Madrid in June 2009. In addition, a task force was created to address the specification for a standardized on-the-wire data-transport protocol (provisionally called the VLBI Transport Protocol or ‘VTP’ protocol) to complement the VDIF specification; hopefully the attendees of the 10th International VLBI Workshop (to be held in Perth, Australia) will be able to ratify a VTP specification and complete the work on this complementary pair of important documents. All of the VLBI standardized specifications, including the VDIF specification, are available at <http://www.vlbi.org/vsi>.

Development of a New VLBI Data Analysis Software

Sergei Bolotin, John M. Gipson, Daniel S. MacMillan

NVI, Inc./NASA Goddard Space Flight Center

Contact author: Sergei Bolotin, e-mail: sergei.bolotin@nasa.gov

Abstract

We present an overview of a new VLBI analysis software under development at NASA GSFC. The new software will replace CALC/SOLVE and many related utility programs. It will have the capabilities of the current system as well as incorporate new models and data analysis techniques.

In this paper we give a conceptual overview of the new software. We formulate the main goals of the software. The software should be flexible and modular to implement models and estimation techniques that currently exist or will appear in future. On the other hand it should be reliable and possess production quality for processing standard VLBI sessions. Also, it needs to be capable of processing observations from a fully deployed network of VLBI2010 stations in a reasonable time. We describe the software development process and outline the software architecture.

1. Introduction

The current VLBI data analysis package, CALC/SOLVE, has served us for more than thirty years. It is the most widely used data analysis software in the geodetic/astrometry VLBI community. CALC/SOLVE software is used for data preparation as well as analysis of VLBI observations. Database output from CALC/SOLVE is input to other VLBI data analysis packages. The current CALC/SOLVE system consists of more than a hundred individual programs most of which are written mostly in FORTRAN90. Many significant results were obtained with CALC/SOLVE in various branches of astronomy, geodesy, and geophysics.

However, the software has certain limitations. CALC/SOLVE was developed as a set of utilities around the Mark III database handler, which was created at the end of the 1970s and then was frozen. Computer hardware limitations that were in effect at that time still constrain the database access library and procedures that use it. On the other hand, since CALC/SOLVE is a production system in the VLBI data flow (preparation of *Version 4* databases and *NGS* files), adding new models and features was usually done as patches over existing code or even as ‘tricks’ to keep the existing general structure of the software. As a result, it is hard to maintain and to extend the current CALC/SOLVE system. Moreover, the forthcoming VLBI2010 system will demand flexibility and performance that the current realization of CALC/SOLVE cannot satisfy.

Therefore, in 2007 the VLBI group at the NASA Goddard Space Flight Center started active work on developing a new VLBI data analysis system. With the help of the geodetic VLBI community new formats for data storage were developed. The NetCDF library was chosen for storing/retrieving of data, corresponding file specifications were determined, and in July 2009 the first conversion from Mark III database to NetCDF files was performed.

The process of software development started in August 2009. We selected the *evolutionary* model for the software production process [1]. This process consists of the following, overlapping-in-time activities: *Conceptualization*: formulating a statement of the problem and establishing core requirements; *Analysis*: developing a model of the system’s behavior, describing the functionality

and performance of the system and necessary resources, producing scenarios of system's behavior; *Design*: creating the architecture for the evolving implementation and establishing common tactical policies, architectural planning, release planning; *Evolution*: growing and changing the implementation through successive refinement, leading to the production system; *Maintenance*: managing post-delivery evolution.

In this article we will discuss *Conceptualization*, a part of *Analysis*, and an upper level of *Design* activities.

2. Conceptualization: What Do We Want from a New Version?

Goals for developing a new version of the software. The VLBI data analysis software is a *tool* for studying Earth rotation, constructing Celestial and Terrestrial reference frames, and investigating various geophysical phenomena. Therefore, the following primary goals have to be achieved with the new software: 1) reliability; 2) ability to easily maintain and extend the software; 3) high performance, and 4) data integrity.

Since the output produced by the software is used by many scientists throughout the world, we must be confident in results obtained. The new software should behave reliably and provide reliable results. Secondly, it should be easy to add new models, new estimated parameters or even types of observables. Further improvement of the software should not force changing of its general design. The third main goal is performance. The software must be efficient enough to process observations from the VLBI2010 system and/or from other techniques of modern geodesy in a reasonable time. User efforts in processing observations should be minimal. It is assumed that data analysis is performed by a group of users. The results of the work of one user should be transparently available to the whole group and the software should provide data integrity in such group work.

In addition, nothing should preclude the following additional goals: combining VLBI with other types of space geodesy observations; implementing different approaches of estimating parameters; supporting efficient interaction with other software; and allowing simulation analysis.

Core Requirements. Based on these goals we determined the core requirements of the software. The first group of requirements concerns reliability. The software should have quality control facilities. This could be test suites that check all the essential procedures of the software, a multilevel logging system, and an error reporting mechanism. The new software should support versioning of input data and solutions. It should be able to reproduce the current CALC/SOLVE results. The software should protect users from making blunders and be capable of automated feedback to stations and correlators. We will pay special attention to data visualization. We will implement a modern graphical user interface with elaborated plotting system. Later we will add the ability to shift from one level of data to another one. For example, to check a specific point in an EOP series, the user could enter a session view, then drill down to some particular baseline, a scan, a group delay, or a fringe plot.

There are several requirements of the software development process. The software should be modular, flexible, and portable. The software development process should be performed with standard software development tools, be a team-oriented work, support multiple versions, and have a multilevel documentation system.

Performance issues can be divided into two parts: consumption of user time and computer time. To increase user performance, the software should be automated and one should be able to

use a script language to set up and run batch jobs. Also, the software should understand various formats of data and use standard network protocols for data transfer. CPU performance can be increased by switching from development to production mode. The part of the code that performs debug calculations and output could be turned off during compilation of a production mode of the software. A more significant increase in performance can be achieved by parallelization of calculations. We expect to use either OpenMP API or threads library on a multi-CPU computer. Alternatively, we could run it on a dedicated computer cluster using one of the standard network protocols.

To ensure data integrity in a multiuser environment the software should perform user administration with different user levels. There should be some file locking mechanism. In addition, the new software should monitor available system resources and resources consumed by each user.

3. Analysis: What Should the System Do?

Overview of the System. The software belongs to the data analysis type of software. It is not a time critical application. As with many similar data analysis softwares, it should read observations in predefined format(s), evaluate theoretical values corresponding to the observables, and with the Least Square Method estimate parameters that have influence on the observable values. In addition, it should perform “cleaning” of the observations: remove outliers, resolve anomalies inherent to a particular observing technique, reweight data, and so on.

There are no special design requirements for the hardware. The system should run on a conventional “personal computer” as well as on a dedicated workstation or even a hardware cluster.

Also, there is no specific requirement for the operating system (OS). We assume POSIX compliance; this could be one of the Linux distributions, Solaris, or FreeBSD. The software could be portable to these families of OS.

There are two prototypes which we will use in the development process. We have the current CALC/SOLVE system which performs the same tasks. We also have SteelBreeze, which could be used for prototyping the Object-Oriented Design and graphical user interface. In general, all time-tested algorithms and approaches realized in these prototypes should be used.

Data flow in the current CALC/SOLVE system is shown on the left in Figure 1. The right part of the figure displays the proposed data flow for the new software. The general structure of the data flow of the new software is kept the same, but there are some significant changes. The data files would be physically separated in two parts: observations and editables. This would prevent observations from unintentional modification by a user. The Mark III database handler format will be replaced by an open source NetCDF library. Several executables that are currently used in data preparation, `calc`, `pxcb`, `xlog` and `dbcal`, will be replaced by one executable block. This executable block, *Editor of Observations*, is intended to interact with a user, while other blocks run mostly in a batch mode. On the other hand, to make the software structure modular, the block `solve` will be split into several independent parts for evaluating (O-C) and the partials, parameter estimation, and further handling of estimated parameters (e.g., writing reports, updating *a priori*). The format conversion filters and network transfer utilities are presented in a separate block.

Functionality of the System. Key function points, or abilities of the system to perform something useful for an end user, are the following: 1) Import observations into a local storage, check reliability of imported data and correct them if it is necessary and possible; 2) Import *a priori* data into a local storage, check them, export them in the appropriate formats; 3) Prepare

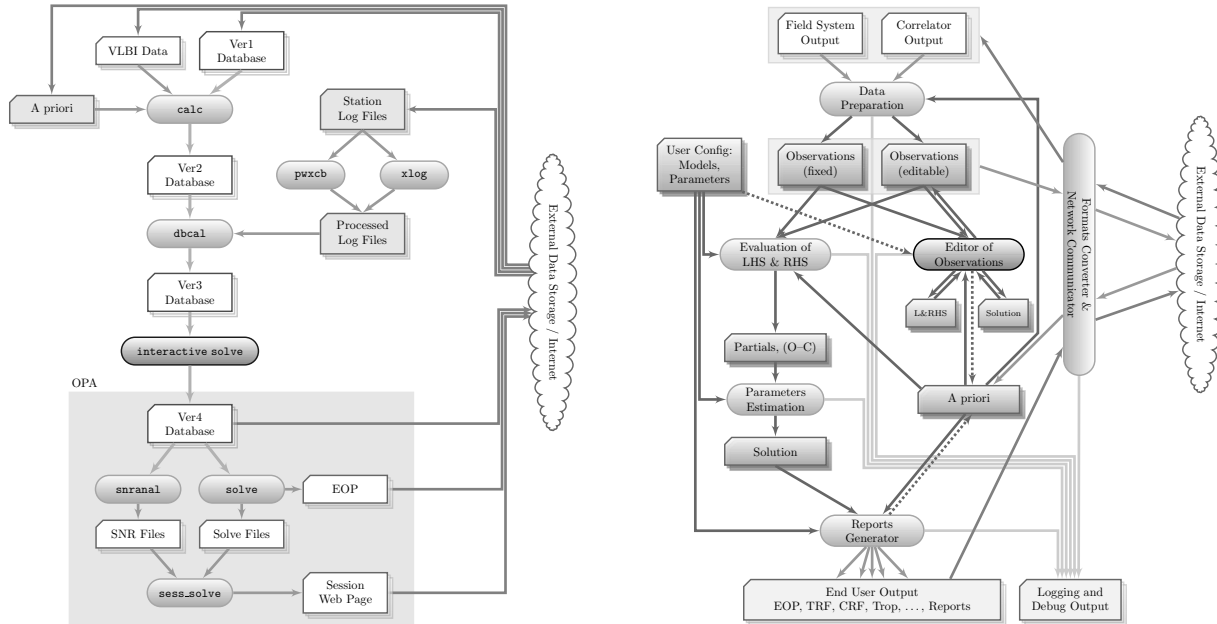


Figure 1. Data flow, current (left) and proposed (right).

newly imported observations for the analysis: check for ambiguities, outliers, clock breaks, new sources/stations, anomalous cable calibration data, perform reweighting, and so on; 4) Edit data; 5) Multi-session analysis: evaluate (O-C) and partial derivatives according to a predefined set of models; form equation systems; obtain a solution; 6) Generate reports and update files with *a priori* data; 7) Send reports to analysts and external data analysis centers; 8) Export checked and validated observations in appropriate formats.

There is another group of function points that are necessary to implement but are not interesting to an end user. They are called system function points. For the new VLBI data analysis software the system function points are: 1) report an error, 2) send and receive a file through a network connection, 3) parse a script for a batch run, 4) check data integrity, 5) monitor available resources (CPU, memory, hard disk space, network connections, open file descriptors), 6) lock a file before writing, unlock it after changes are finished.

4. Architecture Design: How Do We Develop the System?

Architecture Overview. According to the core requirements we performed a decomposition of the system into separate modules. Each module is a block of code that is loosely tied with other parts of the software. In Figure 2 the proposed system decomposition is shown. Each arrow represents a dependency which provides information (e.g., types, function calls, constants). Some blocks in the figure correspond to external software (FITS, NetCDF, LibZ, LibBz2, and Qt libraries) that will be used in the VLBI data analysis software.

Almost all parts of the software will be organized as a shared library, which will allow code reuse for various applications of the geodetic VLBI community.

Common Tactical Policies. Common software development policies are intended to stan-

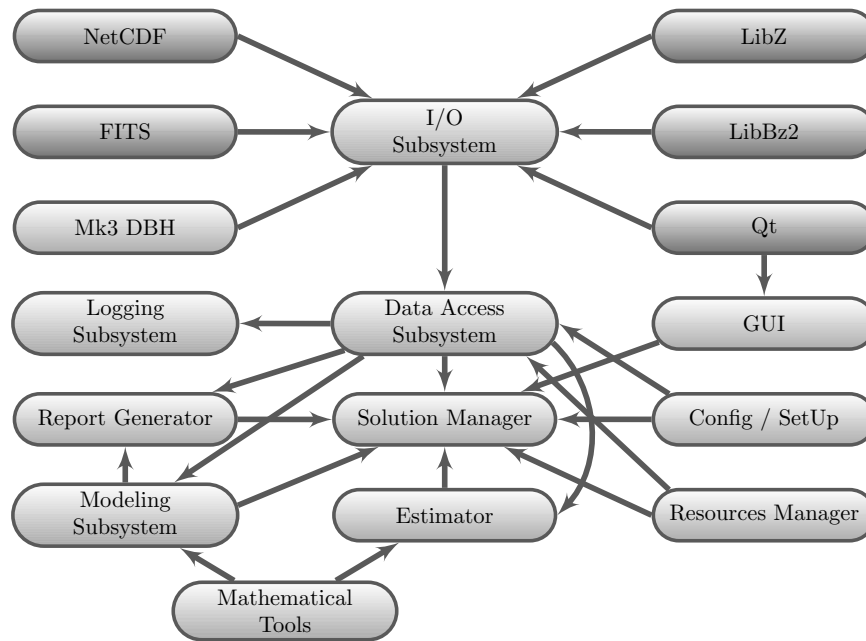


Figure 2. System decomposition.

standardize the development process inside a working group. The policies cover different aspects of the software building process. Using a common *programming style convention* increases readability of the source code for members of the development group. Applying a *test suite* for every essential part of the system assures software quality at the development stage and during distribution to external users. For the portability issues we will use *autogen/autoconf suites*, which are now standard de facto in the open source community. Proper use of these suites allows efficient porting software to a new operating system. Reference documentation will be generated automatically with the *Doxygen utility*. A *version control system* will support simultaneous access to different versions of the software. *Automatic backup* of the source tree will prevent hardware failure.

The Roadmap for future development. The current CALC/SOLVE system will be replaced with the new software piece by piece. We expect to have the first internal release of a replacement for interactive SOLVE by mid-2010. Initially, it will have the minimum functionality and later evolve into mature software that will be able to perform preliminary analysis and editing of new VLBI sessions. The first public release of this new software is planned for the end of 2010. In the spring of 2011 we are going to finish integration of current `pxcb`, `xlog`, and `dbcal` functionality into the new software. Later, work on the replacement of multisession SOLVE and CALC will begin.

References

- [1] G. Booch, Object-Oriented Analysis and Design with Applications. Addison-Wesley, 2nd ed., 1994. ISBN 0-8053-5340-2.

Estimation of Geodetic and Geodynamical Parameters with VieVS

Hana Spicakova, Johannes Böhm, Sigrid Böhm, Tobias Nilsson, Andrea Pany, Lucia Plank, Kamil Teke, Harald Schuh

Institute of Geodesy and Geophysics, Vienna University of Technology

Contact author: Hana Spicakova, e-mail: hana@mars.hg.tuwien.ac.at

Abstract

Since 2008 the VLBI group at the Institute of Geodesy and Geophysics at TU Vienna has focused on the development of a new VLBI data analysis software called VieVS (Vienna VLBI Software). One part of the program, currently under development, is a unit for parameter estimation in so-called global solutions, where the connection of the single sessions is done by stacking at the normal equation level. We can determine time independent geodynamical parameters such as Love and Shida numbers of the solid Earth tides. Apart from the estimation of the constant nominal values of Love and Shida numbers for the second degree of the tidal potential, it is possible to determine frequency dependent values in the diurnal band together with the resonance frequency of Free Core Nutation. In this paper we show first results obtained from the 24-hour IVS R1 and R4 sessions.

1. Introduction

The Vienna VLBI Software VieVS (Boehm et al., 2009 [1]) is a data analysis software, which is developed by the VLBI group at the Vienna University of Technology. The software is written in Matlab with the plan to make it compatible with equivalent non-commercial software, e.g., Octave. One of our main goals is to develop an easy-to-handle software, which will be attractive to our students and thus allow us to easily involve more students in VLBI research. In the modeling part of the software (`vie_mod`) the theoretical VLBI observable (group delay) is computed following the most recent IERS Conventions (McCarthy and Petit, 2004 [7]) and IVS standards like the treatment of thermal deformation of VLBI radio telescopes (Nothnagel, 2009 [9]). The time varying parameters (such as Earth orientation or troposphere parameters) are estimated using piecewise linear offsets at integer fractions of integer hours with a least-squares algorithm to easily allow comparison and combination with estimates from other space geodetic techniques. The VieVS software is extended by an extra program unit for parameter estimation in so-called global solutions, where the connection of the single sessions is done by stacking the normal equations. In this paper we focus on the determination of geodynamical parameters of the solid Earth tides: frequency dependent Love and Shida numbers in the diurnal tidal band together with the Free Core Nutation period.

2. Global Solution in VieVS

Because of the limited computer memory capacity it is essential to keep the equation system small. In the VLBI technique there are parameters in the observation equations which cannot be fixed to a priori values, even if we are not interested in them (e.g., clock parameters). Therefore,

a reduction algorithm is used which is based on a division of the normal equation system into two parts. The first part contains parameters which we want to estimate and the second part the parameters which will be reduced:

$$\begin{pmatrix} N_{11} & N_{12} \\ N_{21} & N_{22} \end{pmatrix} \cdot \begin{pmatrix} dx_1 \\ dx_2 \end{pmatrix} = \begin{pmatrix} b_1 \\ b_2 \end{pmatrix} \quad , \quad (1)$$

where $N = A^T P A$ and $b = A^T P l$. The reduction of dx_2 is done by executing the matrix operation in Equation (1) and introducing the second equation into the first one:

$$\left(N_{11} - N_{12} N_{22}^{-1} N_{21} \right) \cdot dx_1 = b_1 - N_{12} N_{22}^{-1} b_2 \quad \iff \quad N_{reduc} \cdot dx_1 = b_{reduc} \quad . \quad (2)$$

Stacking is used for combining normal equation systems if a parameter is contained in at least two normal equation systems and only one value in the resulting combined system should be estimated. For a combined solution of the identical parameters (dx), the normal matrices (N_{reduc}) and the right hand side vectors (b_{reduc}) from n single sessions have to be summed up:

$$N_{REDUC} = N_{reduc.1} + N_{reduc.2} + \dots + N_{reduc.n} \quad , \quad (3)$$

$$b_{REDUC} = b_{reduc.1} + b_{reduc.2} + \dots + b_{reduc.n} \quad . \quad (4)$$

The final solution is obtained by an inversion of the normal matrix:

$$dx_1 = N_{REDUC}^{-1} \cdot b_{REDUC} \quad . \quad (5)$$

3. Love Numbers and Free Core Nutation Period

Solid Earth deformation arises from the variations in the Earth's gravitational field caused by the Moon and the Sun. Love and Shida numbers (h , l) are dimensionless parameters, which reflect the amount by which the surface of the Earth responds to the tide-generating potential (V^{tid}). Considering the Earth being spherical, non-rotating, elastic, and isotropic—i.e., the most basic model—the tidal displacement (u) at a given latitude and longitude (φ , λ) in the topocentric system is described by equations (6)–(8), where g stands for gravity acceleration and n is the degree of the tide-generating potential.

$$u_R = \sum_{n=2}^{\infty} h_n \cdot \frac{1}{g} \cdot V_n^{tid} \quad , \quad (6)$$

$$u_E = \sum_{n=2}^{\infty} l_n \cdot \frac{1}{g \cdot \cos \varphi} \cdot \frac{\partial V_n^{tid}}{\partial \lambda} \quad , \quad (7)$$

$$u_N = \sum_{n=2}^{\infty} l_n \cdot \frac{1}{g} \cdot \frac{\partial V_n^{tid}}{\partial \varphi} \quad . \quad (8)$$

When a more precise model of the Earth is considered—i.e., ellipticity, rotation, and the elastic mantle/fluid core boundary is taken into account—the relationship between the tide-generating potential and the displacement becomes more complicated. The displacement vector is composed

of deformational parts (δu) of specific harmonic degree and order, and specific frequency inside the band (Wahr, 1981 [14]).

$$\delta u_{R(f)}^{(21)} = -\frac{3}{2} \sqrt{\frac{5}{24\pi}} H_f \delta h_{21(f)} \sin(2\varphi) \sin(\theta_f + \lambda) \quad , \quad (9)$$

where H_f is the Cartwright-Tayler amplitude of the tidal term, $\delta h_{21(f)}$ stands for the difference of the frequency dependent Love number from the constant second degree Love number h_2 , and θ_f is a tidal harmonic argument. The strong frequency dependence of Love numbers in the diurnal band arises from the resonance behavior of the Earth, which is caused by the presence of the fluid core. The rotational axis is slightly inclined w.r.t. the axis of rotation of the mantle. In this situation, forces arise at the elliptical core/mantle boundary, which try to realign the two axes. In the terrestrial reference frame, this phenomenon is seen as a diurnal motion, in the celestial frame it appears as a retrograde motion of the celestial pole with a period of approximately 430 days and is designated as Free Core Nutation (FCN). Because this effect is a free motion with time-varying excitation and damping, resulting in a variable amplitude and phase, an FCN model is not included in the recent precession-nutation model adopted by the International Astronomical Union (IAU 2006/2000A). It means that after taking into account the precession-nutation model a quasi-periodic unmodeled motion of the celestial pole in the celestial frame at the 0.1–0.3 mas level still remains in the measured data (e.g., Lambert, 2007 [6]).

3.1. Estimation of Love Numbers and FCN in VieVS

Basically, three approaches can be used to determine the period of the Free Core Nutation motion. The first option is an indirect estimation from the analysis of the celestial pole offsets obtained from VLBI measurements (e.g., Herring et al., 1986 [4], Vondrak and Ron, 2006 [13]). The FCN effects are also seen in gravity data, where the first determination of the resonant period was done by Neuberger et al. (1987) [8] and was followed by, for instance, Sato et al. (1994, 2004) [11], [12] or Ducarme et al. (2007) [2]. In the VieVS software we implemented the ability to determine the FCN period directly from the analysis of the observed solid Earth tidal displacements of the VLBI antennas, as it was introduced by Haas and Schuh (1996) [3]. For the estimation of the FCN period a resonance formula for the Love numbers in the diurnal band is used, which was published by Wahr (1981) [14]:

$$h_{21}(\omega_T) = h_{21}(\omega_{O1}) + h_{RS} \cdot \frac{\omega_T - \omega_{O1}}{\omega_{FCN} - \omega_T} \quad . \quad (10)$$

$h_{21}(\omega_{O1})$ is the Love number of the O1 tidal wave, whose frequency ω_{O1} is used as reference which is sufficiently distinct from the resonance frequency of the FCN ω_{FCN} . This formula is applied in the least-squares adjustment as a condition equation constraining the estimates of diurnal Love numbers at the tidal waves T , by means of fitting them to the resonance curve, for which also the resonance strength factor h_{RS} was estimated. Because the equation is not linear w.r.t. the ω_{FCN} , iterations have to be carried out.

4. Data and Results

For this paper we used all IVS R1 and R4 sessions, i.e., 24-hour observing sessions which have been performed two times per week since January 2002 using global VLBI networks. Before

the analysis we removed outliers from the observations and excluded sessions with an a posteriori variance of unit weight higher than 1.5. Clock parameters, zenith wet delays, troposphere gradients, and Earth orientation parameters were reduced from the normal equation system and estimated implicitly. The station coordinates and velocities of the 18 VLBI radio telescopes together with the radio source coordinates were fixed to their a priori catalog values, ITRF2005 and ICRF2, respectively. We solved for Love numbers of ten diurnal tidal waves using partial derivatives from Equation (9) and the resonance parameters (i.e., FCN period with the resonance strength factor h_{RS}) were estimated after five iterations from the condition equation (10).

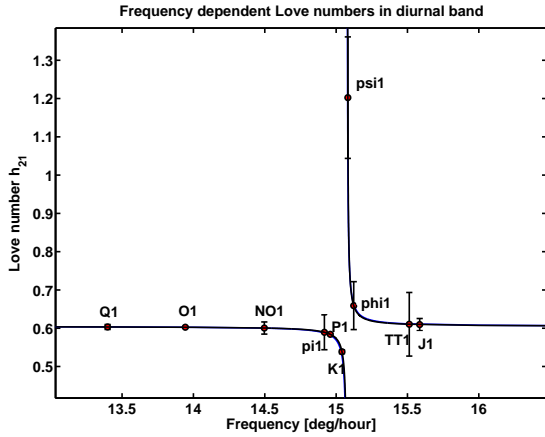


Figure 1. Estimates of the diurnal Love numbers h_{21} and the resonance curve.

Our estimates of the Love numbers (Figure 1, Table 1) are in very good agreement with the recently adopted IERS values. Larger differences can be seen mainly for the tidal waves in the vicinity of the resonance period (phi1, psi1) and for the tides with lower amplitudes (e.g., NO1, pi1, J1). For the resonance period we obtained 413 ± 20 sidereal days in the celestial frame. The large standard deviation of the FCN period might be due to using only eight years of data and the high correlation with the resonance strength factor, as was pointed out in Haas and Schuh (1996) [3]. An apparent time-variation of the FCN period was discussed in Roosbeek et al. (1999) [10] or Hinderer et al. (2000) [5].

Table 1. Estimates of frequency dependent Love numbers for ten diurnal tidal waves, FCN period, and resonance strength factor compared with the IERS values [7] and with the results from Haas and Schuh (1996) [3].

Frequency [$^{\circ}$ /h]	Tide	IERS values [7]	Love number h_{21}	
			this paper	Haas and Schuh (1996) [3]
13.3987	Q1	0.6033	0.6033 ± 0.0065	0.560 ± 0.012
13.9430	O1	0.6026	0.6026 ± 0.0017	0.606 ± 0.002
14.4967	NO1	0.6004	0.6005 ± 0.0158	0.435 ± 0.030
14.9179	pi1	0.5882	0.5895 ± 0.0456	0.623 ± 0.090
14.9589	P1	0.5823	0.5842 ± 0.0027	0.574 ± 0.005
15.0411	K1	0.5261	0.5385 ± 0.0049	0.496 ± 0.002
15.0821	psi1	1.0439	1.2023 ± 0.1587	-0.136 ± 0.228
15.1232	phi1	0.6623	0.6590 ± 0.0626	0.702 ± 0.121
15.5126	TT1	0.6113	0.6104 ± 0.0830	0.934 ± 0.158
15.5854	J1	0.6105	0.6096 ± 0.0159	0.538 ± 0.031
FCN period		432 sid. days	413 ± 20 sid. days	426.3 ± 20.3 sid.days
h_{RS}		–	-0.00217 ± 0.00015	-0.00162 ± 0.00016

5. Summary

The VLBI group at Vienna University of Technology is developing a new data analysis software, called VieVS (Vienna VLBI Software). The first version of the software has been released and can be downloaded by registered users. In this paper we focused on a new module for global adjustment of more sessions, which is implemented in the software. Besides estimation of a new terrestrial reference frame, celestial reference frame, and Earth orientation parameters, the program unit allows the determination of geophysical parameters such as frequency dependent Love and Shida numbers and the Free Core Nutation period from solid Earth tidal deformations.

References

- [1] Boehm, J., H. Spicakova, L. Plank, K. Teke, A. Pany, J. Wresnik, S. Englich, H. Schuh, T. Hobiger, R. Ichikawa, Y. Koyama, T. Gotoh, T. Otsubo, T. Kubooka, Plans for the Vienna VLBI Software VieVS, Proceedings of the 19th European VLBI for Geodesy and Astrometry Working Meeting, edited by G. Bourda, P. Charlot, A. Collioud, pp. 161–164, 2009.
- [2] Ducarme, B., H.-P. Sun, J.-Q. Xu, Determination of the free core nutation period from tidal gravity observations of the GGP superconducting gravimeter network, *J Geod.* 81, pp. 179–187, 2007.
- [3] Haas, R., H. Schuh, Determination of frequency dependent Love and Shida numbers from VLBI data, *Geophys. Res. Lett.* Vol. 23 No. 12/1996, pp. 1509–1512, 1996.
- [4] Herring, T. A., C. R. Gwinn, I. I. Shapiro, Geodesy by radio interferometry: studies of the forced nutations of the Earth, *J Geophys Res* 91(B5), pp. 4745–4754, 1986.
- [5] Hinderer, J., J. P. Boy, P. Gegout, P. Defraigne, F. Roosbeek, V. Dehant, Are the free core nutation parameters variable in time?, *Physics of the Earth and Planetary Interiors* 117, pp. 37–49, 2000.
- [6] Lambert, S., Empirical modeling of the retrograde Free Core Nutation, available at <ftp://hpiers.obspm.fr/eop-pc/models/fcn/notice.pdf>
- [7] McCarthy, D. D., and G. Petit, IERS Conventions 2003, IERS Technical Note 32, Verlag des Bundesamtes fuer Kartographie und Geodaesie. 2004. + electronic updates.
- [8] Neuberg, J., J. Hinderer, W. Zuern, Stacking gravity tide observations in central Europe for the retrieval of the complex eigenfrequency of the Nearly Diurnal Free Wobble, *Geophys. J. R. Astr. Soc.* 91, pp. 853–868, 1987.
- [9] Nothnagel, A., Conventions on thermal expansion modelling of radio telescopes for geodetic and astrometric VLBI, *Journal of Geodesy*, 83, pp. 787–792, 2009.
- [10] Roosbeek, F., P. Defraigne, M. Feissel, V. Dehant, The free core nutation period stays between 431 and 434 sidereal days, *Geophys. Res. Letters.*, 26, 1, pp. 131–134, 1999.
- [11] Sato, T., Y. Tamura, T. Higashi, S. Takemoto, I. Nakagawa, N. Morimoto, Y. Fukuda, J. Segawa, N. Seama, Resonance parameters of Nearly Diurnal Free Core Nutation measured from three superconducting gravimeters in Japan, *J. Geomagn. Geoelectr.* 46, pp. 571–586, 1994.
- [12] Sato, T., Y. Tamura, K. Matsumoto, Y. Imanishi, H. McQueen, Parameters of the fluid core resonance inferred from superconducting gravimeter data, *J. Geodyn.* 38, pp. 375–389, 2004.
- [13] Vondrak, J., C. Ron, Resonant period of free core nutation – its observed changes and excitations. *Acta Geodyn. Geomater.* 3 (143), pp. 53–60, 2006.
- [14] Wahr, J. M., Body tides on an elliptical rotating, elastic and oceanless Earth, *Geophys. J. R. Astron. Soc.*, 64, pp. 677–703, 1981.

VLBI Analysis with the Multi-technique Software GEOSAT

*Halfdan Pascal Kierulf*¹, *Per-Helge Andersen*², *Sarah Boeckmann*³,
*Oddgeir Kristiansen*⁴

¹⁾ *Norwegian Mapping Authority (NMA) and the University of Oslo (UiO)*

²⁾ *Forsvarets forskningsinstitutt (FFI) and the University of Oslo*

³⁾ *Institut für Geodäsie und Geoinformation (IGG-Bonn)*

⁴⁾ *Norwegian Mapping Authority*

Contact author: *Halfdan Pascal Kierulf*, e-mail: `halfdan.kierulf@statkart.no`

Abstract

GEOSAT is a multi-technique geodetic analysis software developed at Forsvarets Forsknings Institutt (Norwegian defense research establishment). The Norwegian Mapping Authority has now installed the software and has, together with Forsvarets Forsknings Institutt, adapted the software to deliver datum-free normal equation systems in SINEX format. The goal is to be accepted as an IVS Associate Analysis Center and to provide contributions to the IVS EOP combination on a routine basis. GEOSAT is based on an upper diagonal factorized Kalman filter which allows estimation of time variable parameters like the troposphere and clocks as stochastic parameters. The tropospheric delays in various directions are mapped to tropospheric zenith delay using ray-tracing. Meteorological data from ECMWF with a resolution of six hours is used to perform the ray-tracing which depends both on elevation and azimuth. Other models are following the IERS and IVS conventions. The Norwegian Mapping Authority has submitted test SINEX files produced with GEOSAT to IVS. The results have been compared with the existing IVS combined products. In this paper the outcome of these comparisons is presented.

1. Introduction

The production of Earth Orientation Parameters (EOPs) for the geodetic community is one of the main products of the IVS. Results from different IVS Analysis Centers (ACs) are combined, and the final IVS combined results are provided. However, the number of different analysis software packages is limited (see [3]), and the combined solution is dominated by the Calc/Solve [7] software. Contributions to the combination from additional independent software packages are strongly desired by the IVS to exclude the probability of deficits in any of the software packages. GEOSAT is a software developed at Forsvarets Forsknings Institutt (FFI). The Norwegian Mapping Authority (NMA) will produce EOP series with GEOSAT in the form of datum-free normal equation systems in SINEX format and thereby contribute to the IVS combination.

To produce VLBI solutions for IVS is the first part of a larger strategic plan from NMA. The next step is to include other geometric geodetic techniques (GNSS and SLR) in a common solution, where the different techniques are combined at the observation level. The long term goal of this large effort is to also include data from the gravity satellites GRACE and GOCE and from satellite altimetry.

In this paper the software will be shortly described (Section 2), and some preliminary results of the comparison with the solutions from other IVS ACs and the IVS combined product will be given (Section 3).

2. The GEOSAT Software

During the last 27 years, FFI has developed a software package called GEOSAT for the combined analysis of VLBI, GNSS (GPS, Galileo, GLONASS), SLR, and other types of satellite tracking data (e.g., DORIS, PRARE, altimetry, gravity, radar, direction, Deep Space Network). The observations are combined at the observation level with a consistent model and consistent analysis strategies. With this procedure, the time-evolution of the common multi-technique parameters (for example EOP, geocenter, troposphere, or clock parameters) is treated consistently across the techniques.

In the combined analysis with GEOSAT the data are processed in arcs of 24 hours defined by the duration of the VLBI session. The result of each analyzed arc is a state vector of estimated parameter corrections and a Square Root Information Filter (SRIF) array containing parameter variances and correlations. The individual arc results are combined into a multi-year global solution using a Combined Square Root Information Filter and Smoother program called CSRIFS. With the CSRIFS program any parameter can either be treated as a constant or a stochastic parameter between the arcs. The estimation of multi-day stochastic parameters is possible and extensively used in the analyses.

A major software component of GEOSAT is a 3D raytracing through the atmosphere. A complete 3D atmospheric model provided daily by ECMWF is input to the software. Based on the available tracking data for that specific date, a set of tables for each active station is automatically generated with information about the time delay in the different elevation and azimuth directions. Also statistical information concerning the variability of relevant parameters is extracted from the ECMWF data. This information is used in the estimation filter as time-dependent parameter constraints. No mapping functions are used when numerical weather model data is available.

The latest electronically updated IERS Conventions have been fully implemented including the new EOP parameterization. Except for the treatment of the troposphere, the analysis strategy follows the recommendation from the IVS Analysis Coordinator. The atmospheric loading is modeled using time series from <http://gemini.gsfc.nasa.gov/aplo> ([6]). The a-posteriori RMS of fit for a VLBI session is typically 15–30 ps. The session-wise VLBI solutions for the IVS are based on NGS cards. Clocks and troposphere zenith wet delay are solved as stochastic parameters, while station positions and EOP are solved as constant parameters. From the session SRIF matrix, the necessary information is extracted, and the unconstrained normal equation is produced.

3. Results

The daily datum-free normal equation systems from GEOSAT are combined and compared with solutions from the other ACs, following the procedure explained in [3]. The overall impression of the results is that they are consistent with the results from the other ACs, except for some systematic differences. In this section we will look at some of the parameters and discuss these differences.

In Figure 1 coordinate time series for Ny-Ålesund are displayed for two different solutions: NMA using the software GEOSAT and Goddard Space Flight Center (GSFC) using the software CALC/SOLVE. The horizontal rate estimates are similar, but the noise level is larger in the NMA solution. The secular uplift is larger in the GSFC solution. However, the non-linear uplift pattern as reported in [4, 5] is seen in both solutions. In Figure 2, the residual time series for all IVS ACs are plotted for Ny-Ålesund (left) and Wettzell (right). We find a consistent pattern between all the

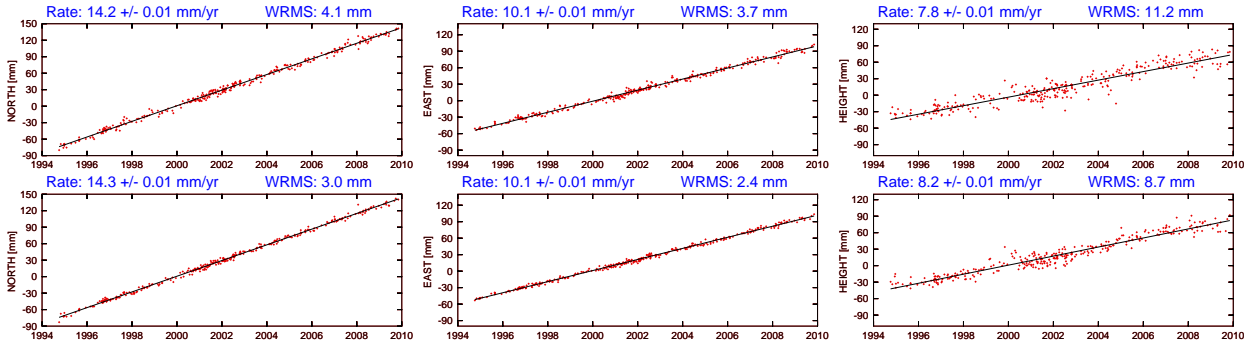


Figure 1. Time series of Ny-Ålesund from NMA (GEOSAT) (upper) GSFC (CALC/SOLVE) (lower).

solutions, but with some systematical differences. For instance, the east and height components for Wettzell are slightly biased both for the NMA and IAA (QUASAR) solutions compared with the other ACs. Similar biases are also found for some other stations.

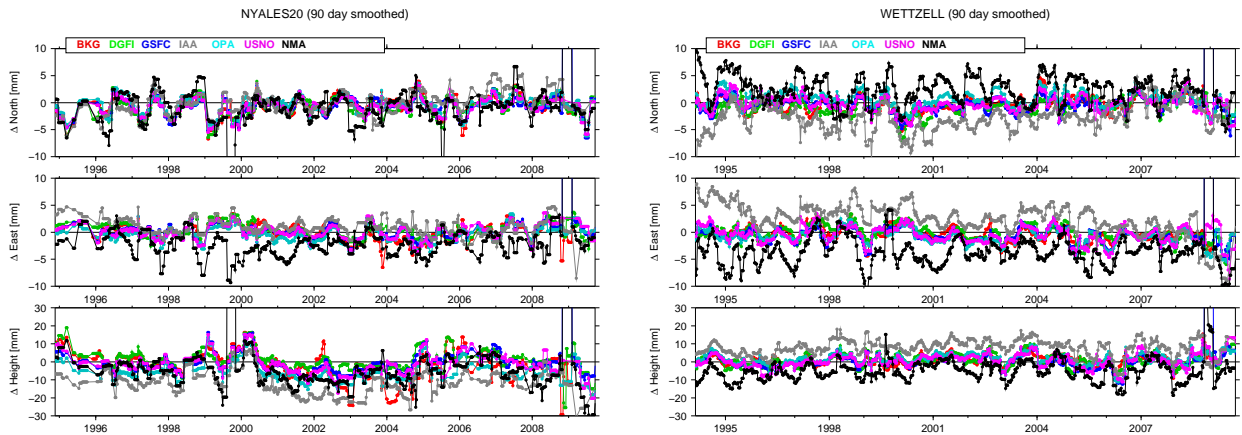


Figure 2. BKG, DGFI, GSFC, IAA, OPA, USNO, and NMA residual time series for Ny-Ålesund (left) and Wettzell (right). Individual time series can be distinguished by color in the electronic version.

The nutation parameters dX and dY of the celestial intermediate pole for all ACs are plotted in Figure 3. We find an annual signal both in the dX and dY components. The signal is similar to what we find in the IAA solution. Some minor errors that can explain the signal were found in the GEOSAT software. They are now fixed, and we expect to see an improvement in the next comparison.

The EOP for all ACs are plotted in Figure 4. The values are relative to the IVS combined solution (left) and the IGS combined solution (right). The X -pole and Y -pole components have similar variations as the other ACs compared to IVS combined. When we compare with the IGS solution, the noise level seems larger. Also the number of outliers is larger. The polar-motion rate (Figure 5) fit very well to the combined solutions and especially to the IGS combined solution. GEOSAT uses midnight as the reference epoch for the EOPs while the other ACs use mid-session. The NMA solutions are therefore extrapolated to mid-session while the rates are constant for the complete days. This may explain why the NMA solution fit the combined polar-motion rates very

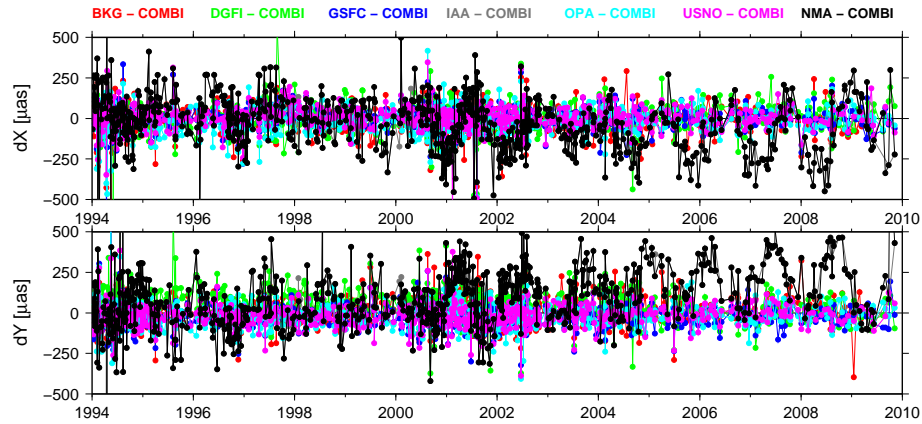


Figure 3. BKG, DGFI, GSFC, IAA, OPA, USNO, and NMA time series of nutation parameters in dX and dY vs. IVS-combined.

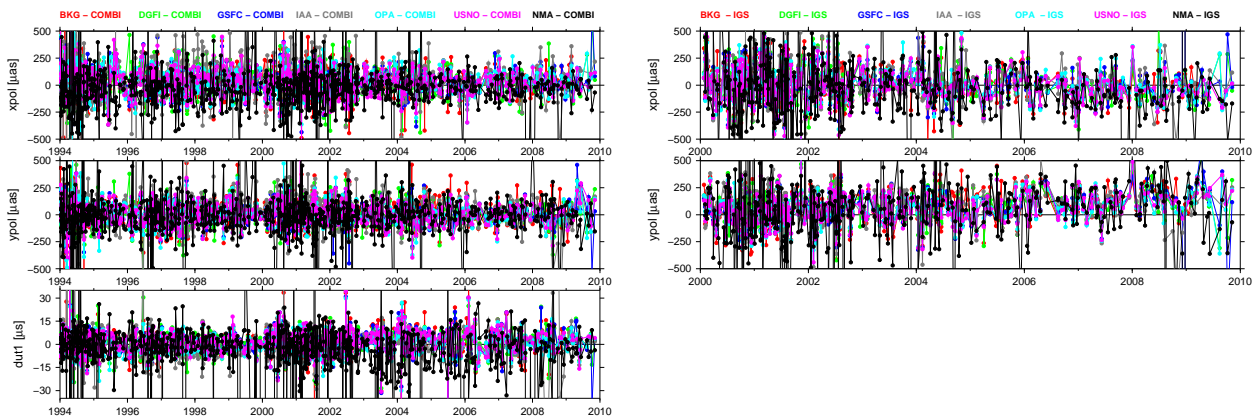


Figure 4. BKG, DGFI, GSFC, IAA, OPA, USNO, and NMA time series of polar motion vs. IVS combined (left) and vs. IGS combined (right).

well, while the fit to the polar-motion parameters seems worse.

For $UT1$ we see several outliers and after around 2003 a number of sessions seem to have an offset. The LOD seems to be a bit noisier than at the other ACs.

As seen above the results for some of the parameters with GEOSAT seem to be somewhat more noisy than the results from the other ACs in the combination. This issue has lately been studied in more detail and has resulted in a strategy that gives more stable normal equations.

4. Conclusions

The overall agreement between the NMA-GEOSAT solution and the solutions from the other ACs is satisfactory for this first comparison. However, some discrepancies have been found. This reveals some issues that have to be investigated further. As soon as the causes for the discrepancies are understood and taken into account, NMA will start to deliver VLBI solutions to IVS regularly.

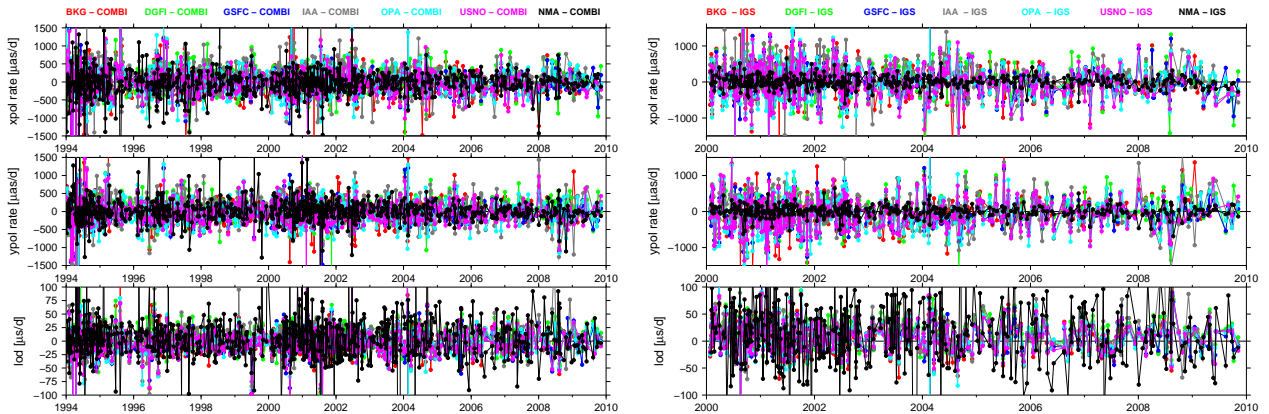


Figure 5. BKG, DGFI, GSFC, IAA, OPA, USNO, and NMA time series of polar motion rate vs. IVS combined (left) and vs. IGS combined (right).

References

- [1] Andersen, P. H., 1995. High-precision station positioning and satellite orbit determination. PhD Thesis, *NDRE/Publication 95/01094*
- [2] Andersen, P. H., 2000. Multi-level arc combination with stochastic parameters. *Journal of Geodesy* 74: **531-551** (doi: 10.1007/s001900000115)
- [3] Böckmann, S., Artz, T., & Nothnagel, A. 2009, VLBI terrestrial reference contribution to ITRF2008. *Journal of Geodesy*, 84, **201-219** (doi: 10.1007/s00190-009-0357-7)
- [4] Kierulf, H. P., Pettersen, B., McMillan, D. S., & Willis, P., 2009. The kinematics of Ny-Ålesund from space geodetic data, *J. Geodynamics*, **37-46** (doi:10.1016/j.jog.2009.05.002).
- [5] Kierulf, H. P., Plag, H.-P., & Kohler, J., 2009. Measuring Surface Deformations Induced by Present-Day Ice Melting in Svalbard, *Geophys. J. Int.*, **1-13** (doi: 10.1111/j.1365-246X.2009.04322.x)
- [6] Petrov, L., & Boy, J.-P. 2004. Study of the atmospheric pressure loading signal in VLBI observations, *Journal of Geophysical Research*, (doi: 10.1029/2003JB002500)
- [7] Petrov, L., 2008. <http://gemini.gsfc.nasa.gov/solve/>

c5++ - Multi-technique Analysis Software for Next Generation Geodetic Instruments

Thomas Hobiger¹, Tadahiro Gotoh¹, Toshimichi Otsubo², Toshihiro Kubooka¹,
Mamoru Sekido¹, Hiroshi Takiguchi¹, Hiroshi Takeuchi³

¹) *Space-Time Standards Group, National Institute of Information and Communications Technology*

²) *Hitotsubashi University and the Space-Time Standards Group, NICT*

³) *Japan Aerospace Exploration Agency, Institute of Space and Astronautical Science (ISAS)*

Contact author: Thomas Hobiger, e-mail: hobiger@nict.go.jp

Abstract

Processing of space geodetic techniques should be carried out with consistent and utmost up-to-date physical models. Therefore, c5++ is being developed, which will act as a framework under which dedicated space geodetic applications can be created. Due to its nature, combination of different techniques as well as automated processing of VLBI experiments will become possible with c5++.

1. Introduction

An analysis software package based on Java and named CONCERTO4 [3] enabled the user to consistently process SLR, GPS, and other satellite tracking data. The next version of this program package will also include VLBI as additional space-geodetic technique. As the software is currently being redesigned and completely re-written in C++, the requirements for VLBI data analysis could be taken into account. Moreover, combination of space geodetic techniques was considered during the design phase.

2. Space Geodesy with c5++

Basically, c5++ provides the framework (Figure 1) under which space geodetic applications can be built. Thus, stand-alone technique specific applications can be developed or multi-technique solutions can be realized. Thereby consistent geophysical and geodetic models, based on the IERS conventions 2003, are applied to each technique, which enables the combination either on the observation level or on the normal-equation level. External libraries, which are available as open source packages, are utilized for data input/output as well as vector and matrix operations. c5++ has been successfully compiled and tested under Windows, Linux, and Mac OS using 32-bit and 64-bit environments. Modules are commented within the code and information is extracted via Doxygen, which outputs on-line the documentation (in HTML) and/or an off-line reference manual.

2.1. Libraries Resp. Classes Contained Within c5++

Table 1 lists the most relevant classes together with their functionality. Space-geodetic software can be built by interfacing the required modules, and other applications can be realized from this framework.

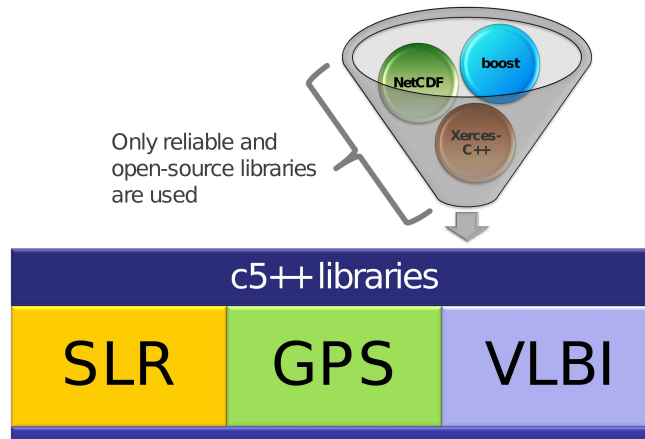


Figure 1. Building space geodetic analysis software for SLR, GPS, or VLBI by interfacing the c5++ libraries.

Table 1. c5++ libraries and their functionality.

Name	Functionality
C5Time	Implements internal time container, allows input of UTC, TAI, TT, MJD, JD and converts between the time systems using an internal storage format.
C5Math	Main math library, which provides dedicated matrix operations and geodetic tools.
Transform	Transforms positions between TRF and CRF
Ephm	Reads JPL binary ephemeris and provides position/velocity of any given celestial body in a user-defined frame
Displacement	Computes solid Earth tides, ocean, and atmosphere loading corrections
Accel	Provides various accelerations respectively forces which act on a satellite
Cowel	Fast and accurate orbit integrator
Param	Is the backbone of c5++ which manages all kind of selectable parameters and carries out automatic interpolation for time-dependent parameters.
ParamIO	Reads and writes parameters/results in XML format
Relativity	Computes relativistic corrections for GPS and SLR and transforms VLBI delays into the TCG frame
C5ObsData	Reads observational data and stores it in an STL container class.
Antenna	Antenna/telescope specific corrections models (deformations, axis offsets, ...)

2.2. VLBI with c5++

Based on the main classes of c5++, a dedicated VLBI analysis chain can be implemented with minimal efforts. Thereby, modules can be attached like building blocks and even dedicated/specialized VLBI software solutions can be realized, without in-depth knowledge of the specific classes. In order to fulfill the requirements of different applications the following observation formats are supported within c5++:

- NGS
- NetCDF
- Mark III
- Raw correlator (K5 format)

In the first stage all modules are designed to work properly and give correct results. Optimization concerning the improvement of processing speed will be made, once the testing and verification phase has been completed.

3. Multi-technique Combination

Since all space-geodetic techniques can utilize the same physical and geophysical models from c5++, consistent combination across the techniques can be realized. Thereby, results can be either combined on the normal-equation level or on the observation level, in accordance with the goals of the Global Geodetic Observing System (GGOS). Moreover, novel applications like spacecraft tracking can be developed, whereas orbit calculations based on multi-technique observations (GNSS, SLR, and VLBI) are expected to provide an utmost accurate 3D trajectory of the satellite.

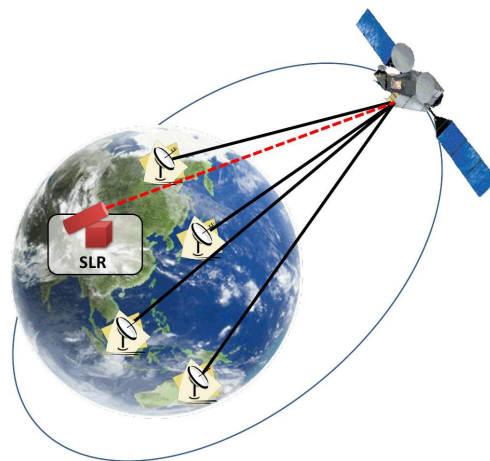


Figure 2. Since c5++ is also designed for satellite techniques, existing modules and models can also be utilized to do space-craft tracking either by VLBI or by a combination of several techniques. E.g., an integration of SLR and VLBI tracking will allow the computation of highly accurate orbit arcs.

4. Automated UT1 Processing

Beside multi-baseline sessions, regular single-baseline VLBI experiments are scheduled in order to provide estimates of UT1 for the international space community. As shown by [4] and [2] the latency of these Intensive experiments could be improved tremendously and results could be made available within less than an hour if e-VLBI and automated processing routines were applied. If the whole processing pipeline works well, results can be obtained even within minutes after the last scan has been recorded, which is highly appreciated by the user community as discussed in [1]. Based on the experience gained over the last two years, the automated processing chain will be improved and the analysis software used until now will be replaced by c5++. Since the correlator output format can be read directly with c5++, no intermediate interface is necessary. Moreover, ambiguity resolution and ionosphere correction can be done within the framework of c5++. Not only the target parameter, i.e., UT1, will be estimated with c5++, but also databases for the VLBI community are expected to be created with that software. As shown in Figure 3, it will also be possible to input a-priori delay models into the correlator in order to achieve highest possible consistency between all the data processing stages.

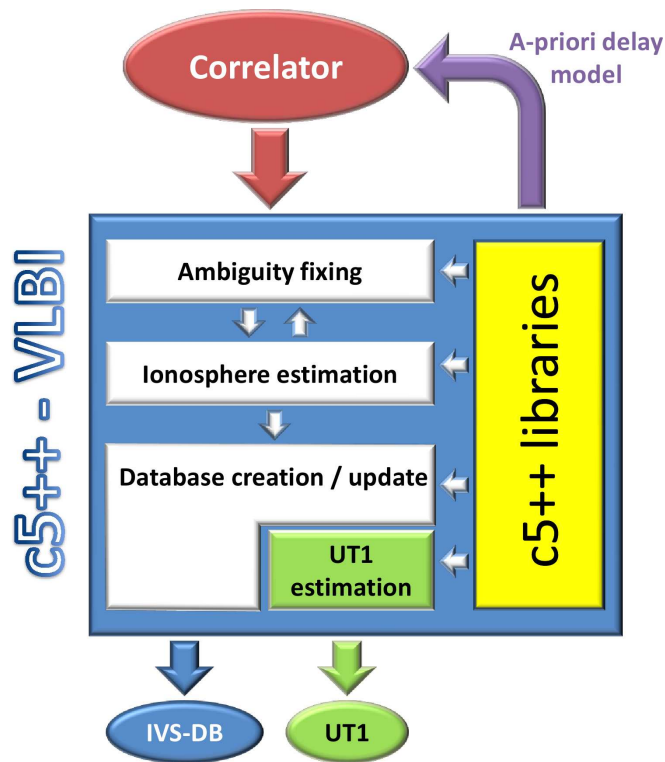


Figure 3. Flow-chart of automated VLBI analysis and UT1 estimation.

A focus will be set on robust and reliable automated ambiguity resolution, in order to allow for completely unattended operation. Additional functions will include automated reporting of results to international services as well as export of standard formats for independent analysis within the space-geodetic community.

Acknowledgments

Parts of this work were supported by a Grant-in-Aid for scientific research (KAKENHI, No. 24241043) from the Japan Society for the Promotion of Science (JSPS). We highly appreciate the support from the VieVS group at Vienna University for helping us with the validation of our modules.

References

- [1] Luzum B. and A. Nothnagel, Improved UT1 predictions through low-latency VLBI observations”, *Journal of Geodesy*, in print, 2010.
- [2] Matsuzaka S., H. Shigematsu, S. Kurihara, M. Machida, K. Kokado and D. Tanimoto, Ultra Rapid UT1 Experiments with e-VLBI, *Proceedings of the 5th IVS General Meeting*, 68–71, 2008.
- [3] Otsubo T. and T. Gotoh, SLR-based TRF Contributing to the ITRF2000 project, *IVS 2002 General Meeting Proceedings*, 300–303, 2002.
- [4] Sekido M., H. Takiguchi, Y. Koyama, T. Kondo, R. Haas, J. Wagner, J. Ritakari, S. Kurihara and K. Kokado, Ultra-rapid UT1 measurement by e-VLBI, *Earth Planets Space*, 60, 8, 865–870, 2008.

Comparison Campaign of VLBI Data Analysis Software - First Results

Lucia Plank, Johannes Böhm, Harald Schuh

Institute of Geodesy and Geophysics, Vienna University of Technology

Contact author: Lucia Plank, e-mail: lucia.plank@tuwien.ac.at

Abstract

During the development of the Vienna VLBI Software VieVS at the Institute of Geodesy and Geophysics at Vienna University of Technology, a special comparison setup was developed with the goal of easily finding links between deviations of results achieved with different software packages and certain parameters of the observation. The object of comparison is the computed time delay, a value calculated for each observation including all relevant models and corrections that need to be applied in geodetic VLBI analysis. Besides investigating the effects of the various models on the total delay, results of comparisons between VieVS and Occam 6.1 are shown. Using the same methods, a Comparison Campaign of VLBI data analysis software called DeDeCC is about to be launched within the IVS soon.

1. Introduction

The calculation of the theoretical delay is one of the main tasks in geodetic VLBI analysis. The comparison of the modeled time delays with the observed values together with their partial derivatives is the basis for the subsequent adjustment procedure. While the results of the adjustment can vary depending on the estimation method and time intervals, the calculated delay relies on theoretical knowledge and should be identical in all software realizations. In practice, different VLBI analysis packages follow different calculation strategies, vary in the usage of correction models, and are sometimes limited in their ability to adopt the latest IERS Conventions. During the development of the Vienna VLBI Software (VieVS) (Böhm et al. 2009 [1]) many comparisons of intermediate results with Occam 6.1 (Titov et al. 2004 [2]) have been performed. While actual VLBI delay models ensure accuracy up to one picosecond (0.3 mm) other parts of geodetic VLBI modeling are much more uncertain, and discrepancies at the millimeter level could be found. The goal of the **Delay** and partial **Derivatives Comparison Campaign** (DeDeCC) is to compare the various software packages used within the IVS in order to detect present deficiencies in the modeling part which might lead to systematic errors in a final solution. In the following we want to give a short insight into the complexity of delay modeling (Section 2), present the main ideas of the campaign setup (Section 3.1) and show first results of comparisons between VieVS and Occam 6.1 (Section 3.2). This report ends with an outline of upcoming activities within DeDeCC (Section 4).

2. The Computed Time Delay

When radio waves emitted by an extragalactic source are received by two widely separated antennas on the surface of the Earth, the time epoch when the same wavefront reaches station 1 and station 2 is usually different. This time delay for each baseline is the main observable of a VLBI experiment and can be accurately determined by the correlation process. On the other

hand, the delay is modeled in the analysis software, which is inspected here. According to Sovers et al. 1998 [3] the geometric time delay in the barycentric coordinate system is

$$\tau_{bary} = (t_2 - t_1)_{bary} = \frac{\vec{k} \cdot \vec{b}/c}{1 - \vec{k} \cdot \beta_2/c} \quad (1)$$

where \vec{k} is the source unit vector in the direction of signal propagation, \vec{b} is the baseline between station 2 and station 1 at the time of signal reception at station 1, β_2 is the barycentric velocity of station 2, and c stands for the velocity of light in vacuum. Considering the fact that the measured time delay is referred to the Earth's surface rather than the barycentric system, as well as the required transformations between the celestial reference frame of the sources and the terrestrial reference frame in which the stations are determined, equation (1) in practice has to be expanded for several relativistic terms. A complete formulation of the VLBI time delay is provided with the IERS consensus model described in Eubanks 1991 [4]. For the calculation of \vec{b} the real station locations are needed, including corrections due to station velocities, solid Earth tides, pole tide, and ocean loading as well as atmosphere loading. For the transformation between the terrestrial and the geocentric reference frame the actual Earth orientation has to be determined beforehand. Besides the geometric delay described above we have to account for the gravitational bending delay τ_{grav} due to celestial bodies and for the propagation delay in the troposphere τ_{trop} . Further corrections due to the ionosphere or clock offsets are often treated separately and are not a matter of comparison here. Generally, the decision of whether a delay correction is either applied directly to the observation or taken into account at the modeled delay is up to each software strategy. This leads to different interpretations of the term *computed delay*. For clarity, equation (2) shows the individual parts which are included in the computed delay used in the comparison campaign.

$$\tau_{comp} = \tau_{geom} + \tau_{grav} + \tau_{trop} + \tau_{axis} + \tau_{thermdef} \quad (2)$$

As shown in Figure 1, the order of magnitude at which the various corrections and models contribute to the total delay ranges from a few millimeters up to some tens of meters. The examined time span covers the first three days of DeDeCC1 (see Section 3.1) and refers to a total delay of approximately $\pm 4,000$ kilometers, corresponding to ~ 13 milliseconds. After the geometry, the biggest effect up to 30 meters comes from the troposphere depending on the local elevation angles. Corrections of some tens of centimeters are made by the antenna axis offsets, the solid Earth tides, and the gravitational influence of the sun. The antenna thermal correction, the gravitational effect of the Earth, and the influence of the ocean on Earth rotation and on station coordinates contribute at the millimeter level.

3. Comparison Campaign

3.1. DeDeCC1

For the first cycle of comparisons, named DeDeCC1, observations of the two stations Westford and Wettzell of the source 0642+449 are examined. The observations are arranged into fifteen 24-hour sessions, fourteen consecutive days from January 1st to January 14th 2001 and a single session one year later, on January 1st 2002. The observation interval is 30 minutes. In the reduced mode, observations with low elevation or beneath the horizon are skipped (every day from 14:00 to 19:30). With an expected agreement at the millimeter level, the usage of identical input parameters

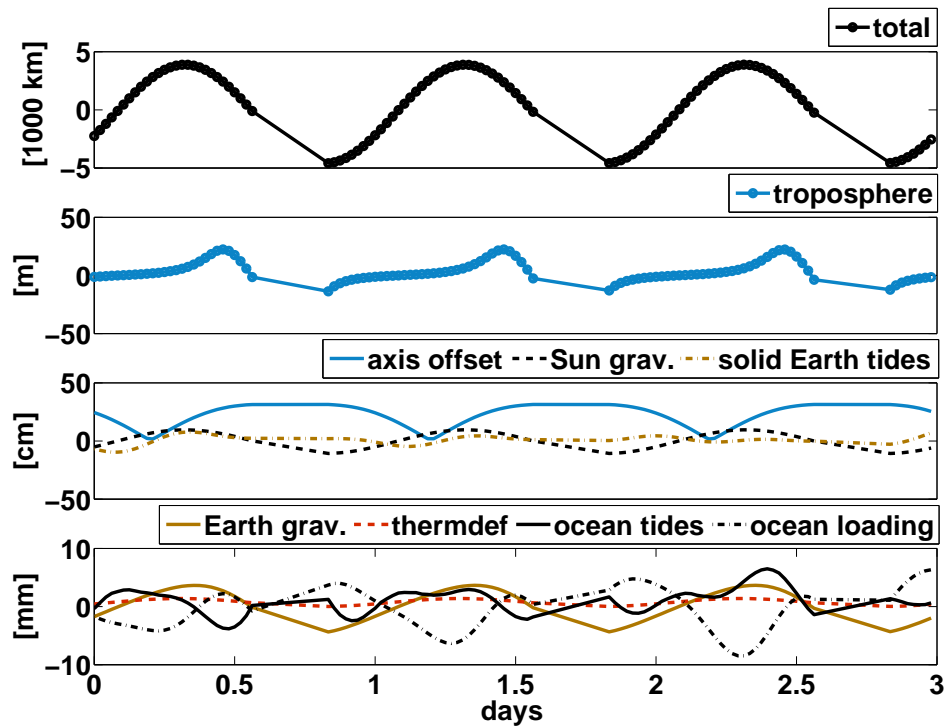


Figure 1. Contribution to the delay at different magnitudes.

and modeling options is essential. Detailed instructions on applied and neglected models, the observation schedule, and the input coordinates can be found at the website of DeDeCC¹. In order to restrain the effect of the various interpolation methods used in existing software the Earth orientation parameters, air pressure, and temperature are fixed to constant values, and atmosphere loading is not considered in DeDeCC.

3.2. VieVS Versus Occam 6.1

A first run of DeDeCC was made with the two software packages available at our institute, the new VieVS and the formerly used Occam 6.1.

As shown in Figure 2, the calculated delays of VieVS and Occam 6.1 differ by ± 2 millimeters during the inspected time periods. The variations are characterized by a dominant daily period and, looking at the longer time spans, additional periods of one year and longer (approx. 5 years) can be detected. Investigations concerning the sources of discrepancies showed that the disagreement due to inconsistencies in the modeling of solid Earth tides, ocean loading, the troposphere, pole tide, thermal correction, and antenna axis offset is below 75 micrometers, which is not critical. The differences more likely originate in the diverse calculation of the Earth rotation angle realized in both programs. Certainly a comparison with at least one further software package needs to be done to clarify the reason for the discrepancies.

¹<http://mars.hg.tuwien.ac.at/~lplank/DeDeCC/>

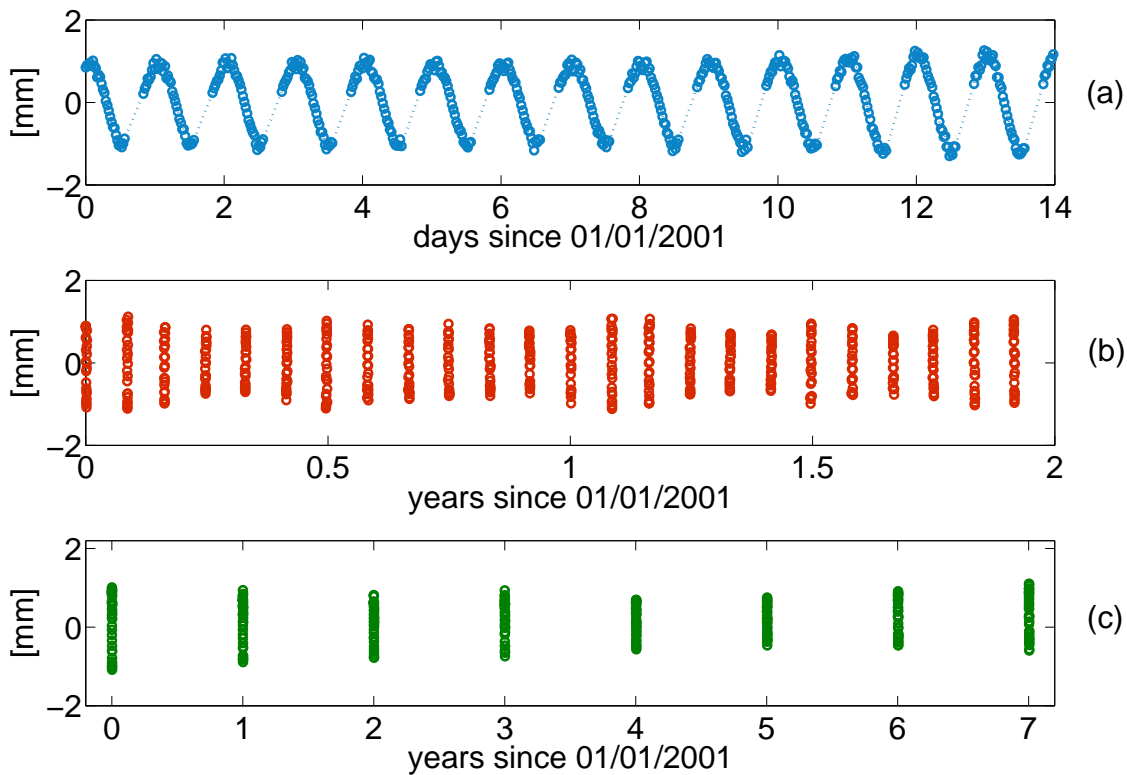


Figure 2. Differences VieVS minus Occam 6.1 of the calculated delays for a period of 14 consecutive days (a), a period of two years with a 24 h session every month (b), and of seven yearly sessions (c).

4. Conclusions and Outlook

So far DeDeCC has helped to detect small bugs and to verify several correction models during the development of VieVS. Under the guidance of the IVS Analysis Coordinator and with the assistance of several IVS analysts, an official Call for Participation in the campaign will be distributed within the IVS soon. Providing comparisons within DeDeCC1 are successful, further investigations including the partial derivatives will follow. Recent developments and upcoming results will be published on the Web (see Section 3.1).

5. Acknowledgements

Lucia Plank is thankful to the Marietta Blau Mobilitatsstipendium of the Vienna University of Technology for subsidizing her participation at the IVS GM2010.

References

- [1] Boehm, J., S. Boehm, T. Nilsson, A. Pany, L. Plank, H. Spicakova, K. Teke, H. Schuh, The new Vienna VLBI Software VieVS, In: IAG Symposia Series, Buenos Aires 2009 (to be published)
- [2] Titov, O., V. Tesmer, J. Boehm, Occam v.6.0 Software for VLBI Data Analysis, In: International VLBI Service for Geodesy and Astrometry 2004 General Meeting Proceedings, NASA/CP-2004-212255, N.R. Vandenberg, K. Baver (eds.), pp 267-271, 2004
- [3] Sovers, O. J., J. L. Fanselow, C. S. Jacobs, Astrometry and geodesy with radio interferometry: experiments, models, results, In: Reviews of Modern Physics, Vol. 70, No. 4, pp 1393-1454, October 1998
- [4] Eubanks, T. M. (ed.), In: Proceedings of the U. S. Naval Observatory Workshop on Relativistic Models for Use in Space Geodesy, U. S. Naval Observatory, Washington, D. C., 1991

Correlations Between the Contributions of Individual IVS Analysis Centers

Sarah Böckmann, Thomas Artz, Axel Nothnagel

Institut für Geodäsie und Geoinformation, Universität Bonn

Contact author: Sarah Böckmann, e-mail: boeckmann@uni-bonn.de

Abstract

Within almost all space-geodetic techniques, contributions of different analysis centers (ACs) are combined in order to improve the robustness of the final product. So far, the contributing series are assumed to be independent as each AC processes the observations in different ways. However, the series cannot be completely independent as each analyst uses the same set of original observations and many applied models are subject to conventions used by each AC. In this paper, it is shown that neglecting correlations between the contributing series yields too optimistic formal errors and small, but insignificant, errors in the estimated parameters derived from the adjustment of the combined solution.

1. Introduction

It is widely accepted that the results of the different space-geodetic techniques are combined in order to fully exploit the strengths of each technique and to overcome the technique-specific weaknesses. In recent years, it has been shown that also a combination of the results achieved by different analysis centers (ACs) using the observations of one technique leads to more robust results (see e.g., [4], [2]). Today, almost all products of the technique-specific services in the International Earth Rotation and Reference Systems Service (IERS) are determined in a so-called intra-technique combination.

As each AC processes the observations in a different way, their results are not identical. However, from a statistical point of view, these intra-technique combinations suffer from the fact that the contributions of different ACs are treated independently despite having been derived from almost the same set of original observations. Mathematically, these dependencies can be expressed by correlations. But, the determination of these correlations and their rigorous consideration presents a delicate problem within today's combination methodologies.

In the work of [5] a first concept is presented to take the impact of the identity, as well as the impact of differences due to independent analysis strategies, into account. So far, this idea has not been adapted for any operational intra-technique combination, most probably because this concept cannot be easily extended to more than two contributions.

Different from [5], in this paper, the dependency of two contributions of real IVS ACs is quantified and rigorously considered by combining directly the observation equations (Section 3). Moreover, the effects on the estimated combined parameters as well as on their formal errors are discussed, and the findings are applied to the operational IVS combination at the normal equation level (Section 4).

2. Mathematical Background

To introduce the basic concept, the most important formulas for the combination of linear equation systems are given for the contributions of two ACs, which can easily be extended for more. These equations are mainly based on [1]. An over-determined system of linear equations

$$\mathbf{l} + \mathbf{e} = \mathbf{A}\hat{\mathbf{x}} \quad (1)$$

with \mathbf{A} being the Jacobian matrix, \mathbf{l} the vector ‘observed minus computed’ observations and \mathbf{e} the vector of residuals is solved in a weighted least squares adjustment by minimizing $\|\mathbf{A}\mathbf{x} - \mathbf{l}\|_P^2$. A combination of two systems simply means to stack the equations so that the elements of the combined system are:

$$\mathbf{l} = \begin{bmatrix} \mathbf{l}_1 \\ \mathbf{l}_2 \end{bmatrix}, \quad \mathbf{e} = \begin{bmatrix} \mathbf{e}_1 \\ \mathbf{e}_2 \end{bmatrix}, \quad \mathbf{A} = \begin{bmatrix} \mathbf{A}_1 \\ \mathbf{A}_2 \end{bmatrix}, \quad (2)$$

if both systems coincide in the parameter vector and its a priori values. In the case of uncorrelated observations, the combined variance-covariance matrix reads as

$$\Sigma\left(\begin{bmatrix} \mathbf{l}_1 \\ \mathbf{l}_2 \end{bmatrix}\right) = \begin{bmatrix} \sigma_1^2 \mathbf{P}_1^{-1} & \mathbf{0} \\ \mathbf{0} & \sigma_2^2 \mathbf{P}_2^{-1} \end{bmatrix} \quad (3)$$

with \mathbf{P} being the weight matrix and σ the variance coefficients. Generally, a least squares solution $\hat{\mathbf{x}}$ can be computed by solving the normal equation system

$$\mathbf{N}\hat{\mathbf{x}} = \mathbf{n} \quad \text{with } \mathbf{N} = \mathbf{A}^T \mathbf{P} \mathbf{A} \quad \text{and } \mathbf{n} = \mathbf{A}^T \mathbf{P} \mathbf{l}. \quad (4)$$

For the computation of the combined normal equation system, this leads to the simple addition of the individual normal equations:

$$\underbrace{\left(\frac{1}{\sigma_1^2} \mathbf{N}_1 + \frac{1}{\sigma_2^2} \mathbf{N}_2\right)}_{\mathbf{N}} \hat{\mathbf{x}} = \underbrace{\frac{1}{\sigma_1^2} \mathbf{n}_1 + \frac{1}{\sigma_2^2} \mathbf{n}_2}_{\mathbf{n}}. \quad (5)$$

However, Eq. (3) and thus Eq. (5) only hold, if the observations \mathbf{l}_1 and \mathbf{l}_2 are uncorrelated. In the case of correlated observations, the combined variance-covariance matrix has to be extended by the cofactor matrices \mathbf{P}_{12} and the covariance coefficient σ_{12} :

$$\Sigma\left(\begin{bmatrix} \mathbf{l}_1 \\ \mathbf{l}_2 \end{bmatrix}\right) = \begin{bmatrix} \sigma_1^2 \mathbf{P}_1 & \sigma_{12} \mathbf{P}_{12} \\ \sigma_{12} \mathbf{P}_{12} & \sigma_2^2 \mathbf{P}_2 \end{bmatrix}^{-1}. \quad (6)$$

The combined parameter vector $\hat{\mathbf{x}}$ can no longer be computed by simply accumulating the individual normal equation systems \mathbf{N}_1 and \mathbf{N}_2 as in Eq. (5). Instead the combined observation equation system has to be solved:

$$\underbrace{\left[\mathbf{A}_1^T \mathbf{A}_2^T\right]}_{\mathbf{N}} \Sigma^{-1} \begin{bmatrix} \mathbf{A}_1 \\ \mathbf{A}_2 \end{bmatrix} \hat{\mathbf{x}} = \underbrace{\left[\mathbf{A}_1^T \mathbf{A}_2^T\right]}_{\mathbf{n}} \Sigma^{-1} \begin{bmatrix} \mathbf{l}_1 \\ \mathbf{l}_2 \end{bmatrix}. \quad (7)$$

Thus, a fully rigorous consideration of the dependency of the individual contributions in an intra-technique combination can only be carried out at the observation equation level.

3. Pilot Study

Since the IVS intra-technique combination is based on datum-free normal equation systems, a rigorous combination taking into account the correlations between the input series is not possible, as the observation equations would be necessary. At the moment, these correlations are neglected. Therefore, the influence of neglecting the correlations on the estimated combined parameters and their formal errors is investigated in this pilot study.

Extensive modifications of the VLBI analysis software Calc/Solve have been carried out to extract the complete observation equations. With this modified version, the continuous 15-day campaign CONT02 has been analyzed by two different ACs using different analysis options as they are used for the contributions to the operational IVS combination as well. Using these observation equations, a combination according to Eq. (7) is carried out. In the first step, the correlations between the contributions are determined in a variance-covariance component estimation as, e.g., described in [3]. In Fig. 1 the correlation coefficients between the contributions of the two ACs estimated for each individual day of the two week period are shown. It is clearly visible that

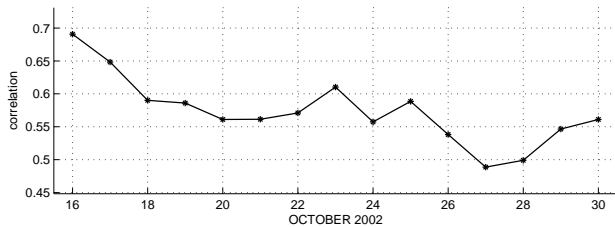


Figure 1. Level of correlations between the two contributions during the two-week CONT02 campaign.

the level of correlation is not constant over the whole campaign; it varies from session to session between 0.5 and 0.7 and naturally depends on the level of the agreement of the analysis options selected by the analysts as well as how much they practically affect the real observations.

In order to understand how much the negligence of these correlations influences the combined results, a combination is carried out twice—first, assuming independent contributions according to Eq. (3), and, secondly, taking the correlations (as presented in Fig. 1) into account with the stochastic model according to Eq. (6). The X-pole estimates and formal errors for the two individual solutions as well as for the combined solutions with and without taking the correlations into account are displayed in Fig. 2. The formal errors are (on average over the two weeks) too opti-

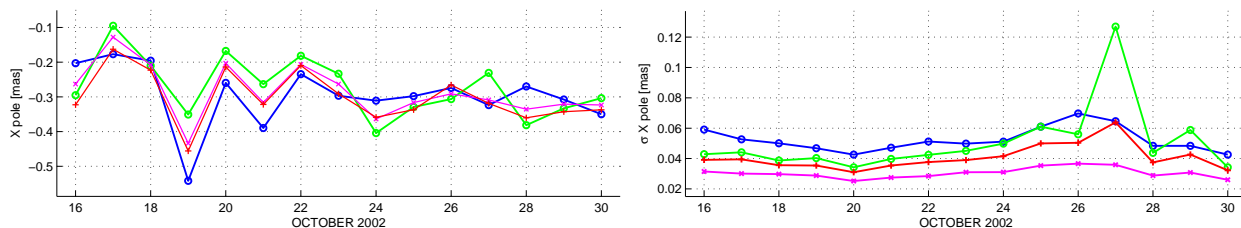


Figure 2. X-Pole estimates (left) and their formal errors (right) for the combined solutions neglecting correlations (magenta, x's) and considering correlations (red, +'s). In blue (dark circles) and green (light circles), the results of the individual solutions are displayed.

mistic by a factor of 1.2 if correlations are neglected. The differences of the combined parameters with and without considering correlation, are within their $1\text{-}\sigma$ formal errors (see Fig. 3) and, thus, insignificant.

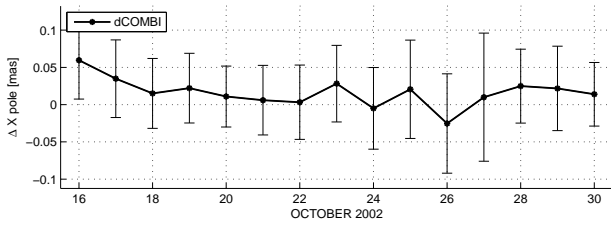


Figure 3. Differences between the estimates of the combined solution neglecting correlations and the estimates of the combined solution where correlations are considered. The error bars display the $1-\sigma$ formal errors of the differences.

4. Impacts on the Operational IVS Combination

Since the dependency of the ACs’ contributions to the operational IVS combination cannot be considered directly in the combination process, at least the knowledge from the pilot study regarding the multiplication factors for the formal errors can be transferred. In the case of two contributions these are too optimistic by a factor of approximately 1.2. Since six and not only two ACs contribute to the operational IVS combination at the moment, the formal errors are expected to be even less realistic. A simplified error propagation assuming six contributions, all correlated amongst each other with 0.6, leads to too optimistic formal errors of the combined parameters by a factor of 2.

In order to investigate if this is realistic, comparisons with independent EOP series can serve as a simple empirical approach. Here, the IGS EOP series (igs00p03.erp) is used as a reference. If the WRMS of the differences of the two series is within the formal errors, the formal errors can be assumed to be realistic. Therefore, the differences of all individual AC’s solutions as well as of the combined solution w.r.t. IGS are computed. For the data of one month each, WRMS values and median formal errors of these differences are calculated and compared for the period 1996.0 to 2009.0.

As displayed in Fig. 4 for the X-pole, the ratio of the median formal errors and the WRMS, both computed over the data of one month with a 7-day sliding window, are less than one for all polar motion components, which indicates that the formal errors are too optimistic. For the individual VLBI series the ratios are about 0.6, while the ratio for the combined solution (without considering correlations) is less than 0.4. However, it is not possible to attribute unambiguously the too optimistic formal errors to the IGS or to the VLBI series. But, here, the goal is that the ratio of the combined series w.r.t IGS equals the level of the ratio of the individual VLBI solutions. This can be achieved by scaling the formal errors of the combined solution by 2 (see Fig. 4) which is exactly the number derived from the pilot study.

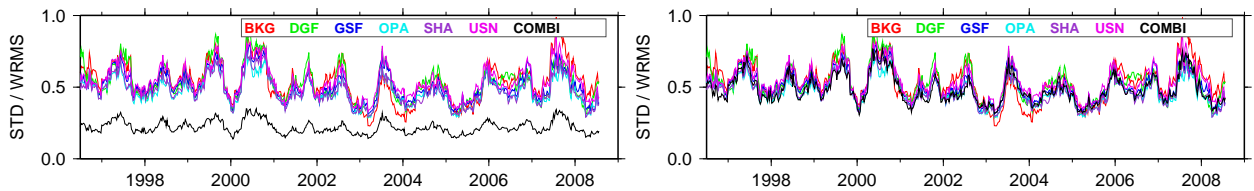


Figure 4. Ratio of the formal errors and the WRMS values of each individual series computed from the normal equation systems and the combined series w.r.t. IGS—(left) without scaling of the formal errors, (right) after scaling the formal errors of the combined solution by a factor of 2.

Figure 5 shows, as an example, the formal errors for the X-pole component between 1996 and 2009 computed from the individual normal equation systems and the combined system itself before

and after scaling. After scaling, the formal errors of the combined solution are clearly closer to the level of the individual series. However, they are still slightly smaller which is realistic because the combined solution contains more information than the individual solution.

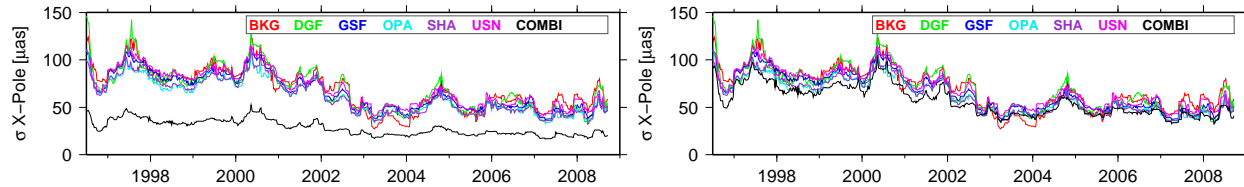


Figure 5. Median smoothed formal errors of the X-pole component between mid-1996 and 2009 for each individual series and the combined series itself, (left) before scaling the combined series, (right) after scaling the combined series by a factor of 2.

5. Summary and Conclusions

Up to now, in intra-technique combinations the dependency of contributions among each other has completely been neglected. Since most of the contributions to the IVS combination uses the same software package for the analysis of the VLBI observations, quite high correlations are expected. In this paper, a study is carried out where the observation equations are used directly for the combination. This allows determination of the level of correlations and investigation of the influence of neglecting the correlations on the estimated combined parameters as well as their formal errors. For the CONT02 data, it turned out that a realistic level of correlations for the contributions to the IVS combination is between 0.5 and 0.7. However, it has to be taken into account that correlations might be smaller using the contributions of different software packages or higher if more similar analysis options are chosen by the analysts. Moreover, it is shown that the negligence of correlations primarily impacts the formal errors of the estimated parameters and not the parameters themselves. For the IVS combined products with six contributing ACs, these are too optimistic by a factor of approximately 2 if the correlations are neglected.

References

- [1] D. Angermann, H. Drewes, M. Krügel, B. Meisel, M. Gerstl, R. Kelm, H. Müller, W. Seemüller, and V. Tesmer, ITRS Combination Center at DGFI: a terrestrial reference frame realization 2003, DKG Reihe B: Angewandte Geodäsie Heft Nr. 313, ISBN 3-7696-8593-8, 1–141, 2004.
- [2] S. Böckmann, A. Nothnagel, T. Artz, and V. Tesmer, International VLBI Service for Geodesy and Astrometry: EOP combination methodology and quality of the combined products, *J Geophys Res*, B04404, 2010, doi: 10.1029/2009JB006465.
- [3] K.-R. Koch. *Parameter Estimation and Hypothesis Testing in Linear Models*, Springer-Verlag, Berlin Heidelberg New York, ISBN 3-540-18840-1, 2nd edition, 1999.
- [4] J. Kouba and Y. Mireault, Analysis coordinator report, In *IGS Annual Report*, pages 55–100, JPL Pasadena CA, 1996, (available electronically at <http://igscb.jpl.nasa.gov/overview/pubs.html>).
- [5] H. Kutterer, M. Krügel, and V. Tesmer, Towards an improved assessment of the quality of terrestrial reference frames, In H. Drewes, editor, *Geodetic Reference Frames*, Vol. 134 of *International Association of Geodesy Symposia*, pages 67–72, 2009, doi: 10.1007/978-3-642-00860-3_10.

VLBI-SLR Combination Solution Using GEODYN

Dan MacMillan ¹, Despina Pavlis ², Frank Lemoine ³, Douglas Chinn ², David Rowlands ³

¹) NVI, Inc./NASA Goddard Space Flight Center

²) SGT, Inc./NASA Goddard Space Flight Center

³) NASA Goddard Space Flight Center

Contact author: Dan MacMillan, e-mail: daniel.s.macmillan@nasa.gov

Abstract

We would like to generate a multi-technique solution combining all of the geodetic techniques (VLBI, SLR, GPS, and DORIS) using the same software and using the same *a priori* models. Here we use GEODYN software and consider only the VLBI-SLR combination. Here we report initial results of our work on the combination. We first performed solutions with GEODYN using only VLBI data and found that VLBI EOP solution results produced with GEODYN agree with results using CALC/SOLVE at the 1-sigma level. We then combined the VLBI normal equations in GEODYN with weekly SLR normal equations for the period 2007–2008. Agreement of estimated Earth orientation parameters with IERS C04 were not significantly different for the VLBI-only, SLR-only, and VLBI+SLR solutions.

1. Introduction

The traditional procedure followed by the IERS for generating an ITRF is to combine technique solutions generated by each technique combination center. Alternatively, we would like to generate a multi-technique solution using the same software and using the same *a priori* models. Our goal is to produce such a solution combining all of the geodetic techniques at the normal equation level using GEODYN [2], but here we consider only the VLBI-SLR combination. The data from each 24-hour session of VLBI data is initially processed with the VLBI CALC/SOLVE [1] software to generate VLBI input files to GEODYN containing: 1) observed delays and 2) solution parameterization. We performed tests to ensure that the VLBI theoretical delay as calculated by the VLBI CALC/SOLVE software is the same as that calculated by GEODYN. Then we ran solutions for independent days with GEODYN using only VLBI data to verify that VLBI results from GEODYN agree with results using CALC/SOLVE. Once this was done, we generated GEODYN VLBI and SLR solutions for 2007–2008. In the next step, we combined the VLBI normal equations in GEODYN with weekly SLR normal equations for the period 2007–2008 for Lageos1/2 and Starlette/Stella to estimate station positions and Earth orientation parameters (EOP). To connect the techniques, we will need to apply the ground ties used by the IERS. Here we report on our progress in generating a VLBI+SLR combination solution.

2. GEODYN Versus CALC/SOLVE VLBI Solution Comparisons

We first compared solutions for single independent 24-hour VLBI solutions using CALC/SOLVE and GEODYN. For these solutions, *a priori* position coordinates are in ITRF2005, and the *a priori* EOP series was IERS C04. The solutions each had a standard set of estimated parameters: site coordinates, daily EOP estimated at session midpoints, 20-minute wet zenith tropospheric delay parameters, 60-minute clocks, and 8-hour gradients.

We compared CALC/SOLVE and GEODYN solutions for CONT08 (15 continuous days of observing from 12-26 August 2008), where each day was processed independently. For the most part, clock and wet zenith delay estimates from the two solutions agree within their formal uncertainties. As a typical example, Figure 1 shows the agreement for the wet zenith delays for Tsukuba, where the WRMS difference is 5 ps and the average formal uncertainty is 7.5 ps. The right-hand panel of Figure 1 shows that for many days there is a diurnal signal in the difference, which points to a likely difference in modeling between the two solutions.

We ran two types of solutions: 1) estimate EOP and fix site positions to ITRF2005 and 2) estimate both EOP and site positions for each session day and apply no-net-translation and no-net-rotation constraints. The differences between the CALC/SOLVE and GEODYN EOP estimates are plotted in Figures 2 and 3. The agreement is generally better for solution type 1. Statistics of the solution differences are given in Tables 1 and 2. There are significant differences between the two solutions for either CALC/SOLVE or GEODYN. In our standard VLBI TRF (terrestrial reference frame) solutions, we estimate global positions and velocities from all VLBI sessions. Fixing the TRF to ITRF2005 as in solution 1 will affect EOP estimates since ITRF2005 was generated from Analysis Center combination solutions from all of the geodetic techniques and clearly differs from our standard VLBI TRF. Estimating site positions in solution type 2 will also affect EOP estimates if there are site position variations during the period of analysis. These two effects are the main contributors to differences seen between solutions 1 and 2.

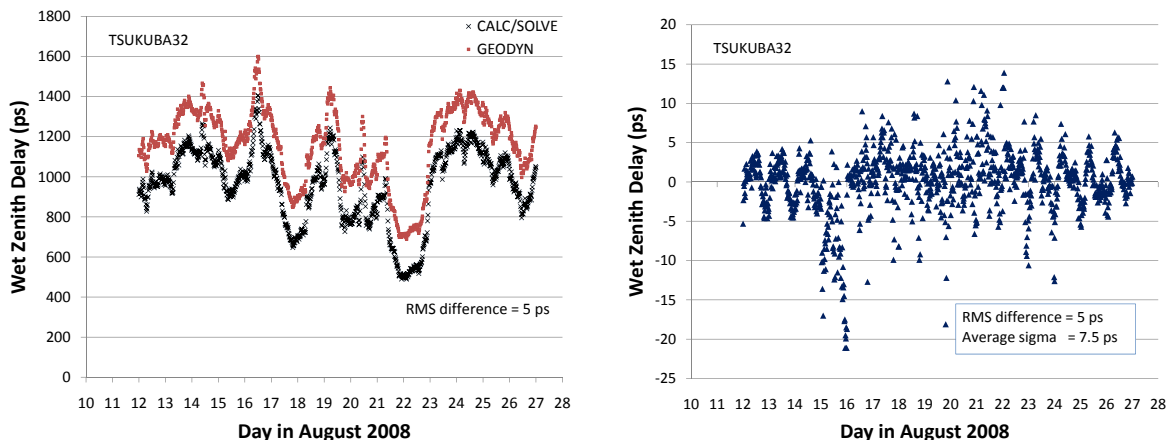


Figure 1. Comparison of the wet zenith delays estimated every 20 minutes at TSUKUB32 using CALC/SOLVE and GEODYN is shown on the left side. The series were offset by 200 ps for clarity. The difference between the CALC/SOLVE and GEODYN series is shown on the right.

3. VLBI and SLR GEODYN Solutions

We developed normal equations for SLR and VLBI data from 2007–2008 using GEODYN. SLR processing used Lageos1, Lageos2, Starlette, and Stella, with the data processed in 7-day arcs. A single combined technique-specific normal equation was created to solve for EOP. We applied the same models to process both sets of data. For example, pole tide, ocean loading with GOT4.7, Tidal EOP, and COM (center of mass) corrections were applied. VLBI session-specific

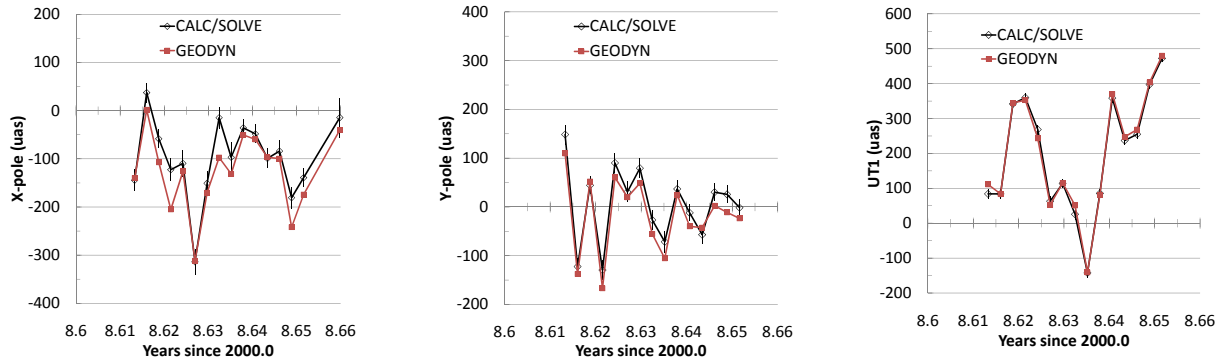


Figure 2. CALC/SOLVE and GEODYN EOP estimates for CONT08 when station positions were fixed in the solution (solution type 1).

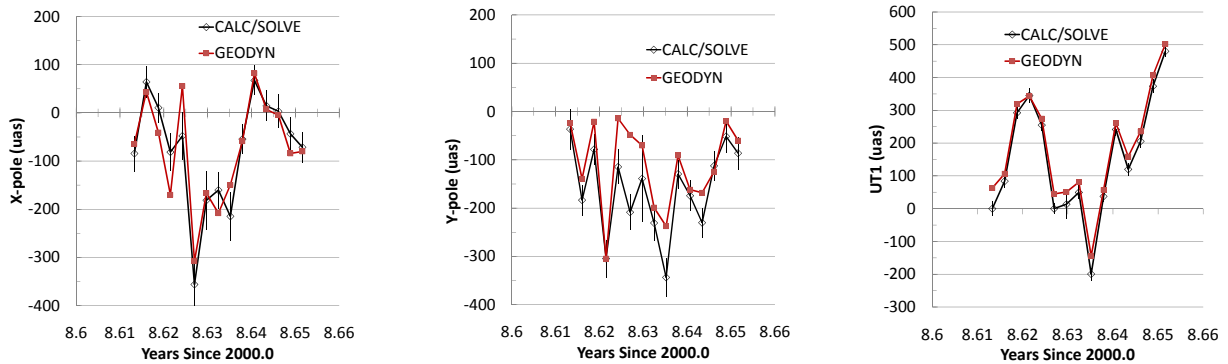


Figure 3. CALC/SOLVE and GEODYN EOP estimates for CONT08 when station positions were also estimated in the solution (solution type 2).

Table 1. EOP differences between CALC/SOLVE and GEODYN solution for 2007–2008 VLBI experiment sessions when site positions are fixed (solution type 1).

Parameter	Bias	WRMS	χ^2
X-pole (μas)	9.6	46	1.31
Y-pole (μas)	-1.2	37	0.97
UT1 (μs)	-0.47	1.9	1.09

parameters (station clocks, wet zenith troposphere delay parameters, gradient parameters) were adjusted separately and back-substituted. Initially, we chose to adjust only EOP in order to compare results and intercompare the GEODYN processing of the two space geodetic techniques. Site coordinates were fixed to *a priori* coordinates, specifically ITRF2005 for VLBI and LPOD2005 for SLR.

The EOP results were compared with IERS C04. When GEODYN solutions are run in standard mode, daily EOP values are estimated at 12 UT. Daily EOP epochs at 12 UT are not optimum

Table 2. EOP differences between CALC/SOLVE and GEODYN solution for 2007–2008 VLBI experiment sessions when site positions are also estimated (solution type 2).

Parameter	Bias	WRMS	χ^2
X-pole (μas)	16.5	64	1.09
Y-pole (μas)	-1.42	71	1.29
UT1 (μs)	-0.41	3.4	1.57

for VLBI, because VLBI 24-hour sessions are not centered on 12 UT. Usually VLBI experiment sessions begin around 18 UT, which means that each VLBI session will contribute to two noon epochs of estimation. To assess the effect of the estimation epochs, we ran two GEODYN VLBI-only solutions—one with a noon epoch and the other at the VLBI session midpoint. Additionally, we ran a CALC/SOLVE solution with session midpoint EOP estimation. Table 3 summarizes the differences relative to IERS C04. The RMS difference for the midpoint GEODYN solution is better than for the noon solution. However, the CALC/SOLVE EOP is much closer to C04. This means that there must be a problem with the GEODYN solution, which requires further investigation.

Table 3. VLBI-only solution EOP differences relative to IERS C04 for 2007–2008 VLBI experiment sessions.

Series	# pts	RMS	Avg	RMS	Avg
		X-pole (mas)	X-pole (mas)	Y-pole (mas)	Y-pole (mas)
GEODYN Noon	422	0.217	-0.033	0.251	-0.024
GEODYN Midpoint	272	0.203	0.044	0.203	-0.039
CALC/SOLVE Midpoint	278	0.132	-0.049	0.131	0.022

Table 4 compares the performance of three GEODYN solutions: 1) SLR-only, 2) VLBI-only, and 3) VLBI+SLR. The RMS differences relative to IERS C04 are not significantly different for these solutions. One would like to see that combining the techniques should produce a better solution.

Table 4. GEODYN Solution EOP differences relative to IERS C04 for 2007–2008 VLBI experiment sessions.

Series	# pts	RMS	Avg	RMS	Avg
		X-pole (mas)	X-pole (mas)	Y-pole (mas)	Y-pole (mas)
SLR	714	0.245	—	0.236	—
VLBI	433	0.212	—	0.247	—
VLBI+SLR	678	0.215	—	0.237	—

4. Conclusions

We have made some initial progress toward the goal of generating a technique combination solution with GEODYN. GEODYN and CALC/SOLVE parameter estimates for 24-hour VLBI sessions mostly agree at about the 1-sigma level: a few mm for site positions and 20–50 μs for EOP. More investigation is required to understand discrepancies between CALC/SOLVE and GEODYN when site positions are estimated along with EOP in independent 24-hour VLBI session solutions. RMS EOP differences between C04 and GEODYN VLBI are 1.5–2 times greater than for CALC/SOLVE VLBI solutions; we need to resolve this. We were able to generate a combined VLBI+SLR solution for 2007–2008. The agreement with C04 of the EOP estimates from this combined solution was insignificantly different from the agreement with C04 of either the SLR or VLBI EOP estimates. Clearly this problem has to be investigated. Other remaining issues are: weighting of different techniques in a combination, accuracy of co-location site ties, and the optimal estimation of common technique parameters such as troposphere and clock parameters.

References

- [1] Ma, C., J.M. Sauber, L.J. Bell, T.A. Clark, D. Gordon, W.E. Himwich, and J.W. Ryan, Measurement of Horizontal Motions in Alaska Using Very Long Baseline Interferometry, *J. Geophys. Res.*, 95, B13, 21,991-22,011, 1990.
- [2] Pavlis, D.E. et al., GEODYN operations manual, NASA Goddard Contractor Report, SGT, Inc., Greenbelt, MD.

Application of Raytracing through the High Resolution Numerical Weather Model HIRLAM for the Analysis of European VLBI

Susana García-Espada ¹, Rüdiger Haas ², Francisco Colomer ¹

¹) *National Geographic Institute (IGN), Spain*

²) *Chalmers University of Technology, Sweden*

Contact author: Susana García-Espada, e-mail: s.gespada@oan.es

Abstract

An important limitation for the precision in the results obtained by space geodetic techniques like VLBI and GPS are tropospheric delays caused by the neutral atmosphere, see e.g. [1]. In recent years numerical weather models (NWM) have been applied to improve mapping functions which are used for tropospheric delay modeling in VLBI and GPS data analyses. In this manuscript we use raytracing to calculate slant delays and apply these to the analysis of Europe VLBI data. The raytracing is performed through the limited area numerical weather prediction (NWP) model HIRLAM. The advantages of this model are high spatial ($0.2^\circ \times 0.2^\circ$) and high temporal resolution (in prediction mode three hours).

1. Introduction

The electromagnetic signals used in space geodetic techniques experience propagation delays on their way through the earth's atmosphere. These propagation delays relate to the refractivity of the medium and they are influenced by temperature, pressure, and humidity. Usually, these effects are taken into account by including atmospheric parameters (zenith parameters and gradients) as unknowns in the data analysis and estimating these together with the other parameters of interest in the geodetic VLBI analysis data like station positions and clock differences.

Mapping functions are used to model these delays and to relate the slant delay at any elevation angle ϵ to a zenith delay value. Today widely used mapping functions are based either on surface meteorological data [2], on climatology, e.g. [3], or to some extent on numerical weather models, e.g. [4], [5]. Raytracing through radiosonde data has often been applied to develop and validate mapping functions used for tropospheric modeling in VLBI and GPS data analyses [6].

As numerical weather models of regional size have improved in terms of accuracy and precision, a new approach is to calculate tropospheric slant delays by raytracing and to apply these directly in the analysis of space geodetic techniques.

2. HIRLAM 3D-var Numerical Weather Prediction Model

The High Resolution Limited Area Model (HIRLAM) project was established in 1985 in order to provide the best available operational short-range forecasting system for the National Meteorological Services in Denmark, Finland, Iceland, Ireland, Netherlands, Norway, Spain, and Sweden. Meteo-France has a research cooperation agreement with HIRLAM. The HIRLAM system is a complete NWP system including data assimilation with analysis of conventional or non-conventional observations and a limited area forecasting model with a comprehensive set of physical parametrization.

The forecast model is a limited area model with a boundary relaxation scheme. The model exists both in a grid-point version and in a spectral version.



Figure 1. HIRLAM horizontal grid.

The HIRLAM model is a synoptic scale model, i.e., representing conditions simultaneously over a broad area. Initial and boundary conditions are taken from the European Centre for Medium Range Weather Forecast (ECMWF). The model is a numerical short-range (< 48 h) weather forecasting system. The most used is the hydrostatic grid point model. The advantages of HIRLAM are:

- High spatial resolution: 22 km to 5 km horizontally, 16 to 60 levels vertically.
- High temporal resolution: analysis: 6 hours assimilation data and analysis (00h, 06h, 12h, 18h) and prediction (3-hour cycle also available).

3. Application in the Analysis of European VLBI

We applied raytracing through the HIRLAM model in the analysis of 15 European VLBI experiments covering EURO75 (22nd March 2005) to EURO89 (3rd September 2007). We used HIRLAM files with 22 km horizontal resolution, 40 vertical levels and 6 hours temporal resolution time (00h, 06h, 12h, 18h). Raytracing was performed for 12 stations: Crimea in Ukraine, DSS65a in Spain; Matera, Noto, and Medicina in Italy; Metsähovi in Finland; Ny-Ålesund in Norway; Onsala in Sweden; Svetloe and Zelenchukskaya in Russia; and Wettzell and Effelsberg in Germany. The Badary station in Russia was also involved in EURO87, but it is not included in the HIRLAM grid so we excluded the station from the VLBI analysis. For each site and epoch we used the HIRLAM grid data to generate vertical profiles of pressure, temperature, and relative humidity for 40 vertical levels. We interpolated spatially between the four nearest points around each site.

We used the ‘*Davis/Herring/Niell Raytrace program*’ [7] to calculate the geometric, wet, and dry delays. The program uses pressure, temperature, and relative humidity profiles starting above sea level to calculate path delay through the atmosphere. The program performs a 1D-raytracing, i.e., the calculation is only elevation dependent but not azimuth dependent. Since the temporal resolution of the applied HIRLAM analysis data was 6 hours only, we had to interpolate temporally to the epochs of the individual VLBI observations.

The resulting raytrace slant delays were introduced as calibrations to the observed delays in the analysis with the software package SOLVE [8]. In the following we compared the analysis results based on this HIRLAM-calibration (H) approach with results from a standard analysis (S) approach. For the S-approach the dry delays were modeled based on observed surface pressure and the NMF dry mapping functions [3], and the wet delays were not modeled but estimated using the corresponding NMF wet mapping functions [3].

3.1. Impact on Estimated Zenith Wet Delays

In a first assessment we compared the estimated zenith wet delays (ZWD) resulting from the H- and S-approaches. As an example, Figure 2 shows time series of estimated ZWDs for DSS65a, Medicina, Onsala, and Wettzell. Blue crosses show results from the S-approach and red diamonds the results from the H-approach. For all stations the estimated ZWD are smaller and closer to zero using the H-approach. Also the variability of the estimated ZWD is reduced when using the H-approach. This can be interpreted to mean that the apriori knowledge about the atmosphere is better when the H-approach is used.

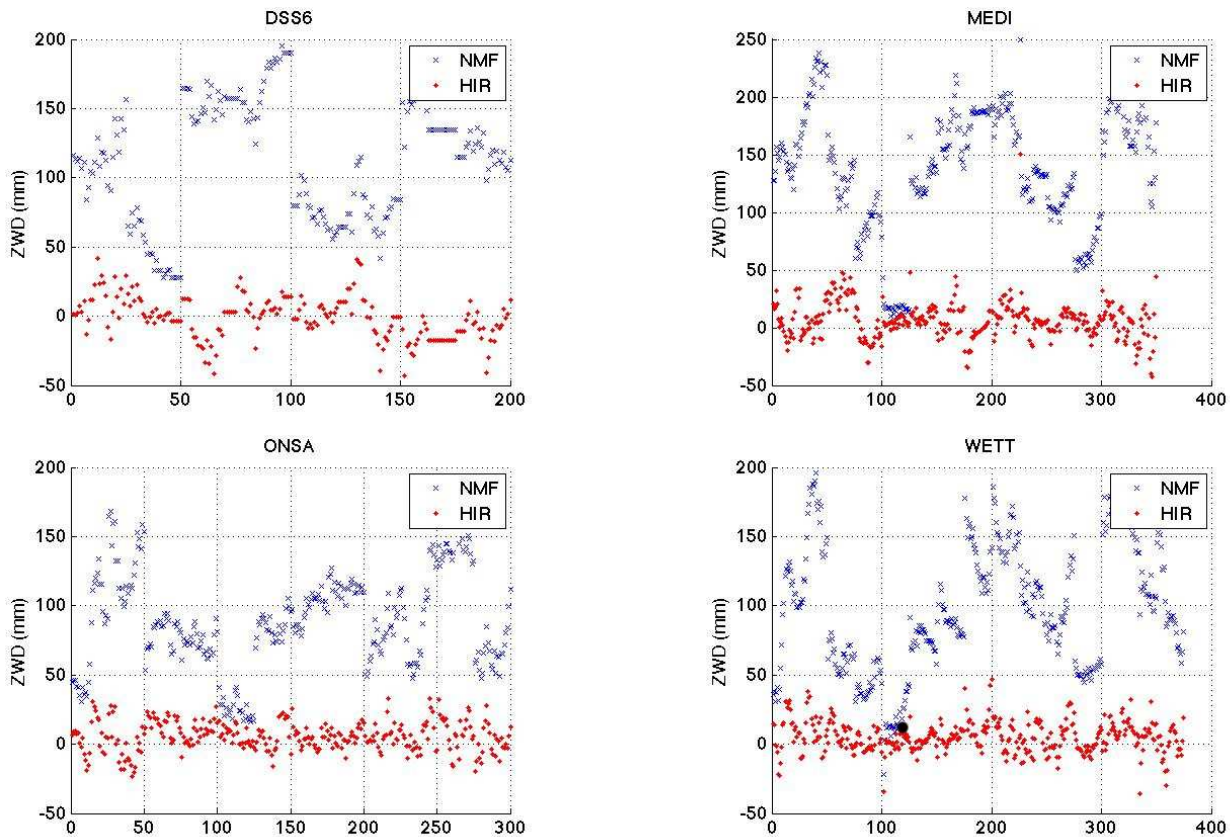


Figure 2. Time series of estimated zenith wet delays for DSS65a, Medicina, Onsala, and Wettzell. Blue crosses show results using the standard analysis approach, while red diamonds show results using the HIRLAM-calibration approach.

3.2. Impact on Baseline Length Repeatabilities

As a next step we assessed the impact of the HIRLAM-calibration on geodetic results. This time we did not estimate any ZWD for the HIRLAM-calibration approach. Other parameters like station positions, clock differences, and gradients were estimated as before. The results of this second HIRLAM-calibration (H2) approach were again compared to the standard analysis (S)

approach. For the S-approach ZWD were estimated as before with 1-hour temporal resolution.

The estimated station positions from both the S- and the H2-approach were used to derive baseline length repeatabilities. Different solutions with different elevation cutoff angles were analyzed. Figure 3 shows baseline length repeatability in terms of weighted root mean-square (wrms) as a function of baseline length for all baselines for elevation cutoff angles of 5° , 10° , 15° , and 19° . The results from the S-approach are depicted as blue circles (NMF) and the results of the H2-approach are shown as red asterisks (HIR).

Baseline repeatabilities are better for the S-approach up to an elevation cutoff angle of 19° . From a cutoff angle of 19° and higher, baseline repeatabilities are better using the H2-approach, i.e., using HIRLAM-calibration and not estimating any ZWD delays.

Best fitting regression lines (offset and rate) were estimated for the baseline repeatability data by least-squares fits. Table 1 shows the corresponding rates and offsets and also the percentage of observations used in the data analysis when using different elevation cutoff angles with respect to a solution with 5° cutoff angle.

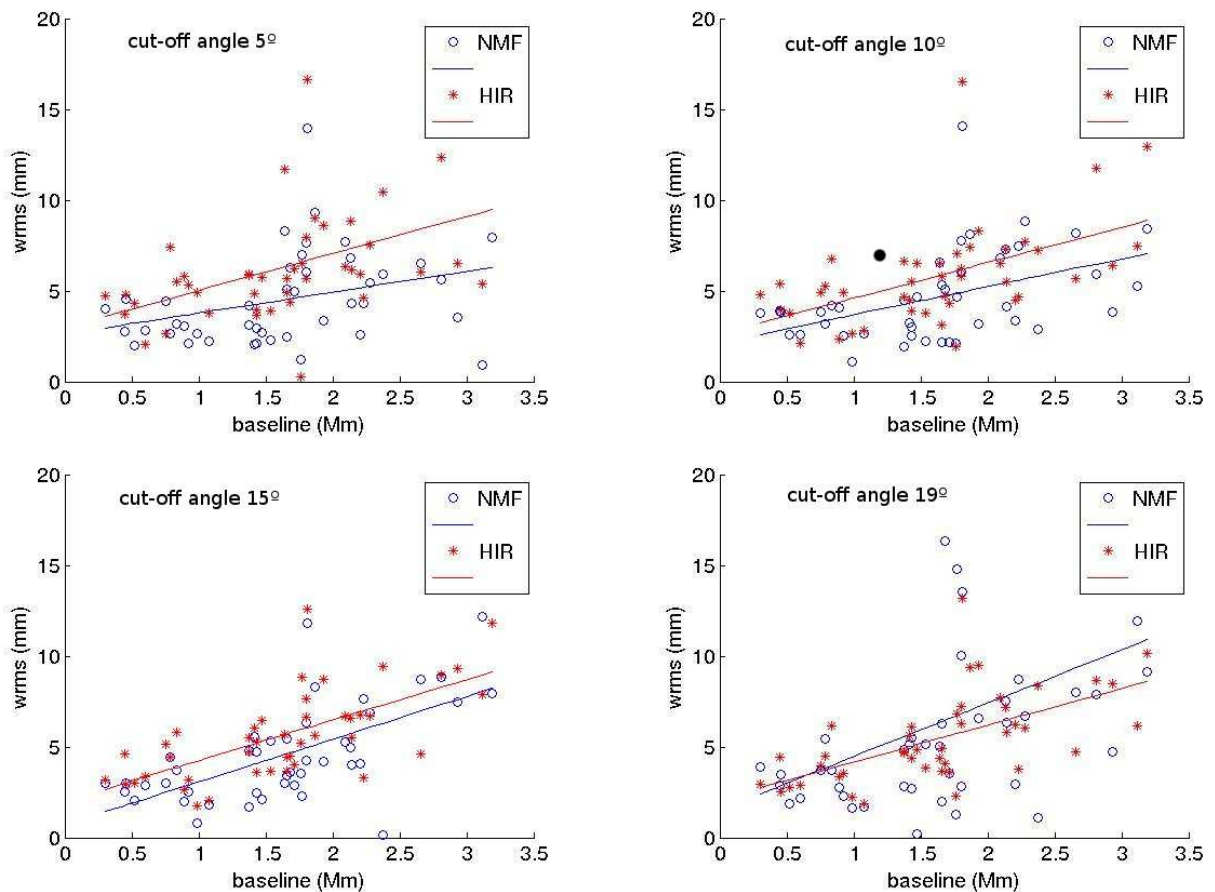


Figure 3. Baseline repeatability for all baselines and different cutoff angles. Weighted root mean-square (wrms) values are plotted against baseline length.

Table 1. Baseline repeability rates and offsets

sol.	Cutoff angle 5°			Cutoff angle 10°			Cutoff angle 15°			Cutoff angle 19°		
	obs. (%)	rate (ppb)	offset (mm)	obs. (%)	rate (ppb)	offset (mm)	obs. (%)	rate (ppb)	offset (mm)	obs. (%)	rate (ppb)	offset (mm)
S	100	1.14	2.6	95	1.54	2.1	86	2.35	0.7	77.1	2.93	1.5
H2		2.04	2.9		1.95	2.6		2.24	1.9		2.03	2.1

4. Conclusions and Outlook

We used the HIRLAM model to derive slant delays with the 1D ‘*Davis/Herring/Niell Raytrace program*’ and applied the results to the analysis of the European VLBI sessions from March 2005 to September 2007. Results from the HIRLAM-calibration were compared to results from a standard analysis.

If we estimate zenith wet delays from both approaches we see that the zenith wet delays and their variation reduce when using the HIRLAM-calibration.

If we do not estimate zenith wet delays in the HIRLAM-calibration approach, but estimate them in the standard analysis, we see that the baseline repeatabilities are better for the HIRLAM-calibration when we use only observations higher than an elevation cutoff angle of 19°.

As a next step we need to investigate how accurate the HIRLAM model is for different sites. Future work will be to develop a 4D-raytracing program that is fully elevation and azimuth dependent. The plan is to use this program with a combination of HIRLAM analysis and forecast profiles in order to additionally improve the temporal resolution. Of course, more databases of the EURO series should be included in the analysis.

References

- [1] Nilsson, T., and R. Haas (2010) Impact of atmospheric turbulence on geodetic very long baseline interferometry. *Journal of Geophysical Research*, **115**, (B03407), 1–11, doi:10.1029/2009JB006579.
- [2] Herring, T. A. (1992) Modelling atmospheric delay in the analysis of space geodetic data, In: Proceedings of Symposium on Refraction of Transatmospheric Signals in Geodesy, J.C. de Munck and T.A.Th. Spoelstra (eds.), Netherlands Geodetic Commission, *Publications on Geodesy*, **36**, New Series, 157–164.
- [3] Niell, A. E. (1996) Global mapping functions for the atmosphere delay at radio wavelengths, *Journal of Geophysical Research*, **101**, B2, 3227–3246.
- [4] Niell, A. E. (2001) Preliminary evaluation of atmospheric mapping functions based on numerical weather models. *Physics and Chemistry of the Earth*, **26**, 475–480.
- [5] Böhm, J., and H. Schuh (2004) Vienna Mapping Functions in VLBI Analyses, In: *IVS 2004 General Meeting Proceedings*, 277–281.
- [6] Stoyanov, B, R. Haas, L. Gradinarsky (2004) Calculating Mapping Functions from the HIRLAM Numerical Weather Prediction Model, In: *IVS 2004 General Meeting Proceedings*, 471–475.
- [7] Davis, J.L, T. A. H. Herring and A. E. Niell (1987–1989) The Davis/Herring/Niell Raytrace program.
- [8] Ma, C., J. M. Sauber, J. L. Bell, T. A. Clark, D. Gordon, W. E. Himwich (1990) Measurement of horizontal motions in Alaska using very long baseline interferometry. *Journal of Geophysical Research*, **95**, (B13), 21991–22011.

Atmospheric Delay Reduction Using KARAT for GPS Analysis and Implications for VLBI

Ryuichi Ichikawa ², Thomas Hobiger ¹, Yasuhiro Koyama ¹, Tetsuro Kondo ²

¹⁾ *Kashima Space Research Center, National Institute of Information and Communications Technology*

²⁾ *National Institute of Information and Communications Technology*

Contact author: *Ryuichi Ichikawa*, e-mail: `richi@nict.go.jp`

Abstract

We have been developing a state-of-the-art tool to estimate the atmospheric path delays by ray-tracing through mesoscale analysis (MANAL) data, which is operationally used for numerical weather prediction by the Japan Meteorological Agency (JMA). The tools, which we have named ‘KASHIMA RAYtracing Tools (KARAT)’, are capable of calculating total slant delays and ray-bending angles considering real atmospheric phenomena. The KARAT can estimate atmospheric slant delays by an analytical 2-D ray-propagation model by Thayer and a 3-D Eikonal solver. We compared PPP solutions using KARAT with that using the Global Mapping Function (GMF) and Vienna Mapping Function 1 (VMF1) for GPS sites of the GEONET (GPS Earth Observation Network System) operated by Geographical Survey Institute (GSI). In our comparison 57 stations of GEONET during the year of 2008 were processed. The KARAT solutions are slightly better than the solutions using VMF1 and GMF with linear gradient model for horizontal and height positions. Our results imply that KARAT is a useful tool for an efficient reduction of atmospheric path delays in radio-based space geodetic techniques such as GNSS and VLBI.

1. Introduction

Radio signal delays associated with the neutral atmosphere are one of the major error sources of space geodesy such as GPS, GLONASS, GALILEO, VLBI, and In-SAR measurements. The recent geodetic analyses were carried out by applying modern mapping functions based on the numerical weather analysis fields with horizontal gradient model with the purpose of better modeling these propagation delays, thereby improving the repeatability of site coordinates. The Global Mapping Function (GMF) [3], and Vienna Mapping Function 1 (VMF1) [2, 4] have been successfully applied to model the zenith hydrostatic delay in recent years. In addition, the lateral spatial variation of the wet delay is reduced by linear gradient estimation [9, 5]. The anisotropic mapping function is also a powerful tool for removing or calibrating the effects of horizontal variability of the atmosphere within GNSS and VLBI analyses. Atmospheric gradients are assumed to have a simple linear form which can be modeled by the anisotropic mapping function. However, it has been suggested that this assumption is not always appropriate in the context of intense mesoscale phenomena such as the passage of a cold front, heavy rainfall, or severe storms. Based on prior work by Ichikawa et al. [8], we have developed a state-of-the-art tool to obtain atmospheric slant path delays by ray-tracing through the mesoscale analysis (MANAL) data from numerical weather prediction with 10 km horizontal resolution provided by the Japan Meteorological Agency (JMA) [6, 7]. The tool, which we have named ‘KASHIMA RAYtracing Tools (KARAT)’, is capable of calculating total slant delays and ray-bending angles considering real atmospheric phenomena. Hobiger et al. preliminarily compared precise point positioning (PPP) estimates using KARAT with those

using the GMF based on GPS data from GEONET operated by Geographical Survey Institute (GSI) [6]. Under the various atmospheric conditions the results imply that the performance of KARAT is almost equal to the solution which is obtained by applying the GMF with gradients. In our study, we have compared PPP processed position solutions using KARAT with those using state-of-the-art mapping functions in order to evaluate the present KARAT potential for longer time periods. In our comparison we processed 57 stations of GEONET data during the year 2008.

2. KARAT

The KARAT have been developed at the National Institute of Information and Communications Technology (NICT), Japan and are capable of calculating total slant delays and ray-bending angles.

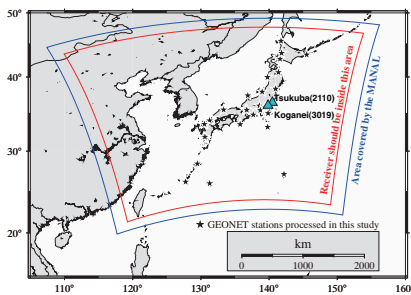


Figure 1. The GEONET stations processed in this study. The boundary of JMA mesoscale analysis data is also shown. The two triangles denote the location of Tsukuba and Koganei GEONET stations, respectively (see Figure 2).

The JMA mesoscale analysis data (which will be called “JMA MANAL data” hereafter), which we used in our study, provides temperature, humidity, and pressure values at the surface and at 21 height levels (which vary from several tens of meters to about 31 km), for each node in a 10 km by 10 km grid that covers the Japanese islands, the surrounding ocean, and East Asia [13]. The 3-hourly operational products have been available from JMA since March 2006. A linear time interpolation is implemented in KARAT to obtain results at arbitrary epochs which allows also to evaluate temporal changes of estimates. Further details of KARAT are described in Hobiger et al. [6, 7].

KARAT can estimate atmospheric slant delays by three different calculation schemes. These are (1) a piece-wise linear propagation, (2) an analytical 2-D ray-propagation model by Thayer [16], and (3) a 3-D Eikonal solver [7].

Although the third scheme can include small scale variability of atmosphere in the horizontal, it has a significant disadvantage due to the massive computational load. In this paper we discuss estimations using the second and the third schemes since we would like to focus on the two more sophisticated methods.

3. Precise Point Positioning Results for GEONET Stations

In order to compare KARAT processing and modern mapping functions we analyzed data sets of GEONET, which is a nationwide GPS network operated by GSI. In our comparison 57 stations from GEONET of the year 2008 were considered for processing. We chose the stations which were not affected by crustal deformations caused by seismic activities. Figure 1 shows the locations of the selected stations in our study. Since these stations are evenly distributed over the Japanese islands, we can investigate effects of various weather conditions on the processing. In addition, we can avoid uncertainties due to the individual difference of equipment in terms of the same type of antenna-receiver set in GEONET.

At first, precise point positioning (PPP) estimates covering the whole period shown above were

obtained for all sites using GPSTOOLS [15]. The troposphere delays were modeled by dry (using the Saastamoinen model [14]) and wet constituents.

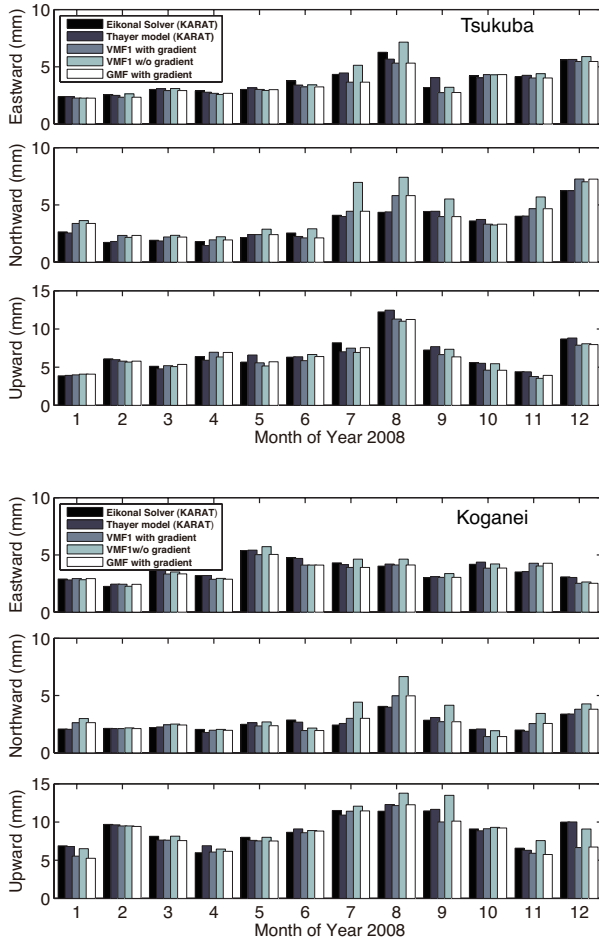


Figure 2. Monthly averaged repeatabilities of station positions at Tsukuba (upper) and Koganei (lower) during 2008.

In this figure five cases of solutions are shown: KARAT solution using Eikonal solver, KARAT solution using the Thayer model, VMF1 solution with gradient, VMF1 solution without gradient, and GMF with gradient. The results of VMF1 without gradient reveal the largest repeatability value for all components at both stations during the summer season (July, August, and September), as one would expect.

Tsukuba and Koganei experienced severe heavy rainfall events during August 26–31, 2008. Especially, the total rainfall around Tsukuba was about 300 mm during these six days. The north-south position errors were caused by steep water vapor gradients associated with an EW rain band at both stations. Such large position errors are partly reduced using the modern mapping functions with gradient model as shown in Figure 2.

On the other hand, the results of the KARAT solutions (both the Eikonal solver and the Thayer model) are much better for the north-south component at both stations during July and

The wet delay was estimated as unknown parameters using the GMF and VMF1 together with linear gradients [5]. Process noise values of zenith delays and linear gradients were set to 0.1 mm and 0.01 mm, respectively. The elevation cutoff angle was set to 10° , and downweighting at lower elevation angles was applied. The ocean loading correction based on the NAO.99b model was applied [10], and no atmospheric loading was applied. The a priori hydrostatic zenith delays were computed from the Saastamoinen model [14] based on standard atmosphere values with the station height correction.

The Kalman-filter estimation interval was set to 300 s, without overlapping data from consecutive days. The daily position estimates from these solutions serve as a reference to which the ray-traced solutions can be compared. In our comparison, PPP estimations using the GMF and VMF1 without linear gradients were also performed.

In order to examine the position error magnitude, the monthly averaged daily repeatabilities for each coordinate component at both stations are displayed in Figure 2. We determined repeatability as the standard deviation of the position solutions with respect to a linear regression.

August. This suggests that both KARAT solutions are quite competitive with the modern mapping functions with gradient model. Figure 3 shows the averaged repeatabilities for all 57 stations. In this figure the results for each coordinate component for all six solutions (i.e., Eikonal solver, Thayer model, VMF1 with gradient, VMF1 without gradient, GMF with gradient, and GMF without gradient) are represented.

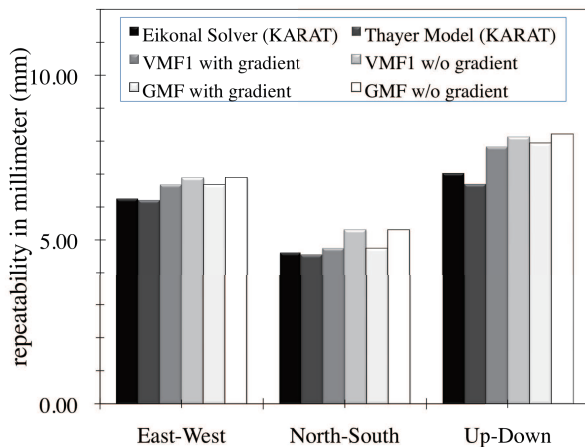


Figure 3. Averaged station position repeatability for 57 GEONET stations shown in Figure 1 for the year 2008.

It indicates that both KARAT solutions are slightly better than the modern mapping functions with gradient solution. However, there are no significant differences between the Eikonal solver and the Thayer model.

One has to consider that the time-resolution of the JMA 10 km MANAL data is three hours, whereas the PPP processing including gradient estimation was performed with a 300-second interval. Under extreme atmospheric conditions such as a severe rainfall event, the three-hour time spacing and the 10 km horizontal resolution of the JMA MANAL data may not be always sufficiently accurate to reduce atmospheric path delay effects.

4. Summary

We have assessed the performance of ray-traced atmospheric delay corrections by comparison between precise point positioning (PPP) solutions using the ray-tracing tool KARAT using JMA MANAL data with those using the modern mapping functions based on numerical weather models. In our comparison 57 stations of GEONET during 2008 were processed. The KARAT solutions are slightly better than the solutions using VMF1 and GMF with a linear gradient model for both horizontal and height positions. On the other hand, there were no significant differences between the two KARAT solutions, i.e., Eikonal solver and Thayer model. We need further investigations to evaluate the ability of KARAT to reduce atmospheric path delays under various topographic and meteorological regimes. One advantage of KARAT is that the reduction of atmospheric path delay will become more accurate each time the numerical weather model is improved (i.e., time and spatial resolution, including new observation data). In spite of the present model imperfection and coarse time resolution, we think that KARAT will help to support station position determination by improving the numerical stability due to a reduction of unknown parameters.

5. Acknowledgements

We would like to thank the Geographical Survey Institute, Japan for providing the GEONET data sets. We also thank the Japan Meteorological Agency for providing data and products. This study was supported by a Grant-in-Aid for Scientific Research A (No. 21241043) from the Japan

Society for the Promotion of Science.

References

- [1] Lanotte, R., G. Bianco, Matera CGS VLBI Analysis Center, In: International VLBI Service for Geodesy and Astrometry 2000 Annual Report, NASA/TP-2001-209979, N. R. Vandenberg and K. D. Baver (eds.), 207–209, 2001.
- [2] Boehm, J. and H. Schuh, Vienna Mapping Functions in VLBI Analyses, *Geophys. Res. Lett.*, *31*, L01603, doi:10.1029/2003GL018984, 2004.
- [3] Boehm, J., A. Niell, P. Tregoning, and H. Schuh, Global Mapping Function (GMF): A new empirical mapping function based on numerical weather model data, *Geophys. Res. Lett.*, *33*, L07304, doi:10.1029/2005GL025546, 2006a.
- [4] Boehm, J., B. Werl, and H. Schuh, Troposphere mapping functions for GPS and very long baseline interferometry from European Centre for Medium-Range Weather Forecasts operational analysis data, *J. Geophys. Res.*, *111*, B02406, doi:10.1029/2005JB003629, 2006b.
- [5] Chen, G. and T. A. Herring, Effects of atmospheric azimuthal asymmetry on the analysis of space geodetic data, *Geophys. Res. Lett.*, *102*, 20489–20502, 1997.
- [6] Hobiger, T., Ichikawa R., Takasu T., Koyama Y. and Kondo T., Ray-traced troposphere slant delays for precise point positioning, *Earth Planets Space*, *60*, e1–e4, 2008a.
- [7] Hobiger, T., Ichikawa R., Koyama Y. and Kondo T., Fast and accurate ray-tracing algorithms for real-time space geodetic applications using numerical weather models, *J. Geophys. Res.*, *113*, D203027, 1–14, doi:10.1029/2008JD010503, 2008b.
- [8] Ichikawa, R., Kasahara M., Mannoji N., and Naito I., Estimations of atmospheric excess path delay based on three-dimensional, numerical prediction model Data, *J. Geod. Soc. Japan*, *41*, 379–408, 1995.
- [9] MacMillan, D. S., Atmospheric gradients from very long baseline interferometry observations, *Geophys. Res. Lett.*, *22*, pp.1041–1044, 1995.
- [10] Matsumoto, K., Takanezawa T., and Ooe M., Ocean tide models developed by assimilating TOPEX/POSEIDON altimeter data into hydrodynamical model: a global model and a regional model around Japan, *Journal of Oceanography*, *56*, 567–581, 2000.
- [11] Niell, A. E., Global mapping functions for the atmosphere delay at radio wavelengths, *J. Geophys. Res.*, *101(B2)*, 3227–3246, 1996.
- [12] Niell, A. E., Preliminary evaluation of atmospheric mapping functions based on numerical weather models, *Phys. Chem. Earth*, *26*, 475–480, 2001.
- [13] Saito, K., et al., The operational JMA nonhydrostatic mesoscale model, *Mon. Weather Rev.*, *134*, 1266–1298, DOI: 10.1175/MWR3120.1, 2006.
- [14] Saastamoinen, J., Contributions to the theory of atmospheric refraction, part 2, *Bull. Géodésique*, *107*, 13–34, 1972.
- [15] Takasu, T. and Kasai S., Evaluation of GPS Precise Point Positioning (PPP) Accuracy, *IEICE Technical Report*, *105(208)*, 40–45, 2005.
- [16] Thayer, G. D., A rapid and accurate ray tracing algorithm for a horizontally stratified atmosphere, *Radio Sci.*, *1(2)*, 249–252, 1967.

Use of GPS TEC Maps for Calibrating Single Band VLBI Sessions

David Gordon

NVI, Inc./NASA Goddard Space Flight Center

e-mail: David.Gordon-1@nasa.gov

Abstract

GPS TEC ionosphere maps were first applied to a series of K and Q band VLBA astrometry sessions to try to eliminate a declination bias in estimated source positions. Their usage has been expanded to calibrate X-band only VLBI observations as well. At K-band, ~60% of the declination bias appears to be removed with the application of GPS ionosphere calibrations. At X-band however, it appears that up to 90% or more of the declination bias is removed, with a corresponding increase in RA and declination uncertainties of ~0.5 mas. GPS ionosphere calibrations may be very useful for improving the estimated positions of the X-only and S-only sources in the VCS and RDV sessions.

1. GPS TEC Maps

GPS TEC (total electron content) maps are global maps of the ionosphere as determined from GPS observations. Several analysis centers of the International GNSS Service (IGS) [1] produce these maps and submit them to the IGS Data Centers (such as cddis.gsfc.nasa.gov). These maps have a latitude/longitude resolution of 2.5/5.0 degrees and cover a 2-hr period. Each daily file contains 13 maps, from 0:00 hrs to 24:00 hrs. Such maps exist from 1998 through the present.

A set of Fortran subroutines to read, interpolate, and give TEC values for a specific time, location, azimuth, and elevation angle is available from the Institute for Astronomy, University of Berne, at web site <ftp://ftp.unibe.ch/aiub/ionex/source>. With these subroutines, the ionosphere is treated as a thin spherical shell at a specified height (typically 400 or 450 km). This software has several interpolation options. The one recommended is the rotated map option, where the longitudes on the two bracketing maps with the same sun angle as the target observation are used.

The author incorporated the above software into a database program to compute VLBI ionospheric delays and place them in VLBI databases. It was originally intended for use in calibrating the K-band (~24 GHz) and Q-band (~43 GHz) VLBA¹ reference frame sessions taken by the K/Q collaboration group [2]. In these sessions, it appeared that the lack of ionospheric calibrations was producing declination biases in the estimation of source positions.

To demonstrate the usefulness of these GPS ionospheric delays, we present in Figure 1 plots of the X/S ionosphere corrections versus the corrections estimated from the GPS ionosphere maps for two baselines in a typical VLBI session. The X/S ionosphere values are instantaneous direct measurements and are believed to be very accurate, except that they contain arbitrary offsets due to the different signal paths of the X and S band systems (which do not affect the VLBI results). The GPS ionosphere values suffer from low spatial and temporal resolution, and thus should be noisy on a point-by-point basis. However, if their longer term average values are accurate, then

¹The VLBA is a facility of the National Radio Astronomy Observatory (NRAO) which is operated by Associated Universities Inc., under cooperative agreement with the National Science Foundation.

their use in VLBI should remove most of the systematic ionospheric effects on global source position estimation. Plots of X/S ionosphere delay corrections vs. GPS ionosphere delay corrections should have slopes of 1.0. But in reality, the slopes typically vary from ~ 0.8 to ~ 1.2 , and can show large scatter.

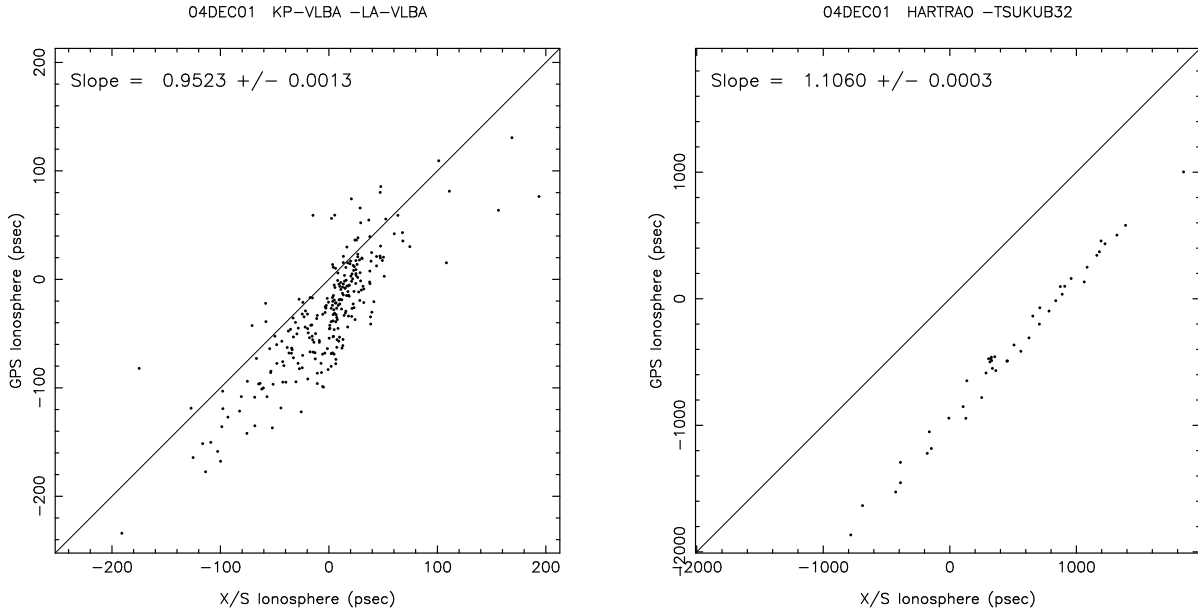


Figure 1. Comparison of X/S ionosphere delay corrections with GPS ionosphere delay corrections for a KP-VLBA to LA-VLBA baseline and a HARTRAO to TSUKUB32 baseline. Slope = 1.0 lines are shown for reference.

2. Application of GPS Ionospheres

GPS ionosphere calibrations were applied to three classes of VLBI sessions: twelve K-band and four Q-band VLBA sessions; ten X/S-band RDV sessions; and thirteen X/S-band VLBA Calibrator Survey (VCS) sessions.

2.1. K and Q Band Results

Twelve K-band reference frame sessions were taken from 2002-2008 on the VLBA. When analyzed with no ionospheric calibration, we find a declination bias (slope of a linear fit) in the Calc/Solve determined source positions of $.00635 \pm .00059$ mas/deg (Figure 2 left), compared to a standard X/S source catalog. The ionosphere causes sources to appear higher in the sky. This displacement will tend to average out in right ascension, but not in declination. When GPS ionosphere calibrations are applied, this declination bias is reduced to $.00253 \pm .00059$ mas/deg (Figure 2 right). A similar effect is seen for the four Q-band sessions, from 2002-2003.

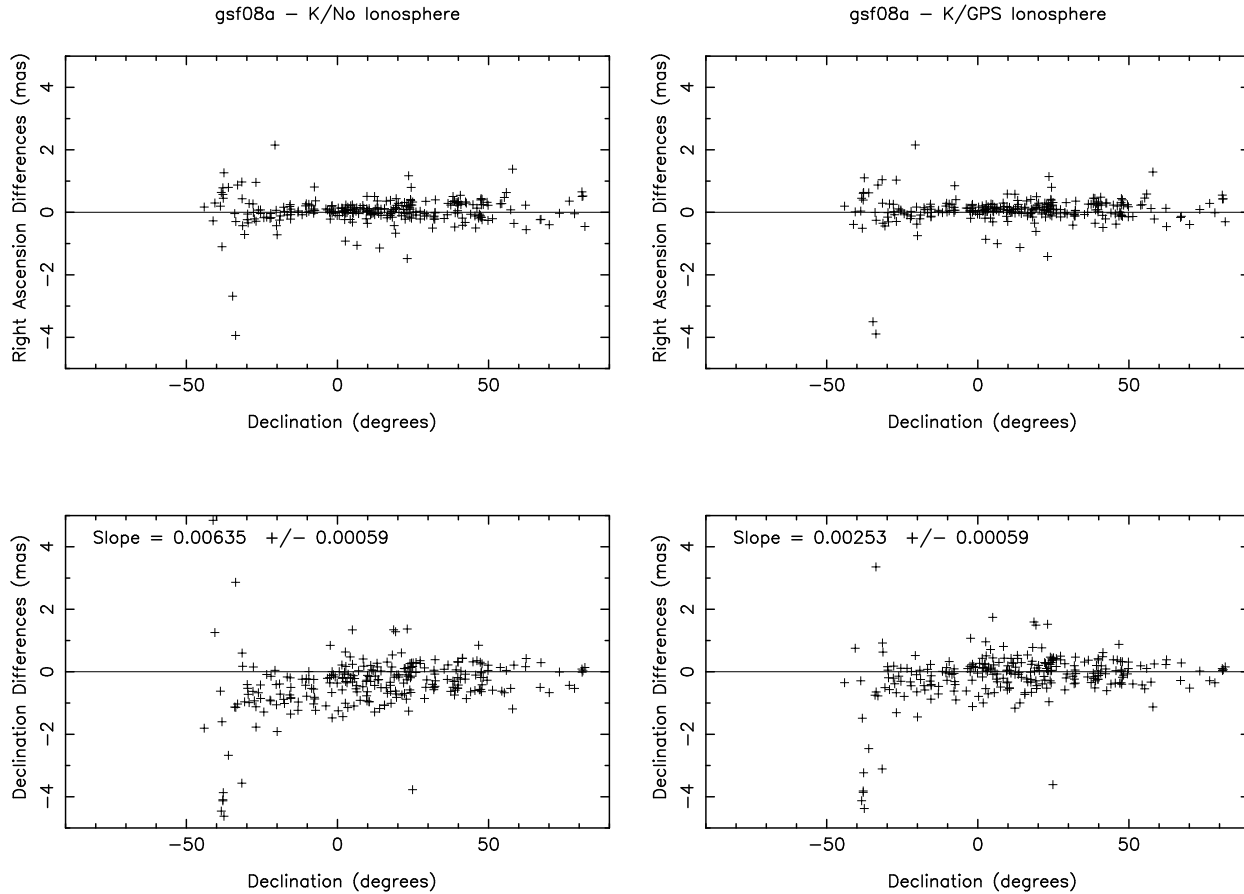


Figure 2. Position differences between a standard GSFC X/S solution vs. K-band only positions (left) and vs. K-band positions calibrated with GPS ionospheres (right).

2.2. RDV Results

For comparison with the K-band results, ten RDV sessions closest in time to the first ten K-band sessions were selected. Using only the VLBA stations, we solved for source positions using the normal X/S ionosphere free combination, using X-band only (no ionosphere), and using X-band with GPS ionosphere corrections applied. We get the following declination biases:

No Ionosphere:	$+0.02659 \pm .00024$ mas/deg	(Figure 3 left)
X/S Ionosphere:	$+0.00011 \pm .00025$ mas/deg	(Figure 3 center)
GPS Ionosphere:	$-.00266 \pm .00024$ mas/deg	(Figure 3 right)

These are plotted in Figure 3. A clear bias is seen when there is no ionosphere correction, and the linear fit is clearly inadequate. The X/S ionosphere case shows no bias, as expected. The GPS ionosphere case shows more scatter, and may slightly overcorrect. When the X/S and X/GPS catalogs are compared, we get WRMS differences of ~ 0.5 mas in both RA and declination, indicating that GPS ionosphere usage adds ~ 0.5 mas of additional uncertainty to source positions at X-band, in an RSS manner.

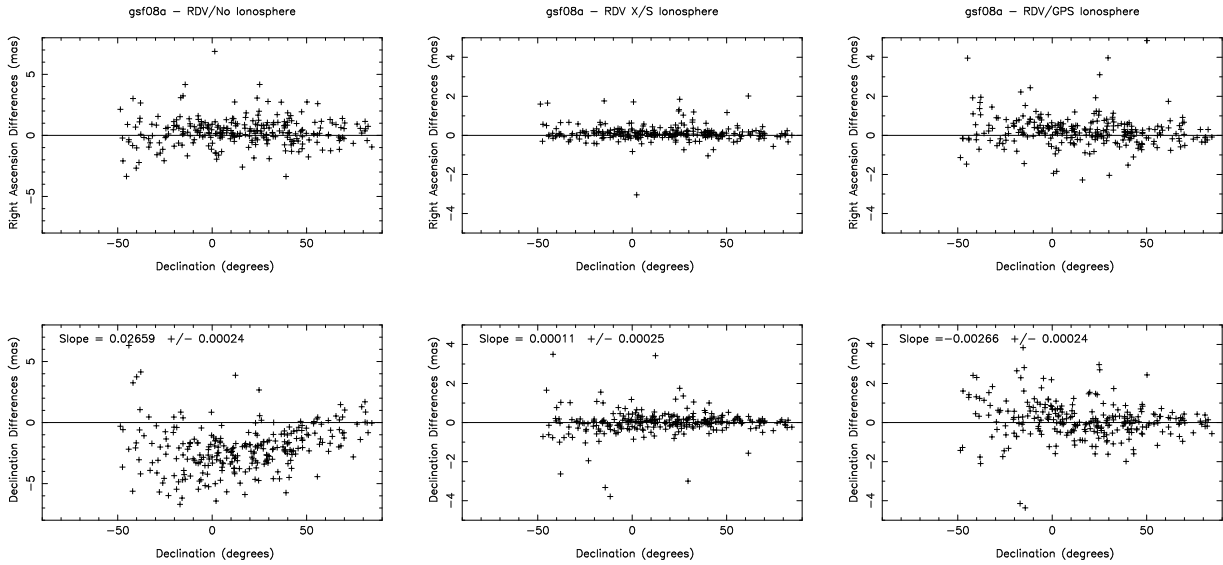


Figure 3. Differences from a standard GSFC X/S CRF solution for: X-band only positions for ten RDVs (left); X/S positions for ten RDVs (center); and X-band positions calibrated with GPS ionospheres for ten RDVs (right).

2.3. VCS Results

We made a similar comparison using the thirteen VCS sessions taken during the VCS2–VCS6 campaigns from 2002–2007 [3, 4, 5, 6, 7]. (The earlier VCS1 sessions [8] from 1994–1997 were too early for GPS ionospheres.) The declination biases found are:

$$\begin{aligned}
 \text{No Ionosphere:} & \quad +.03928 \pm .00032 \text{ mas/deg} & \text{(Figure 4 left)} \\
 \text{X/S Ionosphere:} & \quad +.00315 \pm .00026 \text{ mas/deg} & \text{(Figure 4 center)} \\
 \text{GPS Ionosphere:} & \quad +.00442 \pm .00032 \text{ mas/deg} & \text{(Figure 4 right)}
 \end{aligned}$$

These are plotted in Figure 4. A bias is clear when no ionosphere correction is used, but not so clear with the two ionosphere options. Both actually show small numerical biases, even the X/S case. This could be due to the lower emphasis on tropospheric sampling in these sessions.

With the VCS/GPS solution, we were also able to solve for an additional 135 sources that do not appear in the X/S analysis. These are sources that are detected in X-band only. The VCS sessions also have a number of S-band only sources, so presumably more additional sources could be solved for in an S/GPS analysis. Also, in the 78 RDV sessions to date, there are some X-only and S-only sources that could probably also be picked up using GPS ionosphere calibrations.

3. Conclusions

The use of GPS ionosphere corrections appears to remove $\sim 60\%$ of the declination bias at K and Q bands, and $\sim 90\%$ at X band. The reason for this difference is not clear. At X-band, GPS ionosphere calibrations appear to add ~ 0.5 mas to source position RA and DEC uncertainties, in an RSS sense. Application of GPS ionosphere calibrations at X and S bands to VCS and RDV sessions could significantly improve the positions of some 200 or more single band sources in the

astrometric catalogs. Future work will concentrate on accomplishing this.

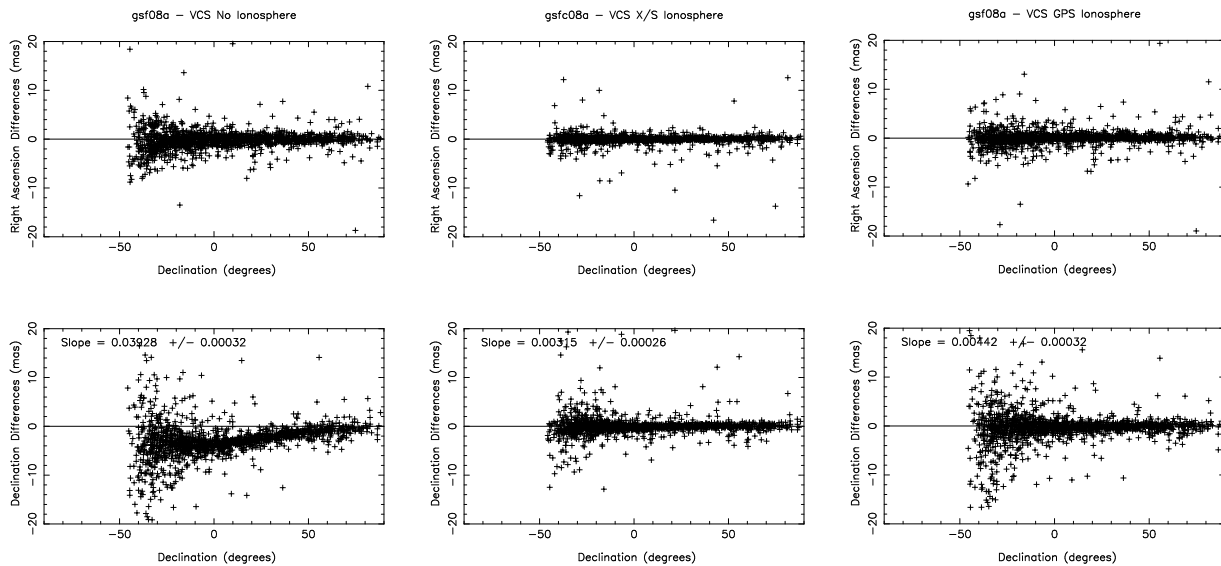


Figure 4. Differences from a standard GSFC X/S CRF solution for: X-band only VCS positions (left); X/S VCS positions (center); and X-band VCS positions calibrated with GPS ionospheres (right).

References

- [1] Dow, J.M., R.E. Neilan, G. Gendt, *Adv. Space Res.*, **36**, 320, 2005.
- [2] Lanyi, G.E., D.A. Boboltz, P. Charlot, A.L. Fey, E.B. Fomalont, B.J. Geldzahler, D. Gordon, C.S. Jacobs, C. Ma, C.J. Naudet, J.D. Romney, O.J. Sovers, L.D. Zhang, *The Celestial Reference Frame at 24 and 43 GHz. I. Astrometry*, *AJ*, **139**, 1695–1712, 2010.
- [3] Fomalont, E.B., L. Petrov, D.S. McMillan, D. Gordon, C. Ma, *The Second VLBA Calibrator Survey - VCS2*, *AJ*, **126** (N5), 2562–2566, 2003.
- [4] Petrov, L., Y.Y. Kovalev, E.B. Fomalont, D. Gordon, *The Third VLBA Calibrator Survey - VCS3*, *AJ*, **129**, 1163–1170, 2005.
- [5] Petrov, L., Y.Y. Kovalev, E.B. Fomalont, D. Gordon, *The Fourth VLBA Calibrator Survey - VCS4*, *AJ*, **131**, 1872–1879, 2006.
- [6] Kovalev, Y.Y., L. Petrov, E.B. Fomalont, D. Gordon, *The Fifth VLBA Calibrator Survey - VCS5*, *AJ*, **133**, 1236–1242, 2007.
- [7] Petrov, L., Y.Y. Kovalev, E.B. Fomalont, D. Gordon, *The Sixth VLBA Calibrator Survey - VCS6*, *AJ*, **136**, 580–585, 2008.
- [8] Beasley, A.J., D. Gordon, A.B. Peck, L. Petrov, D.S. McMillan, E.B. Fomalont, C. Ma, *The VLBA Calibrator Survey - VCS1*, *ApJS*, **141**, 13–21, 2002.

Antenna Axis Offset Estimation from VLBI

Sergey Kurdubov, Elena Skurikhina

Institute of Applied Astronomy RAS

Contact author: Sergey Kurdubov, e-mail: ksl@quasar.ipa.nw.ru

Abstract

The antenna axis offsets were estimated from global solutions and single sessions. We have built a set of global solutions from R1 and R4 sessions and from the sets of sessions between SVETLOE repairs. We compared our estimates with local survey data for the stations of the QUASAR network. Svetloe station axis offset values have changed after repairs. For non-global networks, the axis offset value of a single station can significantly affect the EOP estimations.

1. Axis Offset Estimation

The main task of this study is to check the stability of the axis offset value after repairs. The axis offset estimations from single sessions are very unstable (see Fig. 1), therefore we use global solutions [3] over several time intervals. For the estimation of the SVETLOE axis offset we used the R1 and R4 sessions divided into four intervals:

- 2003.03.06-2005.05.26, 55 sessions, from start of operation until test rail repair
- 2005.07.21-2006.05.04, 40 sessions, from test rail repair until full rail repair and removing of large equipment cabin
- 2006.08.03-2007.06.21, 55 sessions, from full rail repair until repair of the bearings
- 2007.08.30-2009.06.25, 141 sessions, from bearings repair until now

1.1. Comparison of Our Results with the On-site Measurement Data

We have three on-site measurements of the SVETLOE axis offset: in 2005 and 2006 by Igor Shahnabiev and in 2009 by “Yustas Ltd”. Comparison of our estimated values (designated as “VLBI”) and on-site Local Geodetic Surveying measurement (designated as “On-site”) are presented in Table 1.

Table 1. Values of SVETLOE axis offset from VLBI and on-site measurement (in mm).

	2003.03.06- 2005.05.26	2005.07.21- 2006.05.04	2006.08.03- 2007.06.21	2007.08.30- 2009.06.25
VLBI	-15.5 ± 3.2	-15.9 ± 3.6	-10.0 ± 2.8	$+1 \pm 2$
On-site	$-12.5 \pm ??$		-7.5 ± 0.5	-3.0 ± 1.5

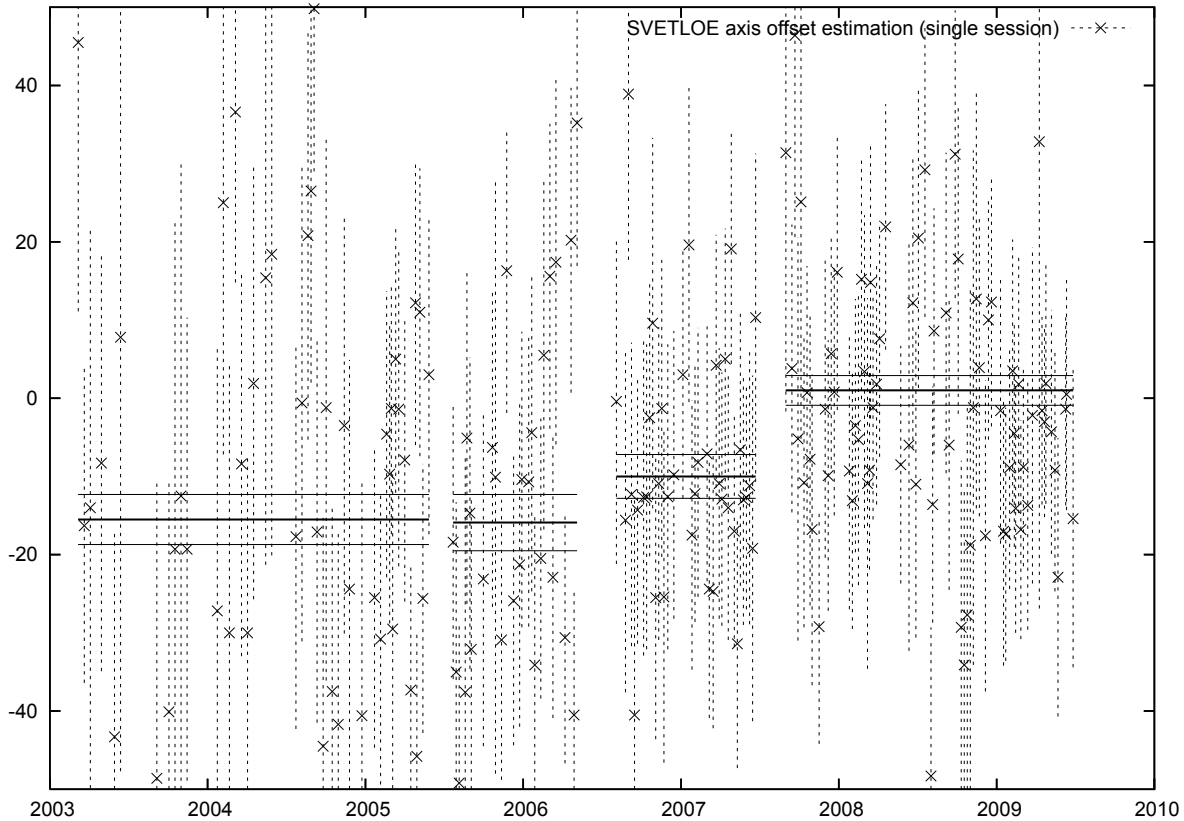


Figure 1. Estimated SVETLOE axis offset from single sessions (crosses) and four global solutions (black solid lines), in mm. The dashed lines indicate error bars.

1.2. Influence of Axis Offset on Estimation of EOP from Local Network

In order to determine how the difference in axis offset can affect our EOP estimations from local network observations, we have processed 41 sessions of our domestic Ru-E [2] program. Ru-E observes 24-hour sessions with Network “Quasar” [1] with the three observatories Svetloe, Zelenchukskaya, and Badary scheduled for the EOP estimation. The biases and RMS (after removing bias) between obtained EOP and IERS 05 C04 series are presented in Tables 2–6. For the results presented in Tables 2–4 the single value of SVETLOE axis offset was used for all sessions. For the results in Table 5 and Table 6 the estimated and measured values were taken for corresponding time intervals.

One can see from a comparison of Table 3 and Table 4 that a difference of 1 cm in axis offset can give a difference up to 0.5 mas in the Y-pole coordinate for our network configuration. The differences in axis offset did not have much impact on the RMS, but it can introduce systematic biases in EOP.

1.3. Conclusion

The value of antenna axis offset can significantly affect parameters estimated from VLBI data processing. Offsets may change after repair work at a station. In order to improve the accuracy of VLBI results it is necessary to estimate the axis offset after a station repair by on-site measurement or from reprocessing of observations. The differences between estimated and measured values need to be investigated.

Table 2. Biases and RMS vs. IERS EOP 05 C04 of EOP estimations with SVETLOE offset = -7.5 mm.

	bias	rms
Xp, mas	-0.114 ± 0.165	0.952
Yp, mas	0.588 ± 0.212	1.225
UT, ms	0.009 ± 0.008	0.046
Xc, mas	-0.608 ± 0.120	0.695
Yc, mas	-0.093 ± 0.114	0.660

Table 3. Biases and RMS vs IERS EOP 05 C04 of EOP estimations with SVETLOE offset = -3 mm

	bias	rms
Xp, mas	-0.109 ± 0.166	0.959
Yp, mas	0.790 ± 0.211	1.221
UT, ms	0.005 ± 0.008	0.046
Xc, mas	-0.596 ± 0.118	0.684
Yc, mas	-0.094 ± 0.113	0.652

Table 4. Biases and RMS vs IERS EOP 05 C04 of EOP estimations with SVETLOE offset = -12.5 mm

	bias	rms
Xp, mas	-0.101 ± 0.157	0.908
Yp, mas	0.342 ± 0.210	1.216
UT, ms	0.012 ± 0.008	0.046
Xc, mas	-0.619 ± 0.118	0.679
Yc, mas	-0.104 ± 0.109	0.631

Table 5. Biases and RMS vs IERS EOP 05 C04 of EOP estimations with estimated SVETLOE offsets = -16 mm, -10 mm, 1 mm for corresponding intervals

	bias	rms
Xp, mas	-0.111±0.161	0.956
Yp, mas	0.690 ±0.210	1.213
UT, ms	0.006±0.008	0.046
Xc, mas	-0.615±0.116	0.667
Yc, mas	-0.087±0.111	0.641

Table 6. Bias and WRMS vs IERS EOP 05 C04 of EOP estimations with measured SVETLOE offsets = -12.5 mm, -7.5 mm, -3 mm for corresponding intervals.

	bias	rms
Xp, mas	-0.090 ± 0.161	0.932
Yp, mas	0.590 ± 0.210	1.210
UT, ms	0.008 ± 0.008	0.046
Xc, mas	-0.602 ± 0.120	0.693
Yc, mas	-0.110 ± 0.115	0.644

References

- [1] A. Finkelstein, A. Ipatov, S. Smolentsev. The Network “Quasar”: 2008–2011. Measuring the Future, Proceedings of the Fifth IVS General Meeting, ed. A. Finkelstein, D. Behrend, St-Petersburg, “Nauka”, pp. 39–46, 2008.
- [2] A. Finkelstein, E. Skurikhina, I. Surkis, A. Ipatov, I. Rahimov, S. Smolentsev. QUASAR National Programs of EOP Determinations. Measuring the future Proceedings of the Fifth IVS General Meeting, ed. A. Finkelstein, D. Behrend, St-Petersburg, “Nauka”, pp. 319–323, 2008.
- [3] S. Kurdubov. QUASAR software in IAA EOP service: Global Solution and Daily SINEX. Proceedings of the 18th European VLBI for Geodesy and Astrometry Working Meeting, ed. by Johannes Boehm, Andrea Pany, and Harald Schuh, GEOWISSENSCHAFTLICHE MITTEILUNGEN, Heft Nr.79, pp. 79–82, 2007.

Prospects for UT1 Measurements from VLBI Intensive Sessions

Johannes Böhm, Tobias Nilsson, Harald Schuh

Vienna University of Technology

Contact author: Johannes Böhm, e-mail: johannes.boehm@tuwien.ac.at

Abstract

Very Long Baseline Interferometry (VLBI) Intensives are one-hour single baseline sessions to provide Universal Time (UT1) in near real-time up to a delay of three days if a site is not e-transferring the observational data. Due to the importance of UT1 estimates for the prediction of Earth orientation parameters, as well as any kind of navigation on Earth or in space, there is not only the need to improve the timeliness of the results but also their accuracy. We identify the asymmetry of the tropospheric delays as the major error source, and we provide two strategies to improve the results, in particular of those Intensives which include the station Tsukuba in Japan with its large tropospheric variation. We find an improvement when (1) using ray-traced delays from a numerical weather model, and (2) when estimating tropospheric gradients within the analysis of Intensive sessions. The improvement is shown in terms of reduction of rms of length-of-day estimates w.r.t. those derived from Global Positioning System observations.

1. Introduction

Very Long Baseline Interferometry (VLBI) is the primary technique for the determination of the Earth Orientation Parameters (EOP), in particular for nutation and Universal Time (UT1). Typically, 24-hour VLBI sessions with five to eight participating stations are observed on about three days per week to provide the EOP with a latency of about two weeks and a UT1 accuracy of approximately 6 to 7 μ s. Additionally, so-called one-hour Intensive sessions are observed every day to provide UT1 with latencies between 3 minutes and 3 days. These Intensive sessions usually only contain single baseline observations and yield UT1 estimates with an accuracy of about 15 μ s when compared to the IERS 05 C04 series (Bizouard and Gambis, 2009, [1]) from the International Earth Rotation and Reference Systems Service.

So-called INT1 sessions are observed from Monday to Friday on the baseline Wettzell (Germany) - Kokee Park (Hawaii, U.S.A.) at 18:30 UT, INT2 sessions from Saturday to Sunday on the baseline Wettzell - Tsukuba (Japan) at 7:30 UT, and additionally INT3 sessions on Monday at 7:00 UT between Wettzell, Tsukuba, and Ny-Ålesund (Spitsbergen, Norway). UT1 estimates in near-real time are crucial for the prediction of EOP, and EOP in real-time are needed for any kind of navigation and positioning on Earth and in space. In particular, the prediction of Global Navigation Satellite Systems (GNSS) orbits benefit from better EOP prediction. Luzum and Nothnagel (2010, [8]) have shown that there is an improvement of 50% in rapid combination and 20% in short term prediction if UT1 estimates are available in near real-time, which is the case for INT3 sessions and in the foreseeable future also for INT1 and INT2 sessions. In this paper, we do not assess questions of timeliness, but we discuss the accuracy of UT1 estimates from Intensive sessions.

2. VLBI Analysis

We analyzed all Intensive sessions of the International VLBI Service for Geodesy and Astrometry (IVS; Schlüter and Behrend, 2007, [12]) from 2007.0 to 2010.0 with the Vienna VLBI Software (VieVS, Böhm et al., 2010a, [3]). Station and source coordinates were fixed to VTRF2008 (Böckmann et al., 2010, [2]) and ICRF2 (Fey et al., 2009, [6]), respectively. We fixed nutation offsets and polar motion to the values provided in the IERS 05 C04 series and modeled the high-frequency variations in polar motion as recommended by the IERS Conventions 2003 (McCarthy and Petit, 2004, [9]). Five parameters were estimated for each single baseline Intensive session: offset and rate between the clocks, one zenith wet delay offset at each station, and one UT1 offset parameter. In the standard solution, no gradients were applied (neither a priori nor as estimated parameters), nor did we use a cutoff elevation angle or downweighting of low observations. Figure 1 shows UT1 estimates for the INT1 and INT2/3 sessions. (We treat the INT2 and INT3 sessions as one common series INT2/3).

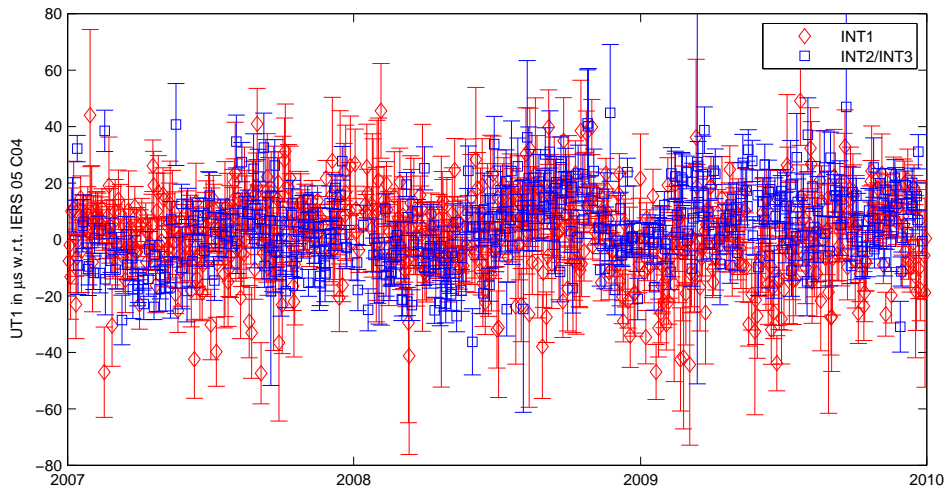


Figure 1. UT1 estimates and formal errors from IVS Intensive sessions from 2007.0 to 2010.0 w.r.t. IERS 05 C04.

We analyzed 675 INT1 sessions and 393 INT2/3 sessions from January 2007 until December 2009, from which we had to remove 17 and 9 sessions as outliers, respectively (with estimates larger than $\pm 50 \mu\text{s}$ or uncertainties larger than $100 \mu\text{s}$). The median biases are 2.4 and $3.7 \mu\text{s}$, and the rms values of the UT1 estimates are 15.0 and $14.7 \mu\text{s}$ w.r.t. the IERS 05 C04 series. On the other hand, the formal uncertainties are 10.9 and $7.3 \mu\text{s}$, which suggests that modeling deficiencies exist and need to be investigated.

A discussion of the influence of nutation and polar motion errors on UT1 estimates from Intensive sessions was provided by Nothnagel and Schnell (2008, [11]) who report maximum values of $30 \mu\text{s}$ in UT1 per mas in nutation or polar motion. However, when using sophisticated forecasts of daily polar motion (e.g., from the International GNSS Service IGS) and nutation offsets (e.g., from the IERS), this is a minor error source. Presently more important is the high-frequency model for polar motion, which has a significant impact on UT1 estimates from Intensive sessions. Figure 2

shows the differences in UT1 when using the empirical model as provided by English et al. (2008, [5]) w.r.t. to applying the model recommended by the IERS 2003 Conventions (McCarthy and Petit, 2004, [9]). In recent years, general awareness has grown that there is a need to replace the IERS 2003 model ('Eanes model') by an improved high-frequency model which is either determined empirically from observations, from improved ocean models, or from a combination of both. With such a new model, the a priori high-frequency polar motion will contribute less as an error source to the determination of UT1 from Intensive sessions.

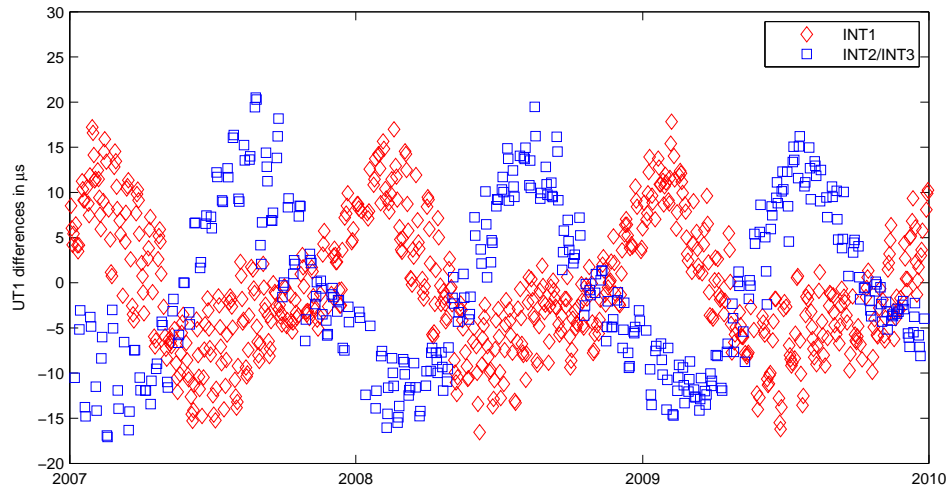


Figure 2. UT1 differences in μs when using the empirical model by English et al. (2003) for polar motion instead of the IERS 2003 'Eanes' model.

Unlike the error sources described above, asymmetries in the tropospheric delays cannot be accounted for easily. Böhm et al. (2010b, [4]) show that the influence of those asymmetries of the tropospheric delays on UT1 estimates from Intensive sessions is about $\pm 10 \mu\text{s}$ but can be as large as $50 \mu\text{s}$ during extreme weather conditions. As a rule of thumb, an unmodeled east gradient of 1 mm (= sum of total east gradients at both stations) causes UT1 to change by about $15 \mu\text{s}$. Considering that gradients can reach values of up to 3 mm (corresponding to about 0.3 m delay at 5 degrees elevation) this is a very large error source, which needs to be considered. Böhm et al. (2010b, [4]) investigated the application of external information about tropospheric delays for the analysis of INT2 sessions, and they found a slight improvement when applying ray-traced delays at Tsukuba (Hobiger et al., 2008, [7]). Since the IERS 05 C04 series is not good for comparison as they already contain information from a standard analysis of Intensive sessions (Bizouard and Gambis, 2009, [1]), Böhm et al. (2010b, [4]) compared length-of-day (LOD) between two Intensive sessions on consecutive days to LOD derived from Global Positioning System (GPS) observations, and the rms of LOD decreased from 23.7 to $22.8 \mu\text{s}$ for a sample of 70 LOD values when using ray-traced delays.

3. Estimation of Gradients

Nilsson et al. (2010, [10]) investigated single baseline observations over time spans of two hours that were extracted from CONT08, which was a special VLBI campaign over 15 days in August 2008 to demonstrate the best accuracy that can presently be achieved with VLBI. This procedure allowed Nilsson et al. (2010, [10]) not only to have optimum reference values for UT1 from the full CONT08 solution but also to have good a priori values for zenith wet delays or gradients. However, one of their findings was that there is an improvement in the estimation of UT1 when gradients are estimated from those single baseline two-hour sessions, in particular when Tsukuba is one of the observing stations.

Although the number of observations is small (below 30), we followed the findings by Nilsson et al. (2010, [10]) and tested the estimation of gradients in ‘real’ IVS Intensive sessions. In a first run, we estimated north and east gradient offsets which are constrained to zero by ± 1 mm. In a second test, we only estimated east gradient offsets (constrained to zero by ± 1 mm), because the east component is most important for UT1. The constraints are necessary to avoid singularity of the normal equation matrix. As already mentioned above, a quality assessment of the UT1 estimates cannot be done by comparison to the IERS 05 C04 values because the latter already contain UT1 information from a standard solution of IVS Intensive sessions without the estimation of gradients. Thus, we again compare LOD values from Intensive sessions on consecutive days to LOD values from the GPS solution as provided by the Center for Orbit Determination (CODE) in Bern. Table 1 shows that we find a considerable improvement when estimating gradients in the INT2 sessions, and even more improvement when only estimating east gradients. The reduction in rms of LOD values is from 24.1 to 21.6 μs when estimating east gradients at Tsukuba and Wettzell in the INT2 sessions. On the other hand, there is hardly any improvement when estimating gradients in INT1 sessions. This is due to the fact that the largest gradients are at Tsukuba, which also confirms the findings by Nilsson et al. (2010, [10]).

Table 1. Rms of UT1 and LOD w.r.t. IERS 05 C04 and GPS, respectively. Considerable improvement is found for the rms of LOD w.r.t. LOD from GPS when only east gradients are estimated.

	rms w.r.t. UT1 from IERS 05 C04		rms w.r.t. LOD from GPS	
	INT1	INT2/3	INT1	INT2/3
samples	657	384	258	224
no gradients	15.0 μs	14.7 μs	27.6 μs	24.1 μs
north and east gradients	16.1 μs	15.6 μs	27.9 μs	22.3 μs
east gradients	16.2 μs	15.9 μs	27.0 μs	21.6 μs

4. Summary and Outlook

We discussed possible error sources for the estimation of Universal Time (UT1) from Intensive sessions, and we identified the asymmetry of tropospheric delays as one—if not the most important—of these error sources. Although the number of observations is typically small (below 30) we found an improvement when estimating (constrained east) gradients in INT2 sessions including Tsukuba. In future investigations we will determine the improvement when estimating

east gradients only at one station (e.g., Tsukuba). Complementarily, we recommend to continue the research in using ray-traced delays for the analysis of IVS Intensive sessions. In future accuracy assessments we plan to use different UT1 reference series, e.g., a Kalman Filter series which does not include information from IVS Intensive sessions (Ray, 2010, personal communication).

5. Acknowledgements

This study made use of VLBI data provided by the International VLBI Service for Geodesy and Astrometry (IVS; Schlüter and Behrend, 2007), and the authors would like to thank all IVS components. We also acknowledge the Deutsche Forschungsgemeinschaft (DFG) for supporting this work (Project SCHUH 1103/3-2).

References

- [1] Bizouard C, Gambis D (2009) The combined solution C04 for Earth Orientation Parameters consistent with International Terrestrial Reference Frame. In Drewes H (ed.) Geodetic Reference Frames, IAG Symposium Munich, Germany, 9-14 October 2006, Vol 134, pp 265-270.
- [2] Böckmann S, Artz T, Nothnagel A, (2010) VLBI terrestrial reference frame contributions to ITRF2008, *J. of Geodesy*, 84(3), 201-219, doi:10.1007/s00190-009-0357-7.
- [3] Böhm J, Böhm S, Nilsson T, Pany A, Plank L, Spicakova H, Teke K, Schuh H (2010a) The new Vienna VLBI Software. IAG Scientific Assembly Proceedings, Buenos Aires.
- [4] J. Böhm, T. Hobiger, R. Ichikawa, T. Kondo, Y. Koyama, A. Pany, H. Schuh, K. Teke (2010b), Asymmetric tropospheric delays from numerical weather models for UT1 determination from VLBI Intensive sessions on the baseline Wettzell-Tsukuba, *J Geod*, 84:319-325, doi:10.1007/s00190-10-0370-x.
- [5] Englich S, Heinkelmann R, Schuh H (2008) Re-assessment of Ocean Tidal Terms in High-Frequency Earth Rotation Variations Observed by VLBI. The 5th IVS General Meeting Proceedings (ed. by Finkelstein A, Behrend D), 2008, pp 314-318.
- [6] Fey A, Gordon D, Jacobs CS (eds.) (2009) The Second Realization of the International Celestial Reference Frame by Very Long Baseline Interferometry. Presented on behalf of the IERS / IVS Working Group. IERS Technical Note 35, Frankfurt am Main: Verlag des Bundesamts für Kartographie und Geodäsie, 204 p., ISBN 3-89888-918-6 (print version).
- [7] Hobiger T, Ichikawa R, Koyama Y, Kondo T (2008) Fast and accurate ray-tracing algorithms for real-time space geodetic applications using numerical weather models. *J Geophys Res* 113(D20302). doi:10.1029/2008JD010503.
- [8] Luzum B, Nothnagel A (2010) Improved UT1 predictions through low-latency VLBI observations. *J Geod*. doi:10.1007/s00190-010-0372/8.
- [9] McCarthy D, Petit G (2004) IERS Conventions 2003. IERS Technical Note No. 32, Verlag des Bundesamtes für Kartographie und Geodäsie, Frankfurt am Main.
- [10] Nilsson T., Böhm J., Schuh H (2010), Universal Time from VLBI Single-Baseline Observations during CONT08, to be submitted to *Journal of Geodesy*.
- [11] Nothnagel A, Schnell D (2008) The impact of errors in polar motion and nutation on UT1 determinations from VLBI Intensive observations. *J Geod* 82(12):863-869. doi:10.1007/s00190-008-0212-2.
- [12] Schlüter W, Behrend D (2007) The International VLBI Service for Geodesy and Astrometry (IVS): current capabilities and future prospects. *J Geod* 81(6-8):379-388. doi:10.1007/s00190-006-0131-z.

Strategies for Improving the IVS-INT01 UT1 Estimates

Karen Baver, John Gipson

NVI, Inc./NASA Goddard Space Flight Center, Greenbelt, MD, 20771

Contact author: Karen Baver, e-mail: karen.d.baver@nasa.gov

Abstract

We discuss an alternative scheduling strategy for the IVS-INT01 sessions and demonstrate that it is more robust and produces lower formal errors than the strategy used for the operational Intensives.

1. Introduction

The primary purpose of the IVS-INT01 sessions is the estimation of UT1. Improving the accuracy and the precision of the UT1 estimates is an important goal in the scheduling of these sessions. In 2009 the GSFC VLBI Analysis Center requested and received the use of four IVS R&D sessions, RD0907 through RD0910, for the evaluation of a new strategy for scheduling the IVS-INT01 sessions. In this paper we present some preliminary results from our analysis of RD0907 through RD0909, and we discuss future work.

2. Labeling the Intensives

In this paper we consider different kinds of one-hour sessions observing the Kokee—Wettzell baseline. We will refer to all of these sessions as Intensives. In order to distinguish them, we need a simple way of labeling them. Where necessary, we will distinguish them by type (USNO, STND, or TEST) and/or by Greenwich Sidereal Time (GST).

USNO vs. STND vs. TEST. We will refer to the operational Intensives scheduled by USNO as USNO Intensives, or USNO for short. These use a restricted list of sources. In our study we scheduled two different kinds of Intensives. The STND (standard) Intensives used the restricted USNO source list. The TEST Intensives used an enlarged list containing all sources that are mutually visible at Kokee and Wettzell.

Greenwich Sidereal Time. Because the sessions in our study are single baseline and of short duration, they only sample a small slice of the sky. The slice changes depending on the date and time of the Intensive. Intensives scheduled on the same date, but at different times, can sample very different slices of the sky. Similarly, Intensives scheduled on different dates can observe the same slice of the sky. To be able to compare sessions, we make use of the fact that Intensives that start at the same Greenwich Sidereal Time (GST) sample the same slice of the sky, regardless of the date or UT time of the session.

3. Designing the Sessions

We divided the R&D network into two parts: the single baseline Kokee—Wettzell network and a network consisting of approximately five remaining stations. We scheduled each network

independently. The primary purpose of the larger network was to serve as an independent check on UT1, and we scheduled it similarly to the R1s and R4s, using the standard R1 observing sequence.

Table 1. Scheduled Intensive Study R&D Sessions.

Start time of R&D Sessions								
	RD0907		RD0908		RD0909		RD0910	
Date	2009Jul08		2009Sep23		2009Oct06		2009Dec16	
	UT	GST	UT	GST	UT	GST	UT	GST
Start	18:00	13:07	18:00	18:10	17:30	18:32	18:00	23:42
Alternating Intensives in GST order.								
STND	5:00	0:09	0:00	0:11	23:10	0:12	USNO	
TEST	6:00	1:09	1:00	1:11	0:10	1:13	19:30	1:12
STND	7:00	2:09	2:00	2:12	1:10	2:13	20:30	2:12
TEST	8:00	3:09	3:00	3:12	2:10	3:13	21:30	3:12
STND	9:00	4:09	4:00	4:12	3:10	4:13	22:30	4:12
TEST	10:00	5:09	5:00	5:12	4:10	5:13	23:30	5:12
STND	11:00	6:10	6:00	6:12	5:10	6:13	0:30	6:13
TEST	12:00	7:10	7:00	7:12	6:10	7:14	1:30	7:13
STND	13:00	8:10	8:00	8:13	7:10	8:14	2:30	8:13
TEST	14:00	9:10	9:00	9:13	8:10	9:14	3:30	9:13
STND	15:00	10:10	10:00	10:13	9:10	10:14	4:30	10:13
TEST	16:00	11:10	11:00	11:13	10:10	11:14	5:30	11:13
STND	17:00	12:11	12:00	12:13	11:10	12:14	6:30	12:14
TEST	USNO		13:00	13:13	12:10	13:15	7:30	13:14
STND	Intensive		14:00	14:14	13:10	14:15	8:30	14:14
TEST	20:00	15:07	15:00	15:14	14:10	15:15	9:30	15:14
STND	21:00	16:07	16:00	16:14	15:10	16:15	10:30	16:14
TEST	22:00	17:07	17:00	17:14	16:10	17:15	11:30	17:14
STND	23:00	18:08	USNO		USNO		12:30	18:15
TEST	0:00	19:08	Intensive		Intensive		13:30	19:15
STND	1:00	20:08	20:00	20:11	19:10	20:12	14:30	20:15
TEST	2:00	21:08	21:00	21:11	20:10	21:12	15:30	21:15
STND	3:00	22:08	22:00	22:11	21:10	22:12	16:30	22:15
TEST	4:00	23:08	23:00	23:11	22:10	23:12	Intensive	

Session start times are indicated in **bold**.

“USNO Intensive” indicates periods when Kokee & Wettzell participated in USNO Intensives and were unavailable for the R&D sessions.

USNO Intensives on R&D Days								
	I09189		I09266		I09279		I09350	
Start	18:30	13:37	18:30	18:40	17:30	18:32	18:00	23:42
End	19:30	14:37	19:30	19:40	18:30	19:32	19:00	00:42

Because Kokee and Wettzell are used in the USNO Intensives, they were not available for the

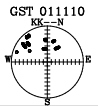
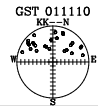
two-hour period immediately prior to, during, and after the USNO Intensives. In the first R&D the stations became available at 19:45 UT. Starting at 20:00 UT we scheduled a series of 22 alternating TEST and STND Intensives. We adjusted the start times of the Intensives in the remaining R&Ds so that we sampled the same slices of the sky; all of the STND Intensives start close to the even hours in GST, while all of the TEST Intensives start close to the odd hours.

Table 1 lists the four R&Ds scheduled for our study¹. The top of the table displays the name and date of each R&D session. Each start time is specified in both UT and GST. Following this are the start times of the alternating Intensives in each session. Rows are organized to clearly indicate the correspondence in GST across the sessions. The first column indicates the scheduling strategy—STND or TEST, and the remaining columns give the start times in UT and GST. We indicate the first Intensive in each R&D session by **bold face**. The remaining Intensives are found by reading down to 23:xx GST, and then starting at the top.

4. Differences between Observing Strategies

The effect of the different source lists had a marked difference on the schedules generated. This is summarized in Table 2, which shows two typical schedules. The STND strategy has more observations because it uses a few strong sources. The TEST strategy uses more, but weaker, sources. Because of this it has fewer observations, but its sky coverage is better.

Table 2. Comparison of Intensive scheduling strategies.

	STND	TEST
Typical Sky Coverage		
Average number of observations	28.3	23.2
Average number of sources	10.6	18.5
Source Strength	Stronger	Weaker
Sky coverage	Narrower	Wider

Bold indicates the strategy that is better for UT1 estimates.

5. Current Strategy and Source Dropouts

Better sky coverage is empirically linked with improved precision and accuracy of the UT1 estimates. The current USNO strategy uses only the strongest sources, but because strong sources are unevenly distributed, only a few are available at some times of the year, which can result in poor sky coverage. Furthermore, because the number of available sources is small, the USNO strategy tends to schedule sources many times in one session. The loss of a single source can lead to dramatic changes in sky coverage, which in turn has a large effect on the UT1 formal errors, as illustrated in Table 3 for three schedules. For each schedule we deleted a single source. The effect ranges from minimal (10% degradation in sigma) to doubling the formal error.

¹RD0910 was not correlated in time for this study, so the analysis only includes RD0907 through RD0909.

Table 3. Effect of losing one source on UT1 formal errors.

Sky Coverage	When	Charts
Good	GST 07:12 April 1-5	
Intermediate	GST 17:11 Sep 1-5	
Bad	GST 19:12 Oct 1-4	

6. Robustness of the TEST and the USNO Schedules

Sessions are prone to lose observations. Ideally, we would like the estimated parameters to be insensitive to this loss. A session is robust if the parameters do not change very much with the loss of a single source. To compare the robustness of the techniques, we selected four USNO Intensives with varying levels of sky coverage ranging from good to bad, and we paired these with TEST Intensives. For each session we ran a set of solutions in which we suppressed a single source and estimated UT1. We did this for all sources in the session, and then computed the scatter of the estimates. These results are summarized in Table 4. The TEST schedules are much more robust because their sky coverage is better and because they use more sources. Hence the loss of a single source does not change the sky coverage as much as in the USNO Intensives.

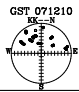
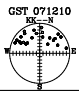
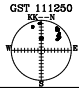

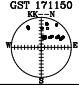
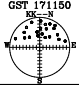
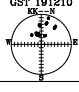
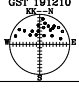
7. Comparison of the TEST and the USNO Schedules

We purposely designed our study so that the TEST sessions would sample the same slice of the sky as other TEST sessions, and the same for the STND sessions. This has the advantage that, for a particular GST, we have more sessions of a given kind. It has the disadvantage that it makes it difficult to directly compare the TEST and the STND sessions.

One way around this is to compare the TEST sessions with USNO sessions. The advantage of doing so is that you can ensure that you are sampling the same slice of the sky. The disadvantage is that the weather, which influences the noise, will be different, since these sessions are at different times of the year.

Our TEST sessions sample 12 slices of the sky. We looked at all USNO Intensives from 2007—2009 that started at the same GST as the TEST sessions. For each of the two Intensive sets, we calculated the average UT1 formal error σ and the average session fit. These are summarized in Table 5. The TEST strategy generally has lower UT1 formal errors. Examination of the exceptions indicates that the TEST strategy can introduce weaker sources that drive up a session’s fit and

Table 4. RMS scatter in UT1 estimates after deletion of successive single sources.

Sky Coverage	GST	USNO	RMS	TEST	RMS
Good	07:12		5.3		4.4
Intermediate	11:12		12.2		7.4
Intermediate	17:11		13.2		2.9
Bad	19:12		21.6		4.4
Average RMS			13.1		4.8

in turn its UT1 formal error. If the USNO schedule has especially good sky coverage, the TEST schedule may suffer in comparison. It may be possible to compensate for this by excluding weaker sources in the TEST schedules.

Table 5. Comparison of USNO and TEST UT1 formal errors (σ) and session fits².

	USNO		TEST	
	$\sigma(\mu s)$	Fit (ps)	$\sigma(\mu s)$	Fit (ps)
Average	14.5	47.5	10.9	54.3
StdDev	4.8	9.7	3.3	13.9

8. Conclusions and Future Work

The results of the TEST scheduling strategy are very encouraging. The TEST strategy yields schedules which are more robust than the USNO Intensives, and on average the UT1 formal errors are 30% better for the TEST sessions. In cases where the TEST formal errors are worse, changing a parameter of the TEST algorithm might compensate. Much of the improvement in the TEST schedules compared to the USNO schedules is due to having more sources and better sky coverage.

We requested, and were granted, the use of five more R&D sessions in 2010. In these new sessions the TEST and STND series will trade the slices of the sky they sampled in RD0907 through RD0910. This will allow us to directly compare the TEST and STND strategies.

The authors would like to thank David Gordon for providing helpful advice about using Greenwich Sidereal Time to compare the Intensive sessions.

²Due to space limitations, only a partial version of this table is presented here. Please refer to ftp://ivscg.gsfc.nasa.gov/pub/general-meeting/2010/presentations/GM2010_S3P07_baver.pdf for the full table.

CPO Prediction: Accuracy Assessment and Impact on UT1 Intensive Results

Zinovy Malkin

Central Astronomical Observatory at Pulkovo of Russian Academy of Sciences

e-mail: malkin@gao.spb.ru

Abstract

The UT1 Intensive results heavily depend on the celestial pole offset (CPO) model used during data processing. Since accurate CPO values are available with a delay of two to four weeks, CPO predictions are necessarily applied to the UT1 Intensive data analysis, and errors in the predictions can influence the operational UT1 accuracy. In this paper we assess the real accuracy of CPO prediction using the actual IERS and PUL predictions made in 2007-2009. Also, results of operational processing were analyzed to investigate the actual impact of EOP prediction errors on the rapid UT1 results. It was found that the impact of CPO prediction errors is at a level of several microseconds, whereas the impact of the inaccuracy in the polar motion prediction may be about one order of magnitude larger for ultra-rapid UT1 results. The situation can be amended if the IERS Rapid solution will be updated more frequently.

1. Introduction

Rapid VLBI UT1 observations are vital for the accuracy of the rapid IERS EOP solution and its prediction. To decrease rapid UT1 latency, special single-baseline 1-hour sessions are conducted practically every day with a delay in processing from several hours to several days. As shown in previous studies [1–3] UT1 estimates obtained from the single-base Intensive programs heavily depend on the celestial pole motion model used during analysis. For the most exacting applications, the celestial pole coordinates are computed as the sum of theoretical values given by an adopted theory of precession-nutation, IAU2000A nowadays, and corrections called celestial pole offset (CPO) that are obtained from observations, exclusively VLBI nowadays. The CPO comprises trends and (quasi)periodic components, Free Core Nutation (FCN) in the first place, caused by the inaccuracy of Earth Rotation theory.

The most accurate CPO is obtained from 24-hour VLBI sessions and is available, as a rule, with a delay from two to four weeks¹. Therefore CPO predictions are necessarily applied to the UT1 Intensive data analysis, and errors in the predictions can influence the rapid UT1 accuracy. In this paper the real accuracy of CPO predictions is assessed using the actual predictions made by IERS (USNO) and PUL IVS Analysis Center (Pulkovo Observatory). The required prediction length can be found from analysis of the IVS combination delay, i.e., the time between the date of publication of the IVS combined solution and the last EOP epoch in this solution. For 2009, the median delay was 18 days, while the maximum delay was 37 days. We extend our analysis to the longer length, which may be interesting for other applications. Of course, the IVS series is then updated with new observations processed, but these changes in the IVS data are small enough to significantly influence rapid UT1 results.

¹Strictly speaking, CPO results from individual Analysis Centers are available with lower delay, but we consider the IVS combined CPO series as the most suitable for the EOP service applications.

This paper is aimed at an accuracy assessment of the CPO predictions computed with different models. As usual, the prediction accuracy is derived from a comparison of predicted values with the final ones. For a proper interpretation of the results obtained in this study, the following circumstance should be taken into account. Each CPO model is a result of the fitting of observed CPO series. The models differ not only by the method of fitting, but also by the CPO data used in the analysis, which makes results from the accuracy assessment somewhat ambiguous. One may consider the prediction accuracy with respect to the model itself, which is, in fact, the accuracy of representation of the given model. However, we are interested in the accuracy of the representation of the actual celestial pole motion, which is the most important for the majority of users. For this reason we use a comparison of CPO predictions with the IVS combined CPO series, which is intended to be an official standard.

2. Data Used

In this study we present results of processing VLBI observations made in the framework of the IVS UT1 Intensive observing program with different delay and different CPO models. The following data were used:

- INT1 sessions, observed on the workdays on the stations KOKEE (Kk) and WETTZELL (Wz); the database is normally available in 2–5 days.
- INT2 sessions, observed on weekends on the stations TSUKUB32 (Ts) and WETTZELL; the database is normally available in 1–2 days.
- INT3 sessions, observed on Monday on the stations NYALES20 (Ny), TSUKUB32, and WETTZELL; the database is normally available on the same day.

The following actual and publicly available CPO models were tested:

- IERS final EOP series computed at the Paris Observatory (C04 series) [4]. It does not contain prediction and thus is equivalent to a zero model for rapid data processing.
- IERS rapid EOP series computed at the USNO (NEOS model) [4]. It is constructed from analysis of the NEOS combined CPO series and updated daily.
- Lambert’s FCN series computed at the Paris Observatory (SL model) [5]. As a matter of fact, it can represent only the FCN contribution to CPO. However, this model is recommended by the IERS Conventions (2003) as the substitute for CPO. It is constructed from the analysis of the IERS combined series C04 and updated every several months.
- The author’s ZM2 model computed at the Pulkovo Observatory [6]. It is constructed from the analysis of the IVS combined CPO series and updated daily.

Comparison of these models with IVS data is shown in Fig. 1.

3. Accuracy of CPO Predictions

As usual, the accuracy of CPO predictions was estimated by a comparison of predicted and final values. Predictions made in the period from December 30, 2006 through December 25, 2009 were used. Both the rms and maximum prediction errors were computed; the latter causes the maximum dilution in the UT1 accuracy and thus is very important. Results are presented in Figs 2 and 3. One can see that ZM2 model provides the best accuracy of CPO prediction.

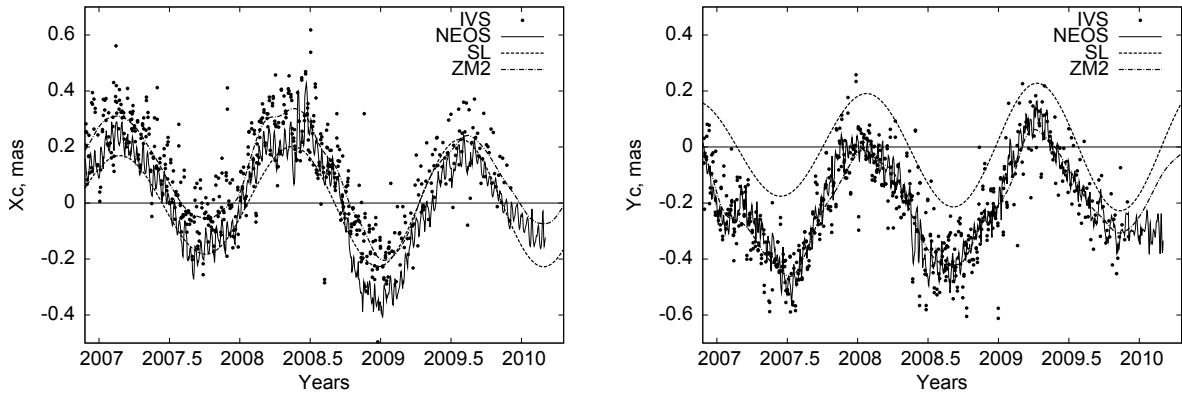


Figure 1. CPO models compared with the IVS combined CPO series.

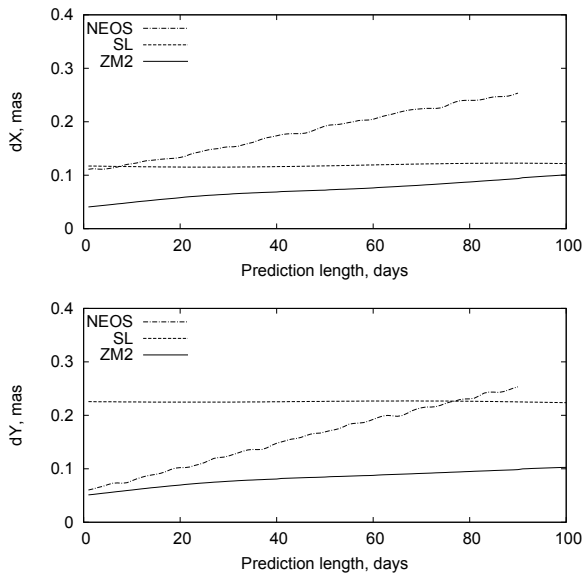


Figure 2. The rms error of CPO prediction for different models.

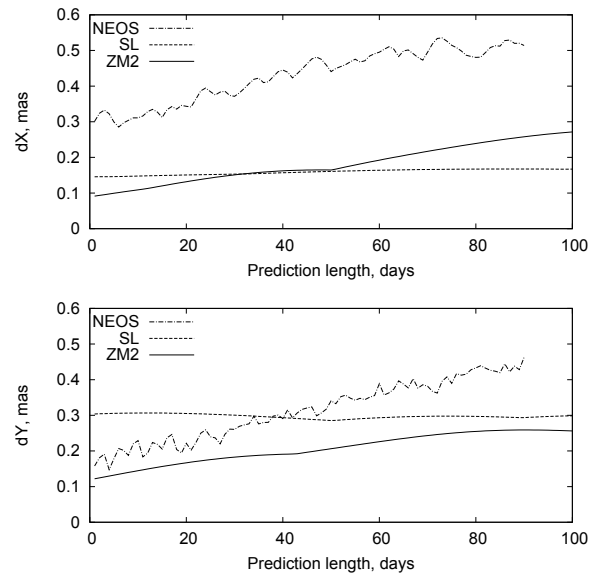


Figure 3. The maximum absolute error of CPO prediction for different models.

4. Impact of Prediction Errors on Rapid UT1

To investigate the impact of the CPO prediction error on the rapid UT1 estimates, we started an experimental processing of INT1, INT2, and INT3 sessions with different CPO models in October 2009. All the computations presented here were made with the ZM2 model. Using other models gave similar results. Each session was processed three times:

1. immediately after the database is available (O); during INT1 and INT2 processing interpolated polar motion (PM) and extrapolated CPO are used, and during INT3 processing both CPO and PM are extrapolated;
2. 5-7 days after the date of observations (O2); in this case practically the final PM is available, but CPO is still extrapolated;

3. at least 10 days after the IVS combined CPO for the date is available (F); during this processing practically both the final CPO and PM are available.

In the beginning of this work, only operational processing (O) was performed. The first O2 processing was made in December 2009. The differences between the UT1 estimates obtained with different delays for several sessions are shown in Tables 1 and 2. These results are quite representative for all the computations. Comparisons of F-O, O2-O, and F-O2 differences show that errors in extrapolated PM coordinates have a more significant impact on the UT1 estimates than on the CPO prediction errors. This can be explained by the fact that, while the maximum CPO 30-day prediction error during the last three months was about 0.15 mas (for ZM2 model), the maximum PM error for the IERS Bulletin A 1-day PM prediction during the same period was about 1.7 mas and 0.94 mas for X and Y pole coordinates, respectively. Consequently, the impact of the PM prediction errors is about one order of magnitude larger than the impact of the CPO prediction errors. The latter is at a level of a few microarcseconds, much less than the uncertainty of UT1 estimates. This result is in good agreement with Nothnagel's estimate of a single-baseline UT1 bias at the level of 1 microsecond for a 40-microarcsecond bias in CPO or PM [2]. One can see that INT3 results obtained for the whole 3-station network NyTsWz are similar to the single-baseline solutions TsWz for the same sessions.

5. Conclusion

The impact of a CPO prediction error on the rapid UT1 results seems not to be very significant, much less than the impact of the PM prediction error. The very rapid UT1 observations of the INT3 observing program that are correlated on the day of the observations—so that the database is normally available before the IERS Rapid combination used as a priori EOP is updated—sometimes show very large biases up to several tens of microseconds as compared with results of processing made after interpolated IERS PM data is published. The situation can be amended if the IERS Rapid solution will be computed and published more frequently, say every 6 hours, after the ultra-rapid IGS combination is ready. Such an approach seems to be much more preferable than a user doing a home-bred combination of the IERS and IGS data.

More details of this study are given in [7].

References

- [1] Titov O.A. (2000) In: Proc. IAU Coll. 180, Washington DC, 27–30 Mar 2000, Eds. K.J.Johnston, D.D.McCarthy, B.J.Luzum, G.H.Kaplan, 259–262.
- [2] Nothnagel A. and Schnell D. (2008) *J. Geodesy*, V. 82, 863–869.
- [3] Malkin Z. (2009) Presented at the IERS Workshop on EOP Combination and Prediction, Warsaw, 19–21 Oct 2009, http://www.cbk.waw.pl/EOPPW2009/contributions/session1/session1.1/mon10_Malkin.pdf, visited on January 25, 2010.
- [4] IERS Annual Report 2007, Verlag des Bundesamts für Kartographie und Geodäsie, Frankfurt am Main, 2009.
- [5] Lambert S.B. (2009) <http://syrte.obspm.fr/~lambert/fcn/notice.pdf>, visited on January 25, 2010.
- [6] Malkin Z.M. (2007) *Solar System Research*, V. 41, 492–497.
- [7] Malkin Z.M. (2010) *Astronomy Reports*, in press.

Table 1. Differences between UT1 estimates obtained using different delays (μ s): INT1 (KkWz). See text.

Session code	Week-day	UT1 differences			Session code	Week-day	UT1 differences		
		F-O	F-O2	O2-O			F-O	F-O2	O2-O
I09357	Wed	-2.0	-2.0	0.0	I09348	Mon	-2.2	-2.2	0.0
I09362	Mon	-1.5	-1.6	0.1	I09349	Tue	-2.1	-1.6	-0.5
I09363	Tue	-1.7	-1.5	-0.2	I09350	Wed	-0.2	-1.3	1.1
I09364	Wed	-1.5	-1.1	-0.4	I09351	Thu	-0.8	-0.8	0.0
I09365	Thu	-1.9	-1.6	-0.3	I09352	Fri	-0.9	-0.8	-0.1
I10004	Mon	-0.3	-1.6	1.3	I09355	Mon	-1.3	-1.3	0.0
I10005	Tue	-1.8	-1.8	0.0	I09356	Tue	-1.6	-1.6	0.0

Table 2. Differences between UT1 estimates obtained using different delays (μ s): INT2 and INT3. See text.

Session code	Week-day	UT1 differences					
		TsWz (INT2)			NyTsWz (INT3)		
		F-O	F-O2	O2-O	F-O	F-O2	O2-O
K09299	Mon	-1.6					
K09304	Sat	-3.2					
K09305	Sun	9.4					
K09306	Mon	47.1					
K09311	Sat	-3.1					
K09312	Sun	1.6					
K09313	Mon	8.4					
K09318	Sat	1.5					
K09319	Sun	-0.4					
K09320	Mon	0.3					
K09325	Sat	-1.6					
K09326	Sun	-1.0					
K09327	Mon	20.8					
K09332	Sat	0.6					
K09333	Sun	5.7					
K09334	Mon	-1.6					
K09339	Sat	-1.0					
K09340	Sun	0.6					
K09341	Mon	-0.9					
K09346	Sat	-0.5	0.5	-1.0			
K09347	Sun	0.2	1.6	-1.4			
K09348	Mon	-9.2	0.1	-9.3			
K09353	Sat	-1.3	-0.6	-0.7			
K09354	Sun	0.2	0.0	0.2			
K09355	Mon	3.5	-0.6	4.1			
K09360	Sat	-1.0	-1.0	0.0			
K09361	Sun	1.7	-1.3	3.0			
K10002	Sat	-2.8	-2.7	-0.1			
K10003	Sun	-1.2	-2.7	1.5			
K10004	Mon	2.9	-1.7	4.6	0.5	-2.1	2.6
K10011	Mon	5.7	-3.0	8.7	6.4	-2.6	9.0
K10018	Mon	-15.3	-2.8	-12.5	-13.3	-2.7	-10.6
K10025	Mon	-4.7	-2.5	-2.2	-4.6	-2.5	-2.1
K10032	Mon	-11.9	-3.2	-8.7	-10.7	-3.1	-7.6

Application of Geodetic VLBI Data to Obtaining Long-term Light Curves for Astrophysics

Masachika A. Kijima

(1) SOKENDAI (*The Graduate University for Advanced Studies*) and (2) National Astronomical Observatory of Japan

e-mail: `masachika.kijima@nao.ac.jp`

Abstract

The long-term light curve is important to research on binary black holes and disk instability in AGNs. The light curves have been drawn mainly using single dish data provided by the University of Michigan Radio Observatory and the Metsähovi Radio Observatory. Hence, thus far, we have to research on limited sources. I attempt to draw light curves using VLBI data for those sources that have not been monitored by any observatories with single dish. I developed software, analyzed all geodetic VLBI data available at the IVS Data Centers, and drew the light curves at 8 GHz. In this report, I show the tentative results for two AGNs. I compared two light curves of 4C39.25, which were drawn based on single dish data and on VLBI data. I confirmed that the two light curves were consistent. Furthermore, I succeeded in drawing the light curve of 0454-234 with VLBI data, which has not been monitored by any observatory with single dish. In this report, I suggest that the geodetic VLBI archive data is useful to obtain the long-term light curves at radio bands for astrophysics.

1. Introduction

Long-term light curves and VLBI images are useful to investigate the physics of AGNs, binary black holes, and disk instability [1][2][3]. The most extensive monitoring campaigns have been conducted by two observatories, the University of Michigan Radio Observatory (UMRAO) and the Metsähovi Radio Observatory (MRO). The UMRAO has observed over 170 sources at 4.8, 8.0, and 14.5 GHz for over three decades [4]. At higher frequencies, the MRO has published observational measurements at 22, 37, and 87 GHz of over 200 extragalactic radio sources, many of which have been observed for over 10 years [5][6][7]. The studies of AGN variability have been mainly based on the data obtained by the UMRAO and the MRO.

Geodetic VLBI has been conducted for 30 years. The numbers of sources are above 1000 and 3000 at X- and S-band, respectively. Geodetic VLBI archive data can also allow us to draw the long-term light curves as well as hitherto single dish observations.

2. Data Reduction

2.1. Procedure

In this section, the procedure to estimate total flux density is described briefly (Fig.1). The detail and parameters used in each program module are described in the next section.

- “Raw-data” is the archive-data file publicly available at the IVS Data Centers. The number of the files is above 20,000.

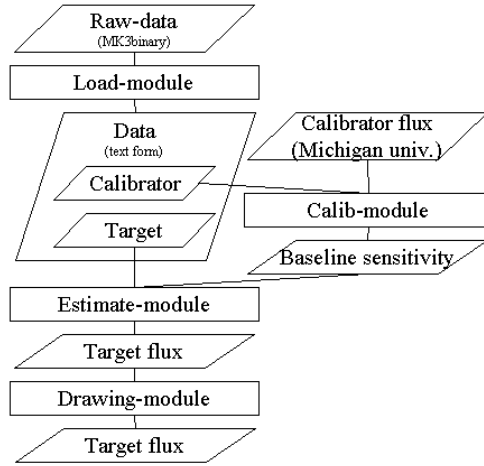


Figure 1. The schematic flow. The parallelograms and rectangles indicate data files and program modules, respectively.

- “Load-module” converts the data format from MK3binary to text form. The module also extracts and collects observational parameters into the one file. The observational parameters are observing date, time, names of the two antennas comprising the baseline, name of the target source, spatial frequencies (u , v , and w), and normalized correlation coefficient (hereafter $\rho_{i,j}$). i and j are i th- and j th-antenna, respectively.
- “Calibration-module” estimates baseline sensitivity ($SEFD_{i,j}$). The sensitivity is estimated with Eq.(1).

$$SEFD_{i,j} = \frac{S_{UMRAO}^{calibrator}}{\rho_{i,j}^{calibrator}} \quad (1)$$

The sources which have been observed frequently are chosen as flux calibrators. The total flux density ($S_{UMRAO}^{calibrator}$) of the calibrator with a long period is provided by the UMRAO. $\rho_{i,j}^{calibrator}$ is the normalized correlation coefficient of the calibrator obtained by geodetic VLBI observations.

- “Estimate-module” estimates the correlation flux of the target source ($S_{i,j}^{target}$) with Eq.(2) for each baseline.

$$S_{i,j}^{target} = SEFD_{i,j} \times \rho_{i,j}^{target} \quad (2)$$

$\rho_{i,j}^{target}$ is the normalized correlation coefficient of the target obtained by geodetic VLBI observations.

- “Drawing-module” estimates the total flux density of the target with the correlation flux densities of all baselines ($S_{i,j}^{target}$ for all i,j). The module divides data by time-bin, draws histograms of $S_{i,j}^{target}$. The total flux density (S^{target}) is estimated with the most frequent value (mode) of the histogram.

2.2. Example

In this section, the calculation and parameters of each module are described with a schematic example (Fig. 2).

Load-module: In the analysis so far, the source structure of the targets and the calibrators is not considered. The visibility data with uv-distance less than “uv range”, set to 50 Mλ in this example, is selected.

Calib-module: The $S_{UMRAO}^{calibrator}$ separated within the interval of the “polate range” are interpolated, and re-sampled at the rate of 1 day. The module makes pairs of $S_{UMRAO}^{calibrator}$ and $\rho_{i,j}^{calibrator}$, and calculates $SEFD_{i,j}$ with Eq.(1).

Estimate-module: The $SEFD_{i,j}$ within the interval “calib range” of $\rho_{i,j}^{target}$ are averaged. The module makes pairs of $SEFD_{i,j}$ and $\rho_{i,j}^{target}$, and calculates $S_{i,j}^{target}$ with Eq.(2).

Drawing-module: The module collects $S_{i,j}^{target}$ separated within the interval of “estim range” for all baselines, and draws histogram of $S_{i,j}^{target}$. The most frequent value (mode) of the histogram is estimated as S^{target} .

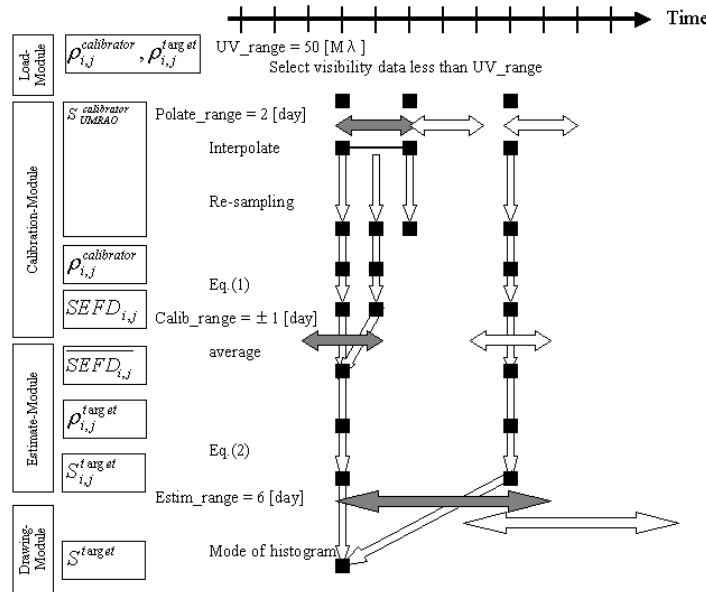


Figure 2. Schematic example. The filled square, the downwards-double arrow, and the left-right-double arrow express the data point, the calculation, and the range of parameter, respectively.

3. Preliminary Results

Initial results are shown in Fig. 3 and 4. For 4C39.25 (Fig. 3), we can see that the black and the gray light curves are consistent with each other. This result implies that we can use the VLBI data as well as single dish data to draw a light curve. For 0454-234 (Fig. 4), the UMRAO has

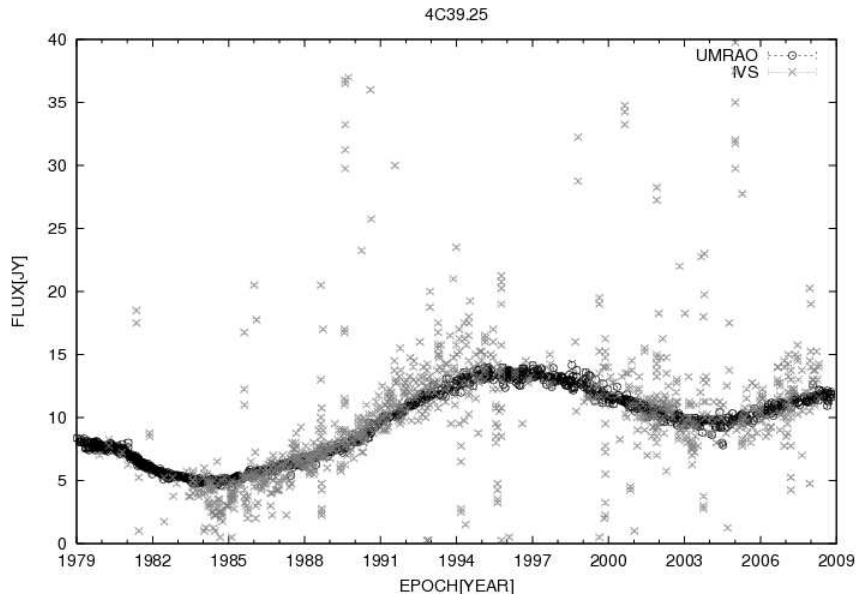


Figure 3. The light curves of 4C39.25. The black light curves are drawn with single dish data provided by the UMRAO at 8 GHz (private communication). The gray light curves are drawn with IVS data, estimated with my analysis at 8 GHz. Please note, the bar of the gray plot is not the error bar. The bar is the class interval width of the histogram drawn by the “Drawing-module”, see text.

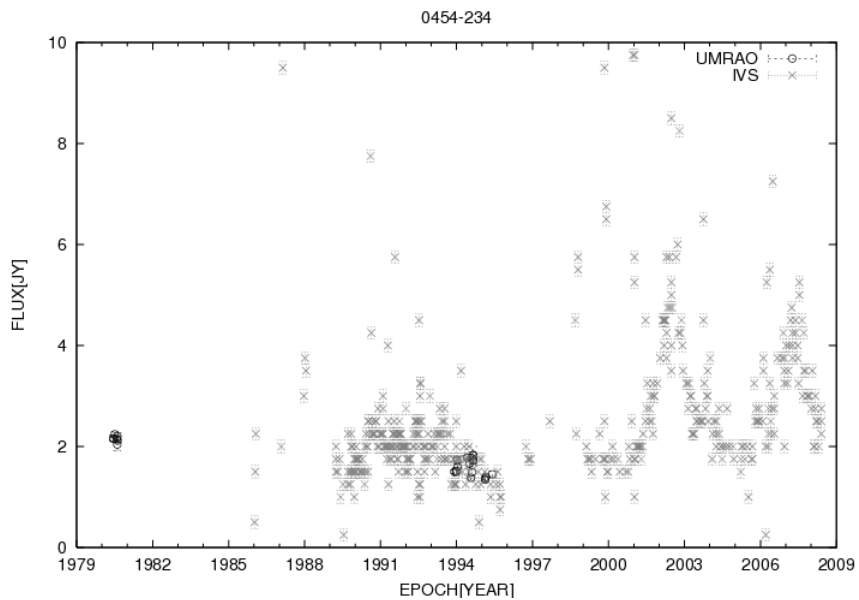


Figure 4. The light curves of 0454-234. The symbol usage is the same as in Fig. 3.

observed this source in 1980 and 1994 only. Based on IVS data, we can find two outbursts in 2002

and 2007. I suggest that the geodetic VLBI archive data is useful for obtaining the long-term light curves at radio bands for astrophysics.

4. Acknowledgements

This study could not have been conducted without the IVS community. I am much obliged for the tireless observations, analyzing, and archiving conducted by the community. My program partially uses MK3TOOLS provided by Thomas Hobiger, National Institute of Information and Communications Technology. This research has made use of data from the University of Michigan Radio Astronomy Observatory which has been supported by the University of Michigan and by a series of grants from the National Science Foundation, most recently AST-0607523. My participation in the “Sixth IVS General Meeting” was partially supported by “Foundation for Promotion of Astronomy”. I would like to thank K. Yamashita for support and helpful discussions.

References

- [1] Mutel R.L., Su Bumei, Bucciferro R.R., Phillips R.B., 1990, ApJ 352, 81
- [2] Caproni A., Abraham Z., 2004b, MNRAS, 349, 1218
- [3] Ohsuga K., 2006, ApJ, 640, 923
- [4] Aller, M. F., Aller, H. D., & Hughes, P.A. 1985, ApJ, 298, 296
- [5] Teräsranta H. et al., 1998, A&AS, 132, 305
- [6] Teräsranta H. et al., 2004, A&A, 427, 769
- [7] Teräsranta H., Wiren S K. P., Saarinen V., Hovatta T., 2005, A&A, 440, 409



Session 4 - Interpretation of VLBI Results in Geodesy, Astrometry and Geophysics

The Second International Celestial Reference Frame (ICRF2)

Chopo Ma

Goddard Space Flight Center, NASA

*e-mail: chopo.ma@nasa.gov*¹

Abstract

The ICRF2 catalog was constructed by the IERS/IVS Working Group with oversight by the IAU Working Group. Derived using data from August 1979 through March 2009, it is a great improvement over the original ICRF with 3414 extragalactic radio source positions, a noise floor of 40 microarcsec, and axis stability of 10 microarcsec. Significant refinements were made in the selection of defining sources, modeling, and the integration of CRF, TRF, and EOP. The adoption of the ICRF2 was approved by the IAU in Resolution B3 at the XXVII IAU General Assembly and became effective 1 January 2010.

1. Introduction¹

The ICRF (International Celestial Reference Frame) [1], adopted by the IAU in 1997 and effective on 1 January 1998, embodied a fundamental conceptual change from the previous optical, stellar, geocentric (equator, ecliptic), and epoch-dependent realization of celestial coordinates based on 1535 fundamental stars [2]. It used instead a smaller number of extragalactic radio objects measured by VLBI with much higher accuracy and established celestial coordinate axes independent of equator, ecliptic, and epoch. Although the ICRF was extended and improved using newer data as available in ICRF-Ext.1 and ICRF-Ext.2 [3], a decade after the ICRF analysis it was evident that much better astrometric and source structure data as well as refined geophysical models were in hand for a second realization. The analysis task was given to a joint IERS/IVS Working Group for the Second Realization of the ICRF and oversight on behalf of the astronomical community was provided by an IAU Working Group. Both groups were formed following discussions in Commission 19 and Division 1 at the XXVI IAU General Assembly in Prague in 2006. The charters and membership of the IERS/IVS Working Group and IAU Working Group are as follows.

IERS/IVS WG Charter: The purpose of the working group is to generate the second realization of the ICRF from VLBI observations of extragalactic radio sources, consistent with the current realization of the ITRF and EOP data products. The working group will apply state-of-the-art astronomical and geophysical models in the analysis of the entire relevant S/X astrometric and geodetic VLBI data set. The working group will carefully consider the selection of defining sources and the mitigation of source position variations to improve the stability of the ICRF. The goal is to present the second ICRF to relevant authoritative bodies, e.g. IERS and IVS, and submit the revised ICRF to the IAU Division I working group on the second realization of the ICRF for adoption at the 2009 IAU General Assembly.

¹This paper represents the work of the IERS/IVS Working Group for the Second Realization of the ICRF and an IAU Working Group tasked with oversight of the IERS/IVS Working Group.

Table 1. Members of the IERS/IVS Working Group.

O. Titov, Australia	R. Heinkelmann, Austria	G. Wang, China
F. Arias, France	P. Charlot, France	A.-M. Gontier, France
S. Lambert, France	J. Souchay, France	G. Engelhardt, Germany
A. Nothnagel, Germany	V. Tesmer, Germany	G. Bianco, Italy
S. Kurdubov, Russia	Z. Malkin, Russia	E. Skurikhina, Russia
J. Sokolova, Russia	V. Zharov, Russia	S. Bolotin, Ukraine
D. Boboltz, USA	A. Fey, USA	R. Gaume, USA
C. Jacobs, USA	C. Ma, USA (Chair)	L. Petrov, USA
O. Sovers, USA		

IAU WG Charter: The purpose of the working group is to oversee the generation of the second realization of the ICRF from VLBI observations of extragalactic radio sources. The reference frame will apply state-of-the-art astronomical and geophysical models in the analysis of the entire relevant S/X astrometric and geodetic VLBI data set. The working group will ensure the selection of defining sources and the mitigation of source position variations and the consistency with the ITRF and the IERS EOP to improve the stability of the ICRF. The goal is to present the second ICRF at the 2009 IAU General Assembly.

Table 2. Members of the IAU Working Group.

Alexandre Andrei, Brazil	Felicitas Arias, France
Bob Campbell, Netherlands	Patrick Charlot, France
Alan Fey, USA	Ed Fomalont, USA
Ralph Gaume, USA	Chopo Ma, USA (Chair)
Jean Souchay, France	Yaroslav Yatskiv, Ukraine
Norbert Zacharias, USA	

The IERS/IVS Working Group accomplished its work through correspondence and in-person meetings, the last in Bordeaux in March 2009. Significant contributions were also made, especially in the later stages, by C. Barache, S. Böckmann, A. Collioud, J. Gipson, D. Gordon, S. Lytvyn, D. MacMillan, and R. Ojha. The finished work was described in IERS Technical Note 35 [4], which was made available electronically to the IVS and IERS. After approval by the IVS and IERS, the IAU Working Group agreed that the ICRF2 was satisfactory, drafted the supporting resolution B3, led the discussions in Division 1 and Commission 19, and presented the resolution to the XXVII IAU General Assembly on August 13, 2009, where it was accepted without dissent. The effective date of the ICRF2 was 1 January 2010.

2. Data

The ICRF2 included 30 years of simultaneous S/X-band (2.8/8.4 GHz) observing from a heterogeneous global network, ~ 6.5 million group delays from more than 4500 24-hr sessions. The data quality clearly improved in the early 1990s, but the older data were included for continuity

with the first ICRF and to extend the source position time series. The VLBA contributed $\sim 28\%$ of the observations, an indication of its importance to global astrometry. In addition to its participation in the IVS observing program, the VLBA was also used for the VLBA Calibrator Survey (VCS) [5], which observed a large number of sources but each target source only in a single session. More details can be found in section 2 of IERS TN 35.

3. Software

Several software packages have been developed independently over the years by different groups for analysis of VLBI geodetic and astrometric data. Four such packages were used in studying the data included in the ICRF2 and in the preliminary and final solutions: CALC/SOLVE (NASA's Goddard Space Flight Center), SteelBreeze (Main Astronomical Observatory (MAO) of the National Academy of Sciences of Ukraine), OCCAM (Geoscience Australia), and QUASAR (Institute of Applied Astronomy of the Russian Academy of Sciences). Preliminary solutions were submitted by seven analysis centers using these analysis packages, and a combination catalog was also generated at MAO. Comparisons of individual catalogs and the combination catalog were used to investigate systematic effects, which were found to be at the 50 microarcsec level. Additional details can be found in section 8 of IERS TN 35.

4. Special Handling Sources

Source position time series generated by several analysis centers were examined to identify sources so variable as to require special handling. Some characteristics of such sources were irregular apparent motion and excessive noise in the time series. These apparent motions are related to changes in source structure or the position of the brightest component rather than physical translations. Unfortunately no single statistical test was found that could unambiguously identify such poorly behaved sources, in large part because the temporal density and continuity of observations varied so widely from source to source. Using several criteria, D. Gordon selected 39 special handling sources whose positions were treated as "arc" parameters in subsequent analysis, i.e. estimated independently for each session in which the source was sufficiently observed, in order to mitigate the effect of these source position variations on the overall catalog. Further details are given in section 4 of IERS TN 35.

5. Modeling and Catalog Solution

State-of-the-art geophysical and astronomical models were used in the solution that generated the (relative) source positions that are in the ICRF2 catalog. These included estimated tropospheric gradients with appropriate a priori starting values and constraints, the VMF1 tropospheric mapping function, thermal variation in antenna structures, and atmospheric pressure loading. The goal was to achieve the greatest consistency among the CRF, TRF, and EOP without propagating systematic errors of one into the others. Consequently the full treatment of station position anomalies was included in the analysis, and CRF, TRF, and EOP were estimated simultaneously. Comparisons of the integrated CRF, TRF, and EOP solutions with CRF-only solutions showed insignificant differences. Additional details are in section 6 of IERS TN 35.

The culminating solution of the ICRF2 analysis was performed with CALC/SOLVE at Goddard

Space Flight Center rather than through a combination of solutions from various analysis centers. There were a number of factors behind this choice including the desire to preserve the consistency of CRF, TRF, and EOP, the marginally better quality of earlier Goddard solutions compared to others, and the absence of a tested mechanism and experience with “rigorous” combination in the mode of the ITRF.

The catalog solution includes 4540 sessions from 1979 August 3 through 2009 March 16 with 6.5 million group delays, 3375 “global” source positions, and 39 “arc” sources. Based on decimation tests and comparisons, the final source position uncertainties were derived from the solution formal errors by a multiplicative factor of 1.5 and a root-sum-square addition of 40 microarcsec. More detail can be found in sections 7 and 9 of IERS TN 35.

6. Selection of Defining Sources

The selection of defining sources balanced two conflicting conditions: the need for uniform coverage of the entire sky and the uneven distribution of source position quality systematically by declination and by source. These limitations arise from the skewed geographic distribution of VLBI observing stations (overwhelmingly in the Northern Hemisphere) and the unequal allocation of observing ($> 95\%$ of observations on a limited (~ 150) set of sources used for geodesy). Consequently the minimum criteria for defining sources are still rather weak, ≥ 10 sessions and > 2 -yr span of observations. The sources were ranked by position stability from the position time series, formal errors from the culminating solution, and the continuous source structure index, which was developed specifically for the ICRF2 analysis. A separate analysis determined the optimum number of defining sources accounting for the actual distribution of source position uncertainties. To populate the sky evenly, the ranking was performed independently in five declination bands. Otherwise the defining sources, those with the highest overall ranking, would be largely in the northern sky. There was structure information for 707 sources, much more than for the first ICRF through the long-term efforts of USNO and Bordeaux Observatory, although only a single epoch for 337 sources. In general the position and structure rankings agreed, but sources with index > 3.0 were rejected. The source structure and ranking analysis are described in detail in sections 5 and 11 of IERS TN 35, respectively.

7. Alignment of ICRF2 Onto ICRS

To align the ICRF2 positions with the ICRS as realized by the initial 1997 ICRF, 138 sources were used. Of these 97 were defining sources in both ICRF and ICRF2 (mostly in the north) and 41 were ICRF2 defining sources with positions in ICRF-Ext.2 (mostly in the south). Three rotation angles and a declination bias were estimated, but only the rotations were applied since the declination bias was considered to be a systematic error in ICRF. The axis stability of ICRF2 is ~ 10 microarcsec. The details of the alignment are given in section 12 of IERS TN 35.

8. ICRF2 Summary

Figure 1 shows the 295 ICRF2 defining sources. Figure 2 shows the 1448 sources in the catalog with multiple sessions. Figure 3 shows the 1966 sources observed in only one session, largely from the VCS program. Figure 4 shows the distribution of uncertainties for the non-VCS sources.

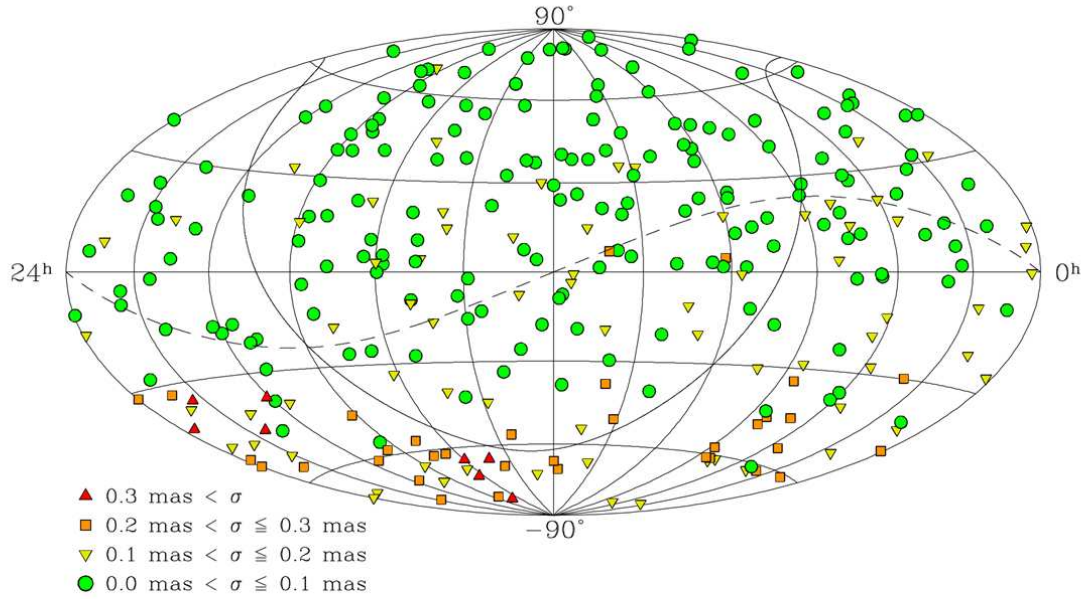


Figure 1. The 295 ICRF2 defining sources.

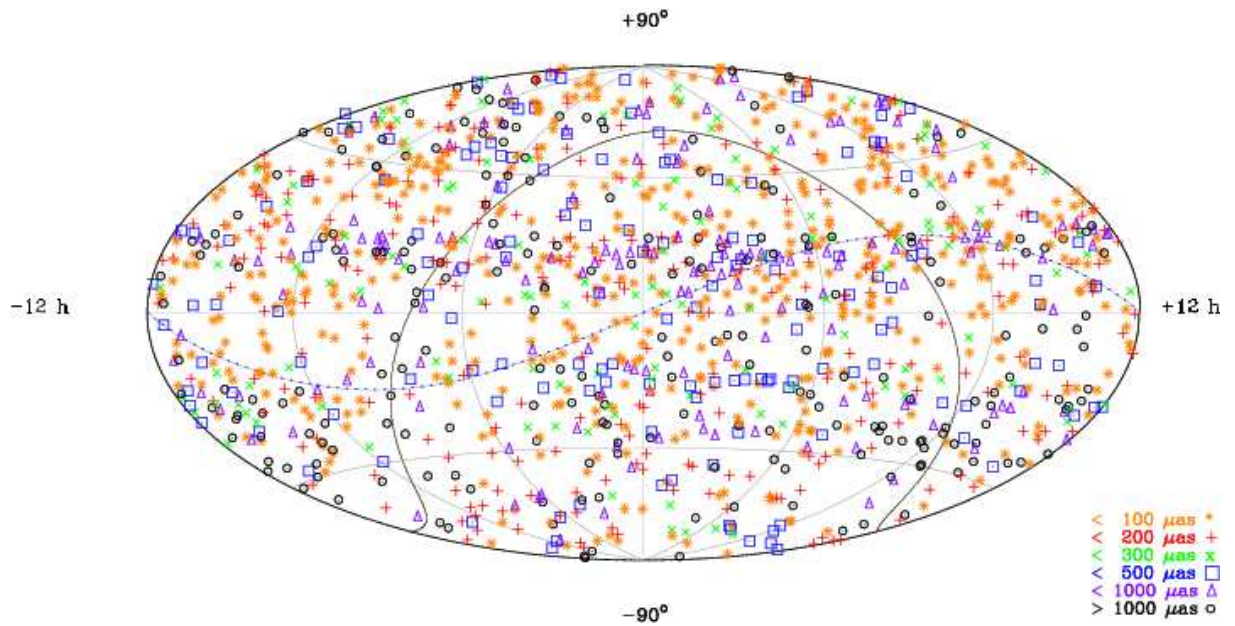


Figure 2. 1448 ICRF2 sources observed in multiple sessions. The formal errors are indicated by the key.

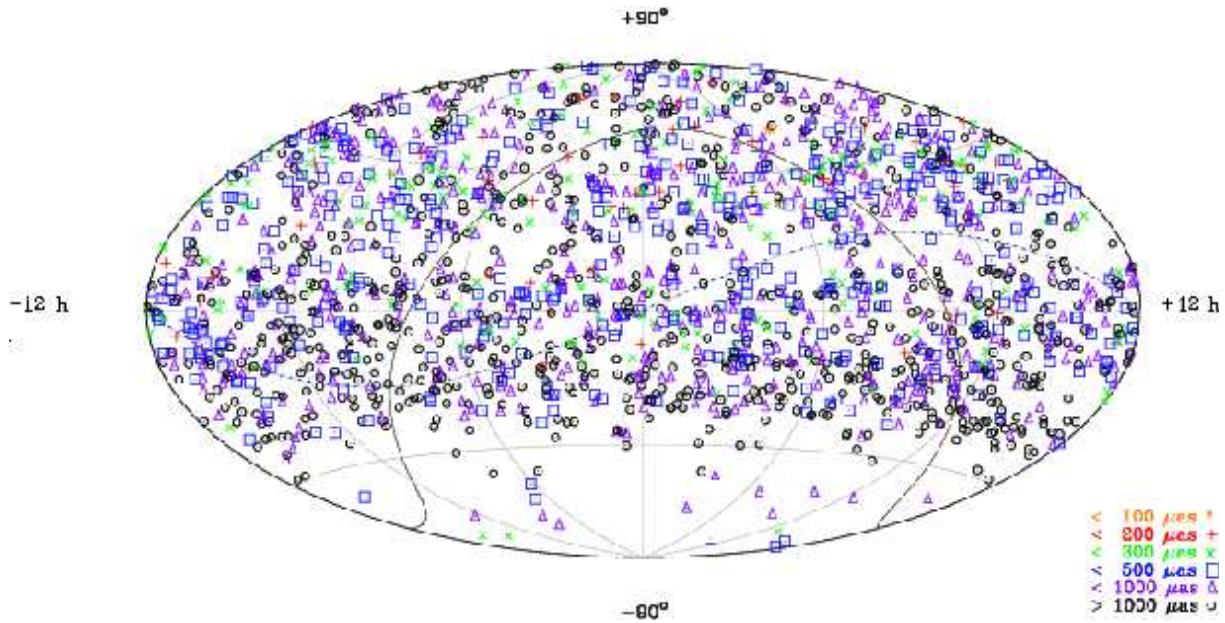


Figure 3. 1966 ICRF2 sources observed in only one session. The formal errors are indicated by the key. These are mostly VLBA Calibrator Survey (VCS) sources.

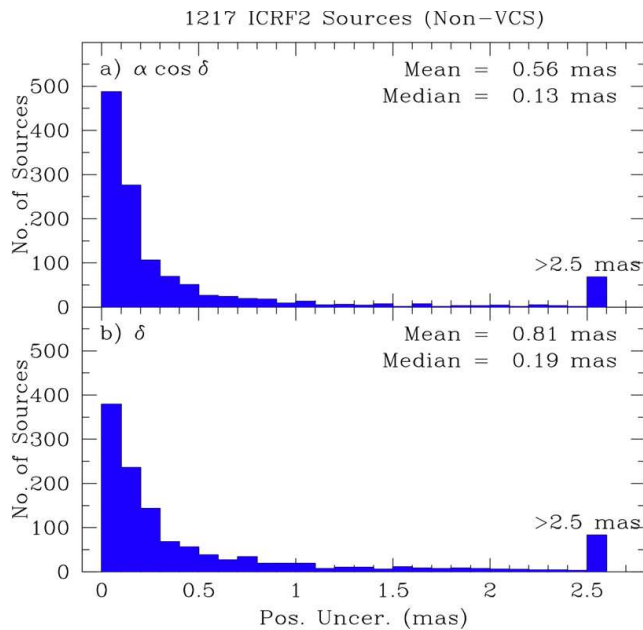


Figure 4. Histograms showing the inflated position uncertainties for the 1217 non-VCS ICRF2 sources.

9. Acknowledgements

The ICRF2 was completed under a very tight schedule through the careful, creative thinking, detailed analysis, and burning the midnight oil by the members of the working groups and the other contributors, whose assistance was invaluable. There was a can-do spirit and collaboration that pushed forward despite difficulties. In particular the editors A. Fey, D. Gordon, and C. Jacobs made the IERS Technical Note 35 a coherent document. The work of the IERS Central Bureau in preparing the final version of TN 35 and making it available was an essential and critical step to the success of the ICRF2 effort. As with all such endeavors the results are not perfect, but they are a significant step forward.

References

- [1] Ma, C., E. Arias, T. Eubanks, A. Fey, A.M. Gontier, et al., AJ 116, 516-546, 1998.
- [2] Fricke, W., H. Schwann, T. Lederle, Fifth Fundamental Catalogue (FK5), Part I, Veröff. Astron. Rechen-Inst. Heidelberg 32, 106 pp, 1988.
- [3] Fey, A., C. Ma, E. Arias, P. Charlot, M. Feissel-Vernier, et al., AJ 127, 3587-3608, 2004.
- [4] The Second Realization of the International Celestial Reference Frame by Very Long Baseline Interferometry, IERS / IVS Working Group, A. Fey, D. Gordon and C. Jacobs (eds.). (IERS Technical Note 35) Frankfurt am Main: Verlag des Bundesamts für Kartographie und Geodäsie, 2009. 105 p.
- [5] Beasley, A.J., D. Gordon, A.B. Peck, L. Petrov, D. S. MacMillan, et al., Astrophys. J. Supp. Series 141, 13-21, 2002.

Time-dependent Selection of an Optimal Set of Sources to Define a Stable Celestial Reference Frame

Karine Le Bail, David Gordon

NVI, Inc./NASA Goddard Space Flight Center

Contact author: Karine Le Bail, e-mail: karine.lebail@nasa.gov

Abstract

Temporal statistical position stability is required for VLBI sources to define a stable Celestial Reference Frame (CRF) and has been studied in many recent papers. This study analyzes the sources from the latest realization of the International Celestial Reference Frame (ICRF2) with the Allan variance, in addition to taking into account the apparent linear motions of the sources. Focusing on the 295 defining sources shows how they are a good compromise of different criteria, such as statistical stability and sky distribution, as well as having a sufficient number of sources, despite the fact that the most stable sources of the entire ICRF2 are mostly in the Northern Hemisphere. Nevertheless, the selection of a stable set is not unique: studying different solutions (GSF005a and AUG24 from GSFC and OPA from the Paris Observatory) over different time periods (1989.5 to 2009.5 and 1999.5 to 2009.5) leads to selections that can differ in up to 20% of the sources. Observing, recording, and network improvement are some of the causes, showing better stability for the CRF over the last decade than the last twenty years. But this may also be explained by the assumption of stationarity that is not necessarily right for some sources.

1. Introduction

The purpose of this study was primarily to apply methods developed in 2003 by M. Feissel-Vernier [1] to new sets of VLBI source position time series. In 2009, Lambert & Gontier [4] did some preliminary analysis in this sense, using a former set of source time series. This paper is inspired by these two papers, but extended to the second realization of the International Celestial Reference Frame (ICRF2) sources and seen with a new point of view. The goal is to select stable sources using the Allan variance as the statistical tool to judge source stability, taking into account their linear trend components.

2. Data

Three sets of VLBI position time series were analyzed, all produced with Calc/Solve software. The first two (from D. Gordon at GSFC) are series GSF005a, which used only global VLBI sessions from August 1979 through February 2009, and series AUG24, which used global, mobile, and some regional VLBI sessions through August 2009. Mobile and regional VLBI sessions used weaker stations and smaller networks, and thus will give noisier results. The third series, OPA (from S. Lambert at the Paris Observatory) used a different approach in its analysis strategy. The analysis was done over two different periods of time. The first covered the approximately twenty years of the best VLBI, from 1989.5—2009.5, and the second covered the last ten years from 1999.5 to 2009.5.

3. Allan Variance as a Tool to Qualify the Stability of VLBI Sources

3.1. Source Stability Index

The following is a quick reminder of the mathematical expression of the Allan variance. If $(x_i)_i$ are the measurements and T the sampling time, the Allan variance is $\sigma_A^2(T) = \frac{1}{2} \langle (\bar{x}_{i+1} - \bar{x}_i)^2 \rangle$. By analogy with the power spectral density, the slope of the Allan variance curve in a log-log plot indicates the type of noise. White noise will give a slope equal to -1 , flicker noise to 0 , and random walk to $+1$. More details can be found in [6].

The stability index SI used in this study is calculated as a combination of the normalized values of the slope coefficients (computed over all data studied) and the Allan variance at one-year sampling time, on both coordinates (right ascension and declination): $SI(source_k)$ is the sum of the normalized values of $slopeRA_k$, $slopeDEC_k$, $\sigma_{RA_k}^2(1yr)$, and $\sigma_{DEC_k}^2(1yr)$.

3.2. Celestial Reference Frame Stability Indicator



Figure 1. Stability test scheme. This figure illustrates the method used to judge the stability of a subset of sources by comparing yearly averaged Celestial Reference Frames $(CRF)_i$ to a mean CRF.

To judge the stability of a subset of chosen sources, we compare two Celestial Reference Frames (CRFs) realized by this subset (see Figure 1): one is the yearly mean realization $(CRF)_i$, while the other is the mean being computed over the full period. To do so, we process three rotations (A_1, A_2, A_3) and a fictitious declination bias dz (cf., [2], [3]) by the following equation:

$$\begin{cases} (\alpha_m - \alpha_i) \cos \delta_m &= A_1(i) \tan \delta_i \cos \alpha_i + A_2(i) \tan \delta_i \sin \alpha_i - A_3(i) \\ \delta_m - \delta_i &= -A_1(i) \sin \alpha_i + A_2(i) \cos \alpha_i + dz(i) \end{cases}$$

where i indicates the year of the average of the coordinates and m the mean coordinates computed over the entire studied period. The stability criteria is obtained by looking at the $(A_1(i), A_2(i), A_3(i), dz(i))_i$ parameter time series for different subsets of sources.

3.3. Statistical Analysis Scheme Used in This Study

The following describes the analysis of the entire set of sources:

1. Some sources can not be analyzed for some statistical reasons of consistency (time series shorter than five years, data gaps bigger than four years, needing more than 50% of gap filling for the regularization of the time series). These are eliminated from the analyzed set.
2. For each source remaining, the stability index SI explained previously is computed (combination of drift slopes and Allan variances at one-year for each coordinate). The sources are then sorted from the most stable (lowest SI value) to the least stable (largest SI value).

3. N bins B_j of sources are created (the 50 most stable sources in bin B_1 , then the 60 most stable sources in bin B_2 , then the 70 most stable in bin B_3, \dots until the entire set of analyzed sources is reconstructed in bin B_N).
4. A set of $(A_1(i, j), A_2(i, j), A_3(i, j), dz(i, j))_i$ where i is the year and j the number of the bin, is computed for each bin $(B_j)_{j=1..N}$.
5. For each bin $(B_j)_{j=1..N}$, we compute standard deviations and means of those four parameters time series, and we sum them together. Finally, we obtain one couple $(S_j, M_j)_{j=1..N}$ per bin $(B_j)_{j=1..N}$ where $S = \sigma(A_1) + \sigma(A_2) + \sigma(A_3) + \sigma(dz)$ and $M = \overline{A_1} + \overline{A_2} + \overline{A_3} + \overline{dz}$.

4. Results

4.1. Evaluation of the Defining Sources

In ICRF2, 295 sources are defining sources. They were chosen taking into account different criteria (cf., [5]), such as even sky distribution (the sky was divided into four divisions based on declination), the quality of the observations (computed by the positional stability of right ascension and declination, meaning a combination of WRMS, χ^2 , and formal error), and the compactness of the sources (source structure index).

In this section, only solution GSF005a is studied. The entire set of sources consists of 1206 sources, but only 519 passed the first step of elimination as showing good characteristics of consistency for statistical study, removing at this step 20% of the defining sources.

We looked at the sky distribution of the stable sources. If we stop the selection at the 50 most stable sources, 75% are defining sources. If we stop at 260, 60% are defining sources, and if we look at the overall sky distribution of those 260 sources, 80% of them are in the Northern Hemisphere. The less stable sources are then the ones in the Southern Hemisphere.

The full overview of the distribution of the most stable sources shows that the choice of the defining sources is finally a good compromise of statistical stability and good sky distribution.

4.2. Comparison Between Different Solutions

We compare here the three solutions (GSF005a, AUG24, and OPA) over two different periods (1989.5-2009.5 and 1999.5-2009.5). We plot $(S_j, M_j)_{j=1..N}$ as a function of the bin number considered as an increasing number of sources and we obtain the plots in Figure 2.

These plots show various information. First, solutions GSF005a and OPA show similar results, whereas AUG24 has the highest values of S_j per number of sources, implying that the non-global sessions are increasing the level of noise and decreasing the stability of the Celestial Reference Frame. Second, when we compare the two periods of time, the past ten years shows better stability than the last twenty years of VLBI observation. This can be attributed to various improvements in VLBI observing and data taking, such as receiver improvements, use of new strong stations (such as the ten VLBA antennas), increased spanned bandwidths, increased recorded bandwidths, and larger network sessions (such as the weekly 6-8 station R1 and R4 sessions). Finally, the comparison between GSF005a and OPA shows that the selection of a set of stable sources is not unique and depends on the analysis strategy. Indeed, if we take for example the bin containing 200 stable sources for GSF005a and the bin of 200 stable sources for OPA, the sources obtained are not the same: only 80% of the sources are common.

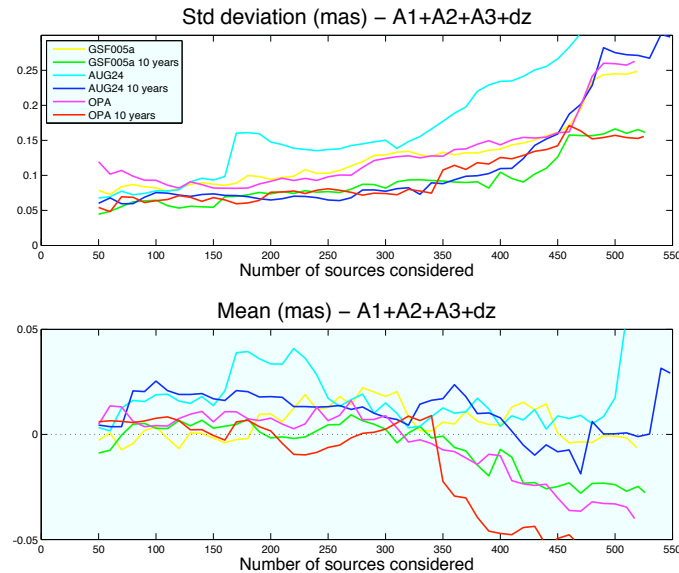


Figure 2. ICRF2 stability comparison. Three solutions are studied over two different periods of time (1989.5 to present and 1999.5 to present): GSF005a and AUG24, processed at GSFC (AUG24 contains the bad and the mobile sessions), and OPA at the Paris Observatory. These graphs compare the stability of the subsets of stable sources selected in each solution, by computing the standard deviation and the mean of the sum of the parameters of transformation between a yearly and a mean CRF realization of these subsets. These parameters are three rotations (A_1, A_2, A_3) and a fictitious declination bias dz .

5. Discussion on the Source Noise Stationarity Assumption

To explain why a set of stable sources is not unique and by noticing the better stability over the ten last years, we investigated the noise stationarity assumption in the different time series. For a set of twenty sources, the statistical study over two different periods of the time series show two completely different conclusions. The example of 3C418 is given in Figure 3. A first study processing the data from 1989 to 1993 shows white noise at the level of $100\mu\text{as}$ for both coordinates (Allan variance plots on the left side of the figure) and another study processing 1997 to 2009.5 shows a combination of white noise and flicker noise, with a level for the flicker noise as low as $50\mu\text{as}$ for both coordinates (Allan variance plots on the right side of the figure).

6. Conclusion

The statistical analysis of this study shows the 295 ICRF2 defining sources are a good compromise of statistical stability and good sky distribution. When looking at the full set of ICRF2 sources, we noticed that the selection of a set of stable sources is not unique and depends on the analysis strategy used for the processing (sessions used, analysis strategy). It may be of interest to compare in detail the impact of differences in the analysis strategy as well as the software used.

The investigation over the last ten years shows better stability, pointing to various VLBI improvements in the last decade, but also that the noise of the source time series is not a stationary

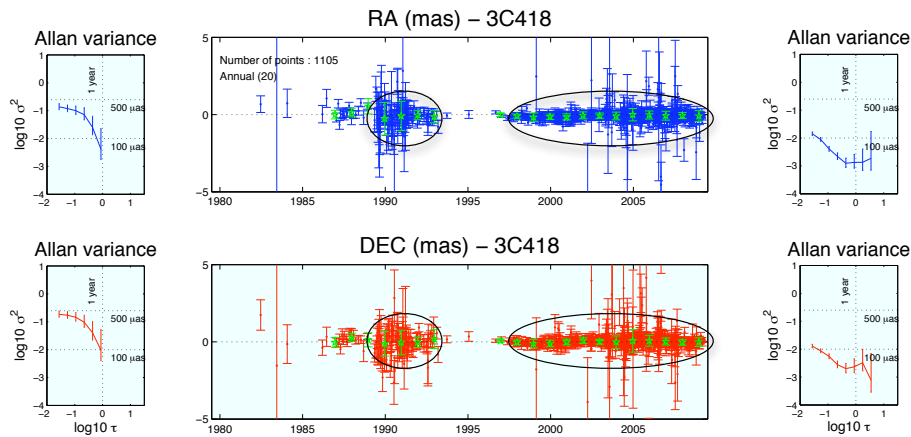


Figure 3. Example of non-stationarity: 3C418. The central part of the figure is the time series of the ICRF2 coordinates of 3C418 in mas (Up: Right ascension \times cos (declination); Bottom: Declination). On the left side, the Allan variances are computed from the 1989-1993 time series, on the right side, from the 1997 to 2009.5 time series. The Allan variance plots show the Allan variance (σ^2) function of the sampling time (τ) in a log10-log10 base.

process. An alternative in the selection of stable sources could be to consider only the stable periods of observation of the sources, instead of keeping only as a base for the Celestial Reference Frame the sources showing good statistical stability over their entire observation period.

7. Acknowledgements

The authors would like to thank Sébastien Lambert and Anne-Marie Gontier at OPA for providing their source position time series solution and for discussing some results of this study.

References

- [1] Feissel-Vernier, M., Selecting stable extragalactic compact radio sources from the permanent astro-geodetic VLBI program, In: *Astronomy & Astrophysics*, 403:105–110, 2003.
- [2] Feissel-Vernier, M., C. Ma, A.-M. Gontier, C. Barache, Analysis strategy issues for the maintenance of the ICRF axes, In: *Astronomy & Astrophysics*, 452:11071112, 2006.
- [3] Gontier, A.-M., K. Le Bail, M. Feissel, T.M. Eubanks, Stability of the extragalactic VLBI reference frame, In: *Astronomy & Astrophysics*, 375:661–669, 2001.
- [4] Lambert, S., A.-M. Gontier, On radio source selection to define a stable celestial frame, In: *Astronomy & Astrophysics*, 493, 317–323, 2009.
- [5] Lambert, S., P. Charlot, A.-M. Gontier, Selection of ICRF2 Defining Sources, In: *The Second Realization of the International Celestial Reference Frame by Very Long Baseline Interferometry*, IERS Technical Note No. 35, A. L. Fey, D. Gordon and C. S. Jacobs (eds.), 73–78, 2009.
- [6] Le Bail, K., Estimating the noise in space-geodetic positioning: the case of DORIS, In: *DORIS Special Issue*, *Journal Of Geodesy*, P. Willis (ed.), 80(8-11):541–565, 2006.

X/Ka Celestial Frame Improvements: Vision to Reality

C. S. Jacobs¹, D. S. Bagri¹, M. J. Britcliffe¹, J. E. Clark¹, M. M. Franco¹,
C. Garcia-Miro², C. E. Goodhart¹, S. Horiuchi³, S. T. Lowe¹, V. E. Moll²,
R. Navarro¹, S. P. Rogstad¹, R. C. Proctor¹, E. H. Sigman¹, L. J. Skjerve¹,
M. A. Soriano¹, O. J. Sovers¹, B. C. Tucker¹, D. Wang¹, L. A. White¹

¹⁾ *Jet Propulsion Laboratory, California Institute of Technology/NASA*

²⁾ *Ingenieria y Servicios Aeroespaciales, Instituto Nacional de Técnica Aeroespacial/NASA*

³⁾ *C.S.I.R.O. Astronomy and Space Science/NASA*

Contact author: C. S. Jacobs, e-mail: Christopher.S.Jacobs@jpl.nasa.gov

Abstract

In order to extend the International Celestial Reference Frame from its S/X-band (2.3/8.4 GHz) basis to a complementary frame at X/Ka-band (8.4/32 GHz), we began in mid-2005 an ongoing series of X/Ka observations using NASA's Deep Space Network (DSN) radio telescopes. Over the course of 47 sessions, we have detected 351 extra-galactic radio sources covering the full 24 hours of right ascension and declinations down to -45 degrees. Angular source position accuracy is at the part-per-billion level.

We developed an error budget which shows that the main errors arise from limited sensitivity, mis-modeling of the troposphere, uncalibrated instrumental effects, and the lack of a southern baseline. Recent work has improved sensitivity by improving pointing calibrations and by increasing the data rate four-fold. Troposphere calibration has been demonstrated at the mm-level. Construction of instrumental phase calibrators and new digital baseband filtering electronics began in recent months. We will discuss the expected effect of these improvements on the X/Ka frame.

1. Introduction

For over three decades, radio frequency work in global astrometry, geodesy, and deep space navigation has been done at S/X-band (2.3/8.4 GHz) [10]. This well known work has been tremendously successful in producing sub-100 μas level global astrometry (e.g.[7]) and sub-cm geodesy. Less well known is that at the same time when S/X work started—the late 1970s—visionary colleagues, e.g. [2, 8], started to lay the foundation for one day doing X/Ka-band (8.4/32 GHz) VLBI. Only now, in the last decade, have technological and programmatic developments allowed that vision to blossom. This paper will report on the current status of X/Ka-band VLBI, present our plan for improving X/Ka-band astrometry, and assess our progress towards realizing that plan.

Ka-band pros: Increasing observing frequencies by a factor of four promises several advantages. For the Deep Space Network, the chief driver is the potential for higher telemetry rates to space probes. Other advantages include 1) sources become more compact lending hope that the positions will be more stable over time, 2) radio frequency interference at S-band would be avoided, 3) Ionosphere and solar plasma effects on delay and signal coherence are reduced about ~ 15 -fold.

Ka-band cons: While these are significant advantages, there are also disadvantages. The change from 2.3/8.4 GHz to 8.4/32 GHz moves one closer to the water vapor line at 22 GHz and thus increases the system temperature to 6–15 Kelvins per atmosphere or more, thereby increasing weather sensitivity. Many sources become weaker and/or resolved. Coherence times are shortened so that practical integration times are a few minutes or less—even in relatively dry climates.

Antenna pointing accuracy must be tightened by the factor-of-4 wavelength reduction. These effects all combine to lower the system sensitivity. Thus counter-measures are needed.

This paper is organized as follows: We will briefly review present X/Ka-band astrometry including an estimate of its accuracy based on comparison to the S/X-band ICRF2. A simplified error budget consisting of errors from sensitivity limitations, instrumental errors, and troposphere mismodeling will guide our discussion of plans for reducing each of those error sources. We will emphasize how our vision for reducing errors is becoming a reality.

2. Observations and Current Accuracy

The results presented here are from 47 Very Long Baseline Interferometry (VLBI) observing sessions of 24 hour duration done from July 2005 until December 2009 using NASA's Deep Space Stations (DSS) 25 or 26 in Goldstone, California to either DSS 34 in Tidbinbilla, Australia or DSS 55 outside Madrid, Spain to form interferometric baselines of 10,500 and 8,400 km length, respectively.

We recorded simultaneous X (8.4 GHz) and Ka-band (32 GHz), sampling each band at 56 Mbps. Each band's 7 channels (each ± 2 MHz) spanned a bandwidth of ≈ 360 MHz. For the three most recent sessions, the data rates were doubled to 224 Mbps—split between bands as 80/144 Mbps.

In all, we detected 351 extragalactic radio sources which covered the full 24 hours of RA and declinations down to -45° . In Figure 1, these sources are plotted using an Aitoff projection to show their locations on the sky. Note that the declination precision decreases as one moves toward the south. This is a result of having significantly less data on the California to Australia baseline combined with the need to observe sources closer to the horizon as declination moves south, thus incurring greater error from higher system temperatures and tropospheric mismodeling.

An external estimate of the accuracy of our astrometry was made by comparing X/Ka source positions to the S/X-based ICRF2 [7]. For 323 common sources, the weighted RMS (wRMS) differences are 190 μas in RA $\cos(\text{dec})$ and 265 μas in declination [5]. Examination of the differences revealed decreasing accuracy in RA and declination as one moves southward (see Fig. 1).

3. Error Budget: Sensitivity, Instrumentation, Troposphere

Having presented the number, spatial distribution, and accuracy of our source positions, we now discuss the major errors currently limiting X/Ka accuracy. The median delay thermal error was ≈ 45 psec. Fig. 2's plot of data scatter vs. the nominal SNR sheds light on the error budget. For SNRs < 15 dB the thermal error dominates. For higher SNRs, the data scatter is limited by a noise floor caused by tropospheric and instrumental errors. Let's now look in more detail at these three main errors: SNR, instrumentation, and troposphere.

Sensitivity: Relative to S and X-bands, Ka-band has higher system temperatures, worse pointing, and larger coherence losses, all of which lower sensitivity and increase delay scatter. Much work was done to minimize signal loss due to mis-pointing, resulting in recovery of roughly +3 dB gain in our Ka-band sensitivity [9].

Fortunately, it is feasible and affordable to further increase sensitivity by increasing the recorded bit rate using recent advances [11]. Thus, while most of the X/Ka data presented in this paper used the same 112 Mbps recording rate as used in much previous S/X work, we have recently

begun to leverage the Mark 5A system's potential by recording at 448 Mbps (Fig. 3). We plan to use 896 Mbps (split as 320/576 Mbps) within the next year, thereby improving the SNR by a factor of 3.2 which would reduce the median thermal errors to ≈ 15 psec—below the instrumental and tropospheric floor! Within 2–3 years, deployment of Mark 5C recorders is expected to increase maximum data rates from 1024 Mbps to 4096 Mbps [11] thereby further improving sensitivity.

Instrumentation: A prototype Ka-band phase calibrator [3] based on A.E.E. Rogers's tunnel diode concept revealed approximately diurnal instrumental effects with ≈ 180 psec amplitude (see Fig. 4). Although the VLBI data have been used to partially parameterize these effects, in order to achieve better than 200 μas accuracy in a timely manner, we have begun building operational calibrators for deployment within the next few years. Fig. 5 shows our first production unit.

Further instrumental improvements are expected from replacing aging Mark IV video converters with Digital Back Ends (DBE). The DBE's phase-linear Finite Impulse Response (FIR) filters will reduce phase errors and increase the spanned bandwidth from 360 to 500 MHz thus reducing both systematic and random group delay errors.

Troposphere: Work started in the 1990s led to JPL's Advanced WVR (A-WVR) which demonstrated the ability to calibrate tropospheric delay fluctuations on inter-continental baselines with 1 mm accuracy [4, 1]. Recent work has focussed on modifying commercial designs to retain mm-level accuracy while being smaller and lighter so as to enable the WVR to be mounted on the VLBI subreflector. This will improve beam alignment and automate co-pointed observing.

4. Conclusions

The S/X-band ICRF has now been extended to the four times higher frequency of X/Ka-band (8.4/32 GHz). A total of 351 sources have been successfully detected. For the 323 sources with sufficient observations to warrant comparison to the ICRF2's S/X results, the wRMS positional agreement was 190 μas in RA $\cos(\text{declination})$ and 265 μas in declination.

Our current limiting errors are SNR, lack of instrumental calibration, and troposphere mis-modeling. SNR errors are being reduced by improving pointing and increasing the data rate. Instrumental errors will be reduced by phase calibrators and DBEs being built for deployment within the next few years. We are working to make mm-level WVR troposphere calibration less expensive and lighter weight to enable its operational use. If all these improvements are achieved, we expect 200 μas or better accuracy within a few years.

5. Acknowledgements

The research described herein was performed at the Jet Propulsion Laboratory of the California Institute of Technology, under a contract with the National Aeronautics and Space Administration. Copyright 2010 © California Institute of Technology. Government sponsorship acknowledged.

References

- [1] Bar-Sever et al, 'Atmospheric Media Calibration for the Deep Space Network,' Proc. IEEE (Special issue), 95, 11, Nov. 2007. <http://ieeexplore.ieee.org/stamp/stamp.jsp?arnumber=04390031>
- [2] deGroot, N.F., 'Ka-band (32 GHz) Allocations for Deep Space,' TDA Prog. Rept. 42-88, pp. 104–109. 15 Feb 1987. http://tmo.jpl.nasa.gov/progress_report/42-88/88N.PDF

- [3] Hammel, Tucker, & Calhoun, ‘Phase Cal. Generator,’ IPN Prog. Rep. 42-154, Pasadena, CA, 2003. http://tmo.jpl.nasa.gov/progress_report/42-154/154H.pdf
- [4] Jacobs et al, ‘Improving Astrometric VLBI by using WVR Calibrations,’ BAAS, 36, 5, 2004. <http://www.aas.org/publications/baas/v36n5/aas205/716.htm>
- [5] Jacobs & Sovers, ‘X/Ka-band Global Astrometric Results,’ Proc. 19th EVGA, Bordeaux, France, 2009. <http://www.u-bordeaux1.fr/vlbi2009/proceedgs/03-Jacobs.pdf>
- [6] Ma *et al*, ‘The ICRF as Realized by VLBI,’ AJ, 116, 1, 516–546, Jul 1998. doi: 10.1086/300408 <http://iopscience.iop.org/1538-3881/116/1/516/>
- [7] Ma et al, ‘The 2nd Realization of the ICRF by VLBI,’ IERS, Frankfurt, Germany, Oct. 2009. http://www.iers.org/nn_11216/IERS/EN/Publications/TechnicalNotes/tn35.html
- [8] Potter. P.D., ‘Use of Ka-band for Radio Metric Determination,’ NASA TDA Prog. Rept. 42-58, pp. 59–66, 15 Aug 1980. http://tmo.jpl.nasa.gov/progress_report/42-58/58N.PDF
- [9] Rochblatt, D., P. Richter, P Withington, M. Vazquez, and J. Calvo, ‘New Antenna Calibration Techniques in the Deep Space Network,’ NASA JPL IPN Progress Report, 42-169, pp. 1–34, 15 May 2007. http://tmo.jpl.nasa.gov/progress_report/42-169/169A.pdf
- [10] Sovers, Fanselow, & Jacobs, ‘Astrometry, Geodesy with Radio Interferometry: Expts., Models, Results,’ Rev. Mod. Phys., 70, 4, 1393–1454, Oct. 1998. <http://link.aps.org/doi/10.1103/RevModPhys.70.1393>
- [11] Whitney, Ruszczyk, Romney, & Owens, ‘Mark 5C VLBI Data System,’ this volume, 2010. ftp://ivscc.gsfc.nasa.gov/pub/general-meeting/2010/presentations/GM2010_S5T01_whitney.pdf

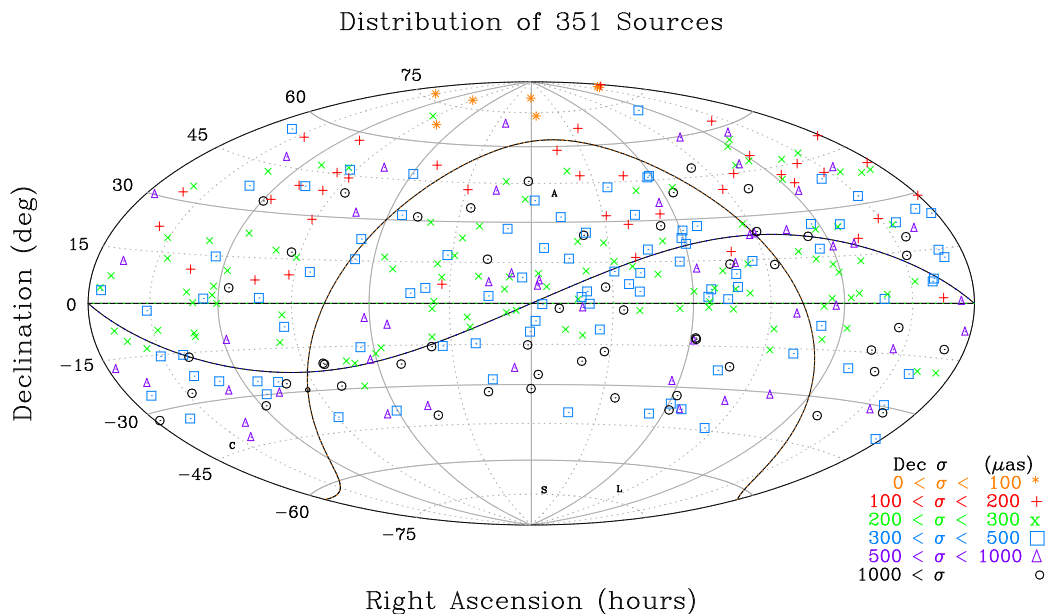


Figure 1. Distribution of 351 X/Ka-band sources detected to date. Symbols indicate 1- σ formal declination uncertainties as defined in the legend at lower right. $(\alpha, \delta) = (0, 0)$ is at the center. The ecliptic plane is indicated by the sinusoidal line. The galactic plane is indicated by the Ω -shaped line. Note the trend for decreasing declination precision moving southward. Local galactic neighborhoods indicated by A, C, S, L: Andromeda, Centaurus-A, Small & Large Magellanic clouds (none observed at X/Ka).

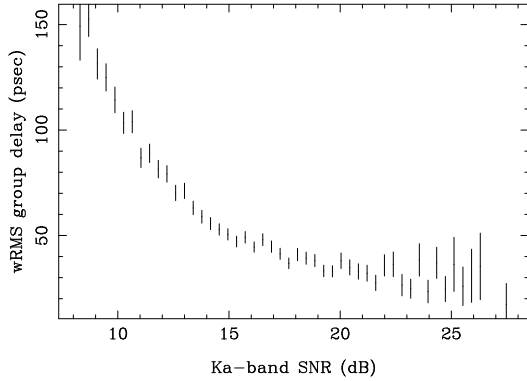


Figure 2. The wRMS residual group delay vs. Ka-band SNR. Thermal error dominates the VLBI residuals for SNR < 15 dB. As SNR increases past that point, a noise floor of ≈ 30 psec from tropospheric and instrumental errors is asymptotically approached.

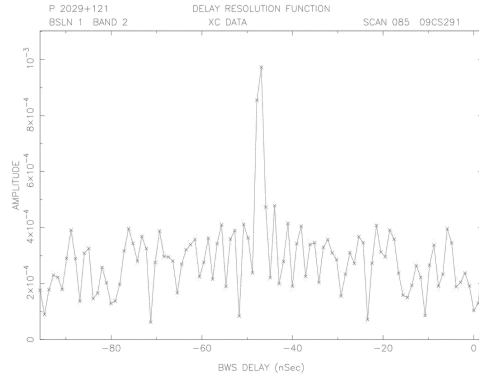


Figure 3. The first 448 Mbps fringes at X/Ka-band using the DSN: Day 291 of 2009, Goldstone to Madrid baseline using source P 2029+121 (one of several sources detected).

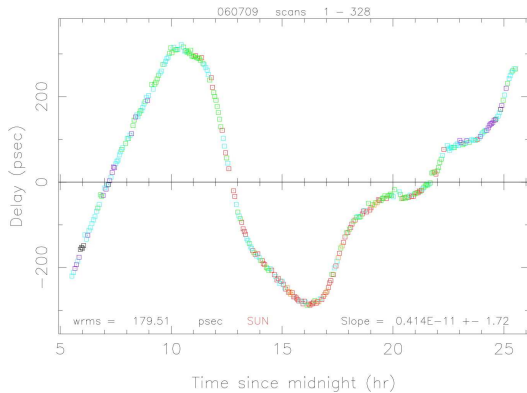


Figure 4. Ka-band proto-type phase calibrator group delays vs. time from 9 Jul 2006. Diurnal variation is driven by thermal changes in cables and other instrumentation. Color code indicates the sun angle (in order closest to farthest: orange, red, green, cyan, purple, black).

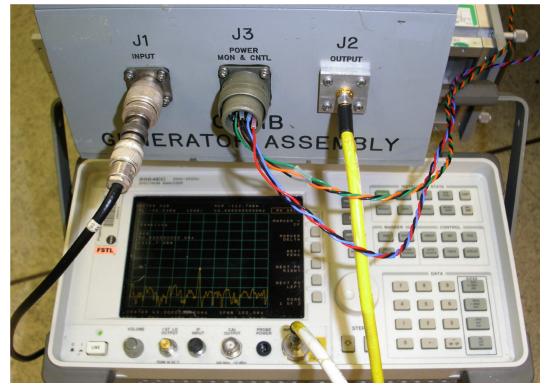


Figure 5. The first production Ka-band Phase Calibrator being tested on a spectrum analyzer. The calibration pulses are generated using a tunnel diode allowing operation up to 32 GHz. Design by Hammel, Tucker, & Calhoun (2003) based on a concept by A.E.E. Rogers.

Long-term Variations of the EOP and ICRF2

Vladimir Zharov ¹, Mikhail Sazhin ², Valerian Sementsov ², Olga Sazhina ²

¹) *Physics Department of Moscow State University*

²) *Sternberg State Astronomical Institute of Moscow State University*

Contact author: Vladimir Zharov, e-mail: zharov@sai.msu.ru

Abstract

We analyzed the time series of the coordinates of the ICRF radio sources. We show that part of the radio sources, including the “defining” sources, shows a significant apparent motion. The stability of the celestial reference frame is provided by a no-net-rotation condition applied to the defining sources. In our case this condition leads to a rotation of the frame axes with time. We calculated the effect of this rotation on the Earth orientation parameters (EOP). In order to improve the stability of the celestial reference frame we suggest a new method for the selection of the defining sources. The method consists of two criteria: the first one we call “cosmological” and the second one “kinematical”. It is shown that a subset of the ICRF sources selected according to cosmological criteria provides the most stable reference frame for the next decade.

1. Introduction

The first realization of the International Celestial Reference Frame (ICRF) was based on the positions of 608 compact extragalactic radio sources (quasars, active galactic nuclei (AGN), and blazars) [6]. The stability of the system axes is guaranteed by the precise positions of the “defining” radio sources. One assumes that the coordinates of these sources are known as precisely as possible. These sources are unresolved on VLBI baselines comparable to the Earth diameter, and it was assumed that variations of their coordinates are negligible.

The second realization of the International Celestial Reference Frame (ICRF2) was established in 2009. The ICRF2 contains five times more radio sources, and the noise floor is of the order of 40 μ as which leads to an axis stability of approximately 10 μ as [5]. Regardless of these values we

- show that many of the new defining sources show significant apparent motion;
- show that a small rotation of the CRF is transformed into long-term variations of the EOP;

and

- suggest a new source selection method to improve the stability of the reference frame.

To obtain the time series of the ICRF source coordinates we used the ARIADNA software. Solution “sai2009a.eops” was based on accepted positions of ICRF2 sources and precession-nutation model IAU2000. The terrestrial reference frame was fixed to the VTRF2008 coordinates and velocities of stations. Solution “sai2009b.eops” differs from the previous one by adding velocities for the sources. To calculate them we used the approximation of time series of coordinates by a polynomial model. The linear model with respect to regression polynomial coefficients β_i ($i = 0, 1, 2$) is

$$y(t) = \beta_0 + \beta_1 t + \beta_2 t^2 + \varepsilon(t), \quad (1)$$

where t is time, $y(t)$ are corrections ($\Delta\alpha \cos \delta$, $\Delta\delta$) to the ICRF coordinates (right ascension or declination) of a source, and $\varepsilon(t)$ are residuals. The coefficients of polynomials were found by regression analysis. The power of the polynomial was determined by R^2 statistics, where

$$R^2 = \frac{\sum(\hat{y}_j - \bar{y})^2}{\sum(y_j - \bar{y})^2} = 1 - \frac{\sum(y_j - \hat{y}_j)^2}{\sum(y_j - \bar{y})^2}. \quad (2)$$

Here y_j is the correction of right ascension or declination at the moment $t = t_j, j = 1, 2, \dots, N$, and \hat{y}_j is the estimation of the polynomial function at t_j , and \bar{y} is the average value of the series over whole interval. The value R depends on the correlation between y and \hat{y} [4]. Obviously, if the polynomial model is correct, that is values \hat{y}_j are equal to y_j , the coefficient $R = 1$. Actually, $\hat{y}_j \neq y_j$ and $R < 1$, but the maximal value of R corresponds to the best fitting model.

Below we show several examples of our data analyses. These figures represent a variation of the celestial coordinates as polynomial function of time. One can see that all of these sources, which are defining sources in the ICRF2 catalog, have significant apparent motion.

The motion of the source 0106+013, which was an “other” source in the ICRF, is shown in Fig. 1. The total number of observations is more than 1500. The motion is modeled by the linear function 41.6 ± 1.6 for α and 13.3 ± 2.0 for δ (in $\mu\text{as}/\text{year}$). The total number of observations of the former “candidate” source 0229+131 was more than 2500. The motion of it is quadratic along right ascension $2.1 \pm 0.1 \mu\text{as}/\text{year}^2$ and linear $1.8 \pm 1.5 \mu\text{as}/\text{year}$ along declination. And in the bottom part of Fig. 1 the motion of the “other” source 0536+145, which was observed ~ 50 times, is shown. The motion is linear with -8.9 ± 13.6 for α and -38.1 ± 19.8 for δ (in $\mu\text{as}/\text{year}$). The defining source 0556+238 of both the ICRF and ICRF2 has a significant linear motion along α (-19.8 ± 3.1) and δ (-15.2 ± 4.8 in $\mu\text{as}/\text{year}$). As we can see the values of velocities of the defining sources can reach a few tens of microarcseconds per year.

The fact that the ICRF sources have apparent motion was observed by several authors [7, 8, 11, 12], and special methods were developed for ranking of sources [5]. They are based on statistical properties of the position time series.

To increase the stability of the celestial reference frame we propose the following method for source selection. First of all, we consider kinematical characteristics of sources. We can predict the value of y_{N+1} and its confidence intervals outside the observed data span when we have a well-fit polynomial model of motion. We call a source stable if it has a small apparent motion, i.e., the confidence intervals of predicted corrections to right ascension and declination include zero value. Otherwise, if the model shows a significant difference of the correction to α or δ from zero, we can call this source unstable (at corresponding confidence level).

The analysis of data shows that many of the ICRF sources reveal significant apparent linear motion—their confidence intervals increase rapidly and do not include zero. Therefore we must consider them as unstable. Actually, one can subtract a well-predicted linear trend, and afterwards the confidence intervals include zero and this source can be considered as “stable”. To substantiate this possibility we consider the physical model of an ICRF source.

2. Blandford–Rees Model of Extragalactic Radio Sources

The apparent motion of extragalactic sources is a very intriguing fact. There are two reasons for such motion. The first one is that there are some real kinds of motion inside the source. The second one is that the light (radio waves) is refracted in a stochastic extragalactic media propagating from source to observer, which originates apparent motion of the source image.

From our point of view, the more realistic possibility is that there are motions inside the sources. The more appropriate model of the ICRF source is the unified AGN model [1, 2]. The main idea

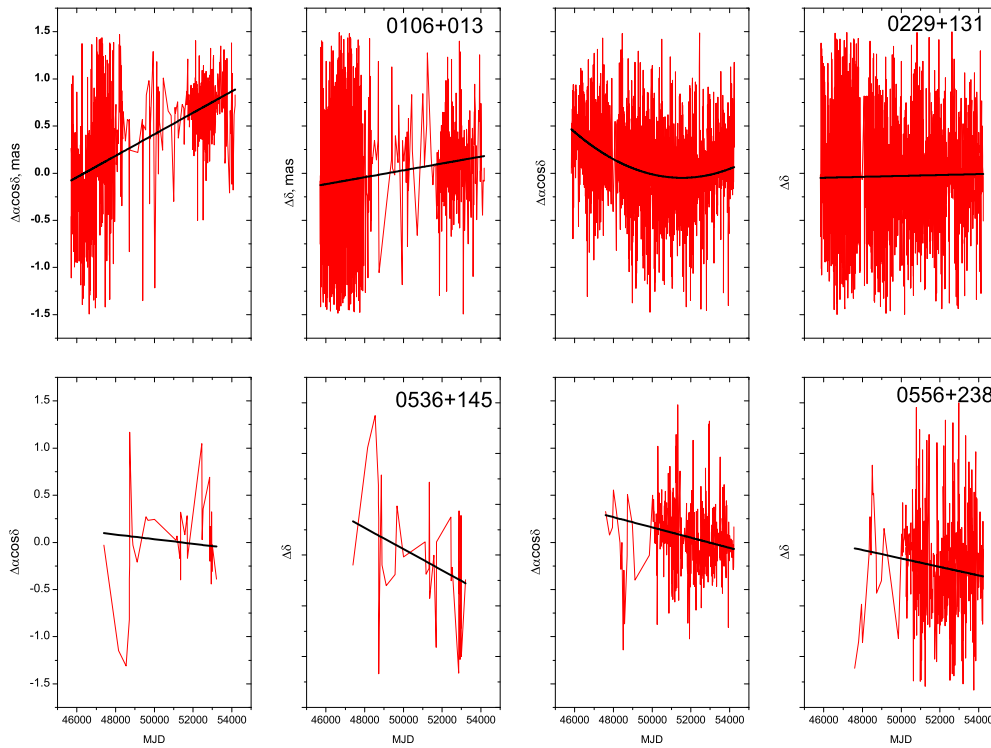


Figure 1. Right ascension (left) and declination (right) variations of the defining sources 0106+013, 0229+131, 0536+145, 0556+238 as function of time (MJD 46000 through 54000).

is that the quasars and AGN are objects that represent a system of a massive black hole and jets [15]. The optical radiation is formed in the black hole accretion disk while the radio emission is created in the jet, at some distance from the optical source (see also the recent discussion on the unification scheme of extragalactic radio sources in [3]). Below we refer to the radio source as “jet-core” instead of the optical core which coincides with the position of the massive black hole.

Taking into account the main properties of this model one can conclude that

- the ICRF radio source is the emission region (or jet-core) inside the jet;
- the position of the ICRF source is the position of the brightness center of the jet-core;
- the linear motion of the ICRF source can be explained by the jet precession mechanism [9, 13];
- the quadratic motion suggests some acting force and can be explained by acceleration of dense clouds inside the jet.

We assume that the linear apparent motion can be explained by the precession of the jet while quadratic apparent motion can be explained by the stochastic process of interaction of the jet particles with interstellar clouds. The period of jet precession is expected to be $10^3 \dots 10^6$ years [13]. One can expect that the stability of the jet precession angular velocity in such an object would be as low as several percent [10]. As the precession periods of the jets are significantly larger than the time of observation, the source motions can be treated as linear, stable, and predictable

with high accuracy for the time interval of VLBI observation of ~ 30 years, while the quadratic motion is stochastic and is unpredictable. As a result we restrict our consideration to two models

$$y(t) = \beta_0 + \beta_1 t + \varepsilon(t), \quad y(t) = \beta_0 + \beta_2 t^2 + \varepsilon(t),$$

and the decision of which model is valid is taken with the following criteria. We calculated R_1^2 (2) for the linear model and R_2^2 (2) for the quadratic model. If and only if $R_2^2/R_1^2 > 5$, we accept the quadratic model of apparent motion. Approximately two thirds of the sources show linear motion, and one third shows quadratic motion. As long as the linear motion is predictable and stationary for a long time, one can subtract the linear trend of the data and work with these “residual” data.

3. Cosmological Criterion for Choosing ICRF Sources

All other motions inside the radio source represent noise components of the astrometric observation. These motions occur inside some linear scale. The smaller the scale, the smaller the angular displacement seen by an observer. Hence, to decrease astrometric noise and to improve the coordinate system stability, we have to choose the most remote sources. It is correct in the Euclidean space: the more remote a source, the less the angular scale of its apparent motion. In the Friedman model of the expanding Universe it is not correct. Extragalactic objects have to be considered in expanding space-time and in the framework of the Standard Cosmological Model.

According to this model, the apparent angular size of the source has a minimum for redshift $z = 1.63$. An object located at this distance with a physical size of about 1 pc has an angular size of $\theta = 116 \mu\text{as}$. This is the minimal angular size of an object, and it will increase for $z < 1.63$ and for $z > 1.63$. It was shown that the redshift interval $0.8 \leq z \leq 3.0$ is the most favorable in terms of the physical shift inside such sources corresponding to the minimal apparent angular shift of a “jet-core”. Details of these calculations can be found in [9]. After tagging sources as “unstable” and “stable” according to the “kinematical” and “cosmological” criteria, we obtained a final list of 137 sources (see Table 1 in [9]).

4. The ICRF System Instability

As was pointed out, the main purpose of selecting “stable” sources is the improvement of the stability of the celestial reference frame that is connected with the predictability of source motion. The variation of the ICRF source coordinates leads to a small rotation of the reference frame. To estimate the stability of the frame three small angles $\theta_1, \theta_2, \theta_3$, which describe the small rotation, were calculated:

$$\mathbf{s}(t) = \begin{pmatrix} 1 & -\theta_3 & \theta_2 \\ \theta_3 & 1 & -\theta_1 \\ -\theta_2 & \theta_1 & 1 \end{pmatrix} \mathbf{s}(t_0)$$

where $\mathbf{s}(t), \mathbf{s}(t_0)$ are unit vectors of a source at moments t and $t_0 = J2000.0$. As was shown in [14] the method of “cosmological” selection improves the stability of the ICRF over the next decade.

The rotation of the reference frame is transformed to the secular variations of the EOP. From the difference of solutions “sai2009a.eops” and “sai2009b.eops” a linear trend in the x-coordinate of the pole equal to $-2.77 \pm 0.22 \mu\text{as}/\text{year}$ was found. The variations of the y-coordinate of the pole and the nutation in longitude and obliquity are $1.60 \pm 0.15 \mu\text{as}/\text{year}$, $0.47 \pm 0.46 \mu\text{as}/\text{year}$, and $-0.54 \pm 0.15 \mu\text{as}/\text{year}$, respectively; and UT is $0.144 \pm 0.007 \mu\text{s}/\text{year}$.

5. Conclusions

The physical basis of the “cosmological” and “kinematical” criteria is the assumption that the apparent motion of the ICRF radio sources is connected with real motion inside quasars. Therefore apparent angular motion corresponds to a real physical shift of the “jet-core” inside a radio source. The motion of the defining sources is transformed to secular variations of the EOP.

The red-shift interval $0.8 \leq z \leq 3.0$ is the most favorable in terms of the physical shift inside such sources corresponding to a minimal apparent angular shift of a “jet-core”. The method of “cosmological” selection improves the stability of the ICRF over the next decade.

Acknowledgements

This work has been supported by the Russian Foundation for Basic Research grants 10-02-00961-a and 08-02-00971, grant of the President of RF MK-473.2010.2 (O.S.).

References

- [1] Begelman M.C., Blandford R.D., Rees M.J., 1984, *Rev. Mod. Phys.*, **56**, 255
- [2] Blandford R.D., Königl A., 1979, *AJ*, **232**, 34
- [3] Browne, I.W.A. The Role of VLBI in Astrophysics, Astrometry and Geodesy. Proc. of the NATO Advanced Study Institute, held September 17-29, 2001, in Bologna, Italy. Series II, mathematics, physics and chemistry, Vol. 135. Edited by Franco Mantovani and Andrzej Kus. Published by Kluwer Academic Publishers, Dordrecht, The Netherlands, 2004, p.175
- [4] Draper N.R., Smith H. Applied Regression Analysis. 3-rd edition. John Wiley & Sons, Inc. 1998.
- [5] The Second Realization of the International Celestial Reference Frame by Very Long Baseline Interferometry Presented on behalf of the IERS. Alan L. Fey, David Gordon, and Christopher S. Jacobs (eds.) IERS Technical Note No. 35. Verlag des Bundesamts für Kartographie und Geodäsie. Frankfurt am Main 2009.
- [6] Ma C., Arias E.F., Eubanks T.M., et al., *AJ*, **116**, 516, 1998.
- [7] MacMillan D.C., 2003, in Romney J.D., Reid M.J., eds, Future Directions in High Resolution Astronomy, (The 10th Anniversary of the VLBA ASP Conference series). astro-ph/0309826
- [8] MacMillan D.S., & Ma C. 2007, *J. of Geodesy*, **81**, 443
- [9] Sazhin M.V., Sementsov V.N., Zharov V.E., Kuimov K.V., Ashimbaeva N.T., Sazhina O.S., 2009, arXiv:0904.2146v1
- [10] Davydov V.V., Esipov V.F., Cherepashchuk A.M., *Astronomy Reports*, **52**, p. 487, 2008.
- [11] Titov O., 2008, Proper motion of reference radio sources, arXiv:0804.1403
- [12] Titov O., 2008, Systematic effects in apparent proper motion of radio sources, arXiv:0805.1099
- [13] Zharov V.E., Sazhin M.V., Sementsov V.N., Kuimov K.V., Sazhina O.S., *Astron. Rep.*, **53**, 579, 2009.
- [14] Zharov V.E., Sazhin M.V., Sementsov V.N., Kuimov K.V., Sazhina O.S., and Ashimbaeva N. T., 2009, The celestial reference frame stability and apparent motions of the radio sources. In Proc. IAU Symposium No. 261, S. A. Klioner, P. K. Seidelman & M. H. Soffel, eds. p.50–55.
- [15] Zensus J. Anton. *Annu.Rev.Astron.Astrophys.* 1997, v.**35**, p.607-636.

Long-term Stability of Radio Sources in VLBI Analysis

Gerald Engelhardt, Volkmar Thorandt

Bundesamt für Kartographie und Geodäsie

Contact author: Gerald Engelhardt, e-mail: gerald.engelhardt@bkg.bund.de

Abstract

Positional stability of radio sources is an important requirement for modeling of only one source position for the complete length of VLBI data of presently more than 20 years. The stability of radio sources can be verified by analyzing time series of radio source coordinates. One approach is a statistical test for normal distribution of residuals to the weighted mean for each radio source component of the time series. Systematic phenomena in the time series can thus be detected. Nevertheless, an inspection of rate estimation and weighted root-mean-square (WRMS) variations about the mean is also necessary. On the basis of the time series computed by the BKG group in the frame of the ICRF2 working group, 226 stable radio sources with an axis stability of $10 \mu\text{as}$ could be identified. They include 100 ICRF2 axes-defining sources which are determined independently of the method applied in the ICRF2 working group. 29 stable radio sources with a source structure index of less than 3.0 can also be used to increase the number of 295 ICRF2 defining sources.

1. General Information

Presently, complete global geodetic VLBI solutions with nearly 30 years of data are possible. Stable compact radio sources can be modeled with only one source position for the whole time span. Unstable radio sources known to have high-level source structure complexity are not suitable for this. They would cause a modeling error. So the question arises: which radio sources are stable? Possible approaches for the answer to this question are the estimation and analysis of time series of radio source positions or, independently of this statistical method, the use of the list of structure indices of radio sources determined by P. Charlot (2009) [1].

2. Time Series for Radio Source Positions

Our basis for deriving time series of radio source positions is a complete global VLBI solution with 24-hour VLBI sessions from January 1984 to July 2007. The main parameter types are globally estimated station coordinates and their velocities and 183 preliminarily stable radio source positions from former investigations [2]. The datum definition was realized by applying no-net-rotation and no-net-translation conditions for 26 selected station positions and velocities with respect to VTRF2005 and a no-net-rotation condition for 183 preliminarily stable sources with respect to ICRF1. All other source positions were estimated in a local mode in each session for generating the time series. This solution is called base solution 1. But there is a problem. This solution does not produce time series for the 183 preliminarily stable radio sources. One possibility for solving this is to reduce the set of stable radio sources for the datum definition by one source. A separate solution with no other changes referring to the base solution 1 yields estimates of local source positions for this selected radio source in the respective sessions. An advantage of this procedure is that there is nearly no change in datum definition for generating time series for all

radio source positions. A disadvantage is the separate calculation for each of the 183 preliminarily stable radio sources. After these additional computations time series for all radio sources are available.

3. Weighted Mean and Outlier Detection for Each Radio Source

On the condition that all radio sources are stable, the weighted mean for each radio source component can be estimated from the time series with locally determined source positions and their standard deviations. To increase the reliability of the used data, an outlier test [2] was applied, which tested the maximum amount of the residual w.r.t. the weighted mean. If an outlier was detected, the corresponding data point was not used in the new estimation of the weighted mean.

4. Test for Normal Distribution

Based on time series of radio source positions, residuals to the weighted mean of a radio source component can be tested for normal distribution. At least 12 sessions should be available for a radio source. Time series with less than 12 sessions are not considered for the test. The purpose of the test is to detect systematic phenomena in the time series of radio source positions. The basis is a smooth test between the empirically determined distribution and the theoretical normal distribution [2]. The parameters of the normal distribution are the mean value and the variance s^2 computed from the sample (residuals). The test statistic χ^2 is computed by

$$\chi^2 = \sum_{m=1}^r \frac{(h_m - np_m)^2}{np_m}$$

where

r number of classes ($r = 10$), class width = $s/2$,

m current number of classes,

n number of values in the time series of a source component,

h_m empirical absolute frequency of class m , and

p_m theoretical probability of class m .

The confidence level χ_s^2 is listed in a table of the chi-square distribution with the significance level of 1 percent. The decision rule says here, if $\chi^2 < \chi_s^2$ than the distribution of the sample (residuals) is in no contradiction with the assumption that it comes from a statistical universe. So systematic phenomena could not be proven. But if $\chi^2 > \chi_s^2$ than the distribution of the sample (residuals) is in contradiction with the assumption that it comes from a statistical universe. So systematic phenomena could be proven: e.g., instabilities of radio source components exist.

5. Further Inspections

The sources with a successful test for normal distribution of the residuals to the weighted mean were also checked concerning the following empirically determined criteria. The computed rate in the time series of right ascension and declination of the radio source should be less than or equal

to $|0.1|$ mas per year, the ratio of rate and error of rate should be less than $|3.5|$, the WRMS should be less than or equal to 1 mas, and the total time span of observations per source should be greater than 3 years.

6. Results

Altogether 1189 radio sources with position time series were available, 482 of which were investigated with at least 12 sessions. The normal distribution was not rejected for 226 radio sources ($\chi^2 < \chi_s^2$), i.e. 194 sources in both components and 32 sources in only one component. The further inspections of rate, sigma of rate, WRMS, and the total time span per source were successfully tested as well. The distribution of the 226 stable radio sources are depicted in Figure 1. The identified 226 stable sources can be compared with the mean source structure index (SI) values determined by Charlot (2009) [1]. SI values for 215 sources are available. 116 sources could be found with SI less than 3.0. That is the limit for the selection of the ICRF2 defining sources [3]. 99 sources have an SI greater than or equal to 3.0.

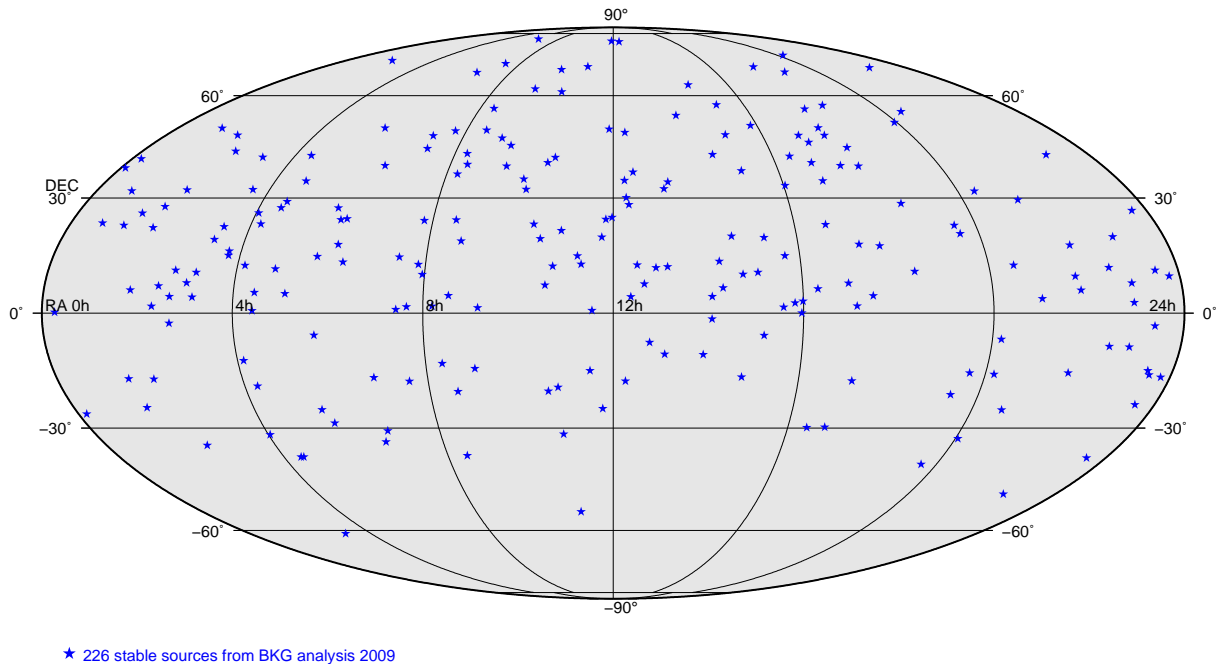


Figure 1. Distribution of 226 stable radio sources from BKG analysis 2009.

Another comparison can be made with the official 295 ICRF2 defining sources [3]. The number of identical sources is 100. The number of sources with insufficient data in the BKG analysis is 46 and there are no data for 31 sources. The number of sources which did not comply with the BKG stability criteria is 118. An important fact is that 29 stable sources from the BKG analysis with SI less than 3.0 are stable enough to increase the official 295 ICRF2 defining sources (Figure 2).

Time series and results are available at <http://ivs.bkg.bund.de/vlbi> or ftp://ivs.bkg.bund.de/pub/analysis/radio_source_positions_time_series.

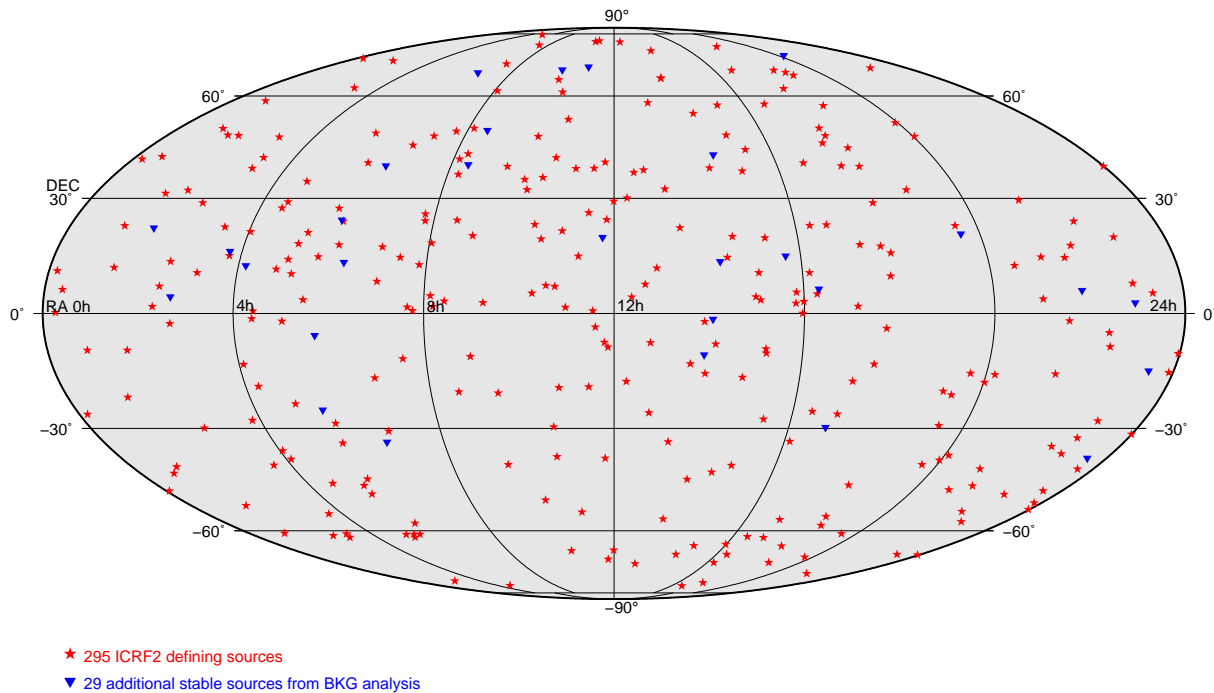


Figure 2. Distribution of the 295 ICRF2 defining sources and 29 additional stable sources from the BKG analysis 2009.

7. Axis Stability

To assess the axis stability by a set of radio sources the following procedure was applied. Radio source position time series are the basis for the computation of annual reference frames. The next step is the estimation of the relative orientation between the annual reference frames and a reference catalog. The scatter (WRMS) of the rotation parameters from the annual reference frames is then a measure for the stability of the axes of the ICRF. The equation for the estimation of the rotation parameters ϵ for one source position is

$$\begin{pmatrix} X_i \\ Y_i \\ Z_i \end{pmatrix}_{time\ series} = \begin{pmatrix} 1 & \epsilon_Z & \epsilon_Y \\ -\epsilon_Z & 1 & \epsilon_X \\ \epsilon_Y & -\epsilon_X & 1 \end{pmatrix} \begin{pmatrix} X_{ref} \\ Y_{ref} \\ Z_{ref} \end{pmatrix}_{reference\ catalog}$$

with previous source position transformation from right ascension and declination to X, Y, Z. Least squares estimation in consideration of source position errors was applied to get the yearly rotation parameters. Table 1 shows the scatter (WRMS) of the rotation parameters derived from different sets of sources.

The accuracy of ϵ_{XYZ} for the sets with 226 stable BKG sources and 295 ICRF2 defining sources is nearly the same, but it is almost two times better compared to the set of the 212 ICRF1 defining sources.

Table 1. Scatter (WRMS) of rotation parameters derived from different sets of sources with input time series bkg000c.ts and reference catalog gsf008a.cat

Set of sources	Number of sources available	WRMS	WRMS	WRMS	WRMS
		ϵ_X	ϵ_Y	ϵ_Z	ϵ_{XYZ}
		μas	μas	μas	μas
212 ICRF1 defining sources	211	15.2	7.4	24.3	16.5
226 stable BKG sources	226	3.4	6.2	14.6	10.4
295 ICRF2 defining sources	264	8.3	8.8	9.1	8.8

8. Conclusions

Generating and statistically analyzing time series of radio source positions are useful to get more information about long-term stability of radio sources. After a successful test for normal distribution of residuals to the weighted mean of both radio source components also an inspection of rate, sigma of rate, WRMS, and total time span per source are necessary to identify stable sources.

A set of 226 stable radio sources could be identified by this method with an axis stability of 10 μas . 100 ICRF2 axes-defining sources could be verified independently of the method applied in the ICRF2 working group. 29 stable sources from the BKG analysis 2009 with an SI value less than 3.0 can be used to increase the number of the official 295 ICRF2 defining sources.

References

- [1] Charlot Patrick et al (2009): Characterization of Source Structure, In: IERS Technical Note No. 35: The Second Realization of the International Celestial Reference Frame by Very Long Baseline Interferometry, edited by A. Fey, D. Gordon, C. Jacobs (2009).
- [2] Engelhardt G., Thorandt V. (2006): First steps to Investigate Long-Term Stability of Radio Sources in VLBI Analysis, In: IVS 2006 General Meeting Proceedings, Concepcion, Chile, edited by D. Behrend and K.D. Baver, NASA/CP-2006-214140, p.281-285.
- [3] Lambert Sebastien et al (2009): Selection of ICRF2 Defining Sources, In: IERS Technical Note No. 35: The Second Realization of the International Celestial Reference Frame by Very Long Baseline Interferometry, edited by A. Fey, D. Gordon, C. Jacobs (2009).

The Position/Structure Stability of Four ICRF2 Sources

Ed Fomalont ¹, Kenneth Johnston ², Alan Fey ², Dave Boboltz ², Tomoaki Oyama ³,
Mareki Honma ³

¹) *National Radio Astronomy Observatory*

²) *United States Naval Observatory*

³) *National Astronomical Observatory of Japan*

Contact author: Ed Fomalont, e-mail: efomalon@nrao.edu

Abstract

Four compact radio sources in the International Celestial Reference Frame (ICRF2) catalog were observed using phase referencing with the VLBA at 43, 23, and 8.6-GHz, and with VERA at 23-GHz over a one-year period. The goal was to determine the stability of the radio cores and to assess structure effects associated with positions in the ICRF2. Conclusions are: (1) 43-GHz VLBI high-resolution observations are often needed to determine the location of the radio core. (2) Over the observing period, the relative positions among the four radio cores were constant to 0.02 mas, suggesting that once the *true* radio core is identified, it remains stationary in the sky to this accuracy. (3) The emission in 0556+238, one of the four sources investigated and one of the 295 ICRF2 defining sources, was dominated by a strong component near the core and moved 0.1 mas during the year. (4) Comparison of the VLBA images at 43, 23, and 8.6-GHz with the ICRF2 positions suggests that the 8-GHz structure is often dominated by a bright non-core component. The measured ICRF2 position can be displaced more than 0.5 mas from the radio core and partake in the motion of the bright jet component.

1. Source Selection, Observations, Reductions, and Imaging

The Second Realization of the International Celestial Reference Frame (ICRF2) is defined by the positions of 295 compact radio sources located around the sky [1]. The position uncertainties for many of these sources is less than 0.06 mas, obtained by averaging decades of observations. This positional accuracy is presently limited by residual variable tropospheric refraction; however, with the improved modeling of the troposphere, the effects of variable source structure is becoming a comparable error component in determining the position of an ICRF2 source. Using interferometric phase referencing among four sources within a three-degree radius, the tropospheric effects largely cancel, and the structure effects with time and frequency can be more accurately determined.

The sources were selected to accommodate observations by the VLBI Exploration of Radio Astrometry (VERA) four-element VLBI array in Japan that can observe two sources simultaneously if they are separated by no more than 2.2°. A search of the 8.6-GHz ICRF2 catalog found several groups of sources, and we chose 0547+234, 0554+242, 0556+238, and 0601+245. They are all compact, and the source 0556+238 is one of the 295 defining sources in the ICRF2 catalog.

Four VERA sessions at 23-GHz and six VLBA sessions at 23-GHz and 43-GHz were observed between Apr 2008 and Dec 2009. One VLBA session at 8.6-GHz was added in Jan 2010. Because of the higher resolution of the VLBA and the use of 43-GHz, the major results of this paper will be obtained from the VLBA sessions alone. However, the VERA images were consistent with that of the VLBA.

For each VLBA session, the observing sequence used was a repetition of 0556-0547-0556-0554-0556-0601-0555-0547. Each scan was 18 sec in length, with 10 sec needed for source switching. The

separation between the center of two 0556+238 scans was only 55 sec, sufficiently close in time to maintain phase coherence at 43-GHz except under adverse weather conditions or for observations at low elevations. The basic sequence among the four sources took 3 min, and ten sequences were made over a 30-minute period. These 30-minute blocks were then alternated between 23-GHz and 43-GHz observing frequencies. The center frequencies were at 22.45-GHz and 43.41-GHz.

The data were calibrated using 0556+238 as the primary reference to determine the delay and phase associated with the clock offsets, the astrometric model errors, and the troposphere delay in the vicinity of the sources. After calibration, each source for each session and frequency was imaged, cleaned and then phase self-calibrated, using the initial reference image. In this way, the image quality was improved, but the astrometric information was unchanged to a level of 0.01 mas.

2. The Morphology and Evolution of Each Source

The VLBA images for five sessions for the sources at 43 and 23-GHz are shown in Figure 1. From analysis of the images, the radio core component for each source could be ascertained using some or all of the following properties: flat spectral index, location at the end of the structure, compactness, and lack of proper motion. The core components are labeled for each source by the symbol **0**, with other numbers used to designate other components. Without these high-resolution high-frequency data, determination of the core would have been ambiguous for 0554+242, 0556+238, and 0601+245.

The images, all registered with respect to 0556+238, showed that the radio cores of 0547+234, 0554+242, and 0601+245 were moving in the southern direction by about 0.1 mas/year! This suggested an astrometric problem with the phase reference calibrator. Careful modeling of its structure at 23 and 43-GHz showed that the source was composed of two close components: the brighter component to the north and a fainter component to the south, with a separation that increased from 0.1 to 0.2 mas during the year. The weaker southern component has a flat spectral index and its motion was consistent with the other three radio cores. Hence, it is the radio core for 0556+238 and has been labeled as **0** in Figure 1. Additional analysis of previous observations of this source at 23-GHz and 8.6-GHz also suggest that its position over the years has been somewhat unstable [3, 4].

The relative position of the four radio cores change by less than about 0.02 mas/yr over the observational period. This result demonstrates that once the location of the radio core is identified with the emission from a radio source, its position is stable to the above accuracy. Future comparison of the core position of radio sources and the position from future space-optical interferometers can, thus, in principle be made at the tens of microarcsecond level.

3. Comparison with the ICRF2 and the VLBA 8.6-GHz Positions

The comparison of the ICRF2 position, the VLBA 43-GHz image and the VLBA 8.6-GHz image (Jan 2010) for each source is shown in Figure 2. For the three sets of images, 0556+238, even with its internal structure changes, was used to align the VLBA 43 and 8.6-GHz positions with the ICRF2 catalog. The position of $\alpha = 05^h59^m32.03313165^s$, $\delta = 23^\circ53'53.9267683''$, with an estimated error of 0.04 mas in both coordinates, was assumed to lie between the two components at 43-GHz with an estimated error of about 0.1 mas to overlap either component. For the VLBA 8.6-GHz image, the northern component is much brighter than the southern component, hence

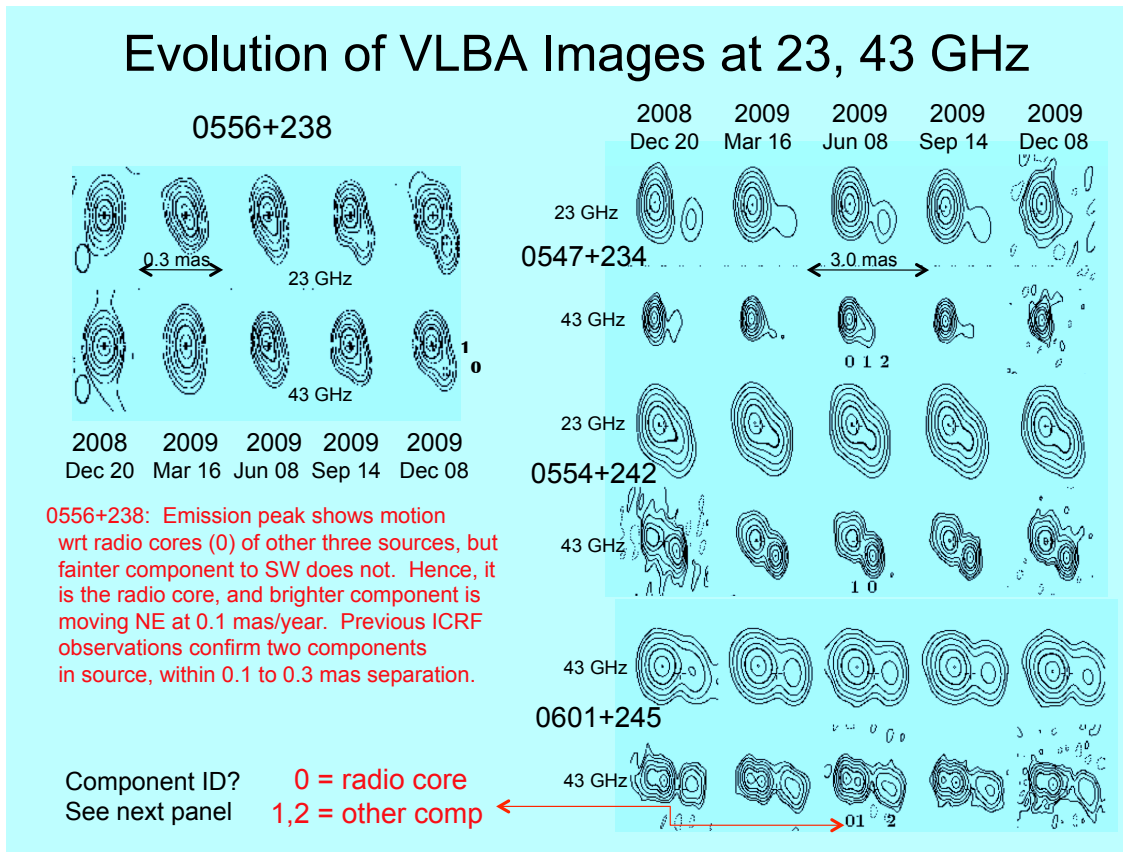


Figure 1. Evolution of the four sources: The left side of the figure shows the structure change of 0556+238. The radio core is identified with the southern component that is clearly seen in the last two sessions. The right side of the figure shows the evolution of the other three sources. The number labels are for the components in each source: 0 is the radio core; 1 and 2 are the additional components. The + shows the location of the assumed phase center for each source.

the peak intensity at this frequency was assumed to be located at the peak emission location of the northern component of the 43-GHz image. These alignment uncertainties, however, are considerably smaller than the large position offsets described in the next few paragraphs.

Although 0547+234 is dominated by a strong radio core, the ICRF2 position, the 43-GHz core position, and the 8.6-GHz position in Jan 2010 are all significantly different. Since this source was not frequently observed during the ICRF2 sessions over the last few decades, the estimated position error may be underestimated. The displacement in the VLBA 43-GHz and VLBA 8.6-GHz position is significant, however. The position at 8.6-GHz may be influenced by the blending of the diffuse emission to the west, blending with the core more strongly at the lower frequency. This source gives a good example of core-shifts with frequency that have been observed for other compact radio sources [5].

The double structure of 0554+242 produces different position estimates, depending on the frequency and resolution. At 43-GHz, the western component is clearly identified as the radio core, and its position should be associated with that of the source. The 8.6-GHz VLBA image, on the other hand, is dominated by the strong, steep-spectrum eastern component, and its position is

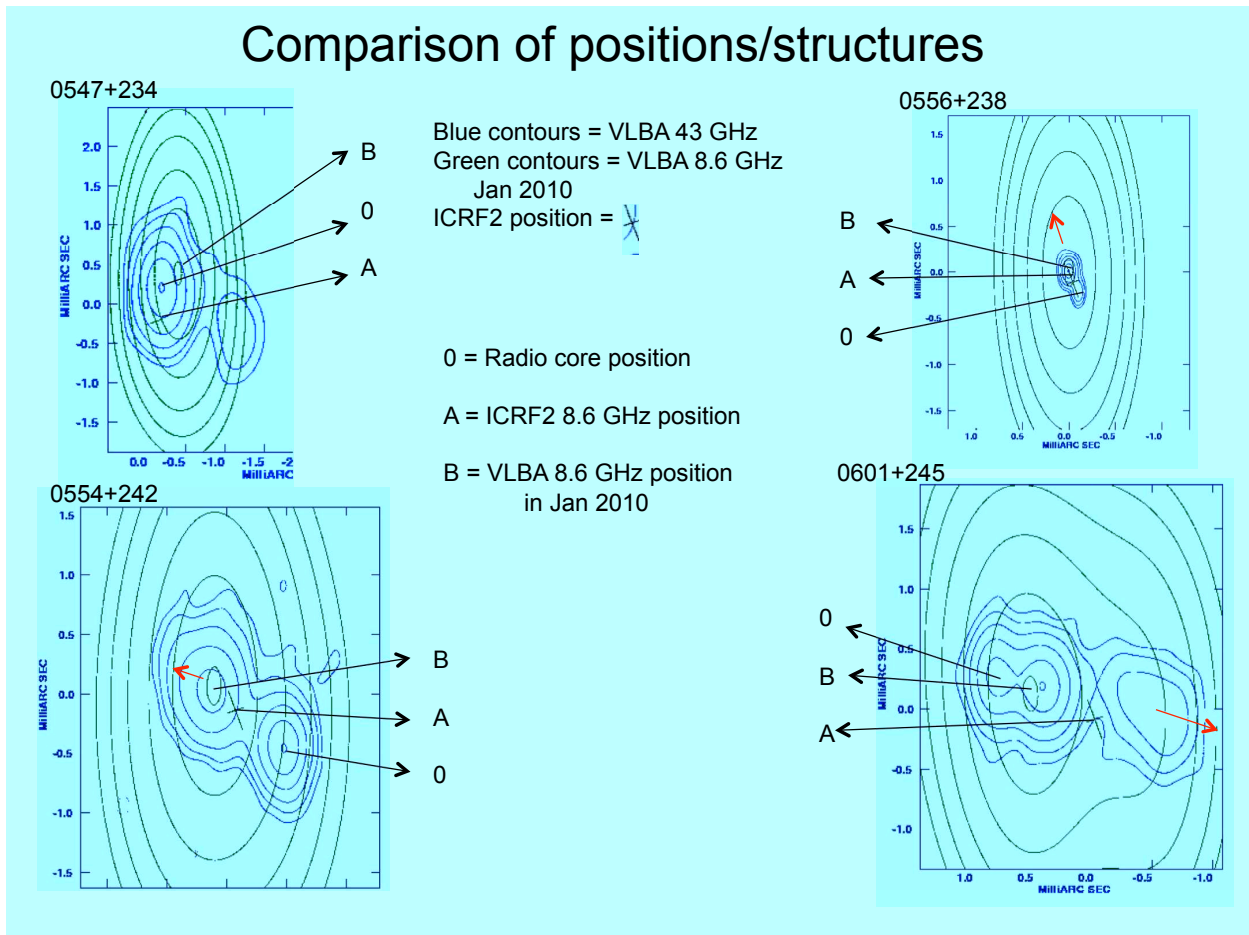


Figure 2. The comparison of the positions and structure of the four sources: The 8.6-GHz Jan 2010 VLBA structures are shown by the green contours (the larger oval and quasi-oval lines). The 43-GHz Dec 2009 VLBA structures are shown by the blue contours that are well within the 8.6-GHz structure. The ICRF2 position is shown by the tilted cross and is labeled by **A**. The radio core position is labeled by **O**, and the VLBA 8.6-GHz position in 2010 is labeled by **B**. The motions of some components are indicated by the arrows.

considerably east of the radio core. The ICRF2 position of 0554+242 is located between the two components, about 0.6 mas from the core position. The difference in the ICRF2 position and the VLBA 8.6-GHz position is likely caused by the motion of the eastern component away from the core over the last ten years.

The source structure of 0601+245 is complex, but analysis of the 23 and 43-GHz images suggests that the radio core is associated with the component at the eastern part of the emission. The peak of the VLBA 8.6-GHz image (hence its position) is near the middle component which has

a relatively steep spectral index and would thus dominate the emission at 8.6-GHz. The ICRF2 position is displaced about 0.7 mas to the west of the radio core. Without a detailed reanalysis of the many ICRF2 observations that contributed to the position determination of this source, the cause of the displacement cannot be ascertained. It is possible that its position may be weighted from previous observations when the western component was brighter and closer to the radio core.

4. Summary

Using phase referencing at 43-GHz on four close sources, the relative positions of the sources were obtained to about 0.02 mas accuracy. The radio cores of the sources were identified, but 43-GHz and 23-GHz VLBI observations over one year were required to determine the location of the radio core. The relative positions of the radio cores in the four sources remain constant to within 0.02 mas over the year.

The comparison of the ICRF2 positions with the radio images obtained with the VLBA at 43-GHz and 8.6-GHz show structure-induced offsets between the ICRF2 position and that of the radio core. These offsets can be as large as 1.0 mas and vary with time. The development of a celestial reference frame at frequencies higher than 8.6-GHz would alleviate the positional error induced by structure, and recently observations to determine an all-sky catalog at 23 and 43-GHz were initiated for this reason [3, 4]. Future comparison with GAIA will also require the location of the radio core.

References

- [1] Fey, Alan L., Gordon, David, & Jacobs, Christopher S. 2010, IERS / IVS Working Group, “The Second Realization of the International Celestial Reference Frame by Very Long Baseline Interferometry”, IERS Technical Note No. 35: <http://www.iers.org/IERS/EN/Publications/TechnicalNotes/tn35.html>
- [2] Mioduszewski A. & Kogan, L. 2010, AIPS memo 110
<ftp://ftp.aoc.nrao.edu/pub/software/aips/TEXT/PUBL/AIPSMEM110.PS>
- [3] Charlot, P., Boboltz, D. A., Fey, A. L., Fomalont, E. B., Geldzahler, B. J., Gordon, D., Jacobs, C. S., Lanby, G. E., Ma, C., Naudet, C. J. et al. 2010, AJ, 139, 1695
- [4] Lanyi, G. E., Boboltz, D. A., Charlot, P., Fey, A. L., Fomalont, E. B., Geldzahler, B. J., Gordon, D., Jacobs, C. S., Ma, C., Naudet, C. J. et al. 2010, AJ, 139, 1695
- [5] Kovalev, Y. Y., Lobanov, A. P., Pushkavev, A. B. & Zensus, J. A. 2008, A&A, 483, 759

Rotational Alignment Altered by Source Position Correlations

C. S. Jacobs, M. B. Hefflin, G.E. Lanyi, O. J. Sovers, J. A. Steppe

Jet Propulsion Laboratory, California Institute of Technology

Contact author: C. S. Jacobs, e-mail: Chris.Jacobs@jpl.nasa.gov

Abstract

In the construction of modern Celestial Reference Frames (CRFs) the overall rotational alignment is only weakly constrained by the data. Therefore, common practice has been to apply a 3-dimensional No-Net-Rotation (NNR) constraint in order to align an under-construction frame to the ICRF. We present evidence that correlations amongst source position parameters must be accounted for in order to properly align a CRF at the 5–10 μas level of uncertainty found in current work. Failure to do so creates errors at the 10–40 μas level.

1. Introduction to No-net-rotation Constraint Equations

Since the adoption of the ICRF [4] by the IAU in 1997 [1], the axes which define Right Ascension and declination have been realized by an ensemble of quasar positions. Subsequent frames, most notably the ICRF2 [5], have been aligned to the original ICRF by imposing a 3-dimensional No-Net-Rotation (NNR) constraint in the form of the cross-product (see full derivation in appendix),

$$\sum_{i=1}^{N_{src}} s_{0i} \times \Delta s_i = 0 \quad (1)$$

where for a set of N_{src} sources,

$$s_{0i} = (\cos \alpha_{0i} \cos \delta_{0i}, \sin \alpha_{0i} \cos \delta_{0i}, \sin \delta_{0i}) \quad (2)$$

is the unit vector in the reference source direction for the i^{th} source of coordinates $(\alpha_{0i}, \delta_{0i})$ and Δs_i is the difference of the reference position from the estimated position.

$$\begin{aligned} s_{0i} \times \Delta s_i = & [-\cos \alpha_{0i} \sin \delta_{0i} \cos \delta_{0i} \Delta \alpha_i + \sin \alpha_{0i} \Delta \delta_i], \\ & [-\sin \alpha_{0i} \sin \delta_{0i} \cos \delta_{0i} \Delta \alpha_i - \cos \alpha_{0i} \Delta \delta_i], \\ & [\cos^2 \delta_{0i} \Delta \alpha_i] \end{aligned} \quad (3)$$

The above triplet of constraints affects both the estimated set of α_i and δ_i and their associated covariance including the correlations amongst parameters.

The MODEST linear least squares fit software [7] requires the coefficient with respect to $\Delta \alpha_i$ and $\Delta \delta_i$ of each rotation constraint, $C_j = (\sum_i s_{0i} \times \Delta s_i)_j$ where j goes from 1 to 3. The result is

$$\partial C_1 / \partial \Delta \alpha_i = -\cos \alpha_{0i} \sin \delta_{0i} \cos \delta_{0i}, \quad \partial C_1 / \partial \Delta \delta_i = \sin \alpha_{0i} \quad (4)$$

$$\partial C_2 / \partial \Delta \alpha_i = -\sin \alpha_{0i} \sin \delta_{0i} \cos \delta_{0i}, \quad \partial C_2 / \partial \Delta \delta_i = -\cos \alpha_{0i} \quad (5)$$

$$\partial C_3 / \partial \Delta \alpha_i = \cos^2 \delta_{0i}, \quad \partial C_3 / \partial \Delta \delta_i = 0 \quad (6)$$

Note that the constraint Eq. (1) is unweighted in the position parameters, s . The MODEST software implements constraints by treating them as pseudo-observations with given uncertainties. Specifying a vanishingly small uncertainty is equivalent to using an absolute constraint.

Using the preceding partials (Eqs. 4, 5, 6), each C_j was separately constrained to be zero to within a tight constraint uncertainty of $\sigma_j = 10^{-10}$ radians.

2. Sensitivity of S/X, K, and X/Ka Frame Alignment to Correlations

Our procedure was first to estimate source positions under the influence of unweighted NNR constraints (Eq. 1) to the ICRF2 defining sources. We used only sources with at least three sessions, ten delay observations, and a formal error ellipse major axis smaller than 5 nrad, and which were also in the ICRF2 defining list.

Second, we did an after-the-fact verification that the NNR constraints indeed kept the positions from rotating with respect to the defining sources by estimating a 3-D rotation with respect to the ICRF2 defining sources.

This second step was done using alternately diagonal-only parameter covariance and full covariance for the Celestial Reference Frame (CRF) being constrained. The reference, ICRF2, always used diagonal covariances because the off-diagonal correlations are not published.

The results for three data sets are given in Table 1 with descriptions of the sets as follows:

- The S/X data set included observations from October 1978 to September 2009 totalling 5.3M observations from 1709 sources. The NNR constraint used 267 ICRF2 defining sources.
- The K-band data set [3] covers 2002 to 2009 with over 100,000 observations of 275 sources. The NNR constraint used 125 ICRF2 defining sources.
- The X/Ka-band data set [2] covers 2005 to 2010 with over 10,000 observations of 387 sources. The NNR constraint used 153 ICRF2 defining sources.

Table 1. 3-D Rotations (μas) estimated *with* vs. *without* correlations.

CRF	N_{Def}	R_1	σ_{R_1}	R_2	σ_{R_2}	R_3	σ_{R_3}
S/X with corr.	267	1.4	± 5.4	2.4	± 5.6	2.0	± 4.4
without corr.	267	-25.8	± 4.9	9.4	± 4.9	-1.6	± 4.3
K with corr.	125	0.1	± 6.8	1.2	± 7.4	-0.1	± 5.2
without corr.	125	-20.5	± 11.5	-17.7	± 11.9	-8.2	± 7.9
X/Ka with corr.	153	0.3	± 6.3	2.9	± 6.6	-0.1	± 4.9
without corr.	153	-35.1	± 17.9	31.1	± 18.3	38.6	± 11.2

3. Discussion

NNR Constraint Weighting: Given that the NNR constraint to the ICRF2 was unweighted, there may be problems caused by using a diagonal weighting for our after-the-fact check of rotational alignment. Our alignment check used the sum of the covariance of the frame under study and the diagonal ICRF2 covariance (note that the ICRF2 off-diagonal terms have not been made

available). For the three cases studied above, the X/Ka frame has the largest uncertainties, which are expected to dominate the combined X/Ka + ICRF2 covariance. The K-band uncertainties are somewhat larger than the ICRF2 and will partially dominate the combined covariance. However, because the S/X frame comes from almost the same data as the ICRF2, its uncertainties are comparable to those of the un-inflated ICRF2. Once the ICRF2 diagonal covariances are inflated by a scale factor of 1.5 and then have a 40 μs noise floor RSS'ed into each position coordinate, the ICRF2 covariance dominates the diagonal uncertainties.

These remaining nuances in weighting may explain why—even with full covariance—our after-the-fact check shows a few μs residual non-alignment. We have not yet studied these issues closely and can only say that the subject deserves more careful investigation.

Nutation constraints: One important lesson learned in the course of our comparisons is that other constraints can distort the desired effect of the NNR constraint. In the case of our K-band solution, our a priori nutation model was the IAU 2000 standard of Matthews, Herring, Buffet (MHB) [6]. Because there was evidence external to our study that the MHB model had 100–150 μs errors, we at first estimated nutation corrections with “weak” 200 μs a priori uncertainties on the nutation angles for each of twelve day-long sessions. Noting that a priori constraints act as pseudo-measurements, this effectively added 12 observations of the nutation pole each with 200 μs uncertainty. Thus, in retrospect, we realized that we had added a global constraint on the nutation pole of 200 μs / $\sqrt{12}$ = 58 μs which was strong enough to bias the 3-D rotational alignment of our celestial reference frame. This example is shared as a reminder that celestial frame alignment at the level of 10 μs requires careful attention to many details.

4. Conclusions

The celestial frame No-Net-Rotation constraint, $\sum s_{0i} \times \Delta s_i = 0$, alters the α - δ full covariance produced by a CRF solution. The correlations contain significant information which is needed to correctly estimate 3-D rotations and associated sigmas. At the 5–10 μs levels of axial alignment precision found in current CRF work, these correlations must be accounted for in order to avoid statistically significant misalignment of a given CRF.

5. Acknowledgements

The research described herein was performed at the Jet Propulsion Laboratory of the California Institute of Technology, under a contract with the National Aeronautics and Space Administration. Copyright 2010 © California Institute of Technology. Government sponsorship acknowledged.

References

- [1] IAU General Assembly XXIII, Resolution B2-d, Kyoto, Japan, August 1997.
iau.org/static/resolutions/IAU1997.French.pdf
- [2] Jacobs, C. & O. Sovers, ‘X/Ka Global Astrometry,’ Proc. 19th EVGA, Bordeaux, France, 24 Mar 2009.
www.u-bordeaux1.fr/vlbi2009/index.php?numpage=13&nompage=Proceedings
- [3] Lanyi, G.E., et al, ‘The Celestial Frame at 24 and 43 GHz I. Astrometry,’ AJ, 139, 5, p. 1695, 2010.
doi: 10.1088/0004-6256/139/5/1695
iopscience.iop.org/1538-3881/139/5/1695

- [4] Ma, Arias, Eubanks, Fey, Gontier, Jacobs, Sovers, *et al*, ‘ICRF as Realized by VLBI,’ *AJ*, 116, 1998. doi: 10.1086/300408
iopscience.iop.org/1538-3881/116/1/516/
- [5] Ma, C., *et al*, ‘The Second Realization of the ICRF by Very Long Baseline Interferometry,’ IERS Tech. Note 35, editors: A. L. Fey, D. Gordon, & C. S. Jacobs, Frankfurt, Germany, Oct. 2009. www.iers.org/nn_11216/IERS/EN/Publications/TechnicalNotes/tn35.html
- [6] Matthews, P. M., T. A. Herring, and B. A. Buffet, ‘Modeling of Nutation and Precession: New nutation series for Nonrigid Earth and Insights into the Earth’s Interior,’ *JGR*, vol. 107, no. B4, 10.1029/2001JB000390, Apr. 2002.
www.agu.org/journals/jb/jb0204/2001JB000390/
- [7] Sovers, O. J., J. L. Fanselow, and C. S. Jacobs, ‘Astrometry and Geodesy with Radio Interferometry: Experiments, Models, Results’, *Rev. Mod. Phys.*, vol. 70, no. 4, pp. 1393–1454, Oct. 1998. doi: 10.1103/RevModPhys.70.1393
rmp.aps.org/abstract/RMP/v70/i4/p1393_1

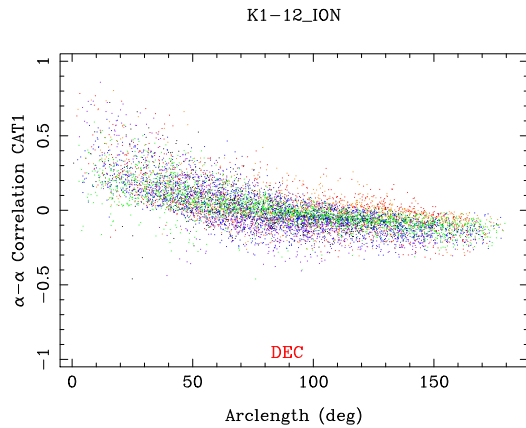


Figure 1. K-band (24 GHz) 12-session distribution of α - α correlations vs. arclength for all combinations of two sources. The correlations are systematically positive for short arcs and become negative for the longest arcs. These trends alter both the estimated rotations and their uncertainties. Color coding of 22.5° dec. bands: low to high (orange, red, green, blue, purple, black).

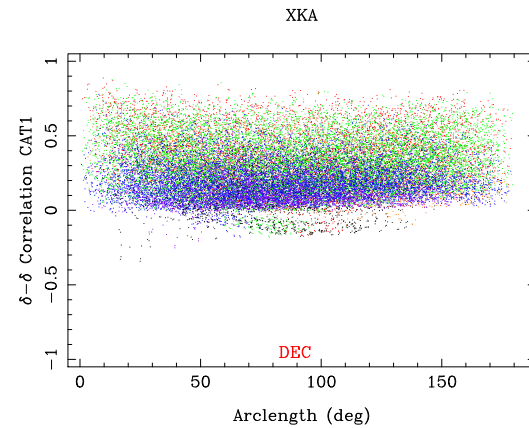


Figure 2. X/Ka (8.4/32 GHz) CRF’s distribution of δ - δ correlations vs. arclength. The correlations remain systematically positive over the full range of arc lengths, thus altering both the estimated rotations and their uncertainties. Color coding is the same as in the preceding figure. Note the tendency for low declination to be more strongly correlated.

6. Appendix: Derivation of NNR Constraint Equation

Given two sets of sources forming two frames, one frame is a priori assigned the role of the absolute reference and the other frame we wish to estimate from our data. Next, we establish the mathematical formula which describes the angular rotational offset between these two frames. Then we estimate the positions from data by least squares such that the rotational offset is zero.

Let s_{0i} be the reference position vector of the i^{th} source, and let s_i be the estimated position. Denote the difference as $\Delta s_i = s_{0i} - s_i$. Suppose an approximately infinitesimal rotation, $R(\vec{\epsilon})$, is applied to s_i . Then the rotated position is

$$R(\vec{\epsilon}) s_i = s_i + \vec{\epsilon} \times s_i \quad (7)$$

We want the rotation $R(\vec{\epsilon})$ that minimizes the mean square angular position difference:

$$(\Delta\theta)^2 = \frac{1}{N_{src}} \sum_{i=1}^{N_{src}} (\Delta s_i - \vec{\epsilon} \times s_i) \cdot (\Delta s_i - \vec{\epsilon} \times s_i) \quad (8)$$

We minimize with respect to variations in ϵ_j by setting the derivative, $\partial (\Delta\theta)^2 / \partial \epsilon_j = 0$

$$\sum_{i=1}^{N_{src}} \left[\frac{\partial}{\partial \epsilon_j} (\Delta s_i - \vec{\epsilon} \times s_i) \right] \cdot (\Delta s_i - \vec{\epsilon} \times s_i) + (\Delta s_i - \vec{\epsilon} \times s_i) \cdot \left[\frac{\partial}{\partial \epsilon_j} (\Delta s_i - \vec{\epsilon} \times s_i) \right] = 0 \quad (9)$$

$$\sum_{i=1}^{N_{src}} \left(-\left(\frac{\partial}{\partial \epsilon_j} \vec{\epsilon} \right) \times s_i \right) \cdot (\Delta s_i - \vec{\epsilon} \times s_i) + (\Delta s_i - \vec{\epsilon} \times s_i) \cdot \left(-\left(\frac{\partial}{\partial \epsilon_j} \vec{\epsilon} \right) \times s_i \right) = 0 \quad (10)$$

Since dot products commute, this can be re-written:

$$\sum_{i=1}^{N_{src}} (-2)(\Delta s_i - \vec{\epsilon} \times s_i) \cdot \left(\left(\frac{\partial}{\partial \epsilon_j} \vec{\epsilon} \right) \times s_i \right) = 0 \quad (11)$$

We want the above derivative to be zero, $\partial(\Delta\theta)^2/\partial\epsilon_j = 0$ when evaluated at $\vec{\epsilon} = 0$, thus

$$\sum_{i=1}^{N_{src}} (\Delta s_i) \cdot \left(\left(\frac{\partial}{\partial \epsilon_j} \vec{\epsilon} \right) \times s_i \right) = 0 \quad \text{for } j = 1, 2, 3 \quad (12)$$

Using the general vector property $v_1 \cdot (v_2 \times v_3) = v_2 \cdot (v_3 \times v_1)$ we have:

$$\sum_{i=1}^{N_{src}} \left(\frac{\partial}{\partial \epsilon_j} \vec{\epsilon} \right) \cdot (s_i \times \Delta s_i) = 0 \quad \text{for } j = 1, 2, 3 \quad (13)$$

Since $\frac{\partial}{\partial \epsilon_j} \vec{\epsilon}$ is just the elementary unit vector on the j^{th} axis, this represents three equations which can be combined into the vector equation:

$$\sum_{i=1}^{N_{src}} s_i \times \Delta s_i = 0 \quad (14)$$

Noting that $s_i \times \Delta s_i = (s_{0i} - \Delta s_i) \times \Delta s_i = s_{0i} \times \Delta s_i - \Delta s_i \times \Delta s_i = s_{0i} \times \Delta s_i$ since for any vector, v , $v \times v = 0$, we have:

$$\sum_{i=1}^{N_{src}} s_{0i} \times \Delta s_i = 0 \quad (15)$$

Global VLBI Observations of Weak Extragalactic Radio Sources: Imaging Candidates to Align the VLBI and Gaia Frames

Géraldine Bourda¹, Arnaud Collioud¹, Patrick Charlot¹, Richard Porcas²,
Simon Garrington³

¹) *Laboratoire d'Astrophysique de Bordeaux, Université de Bordeaux, CNRS/UMR5804*

²) *Max Planck Institute for Radio Astronomy, Bonn*

³) *University of Manchester, Jodrell Bank Observatory*

Contact author: Géraldine Bourda, e-mail: bourda@obs.u-bordeaux1.fr

Abstract

The space astrometry mission Gaia will construct a dense optical QSO-based celestial reference frame. For consistency between optical and radio positions, it will be important to align the Gaia and VLBI frames (International Celestial Reference Frame) with the highest accuracy. In this respect, it is found that only 10% of the ICRF sources are suitable to establish this link (70 sources), either because most of the ICRF sources are not bright enough at optical wavelengths or because they show extended radio emission which precludes reaching the highest astrometric accuracy. In order to improve the situation, we initiated a multi-step VLBI observational project, dedicated to finding additional suitable radio sources for aligning the two frames. The sample consists of about 450 optically-bright radio sources, typically 20 times weaker than the ICRF sources, which have been selected by cross-correlating optical and radio catalogs. The initial observations, aimed at checking whether these sources are detectable with VLBI, and conducted with the European VLBI Network (EVN) in 2007, showed an excellent 90% detection rate. This paper reports on global VLBI observations carried out in March 2008 to image 105 from the 398 previously detected sources. All sources were successfully imaged, revealing compact VLBI structure for about half of them, which is very promising for the future.

1. Context

During the past decade, the IAU (International Astronomical Union) fundamental celestial reference frame was the ICRF (International Celestial Reference Frame; [1, 2]), composed of the VLBI positions of 717 extragalactic radio sources, measured from dual-frequency S/X observations (2.3 and 8.4 GHz). Since 1 January 2010, the IAU fundamental celestial reference frame has been the ICRF2 [3], successor of the ICRF. It includes VLBI coordinates for 3414 extragalactic radio sources, with a floor in position accuracy of 60 μas and an axis stability of 10 μas .

The European space astrometry mission Gaia, to be launched in 2012, will survey all stars and QSOs (Quasi Stellar Objects) brighter than apparent optical magnitude 20 [4]. Optical positions with Gaia will be determined with an unprecedented accuracy, ranging from a few tens of μas at magnitude 15–18 to about 200 μas at magnitude 20 [5]. Unlike Hipparcos, Gaia will permit the realization of the extragalactic celestial reference frame directly at optical bands, based on the QSOs that have the most accurate positions. A preliminary Gaia catalog is expected to be available by 2015 with the final version released by 2020.

In this context, aligning VLBI and Gaia frames will be crucial for ensuring consistency between the measured radio and optical positions. This alignment, to be determined with the highest

accuracy, requires several hundreds of common sources, with a uniform sky coverage and very accurate radio and optical positions. Obtaining such accurate positions implies that the link sources must be brighter than optical magnitude 18 [6], and must not show extended VLBI structures.

In a previous study, we investigated the potential of the ICRF for this alignment and found that only 70 sources (10% of the catalog) are appropriate for this purpose [7]. This highlights the need to identify additional suitable radio sources, which is the goal of a VLBI program that we initiated three years ago [8]. This program has been devised to observe 447 optically-bright extragalactic radio sources extracted from the NRAO VLA Sky Survey, a dense catalog of weak radio sources [9]. The observing strategy to detect, image, and measure accurate VLBI positions for these sources is described in [8].

The initial observations, whose goal was to assess the VLBI detectability of the targets, were conducted with the European VLBI Network (EVN) in 2007. These showed an excellent 90% detection rate [8]. Proceeding further with our program, we now report on global VLBI imaging observations carried out in March 2008 to image 105 of the 398 previously detected sources.

2. Observations and Data Reduction

The observations were performed during a 48-hour experiment (hereafter designated as GC030), on 7–9 March 2008, with a global VLBI array recording at 512 Mb/s in a dual-frequency S/X mode. This network was composed of five telescopes from the EVN (Effelsberg, Medicina, Noto, Onsala-20m, and Hartebeesthoek), the DSN 70-m Robledo telescope for part of the time, and nine antennas of the VLBA (Very Long Baseline Array). Sixteen 8-MHz-wide sub-bands were recorded, with eight contiguous bands at each of S- and X-band. On average, a total of three to four 5-minute long scans were scheduled on each of the 105 target sources. In addition, we observed a sample of ten well-distributed ICRF sources, for use as calibrators. In all, about 80% of the allocated time was spent on source, while the rest was used for slewing.

The correlation of GC030 was done with the VLBA correlator at the Array Operations Center in Socorro (New Mexico, USA). The correlated data were then calibrated using the Astronomical Image Processing System (AIPS¹). An initial amplitude calibration for each sub-band was accomplished using system temperature measurements taken during the observations combined with gain curves supplied for each telescope. Prior to fringing the targets, phase offsets between the sub-bands were determined by fringing a short calibrator scan, and then applied to all data. This allowed us to combine all sub-bands together when fringing, thereby increasing the signal-to-noise-ratio and maximizing chances of detection for these weak targets. Calibrators were used in a second stage to estimate amplitude correction factors for each station, each band (S and X), and each sub-band. These corrections, at the level of less than 10% on average, were applied to the calibrated data, which were then exported as FITS files.

The remaining data reduction was conducted with the Caltech DIFMAP² software-package which was used for imaging. Visibility data for each frequency band were self-calibrated, Fourier inverted, and CLEANed following the hybrid-mapping technique [10], using DIFMAP in an automatic mode. A point-source model was used as a starting model for the iterative procedure in all cases. Uniform weighting and, after several iterations, natural weighting, were applied to derive the final images.

¹<http://www.aips.nrao.edu>

²<http://www.astro.caltech.edu/~tjp/citvlb/index.html>

3. VLBI Imaging Results

Based on the analysis described above, VLBI maps at X- and S-bands were successfully produced for each of the 105 target sources observed during GC030. These images have the following characteristics:

- The typical beam has a size of about 1.2×0.5 mas at X-band and 4.2×2.0 mas at S-band.
- The dynamic range (defined as the ratio of the first plotted contour level to the peak brightness) is generally $\sim 1:100$.
- The typical image noise rms is 0.080 mJy/beam at X-band and 0.117 mJy/beam at S-band. This compares well with the theoretical image thermal noise at X- and S-bands, which are 0.050 and 0.082 mJy/beam, respectively.

Figures 1 and 2 show the VLBI maps that we produced for the first six sources of the list (when ordered by increasing right ascension): 0003+123, 0049+003, 0107–025, 0109+200, 0130–083, and 0145+210. The total flux densities for these sources, as integrated from the GC030 images, are respectively: 128 mJy, 49 mJy, 46 mJy, 120 mJy, 78 mJy, 126 mJy at X-band, and 115 mJy, 28 mJy, 56 mJy, 78 mJy, 140 mJy, 268 mJy at S-band. When considering all 105 targets, the total flux density ranges from 23 mJy to 222 mJy at X-band, with a median value of 61 mJy, and from 22 mJy to 397 mJy at S-band with a median value of 65 mJy. Based on the X-band and S-band flux densities, the spectral index α (defined as $S \propto \nu^\alpha$, where S is the source flux density and ν is the frequency) has also been determined. In this definition, the sources with a dominating compact core are expected to have $\alpha > -0.5$. The median value of α for the sources observed during GC030 is -0.05 , with $\alpha > -0.5$ for more than 90% of the targets (97 sources out of 105 sources imaged).

4. Astrometric Quality

The images derived from GC030 show a variety of morphologies, ranging from point-like sources to extended or even double sources. In order to identify the most point-like ones, suitable for the Gaia link, we used the so-called “structure index” (SI) as an indicator of astrometric quality [11, 12]. Accordingly, only sources with $SI < 3$ should be used, since one wants to determine the link with the highest accuracy.

Analysis of the structure index values at X- and S-bands for all 105 sources observed during GC030 indicates that about half of them (47 sources) show point-like or compact structures at X-band ($SI < 3$), whereas the other half show extended structures. The resulting list of suitable sources is given in [13]. We note that these 47 sources increase the number of potential link sources by 70% when added to the 70 suitable sources already identified in [7], which is very promising considering that only one fourth of our targets has been imaged thus far.

5. Future Prospects

It is anticipated that the remaining 293 detected sources from our initial sample will be observed within the coming year and imaged in the same way. Assuming similar statistics, we expect another 150 suitable link sources to be identified. The final stage of this project, dedicated to measuring accurately the VLBI position of those sources, will be engaged in the near future. While making the Gaia link possible, these new VLBI positions will also serve to densify the ICRF at the same time.

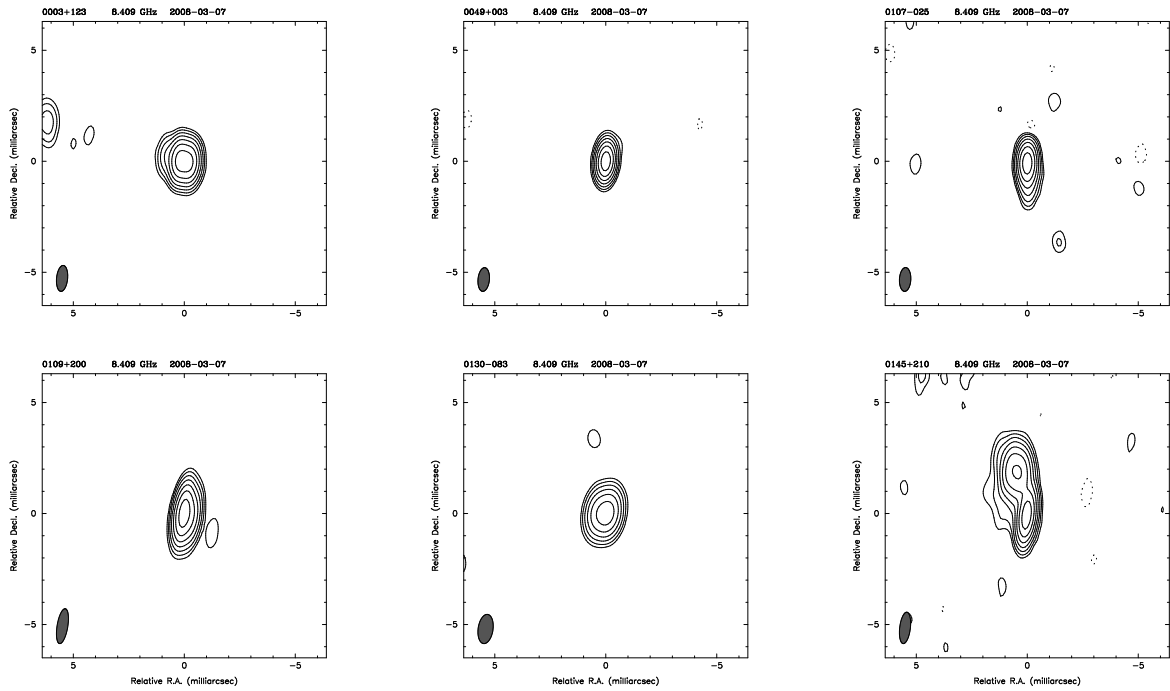


Figure 1. VLBI images at X-band for the first six sources from GC030 (when ordered by increasing right ascension). Contour levels start at 1% or 2% of the peak brightness and increase by a factor of 2 each time.

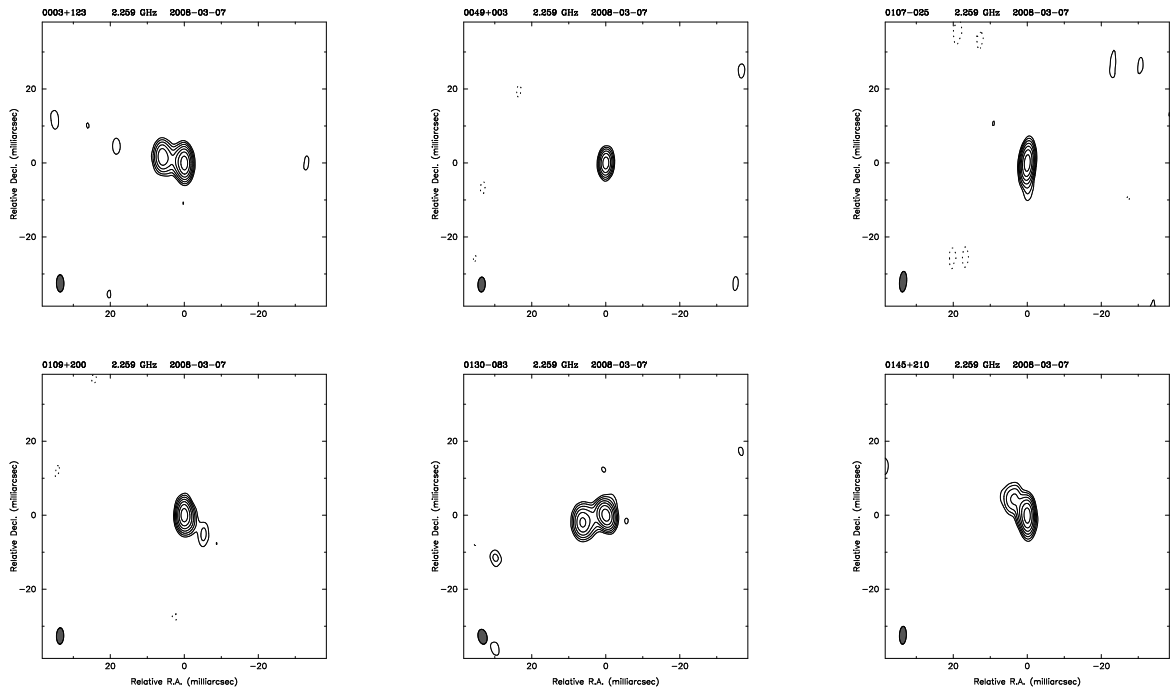


Figure 2. VLBI images at S-band for the first six sources from GC030 (when ordered by increasing right ascension). Contour levels start at 1% or 2% of the peak brightness and increase by a factor of 2 each time.

6. Acknowledgements

The authors would like to thank the VLBI friends at the EVN and VLBA observing stations. This work has benefited from research funding from the European Community's sixth Framework Programme under RadioNet R113CT 2003 5058187. The EVN is a joint facility of European, Chinese, South African, and other radio astronomy institutes funded by their national research councils. The VLBA is part of the National Radio Astronomy Observatory (NRAO), which is operated by Associated Universities, Inc., under cooperative agreement with the National Science Foundation.

G. Bourda would like to thank the International Association of Geodesy, the "Comité National Français de Géodésie et Géophysique" and the "Action Spécifique Gaia" for supporting her travel expenses to this meeting.

References

- [1] Ma, C., E. Arias, T. Eubanks, A. Fey, A.-M. Gontier, et al., *AJ* 116, 516–546, 1998.
- [2] Fey, A., C. Ma, E. Arias, P. Charlot, M. Feissel-Vernier, et al., *AJ* 127, 3587–3608, 2004.
- [3] IERS Technical Note 35, "The Second Realization of the International Celestial Reference Frame by Very Long Baseline Interferometry", A. Fey, D. Gordon & C. Jacobs (eds.), Frankfurt am Main: Verlag des Bundesamts für Kartographie und Geodäsie, 2009.
- [4] Perryman, M., K. de Boer, G. Gilmore, E. Hog, M. Lattanzi, et al., *A&A* 369, 339–363, 2001.
- [5] Lindegren, L., C. Babusiaux, C. Bailer-Jones, U. Bastian, A. Brown, et al., In: Proceedings of IAU Symposium 248, "A Giant Step: from Milli- to Micro-arcsecond Astrometry", W. Wenjin, I. Platais & M. Perryman (eds.), Cambridge University Press, 217–223, 2008.
- [6] Mignard, F., In: Proceedings of IAU General Assembly XXV, Joint Discussion 16: "The International Celestial Reference System: Maintenance and Future Realization", R. Gaume, D. McCarthy & J. Souchay (eds.), 133–140, 2003.
- [7] Bourda, G., P. Charlot, J.-F. Le Campion, *A&A* 490, 403–408, 2008.
- [8] Bourda, G., P. Charlot, R. Porcas, S. Garrington, *A&A* (accepted), 2010.
- [9] Condon, J., W. Cotton, E. Greisen, Q. Yin, R. Perley, et al., *AJ* 115, 1693–1716, 1998.
- [10] Pearson, T., A. Readhead, *ARA&A* 22, 97–130, 1984.
- [11] Fey, A., P. Charlot, *ApJS* 111, 95–142, 1997.
- [12] Fey, A., P. Charlot, *ApJS* 128, 17–83, 2000.
- [13] Bourda, G., A. Collioud, P. Charlot, R. Porcas, S. Garrington, *A&A* (accepted), 2010.

Astrometric “Core-shifts” at the Highest Frequencies

María Rioja ¹, Richard Dodson ²

¹⁾ ICRAR, University of Western Australia AND Observatorio Astronómico Nacional, Spain

²⁾ ICRAR

Contact author: María Rioja, e-mail: maria.rioja@icrar.org

Abstract

We discuss the application of a new VLBI astrometric method named “Source/Frequency Phase Referencing” to measurements of “core-shifts” in radio sources used for geodetic observations. We detail the reasons that astrometrical observations of ‘core-shifts’ have become critical in the era of VLBI2010. We detail how this new method allows the problem to be addressed at the highest frequencies and outline its superior compensation of tropospheric errors.

1. Introduction

In the era of VLBI2010 all aspects of VLBI geodetic analysis need to be much more precise. The target positional accuracy of 1 mm converts to an angular precision of $\sim 30 \mu\text{as}$. Therefore many effects, which have been considered secondary in the past, will now need to be accounted for. Among those is the changing observed position of celestial sources with observing frequency, known as “core-shifts”.

1.1. Effect of Core-shifts in VLBI Geodetic Studies

The standard theory for extragalactic radio sources predicts changes in their positions at different frequencies, although the black-hole “central engine” powering the typical core-jet structures is considered to be stationary [1]. Hence, the observed “apparent” celestial positions correspond to the location down the jet from the central engine at which the optical depth is equal to unity, which is known as the “core”. Prior to this location the emission is self-absorbed. Since the location at which the optical depth is unity is a function of frequency-dependent opacity effects, the “core” appears to move as the observing frequency changes. Such changes in position are termed “core-shifts”. Assuming a simple model for the jet, the distance of the first detectable emission is $r_{\text{core}} \propto \nu^{-1/k_r}$, where ν is the observing frequency and the k_r is a power-law exponent which is commonly taken as unity.

Other than the intrinsic opacity-related effects, as mentioned above, the measured “core-shifts” may have another contribution related to insufficient resolution and structure blending effects at the lower frequencies. We term this contribution as “instrumental core shift”. Figure 1 is a sketch showing both contributions; typical values are listed in Table 1.

There is a wide observational evidence of existence of “core-shifts” revealed by VLBI astrometric techniques, e.g. [11, 3], and other approaches, e.g. [5]. Measurements of “core-shifts” are used in astronomy to probe the environments in the inner-jet regions and need to be accounted for in studies that involve the comparison of images at two or more frequencies to ensure a proper registration.

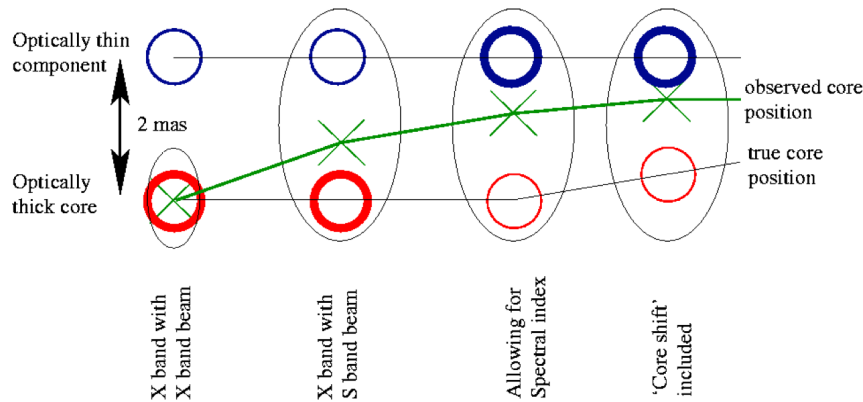


Figure 1. A sketch showing contributions to observed “core-shifts”: *extrinsic*, due to structure blending at lower frequencies (first 3 starting from left), and *intrinsic* opacity (rightmost).

The influence of “core-shifts” in geodetic VLBI observations comes through the basic practice in geodesy of calibrating the ionospheric contribution with simultaneous observations at S/X-bands (2.2GHz/8.4GHz, respectively). This approach works under the critical assumption that the brightness distributions for each source are identical and are co-located at both frequencies. Otherwise, unaccounted “core-shifts” will introduce, in general, errors in the geodetic parameters. Nevertheless, for group-delay VLBI geodesy, as it has traditionally been performed, the effect of the intrinsic “core-shifts” is strongly attenuated in the analysis, and the estimated source positions correspond to those at zero wavelength (assuming k_r is unity) [9]. For phase-delay VLBI geodesy this is no longer the case, and the “core-shifts” will need to be corrected for across the observing frequency bands to avoid the propagation of errors into the estimated geodetic parameters; the same applies for the “instrumental core-shifts” in both phase and group-delay geodetic analysis.

Table 1. Typical sizes of the *intrinsic* opacity and the *extrinsic* instrumental core-shift contributions, along with typical measured “core-shift” values.

	<i>Opacity</i> core shift	<i>Instrumental</i> core shift	Measured core shift
2.2/8.4 GHz	0–1 mas	0 – 2 mas	0 – 1400 μ as
8.4/30 GHz	0–0.25 mas	0 – 0.5 mas	0 – 30 μ as

2. The Basis of the Source/Frequency Phase Referencing Method

The phase referencing astrometric technique is well established and has produced many significant insights. However, the fast telescope switching cycles imposed by the rapid tropospheric fluctuations at higher frequencies has prevented the application of conventional phase referencing techniques beyond 43 GHz, except for a single case at 86 GHz [8]. This is particularly significant

for “core-shift” measurements as it is in the mm-wavelengths that we see the ‘naked’ core, free of the confusing emission structure from the synchrotron jets.

We have proposed an advanced tropospheric calibration method which would allow phase referencing and astrometry under a wider variety of conditions at mm-wavelengths [2]. In previous work, “fast-frequency switching” has been shown to increase the coherence time at mm-wavelengths, but without achieving astrometry [7, 4]. The non-dispersive nature of the troposphere makes it possible to use lower frequency observations to calibrate higher, providing the switching interval between frequencies matches the temporal structure of the tropospheric fluctuations at the lower frequency.

Our SOURCE/FREQUENCY PHASE REFERENCING (SFPR) method adds a source switching to the observing strategy, in addition to the fast frequency switching, to calibrate the residual dispersive contributions remaining in the phase transfer between frequencies. The new method is an enhancement which allows “*bona fide*” astrometric measurements of “core-shifts” in radio sources. The nodding between sources has to match the temporal and spatial structures of ionospheric perturbations (with typical scales of several minutes, and several degrees), and other non-dispersive terms such as instrumental contributions (with typical timescales of many minutes). A complete description of the method is presented in [10], [2], and [12]. We include here a brief outline of the basics:

A pure self-calibration analysis is used for the low *reference* frequency (r) target source (A) observations. Following the standard nomenclature, the residual phase values (ϕ_A^r) are shown as a compound of geometric, tropospheric, ionospheric, and instrumental terms (excluding source structure and phase ambiguity terms, for simplicity):

$$\phi_A^r = \phi_{A,geo}^r + \phi_{A,tro}^r + \phi_{A,ion}^r + \phi_{A,inst}^r$$

The calibration transfer between frequencies involves multiplying the phases by the frequency ratio R . This results in the perfect cancellation of the non-dispersive errors, i.e., tropospheric and geometric (source and antenna coordinates), but not for the dispersive ones, which remain. The *target* frequency (t)-referenced phases are:

$$\phi_A^t - R.\phi_A^r = \phi_{A,str}^t + 2\pi\nu^t/c * (\bar{B}.\bar{\theta}_{A,shift}) + ION + INST$$

where $\bar{\theta}_{A,shift}$ is the “core-shift” in A between both bands; ION/INST are the residual dispersive long time-scale terms which have prevented direct imaging and hence astrometry in previous attempts of frequency-referenced maps.

SFPR enables astrometry by using interleaving observations on a calibrator source (C), with the same observational strategy and analysis as explained above for source A . The results of C are used to correct the A dataset. The calibration transfer between sources is done as in conventional phase referencing. The SFPR-ed phases are:

$$(\phi_A^t - R.\phi_A^r) - (\phi_C^t - R.\phi_C^r) = \phi_{A,str}^t + 2\pi\nu^t/c * (\bar{B}.\bar{\theta}_{A,shift} - \bar{B}.\bar{\theta}_{C,shift})$$

which can be inverted to yield a synthesis image of A at the *target* frequency where the offset from the center is the combined “core-shifts” in A and C , between both frequencies. Figure 2 shows the SFPR map result from our observational demonstration using the VLBA, at 43/86 GHz [2].

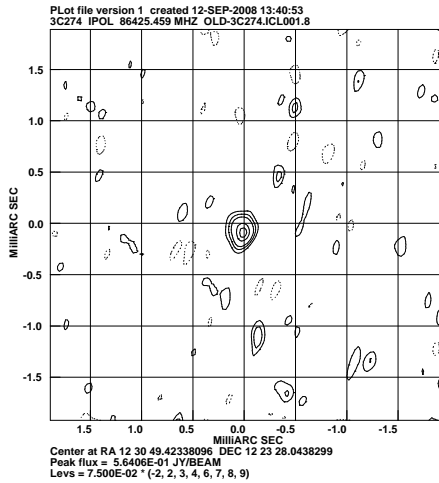


Figure 2. 86-GHz Source Frequency Phase-Referenced image of 3C274, calibrated against 43-GHz and 3C273. We believe that the core-shift seen is real as it matches the predicted values [6]. Typical errors appear to be of the order of 20 μ as.

3. Tropospheric Compensation with the SFPR Method

Of particular interest to astrometric studies is that the SFPR method, by providing a superior tropospheric compensation, achieves high precision estimates at the highest frequencies. There are two major contributions to the tropospheric errors in VLBI observations: the “dynamic component”, due to uncertainties in the water vapor content in the troposphere (i.e., the ‘wet’ part) introduces random temporal variations, and the “static component”, due to slowly varying errors in the tropospheric zenith delay estimates at each station, which propagate into different errors along different line of sights as it is multiplied by the mapping function.

Because SFPR calibrates the high frequency target data using observations along the same line of sight, at a lower frequency, the residuals from the “static component” are naturally zeroed. When SFPR is used in frequency-switching mode (as for example with the VLBA) residual terms arising from “dynamic” random fluctuations in the time span between consecutive same-frequency scans are expected to remain in the high frequency target dataset. However, when simultaneous frequency-band observations are carried out, it eliminates the need for frequency switching and the “dynamic component” is also perfectly compensated for. Arrays like the KVN, and telescopes like Yebes and Haystack allow simultaneous multi-frequency observations, in the high frequency regime, and therefore would result in an exact adaptive tropospheric correction. Figure 3 shows a comparison of tropospheric compensation achieved with different astrometric techniques, for the “dynamic” and “static” contributions.

4. Conclusions

The phenomena of “core-shifts” in radio sources should be accounted for to achieve the VLBI2010 goals. We have presented an astrometric method, SFPR, which allows high precision measurements of “core-shifts” up to highest frequencies, beyond the current threshold for any other technique. The “core-shifts” measurements at high frequencies are expected to be free of “instrumental” effects, and hence could serve to disentangle the nature of the “core-shifts” at the frequencies of interest for the VLBI2010 program.

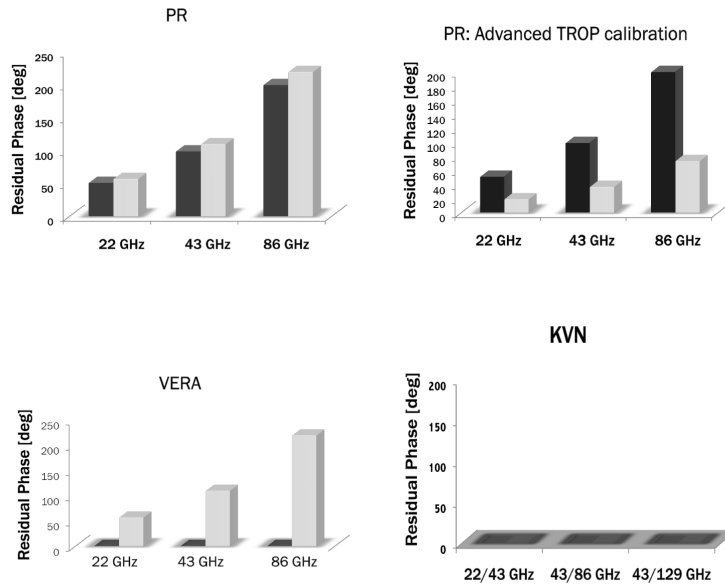


Figure 3. Residual tropospheric errors arising from the *dynamic* (dark) and *static* (light) components, vs. frequency, using **a)** conventional phase referencing techniques: using two sources 2° away and telescope switching 1 minute (PR), plus geodetic setup to estimate tropospheric zenith delay (PR:Advanced), using simultaneous observations of the two sources (VERA); **b)** using SFPR technique, with two frequencies/sources (KVN).

Moreover, the SFPR method enables astrometric studies at the highest frequencies, with a very high precision resulting from the superior tropospheric compensation.

References

- [1] Blandford, R. D. and Konigl, A. (1979). Relativistic jets as compact radio sources. *ApJ*, 232:34
- [2] Dodson, R. and Rioja, M. J. (2008). Astrometric calibration of mm-VLBI using Source Frequency Phase Referenced observations. VLBA Scientific Memo 31, NRAO.
- [3] Guirado, J. C. *et al.*, (1995), *AJ*, 110.
- [4] Jung, T., *et al.*, (2008). In *The role of VLBI in the Golden Age for Radio Astronomy*.
- [5] Kovalev, Y. Y., Lobanov, A. P., Pushkarev, A. B., Zensus, J. A. (2008). *A&A*, 483
- [6] Lobanov, A. P. (1998). *A&A*, 330:79
- [7] Middelberg, E., Roy, A. L., Walker, R. C., and Falcke, H. (2005). *A&A*, 433:897
- [8] Porcas, R. W. and Rioja, M. (2002). In *Proc. 6th EVN Symp.*
- [9] Porcas, R. W. (2009). Radio astrometry with chromatic AGN core positions. *A&A*, 505:L1
- [10] Rioja, M. J., Dodson, R., Porcas, R. W., Suda, H., and Colomer, F. (2005). *arXiv:astro-ph/0505475*.
- [11] Rioja, M. J., Marcaide, J., Elósegui, P., and Shapiro, I. (1997). *A&A*, 325
- [12] Rioja, M. J. and Dodson, R. (2010). *ApJ in prep.*

Forthcoming Occultations of Astrometric Radio Sources by Planets

Victor L'vov, Zinovy Malkin, Svetlana Tsekmeister

Central Astronomical Observatory at Pulkovo of Russian Academy of Sciences

Contact author: Victor L'vov, e-mail: epos-gao@mail.ru

Abstract

Astrometric observations of radio source occultations by solar system bodies may be of large interest for testing gravity theories, dynamical astronomy, and planetary physics. In this paper, we present an updated list of the occultations of astrometric radio sources by planets expected in the coming years. Such events, like solar eclipses, generally speaking can only be observed in a limited region. A map of the shadow path is provided for the events that will occur in regions with several VLBI stations and hence will be the most interesting for radio astronomy experiments.

1. Introduction

Observations of occultations of compact radio sources by Solar System planets may be interesting for several astronomical and physical applications, such as testing GR [1], improvement of planet orbits and their tie to ICRF [2], and planetary research [3, 4].

Our previous computations of occultations of astrometric radio sources by planets and their close approaches were published in [1]. In this paper we present the updated list of the forthcoming occultations that may be of interest for radio astronomy observations. The main differences with respect to the previous work are the use of an extended astrometric source list and the computation of event maps for a better planning of observations.

2. Forthcoming Occultations

Most computations of occultation events of geodetic radio sources by planets were performed using the codes APPROACH and OCCULT, which utilize the Ephemeride Package for Objects of the Solar System (EPOS) data and environment¹. Source coordinates were taken from the catalog of astrometric radio source positions of Leonid Petrov, version 2009c².

The list of occultations is presented in Table 1 with their basic features. One can see that most of the events are visible in regions with radio astronomy observatories, and several of them can be observed by many antennas. The nearest most interesting event is the occultation of the source 1946–200 by Mars in February 2011 visible in North America with VLBA, VLA, GBT, and other radio astronomy facilities.

Figure 1 and Table 2 present more detailed information about several of the nearest events that can be observed in regions with several geodetic VLBI antennas. The shadow path maps are shown in Figure 1. Table 2 lists the detailed parameters of several of the nearest events, such as

¹<http://neopage.pochta.ru/ENG/ESUPP/main.htm>

²http://astrogeo.org/vlbi/solutions/2009c_astro/

Table 1. Occultations of radio sources by planets in 2011–2030 (d is the angular distance from the Sun, and the letter indicates east or west elongation).

Planet	Date			Source	d, deg	Region of visibility
	Y	M	D			
Venus	2011	02	26	1946–200	42W	Antarctic, S. America
Mars	2011	05	03	0127+084	19W	N. America
Venus	2012	12	24	1631–208	23W	S. America, Antarctic, Africa
Venus	2015	08	06	0947+064	15E	America
Jupiter	2016	04	10	1101+077	144E	Australia, SE Asia
Venus	2020	01	16	2220–119	38E	S. America, Europe, Africa
Venus	2020	07	17	0446+178	42W	N. America
Mercury	2022	11	14	1529–195	4E	S. America
Jupiter	2025	09	18	0725+219	65W	America
Mercury	2027	03	21	2220–119	27W	N. America
Saturn	2028	10	24	0223+113	173W	by ring; Asia, Europe, N. Africa
Mercury	2029	01	14	1958–179	5E	Australia, Antarctic, S. Africa
Venus	2029	02	28	2221–116	6W	Africa, SE Asia, Australia
Mercury	2029	04	16	0243+181	19E	Asia, N. America
Mercury	2029	12	27	1858–212	8E	S. America, Australia
Mercury	2030	02	27	2208–137	9W	S. America, Africa

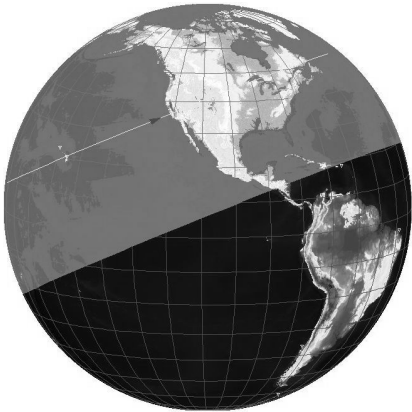
the elevation, azimuth, and position angle on the planetary limb at the beginning and the end of the occultation. Detailed parameters for other events are available on request.

3. Conclusion

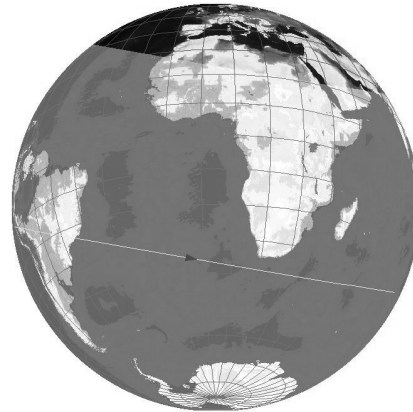
Observations of the occultations of radio sources by planets are attractive for several interesting applications in physics and planetary science. They can effectively supplement the observations of radio source occultations by the Moon and spacecraft radio occultations by planets. The list of occultations presented in this paper can be used for scheduling observations in different modes such as VLBI, connected-element interferometer, or single-dish mode, depending on the scientific task. The list of occultations as well as an updated list of close approaches of planets to radio sources is available at http://www.gao.spb.ru/english/as/ac_vlbi/.

References

- [1] Malkin, Z.M., L'vov, V.N., Tsekmeister S.D. (2009) Forthcoming Close Angular Approaches of Planets to Radio Sources and Possibilities to Use Them as GR Tests. *Solar System Research*, v. 43, No. 4, p. 313.
- [2] Linfield, R.P. (1992) Occultation of a compact radio source by Venus. *Astronomical Journal*, v. 104, p. 880.
- [3] Leblanc, Y., Ladreiter, H.P. (1992) Neptune's radio emissions. *Advances in Space Research*, v. 12, p. 23.
- [4] Black, G., Campbell, D., Nicholson, P., Sault, R. (2000) New Long-Wavelength Radio Source Occultations by Saturn's Rings. *Bulletin of the American Astronomical Society*, v. 32, p. 1086.



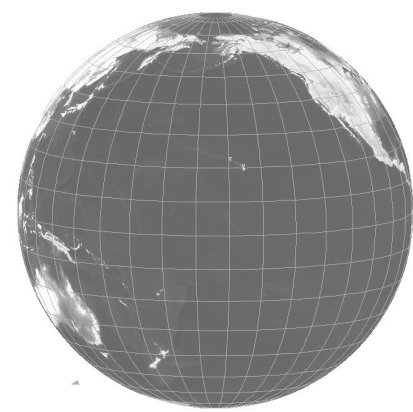
0127+084, Mars, May 03, 2011



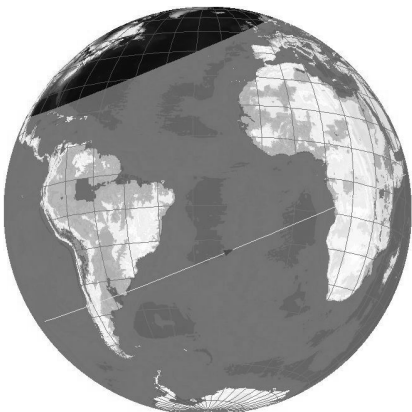
1631-208, Venus, Dec 24, 2012



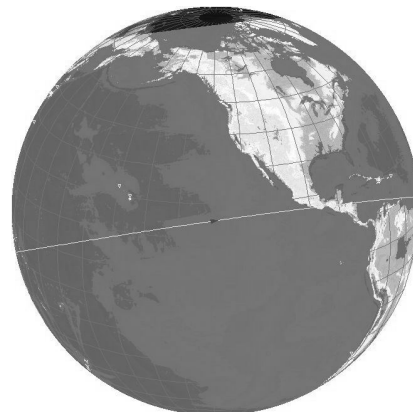
0947+064, Venus, Aug 06, 2015



1101+077, Jupiter, Apr 10, 2016



2220-119, Venus, Jan 16, 2020



0446+178, Venus, Jul 17, 2020

Figure 1. Visibility of selected nearest occultations of radio sources by planets. The visibility regions of the occultations are shown in light (for the 2016 event, the region covers the whole depicted hemisphere).

Table 2. Detailed features of the nearest occultations of radio sources by planets: B — at the beginning, E — at the end.

Planet	Date	Station	Time, TT		El., deg		Az., deg		Pos. angle	
			B	E	B	E	B	E	B	E
Venus	Feb 26, 2011	OHIGGINS	14:18:18	14:22:03	46	45	20	21	35	309
		SYOWA	14:18:20	14:23:11	11	11	118	119	55	290
Mars	May 03, 2011	KOKEE	18:10:19	18:12:26	41	42	278	278	60	256
		MK-VLBA	18:10:19	18:12:28	46	46	278	278	66	250
		OV-VLBA	18:11:31	18:13:40	61	61	345	347	65	251
		DSS13	18:11:32	18:13:41	63	63	348	349	69	247
		KP-VLBA	18:11:38	18:13:45	67	67	359	360	77	239
		BR-VLBA	18:11:43	18:13:45	50	50	347	348	49	266
		PIETOWN	18:11:46	18:13:53	64	64	7	8	75	240
		LA-VLBA	18:11:50	18:13:57	63	63	11	12	74	241
		FD-VLBA	18:11:52	18:13:55	67	67	19	20	84	232
		GILCREEK	18:11:59	18:13:20	28	29	318	319	17	298
		GGAO7108	18:12:37	18:14:41	47	46	55	56	84	232
		HN-VLBA	18:12:42	18:14:48	42	41	57	58	78	237
		WESTFORD	18:12:43	18:14:49	41	41	58	58	79	237
Venus	Dec 24, 2012	FORTLEZA	10:06:07	10:09:25	45	46	244	244	80	300
		OHIGGINS	10:07:13	10:10:03	31	32	286	287	136	244
		HARTRAO	10:08:02	10:11:28	68	67	83	83	87	293
		SYOWA	10:08:11	10:11:16	37	37	43	44	129	252
Venus	Aug 06, 2015	YEBES40M	18:41:27	19:23:00	9	1	91	98	284	68
		FORTLEZA	18:44:31	19:20:16	39	31	79	81	236	117
		SC-VLBA	18:49:35	19:29:43	63	54	68	76	260	94
		WESTFORD	18:53:34	19:32:45	50	46	30	43	284	70
		HN-VLBA	18:53:44	19:32:53	50	46	29	42	284	69
		GGAO7108	18:54:33	19:34:07	55	51	24	39	281	73
		FD-VLBA	19:02:27	19:42:29	63	66	334	357	274	80
		LA-VLBA	19:03:07	19:42:45	58	60	334	353	279	75
		PIETOWN	19:03:41	19:43:28	59	62	330	349	278	76
		KP-VLBA	19:04:48	19:44:46	59	63	322	341	276	78
		DSS13	19:06:13	19:45:56	54	59	318	334	279	75
		OV-VLBA	19:06:34	19:46:03	52	56	318	333	281	73
		BR-VLBA	19 06:39	19:44:22	43	46	324	336	291	63
		GILCREEK	19:10:09	19:43:42	21	23	302	311	305	49
		MK-VLBA	19:17:05	19:58:37	31	41	275	279	269	86
KOKEE	19:17:31	19:59:12	27	37	274	279	271	83		

Table 2. (continued)

Planet	Date	Station	Time, TT		El., deg		Az., deg		Pos. angle	
			B	E	B	E	B	E	B	E
Jupiter	Apr 10, 2016	TIGOCONC	07:02:05	10:07:53	15	-21	68	97	268	133
		LA-VLBA	07:05:34	10:15:00	49	13	54	90	274	128
		KP-VLBA	07:06:09	10:14:31	55	17	52	88	273	128
		DSS13	07:06:55	10:15:16	56	21	42	84	273	128
		OV-VLBA	07:07:09	10:15:37	55	22	38	83	273	128
		BR-VLBA	07:07:37	10:17:21	46	21	29	78	274	128
		GILCREEK	07:10:03	10:20:51	32	26	351	45	274	127
		MK-VLBA	07:12:22	10:16:11	71	58	308	72	271	130
		KOKEE	07:12:53	10:16:52	67	60	306	65	271	130
		USSURISK	07:15:37	10:25:14	7	40	267	305	273	130
		HOBART26	07:16:01	10:15:13	9	34	288	328	265	137
		VERAMZSW	07:16:13	10:24:24	15	48	272	311	272	130
		TSUKUB32	07:16:27	10:24:25	14	50	271	308	272	131
		KASHIM34	07:16:28	10:24:21	14	50	271	308	272	131
		GIFU11	07:16:31	10:24:39	11	48	269	303	272	131
		SESHAN25	07:16:34	10:25:38	-2	38	260	286	272	131
		TIDBIN64	07:16:41	10:16:04	12	41	288	327	266	136
		AIRA	07:16:48	10:24:57	6	45	265	294	271	131
		VERAIRIK	07:16:48	10:24:59	6	45	265	294	271	131
		PARKES	07:16:56	10:16:27	12	43	287	325	266	136
VERAISGK	07:17:13	10:25:02	0	42	262	283	271	132		
CHICHI10	07:17:14	10:23:43	16	56	270	300	271	131		
VERAOGSW	07:17:14	10:23:44	16	56	270	300	271	131		
Venus	Jan 16, 2020		:	:						
Venus	Jul 17, 2020		:	:						

Finding Extremely Compact Sources Using the ASKAP VAST Survey

Hayley E. Bignall¹, David L. Jauncey², James E. J. Lovell³, Roopesh Ojha⁴,
Cormac Reynolds¹

¹) *ICRAR/Curtin University of Technology*

²) *CSIRO Australia Telescope National Facility*

³) *School of Mathematics & Physics, University of Tasmania*

⁴) *US Naval Observatory*

Contact author: Hayley E. Bignall, e-mail: H.Bignall@curtin.edu.au

Abstract

VLBI observations of intraday variable (IDV) quasars found in the MASIV (Micro-Arcsecond Scintillation-Induced Variability) 5 GHz VLA Survey of 500 flat-spectrum sources in the northern sky have shown that these sources are extremely compact, often unresolved, on milliarcsecond scales, and more core-dominated than their non-IDV counterparts. VAST: an ASKAP Survey for Variables and Slow Transients, proposes to observe 10,000 square degrees of southern sky daily for 2 years in the VAST-Wide survey component. This is expected to reveal of order 30,000 compact sources brighter than 10 mJy showing refractive interstellar scintillation (the cause of centimeter-wavelength IDV) at the survey frequency of about 1.4 GHz. Many of these sources may be suitable astrometric calibrators for VLBI at higher frequencies.

1. Introduction

Sufficiently compact radio sources will have their measured intensity modulated due to the effects of scattering in the inhomogeneous, ionized interstellar medium (ISM) of our Galaxy [1, 2, 3]. For observing frequencies between $\sim 1 - 5$ GHz, a source will typically show refractive interstellar scintillation (RISS) if a significant amount of its flux density is in a compact component of angular diameter ~ 0.1 mas or smaller, with the angular size cutoff for a source to show refractive or weak scintillation decreasing towards higher frequencies. For sufficiently compact extragalactic radio sources, the largest amplitude modulations may be observed close to the transition frequency between weak and strong scattering, which is typically a few GHz for sources observed at moderate to high Galactic latitudes, increasing toward lower Galactic latitudes.

The present paper discusses the use of interstellar scintillation as a means of selecting the most compact extragalactic radio sources as potential VLBI calibrators. Section 2 summarizes some results of the Micro-Arcsecond Scintillation-Induced Variability (MASIV) VLA Survey of the northern sky at 5 GHz, as well as results of VLBI follow-up of sources observed in the MASIV Survey. As outlined in Section 3, VAST: an ASKAP Survey for Variables and Slow Transients, will scan the southern sky daily at 1.4 GHz, to discover transient and variable sources. Variability observed in VAST is expected to reveal a large number of candidate astrometric calibrators suitable for higher frequency VLBI observations. This will be potentially important for future VLBI science, especially given the current relatively sparse density in the southern hemisphere of suitable calibrators for phase referencing, astrometry, and geodesy observations.

2. Results of the MASIV VLA Survey and VLBI Follow-up

The MASIV Survey [4] observed approximately 500 compact, flat-spectrum radio sources spread over the northern hemisphere to measure their short-timescale radio variability. The initial Survey comprised four sessions with the NRAO Very Large Array (VLA) observing continuously for 72 hours (96 hours for the 2002 September session), which were spread at ~ 4 month intervals over the course of a year. The observations were performed at 5 GHz, close to the expected transition between weak and strong scattering where the amplitude of ISS is expected to be largest, with the VLA split into 5 subarrays each observing a different declination range. “Strong” and “weak” source samples were observed, with the weak sources selected to have average flux densities ≥ 0.1 Jy, and the strong sources ≥ 0.5 Jy. The final analysis included 443 sources which were unaffected by confusion and unresolved with the VLA in all configurations [5].

Over half of the observed sources showed intraday variability (IDV) in at least one epoch. MASIV showed a clear Galactic dependence of IDV, with a strong correlation between variability amplitude and $H\alpha$ emission measure along the line-of-sight, extracted from the published WHAM Survey [6]. This result demonstrates unequivocally that IDV is linked to the Galactic ISM; i.e., IDV is predominantly interstellar scintillation. The MASIV Survey was able to detect variability on timescales of hours to days. The observed root-mean-square (RMS) fractional variability on a 2-day timescale was typically 2-10%. Figure 1 shows an example of MASIV data for a scintillating source.

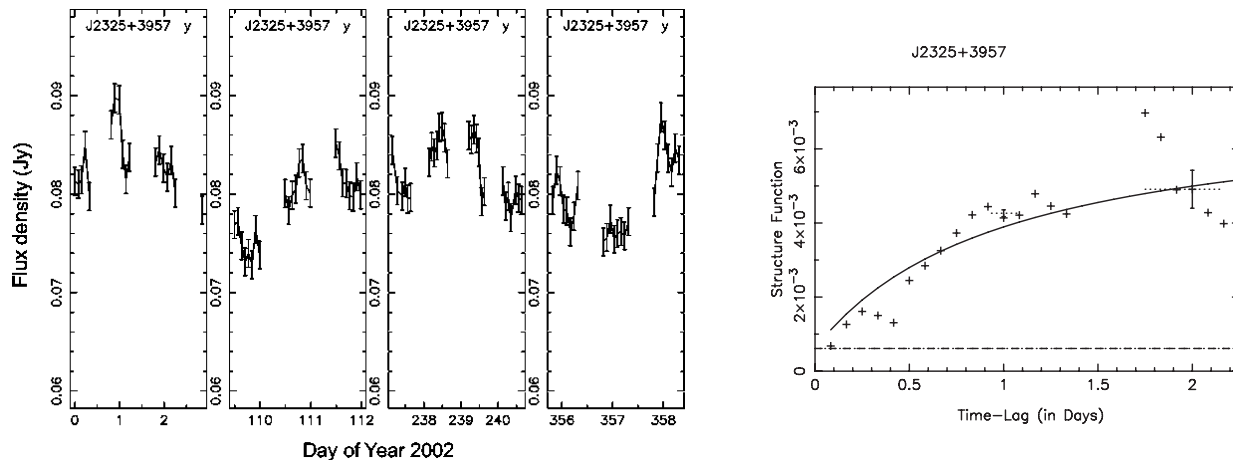


Figure 1. Example of a scintillating source observed in the MASIV Survey, from Lovell et al. 2008 [5]. Left: Flux density versus time for J2325+3957. Right: Structure function calculated from the combined data shown in the left-hand panel. The solid line shows a simple model fit used to characterize the timescale and amplitude of the variations.

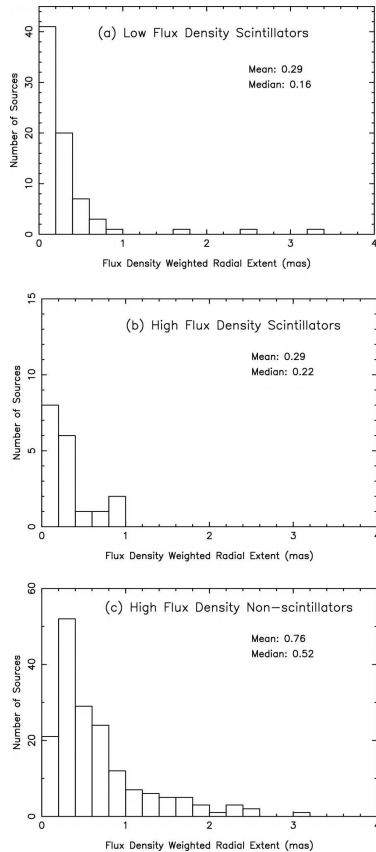


Figure 2. Distribution of flux density-weighted radial extent for samples of scintillating and non-scintillating MASIV Survey sources [7].

Follow-up observations of MASIV Survey sources with the NRAO Very Long Baseline Array (VLBA) [7, 8] showed that scintillating sources on average are more core dominant than non-scintillating sources. Furthermore, the overall angular size of scintillating sources is significantly smaller than that of non-scintillators. This is illustrated in Figure 2, from [7], which shows the 8.4 GHz flux density-weighted radial extent for low flux density scintillators, high flux density scintillators, and non-scintillators selected from the MASIV Survey. The flux density-weighted radial extent, R , is defined as

$$R = \frac{\sum_i S_i r_i}{\sum_i S_i},$$

where r_i is the radius at which the i th CLEAN component has flux density S_i . A Kolmogorov-Smirnov test rejects a common parent population for the scintillating (both low and high flux density) and non-scintillating sources at the 99% confidence level. These results imply that scintillating sources are more compact and core-dominated than non-scintillating sources, and hence are potentially good candidates for astrometric and geodetic calibration.

3. VAST: an ASKAP Survey for Variables and Slow Transients

3.1. The Australian Square Kilometer Array Pathfinder (ASKAP)

The Australian Square Kilometer Array Pathfinder is a next-generation radio telescope currently under construction in Western Australia, led by CSIRO ATNF. It is planned that ASKAP will comprise an array of 36 antennas each 12 m in diameter. The system temperature design goal is 35 K. The specified operational frequency range is from 0.7 to 1.8 GHz, with an instantaneous bandwidth of 300 MHz. ASKAP will use phased array feed technology to provide 30 independent beams, each of 1 square degree, yielding a 30 square degree field-of-view at 1.4 GHz. The specified maximum baseline is 6 km, and full cross-correlation of all antennas is planned. In the first five years of observations, anticipated to start in 2013, it is planned that at least 75% of ASKAP time will be devoted to large surveys. After an open international competition, ten major surveys have been selected to proceed to a design study phase.

3.1.1. ASKAP “BETA” Phase

The Boolardy Engineering Test Array (BETA) will consist of six antennas operating at the Murchison Radio-astronomy Observatory (MRO) by 2011. It is planned that BETA will have the same wide field-of-view as the full ASKAP array, but lower sensitivity due to having only 1/6th of ASKAP collecting area. BETA is therefore potentially useful for large-area sky monitoring surveys for relatively bright sources.

3.2. The VAST Survey

VAST is one of the ASKAP Survey Science Projects now beginning a design study. VAST aims to discover and investigate variable and transient phenomena occurring on timescales of 5 s and longer; e.g., flare stars, intermittent pulsars, X-ray binaries, magnetars, extreme scattering events, intraday variables, radio supernovae, and ‘orphan’ afterglows of gamma ray bursts. VAST will probe hitherto unexplored regions of phase space to search for new classes of radio transient sources. The planned VAST Survey includes wide, deep and Galactic plane components. The VAST-Wide component proposes to observe 10,000 square degrees of southern sky (400 pointings) daily for two years, requiring 6 hours of ASKAP time per day. The total time requested is thus 4380 hours. This assumes 40 seconds per pointing plus overheads, resulting in an RMS sensitivity of 0.5 mJy/beam according to ASKAP specifications.

Based on radio source counts [9, 10], approximately three flat-spectrum radio sources with flux density $S > 10$ mJy are expected per square degree. Based on the findings of the MASIV Survey, a large fraction of these would be expected to show RISS at 1.4 GHz, implying component angular sizes typically no larger than ~ 0.1 mas. While only the most extreme variables would be detected at a 10 mJy flux density limit, VAST should be able to reliably detect variations down to a few percent in sources with total flux density $S \geq 0.1$ Jy.

Due to the strong frequency dependence of the timescale of ISS (expected to be close to ν^{-2} in the refractive scintillation regime, where ν is the observing frequency), timescales of variability at 1.4 GHz are expected to be an order of magnitude longer than those at 5 GHz. Thus, instead of the variability with typical timescales of days observed in the MASIV Survey, the VAST Survey will observe variability with characteristic timescales of weeks to months, except for a very small fraction of sources scintillating through scattering screens in the local ISM which will exhibit shorter characteristic timescales [11]. As was shown in early studies [12], active galactic nuclei which show RISS generally have “flat” or inverted radio spectra and can be expected to be very compact also at higher frequencies where astrometric observations are ideally performed. Moreover, higher frequency VLBI observations avoid the most severe effects of interstellar scattering, such as refractive apparent position shifts and angular broadening, which would decrease astrometric accuracy.

4. Conclusions

Only the most compact, core-dominated sources exhibit interstellar scintillation. The ASKAP VAST Survey is expected to find thousands of good candidate astrometric calibrators in the southern hemisphere. The detection of scintillating sources will also help to provide potential phase-reference calibrators in the vicinity of any transients detected, for rapid VLBI follow-up, e.g., to measure proper motions of Galactic transients and pin down their origin.

5. Acknowledgements

VAST is an international collaboration with over 70 members, led by Tara Murphy (The University of Sydney) and Shami Chatterjee (Cornell University). See <http://www.physics.usyd.edu.au/sifa/vast> for more information.

References

- [1] Narayan, R., *The Physics of Pulsar Scintillation*, Philosophical Transactions: Physical Sciences and Engineering, Volume 341, pp. 151–165, 1992.
- [2] Walker, M. A., *Interstellar scintillation of compact extragalactic radio sources*, Monthly Notices of the Royal Astronomical Society, Volume 294, pp. 307–311, 1998.
- [3] Walker, M. A., *Erratum: Interstellar scintillation of compact extragalactic radio sources*, Monthly Notices of the Royal Astronomical Society, Volume 321, p. 176, 2001.
- [4] Lovell, J. E. J., D. L. Jauncey, H. E. Bignall, L. Kedziora-Chudczer, J.-P. Macquart, B. J. Rickett, A. K. Tzioumis, *First Results from MASIV: The Microarcsecond Scintillation-induced Variability Survey*, The Astronomical Journal, Volume 126, pp. 1699–1706, 2003.
- [5] Lovell, J. E. J., B. J. Rickett, J.-P. Macquart, D. L. Jauncey, H. E. Bignall, L. Kedziora-Chudczer, R. Ojha, T. Pursimo, M. Dutka, C. Senkbeil, S. Shabala, *The Micro-Arcsecond Scintillation-Induced Variability (MASIV) Survey II: The First Four Epochs*, The Astrophysical Journal, Volume 689, pp. 108–126, 2008.
- [6] Haffner, L. M., R. J. Reynolds, S. L. Tufte, G. J. Madsen, K. P. Jaehnig, J. W. Percival, *The Wisconsin H α Mapper Northern Sky Survey*, The Astrophysical Journal Supplement Series, Volume 149, pp. 405–422, 2003.
- [7] Ojha, R., A. L. Fey, D. L. Jauncey, J. E. J. Lovell, K. J. Johnston, *Milliarcsecond Structure of Microarcsecond Sources: Comparison of Scintillating and Nonscintillating Extragalactic Radio Sources*, The Astrophysical Journal, Volume 614, pp. 607–614, 2004.
- [8] Ojha, R., A. L. Fey, T. J. W. Lazio, D. L. Jauncey, J. E. J. Lovell, L. Kedziora-Chudczer, *Scatter Broadening of Scintillating and Nonscintillating AGNs. I. A Multifrequency VLBA Survey*, The Astrophysical Journal Supplement Series, Volume 166, pp. 37–68, 2006.
- [9] Wall, J. V., *Populations of extragalactic radio sources*, Australian Journal of Physics, Volume 47, pp. 625–655, 1994.
- [10] Jackson, C. A., J. V. Wall, *Extragalactic radio-source evolution under the dual-population unification scheme*, Monthly Notices of the Royal Astronomical Society, Volume 304, pp. 160–174, 1999.
- [11] Bignall, H. E., J.-P. Macquart, D. L. Jauncey, J. E. J. Lovell, A. K. Tzioumis, L. Kedziora-Chudczer, *Rapid Interstellar Scintillation of PKS 1257-326: Two-Station Pattern Time Delays and Constraints on Scattering and Microarcsecond Source Structure*, The Astrophysical Journal, Volume 652, pp. 1050–1058, 2006.
- [12] Heeschen, D. S., *Flickering of extragalactic radio sources*, Astronomical Journal, Volume 89, pp. 1111–1123, 1984.

The First Experiment with VLBI-GPS Hybrid System

Younghee Kwak ¹, Tetsuro Kondo ², Tadahiro Gotoh ², Jun Amagai ², Hiroshi Takiguchi ², Mamoru Sekido ², Ryuichi Ichikawa ², Tetsuo Sasao ³, Jungho Cho ⁴, Tuhwan Kim ⁵

¹) *Ajou University / Korea Astronomy and Space Science Institute*

²) *Kashima Space Research Center, NICT*

³) *Yaeyama Star Club*

⁴) *Korea Astronomy and Space Science Institute*

⁵) *Ajou University*

Contact author: Younghee Kwak, e-mail: bgirl102@kasi.re.kr

Abstract

In this paper, we introduce our GPS-VLBI hybrid system and show the results of the first experiment which is now under way. In this hybrid system, GPS signals are captured by a normal GPS antenna, down-converted to IF signals, and then sampled by the VLBI sampler VSSP32 developed by NICT. The sampled GPS data are recorded and correlated in the same way as VLBI observation data. The correlator outputs are the group delay and the delay rate. Since the whole system uses the same frequency standard, many sources of systematic errors are common between the VLBI system and the GPS system. In this hybrid system, the GPS antenna can be regarded as an additional VLBI antenna having multiple beams towards GPS satellites. Therefore, we expect that this approach will provide enough data to improve zenith delay estimates and geodetic results.

1. Motivation

Combination of space geodetic techniques has been one of the fundamental issues in the IERS. Especially, the effective combination of the VLBI and GPS techniques is expected to solve the largest difficulties in current VLBI geodesy: the wet delays and clock offsets [4][5]. There have been several suggestions along this line [1][4][5][6][7][8]. In this study, we observationally tested the feasibility of the newly proposed observation-level combination technique, GPS-VLBI (GV) hybrid system [4][5] (Figure 1).

2. Concept

In the GPS-VLBI hybrid system, VLBI antennas observe quasars just like in a usual geodetic VLBI session. The GPS L1 and L2 signals are received by commercial GPS antennas, down-converted to video-band signals, and then sampled by VLBI samplers. The sampled GPS data are recorded as ordinary VLBI data by VLBI recorders and correlated by a VLBI correlator [4][5]. Observed group delay and delay rate from quasars and GPS satellites are analyzed following the usual VLBI analysis scheme. Thus we can expect to minimize various systematic errors between the two techniques.

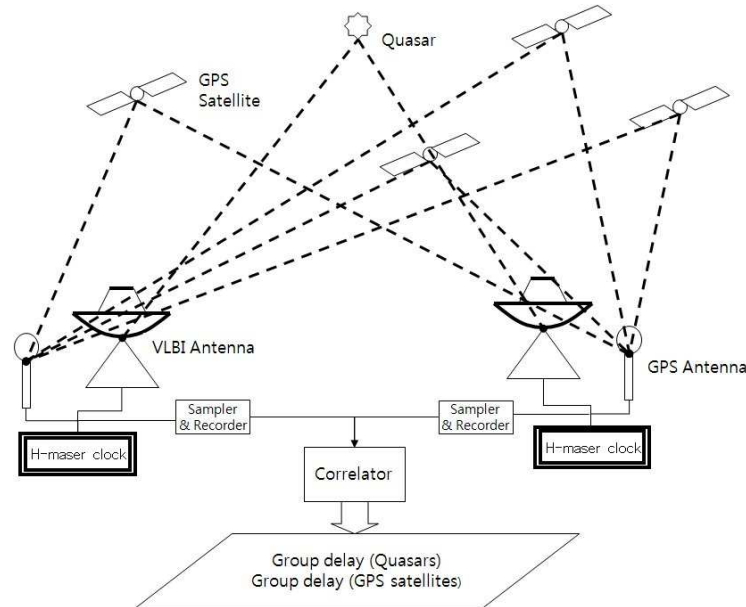


Figure 1. Concept of the GPS-VLBI Hybrid system.

3. Test Experiment of the GPS Part of the GV Hybrid System

Before the GPS-VLBI hybrid observation, we conducted a test experiment to verify that VLBI type observations of GPS satellites can be realized.

3.1. Settings

The test experiment was held at 06:19:00-06:20:00 (UTC) on September 9th in 2009 between Kashima and Koganei, Japan. The baseline length was about 110 km. The signal of each GPS satellite was received together in 32 MHz bandwidth covering 20.46 MHz GPS bandwidth. There were eight satellites above 15 degree cut-off elevation angle.

We used commercial GPS antennas, specially developed GPS down converters (see below), VSSP32 [3], and a software correlator [2] developed by NICT.

3.2. New GPS Down Converter

In a conventional GPS observation, the whole procedure from receiving signals to generating GPS data is accomplished in a normal GPS receiver. In order to record GPS signals with a VLBI system, we need to convert the GPS L1 (1575.42 MHz) and L2 (1227.6 MHz) signals to input signals for the VLBI sampler. One of the authors, J. Amagai, designed a special GPS converter system for this purpose. The outputs of the converter system are 75.42 MHz and 77.6 MHz signals for L1 and L2, respectively, with 32 MHz bandwidth each.

3.3. Results

As correlation results for 1 minute integration time, we simultaneously obtained clear fringes (Figures 2, 3) from all eight satellites above 15 degree cut-off elevation angle. If we approximate the GPS signals by white noise for simplicity, 87.5% and 12.5% of resultant signal-to-noise ratios (SNR) for L1 and L2 signals, respectively, already reach the typical VLBI group delay precision of 0.1 nsec.

4. Future Work and Perspectives

These results show that VLBI type observation of GPS satellites is readily realized in the GPS-VLBI hybrid system. Based on this test experiment, we successfully performed a 24-hour GPS-VLBI hybrid observation last December. The data are now in the correlation stage. After correlation, we will develop an analysis model for GPS satellites.

We expect the GPS-VLBI hybrid system to contribute to the following aspects:

- Better estimation of wet delays by using a large amount of GPS data,
- Better estimation of clock offsets by using identical H-maser clocks for both GPS and VLBI observations,
- Observation-level combination of space geodetic techniques,
- Direct connection of GPS satellite orbits to the International Celestial Reference Frame [1][4],
- Better UT1 determination using GPS [4][5],
- Connection of the origin of VLBI Terrestrial Reference Frame (TRF) with the Earth center of mass position [1].

References

- [1] Dickey, J., 2010, Proceedings of the 6th General Meeting of the IVS, in press (this volume).
- [2] Kondo T., Koyama Y., and Osaki H., Current Status of the K5 Software Correlator for Geodetic VLBI: IVS CRL-TDC News No. 23, pp.18-20, 2003.
- [3] Kondo, T., Y. Koyama, R. Ichikawa, M. Sekido, E. Kawai, and M. Kimura, Development of the K5/VSSP system, Journal of the Geodetic Society of Japan, Vol.54, No.4, pp.233-248, 2008.
- [4] Kwak, Y., T. Sasao, J. Cho, T. Kim, New Approach to VLBI-GPS Combination, 5th IVS General meeting, 2008.
- [5] Kwak, Y., T. Sasao, J. Cho, T. Kim, New suggestion for VLBI-GPS combined observation, AOGS, Busan, Korea, 2008.
- [6] Petrachenko, B., Corey, B., Himwich, E., Ma, C., Malkin, Z., Niell, A., Shaffer, D. and Vandenberg, N. 2004, Report of IVS WG3.1 - Observing strategies, available at <http://ivscg.gsfc.nasa.gov/about/wg/wg3/index.html>
- [7] Thaller, D., Rothacher, M., GPS and VLBI Antenna Behaviour Derived From A GPS Antenna On The Wettzell Radiotelescope, EGS XXVII General Assembly, Nice, 21-26 April 2002.
- [8] Tornatore, V. and Haas, R., 2010, Proceedings of the 6th General Meeting of the IVS, in press (this volume).

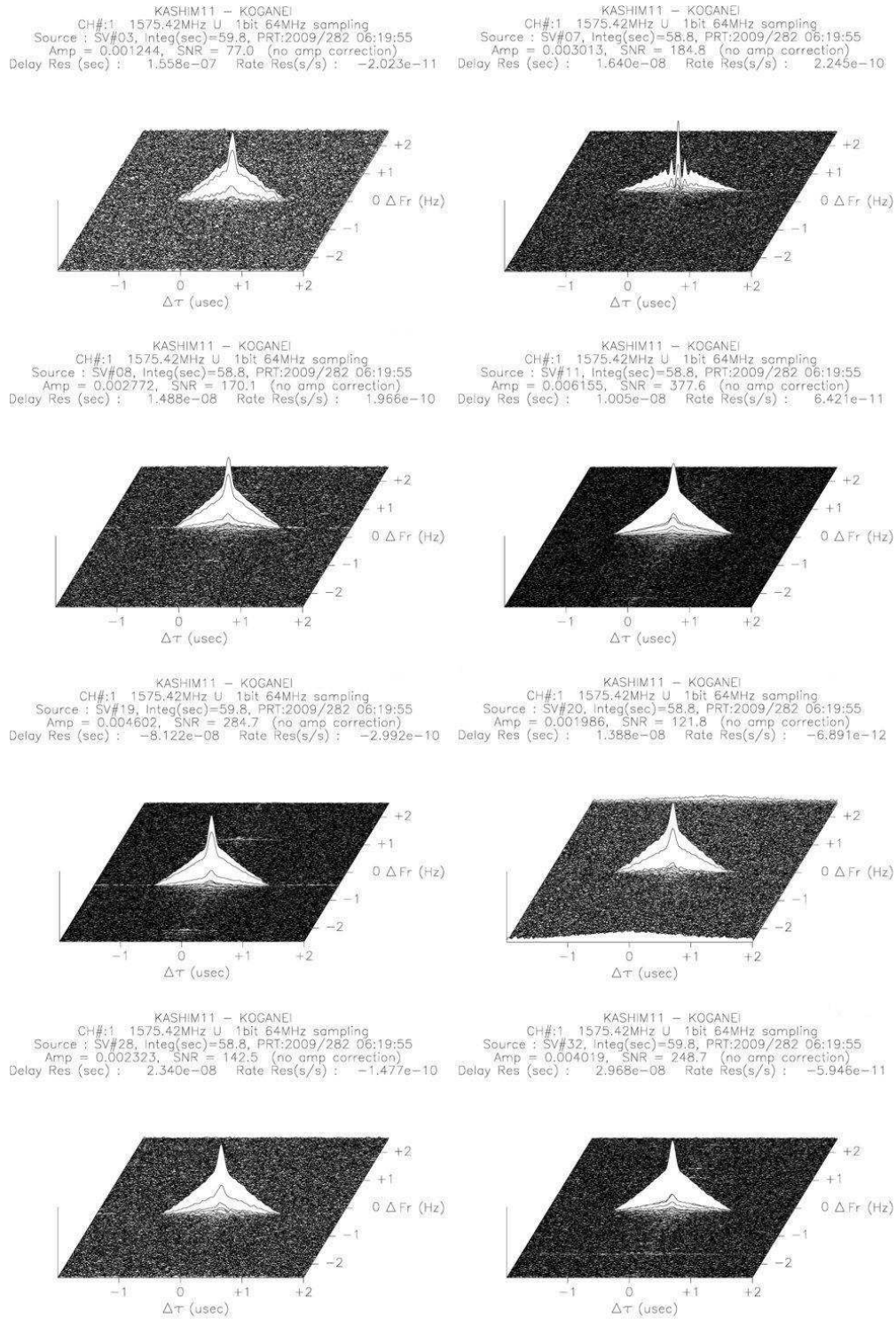


Figure 2. Fringe peaks for GPS L1 signal.

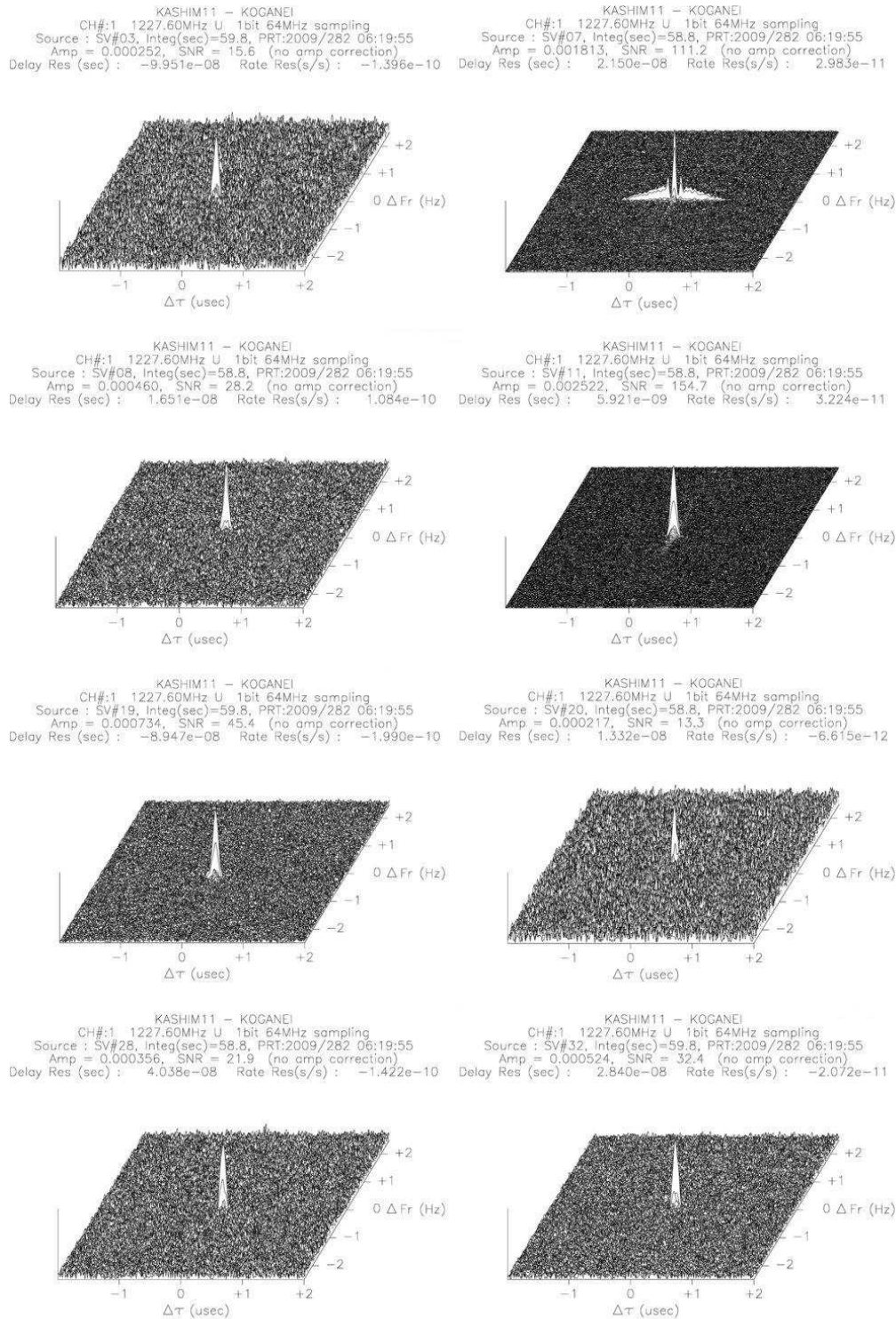


Figure 3. Fringe peaks for GPS L2 signal.

Ionospheric Response to the Total Solar Eclipse of 22 July 2009 as Deduced from VLBI and GPS Data

L. Guo ¹, F.C. Shu ¹, W.M. Zheng ¹, T. Kondo ³, R. Ichikawa ², S. Hasegawa ², M. Sekido ²

¹) *Shanghai Astronomical Observatory, CAS*

²) *Kashima Space Research Center, NICT*

³) *Kashima Space Research Center, NICT, and Ajou University, Korea*

Contact author: L. Guo, e-mail: kent-gl@shao.ac.cn

Abstract

A total solar eclipse occurred over China at latitudes of about 30°N on the morning of 22 July 2009, providing a unique opportunity to investigate the influence of the sun on the earth's upper ionosphere. GPS observations from Shanghai GPS Local Network and VLBI observations from stations Shanghai, Urumqi, and Kashima were used to observe the response of TEC to the total solar eclipse. From the GPS data reduction, the sudden decrease of TEC at the time of the eclipse, amounting to 2–8 TECU, and gradual increase of TEC after the eclipse were found by analyzing the diurnal variations. More distinctly, the variations of TEC were studied along individual satellite passes. The delay in reaching the minimum level of TEC with the maximum phase of eclipse was 5–10 min. Besides, we also compared the ionospheric activity derived from different VLBI stations with the GPS results and found a strong correlation between them.

1. Introduction

The ionosphere undergoes substantial changes during a solar eclipse. The eclipse causes a change of ionization in the E-region and F-region of the ionosphere where dynamic processes play an important role. During the eclipse, the Total Electron Content (TEC) is a good indicator of the state and dynamics of the F-region of the ionosphere. Consequently, experimental observations of the ionosphere at such time provide a unique opportunity to investigate the ionospheric response to the change in the solar flux emission towards the earth.

Different techniques have been used to study the eclipse-induced ionospheric changes including the earlier beacon satellite, then predominantly ionosonde measurements, and today the widely used Global Positioning System (GPS)-based TEC measurements. The response of GPS-based TEC variations to the solar eclipse under low solar activity was studied by several authors [1][2][3][4]. Baran et al. (2003) [3] detected the effect of the eclipse on 11 August 1999 over Europe in diurnal variations and found trough-like variations with gradual decrease, followed by increase of TEC at all European stations. The depression of TEC of this eclipse amounted to 2–8 TECU (TEC Unit, 1 TECU = 1×10^{16} electron/m²) and the delay in reaching the minimum TEC with respect to the maximum phase of the eclipse was 10–20 min. Observations by Afrainmovich and Lesyuta 2002 [4] for the total eclipse of 21 June 2001 using data from three African GPS stations showed a low level of geomagnetic disturbance and a clearly pronounced effect of a depression of TEC for all GPS stations during the eclipse period. The delay between the smallest TEC with respect to eclipse totality was 9–37 min, and the depth and duration of the TEC decrease were 0.5–0.9 TECU and 30–67 min, respectively. Using data from a GPS network in Antarctica on 23

November 2003, Zainol et al. 2006 [5] analyzed in detail the signature of a Traveling Ionospheric Disturbance (TID) event and the different values of sudden TEC depressions at different stations. A linear relationship between the eclipse magnitude and TEC depletion was also detected. And before and after the eclipse day the observation of the TID waves suggested that the TID event on the eclipse period did not result from the solar eclipse but had tropospheric origin. Observation results by Jakowski et al. 2008 [6] showed the response of TEC to the total solar eclipse on 3 October 2005 with European GPS network. They also detected the depression of TEC of 3–4 TECU and the delay of a minimum level of TEC with respect to the maximum phase of the eclipse at 20–30 min by diurnal variation analysis. The two-dimensional TEC maps with 5-min interval temporal resolution showed that the eclipse produced remarkable changes in the structure of the ionosphere. Such response of TEC to the solar eclipse depends on the latitude as well as the longitude.

In addition, Very Long Baseline Interferometry (VLBI) can measure the difference of TEC in the ray path to the radio source between two stations of a baseline due to the nature of the dual frequency observations. By comparing VLBI with GPS-based TEC values, we can get the difference between the two techniques, and such comparisons have been used by many researchers [8][9][10]. From the published results, ionospheric parameters derived by VLBI and GPS show similar trends and differ by a few TECU or by a large system constant. And such systematic difference is due to the S/X VLBI receiver offsets.

In this paper we present the ionospheric response to the total solar eclipse on 22 July 2009 using three VLBI stations at Shanghai, Urumqi, and Kashima, GPS co-located receivers, and the Shanghai GPS Local Network to study the TEC diurnal variations during the eclipse day. The event took place under low solar activity.

2. The Geometry and General Information about the Total Solar Eclipse

The total solar eclipse took place on 22 July 2009. The three curved lines with bars in Figure 1 show the central path of the total eclipse by the central line and zones of partial eclipse by the outer lines. Shanghai and Wuhan are located very near to the central path of the total eclipse. Besides, two other VLBI stations (Urumqi and Kashima) carried out observation experiments during the event. At Shanghai station, the partial eclipse began at Universal Time (UT) 00:23:26 (first contact) and ended at UT 03:01:38 (fourth contact) with the maximum eclipse occurring at UT 01:36:48 [11].

Different methods were used for the analysis of the TEC behavior during the eclipse. A single technique was employed for diurnal TEC variations by averaging GPS measurements for satellites in different directions. The comparison of VLBI- and GPS-based TEC was also presented. VLBI measures the difference of TEC in the ray path to a radio source between two stations, whereas GPS measures the TEC along the ray path from a GPS satellite to the stations. To compare results between them, firstly the vertical TEC value at the VLBI station is calculated. Then slant TEC is obtained from vertical TEC by applying an ionosphere mapping function according to the VLBI observation elevation at the two stations. Lastly the difference of the slant TEC is easily computed [8].

3. The Eclipse Effect on TEC by GPS Measurements

For GPS-based TEC reduction, we used the widely-used local ionosphere model as a single, infinitesimally thin layer at a fixed height of 375 km and a simple mapping function to convert the slant TEC along the ray path into vertical TEC. Figure 2 shows the diurnal variations of TEC from the phase measurement along satellite passes at four different stations on eclipse day and reference quiet days. In Figure 2 we can clearly see an obvious depression of TEC, amounting to 2–6 TECU, at eclipse day compared with that on the reference day. The time of the maximum phase of the eclipse varied in Universal Time (UT) from 01:30 to UT 01:35, so the delay of the minimum TEC with respect to such maximum phase of the eclipse was in the range of 5–10 min combined with the minimum TEC value shown in Figure 2. As the stations were close, the levels of TEC depression observed by the same satellite and different stations were similar to each other.

Figure 3 shows the diurnal variations of the vertical TEC over a single station (SHAO) for the eclipse day (22 July 2009) and a reference quiet day (21 July 2009). By comparing the TEC on the eclipse day with that of the reference quiet day, we can study the eclipse effect on the TEC variations. It is shown in Figure 3 that the obviously sudden depression of the TEC value occurred for the eclipse day. The time for the minimum TEC value was close to the maximum phase of the eclipse, and its depression reached 6–8 TECU. In the following approximately 2 hours, the TEC value gradually reached the regular level.

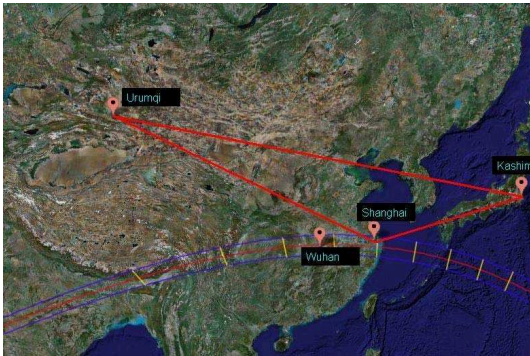


Figure 1. Map of the total solar eclipse path on 22 July 2009, and distributions of VLBI and GPS sites. Shanghai and Wuhan are located very near the central path of the total eclipse.

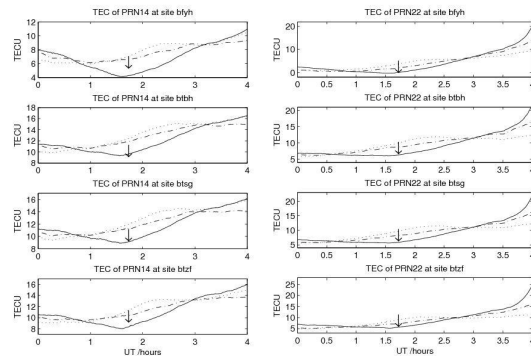


Figure 2. Temporal TEC variations along individual satellite passes for PRN 14 (left) and 22 (right) observed at BFYH, BTBH, BTSG, and BTZF stations on 22 July (black solid line—the eclipse day), 21 July (dashed line—quiet day) and 23 July (dotted line—quiet day). The arrows show the time of TEC minima.

4. Comparison of VLBI- and GPS-based TEC

To detect the TEC variations by VLBI, a 9-hour VLBI experiment for ionospheric TEC measurement during the eclipse was carried out in S/X dual-band with participation of Shanghai, Urumqi, and Kashima stations. The observation target was a strong extragalactic source, 4C39.25, at the solar angle of 25° . The difference of TEC in the ray path to the source was determined

by VLBI group delay measurements. The method for comparing the differences of TEC by the VLBI- and GPS-based measurements was described in section 2. The differences between them on eclipse day are shown in Figure 4. The jump in VLBI-based TEC differences at about UT 02:40 needs further analysis.

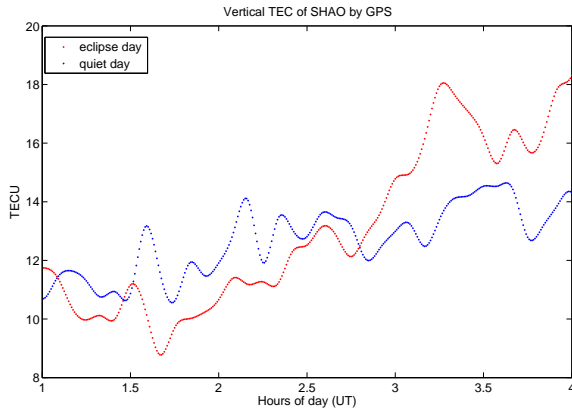


Figure 3. Diurnal VTEC variations observed at SHAO station on 22 July (the eclipse day) and 21 July (the quiet day). The line with the larger initial value is the eclipse day line.

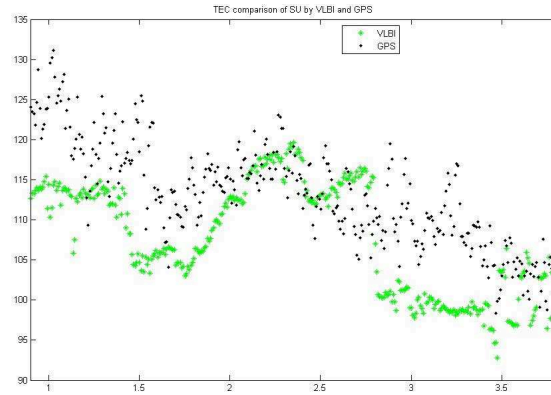


Figure 4. Correlation between GPS and VLBI data: Shanghai-Urumqi baseline on eclipse day 22 July 2009. The RMS of the difference was 4 TECU. The offset was caused by S/X VLBI receiver offset.

5. Conclusions

We presented the TEC variations' response to the eclipse over the Shanghai GPS Local Network and a comparison of VLBI- and GPS-based TEC. By analysis of the diurnal TEC variations, the sudden TEC depression amounted to 2–8 TECU for the eclipse day, and the delay of minimum TEC with respect to the time of maximum phase of the eclipse was in the range of 5–10 min.

The comparison of VLBI- and GPS- based TEC variations was also presented. The offsets between them were caused by S/X VLBI receiver offsets. We also found a jump in the VLBI-based TEC differences at UT 02:40; this jump needs further analysis.

References

- [1] Espenak, F., and Anderson J., Predictions for the Total Solar Eclipses of 2008, 2009, and 2010, Proc. IAU Symp.233, Solar Activity and its Magnetic Origins, Cambridge University Press, pp. 495–502, 2006.
- [2] Afrainmovich E. L., Kosogorov, E. A., Lesyuta O. S., Ionospheric effects of the August 11, 1999 total solar eclipse as deduced from European GPS network data, Advances in Space Research, Volume 27, Issues 6-7, pp. 1351–1354, 2001.
- [3] Baran W. L., Ephishov L. I., Shagimuratov I. I., et al., The response to the ionospheric total electron content to the solar eclipse on August 11, 1999, ASR, Volume 31, Issue 4, pp. 989–994, 2003.
- [4] Afrainmovich E. L., Lesyuta O. S., Ionospheric response to the total solar eclipse of June 21, 2001 as

- deduced from the data from the African GPS network, 2002. arXiv:physics/0201047v1 [physics.geo-ph] 24 Jan 2002.
- [5] Zainol Abidin Abdul Rashid, Mohammad Awad Momani, Sumazly Sulaiman, et al. GPS ionospheric TEC measurement during the 23rd November 2003 total solar eclipse at Scott Base Antarctica, *Journal of Atmospheric and Solar-Terrestrial Physics*, Volume 68, Issue 11, pp. 1219–1236, July 2006.
 - [6] Jakowski N., Stankov S.M., Wilken V., et al., Ionospheric behavior over Europe during the solar eclipse of 3 October 2005, *Journal of Atmospheric and Solar-Terrestrial Physics*, Volume 70, Issue 6, April 2008, pp. 836–853.
 - [7] Tsai and Liu, Tsai H.F., Liu J.Y., Ionospheric total electron content response to solar eclipses. *J. Geophysical Research* 104 6, pp. 12.657–12.668, 1999.
 - [8] Sekido M., Kondo T., Kawai E., et al., Evaluation of Global Ionosphere TEC by Comparison with VLBI Data, IVS 2004 General Meeting Proceedings. pp. 427–436, NASA/CP-2004-212255, 2004.
 - [9] Bergstrand, S., and Haas, R., Comparison of ionospheric activity derived from GPS and different VLBI networks, IVS 2004 General Meeting Proceedings, pp. 447–451, NASA/CP-2004-212255, 2004.
 - [10] Hobiger T., Boehm J., Todorova S. et al., The Project VLBI ionos- How VLBI contributes to Ionospheric Research. Proceedings of the 16th Working Meeting on European VLBI for Geodesy and Astrometry. Leipzig, pp. 291–298, 2003.
 - [11] Shu F. C., Guo L., Liu M., et al, Ionospheric TEC measurement with VLBI and GPS during the total solar eclipse of 22 July 2009, *Science Technology Review*, vol 27, 15, pp. 19–24, 2009.

The Tropospheric Products of the International VLBI Service for Geodesy and Astrometry

Robert Heinkelmann, Christian Schwatke

Deutsches Geodätisches Forschungsinstitut (DGFI)

Contact author: Robert Heinkelmann, e-mail: heinkelmann@dgfi.badw.de

Abstract

The IVS runs two tropospheric products: The IVS tropospheric parameter rapid combination monitors the zenith wet delay (ZWD) and zenith total delay (ZTD) of the rapid turnaround sessions R1 and R4. Goal of the combination is the identification and the exclusion of outliers by comparison and the assessment of the precision of current VLBI solutions in terms of tropospheric parameters. The rapid combination is done on a weekly basis four weeks after the observation files are released on IVS Data Centers. Since tropospheric and geodetic parameters, such as vertical station components, can significantly correlate, the consistency of the ZTD can be a measure of the consistency of the corresponding TRF as well. The ZWD mainly rely on accurate atmospheric pressure data. Thus, besides estimation techniques, modeling and analyst's noise, ZWD reflects differences in the atmospheric pressure data applied to the VLBI analysis. The second product, called tropospheric parameter long-term combination, aims for an accurate determination of climatological signals, such as trends of the atmospheric water vapor observed by VLBI. Therefore, the long-term homogeneity of atmospheric pressure data plays a crucial role for this product. The paper reviews the methods applied and results achieved so far and describes the new maintenance through DGFI.

1. Tropospheric Model of Radio Techniques

The general station dependent tropospheric model for the delay of radio waves propagating through the neutral atmosphere

$$d_{trop} = m f_h(\epsilon) \cdot ZHD + m f_w(\epsilon) \cdot ZWD + m f_g(\epsilon) \cdot [G_N \cos(\alpha) + G_E \sin(\alpha)] \quad (1)$$

accounts for non-dispersive delaying and bending effects through constituents of the Earth's atmosphere. The variables α and ϵ denote the azimuth and elevation angles of a specific observation at a VLBI antenna. The gradient mapping function $m f_g$ can be taken from [9]

$$m f_g(\epsilon) = m f_h(\epsilon) \cdot \cot(\epsilon) \quad \text{or} \quad m f_g(\epsilon) = m f_w(\epsilon) \cdot \cot(\epsilon) \quad (2)$$

and the hydrostatic and wet mapping functions $m f_{h,w}$ are currently provided by [1]¹. For part of the atmosphere, the assumption of hydrostatic equilibrium approximately holds. The hydrostatic delay at zenith ZHD (mm) can be expressed analytically [3]

$$ZHD = \frac{2.2768 \cdot p}{1 - 0.00266 \cos(2\varphi) - 0.000280h} \quad (3)$$

depending on the surface air pressure p and the position (latitude φ and orthometric height h) of the antenna reference point.

¹<http://ggosatm.hg.tuwien.ac.at/DELAY/>

Water vapor shows rather different dipole characteristics and insufficient mixing with the other (dry) atmospheric gases. The wet delay is considered unknown and is estimated along with the other parameters by classical parameter estimation or filter techniques. The partial derivative of the zenith wet delay reads:

$$\frac{\partial d_{trop}}{\partial ZWD} = m f_w(\epsilon) \quad (4)$$

It is usually represented by constrained linear spline functions [8] or by a random walk stochastic process [7], respectively, in case of filter techniques.

The total zenith delay is the sum of the apriori (here: hydrostatic) and the estimated (here: wet) zenith delay

$$ZTD = ZHD + ZWD \quad (5)$$

2. The Role of Surface Air Pressure for Troposphere Modeling

While φ and h (eq. 3) can be approximated by their respective apriori values, ZHD depends almost entirely on the in-situ surface air pressure, which is usually recorded by meteorological sensors and provided for each observation, e.g., in the NGS file. In some cases, however, the meteorological records are missing, which is indicated by an invalid entry such as -999.99 hPa, or they are erroneous. Unlike temperature measurements, pressure measurements are most unlikely to be affected by artificial trends, such as urban growth or vegetation. Therefore, known inhomogeneities of the measured surface air pressure are mainly breaks of the running mean value due to calibration, replacement, or relocation of the sensor. The usage of inaccurate air pressure in VLBI analysis may have several effects on the estimated parameters:

1. ZHD will be wrong by about 2.3 mm per 1 hPa (eq. 3).
2. Since the hydrostatic and wet mapping functions are similar, the ZWD estimate absorbs most of the inaccurate ZHD and will be biased by about -2.1 mm per 1 hPa.
3. The rest, about -0.2 mm per 1 hPa, propagates into other parameters due to correlations, mainly into the height component of the station.

Following 1. and 2., ZTD (eq. 5) is also affected, by about 0.2 mm per 1 hPa. The estimate (ZWD) does not fully compensate for the wrong apriori (ZHD), because the hydrostatic and wet mapping functions differ. In the past there were approaches modeling the tropospheric delay with a single total mapping function, which would serve better for this particular purpose. Nevertheless, the usage of total mapping functions is significantly less accurate than the models separately accounting for hydrostatic and wet atmospheric constituents. Figures 1 and 2 display examples of ZWD and ZTD at two IVS sites. It is clearly visible that the ZWD differences between the IVS Analysis Centers become much smaller in the case of ZTD at Westford. At Zelenchukskaya, however, the ZWD differences almost totally remain at ZTD. Hence, much larger effects on the station coordinates are to be expected at this site.

For geodesy, 3. must be alarming since the primary geodetic parameters, the station coordinates, are affected. If the surface air pressure used in VLBI analysis deviates from its true value by 5 hPa, the effect on station coordinates will reach the 1-millimeter-level at most of the sites. Therefore, it is not sufficient to replace missing pressure values by a constant value or any simple atmospheric model. An appropriate way to substitute missing pressure values has been introduced by the authors before, cf. [6]. Since numerical weather models (NWM) such as NCEP or ECMWF

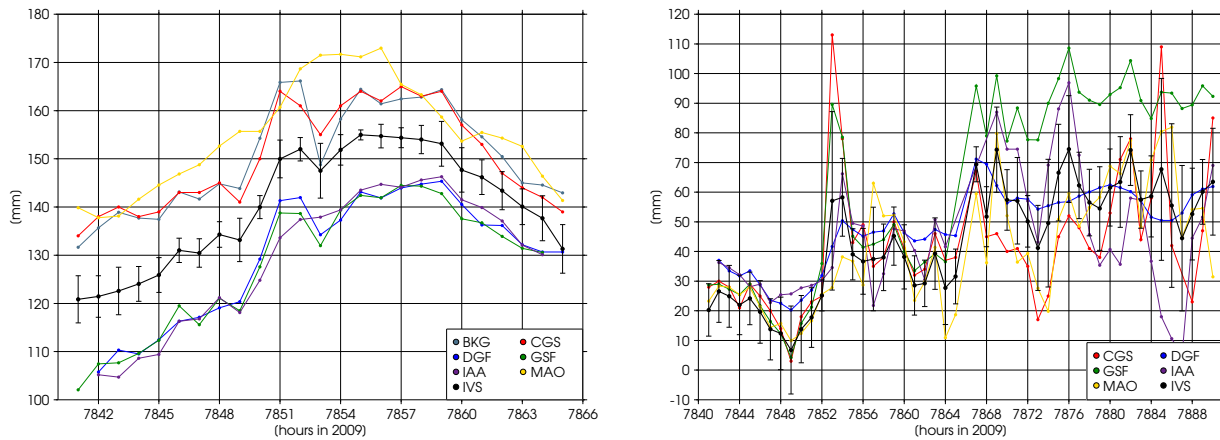


Figure 1. ZWD (mm): Westford, USA (left) and Zelenchukskaya, Russia (right). IVS line has error bars.

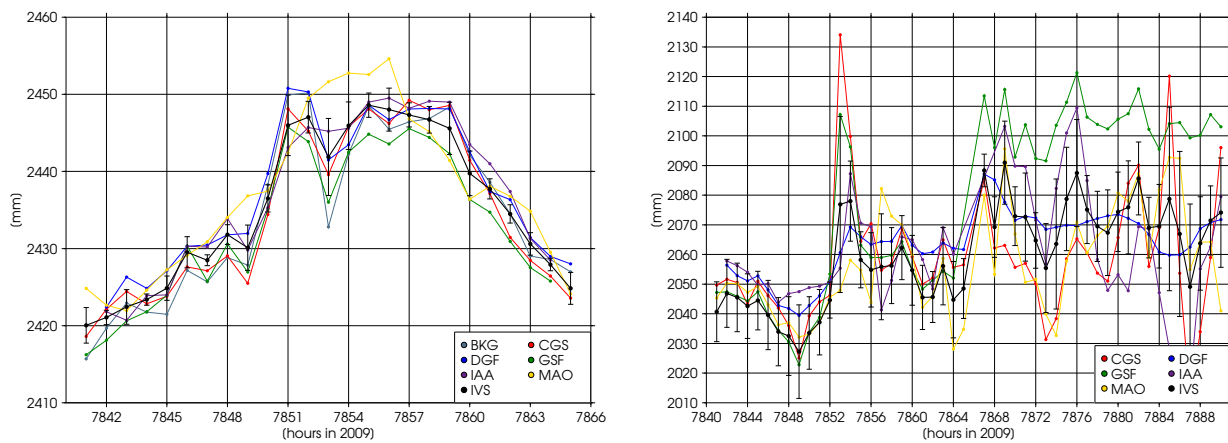


Figure 2. ZTD (mm): Westford, USA (left) and Zelenchukskaya, Russia (right). IVS line has error bars.

show inherent biases, too, it is questionable, whether pressure values interpolated from such models can provide the absolute accuracy target in general. If no particular accuracy is needed or no NWM is available, substitutes can be calculated from GPT [2].

3. Tropospheric Parameter Long-term Combination

- <http://www.dgfi.badw.de/index.php?id=196>
- Relevant publication: [5]
- Considered breaks (> 1 hPa) of the running mean value (Table 1) and outliers of pressure records (Table 2). A positive break in Table 1 means that the pressure values before the specified epoch are larger than the pressure values after the epoch until present day.

Table 1. Pressure breaks > 1 hPa at 8 frequently used observing sites

IVS site	epoch	break (hPa)
Algonquin Park	2003 Jan 17	-2.8
Gilmore Creek	1993 Jun 26	+1.4
Hartebeesthoek	1993 May 04	+15.5
Hobart (26)	1991 Dec 11	+17.4
Kokee Park	2003 Jun 17	+1.6
Ny-Ålesund	1998 Jul 01	+2.8
Shanghai (25)	1995 Apr 25	-7.6
Wettzell	1986 Aug 07	+1.9

Table 2. Possible outliers

solution	site	start epoch	end epoch
aus	all	2000.2	2001.1
	Fortaleza	2003.75	open
	Gilmore Creek	1984.0	1989.5
	Wettzell	1984.0	1989.0
iaa2007a	Westford	1999.4	2000.0
mao2005a	Fortaleza	2003.75	open
	Westford	2000.0	2001.0
	Wettzell	1984.0	1989.0
gsf2005a	Kokee Park	OHIG32, R&D-8	
	Wettzell	T2030, T2031, T2032, T2033	

4. Tropospheric Parameter Rapid Combination

- <http://www.dgfi.badw.de/index.php?id=194>
- Relevant publication: [4]
- Missing pressure records, outliers, and breaks (Tables 3–5) have to be considered.

Table 3. Missing pressure records (%) since 2002

site	%	site	%	site	%
Algonquin Park	0.6	Kokee Park	0.6	Svetloe	1.4
Badary	2.3	Matera	0.5	TIGO Concepción	0.7
Fortaleza	87.4	Medicina	2.6	Tsukuba (32)	0
Gilmore Creek	0	Ny-Ålesund	0.4	Westford	30.1
Hartebeesthoek	0.5	Onsala (60)	0	Wettzell	0
Hobart (26)	0.8	Shanghai (25)	1.5	Zelenchukskaya	38.9

Table 4. Possible outliers of IVS-R1 and R4

site	outlier
Fortaleza	$p = 0\text{hPa!}$
Hobart (26)	IVS-R1054
Matera	IVS-R4368
Westford	$p < 970\text{hPa}, p > 1030\text{hPa}$
Wetzell	$p < 900\text{hPa}, p > 970\text{hPa}$

Table 5. Pressure breaks w.r.t. current mean pressure since 2002

site	epoch	break
Algonquin Park	2003.08	1.6
	2004.5	4.0
	2004.9	2.1
	2006.16	5.1
Hobart (26)	2005.965	3.7
Svetloe	2004.0	-2.2
	2008.96	3.9
Tsukuba (32)	2005.0	0.6
Westford	2005.0	2.1
Zelenchukskaya	2007.5	11.4

References

- [1] Böhm J., B. Werl, H. Schuh, JGR, B02406, doi:10.1029/2005JB003629, 2006.
- [2] Böhm J., R. Heinkelmann, H. Schuh, JoGe, Vol. 81, No. 10, 679–683, 2007.
- [3] Davis J.L., T.A. Herring, I.I. Shapiro, A.E.E. Rogers, G. Elgered, Radio Sci., Vol. 20, No. 6, 1593–1607, 1985.
- [4] Heinkelmann R., J. Böhm, H. Schuh, Proc. of the 17th Working Meeting on European VLBI for Geodesy and Astrometry, INAF – Istituto di Radioastronomia – Sezione di NOTO – Italy, M. Vennebusch, A. Nothnagel (eds.), 79–83, 2005.
- [5] Heinkelmann R., J. Böhm, H. Schuh, S. Bolotin, G. Engelhardt, D.S. MacMillan, M. Negusini, E. Skurikhina, V. Tesmer, O. Titov, JoGe, Vol. 81, Nos. 6–8, 483–502, 2007.
- [6] Heinkelmann R., J. Böhm, H. Schuh, V. Tesmer, In: Geodetic Reference Frames, IAG Symposia, Vol. 134, H. Drewes (ed.), 45–51, 2009.
- [7] Herring T.A., J.L. Davis, I.I. Shapiro, JGR, Vol. 95, No. B8, 12561–12581, 1990.
- [8] Ma C., J.M. Sauber, L.J. Bell, T.A. Clark, D. Gordon, W.E. Himwich, J.W. Ryan, JGR, Vol. 95, No. B13, 21991–22011, 1990.
- [9] MacMillan D.S., GRL, Vol. 22, No. 9, 1041–1044, 1995.

Extracting Independent Local Oscillatory Geophysical Signals by Geodetic Tropospheric Delay

O. J. Botai¹, L. Combrinck², V. Sivakumar³, H. Schuh⁴, J. Böhm⁴

¹⁾ *Department of Geography, Geoinformatics and Meteorology, University of Pretoria*

²⁾ *Hartebeesthoek Radio Astronomy Observatory*

³⁾ *National Laser Center, Council for Scientific and Industrial Research*

⁴⁾ *Institute of Geodesy and Geophysics (IGG), Vienna University of Technology*

Contact author: O. J. Botai, e-mail: joel.botai@up.ac.za

Abstract

Zenith Tropospheric Delay (ZTD) due to water vapor derived from space geodetic techniques and numerical weather prediction simulated-reanalysis data exhibits non-linear and non-stationary properties akin to those in the crucial geophysical signals of interest to the research community. These time series, once decomposed into additive (and stochastic) components, have information about the long term global change (the trend) and other interpretable (quasi-) periodic components such as seasonal cycles and noise. Such stochastic component(s) could be a function that exhibits at most one extremum within a data span or a monotonic function within a certain temporal span. In this contribution, we examine the use of the combined Ensemble Empirical Mode Decomposition (EEMD) and Independent Component Analysis (ICA): the EEMD-ICA algorithm to extract the independent local oscillatory stochastic components in the tropospheric delay derived from the European Centre for Medium-Range Weather Forecasts (ECMWF) over six geodetic sites (HartRAO, Hobart26, Wettzell, Gilcreek, Westford, and Tsukub32). The proposed methodology allows independent geophysical processes to be extracted and assessed. Analysis of the quality index of the Independent Components (ICs) derived for each cluster of local oscillatory components (also called the Intrinsic Mode Functions (IMFs)) for all the geodetic stations considered in the study demonstrate that they are strongly site dependent. Such strong dependency seems to suggest that the localized geophysical signals embedded in the ZTD over the geodetic sites are not correlated. Further, from the viewpoint of non-linear dynamical systems, four geophysical signals—the Quasi-Biennial Oscillation (QBO) index derived from the NCEP/NCAR reanalysis, the Southern Oscillation Index (SOI) anomaly from NCEP, the SIDC monthly Sun Spot Number (SSN), and the Length of Day (LoD)—are linked to the extracted signal components from ZTD. Results from the synchronization analysis show that ZTD and the geophysical signals exhibit (albeit subtle) site dependent phase synchronization index.

1. Introduction

With the increasing ease of collecting and homogenizing tropospheric geodetic data, a long time series of geodetic data sets such as Zenith Tropospheric Delay (ZTD), Water Vapor (WV), and geodetic site coordinates are now available to the scientific community. As a result, the accumulated datasets make it possible to study the geophysical signals embedded in the data. These geophysical signals hold important information about atmosphere–earth system dynamics. However, sequences of these (geodetic) observations have noise, with unknown dependency structure embedded in the data. Until now, the classical techniques of analyzing such series have been subjective and unable to characterize the stochastic structure manifested in the observations. As a result, analyzing such data sets required complex, yet flexible and robust, approaches of objectively manipulating the data.

In non-linear and non-stationary time series, the stochastic global component could be a function which exhibits at most one extremum within a data span or a monotonic function within a certain temporal span (Zhauhua et al., 2007). At first, the mathematical approaches of extracting this component were based on fitting a simple deterministic function (e.g., a linear function) to the data. This method of detrending is clearly suitable for a stationary world and, therefore, may not be robust for real-world applications such as in tropospheric delay due to WV analyses. As the theory of stationary time series developed, the trend was considered as a deterministic component that ought to be removed from the time series in order to make it stationary (Alexandrov et al. 2009). Nevertheless, the deterministic method of trend extraction fails to account for a) the random irregular components, b) the conflicts within the identification of turning points in the trend, and c) the unclear definition of trend, acceptable degree of smoothness, trend-cycles, or long-term structural effects. Some of the prominent approaches of extracting the quasi-period global component in the data include: a) model-based approaches (a stochastic time series model for the data, e.g., ARMA or ARIMA model, are assumed *a priori*); b) nonparametric filtering (which does not require a specification of a model) e.g., the Hodrick-Prescott filter; c) Singular Spectrum Analysis, SSA (a nonparametric methodology that does not require a specification of time series models or a trend *a priori*); d) wavelets; e) Independent Component Analysis (ICA); and f) Empirical Mode Decomposition (EMD). Some of these methods of trend extraction encompass regression analysis or Fourier-based filtering and are based on unjustifiable linearity and stationarity assumptions. Furthermore, the stochastic global component often evolves from the same or part of the same underlying process that generates data, and therefore the temporal structure is often linked to local time scales. As a result, the use of functional forms to represent the unknown embedded trend model could be subjective.

The importance of estimating the slowly evolving changes in tropospheric delay due to WV lies in the role IWV plays in geodetic measurement as well as in climate change. As a result, estimating this stochastic global component is a key element of many studies involving WV variability and its links with the dynamics and precipitation (e.g., Zveryaev and Allan 2005; Trenberth et al. 2005; Schneider et al. 2009). In all these studies, the functional form of the trend is deterministically and subjectively determined. Since the data record under consideration is generated from non-linear and non-stationary underlying processes, a functional form of the trend has to be stochastic and therefore ought not to be pre-selected. Therefore, in order to extract the trend and other (quasi-) periodic components in the data, the process of detrending must be data adaptive (Zhauhua et al. 2007; Alexandrov et al. 2008).

In this study, we examine the use of the combined Independent Component Analysis (ICA) and EMD to extract the local independent components in the tropospheric delay derived from the ECMWF reported by Böhm et al. (2006). Aires et al. (2000) demonstrated a north-south equatorial Atlantic SST linkage by applying the ICA algorithm to study the variability of the tropical sea surface temperature (SST), as well as the links between the variability of ENSO and Atlantic SST. In particular, the Denoising Source Separation (DSS) algorithm (see Särelä and Valpola 2005) can be used to identify hidden geophysical signal components $s_i(t)$ present in the measurements $y_j(t)$ expressed in Equation (1).

$$y_j(t) = \sum_{i=1}^N \beta_{i,j} s_i(t) \quad (1)$$

Here, the index j runs over the independent variable measurements, which could be spatial

locations over the discretized observation period t . This generative model describes how the observed data are generated by a process of mixing the underlying signals $s_i(t)$, which are referred to as the ICs. In matrix formulation, the matrix of observations Y , the matrix of the underlying geophysical sources S , the matrix of linear or non-linear combination of the signals or mixing vectors A , and the Gaussian noise δ are mathematically described by a mixing model expressed in Equation (2).

$$Y = AS + \delta \quad (2)$$

Lastly, the causal links between ICs from different IVS and other geophysical records, such as Sun Spot Number (SSN), Length of Day (LoD), Southern Oscillation Index (SOI), and Quasi-Biennial Oscillations (QBO), are examined by use of the angle strength of the phase angle difference between the series, hereafter the mean phase coherence (Mormann et al. 2000). Documenting these results would be useful for understanding the underlying non-stationary and non-linear geophysical signal structure present in the data and for assessing their dependency on each other with applications for the short-term and long-term variability of the atmosphere. An example of research in this direction has been reported by Paluš and Novotná (2009). These contributions would benefit researchers from a diversity of fields.

2. Data and Method

2.1. Data

ZTD over six geodetic IVS sites (see Table 1) spanning 1998 through 2008 were obtained from the Institute of Geodesy and Geophysics (IGG), Technical University of Vienna, Austria (<http://www.hg.tuwien.ac.at/~ecmwf1/VLBI>). The ZWD and IWV datasets are derived from ECMWF numerical model simulations (Böhm et al. 2006).

The data under consideration were originally computed at six-hour intervals for the entire temporal span. Monthly values of ZTD were computed for the time span under consideration. The top panel in Figure 1 depicts the apparent seasonality in ZTD (40 cm of ZTD has been added to stations except Hobart26 for better visualization) in all six geodetic IVS stations studied. Geophysical data are significantly affected by seasonal variability. In order to avoid strong seasonality that could mask other important signals (with, e.g., annual, interannual, and interseasonal variability), ZTD data sets were seasonally adjusted by use of the Ratio-to-Moving Average method described by Hanke et al. (2001) and have been plotted in the bottom panel of Figure 1 (here only HartRAO is plotted to illustrate the effect of seasonal adjustment to ZTD). Additionally, we have used monthly time series anomalies of four geophysical signals (here the 1998–2008 time epoch is used): the QBO index derived from the NCEP/NCAR reanalysis; the

Table 1. Geodetic IVS stations used in the study and the number of daily data records for the period 1998 to 2008.

Station	Latitude, Longitude, and Height	# recs
HartRAO	−25.89°, 27.69°, 1416.12 m	4191
Hobart26	−42.80°, 147.44°, 65.53 m	4191
Wettzell	49.15°, 12.88°, 669.56 m	4191
Westford	42.61°, 288.51°, 87.20 m	4191
Tsukub32	36.10°, 140.09°, 85.09 m	4183
Gilcreek	64.98°, 212.50°, 332.52 m	4191

SOI anomaly from NCEP; the SIDC monthly SSN available at www.sidc.oma.be; and the LoD, which is an IERS product.

2.2. Extracting Local Oscillatory Signals in ZTD by Use of EEMD-ICA

The study of ZTD variability is of particular interest, a) because of the inherent mixture of different signal components that exhibit large spatio-temporal time-scales, and b) because the inherent variability is governed by several complex periodic and aperiodic phenomena. In the present study, we propose a combination of Ensemble EMD; hereafter EEMD (see Zhaohua and Huang 2009) and ICA to isolate the low frequency components in ZTD and thereafter investigate the phase dynamics of the oscillating independent components without imposing the assumption of linearity on them. Firstly, the data is decomposed into spectrally independent oscillatory modes called the Intrinsic Mode Functions (IMFs). The resulting IMFs contain inherent additive noise, which dominates the high frequency IMFs. As a result, only those IMFs with lower noise contamination are selected for use in the ICA step. The selection of physically significant IMFs to be used in the ICA stage is a two-step process. In the first step, the IMFs are selected based on the level of noise contamination in the sample. If the IMF_1 is assumed to be highly contaminated, then its amplitude could be used as a reference of the amplitude of the noise contaminated IMFs. Statistically independent IMFs are extracted by selecting only those IMFs whose global energy is at least 30% of the energy of IMF_1 . In the second step, ICA reduces the dimensionality of the IMFs adaptively. Given that the number of statistically independent IMFs is smaller than the original IMFs, ICA generally merges the statistically dependent components into the same group and therefore reduces the dimensional space of IMFs.

Furthermore, ICA is a statistical technique that decomposes a series of observations into a linear combination of non-Gaussian random variables that are highly independent components (Hyvärinen 1999). An Extended FastICA (EFICA) algorithm was used to adaptively extract the non-linear components in the data. (FastICA is a Matlab software freely available at <http://www.cis.hut.fi/projects/ica/>.) The EFICA algorithm utilizes the generalized symmetric FastICA as well as the adaptive selection of the first derivative of the non-linear function called the contrast function (Koldovský et al. 2006) followed by a refinement step. In general, the EEMD-ICA algorithm used in this study can be summarized as follows:

1. Add iid white noise of zero-mean and $\sigma_{iid} = \lambda\sigma_0$ to ZWD. Here, the noise parameter was arbitrarily taken as $\lambda \sim 30\%$.
2. Derive the set of ZTD IMFs by applying EMD until the last IMF is a monotonic function or has at most one extremum.
3. Repeat steps 1 and 2 a number of times, each time using a different randomly generated σ_{iid} , resulting in an ensemble of IMFs (120 ensembles have been used).
4. Average over the ensemble to obtain a set of averaged IMFs.
5. Perform EFICA on the IMFs obtained in step 4 via three steps:
 - (a) run the original symmetric FastICA until convergence. In FastICA, the ICs are estimated based on the assumption that the mutually statistically independent components in the mixture exhibit non-Gaussian probability distributions. In order to assess the statistical

independence of the geophysical signals in ZTD, the fourth-order cumulant (kurtosis κ) defined in (3) is used.

$$\kappa(y) = E(y^4) - 3(E(y^2))^2 \quad (3)$$

The kurtosis utilized in computing the statistical independence of the signal present in ZTD could be optimized by using either the fixed-point gradient learning algorithm (Hyvärinen and Oja 1997) or the Newton's method described in Nocedal and Wright (1999).

- (b) different non-linearities (the derivative of the score function) are adaptively selected and used to estimate the score functions of the components derived in step (a) above.
 - (c) components derived from FastICA are fine-tuned using the non-linearities computed in (b) above. This results in an accurate estimation of the unmixing matrix $W (=A^{-1})$.
6. Slowly varying components are selected and multiplied with the mixing matrix to back-reconstruct the selected IMF set.

The causal relationships among the ICs from different stations and between dominant signals of the QBO, SOI, SSN, and LoD are investigated by use of phase synchronization (e.g., Shelter et al. 2007; Kreuz et al. 2007). Synchronization between dynamical systems is an active field of scientific and technical research. For a review and description of the various concepts of synchronization detection, refer to Rosenblum et al. (2001) and Pareda et al. (2005) and others therein.

There are many different approaches of quantifying the degree of synchronization between two systems: linear approaches like the cross correlation or the coherence function, as well as non-linear measures such as mutual information (e.g., Kreuz et al. 2007 and references therein). In the present work, the relation between phases of two geophysical signals and derived tropospheric components over different temporal scales is used as a measure of the presence of interaction between the systems. The relation does not necessarily mean that they are synchronized.

The concept of analytic signal as applied in signal processing is used to define the phase of an arbitrary signal in this work. This analytic signal approach has the advantage that the phase can easily be obtained from scalar time series (Rosenblum and Kurths 1998). For a univariate measurement $x(t)$ the analytic signal $\zeta(t)$ is defined by Equation (4):

$$\zeta(t) = x(t) + j\tilde{x}(t) = A_x^H(t)e^{j\phi_x^H(t)} \quad (4)$$

Here, the function \tilde{x} is the Hilbert transform of $x(t)$ defined by Equation (5);

$$\tilde{x}(t) = \pi^{-1}P \int_{-\infty}^{\infty} \frac{x(\tau)}{t - \tau} d\tau \quad (5)$$

The P in Equation (5) suggests that the integral is taken in the sense of the Cauchy principal value. This implies that the Instantaneous Phases $\phi(t)$ and Instantaneous Amplitude $A(t)$ are uniquely defined from Equation (4). Therefore, given two interacting geophysical signals $x(t)$ and $y(t)$, the phase difference of their analytic signals given by Equation (6) can be used to derive the phase synchronization index defined in Equation (7).

$$\phi_{xy}^H(t) = n\phi_x^H(t) - m\phi_y^H(t) \quad (6)$$

$$\eta = \left| \langle e^{i\phi_{xy}^H(t)} \rangle_t \right| = \sqrt{\langle \cos \phi_{xy}^H(t) \rangle_t^2 + \langle \sin \phi_{xy}^H(t) \rangle_t^2} \quad (7)$$

In Equation (6), n and m are integers defining the phase locking ratio ($n:m$). The synchronization index η ranges from 0 (which suggests that the phase difference is uniformly distributed and there is no phase synchronization) to 1 (which implies that there is perfect synchronization and the phase difference is a constant).

It is worth noting that the use of η to assess the linkage (interaction) between two geophysical signals requires that the independent components in the signal be separated. The rationale behind this analysis is based on the fact that, if the variable represented by one of the series is indeed caused (or at least influenced) by the underlying dynamics in the second series, then the characteristic fluctuations in the ICs derived from the first ICs ought to be preceded by a reaction in the ICs computed from the second series.

3. Results and Discussion

Monthly ZTD delays at the IVS stations (see Table 1) derived from NWP model simulations have been decomposed into the corresponding IMFs. This decomposition stage separates low and high frequency modes. As depicted in Figure 2, the ZTD delay at all the IVS stations (except Tsukub32 which has fewer data records) were decomposed into seven IMFs. We have combined the IMFs with the lowest frequencies (here we have used IMF₆ and IMF₇) in order to generate a weakly oscillating component of the series; hereafter the trend. Figure 2 illustrates a station-dependent trend (this is mode 5 (for Tsukub32) or mode 6 (for all other IVS stations)) with characteristic decadal fluctuations. Additionally, in all the IVS stations, the highly fluctuating IMF (first mode) has oscillating structure with a characteristic period of about one month.

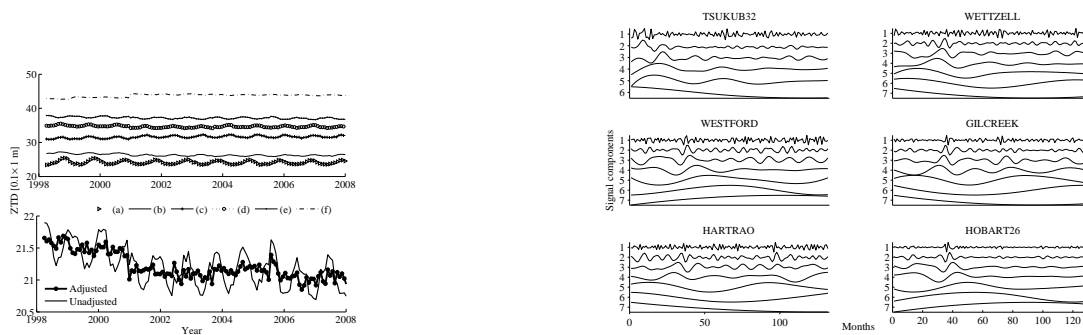


Figure 1. Top panel: tropospheric delay due to water vapor at IVS stations, with 40 mm ZTD added to each station except Hobart26 for better visualization. [a → f: Tsukub32, Wetzell, Westford, Gilcreek, HartRAO, and Hobart26.] Bottom panel: seasonally adjusted and unadjusted ZTD over HartRAO.

Figure 2. Mode Functions (IMFs) of ZTD series over IVS stations.

Higher periods are not visible because the ZTD series is monthly averaged. The second and third oscillation modes in all the IVS stations exhibit intra-annual and seasonal oscillation periods.

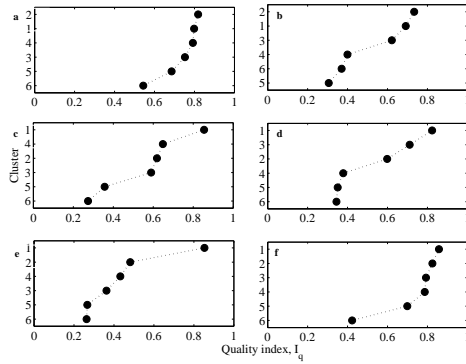


Figure 3. Station dependent quality index I_q of independent components derived from zenith total delay: [a → f: Tsukub32, Wettzell, Westford, Gilcreek, HartRAO, and Hobart26].

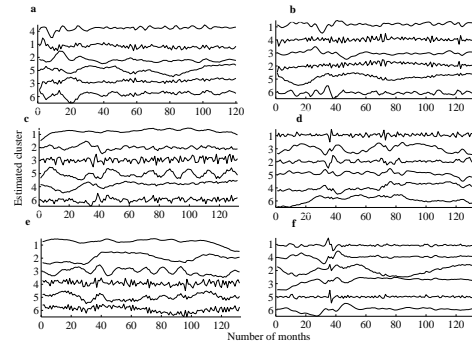


Figure 4. Estimated independent components in zenith total delay: [a → f: Tsukub32, Wettzell, Westford, Gilcreek, HartRAO, and Hobart26].

These modes could be associated with regional or local weather processes at each IVS site. Annual oscillation periods (corresponding to the fourth and fifth modes) are evident in ZTD series for all IVS stations except Tsukub32. This oscillation pattern could be associated with relatively global geophysical processes such as North Atlantic tele-connection patterns and ENSO.

In the present study, the physical causes of variability of ZTD are assessed by extracting the internal regularities, which include linear or non-linear mixtures of different statistically independent components, by use of ICA. Since we do not have information about the signals embedded in the ZTD data a priori, a blind *source* separation procedure is the natural choice (see for example Särelä and Valpola 2005). In the FastICA algorithm (Hyvärinen 1999), where a pre-estimate of the unmixing matrix is computed, the statistically independent IMFs are computed based on optimizing contrast functions, i.e., to solve for the signals embedded in the observations; a cost function that either maximizes the non-Gaussianity or minimizes the mutual information is formulated (Del Negro et al. 2008). The quality index I_q of the clusters used to estimate the ICs in the FastICA algorithm are depicted in Figure 3 (here, a → f corresponds to Tsukub32, Wettzell, Westford, Gilcreek, HartRAO, and Hobart26, respectively). From Figure 3, it can be seen that each of the IVS stations considered in the study contains ICs with unique I_q values. This finding is further evidence that the variability of ZTD at each IVS station is driven primarily by local atmospheric processes.

In all the stations, the magnitude of I_q of all the clusters is generally greater than 0.5. Furthermore, the I_q for all the IVS stations exhibit a knee at cluster 3. This is a strong evidence of some dependence of the geophysical signal derived from ICs at each IVS site as extracted from cluster 3. Therefore, the variability mode of the ZTD could be associated with a geophysical signal with a global geophysical origin such as the climatic tele-connection patterns. Figure 4 depicts the estimated ICs of each cluster (arranged in the order of the clustering quality index) of ZTD at IVS stations. It is evident that the variability structure of the each component is unique at each station. In the present work, the cluster quality index order is used to select the four components that are used to examine the interaction between ZTD and other geophysical signals.

In assessing the nature of linkage between the independent signal components in ZTD with

the geophysical signals, ZTD components that exhibited near Gaussian distribution were selected. Station dependent Gaussian distributed signal components are given in Table 2. Here, a Gaussian shaped distribution depicts a high degree of localization, which suggests that the signal component does not contain spurious components. The linkage between the selected geophysical components (such as those selected in Table 2) is computed and tested by use of the phase synchronization index (see, for instance, Kreuz et al. 2007). In this methodology of non-linear dynamics, the independent components embedded in the mixture of ZWD and other geophysical signals are analyzed focusing on the phases of the fluctuations in each component. From our analysis, it is evident that the signal components extracted from ZTD and the geophysical signals QBO, SOI, SSN, and LoD show some degree of interaction among themselves (see Table 3). As tabulated in Table 3, the phase synchronization index at all IVS stations varies between 0.45 and 0.62 based on the phase locking order 1:1. These values vary across the stations that were considered in this study and, therefore, seem to suggest spatial dependence. As illustrated in Table 3, ZTD observations at Tsukub32 and Westford stations appear not to contain signal components that have dynamical interdependence with QBO, SOI, SSN, and LoD, i.e., the synchronization values are below 0.5.

This signifies weak coupling. The low synchronization index between the ZTD signal components and QBO, SOI, SSN, and LoD could be attributed to strong noise or irregular ZTD fluctuations (which is due to atmospheric dynamics) and non-stationarity (Botai et al. 2009). Further, we observe that Wettzell, Gilcreek, HartRAO, and Hobart exhibit synchronization indices greater than 0.5. The presence of interaction between ZTD measurements and QBO, SOI, SSN, and LoD at the four IVS stations seems to suggest that QBO, SOI, SSN, and LoD signals are indeed embedded in the data.

Table 2. Signal components with approximate Gaussian structure at six IVS stations. Column 2 has selected ZTD components, and column 3 has geophysical signal components.

Station	ZTD	Geophysical
Tsukub32	1, 3, 4	3, 4
Wettzell	1, 2, 3, 4	3, 4
Westford	1, 2, 3	4
Gilcreek	1, 2, 6	3
HartRAO	1, 2	3, 4
Hobart	1, 2, 3	3, 4

Table 3. Synchronization index derived from ZTD and geophysical signals.

VLBI Station	Component pairs	Corresponding phase synchronization index
Wettzell	1-3; 1-4; 2-3; 2-4; 3-3; 3-4; 4-3; 4-4	0.48; 0.58; 0.47; 0.62; 0.43; 0.61; 0.42
Tsukub32	1-3; 1-4; 3-3; 3-4; 4-3; 4-4	0.47; 0.46; 0.47; 0.46; 0.47; 0.45
Westford	1-4; 2-4; 3-4	0.46; 0.49; 0.46
Gilcreek	1-3; 2-3; 6-3	0.55; 0.58; 0.58
HartRAO	1-3; 2-4; 2-3; 2-4	0.54; 0.53; 0.57; 0.50
Hobart	1-3; 1-4; 2-3; 2-4; 3-3; 3-4	0.57; 0.48; 0.57; 0.49; 0.56; 0.48

4. Conclusion

The aim of this study was twofold. Firstly, the combined empirical mode decomposition and independent component analysis methods were used to extract signal components embedded in the tropospheric delay due to water vapor. Results suggest that the tropospheric delay data is a mixture of signal components, each with a different temporal structure. These signal components exhibit spatial dependence suggesting that the high modes of ZTD fluctuations are driven by local atmospheric dynamics. Secondly, in order to assess the linkage of these signal components to geophysical processes, measures of synchronization were done based on the Hilbert transform analytic signal approach. Although further verification on a larger set of IVS stations and other geophysical signals is required, our results reveal that tropospheric delay and the geophysical signals have some dynamical coupling.

References

- [1] Aires F., Chédin A., and Nadal J-P., (2000). Independent component analysis of multivariate time series: Application to the tropical SST variability. *J. Geophys. Res.*, 105(13): 17437-17455.
- [2] Alexandrov T., (2009). A method of trend extraction using singular spectrum analysis, *REVSTAT*, 7(1): 1-22.
- [3] Boehm J., Werl B., and Schuh H., (2006). Troposphere mapping functions for GPS and very processes in geodetic precipitable water vapor time series, Michael G Sideris (ed). *Observing our Changing Earth*, International Association of Geodesy Symposia, Springer Berlin Heidelberg, 133: 625-630, doi: 10.1007/978-3-540-85426-5.
- [4] Botai O. J., Combrinck W. L., and deW Rautenbach C. J., (2008). Nonstationary tropospheric long baseline interferometry from European Centre for Medium-Range Weather Forecasts operational analysis data, *J. Geophys. Res.*, 111(B02406): doi:10.1029.
- [5] Darbellay G. A., (1999). An Estimator for Mutual Information based on criterion for independence, *Computational statistics and data analysis*. 32: 1-17.
- [6] Del Negro C., Greco G., Napoli R., and Nunnari G., (2008). Denoising gravity and geomagnetic signals from Etna volcano (Italy) using multivariate methods. *Nonlin. Processes Geophys*, 15: 735-749.
- [7] Hanke J., Wichern D., and Reitsch A., (2001). *Business forecasting*, Prentice Hall, Upper Saddle River, NJ.
- [8] Hyvärinen A., (1999). Fast and Robust Fixed-Point Algorithms for Independent Component Analysis. *IEEE Trans. Neutr. Net.*, 10(3): 626-634.
- [9] Hyvärinen A., and Oja E., (1997). A Fast Fixed-Point Algorithm for Independent Component Analysis. *Neural computation*, 9(7): 1483 - 1492.
- [10] Huang N. E., Shen Z., Long S. R., Wu M. C., Shih H. H., Zheng Q., Yen N. .C., Tung C. C. and Liu H. H., (1998). The empirical mode decomposition and the Hilbert spectrum for nonlinear and non-stationary time series analysis. *Proc. Roy. Soc. Lond.*, 454: 903-993.
- [11] Koldovský Z., Tichavský P., and Oja E., (2006). Efficient variant of algorithm FastICA for independent component analysis attaining the Cramér-Rao lower bound. *IEEE Trans., on Neural Networks*, 17 (5): 1265-1277.
- [12] Kreuz T., Mormann F., Andrzejak R. G., Kraskov A., Lehnertz K., and Grassberger P., (2007). Measuring synchronisation in coupled model systems: A comparison of different approaches, *Physica D* 225: 29-42.

- [13] Marwan, N., Romano M. C., Thiel M., and Kurths J., (2006). Recurrence plots for the analysis of complex systems, *Physics Reports*, 438: 237-329.
- [14] Mormann F., Lehnertz K., David P., and Elger C. E., (2000). Mean phase coherence as a measure of phase synchronisation and its application to the EEG of epilepsy patients, *Physica, D*, 144: 358-369.
- [15] Nocedal J., and Wright S. J., (1999). *Numerical Optimization*. Springer-Verlag. ISBN 0-387-98793-2.
- [16] Paluš M., and D. Novotná (2009). Phase-coherent oscillatory modes in solar and geomagnetic activity and climate variability, *J. Atmos. Sol.-Terr. Phys.* 71(8-9), 923-930.
- [17] Pareda E., Quiroga R. Q., and Bhattacharya J., (2005). Nonlinear multivariate analysis of neurophysiological signals, *Progress in Neurobiology*, 77: 1-37.
- [18] Rosenblum M., and Kurths J., (1998). Analysing synchronisation phenomena from bivariate data by means of the Hilbert Transform, In: *Nonlinear analysis of physiological data*, H. Kantz, J. Kurths, and G. Mayer-Kress (eds), Springer, Berlin, 91-99.
- [19] Rosenblum M., Pikovsky A., Kurths J., Schafer C., and Tass P. A., (2001). Phase synchronisation: from theory to data analysis, *Handbook of biological physics*, Elsevier Science, A. J. Hoff (series eds), 4, *Neuro-informatics*, F. Moss and S. Gielen (eds) Chapter 9, 279-321.
- [20] Rybski D., Havlin S., and Bunde A., (2003). Phase synchronization in temperature and precipitation records. *Physica A* 320, 601-610.
- [21] Särelä J., and Valpola H., (2005). Denoising source separation. *J. Machine Learning Research*, 6: 233-272.
- [22] Schelter B., Winterhalder M., Timmer J., and Peifer M., (2007). Testing for phase synchronisation, *Physics Letters A*, 366: 382-390.
- [23] Schneider D.P., Ammann C. M., Otto-Bliesner B. L., and Kaufman D. S., (2009). Climate response to large, high latitude and low-latitude volcanic eruptions in the Community Climate System Model, *J. Geophys. Res. Atmosph.*, 104 (D15101): doi: 10.1029/2008JD011222.
- [24] Shannon C. E., and Weaver W., (1949). *The mathematical theory of communication*. University of Illinois press.
- [25] Trenberth K. E., Fasullo J., and Smith L., (2005). Trends and variability in column-integrated water vapour. *Clim. Dyn.*, 24: 741-758, doi: 10.1007/s00382-005-0017-4.
- [26] Zhaohua W. and N. E. Huang, (2009). Ensemble empirical mode decomposition: a noise-assisted data analysis method, *Advances in Data Adaptive Analysis*, 1(1): 1-41.
- [27] Zhauhua W., Huang N. E., Long S. R., and Peng C.K., (2007). On the trend, detrending and variability of nonlinear and nonstationary time series, *PNAS*, 104(38): 14889-14894.

Reliability and Stability of VLBI-derived Sub-daily EOP Models

Thomas Artz ¹, Sarah Böckmann ¹, Laura Jensen ¹, Axel Nothnagel ¹,
Peter Steigenberger ²

¹) *Institut für Geodäsie und Geoinformation, Universität Bonn*

²) *Institut für Astronomische und Physikalische Geodäsie, Technische Universität München*

Contact author: Thomas Artz, e-mail: artz@igg.geod.uni-bonn.de

Abstract

Recent investigations have shown significant shortcomings in the model which is proposed by the IERS to account for the variations in the Earth's rotation with periods around one day and less. To overcome this, an empirical model can be estimated more or less directly from the observations of space geodetic techniques. The aim of this paper is to evaluate the quality and reliability of such a model based on VLBI observations. Therefore, the impact of the estimation method and the analysis options as well as the temporal stability are investigated.

It turned out that, in order to provide a realistic accuracy measure of the model coefficients, the formal errors should be inflated by a factor of three. This coincides with the noise floor and the repeatability of the model coefficients and it captures almost all of the differences that are caused by different estimation techniques. The impact of analysis options is small but significant when changing troposphere parameterization or including harmonic station position variations.

1. Introduction

In the analysis of Very Long Baseline Interferometry (VLBI) observations, a model is used to correct the delays for inter-day Earth orientation variations. When different models are used, differences in the Earth orientation parameters (EOPs)—especially the rates—with an annual (and semi-annual) signature appear. Their amplitudes can easily reach the 100- μ s level.

The International Earth Rotation and Reference Systems Service (IERS) recommends a model based on an ocean tidal model plus components originating from nutation (Tab. 8 and Tab. 5 of the IERS Conventions 2003 [3]). However, VLBI is sensitive to the integral effect of all variations at each tidal line, including e.g., the tidal and thermally driven S1-excitations. Thus, the IERS model is not sufficient. Besides the dominating oceanic part, other forces should be applied, e.g. tidal variations in the atmosphere or variations of non-tidal origins. As these are not completely modeled physically, the next best option is to estimate a model based on space geodetic techniques.

Several investigations were performed, e.g., on the basis of observations of VLBI or Global Navigation Satellite Systems. However, the results are not homogeneous, as different observations and solution set-ups were used. A model for the sub-daily variation of the EOPs (sub-daily EOP model) is composed of poly-harmonic functions for polar motion (PM) and universal time (UT1):

$$\Delta X(t) = \sum_{j=1}^n -p_j^c \cos \psi_j(t) + p_j^s \sin \psi_j(t) \quad (1)$$

$$\Delta Y(t) = \sum_{j=1}^n p_j^c \sin \psi_j(t) + p_j^s \cos \psi_j(t) \quad (2)$$

$$\Delta UT1(t) = \sum_{j=1}^n u_j^c \cos \psi_j(t) + u_j^s \sin \psi_j(t) \quad (3)$$

where n describes the number of tidal terms of the model and $\psi_j(t)$ are the corresponding angular arguments. The model coefficients p_j^c , p_j^s , u_j^c , and u_j^s can be estimated directly from the VLBI observations. This approach has been used, e.g., by [2]. Another possibility—applied, e.g., by [5]—is to solve for highly-resolved EOP time series in a first step, to generate the left hand side of eq. (1)-(3). In a second step, these time series are used as pseudo-observations to solve for the model coefficients. Finally, a solution on the normal equation (NEQ) level can be performed. In this study, NEQs are, therefore, built as in the first step of the solution level approach. However, this equation system is not solved directly. The NEQs are transformed to change the parameterization from highly-resolved EOPs to the model coefficients. Subsequently, all modified NEQ systems are added together and solved. The method of parameter transformation is described, e.g., in [1].

To assess the stability of such empirical sub-daily EOP models, the temporal behavior of the estimated model terms is analyzed in this paper. Furthermore, the noise floor and the formal errors are investigated to define the precision of the estimated model. In addition, several solution set-ups and estimation techniques are compared to describe the reliability of VLBI-derived models.

2. Solution Description of the Standard Approaches

Altogether, three solutions have been performed with almost identical features: for all three approaches, the basic parameterization and modeling is identical. The celestial and terrestrial reference frames are estimated. Axis offsets are estimated if no information based on local surveying is available. Furthermore, the zenith wet delays (ZWD) are estimated with a temporal resolution of 20 min while troposphere gradients are resolved with a 6-h resolution. Stabilizing rate constraints of 50 ps/h are imposed on ZWDs. For the gradients, rate constraints of 2 mm/d and offset constraints of 0.5 mm are added. The nutation is fixed to estimates from a global VLBI solution.

The only difference of the three solutions is characterized by the method used to derive the coefficients of the sub-daily EOP model. The coefficients of the observation-level model, as well as an hourly EOP solution, are estimated in a global solution with Calc/Solve [4], i.e., simultaneously with all other parameters. Subsequently, the time series of hourly spaced EOPs is used as pseudo observations in a separate estimation process to derive the model on the solution level. For the solution on the NEQ-level, session-wise NEQs are generated with Calc/Solve and then transformed as described above. These NEQs are, in turn, added to a global solution, and the reference frames and the model are estimated simultaneously as well.

3. Stability and Accuracy of the Model Coefficients

To investigate the stability of VLBI-derived models, the most stable solution should be found first. To obtain such a solution, altogether 25 solutions have been calculated: the first with observations only from the year 2009, then the observations of 2008 have been added for the second solution and so on. Finally, the last solution has been calculated with all observations from 1984 to 2009. For solutions with observations of less than 18.6 years, terms that differ from each other by less than one cycle in the considered time span are constrained as described by [2].

By analyzing two subsequent solutions, a solution over a time span of 14 years is considered

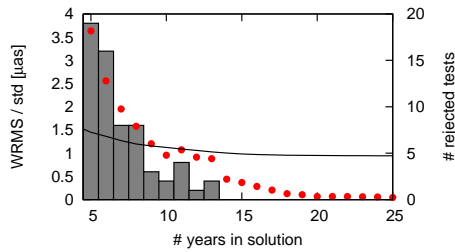


Figure 1. Mean standard deviation (solid line) and WRMS of the differences of one limited solution to the prior one (dots); the number of terms that are different from those in the prior solution with a reliability of 95% for PM (bars).

to be sufficiently stable. The mean standard deviation of the model terms' differences is almost constant from there on (see Fig. 1). Furthermore, the WRMS of the model differences is clearly below the standard deviations. Finally, a simple test indicates that with more than 13 years of data, adding one more year does not yield significant model differences. The gray bars in Fig. 1 indicate how many coefficients differ between two subsequent solutions with a probability of 95%.

To test the stability, 13 models have been estimated with 14 years of observations—starting in 1984—each shifted by one year. For every coefficient, a WRMS value of the difference to the mean value has been calculated. A large WRMS of an individual coefficient is caused by a bad repeatability/stability indicating that this particular coefficient cannot be well determined or is not sufficiently described by a constant amplitude. Figure 2 shows these WRMS values for the PM and UT1 terms. For PM the repeatabilities are in general below $3 \mu\text{as}$, but there are some exceptions. These are the M2 coefficients in the retrograde and the K2 coefficients in the prograde semi-diurnal band. In the prograde diurnal band, bigger deviations appear at K1 and its sidebands, 2Q1 and Q1. For UT1, the repeatability is below $0.2 \mu\text{s}$ for most of the terms. Here, bigger differences can be seen at K1 and K2 and their sidebands. The presence of the sidebands—which would not be separable from the major terms without constraints in this limited time span—might be the reason for the lower stability of these coefficients. Furthermore, for more than one third of the coefficients, a linear evolution can be recognized in the time series. This leads to the suggestion that the estimated coefficients are not constant in time. Besides the information on the repeatability of the estimated terms, these values serve as an additional accuracy measure. This empirically derived standard deviation is approximately three times larger than the formal errors of the least squares adjustment and, thus, indicates too optimistic formal errors.

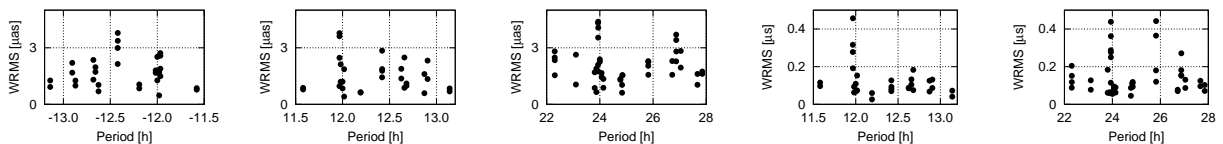


Figure 2. WRMS values of the estimated coefficients. From left to right: retrograde and prograde semi-diurnal PM, diurnal PM, semi-diurnal UT1, and diurnal UT1.

A final measure for the accuracy can be derived by indicating the noise floor of the complete model (not shown here). This noise floor can be evaluated by adding some terms to the model, for which no impact on the EOPs is expected. Following [2], nine terms have been chosen for the PM model and six for UT1. The semi-diurnal band exhibits a lower noise level compared to the diurnal band. For the complete solution, this level is below $6 \mu\text{as}$ (PM) and $0.35 \mu\text{s}$ (UT1). For both, the term with a period of 27.04 h is significantly larger compared to the other ones.

4. Reliability of the Estimated Coefficients

As shown in Sec. 3, almost all coefficients can be estimated producing stable results, and the accuracy of the model coefficients can be reliably described by three times the formal errors. However, this does not yet comprise any information on the reliability of these terms. For this purpose, the impact of changes in the solution set-up and the method of estimating the sub-daily EOP model can be analyzed.

4.1. Impact of Analysis Options

Changes in the analysis set-up, which are not related to the parameterization or modeling of the EOP, should not change the estimated coefficients significantly. Only modifications in the handling of the station or source positions might affect the estimated model. Especially the variations in the settings which are not based on common rules are of interest, as this describes the impact of the analyst’s noise.

Most modifications, such as fixing the reference frames or nutation to results from a formerly performed global VLBI solution, do not lead to significant changes of the model. Moreover, using only VLBI observations since 1990 has no recognizable influence. Furthermore, extending the resolution of the ZWD from 20 min to 60 min and the resolution of the troposphere gradients from 6 h to 24 h, leads to significant differences which are shown in Fig. 3. It has to be mentioned that the higher resolution for the troposphere leads to a slightly better agreement with the IERS model (not shown here) and changing ZWD or the gradients alone does not have a comparable impact.

The biggest effect results from the introduction of non-linear station motion. Calc/Solve provides the opportunity to estimate harmonic station variations. This has been done for the stations with sufficient observations for annual (Sa), semiannual (Ssa), diurnal (S1), and semi-diurnal (S2) components. Subsequently, these station motions are used as a priori information for the global solution to estimate the EOP model. This procedure leads to significant differences of the S1 and S2 coefficients which are shown in Fig. 3 for PM exemplarily. Obviously, station motions are able to absorb EOP variations and vice versa.

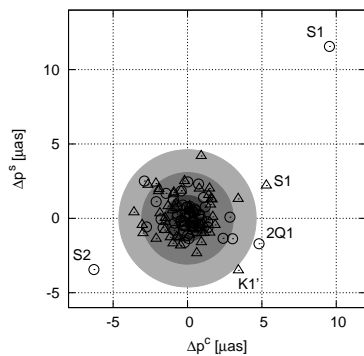


Figure 3. Differences of the PM model terms of the standard solution to a solution where harmonic site positions (circles) or a different parameterization of the troposphere (triangles) is used. The gray colored areas denote 1 (dark) over 2 to 3 σ (light).

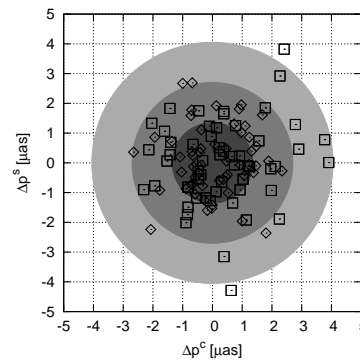


Figure 4. PM model differences of the observation level approach to the NEQ (diamonds) and solution (squares) level approaches.

4.2. Model Comparisons

To assess the impact of the model estimation technique, the NEQ and solution level approaches are compared to the observation level approach. The last is the most strict as the information of each observation is preserved. For the first two approaches, EOPs are converted to discrete, hourly spaced values first; thus, information is lost. The advantage of the NEQ over the solution level approach is the conservation of the full variance and covariance information.

The differences are shown in Fig. 4. These are, in general, below the $3\text{-}\sigma$ level and thus in the range of the model precision as shown in Sec. 3. Furthermore, the assumptions concerning the strictness of the estimation procedure are fulfilled as the model on the observation level is slightly closer to the one on the NEQ level compared to the solution level.

5. Conclusions

The general stability and accuracy of coefficients of a sub-daily EOP model is in the range of three times the formal errors. This is confirmed by the repeatability of the model coefficients from shifted stable (14-year) solutions and by the noise floor of the complete model. For some terms, less stable results are achieved. These are terms for which sidebands are not separable from the major term with observations of less than 18.6 years.

Furthermore, different estimation techniques have been compared. The approach on the observation level and on the NEQ level comprise almost no differences within the derived accuracy level. The differences of the solution level approach are only slightly bigger.

Finally, it was shown that the impact of various analysis options is low but not negligible. Especially the troposphere parameterization leads to significant model differences. Furthermore, harmonic station position variations are able to absorb EOP variations at the same period or vice versa. It is not yet clear whether it is correct to consider such station motions or not.

References

- [1] E. Brockmann, Combination of solutions for geodetic and geodynamic applications of the Global Positioning System (GPS), Geod.-Geophys. Arb. Schweiz, Vol. 55, 1997.
- [2] J. M. Gipson, Very long baseline interferometry determination of neglected tidal terms in high-frequency earth orientation variation, *J Geophys Res*, 101:28051–28064, 1996, doi: 10.1029/96JB02292.
- [3] D. McCarthy and G. Petit, IERS Conventions (2003), Verlag des Bundesamtes für Kartographie und Geodäsie, Frankfurt am Main, 2004, IERS Technical Note 32.
- [4] L. Petrov, Mark-5 VLBI analysis software Calc/Solve, Web document <http://gemini.gsfc.nasa.gov/solve/>, Sept. 2008.
- [5] M. Rothacher, G. Beutler, R. Weber, and J. Hefty. High-frequency variations in Earth rotation from Global Positioning System data, *J Geophys Res*, 106:13711–13738, 2001, doi: 10.1029/2000JB900393.

Simulation of Local Tie Accuracy on VLBI Antennas

Ulla Kallio, Markku Poutanen

Finnish Geodetic Institute

Contact author: Ulla Kallio, e-mail: Ulla.Kallio@fgi.fi

Abstract

We introduce a new mathematical model to compute the centering parameters of a VLBI antenna. These include the coordinates of the reference point, axis offset, orientation, and non-perpendicularity of the axes. Using the model we simulated how precisely parameters can be computed in different cases. Based on the simulation we can give some recommendations and practices to control the accuracy and reliability of the local ties at the VLBI sites.

1. Model

Most of the models used in the calculation of the VLBI antenna reference point have been based on a 3D circle fitting [1], [2]. The main restriction of those models is that observations must be planned so that the tracks of the points form circles in the three dimensional space. If we use the VLBI antenna angle readings as additional observations we can calculate the reference point and axis offset also from scattered points. This kind of model was first presented by Lösler [4]. We parameterized our model differently so that the telescope axes are presented in the same three dimensional Cartesian system as the observed coordinates [3]. The basic assumptions are that points on the antenna structure rotate about the secondary axis and that the secondary axis rotates about the primary axis, but no pre-defined geometry or order of observations are assumed. The model is suitable for different types of telescope mounting and can be used with the data collected during the normal use of a telescope.

The position vector of a target (or a GPS antenna attached to a radio telescope) X is the sum of three vectors: the position vector of the reference point X_0 , the axis offset vector $(E - X_0)$ rotated by angle α about the azimuth axis a , and a vector from the eccentric point E to the antenna point p rotated about the elevation axis e by angle β and about the azimuth axis by angle α (Fig. 1). Unknown parameters are X_0 , E , a , e , and p . Observations are coordinates X for each antenna point and epoch and VLBI antenna angle readings α and β for every epoch. The estimated values of E , e , and p are those of an antenna initial position which may be zero for both angles.

The basic equation and the rotation matrix of our model are

$$X_0 + R_{\alpha,a}(E - X_0) + R_{\alpha,a}R_{\beta,e}p - X = 0 \quad (1)$$

$$R(\alpha, a) = \cos \alpha \begin{pmatrix} 1 & 0 & 0 \\ 0 & 1 & 0 \\ 0 & 0 & 1 \end{pmatrix} + (1 - \cos \alpha) \begin{pmatrix} xx & xy & xz \\ xy & yy & yz \\ xz & yz & zz \end{pmatrix} + \sin \alpha \begin{pmatrix} 0 & -z & y \\ z & 0 & -x \\ -y & x & 0 \end{pmatrix} \quad (2)$$

The axis $a = (x \ y \ z)^T$ is in a three-dimensional Cartesian coordinate system. Because the rotation axes are unit vectors and the reference point is the intersection of the primary axis with the

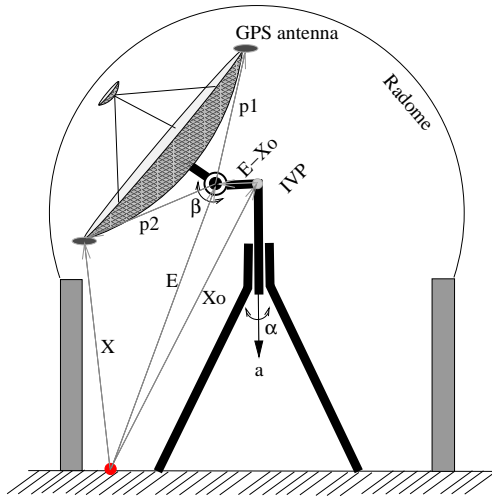


Figure 1. Geometry of the model.

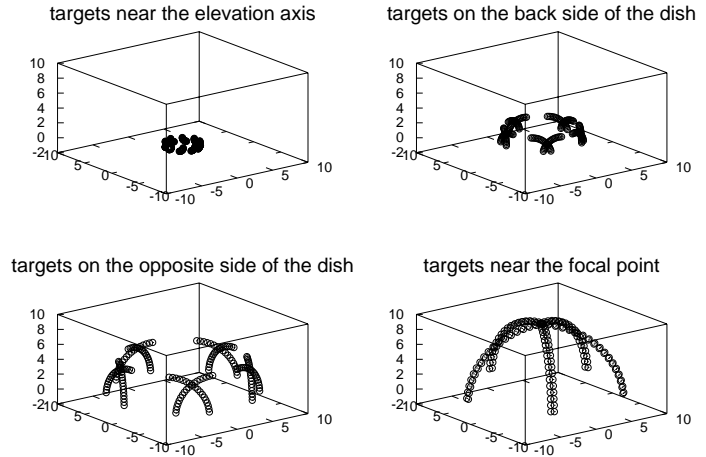


Figure 2. The geometry of observations in the four case studies.

shortest vector between the primary and secondary axes [1], four conditions between parameters are necessary:

$$1) a^T a - 1 = 0; \quad 2) e^T e - 1 = 0; \quad 3) (E - X_0)^T a = 0; \quad 4) (E - X_0)^T e = 0 \quad (3)$$

The solution of the above inverse problem can be reached by iteration in a linearized least squares mixed model with conditions between the parameters. The weight matrix of the observations is the inverse of their covariance matrix. The covariance matrix of parameters is therefore the inverse of the normal equation matrix in the least squares adjustment. The precision of the model parameters is a function of the number and geometry of the observations.

2. Simulation

By simulation we can study e.g. the following questions:

- the limits of the model (minimum number of observations, geometry),
- robustness of the model,
- how good the initial values of the parameters must be for linearization,
- how many target points to choose,
- what is the best place for targets,
- how to choose the antenna positions,
- what is the accuracy of the reference point, the antenna offset and the axes orientation,
- how accurate must the coordinate observations be,
- what is the minimum number of observations to get a reliable solution,
- how the random errors propagate to the solution,
- how the systematic errors propagate to the solution, and
- how the blunders can be detected.

In our simulations we varied the placements and the number of targets, the number of VLBI antenna positions, and the precision of the target points. We calculated the variances of the reference point coordinates, the axis offset, and the angle between the axes using two different strategies.

In the first case we computed the inverse of the normal equation matrix in least squares adjustment which is the covariance matrix of the unknown parameters of the model. Because the axis offset and the angle between axes are not the model parameters they must be calculated. The angle between the axes is

$$\varphi = \arccos(a^T e) \quad (4)$$

and the axis offset

$$o = \pm \sqrt{(E - X_0)^T (E - X_0)} \quad (5)$$

The sign of the offset o is negative if the direction of the offset vector is opposite to the antenna opening direction. The variances of the angle and the offset are reached by using the law of variance propagation.

In the second case we added the normal distributed random errors to observations and repeated the adjustment thousands of times with different observations. Then we calculated the standard deviations from the adjusted parameters and derived axis offsets and angles. Besides the azimuth-elevation type antenna orientation, we tested the model with X/Y- and polar-mount types of antennas. We have also applied the model to the Metsähovi VLBI telescope using real data. In our simulations we used local topocentric coordinate systems. When using real data, the system is chosen according to the target point coordinate system.

2.1. Geometry of Observations and Precision

We simulated four different observation geometries (Fig. 2) to find the best places for the targets:

1. The targets or prisms were near the elevation axis and only a few meters from the azimuth axis (used, e.g., in Onsala local tie measurements [4], [5]).
2. The targets were on the back side of the antenna dish (used, e.g., in the Metsähovi local tie measurements with tacheometers)
3. The target points or GPS antennas were on the opposite side of the dish (used e.g. in the Metsähovi tie measurements with GPS)
4. The targets were near the focal point on the apex of the quadripod (here the target point coordinates were approximated from the Metsähovi telescope dimensions)

In order to get realistic target or GPS point coordinates we used the actual antenna dimensions in the simulations [7]. For comparable results we used in all cases two targets at opposite sides of the telescope, although for example in Onsala they had eight targets in the real measurements [5]. In our simulations we derived the weight matrix of observations from the diagonal covariance matrix of coordinates X for each antenna point and epoch, and VLBI antenna angle readings α and β for every epoch. We varied the precision of the target coordinates between 0.0001–0.05 m for the horizontal components and 0.0002–0.10 m for the vertical components. The precision of the telescope angle readings were 0.0001° in all cases. In each case there were 90 antenna positions. The results of the simulations are presented in Figures 3 and 4.

2.2. Number of Targets, Number of VLBI Antenna Positions and the Precision

For this experiment we chose the first type of observation geometry from our list above: targets were near the elevation axis. We varied the number of targets from two to ten. The precision of the target points was 0.01 m for horizontal and 0.02 m for vertical components. The 18 elevations

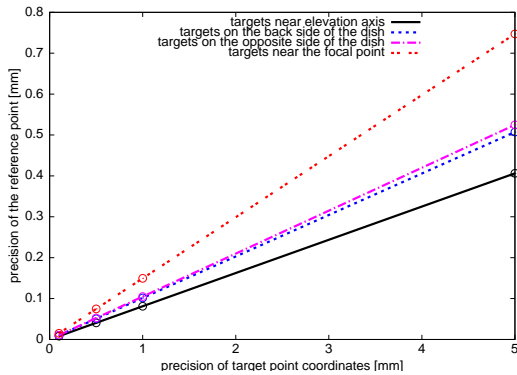


Figure 3. Precision of the reference point in different target geometries.

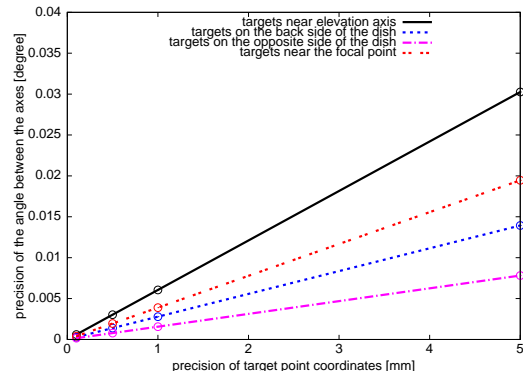


Figure 4. Precision of the angle between the axes in different target geometries.

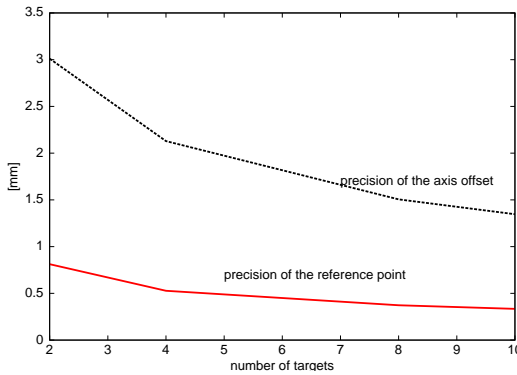


Figure 5. Increasing the number of targets.

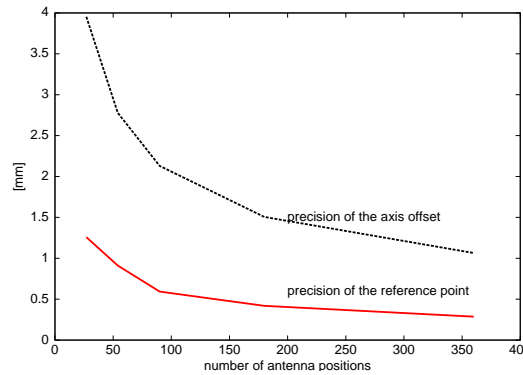


Figure 6. Increasing the antenna positions.

in five azimuths give 90 antenna positions together. In Figure 5 we can see that the precision of the reference point is at sub-mm level with only two targets and 90 antenna positions, but if a mm level precision is required for the axis offset, then the precision of the observations must also be at the mm level.

What happens if we increase the number of antenna positions? We chose the second type of the observation geometry from our list: targets on the back side of the dish. We varied the number of azimuths from three to ten but kept the number of elevations fixed to 18. The number of targets was four and the precision of target points 0.01 m for horizontal components and 0.02 m for vertical components. In Figure 6 we see that the precision of the reference point is below the mm level after 50 antenna positions. Also the axis offset is near the mm level if we increase the number of antenna positions to 360. In our simulation, azimuth values were chosen equally around the azimuth axis.

The model is suitable also for X/Y or polar type mounts. As a demonstration we adopted the dimensions of the Hobart 26 m VLBI antenna with 8.1913 m axis offset [2], [6], and [7]. We used 42 antenna positions (three positions [-20,0,20] for X and 14 positions [-65,65] with steps of 5° for Y) and generated 1000 observation sets with normal-distributed random errors and adjusted the model parameters. In the simulation we assumed that the two GPS antennas or targets were on the opposite side of the dish. With these assumptions we computed the variation of axis offset

and the angle between the axes. 95% of the solutions of the axis offset were between 8.1834 m and 8.1996 m, if the precision of the observed coordinates was 1 cm. When we used mm-level target point precision and the same antenna positions, we got 8.1905 m and 8.1922 m. To achieve better accuracy we need to increase the number of antenna positions where the observations are made.

3. Summary of the Results and Conclusion

The precision of the antenna axis offset depends mostly on the achievable precision of the target coordinates, the number of targets, and the number of VLBI antenna positions. If we use the same number of targets and the same number of antenna positions, all target geometries which we tested gave almost the same precision for the axis offset. The most precise reference point coordinates will be achieved if the targets are placed near the elevation axis. It is possible to achieve a sub-millimeter precision for the coordinates of the reference point and the antenna offset by increasing the number of VLBI antenna positions, even if the precision of target points is on the cm level.

In real measurements it is not possible to choose the places of the targets arbitrarily, but they must instead be installed where they are visible from the observing points. It may not be possible to give unambiguous answers on how many targets or how many antenna positions one must have. It is still recommendable to simulate the accuracy before the measurement work. Our model is powerful and very easy to use for this purpose.

Acknowledgement

The authors would like to thank the personnel of the Aalto University Metsähovi radio observatory for their invaluable help. This project is partly funded by the Academy of Finland, decision number 134952.

References

- [1] Dawson, J., Sarti, P., Johnston, G.M., and Vittuari, L. Indirect approach to invariant point determination for SLR and VLBI systems: an assessment. *J. Geodesy*, **81(6-8)**: 433–441, 2007.
- [2] G. Johnston and J. Dawson. The 2002 Mount Pleasant (Hobart) radio telescope local tie survey. *Geoscience Australia*, **21**, 2004.
- [3] U. Kallio and M. Poutanen. Can we really promise a mm-accuracy for the local ties on a geo-vlbi antenna. In *IAG 2009 Scientific Assembly – Buenos Aires*, 2009. *Submitted for the Proceedings*, 2010.
- [4] Michael Lösler. New mathematical model for reference point determination of an azimuth-elevation type radio telescope. *Journal of Surveying Engineering*, **135(4)**: 131–135, 2009.
- [5] Michael Lösler and Rüdiger Haas. The 2008 local-tie survey at the Onsala space observatory. In Charlot P., A. Collioud and G. Bourda, G. (Ed.) *Proceedings of the 19th European VLBI for Geodesy and Astrometry Working Meeting, March 24–25, 2009, Bordeaux, France*, p. 97–101, 2009.
- [6] A. Nothnagel. Info file for antenna dimensions, reference temperatures, etc., <http://vlbi.geod.uni-bonn.de/ivs-ac/conventions/antenna-info.txt>, 2009.
- [7] A. Nothnagel. Conventions on thermal expansion modelling of radio telescopes for geodetic and astrometric VLBI, *J. Geodesy*, **83**: 787–792, 2009.

VLBI and GPS-based Time-transfer Using CONT08 Data

Carsten Rieck ¹, Rüdiger Haas ², Kenneth Jaldehag ¹, Jan Johansson ¹

¹⁾ *SP Technical Research Institute of Sweden*

²⁾ *Chalmers University of Technology, Onsala Space Observatory*

Contact author: Carsten Rieck, e-mail: carsten.rieck@sp.se

Abstract

One important prerequisite for geodetic Very Long Baseline Interferometry (VLBI) is the use of frequency standards with excellent short term stability. This makes VLBI stations, which are often co-located with Global Navigation Satellite System (GNSS) receiving stations, interesting for studies of time- and frequency-transfer techniques. We present an assessment of VLBI time-transfer based on the data of the two week long consecutive IVS CONT08 VLBI campaign by using GPS Carrier Phase (GPSCP). CONT08 was a 15 day long campaign in August 2008 that involved eleven VLBI stations on five continents. For CONT08 we estimated the worst case VLBI frequency link stability between the stations of Onsala and Wettzell to $\approx 1\text{e-}15$ at one day. Comparisons with GPSCP confirm the VLBI results. We also identify time-transfer related challenges of the VLBI technique as used today.

1. Introduction

Work in the field of time- and frequency-transfer using Very Long Baseline Interferometry (VLBI) originated in the 1970s and was often driven by the need of the Deep Space Network (DSN) ground station time synchronization. Already in the early 1980s VLBI frequency link instabilities on the order of $1\text{e-}14@1\text{d}$ were reported [1], and time-transfer reached ns level precision. The time-transfer accuracy was verified with the help of clock transports [2] or by comparisons with independent techniques, such as Global Positioning System (GPS) or Two Way Satellite Time and Frequency Transfer (TWSTFT) [3]. In order to reach ns and sub-ns uncertainties it is necessary to use differential station calibration techniques [4, 5].

Most recent work presented in [6] resulted in frequency link instabilities surpassing GPS Carrier Phase (GPSCP) with better than $1\text{e-}15@1\text{d}$ modified Allan deviation (MADEV). The intent of this paper is to investigate the potential of VLBI time-transfer and gain a better understanding of the local VLBI system delays.

An additional motivation is the fact that some of the IVS sites maintain UTC realizations. Traditional long distance time-transfer methods are often heavily dependent on active third parties that are not necessarily dependable in the long term. GPS and TWSTFT are today the backbone of international time metrology and can fast become outdated due to economical or political reasons, thus VLBI could become an alternative and independent passive time-transfer method.

2. Time and Frequency Within the VLBI System

The frequency source in a VLBI system is usually a hydrogen maser that supplies the local oscillators (LO) of the front-end, the phase calibration system (PCAL), and the video converters (VC) of the back-end with a 5 MHz reference frequency. The time stamping of the data recording is governed by the time scale that is maintained by the formatter clock. Often the formatter clock

has a 1PPS output that is used to monitor the VLBI clock offset during the experiment. A VLBI time-transfer system needs to assure at least three items on the equipment side:

1. The formatter clock has to be calibrated and constantly measured using a reference delay measurement system to another clock or timescale, such as a UTC(k) representation.
2. The signal chain from the fiducial point of the antenna system to the formatter clock needs to be calibrated by measuring equipment delays or by using differential calibration techniques.
3. Delays induced by environmental changes have to be estimated. PCAL is used for bandwidth synthesis and could also be used to measure the momentary delay of the receiver chain.

We have used a 50 ps time interval counter (TIC) in order to quantify the timing noise level of the Onsala station. Compared to the local timescale the formatter 1PPS output experiences several times as much noise as the source clock at any time interval, with an Allan deviation of about $2.6e-15@1d$ and RMS levels of about 150 ps. It is not clear if the formatter 1PPS output represents the noise that is apparent in the recording time stamps, but a reference delay measurement system based on the formatter clock output will presently dominate the noise of the VLBI time-transfer.

3. VLBI Time-transfer Using the CONT08 Experiment

The continuous sessions of the IVS have been a tool for assessing the VLBI technique and are of special scientific value. The CONT08 experiment was carried out from August 12 through August 26 in 2008 and involved eleven stations on five continents using a 512 Mbit/s recording.

Besides its main scientific goal, the study of high frequency sub-diurnal earth orientation parameters (EOP), CONT08 was also used to assess the improvement of the VLBI technique and its geodetic accuracy, and to make comparisons with co-located techniques like GNSS, SLR, and DORIS. Figure 1 shows the station network of CONT08. All captured data of the experiment were correlated in 24-hour batches by the Washington correlator (WACO) using the Kokee Park station (KOKEE) as its reference.

(<http://ivscc.gsfc.nasa.gov/program/cont08/>)



Figure 1. CONT08 VLBI station network.

3.1. Network Analysis (NA)

The data were processed in batches of 24 hours using Calc/Solve [7]. In the analysis we used ONSALA60 as the clock reference, and the clock offsets of all other stations were estimated as quadratic terms with constraint ($5e-14$ s/s) deviation estimates every 1200 s. The batch processing gives rise to discontinuities at the day-boundaries, which affects all parameters that are expected to be continuous, such as clocks and atmospheric delays. During CONT08 the clock discontinuities are generally on the order of a few hundred picoseconds, often much larger than the formal uncertainties of the estimates, which are on the order of 30 ps. The last two days of the experiment, MJD 54703 and 54704, show excessive day-boundary offsets of about 50 ns with an almost

inverted behavior between the two days. The magnitudes of these offsets are not explainable from the modeling and are believed, but so far unverified, to be an effect of the correlation. Throughout CONT08 the KOKEE station clock experienced an excessive 1 ns diurnal signature likely caused by the environment at KOKEE. This can be one reason for correlator-introduced biases, because the correlation was based on a badly behaving clock/distribution. From a geodetic point of view additional biases are no problem as long as they are constant during one common period of correlation and analysis. These disturbing conditions, i.e. **a)** discontinuities through analysis, and **b)** possible biases from correlation, prevent an absolute time-transfer.

The output of the Calc/Solve analysis allows concatenating two adjacent solutions because of overlapping estimates. This removes any meaning of a phase bias, but can be useful for the evaluation of a frequency-transfer. Day-boundary offset removal likely introduces errors in the estimated frequency offset of the combined time series. Allan deviations (ADEV) for the CONT08 VLBI-derived and 2nd order detrended clock differences, see Figure 2, represent the link stability of VLBI by assuming that the intrinsic stability of the station clocks is better than the link stability during time intervals shorter than one day. Removal of the quadratic phase term removes most of the long term instability of a maser clock. This assumption is dependent on the actual clock performance during the experiment, but can be used to identify a worst case link instability. The Onsala-Wettzell baseline outperforms all other differences with an ADEV of $1.2\text{e-}15@1\text{d}$.

3.2. Clock Constraints in Single Baseline Analysis (SBA)

Because of its good performance in the network analysis we used the Onsala-Wettzell baseline in a single baseline analysis in order to study the effect of **1)** an alternative processing strategy and **2)** the influence of different clock constraints on the time-transfer results. In a geodetic setup the clock parameters are often loosely constrained, e.g., $1\text{e-}13$ s/s at 1 hour sampling, in order to allow the absorption of unmodeled effects, such as certain loading types or errors in the atmospheric delay mapping. For timing purposes the actual clock constraints should be adjusted to the stability of the involved station clocks. Figure 3 shows the Allan deviations of different 2nd order detrended clock solutions. Constraints harder than $5\text{e-}14$ s/s seem to create problems in the processing where the clock performance is overestimated and the LSQ analysis cannot separate the clocks from instrumental noise. The clock difference between the network and single baseline solution for the same constraint is significant and can be seen as a frequency offset of about 50 ps per day. Even the different SBA/NA solutions differ, most noticeably, by phase jumps at the day-boundaries with their magnitude roughly proportional to the constraint difference. This indicates systematic differences in the estimated day-boundaries offsets.

4. GPSCP Time-transfer and Comparative Results

All IVS stations have co-located IGS receivers, where seven out of eleven used a common clock as the frequency source for both the VLBI equipment and the IGS stations. Table 1 summarizes the situation during the CONT08 experiment. In order to assess the correctness of the VLBI derived clock difference frequency offsets we have used comparisons with GPSCP solutions for the seven common clock cases. Due to the global distribution of the stations, Precise Point Positioning (PPP) derived station clocks, using NRCANPPP [8], were differentiated in order to create matching clock differences to the Onsala H-maser. NRCANPPP is capable of continuously processing arbitrary

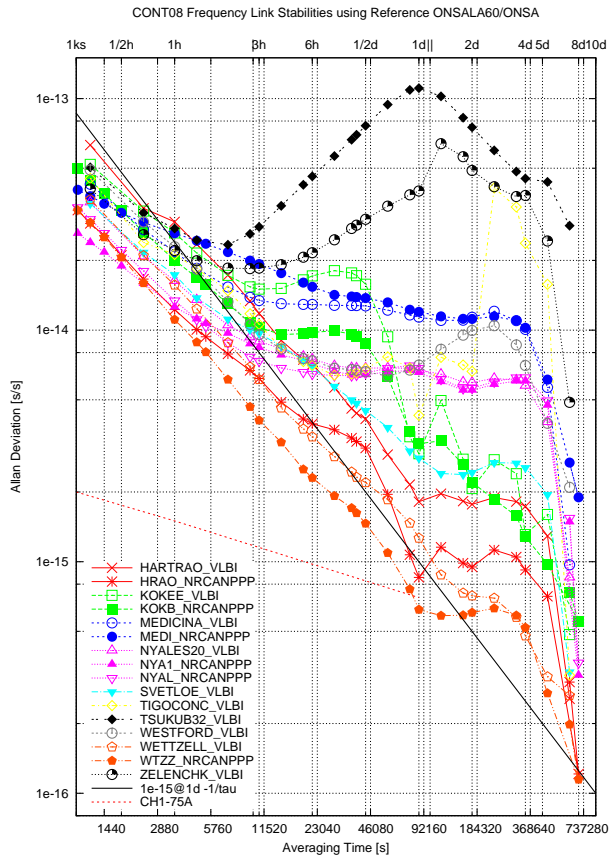


Figure 2. CONT08 VLBI and NRCANPPP derived frequency link stabilities (ADEV) of 2nd order detrended time series. TSUKUB32 experienced a dramatic frequency change during CONT08.

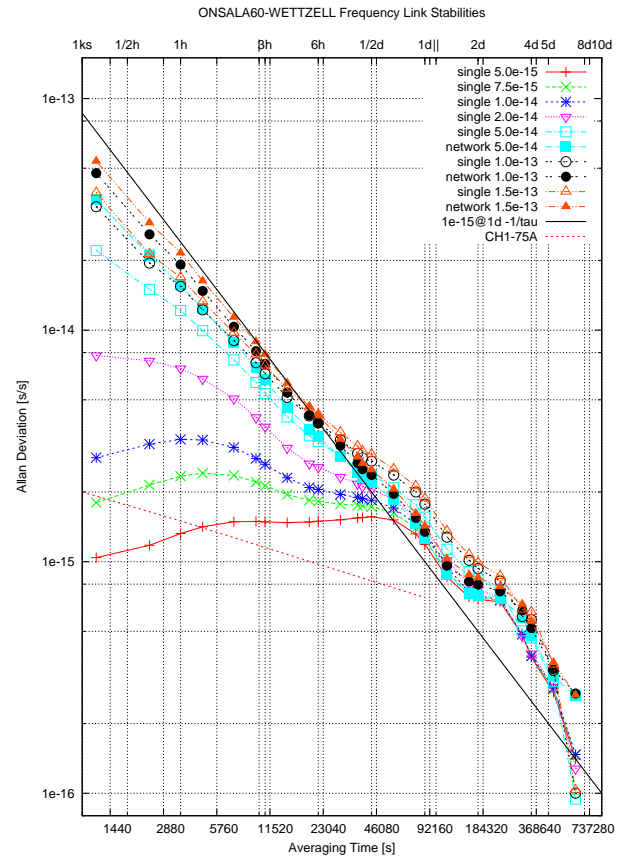


Figure 3. VLBI ADEV stability of ONSALA60-WETTZELL using different analysis strategies and constraint settings. The network solutions exhibit more noise than similar single baseline solutions.

long time series without introducing day-boundary offsets. Figure 2 gives the estimated PPP link stabilities. The last two columns in Table 1 compare VLBI and NRCANPPP. The Onsala-Wettzell baseline, using the WTZZ receiver and the VLBI network solution, show the best agreement and stability. The link difference has a significant relative frequency offset of about $5e-16$. This offset can be attributed to either technique, e.g., the absence of integer ambiguity resolution in PPP and frequency biases introduced by the VLBI day-boundary fix.

5. Conclusions

Day-boundary offsets caused by batch-analysis and possible correlator introduced biases make VLBI time-transfer challenging. CONT08 derived frequency link stabilities of $\approx 1e-15@1d$ (ADEV) do not match results reported in [6]. Practical VLBI time-transfer will require changes to the equipment and processing, a consistent calibration, and a continuous correlation and analysis process. VLBI2010 (http://www.haystack.mit.edu/geo/vlbi_td/2010) with its wideband 24/7 observations may improve the time link noise and may make absolute VLBI time-transfer possible.

Table 1. CONT08 summary. VLBI, NRCANPPP time-transfer results and comparison.

VLBI	IGS	CommonClk	VLBI@1d	GPSCP@1d	GPSCP-VLBI	RMS
HARTRAO	HRAO	Y:EFOS C	1.9e-15	8.5e-16	3.8e-17	260ps
KOKEE	KOKB	Y:SigmaTau	3.0e-15	3.2e-15	7.4e-17	210ps
MEDICINA	MEDI	Y:EFOS 4	1.2e-14	1.2e-14	1.2e-15	340ps
NYALES20	NYAL	Y:APL 2	6.8e-15	6.5e-15	-4.5e-16	110ps
	NYA1			6.8e-15	-6.6e-16	140ps
ONSALA60	ONSA	Y:CH1-75A	CALC/SOLVE/GPSCP CLK REFERENCE			
SVETLOE	SVTL	N:CH1-80/int	2.8e-15	1.1e-12	no common clock	
TIGOCONC	CONT	Y:EFOS24	4.3e-15	no GPS data available		
	CONZ	N:internal		6.1e-9	no common clock	
TSUKUB32	TSK2	N:RH401A	1.2e-13	8.2e-14	no common clock	
	TSKB	5071A(IGS)		6.5e-14	no common clock	
WESTFORD	WES2	N:APL 3/4	7.1e-15	8.4e-14	no common clock	
WETTZELL	WTZR	Y:EFOS 18	1.2e-15	1.9e-14	8.9e-15	1.9ns
	WTZZ			6.2e-16	4.8e-16	70ps
ZELENCHK	ZECK	N:CH1-80/int	4.0e-14	4.1e-10	no common clock	

6. Acknowledgements

This work has been performed as part of the Swedish National Metrology Program, program owner VINNOVA Swedish Agency for Innovation Systems. We would like to acknowledge the work of the following organizations/individuals: Karl-Åke Johansson at OSO, Per Jarlemark at SP, National Resources Canada for the NRCAN GPS PPP software, and the Open Source Community.

References

- [1] Johnston et al.: Precise Time Transfer Using Mark III VLBI Technology, 15th PTTI, p443, 1983.
- [2] Spencer et al.: Comparison of VLBI, TV, and Travelling Clock Techniques for Time Transfer, In: Proc. 13th PTTI, p231, 1981.
- [3] Yoshino et al.: The first comparative experiment of VLBI and two-way time transfer with better than 1 nsec precision, Proc. IEEE IMTC/94, vol. 2, p. 808, 1994.
- [4] Hama et al.: Japan-US time comparison experiment for realizing better than 1-ns accuracy by using a radio interferometric technique, IEEE Transactions on Instrumentation and Measurement, p. 640, 1989.
- [5] Yoshino et al.: Development of VLBI time transfer system toward 0.1 nsec accuracy using transportable ground terminal for calibration, Proc. IEEE IMTC/94, vol.2, p. 806, 1994.
- [6] Takiguchi et al.: VLBI Measurements for Time and Frequency Transfer, Proc. EFTF2008, 2008.
- [7] Ma et al.: Measurement of horizontal motions in Alaska using Very Long Baseline Interferometry. Journal of Geophysical Research, 95(B13), pp. 21991–22011, 1990.
- [8] Orgiazzi et al.: Experimental Assessment of the Time Transfer Capability of Precise Point Positioning (PPP), Proc. of the Joint IEEE Intl. FCS and the PTTI, Vancouver, Canada, 2005.



Session 5 - Progress in Technology Development

The Mark 5C VLBI Data System

Alan Whitney¹, Chester Ruszczyk¹, Jon Romney², Ken Owens³

¹⁾ *MIT Haystack Observatory*

²⁾ *NRAO*

³⁾ *Conduant Corporation*

Contact author: Alan Whitney, e-mail: awhitney@haystack.mit.edu

Abstract

The Mark 5C disk-based VLBI data system is being developed as the third-generation Mark 5 disk-based system, increasing the sustained data-recording rate capability to 4 Gbps. It is built on the same basic platform as the Mark 5A, Mark 5B and Mark 5B+ systems and will use the same 8-disk modules as earlier Mark 5 systems, although two 8-disk modules will be necessary to support the 4 Gbps rate. Unlike its earlier brethren, which use proprietary data interfaces, the Mark 5C will accept data from a standard 10 Gigabit Ethernet connection and be compatible with the emerging VLBI Data Interchange Format (VDIF) standard. Data sources for the Mark 5C system will be based on new digital backends now being developed, specifically the RDBE in the U.S. and the dBBC in Europe, as well as others. The Mark 5C system is being planned for use with the VLBI2010 system and will also be used by NRAO as part of the VLBA sensitivity upgrade program; it will also be available to the global VLBI community from Conduant. Mark 5C system specification and development is supported by Haystack Observatory, NRAO, and Conduant Corporation. Prototype Mark 5C systems are expected in early 2010.

1. Introduction

The Mark 5C is being designed as the next-generation Mark 5 system, with a capability of recording sustained data rates to 4096 Mbps. It will use the same disk modules as the Mark 5A and Mark 5B, thus preserving existing investments in disk modules. The data interface for both recording and playback will be 10 Gigabit Ethernet, which is rapidly becoming a widely supported standard. The use of 10GigE interfaces comes with some significant implications, however. Firstly, data sources must be designed to provide data streams in a format compatible with the Mark 5C requirements. And secondly, data playback through a 10GigE interface is a good match for a rising generation of software correlators. In the interests of backwards compatibility, the Mark 5C will also support a mode which writes disk modules in Mark 5B data format which can be correlated on existing Mark IV correlators that support Mark 5B.

The Mark 5C will be implemented using the existing Amazon StreamStor disk-interface card (used in the Mark 5B+) from Conduant Corporation along with a new 10GigE-specific interface daughterboard being designed by Conduant. Unlike the Mark 5A and Mark 5B, no separate specialized I/O card will be necessary in the Mark 5C.

2. Data Sources

One major implication of the Mark 5C model is that the data source is responsible for all data time-tagging, formatting, and creation of Ethernet packets. This is a departure from the VSI-H

model used by the Mark 5B, which has basically only 32 parallel sample bit-streams, a clock, and 1pps tick flowing between the data source and the Mark 5B, with the Mark 5B being responsible for creating data frames with higher level time-tagging and formatting.

Fortunately, VLBI data sources capable of creating such formatted Ethernet packets are now being developed in both the U.S. and Europe as part of the development of digital downconverters and backends. Several different digital-backend systems with 10GigE output suitable for recording by the Mark 5C are planned to be available in 2010. The details of the data formats to be provided to the Mark 5C are specified in a separate document “Mark 5C Data-Frame Specification”. Normally, each Ethernet packet from the data source will contain sample data from only a single frequency channel, although a Mark 5B-compatible data mode is specified which will write disk modules in a format that can be re-played on a Mark 5B playback unit; this will provide the ability to process the recorded data on existing Mark IV hardware correlators.

3. Correlation

A major shift is currently developing to move from hardware-based correlators to software-based correlators, some of which already exist. Unlike the Mark 5A and Mark 5B, the Mark 5C will have no streaming hardware playback interface. Instead, the data files will appear to the user as standard Linux files and will be read as such. We expect that the standard interface for playback to a correlator will be through a standard 10GigE interface implemented on a commercial NIC. Unlike existing hardware correlators, software correlators do not demand constant-rate streaming inputs. As such, the Mark 5C playback is well-suited for interfacing to software correlators, but not well-suited for or intended to interface to hardware correlators.

4. General Mark 5C Characteristics

The Mark 5C will have the following characteristics:

- Mark 5C will be fully compatible with all existing Mark 5 disk modules; however, some modules with older disks may limit record/playback data rates.
- At data rates above about 2 Gbps, it will be necessary to record to two 8-disk modules simultaneously, in so-called “non-bank” mode, which is not normally used by Mark 5A or Mark 5B/5B+.
- A 10GigE interface for *receive-only* will be implemented on the Amazon StreamStor disk-interface card (currently used in the Mark 5B+) by replacing the FPDP I/O daughterboard on the Amazon card with a newly designed 10GigE daughterboard. This 10GigE interface will be *receive-only*, optimized for sustained real-time recording of *at least* 4096 Mbps from a data source. Received Ethernet packets can be OSI Layer 2 or higher but will only be processed by the Mark 5C at the Layer 2 level. Jumbo Ethernet packets up to 9000 bytes will be supported. The data source is required only to transmit Ethernet packets and is not required to process any received packets.
- The entire data payload from each arriving Ethernet packet, sans a specified length of payload header (which may contain higher OSI Layer parameters or other information), will be recorded to disk. In this sense, the Mark 5C is entirely ‘formatless’; i.e., all data formatting

must be done by the data source. This allows each user to format the recorded data according to his/her needs.

- The Ethernet data payload may contain a user-generated 32-bit “Packet Sequence Number” (PSN), whose position within the data payload can be specified to the Mark 5C. The Mark 5C can be commanded to a “PSN monitor mode” that will parse this serial number from every packet to identify missing or out-of-order packets. Out-of-order packets, within some reasonable limits, will be restored to proper order, while the user data from each missing packet will be replaced by user-specified “fill-pattern” data. The MSB of the PSN may also be used as an ‘invalid’ marker to prevent recording data from a packet. If “PSN monitor mode” is disabled, data are recorded to disk in the order that packets are received; no checks are made for out-of-order or missing packets.
- Similar to the Mark 5A/B, the Mark 5C will record data as “scans”, where a scan is defined as the period between starting and ending the recording of a particular observation. The duration of a scan may be from several seconds to many minutes. The host application software will maintain a directory of scans for easy identification and access. No duplicate-named scans are allowed.
- Scans will appear as normal Linux files to the host PC. Data playback on the Mark 5C will be through a 10GigE NIC interface on the host PC. A planned upgrade by Conduant of the Amazon card, which interfaces to the PCI-X bus, will support the PCI-e bus to allow substantially higher playback rates from Mark 5 disk modules.

5. Physical Connections

Because the interconnection between the data source and the Mark 5C is a standard 10 Gigabit Ethernet connection, there is considerable flexibility in connection topology between data-source units and Mark 5C units. Figure 1 illustrates the general case where multiple data-source units provide data to multiple Mark 5C units through a standard Ethernet switch. The Ethernet switch allows Ethernet packets from either of the two DBE2 units to be arbitrarily routed to any of four Mark 5C units, providing an easy way to manage route data packets in an arbitrary manner, but it is particularly useful to manage data-rate mismatches between individual data sources and individual Mark 5Cs. For example, an 8 Gbps packet stream from a single DBE2 could be separated into two 4 Gbps packet streams to two Mark 5C units.

6. Data-organization Philosophy

Previous generations of VLBI data recorders, such as Mark III/3A/4/5A/5B have generally formatted multiple observing frequency channels as multiple-parallel bit-streams representing simultaneous samples from all channels. Also, typically, the per-channel data rate is constrained to 2^n Mbps, and the number of channels is also usually constrained to be integer powers of 2, thereby also constraining total data rates to be 2^n Mbps. This type of data organization has been satisfactory for the type of hardware correlators that have been predominant over the past 30 years, but it is not well matched to today’s needs.

Modern VLBI data management relies increasingly heavily on the use of standardized local and global computer networks whose capacities are not well matched to the 2^n Mbps paradigm

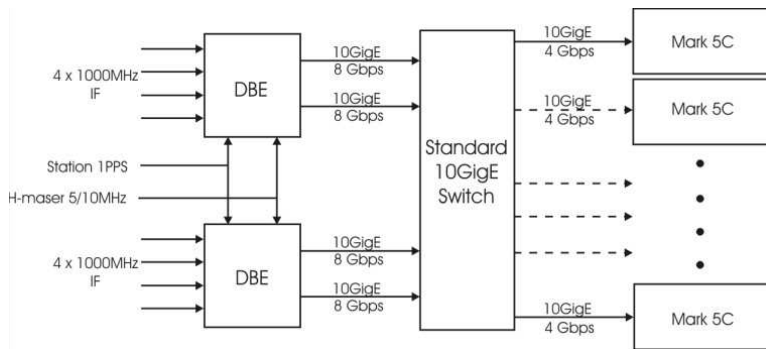


Figure 1. Generic signal-connection diagram for Mark 5C.

of established VLBI data systems. Furthermore, VLBI correlation processing is moving rapidly towards fully software solutions operating on clustered computer networks. Both of these trends argue for improved flexibility in aggregate VLBI data rates and repackaging of data into more convenient forms for processing by standard computer hardware.

7. Mark 5C Data-frame Format

The Mark 5C itself is data-format independent and simply records Ethernet packets which are sent to it. However, most usage of the Mark 5C is expected to utilize the VLBI Data Interchange Format (VDIF) specification ratified by the global VLBI community in 2009.

The primary elements of the VDIF specification, as applied to the Mark 5C, are as follows:

1. Each Ethernet packet arriving at the Mark 5C contains one self-identifying VDIF Data Frame.
2. Each Data Frame contains a 16-byte or 32-byte Data Frame Header followed by a Data Array.
3. The Data Array of a Data Frame may contain either single-channel or multi-channel data, but most Mark 5C usage is expected to utilize multiple “threads” of single-channel Data Frames.
4. The Data Frame length must be constant during a given scan (defined as the period between starting and ending the recording of a particular observation) but can vary from scan to scan if necessary.
5. The Data Frame length (including header) must meet the following three criteria:
 - (a) Must be within the range 64-9000 bytes
 - (b) Must be a multiple of 8 bytes for compatibility with the StreamStor disk-addressing algorithm
 - (c) Must result in an integer number of complete Data Frames per second

The currently proposed format of a VDIF data-frame header is shown in Figure 2.

Some of the fields in the VDIF data-frame header are self-explanatory. The detailed VDIF specification is available at http://vlbi.org/docs/VDIF_specification_Release_1.0_ratified.pdf.

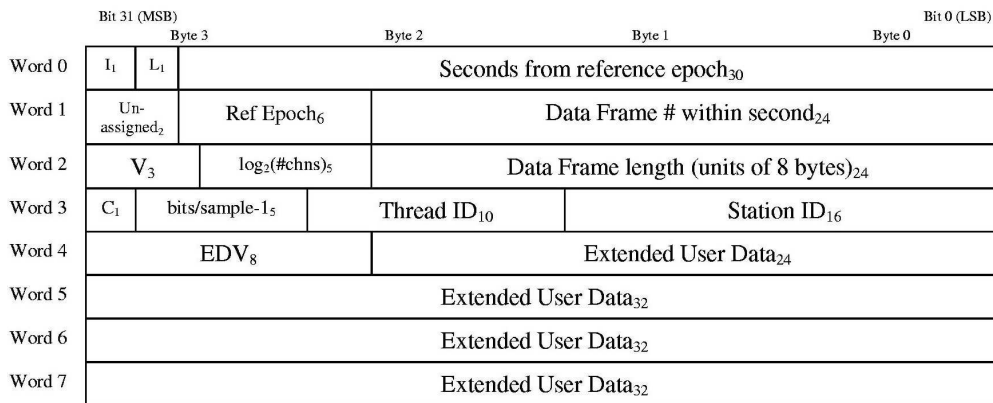


Figure 2. VDIF Data Frame Header format; subscripts are field lengths in bits.

8. Slow-disk Management

Considerable experience has shown a low, but significant, occurrence of “slow” disks, that is disks that still function to read and write, but at a reduced data rate due presumably to marginal or bad sectors on the disk. Normal RAID systems will simply slow down to accommodate such disks in a RAID array since they are not designed for real-time operation. The StreamStor disk-interface cards in the Mark 5 units are designed to re-distribute the load to normal-performing disks in the face of one or more “slow” disks in the recording array so as not to lose critical real-time data. Playback through a software correlator is generally non-critical as to playback rate, though the correlation speed may be slower than normal. If correlation speed is important, a playback mode may be invoked whereby data not received in time from slow disks will be replaced with a specified “fill pattern”.

9. Upgrade Path from Mark 5A, Mark 5B, or Mark 5B+

The Mark 5C requires an Amazon StreamStor card (\sim \$9500) plus a 10 Gigabit/sec Ethernet daughterboard (\sim \$3–4K); no VLBI-specific I/O board is required. To upgrade from Mark 5A or Mark 5B requires an Amazon board and a 10GigE daughterboard. To upgrade from a Mark 5B+ requires only a 10GigE daughterboard.

10. Summary

The Mark 5C development is being supported by Haystack Observatory, NRAO, and Conduant Corporation. Prototype Mark 5C systems are expected in early 2010 and should be available to the VLBI community in the latter half of 2010.

Detailed specifications for the Mark 5C are available at http://www.haystack.edu/tech/vlbi/Mark5/Mark_5_memos in memo number 57; other information related to Mark 5C is also available at this URL.

Next-generation A/D Sampler ADS3000+ for VLBI2010

Kazuhiro Takefuji¹, Hiroshi Takeuchi², Masanori Tsutsumi¹, Yasuhiro Koyama¹

¹) *Kashima Space Research Center, National Institute of Information and Communications Technology (KSRC/NICT)*

²) *Institute of Space and Astronautical Science Japan Aerospace Exploration Agency (ISAS/JAXA)*

Contact author: Kazuhiro Takefuji, e-mail: takefuji@nict.go.jp

Abstract

A high-speed A/D sampler, called ADS3000+, has been developed in 2008, which can sample one analog signal up to 4 Gbps to versatile Linux PC. After A/D conversion, the ADS3000+ can perform digital signal processing such as real-time DBBC (Digital Base Band Conversion) and FIR filtering such as simple CW RFI filtering using the installed FPGAs. A 4 Gbps fringe test with the ADS3000+ has been successfully performed. The ADS3000+ will not exclusively be used for VLBI but will also be employed in other applications.

1. Introduction

The National Institute of Information and Communications Technology (NICT) has been developing VLBI observation systems and data processing systems since the 1970s. The K5 VLBI system is designed with the commodity products such as personal computers, hard disks, and network components. This strategy has been quite successful for developing highly flexible and high-performance observation systems and data processing systems for VLBI. K5/VSI series are realized by high-speed AD sampler units and a commodity Linux PC system to record data according to the VSI-H (VLBI Standard Interface - Hardware) specifications. VSI-H was proposed to define a standard interface for the high-speed data transfer between data input modules, data transfer modules, and data output modules to improve the compatibility between next generation VLBI observing systems and the correlator systems. Three high-speed AD sampler units, ADS1000, ADS2000, and ADS3000, have been developed to date to support various sampling modes. ADS1000 can sample one baseband channel at a sampling rate of 1024 Msps/2bit. ADS2000 can sample 16 baseband channels at the sampling rate of 64 Msps suitable for geodetic VLBI observations with the bandwidth synthesis method. ADS3000 can sample a wide range of the baseband frequency band up to 1024 MHz with a sampling rate of 2048 Msps [2]. Currently, ADS3000+ is under development to support 4 Gbps x 1 ch, 2 Gbps x 2 ch, and 1 Gbps x 4 ch sampling modes by using a faster AD sampler chip [1]. ADS3000 and ADS3000+ are equipped with FPGA chips to realize digital baseband converter (DBBC) with user-selectable bandwidth of 4–32 MHz. We will present more details about the newly designed ADS3000+ system in this article.

2. The Next-generation A/D Sampler ADS3000+

The ADS3000+¹ is a newly-extended A/D sampler from the ADS3000 system that supports various sampling modes. A faster A/D sampler chip and two new FPGA chips replace a simple

¹More information is available in <http://www2.nict.go.jp/w/w114/stsi/K5/>



Figure 1. Front view of the ADS3000+ unit. Many status settings can be displayed and monitored.

Size	EIA 2U (480mm x 88mm x 430mm)
Reference	10MHz 0dBm+-3dBm, 1PPS (50ohm)
IF input	+/-250m Vp-p (50ohm)
Output	VSI-H compliance
Control	RS232-C (D-sub 9pin male),100Base-Tx
Power supply	AC100-240V
A/D chip	e2V EV8AQ160
FPGA chip 1	Xilinx Virtex5 XC5VLX110
FPGA chip 2	Xilinx Virtex5 XC5VLX220
Sampling Modes	4096 Msps x 1 ch 2048 Msps x 2 ch 1024 Msps x 4 ch (DBBC mode)

Figure 2. Specifications of the ADS3000+ unit. The FPGA chip can be replaced by a larger one (e.g., XC5VLX330).

FPGA chip. It has the capability of sampling analog data up to 5 GHz at the highest speed. However, one VSI-H (VLBI Standard Interface) interface is connected to a PC up to 2 Gbps (Giga bit per second). The maximum sampling speed via two VSI-H connections becomes 4 Gbps. ADS3000+ has four VSI-H output ports, so 8 Gbps recording is possible, if a PC is connected to every port.

The ADS3000+ digitizes analog signal 4 Gbps x 1 ch, 2 Gbps x 2 ch, and 1 Gbps x 4 ch. Moreover, various signal processing steps such as DBBC (Digital Base-Band Converter) can be performed with the FPGA chips inside the ADS3000+. Figure 2 shows the major specifications of the ADS3000+ system. Standard sampling modes up to 4 GHz have already been evaluated [3].

3. First Fringe Detection at 4 Gbps

Before doing a 4 Gbps fringe experiment, the VSI-H limitation (connection between ADS3000+ and PC) has to be considered. The VSI-H data rate at one channel is 2 Gbps at maximum, so that a 4Gbps@1bit experiment is not possible with one port output. A workaround of simulating two VSI-H ports has been applied to ADS3000+. Specifically, the digitized data is sequentially divided into one-byte or four-byte samples and allocated to the two VSI-H outputs. The two digital data streams are assembled by a software program to obtain 4 Gbps data. It is an adaptation of a high-performance look-up-table method.

A fringe test was carried out on 27 April 2009. The Kashima 34m antenna and 11m antenna were used with ADS3000+ units at the two stations. The phase calibration signal was shut off to detect fringes correctly. After sampling at 4 Gbps speed with 1bit quantization, the whole bandwidth spectrum of X-band is fully shown in Figure 3. A first fringe of 3C273B at 4 Gbps could be successfully detected after correlation. This is shown in Figure 4. A signal-to-noise-ratio (SNR) of the 3C273B fringe is estimated to be about 8.6 at 8 ms integration. The speed of the 4 Gbps fringe is a world record [3].

4. Real-time FIR Filtering, RFF Mode

With FPGA, a real-time FIR filtering signal process, called RFF mode, can be realized with 2 Gbps x 2 ch at maximum. We adapted the RFF mode to the radio signal environment of Kashima

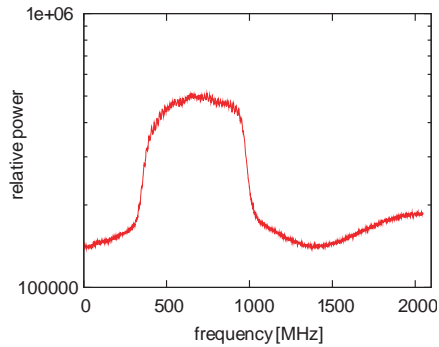


Figure 3. X-band spectrum of Kashima 11m antenna. The bandwidth is 500 MHz; however, the 4 Gbps mode detects up to Nyquist-rate 2 GHz. The whole X-band bandwidth spectrum can be obtained at one time.

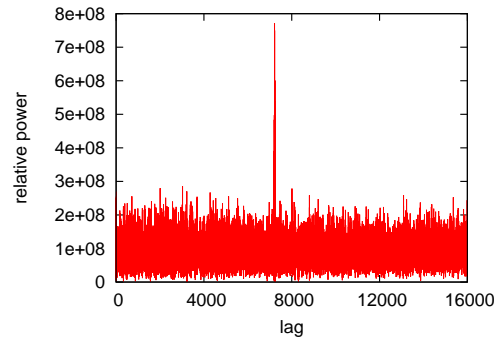


Figure 4. First fringe of 3C273B at 4 Gbps speed with ADS3000+ in 8 ms integration time between Kashima 34m and 11m antennas on 27 April 2009. The 4 Gbps fringe is a world speed record.

Space Research Center. This is shown in Figure 5. In this case, we designed a band elimination filter (BEF) for suppressing strong signals. In RFF mode, the filter coefficient is limited to 65taps 8bit range. However, any filter can be designed for these conditions. The RFF is also used for VLBI purposes. For example, a real-time Hilbert transform can be used, which makes 90 degree shift like 90 degree hybrid. One channel of RFF is Hilbert-transformed, and another channel is used for delay synchronization. We plan to use this RFF mode to convert linear polarization to circular polarization.

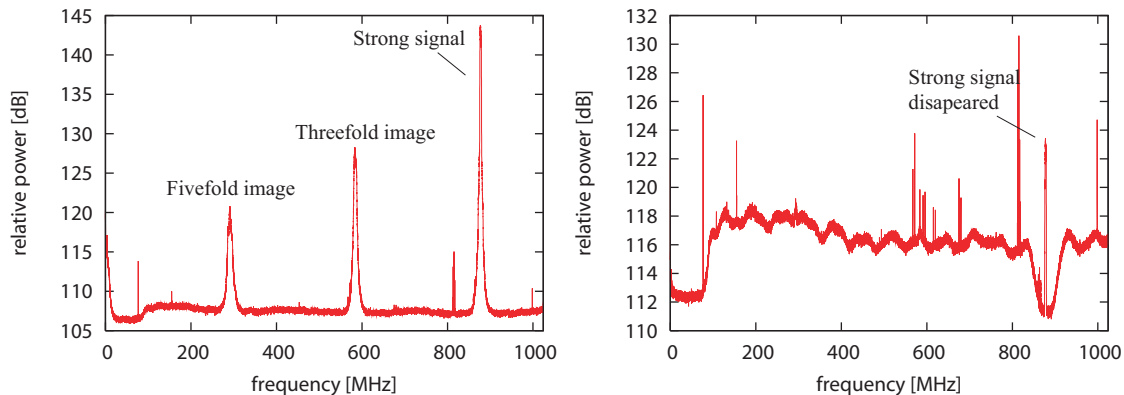


Figure 5. (left) With an omni-directional antenna and a wide-band receiver of 100–1024 MHz, the radio conditions around Kashima Space Research Center were determined. At 880 MHz, a strong radio signal from the base station can be seen. The base station signal is too strong to obtain a proper dynamic range. (right) With BEF, the strong base station signal weakens, and it is possible to measure other radio signals with an improved dynamic range.

5. DBBC on the ADS3000+

Digital sampling DSP with ADS3000+ is realized via DBBCs. There are 16-ch DBBCs inside ADS3000+. The DBBC specifications are shown in Table 1. The output formats of 16-ch DBBCs at 2 bit or 8-ch DBBCs at 4 bit can be selected. Figure 6 shows a DBBC flow chart. First digital data comes from A/D, and it is multiplied by NCO (numerical controlled oscillator), which makes it possible to tune the frequency by 1Hz resolution and angular acceleration. After frequency shift, filtered CIC and FIR follow. CIC (Cascade Integrator Comb) is not only a small circuit but also a useful LPF. Finally, complex or real (USB or LSB) signal is generated. A delay between 16-ch DBBCs is calibrated to zero in all modes. The user does not need to care about delay inside DBBCs. Following the final check of the DBBC, we will perform a fringe test between analog BBC and DBBC systems. The bandwidth of the analog BBC has a slope characteristic due to image rejection mixer. It will be more meaningful to compare analog-analog BBC and DBBC-DBBC.

Table 1. Specifications of the ADS3000+ DBBC mode. One VSI-H of DBBC generates 16 ch x 2 bit or 8 ch x 4 bit. The VSI clock speed can be fixed or variable. So far, only 1024 Msps x 4 ch is supported in DBBC mode.

Sample speed	Quantization	VSI clock
8 Msps	4 bit	Fixed: 64 MHz, Variable 8 MHz
16 Msps	4 bit	Fixed: 64 MHz, Variable 16 MHz
32 Msps	4 bit	Fixed: 64 MHz, Variable 32 MHz
64 Msps	4 bit	Fixed: 64 MHz, Variable 64 MHz
1024 Msps	1 bit, 2 bit	Fixed: 64 MHz

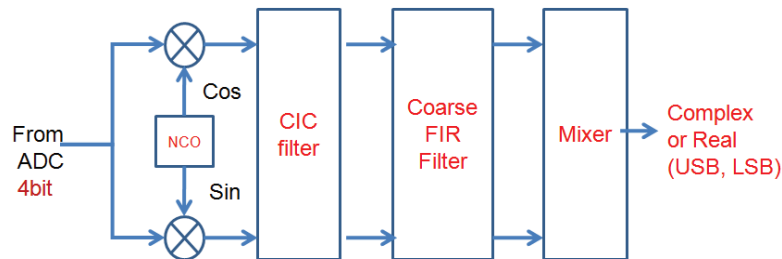


Figure 6. ADS3000+ DBBC flowchart. The DBBC follows a modified Weaver method which is multiplied by NCO and filtered out. To suit the FPGA capacity, a CIC filter (Cascade Integrator Comb) is applied. There are 16 DBBCs in ADS3000+. Each DBBC can generate Complex or Real (USB or LSB) with 4, 8, 16, or 32 MHz bandwidth.

6. Discussion

The National Astronomical Observatory of Japan (NAOJ) currently checks the connection between ADS3000+ and Mark 5B recording system. The compliance of ADS3000+ with VSI-H

output is kept; hence, a good result is expected. Currently ADS3000+ has a VSI-H output interface which connects PC with 2-Gbps speed at maximum. Four VSI-H output ports on ADS3000+ yield an 8-Gbps speed. However, to divide data inside ADS3000+ and to assemble data after recording to PC could be useless. By A/D chip specification of ADS3000+, it is possible to convert to digital signal up to 5 Gsps and 8bit quantization. Total 40 Gsps data is impossible to record via VSI-H and 10GbE interfaces. Currently 40GbE, 100GbE, and USB3.0 is more familiar. When considering 40GbE and 100GbE for the future equipment, it will be necessary to further develop not only the recorder system but also the e-VLBI network transfer. USB3.0, on the other hand, tends toward greater use at 5 Gbps. In case of using USB3.0, it is more convenient and cheaper. USB3.0 has the potential to create K5/VSI3.0 system with ADS3000+.

7. Summary and Outlook

We were able to obtain the speed record for 4 Gsps fringe in 2009. ADS3000+ will not only be a powerful converter for the current receiver system, but it is also suitable for a wide-band receiver of the next-generation VLBI (VLBI2010). The SNR is proportional to the bandwidth, and finer phenomena can be captured with high-speed sampling, so that the ADS3000+ will hopefully break new ground in VLBI, astronomy, and science.

Development of the ADS3000+ system is a cooperative effort between NICT, JAXA/ISAS, and COSMO RESEARCH Corp². The authors would like to thank the Kashima VLBI team for their cooperation.

References

- [1] Koyama, Y., T. Kondo, M. Sekido, and M. Kimura, Developments of K5/VSI System for Geodetic VLBI Observations TDC News, IVS NICT-TDC News, **No.29**, pp.15-18, 2008.
- [2] Takeuchi, H., M. Kimura, J. Nakajima, T. Kondo, Y. Koyama, R. Ichikawa, M. Sekido, and E. Kawai, Development of 4-Gbps Multi-functional VLBI Data Acquisition System, Publications of the Astronomical Society of the Pacific, **Vol.118**, pp.1739-1748, 2006.
- [3] Takefuji, K., H. Takeuchi, and Koyama, Y., First Fringe Detection with Next-Generation A/D Sampler ADS3000+ TDC News, IVS NICT-TDC News, **No.30**, pp.17-21, 2009.

²<http://www.cosmoresearch.co.jp>

VLBI Technology Development at SHAO

*Xiuzhong Zhang, Fengchun Shu, Ying Xiang, Renjie Zhu, Zhijun Xu, Zhong Chen,
Weimin Zheng, Jintao Luo, Yajun Wu*

Shanghai Astronomical Observatory, Chinese Academy of Sciences

Contact author: Xiuzhong Zhang, e-mail: xzhang@shao.ac.cn

Abstract

VLBI technology development made significant progress at SHAO in the last few years. The development status of the Chinese DBBC, the software and FPGA-based correlators, and the new VLBI antenna, as well as VLBI applications are summarized in this paper.

1. Introduction

In 1972 Shanghai Astronomical Observatory (SHAO) prepared and started to develop a VLBI system in China. The project was proposed in 1975, and it was approved in 1978. Three years later, the first successful VLBI experiment was observed between a 6-m antenna at SHAO and the 100-m antenna at Effelsberg at L-band. After that, SHAO started to build a 25-meter telescope. The telescope was put into full operation in 1987. With the strong support of the Chinese Lunar Project, four VLBI stations and one data processing center were built in 2006. They form the Chinese VLBI Network (CVN). The Shanghai Astronomical Observatory is an organizer and technical supporter of CVN.

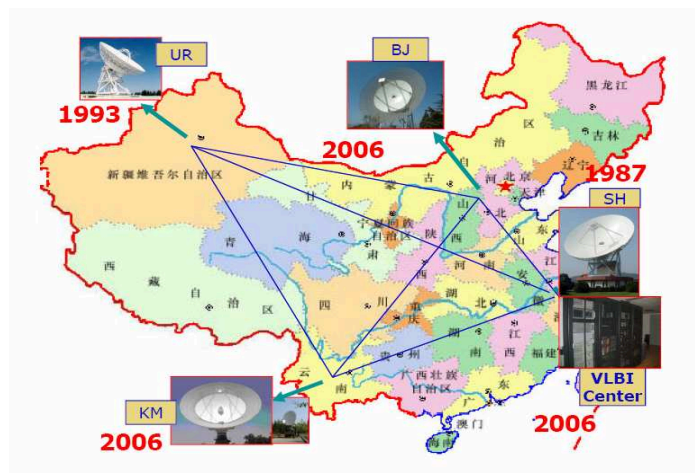


Figure 1. The location of the CVN stations.

2. The CVN

There are four VLBI stations in China. They are named Sheshan (Sh), Nanshan (Ur), Kunming (Km), and Miyun (Bj). The longest baseline of the CVN is 3249 km (Sh to Ur). There are fiber connections between the VLBI stations and the data processing center. The data rate is about one Gbps for Sheshan and 100 Mbps for the other three stations. Figure 1 shows a map with the locations of the CVN stations.

3. The Digital Backend System

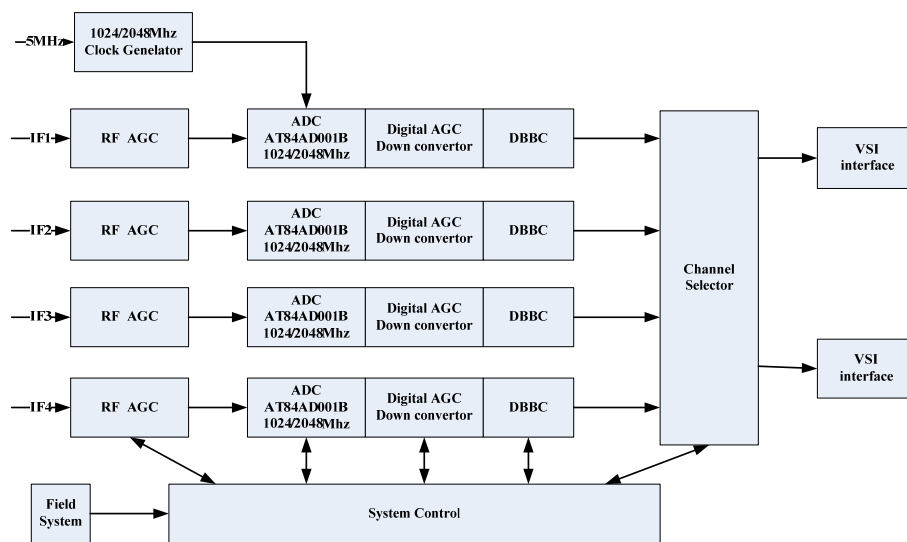


Figure 2. Diagram of the Chinese Data Acquisition System CDAS.



Figure 3. Collage of photos showing the CDAS at the four CVN stations.



Figure 4. Two CDAS systems integrated into one box.

The data acquisition system is the key equipment at a VLBI station. The traditional DAS systems with analog base band converters are used at most VLBI stations in the world. Unfortunately, this type of data acquisition system is no longer manufactured. The new type of data acquisition system with digital base band converters is coming slowly into the market. After a long discussion, SHAO started the development of a data acquisition system with digital base band converters at the beginning of 2007. The system will be integrated and operated at the four Chinese VLBI stations. The name of this digital base band converter is “Chinese VLBI Data Acquisition System”, abbreviated to CDAS. It is compatible with the traditional data acquisition system, which currently operates at the VLBI stations. But the total bandwidth of the CDAS is 2 GHz. There are two VSI data output interfaces in CDAS. With a different IP core, the CDAS could be compatible with the DBBC and DBE, which are being developed by the EVN and at Haystack Observatory respectively. CDAS has the following characteristics:

- use of 5 MHz as standard frequency signal input
- use of 1 pps as a time signal input
- four channel IFs input (the bandwidth of each IF may be 512MHz/1024MHz)
- two VSI interfaces to Mark 5B Disk Array
- fully compatible FS interface of traditional DAS (hardware and software)
- PCAL and total power output
- any two channels auto and cross spectrum monitor
- PCI interface for control

Figure 2 shows the diagram of CDAS. CDAS consists of three parts: RF AGC, Digital Part, and Output Module.

Figure 3 shows photos of CDAS which are integrated at the CVN stations now. Figure 4 shows the new CDAS version, which is configured with two CDAS in one box. Both CDAS have an individual power supply and input/output signal interface. For more details of CDAS characteristics, see [5].

4. The Correlator

The CVN data processing center has two correlators. One is a software correlator which is described by Dr. Zheng [6]. The other is an FPGA-based correlator. This is a 5-station FX-type correlator. It was specifically designed for the first Chinese Lunar satellite (CE-1) mission. The data rate of this correlator is 256 Mbps. Some functions of this correlator have been improved for the second Chinese Lunar satellite (CE-2). The VSI and network interface have been integrated into the modified correlator. Figure 5 shows a diagram of the FPGA-based correlator. A more

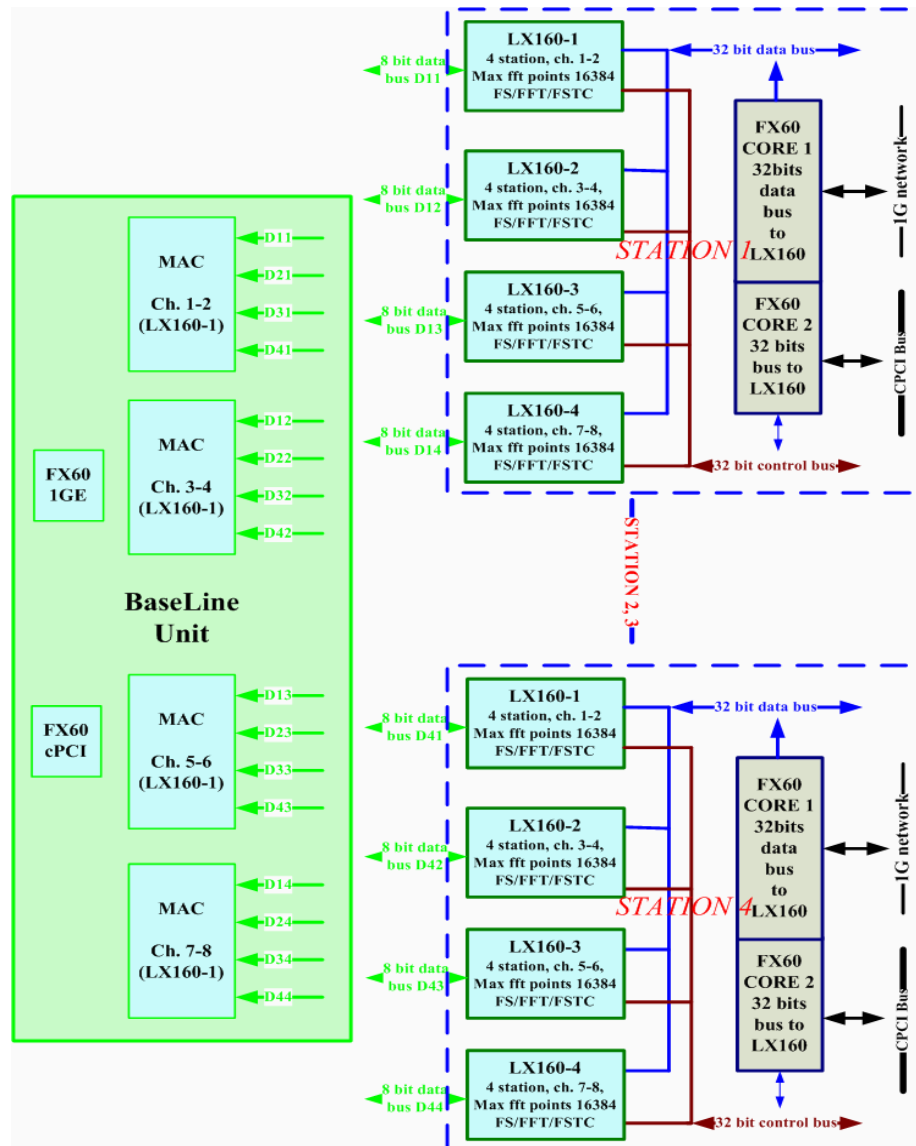


Figure 5. Diagram of the new FPGA-based correlator for the CE-2 project.

detailed description can be found in [7]. SHAO has become an official member of RadioNet. We recently joined the Uniboard project and plan to use the Uniboard to build a new FPGA-based e-VLBI correlator for astrophysics, astrometry, and geodesy applications.

5. New Telescope

The CVN showed excellent efficiency in the first Chinese Lunar Project. The people realized the advantage of VLBI technology for spacecraft tracking. With the support of the local government of Shanghai, the Chinese Academy of Sciences, and the Chinese Lunar Project, SHAO has an opportunity to build a new 65-meter telescope. The frequency of the Shanghai 65-meter telescope will cover L, S, C, X, Ku, K, Ka, and Q bands. In 2012, the 65-meter telescope will be observing in L, S/X, and C bands. The full facility of this telescope will be finished in 2015. Figure 6 shows the structure of the Shanghai 65-meter telescope. More information can be found on the Web at <http://202.127.24.8/eng.aspx>.

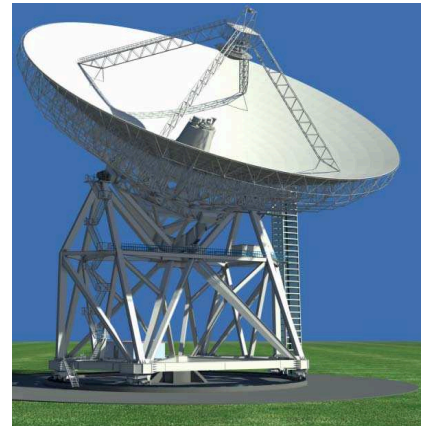


Figure 6. Artist's rendition of the structure of the Shanghai 65-meter antenna.

6. Conclusion

The CVN accomplished very successfully the CE-1 tracking task. CVN will continue to work on astrophysics, astrometry, and geodesy applications. With new VLBI equipment, the CVN plans to join international and domestic observations more actively.

References

- [1] XZ Zhang, et al., CVN Correlator and its Future, *New Technologies in VLBI*, Astronomical Society of the Pacific Conference Series Volumes, Vol. 306, 287–300, 2003.
- [2] Zhijun Xu, et al., Real Time Correlator in FPGA, *IVS 2006 General Meeting Proceedings*, p. 89–92.
- [3] Gino Tuccari, et al., DBBC - A Flexible Platform for VLBI Data Processing, *IVS 2006 General Meeting Proceedings*, p. 185–189
- [4] Alan R. Whitney et al., A Wide-Band VLBI Digital Backend System, *IVS 2006 General Meeting Proceedings*, p. 72–76.
- [5] Renjie Zhu, et al., this volume.
- [6] Weimin Zheng, et al., CVN Software Correlator Applications in Deep-Space Exploration, *Proceedings of SPIE*, Vol. 6795, 2007.
- [7] Weimin Zheng, et al., this volume.

The Progress of CDAS

*Renjie Zhu, Xiuzhong Zhang, Wenren Wei, Ying Xiang, Bin Li, Yajun Wu, Fengchun Shu,
Jintao Luo, Jinqing Wang, Zhuhe Xue, Rongbin Zhao, Lan Chen*

Shanghai Astronomical Observatory, CAS

Contact author: Renjie Zhu, e-mail: zhurj@shao.ac.cn

Abstract

The Chinese Data Acquisition System (CDAS) based on FPGA techniques has been developed in China for the purpose of replacing the traditional analog baseband converter. CDAS is a high speed data acquisition and processing system with 1024 Msps sample rate for 512M bandwidth input and up to 16 channels (both USB and LSB) output with VSI interface compatible. The instrument is a flexible environment which can be updated easily. In this paper, the construction, the performance, the experiment results, and the future plans of CDAS will be reported.

1. Introduction

In China, VLBI technology has been applied to orbit monitoring and orbit determination of spacecraft. Several radio telescopes have been established, such as the 50m antenna in Beijing and the 40m antenna in Kunming. Additionally, another 65m antenna is under construction in Shanghai. Including the two 25m antennas built earlier in Shanghai and Urumqi, there are four antennas now, and five or more will serve in the future as the VLBI network in China.

With the development of digital techniques, traditional VLBI terminals will be replaced by digital ones. The need for such replacement is well known and motivated by the necessity of both renewing an obsolete system whose components' replacement is every day more difficult and of achieving better performance making use of more predictable digital techniques [1].

Nowadays, high performance ADCs and high performance FPGAs are widely used. They can also meet the requirements of VLBI digital terminals, which would be economically convenient, and they are flexible and of high resolution.

2. The Overview of CDAS

CDAS is the abbreviation of Chinese Data Acquisition System. The concept of CDAS is shown in Figure 1. CDAS has:

- 1024 MHz sampling rate per channel;
- Up to 4 IFs input and 16 channels output;
- 32MHz/16MHz/8MHz/4MHz/2MHz/1MHz bandwidth output selectable; and
- 1/2/4 or 8-bit sampling selectable Mark IV or VSI-H interface compatible.

CDAS has about 20dBm dynamic range of input power level from -44dBm to -4dBm with analog AGC. As Figure 2 shows, for each IF, there are one ADC and four FPGAs used for data processing including DDS, down conversion, and filtering. And in order to fit for tracking

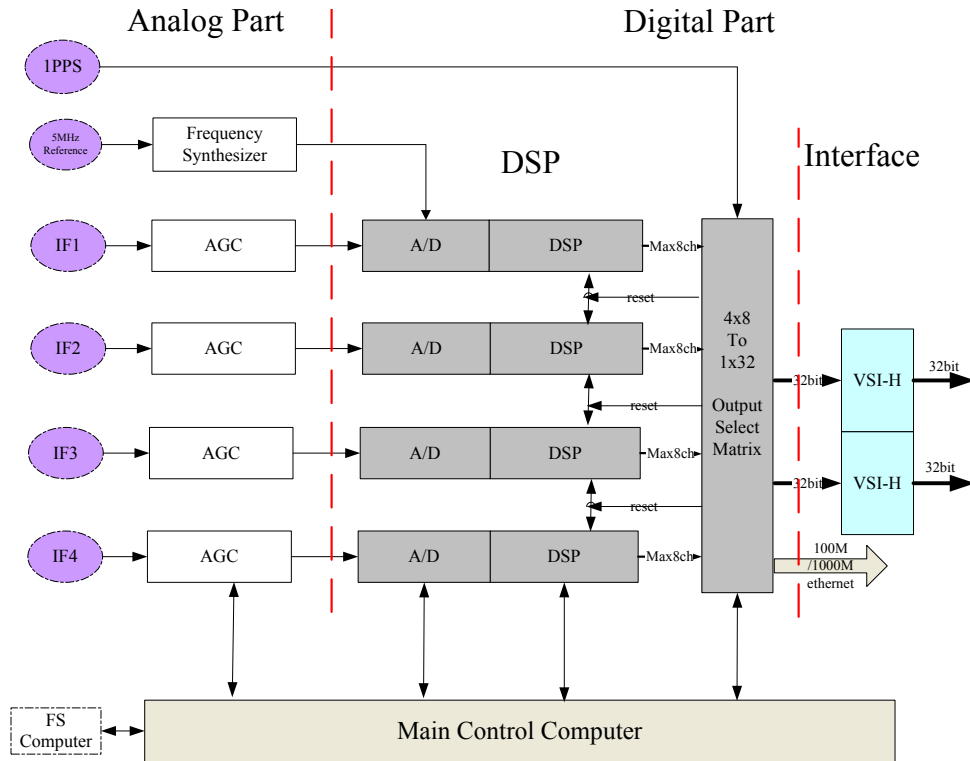


Figure 1. The concept of CDAS.

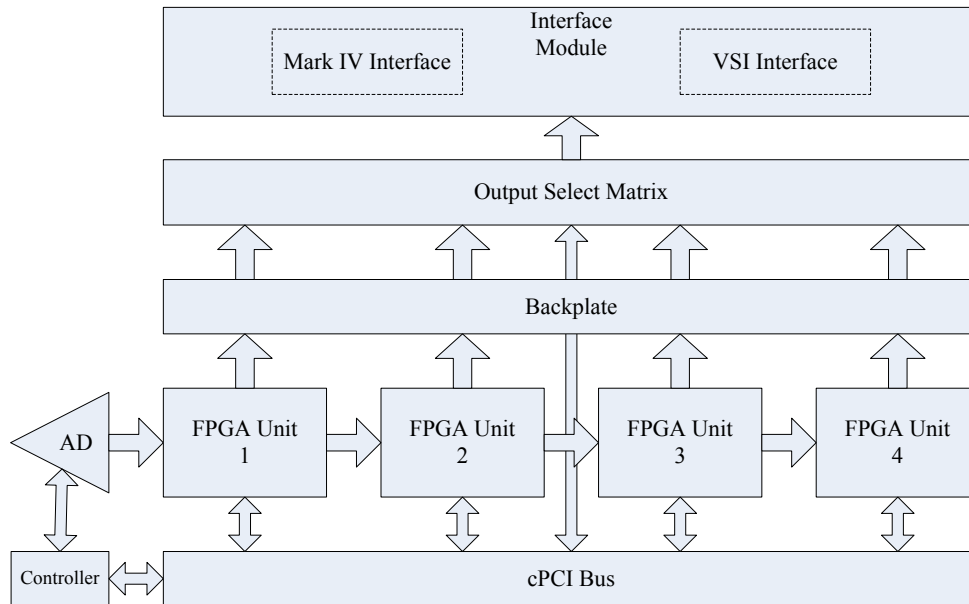


Figure 2. Signal Process Diagram.

spacecraft, the power level is calculated in each channel in order to avoid overflow. Each FPGA can produce one BBC including both USB and LSB. Another FPGA with PPC440 embedded is responsible for control and communication including ePCI bus control and communication with the Master Control Computer. The output select matrix module will select signals from the back plate and send them to the interface. The interface can be connected to a Mark IV formatter or a Mark 5B VSI-H interface.

3. Observation Results Comparison

Some comparisons between analog BBC (ABBC) and CDAS are shown below:

Figure 3 shows the result of a zero baseline test. The utilization of bandwidth is from about 75% (ABBC) up to 95% (CDAS).

Figure 4 shows the SNR comparison of a long baseline experiment between Shanghai and Kunming on 6 September 2009. The SNR of CDAS is much better than ABBC.

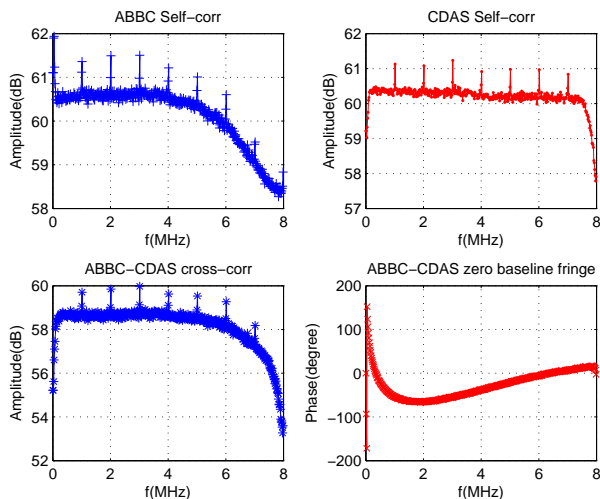


Figure 3. Bandwidth Comparison.

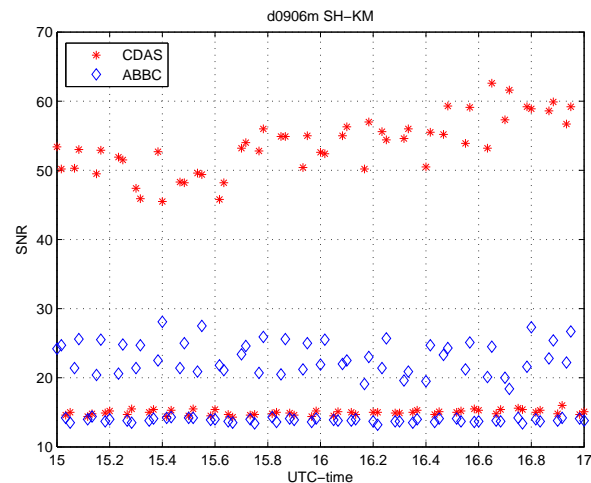


Figure 4. SNR Comparison.

4. CDAS at the Stations

Since January 2008, CDAS has been installed at Shanghai, Beijing, Kunming, and Urumqi—four VLBI stations. Figures 5 and 6 show the whole CDAS system at the Urumqi and Kunming stations, including FS Computer, Mark 5B, and LCD monitor.

After that, firmware and software have been updated several times during the past two years. CDAS will be applied in Chinese lunar projects in the future.

5. Future Plans

The sample rate of ADC is increasing from 1024 Msps to 2048 Msps, and this will double the total bandwidth of CDAS.



Figure 5. CDAS in Urumqi.



Figure 6. CDAS in Kunming.

10GigE and VDIF will also be supported to be compatible with Mark 5C in the future.

References

- [1] Gino Tuccari, INAF-IRA In: IVS 2004 General Meeting Proceedings, pp. 234–237.

DBBC2 Backend: Status and Development Plan

Gino Tuccari ¹, Walter Alef ², Alessandra Bertarini ³, Salvatore Buttaccio ¹,
Giovanni Comoretto ⁴, Dave Graham ², Alexander Neidhardt ⁵, Pier Raffaele Platania ¹,
Antonietta Russo ⁴, Alan Roy ², Michael Wunderlich ², Reinhard Zeitlhöfner ⁶,
Ying Xiang ⁷

¹) *Istituto di Radioastronomia – INAF*

²) *Max-Planck-Institut für Radioastronomie Bonn*

³) *Institut für Geodäsie und Geoinformation, Universität Bonn*

⁴) *Osservatorio di Arcetri – INAF*

⁵) *FESG München*

⁶) *BKG Wettzell*

⁷) *Shanghai Astronomical Observatory – CAS*

Contact author: Gino Tuccari, e-mail: g.tuccari@ira.inaf.it

Abstract

The DBBC2 system is in a mature phase now, and the deployment is continuing. A review of the backend is shown, and the new functionalities in development are reported.

1. Hardware

The DBBC2 hardware system is composed of a class of boards able to support different platforms and thus different system configurations. In the VLBI backend implementation, mainly two observing types are required: tunable configuration and fixed contiguous bands. The first is adopted to emulate the present Mark IV terminal and is required for both geodetic and astronomical observing modes. The second is for astronomical millimeter observations and the new coming VLBI2010 geodetic modes. Both modes are required in the same terminal to be used depending on the observation to be performed, so some efforts have been put into accomplishing these modes in a unique hardware architecture.

The interface between the receivers and the backend is included in the DBBC2. It is based on the Conditioning Module, with the possibility of selecting the Nyquist band on which to operate and the total power measurements. An automatic gain control allows the regulation of the signal levels to be transferred to the analog-to-digital conversion ADB boards. Two types of such sampling elements are available with an instantaneous band for VLBI of 512 or 1024 MHz. Additional possibilities are available up to an instantaneous 2048 MHz, described in the new hardware development section (Section 3).

The ADB1 board operates with a sampling 1024 MHz clock, for converting an input signal in the range 10–2200 MHz, while the ADB2 operates at 2048 MHz with an input signal up to 3500 MHz. The ADB2 is able to operate in ADB1 mode and, moreover, can adopt as piggy-back a FILA10G board, to transfer pure sampled data using optical fibers with a 10G Ethernet connection. The ADB2 board was widely tested and is ready to be inserted in the standard DBBC2 stack.

The processing unit Core2 board is also fully operative and represents the element adopted to generate the down-converted channels in both modes: tunable and fixed tuning. The board is compatible with ADB1 and ADB2 and supports a minimal equivalent of four Core1 functionality. The pcb has 40 equivalent layers, and all the connections for signal transfer are differential, twisted, and matched in delay and impedance between the pads of the dice and the pins of the bus connectors. A piggy-back element can be adopted for additional functionalities.

One Core2 board is able to emulate the complete functionality of four analogue BBCs, or to generate a fixed tuning version of fifteen 32-MHz-wide baseband channels, covering an input 512 MHz receiver band.

The CaT2 board (Clock and Timing) is able to generate a highly flexible number of synthesized sampling clock values (e.g., 2048 MHz, 1024 MHz), phase locked with an external 10 MHz. Low phase-noise and very small sensitivity to temperature are the main performance characteristics. The board is also producing 1PPS synchronization signals for all the ADB boards and the entire digital chain. Frequency selection is performed with the DBBC2 internal PC Set.

The FiLa10G can be used as piggy-back board of any ADB2 sampler, giving the possibility to transmit and receive in the same time a high data rate of 20 Gbps + 20 Gbps. The bidirectional functionality could be required for instance when an RFI mitigation is needed to be realized in a remote position with respect to the sampling and processing site. With the typical sampling frequency of 2048 MHz and the full 10-bit data representation, a double optical fiber set meets the full data handling requirement. Moreover, the board is equipped with two additional transceivers able to operate at 1-2-4 Gbps for slower connections.

2. Firmware

The DBBC2 VHDL firmware was completely rewritten in a platform-independent fashion. This was accomplished with a great reduction in complexity producing very compact and efficient code. Performance improvement guarantees a bit-by-bit identical output from a set of BBCs belonging to the same Core2 board, having of course the same tuning settings and input data. Still some debugging is under way to check the entire new code.

The fixed tuned (FT) configuration firmware is also available: it produces a set of 16 (15 usable) contiguous 32 MHz bands from a 512 MHz input range, in any of the Nyquist zones available from the ADB1/2 boards. This configuration is available for the VLBI2010 mode or for the millimeter VLBI network.

Firmware under development covers the following tasks: a) fully tunable 1 GHz input bandwidth, b) fully tunable 2 GHz input bandwidth, c) 1 GHz FT with 31 channels 32 MHz bandwidth, and d) 2 GHz FT with 63 channels 32 MHz bandwidth.

Additional firmware configurations are under development, including a multichannel spectrometer, the linear-to-circular (L2C) polarization digital conversion, and a polarimeter. In particular the L2C configuration was fully simulated and proved efficient. Now the adequate processing board (Core3, see in the new hardware development section) is expected for taking care of the necessary processing capability.

3. New Hardware Development

New hardware parts to be integrated in the system are under development. This covers the interfacing, input bandwidth, and processing capability.

The FILA10G board is the interface between the system and the Mark 5C recorder or the network. The main connections are two optical fibers operating each at a maximum rate of 10 Gbps. In VLBI standard this is limited by 8.192 Gbps, and for the present recording capability the limitation is 4 Gbps. The data rate is fully bidirectional and compliant with standard Ethernet networks, under UDP protocol. At present the development status sees the hardware defined and available with some prototypes, and the firmware development at a good stage: VLBI VDIF and Mark 5B modes are almost complete. Some communication experiments have been done with a Mark 5C recorder.

The 10G network FILA10G board is adopting optical fibers. In order to be connected with one or two Mark 5C recorders, which adopt the copper CX4 standard, it needs to be interfaced with a commercial 10G switch having both types of ports. As an alternative, a bi-directional interface was developed that can be used for such purpose. It is named GLAPPER to recall its functionality to be a transit between GLAss and coPPER.

In order to increase the instantaneous input bandwidth, an ADB3 Module has been defined. It is able to support 2048 MHz input bandwidth with a 2.048 GHz sampling clock. Nyquist input bands possible are 10–2048 MHz and 2048–3500 MHz. The main use of this module is with a fixed tuned bands configuration for a significant sensitivity improvement. Prototypes of the ADB3 Module are available and fully debugged.

The Core3 board is an evolution of the present Core2 processing board. It is mainly devoted to very high demanding processing capabilities. It is planned to be used as a digital preprocessor for L2C polarization conversion, for VLBI2010 FT configurations with 1 or 2 GHz input bandwidth, and in applications such as a spectrometer with a very high number of channels. The hardware has been fully defined, and the boards are expected before the end of 2010. Firmware applications are already simulated and ready to be debugged in the real board.

4. HAT-Lab

HAT-Lab is a spin-off company supported by INAF for the DBBC production. The company has agreements with IRA-Noto, where laboratories are placed for a part of the production, and MPI in Bonn where other phases of the production are realized. A certain number of operations are realized by external specialized companies to simplify and optimize the production of the complex boards. Assembly and testing is fully realized in HAT-Lab, IRA, and MPI.

At present eight systems have been deployed by IRA, and HAT-Lab is going to deliver eight additional systems. In the second half of 2010, the same number of units are expected to be produced. The production capability of HAT-Lab is around twelve systems per year, and production time is close to six months.

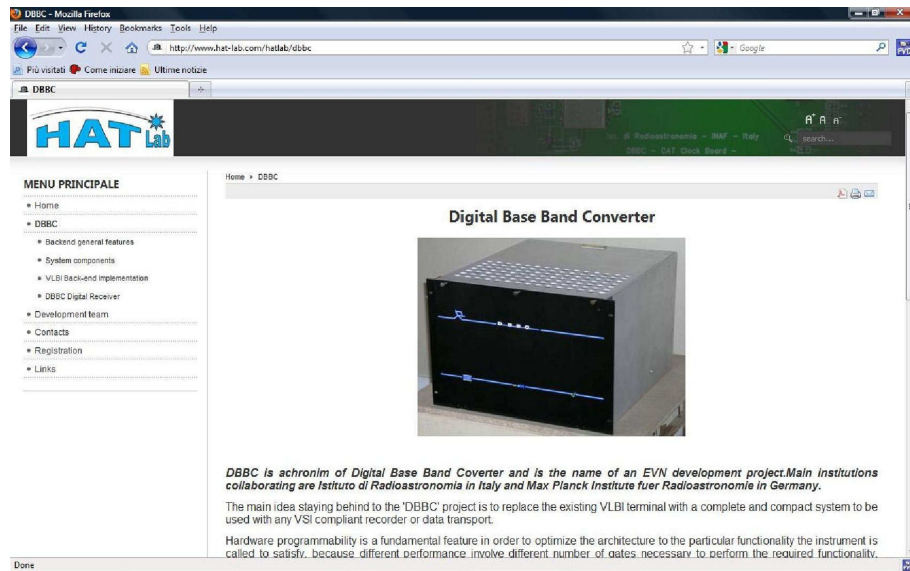


Figure 1. HAT-Lab Web site.

RDBE Development and Progress

A. Niell¹, M. Bark², C. Beaudoin¹, W. Brisken², H. Ben Frej², S. Doeleman¹,
S. Durand², M. Guerra², A. Hinton¹, M. Luce², R. McWhirter¹, K. Morris², G. Peck²,
M. Revnell², A. Rogers¹, J. Romney², C. Ruzsczyk¹, M. Taveniku³, R. Walker²,
A. Whitney¹

¹) *MIT Haystack Observatory*

²) *NRAO*

³) *XCube Communication, Inc.*

Contact author: A. Niell, e-mail: aniell@haystack.mit.edu

Abstract

A digital backend based on the ROACH board has been developed jointly by the National Radio Astronomy Observatory and MIT Haystack Observatory. The RDBE will have both Polyphase Filterbank and Digital Downconverter personalities. The initial configuration outputs sixteen 32-MHz channels, comprised of half the channels from the PFB processing of the two IF inputs, for use in the VLBI2010 geodetic system and in the VLBA sensitivity upgrade project. The output rate is 2×10^9 bits/second (1×10^9 bits/sec = 1 Gbps) over a 10 GigE connection to the Mark 5C with the data written in Mark 5B format on disk.

1. The RDBE Development

The need for increased accuracy and sensitivity in radio astronomy has led to the development of primarily digital systems for the complete backend. The first digital backend developed at Haystack Observatory, called the DBE1, was based on the CASPER iBOB. Data were output at a rate of 2 Gbps on VSI-H connections from each of two IF inputs, writing each to a Mark 5B+ for a total data rate of up to 4 Gbps. The digital signal processing utilized a polyphase filterbank (PFB) approach to provide sixteen channels of 32 MHz bandwidth from each IF. However, the size of the FPGA on the iBOB inhibited the addition of any other capabilities. At the same time, NRAO was seeking an optimal approach to a digital backend for its VLBA Sensitivity Upgrade project. Thus, a collaborative development was initiated, with the hardware design and construction led by NRAO and the software/firmware development led by Haystack. NRAO collaborated separately with the South African KAT project and the UC Berkeley CASPER Laboratory to develop the ROACH hardware platform for the new RDBE (ROACH Digital BackEnd).

Some of the achieved and planned features of the RDBE are:

- PFB channelization into sixteen 32-MHz channels from each 512 MHz IF:
 - each IF output to one Mark 5C (4 Gbps total output rate) (in development)
 - eight channels from each IF combined on one output (2 Gbps total rate) (complete)
 - selection of which eight channels are recorded from both IFs (the same eight) (complete)
- output over one or two 10 GigE Ethernet ports:
 - Mark 5B format (complete)

- VDIF format (in development)
- threshold adjustment to obtain proper state statistics for each 32 MHz channel (complete)
- adjustable input attenuator setting for level control to the samplers (complete)
- synchronous detection of the added power from a noise diode for system temperature measurement (in development)
- implementation of a digital down-converter personality (in development)
- phase cal signal extraction (planned)

2. The RDBE Structure

The basic components of the RDBE are the input Analog Level Control (ALC) board, samplers (iADC), ROACH board, and a synthesizer/timing board. The iADC was developed by the CASPER Laboratory, while the ALC and synthesizer board were developed by the NRAO-Socorro Electronics division. A schematic of the physical organization of the RDBE is indicated in Figure 1. The fully constructed RDBE is shown in Figure 2a.

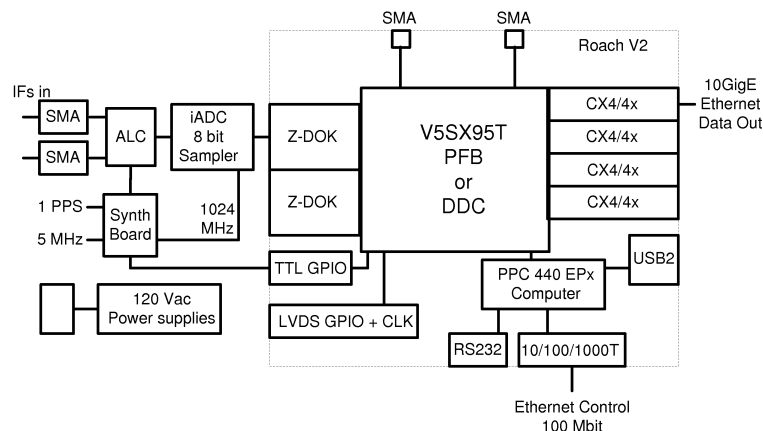


Figure 1. Layout of the RDBE.

A functional block diagram is shown in Figure 2b. The inputs are one or two 512 MHz data lines, a 1-pulse-per-second signal, and the 5 MHz reference frequency from which the 1024 MHz clock rate is synthesized. The digital signal processing of the RDBE is carried out in a XILINX SX95T-1 FPGA chip on the ROACH board, which is programmed in VHDL. Commands (which must follow VSI-S standards) and communications are received and transmitted over a 1 Gbps Ethernet to the Power PC on the ROACH board. The commands, defined in the DBE command set document (in preparation), are processed by the RDBE Application Server and passed to the FPGA via the Hardware Application Layer (HAL) over the external bus control (EBC) interface. This method was adopted to isolate the FPGA firmware from the PPC software applications, thus allowing different FPGA personalities (e.g., PFB or DDC) to be loaded without modifying the software. Having been processed by the PFB or DDC firmware in the FPGA, the data are output through one or two 10 GigE ports on CX4 connectors.

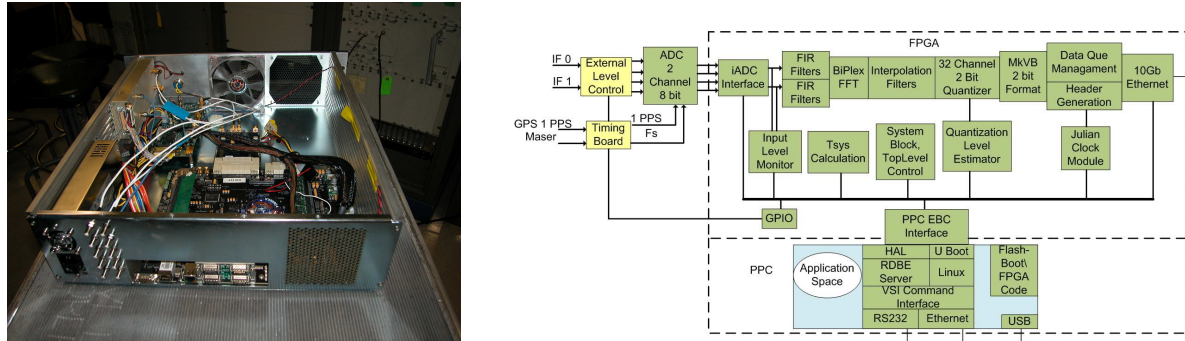


Figure 2. a) The RDBE. b) Functional diagram of the RDBE.

3. Test of PFB Functionality in Geodetic/VLBA Mode

The PFB capability of the RDBE has been demonstrated in several short-baseline VLBI tests, without many of the functions required for an operational system. For these tests, the signal from each IF was filtered to be in the second Nyquist zone of the iADC (512-1024 MHz) and thus appears as net lower sideband. The PFB FPGA personality (functionality) selected eight odd-numbered channels (1, 3, ..., 15) from both IFs and interspersed them in the output stream, thus producing sixteen 32-MHz channels. Output to the Mark 5C recorder was transmitted through one 10 GigE port at 2 Gbps in Mark 5B format. Data were recorded in parallel using existing systems to verify that the setups were correct in case the RDBE/Mark 5C failed to produce fringes.

Tests by Haystack used RDBEs at the 18-m Westford, MA, antenna and at the 5-m MV3 antenna in Greenbelt, MD. These two antennas are separated by approximately 800 km and have been used extensively for testing the VLBI2010 broadband proof-of-concept system ([1]). Both antennas used the broadband system, with a DBE1 and Mark 5B+ as output for one band, and an RDBE and Mark 5C processing and recording signals from the other. The data were correlated on the Mark IV correlator at Haystack. A single scan on the source 4C39.25 was used to validate the basic functionality of the RDBEs. The observations were made in the frequency band 8.6 to 9.1 GHz, and fringes were found within one microsecond of the expected clock difference as measured relative to GPS at each site

Tests by NRAO used RDBEs and Mark 5C units, installed in parallel with the existing equipment, in a “piggyback” mode during normal VLBA observations. Fringes from a continuum calibrator, 0823-223, were detected in the 8.6-9.1 GHz band between the Los Alamos and Pie Town stations, using the VLBA’s DiFX correlator. Single-dish spectra of 22-GHz water masers in Orion A were also obtained at Los Alamos.

4. Next Steps

Several important functions remain to be implemented before the PFB personality can be used operationally.

- Access to the 1 second marker within the FPGA for processing by the PPC. This will enable display of the actual time being encoded in the data output stream at the beginning of each second, as well as comparison with GPS time.

- Measurement of system noise temperature in each channel by synchronously detecting the power from a noise source, injected in the front end at a switch rate of 10 to 100 Hz.
- Support for other 2-Gbps channel subsets, in addition to the alternating channel scheme used in the tests.

In addition to the PFB personality implemented at Haystack, a digital down converter (DDC) personality is being developed at NRAO. It is expected that up to sixteen DDCs will be supported, with bandwidths between 0.0625 MHz and 128 MHz (with the number of DDCs times the bandwidth not exceeding 512 MHz). The DDCs will be tunable to any frequencies covered by the two IFs, and each DDC can be either upper or lower sideband.

Longer-term PFB data processing capability is also being planned.

- Extraction of phase cal tones
- Output in VDIF format [2]
- Output of each IF through a CX4 to a Mark 5C (4 Gbps total on two Mark 5Cs)
- Output of both IFs through one CX4 to one Mark 5C (4 Gbps total); this requires completion of so-called non-bank mode recording in the Mark 5C (spreading the input data across two modules).
- The addition of a second iADC to the ROACH board to accept a total of four 512 MHz IFs; production of a single 512 MHz channel from each for a total data rate of 8 Gbps out of two CX4s.

5. Acknowledgments

Work on this project at MIT Haystack Observatory was supported by NSF grant AST-0521233 and by NASA contract NNG10HP00C.

The National Radio Astronomy Observatory is a facility of the National Science Foundation operated under cooperative agreement by Associated Universities, Inc.

References

1. Niell, Arthur, and the Broadband Development Team, The NASA VLBI2010 Proof-of-Concept Demonstration and Future Plans, this volume.
2. Whitney, A, M. Kettenis, C. Phillips, M. Sekido, VLBI Data Interchange Format (VDIF), Feb 2010, http://vlbi.org/vdif/docs/WhitneyVDIF_paper_for_IVS_GM_Tasmania.pdf

The Digital Data Acquisition System for the Russian VLBI Network of New Generation

Leonid Fedotov, Eugeny Nosov, Sergey Grenkov, Dmitry Marshalov

Institute of Applied Astronomy of RAS

Contact author: Leonid Fedotov, e-mail: flv@ipa.rssi.ru

Abstract

The system consists of several identical channels of 1024 MHz bandwidth each. In each channel, the RF band is frequency-translated to the intermediate frequency range 1 – 2 GHz. Each channel consists of two parts: the digitizer and Mark 5C recorder. The digitizer is placed on the antenna close to the corresponding Low-Noise Amplifier output and consists of the analog frequency converter, ADC, and a device for digital processing of the signals using FPGA. In the digitizer the subdigitization on frequency of 2048 MHz is used. For producing narrow-band channels and to interface with existing data acquisition systems, the polyphase filtering with FPGA can be used. Digital signals are re-quantized to 2-bits in the FPGA and are transferred to an input of Mark 5C through a fiber line. The breadboard model of the digitizer is being tested, and the data acquisition system is being designed.

1. Digital Data Acquisition System

A new generation national VLBI network based on small radiotelescopes is primarily intended for the daily monitoring of UT. Therefore it is not necessary to ensure compatibility with the existing “Quasar-KVO” VLBI network. But it is necessary to provide extremely high sensitivity of each receiver channel in order to ensure access to the maximum number of reference radio sources. The most obvious way to increase the sensitivity is to expand the bandwidth of the receiver channels from 16 – 32 MHz to 0.5 – 1 GHz with a corresponding increase of the data stream record rate. In addition, it is also necessary to expand the bandwidth of the intermediate frequencies (IF) to improve the accuracy of the VLBI measurements.

A significant expansion of the DAS channels’ bandwidth up to 1 GHz and a corresponding increase of the output data rate up to 4 Gb/s per channel can be achieved by using analog-to-digital conversion and digital signal processing directly in the IF range. Modern analog-to-digital converters (ADCs) can digitize IF signals and avoid a signal transfer to baseband using analog methods. The sampling frequency of such ADCs is able to achieve a few GHz, the number of bits reaches up to 10, and the input bandwidth reaches up to 5 GHz [1], [2], [3].

The new generation digital DAS developed at Institute of Applied Astronomy consists of a 10-channel RF/IF downconverter and four identical digital signal processing (DSP) units (Figure 1). **The RF/IF downconverter** converts input signal spectra from a multi-band radio irradiator of the radiotelescope (*C*, *X*, *S* and *Ku* bands) to the IF range of 1–2 GHz. Eight of ten channels of the RF/IF downconverter can be tuned in the wide frequency range of 3–14 GHz. There is no downconversion in the other two channels intended for S-band, because it can be directly digitized by ADC; but the signal is amplified and filtered. The downconverter receives the signals of five bands (*S*, *C – low*, *C – high*, *X*, *Ku*) in two polarizations (two channels for each band) simultaneously. Each DSP unit can be connected to the outputs of the RF/IF downconverter through an IF switch.

The DSP unit is the basis of the DAS and contains the following devices (Figure 2):

- ADC,
- FPGA,
- Clock oscillator,
- Demultiplexer of the ADC output signal,
- Flash RAM to store FPGA firmware,
- Microcontroller,
- Optical transmitters.

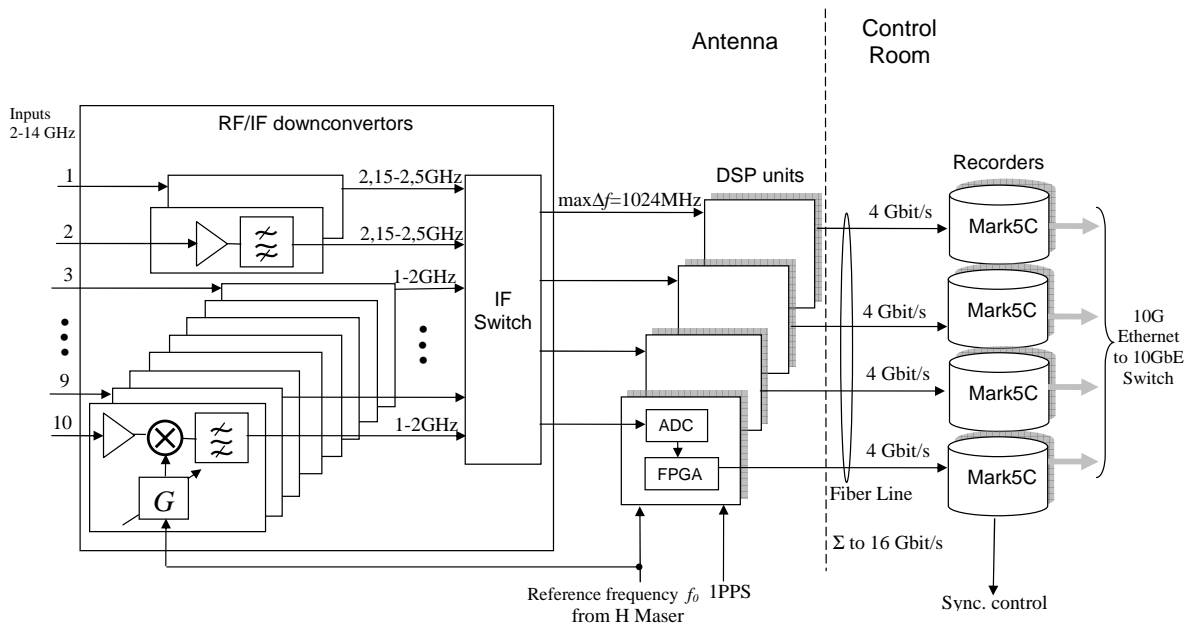


Figure 1. The Digital Data Acquisition System for the Russian VLBI-network of new generation.

It will be implemented as a single multilayer-printed circuit board (PCB).

The sampling rate of the ADC is 2048 MSamples/s. It corresponds to an IF bandwidth of 1024 MHz and a total output data stream rate of the ADC of about 20 Gb/s. It is necessary to decrease the sample arrival rate in order to transmit the stream into FPGA. This can be done by the demultiplexer at the ADC output. The demultiplexer 1 : 4 decreases the sample arrival rate to 512 MSamples/s. The use of the sampling frequency of 2048 MHz instead of 2000 MHz simplifies the coupling of the digital DAS with the existing data recording systems which usually use clock frequencies that are powers of 2 (e.g., 32 or 64 MHz in devices using VSI-H format [4]). Each DSP unit is synchronized by a hydrogen maser to ensure a long-term stability of the clock frequencies.

The FPGA performs the following operations: measurement of the rms level of the input signal, division of the fullband input signal into narrowband channels and converting it to the baseband (if necessary), calculation of the rms level of the narrowband channels, 2-bit quantization of the

output signals, generation of a test vector to check the transmission line and data recording system, formatting the output data in accordance with a data recording system interface, and sending them to the optical transmitters.

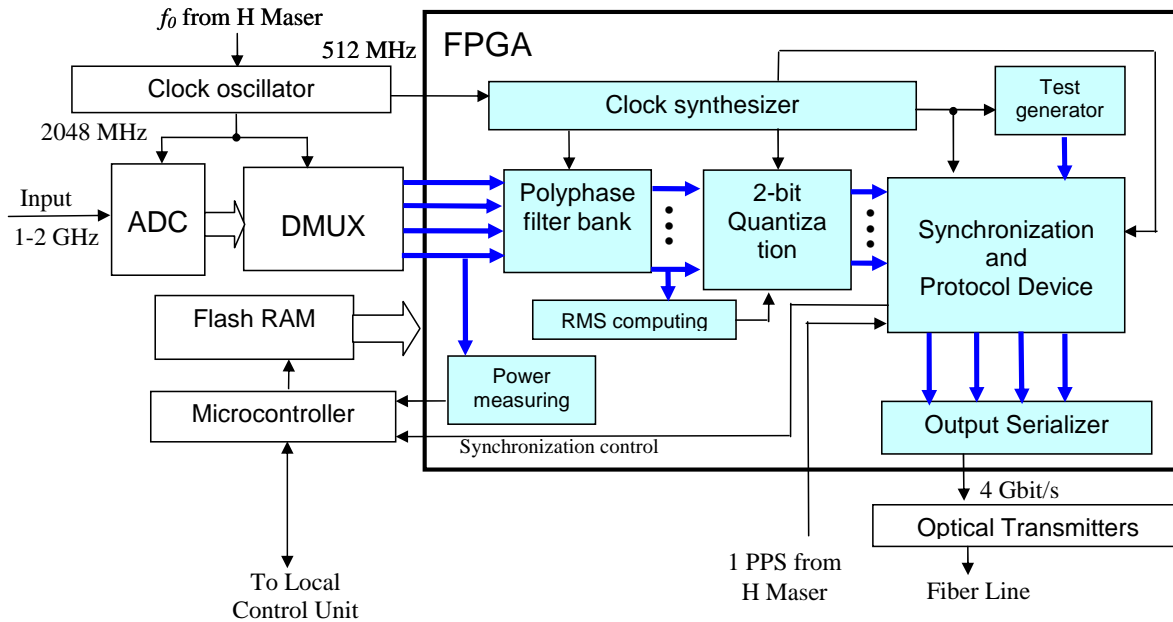


Figure 2. The DSP unit of the Digital Data Acquisition System.

The microcontroller provides the communication with the local control unit, execution of its commands, and loading of the appropriate firmware to the FPGA.

The previous DAS can be replaced by the DSP unit which is only one PCB. So the new digital DAS has lower weight and smaller size. That is why it can be mounted on the antenna. Output data streams are transmitted from the DAS to the data recording systems located in a control room.

The basic principles of the new generation DAS can be formulated as follows:

1. *The DAS should be a modular system consisting of identical RF/IF downconverter channels and DSP units with frequency bandwidth of 1024 MHz.*

The modular structure of the DAS is easily scalable and configurable for the required tasks.

2. *Using undersampling.*

Undersampling is a sampling technique that utilizes the aliasing signal caused by using a sampling frequency lower than the Nyquist frequency. In this technique the signal is sampled and simultaneously converted to low frequency [5], [6].

Undersampling allows the use of a sampling frequency of 2048 MHz to digitize IF signal of 1024 – 2048 MHz frequency range.

3. *Using a fiber-optical communication line for the transmission of signals from the antenna to the control room.*

As the DAS is located on the antenna, the signal is transmitted to the control room by a

fiber-optic line in digital form. It excludes any communication line influence on the signal.

4. Using an existing data recording system.

The DAS output data streams must be recorded with a data rate of 4 Gb/s per channel. This data rate is achievable by the Mark 5C recording system of Conduant Corp [7]. For each channel of the DAS, one Mark 5C is required.

5. Using a polyphase filter bank for dividing the fullband input signal into narrowband channels to work with previous DASs.

When the bandwidth of the DAS channels is 1024 MHz, the main processing operation is 2-bit quantizing of the input signal. No filtering is required in this case, which means that only a bit of computing resources of FPGA are used. There is an opportunity to carry out consistent observations by using the existing and digital DAS simultaneously. For this purpose the input 1024 MHz bandwidth of the digital DAS can be divided into narrowband channels.

The dividing into channels can be performed by a polyphase filter bank [6].

6. Supervision of the data streams.

The FPGA in each DSP unit measures the rms level of the input digital signal and the output channels. The measured levels are used for the calibration of the radio telescope, automatic setting of the optimal input signal level of the ADC, and determination of the quantizing threshold. Supervision of the amplitude-frequency characteristic, a phase calibration signal and an output 2-bit signal are distributed through each channel by the data recording system by making a short time trial recording just before an observation and analyzing it. The data recording system also verifies the transferred data for errors. The state of the equipment is written to the log-file in the local control unit during the observation and is then transmitted to the correlation center.

The DAS described above provides a flexible architecture consisting of identical channels. The new generation digital DAS allows a significant increase of the sensitivity of VLBI in comparison to the existing analog DAS. It gives the opportunity of using antennas of smaller diameter.

A prototype of the DSP unit (Figure 3) was made to check the basic principles. The prototype consists of evaluation boards of the following devices:

- 10-bit ADC (AT84AS008-EB),
- High-frequency demultiplexer 1:4 (AT84CS001-EB),
- FPGA XC5VFX70T (ML507),
- Optical transceiver AFCT-5710LZ.

The following tests have been made by using the prototype:

- Transmission of an internally generated test signal from ADC through demultiplexer to FPGA,
- Transfer of the test signal from one FPGA to another by fiber-optical line,
- Digitization of a signal from an external signal generator,
- Measuring of the input signal power.

The tests of the prototype provide the opportunity to implement the digital DAS with modern electronic components.

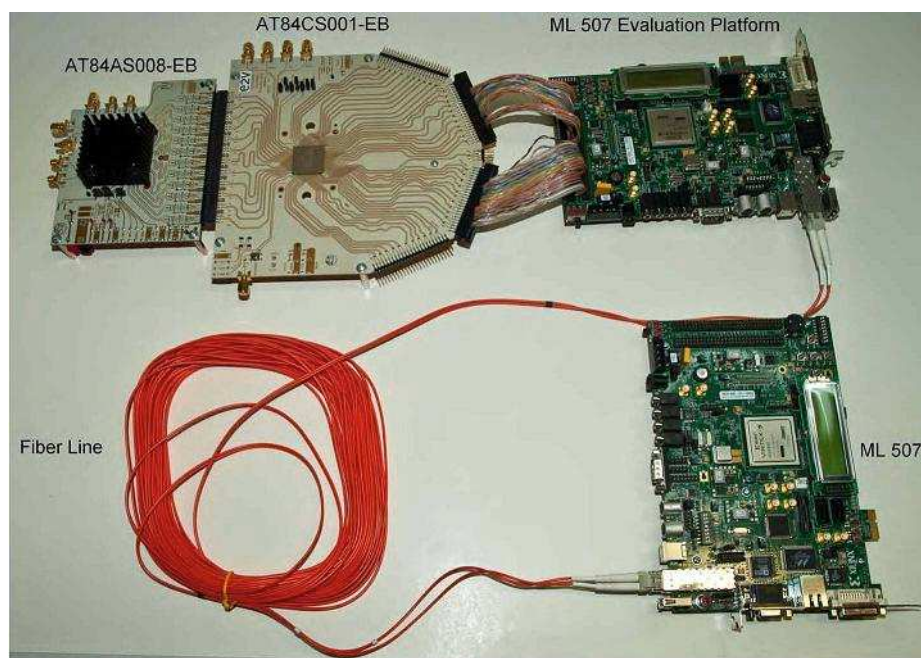


Figure 3. The prototype of the DSP unit of the Digital Data Acquisition System.

References

- [1] ADC081500 High Performance, Low Power, 8-Bit, 1,5 GSPS A/D Converter from Power Wise Family. www.national.com/pf/DC/ADC081500.html.
- [2] AT84AS008, EV10AS150A, EV10AQ190. www.e2v.com/products-and-services/specialist-semiconductors/broadband-data-converters/datasheets.
- [3] MAX109 8-bit, 2,2 Gbps ADC with Track/Hold Amplifier and 1:4 Demultiplexed LVDS Outputs. www.maxim-ic.com/quickview2.cfm/qv_pk/5391.
- [4] A. Whitney, VLBI Standard Hardware Interface Specification — VSI-H, 2002. www.haystack.mit.edu/tech/vlbi/vsi/docs/2002_12_12_vsi-h_draft_rev_1.1.pdf.
- [5] Yoshio Kunisawa, Study on a multiple signal receiver using undersampling scheme. Proceedings of the SDR 05 Technical Conference and Product Exposition.
- [6] Alexander B. Sergienko, Digital Signal Processing. St.-Petersburg: Piter, 2006.
- [7] Alan R. Whitney, The Mark 5 VLBI Data System. Proceedings of the 18th VLBI for Geodesy and Astrometry Working Meeting, 12–13 April 2007, Vienna, P. 33–38.

First Phase Development of Korea-Japan Joint VLBI Correlator and Its Current Progress

Se-Jin Oh ¹, Duk-Gyoo Roh ¹, Jae-Hwan Yeom ¹, Hideyuki Kobayashi ²,
Noriyuki Kawaguchi ²

¹) *KVN, Korea Astronomy and Space Science Institute*

²) *VERA, National Astronomical Observatory of Japan*

Contact author: Se-Jin Oh, e-mail: sjoh@kasi.re.kr

Abstract

The first phase of the Korea-Japan Joint VLBI Correlator (KJJVC) development has been completed and installed to correlate the observed data from KVN (Korean VLBI Network) and VERA (VLBI Exploration of Radio Astrometry) in October 2009. KJJVC is able to process 16 stations, a maximum of 8 Gbps/station, and 8,192 output channels for VLBI data. The system configuration, the experimental results, and future plans are introduced in this paper.

1. Introduction

Recently, it has been suggested to continue the research in close cooperation with East-Asian region research group using the VLBI network. Especially in the case of Korea and Japan, a Memorandum of Understanding (MOU) has been signed between Korea Astronomy and Space Science Institute (KASI) and National Astronomical Observatory of Japan (NAOJ) to build a Korea-Japan Joint VLBI Network (KJJVN) and to perform joint observation research using the Korean VLBI Network (KVN) and the VLBI Exploration of Radio Astrometry (VERA). KVN has three stations with 21-m diameter antennas and has been operating at 22 and 43 GHz since 2008. VERA has four stations with 20-m diameter antennas and has been operating at 2, 8, 22, and 43 GHz since 2002. KVN plans to extend the observation frequency to 86 and 129 GHz by 2011 [1]. Including VSOP-2 after 2012, the East-Asian VLBI Network (EAVN) [2] will obtain the effectiveness of a ground-based 6,000 km diameter VLBI radio telescope. To process the observation data of EAVN, the need for a new correlator has been strongly considered. The new correlator development project for KVN was begun in 2004. The VERA also needs to develop a substitute correlator for the Mitaka FX correlator as a back-up. Therefore, a MOU was signed between KVN and VERA in 2005 to jointly develop a new correlator and to extend the number of stations of the EAVN. The Korea-Japan Joint VLBI Correlator (KJJVC) development project was started in 2006.

In this paper, the specification and technical design of each component will be introduced briefly. The paper is organized as follows: In Section 2, we briefly introduce the East-Asian VLBI Network. In Section 3, each component of KJJVC is introduced. Finally, the current progress and future plans are summarized in Section 4.

2. East-Asian VLBI Network

Radio interferometers get good quality observation data in proportion to the square of the number of stations observing at the same time. So it is better that Korea and Japan cooperate rather than independently operate in order to get good science research.

KVN, which has been operated by KASI since 2008, consists of three radio telescopes with 21-m diameter dishes and baseline lengths of about 500 km, which is half the size of the Korean Peninsula. The KVN will employ a unique multi-frequency band receiver system which is able to achieve simultaneous observations at up to four frequencies (22, 43, 86, and 129 GHz). The phase of a source at 22 GHz can be used to calibrate the phase of the same source at higher frequency bands. To do this, the KVN Data Acquisition System (DAS) [3] was developed and installed at each site for measuring simultaneously four frequencies.

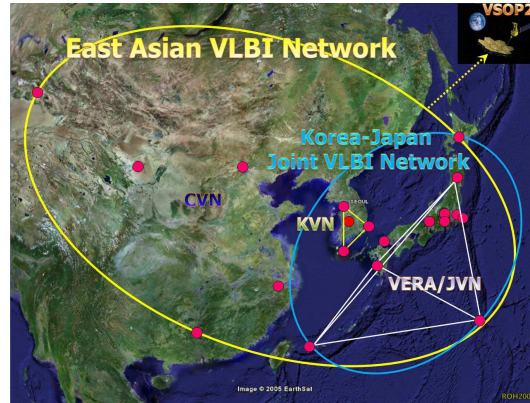


Figure 1. East-Asian VLBI Network with KVN, VERA/JVN, KJJVN, and CVN including VSOP-2.

In the case of Japan, VERA is also operated by using a unique dual beam system at four stations of NAOJ since 2002. VERA plans to improve the DAS in order to be able to process at maximum 8 Gbps for LHCP and RHCP observation simultaneously including the 86 GHz frequency band. As shown in Figure 1, the EAVN, which is based on the KJJVN in connection with the Chinese VLBI Network (CVN), will be realized in 2011. The next generation space VLBI satellite (VSOP-2) will be launched after 2012, so it will be a huge size radio telescope of 36,000 km. It is necessary to build a correlation Data Center for providing large capacity correlation, as 16 stations will be operated simultaneously according to the new VLBI network expansion plan.

3. Korea-Japan Joint VLBI Correlator

Figure 2 (a) is the conceptual configuration of KJJVC. There are several VLBI data playback systems which will be used in our combined VLBI network, such as Mark 5B, VERA2000, K-5/OCTA DISK and some kind of optical fiber which will be introduced in the near future. Some of them have the VSI-H compatible interface, but others use a different interface for data transmission. Furthermore they have their own maximum data recording/play back rates, respectively. To absorb all of these differences and in homogeneity among these existing VLBI data playback systems, the Raw VLBI Data Buffer (RVDB) was introduced, which is in fact a big data server with many large RAID disks and several kinds of VLBI data interfaces. The VLBI Correlation Subsystem (VCS) will receive the VLBI data from the RVDB system, will calculate the correlation between every possible pair of data inputs with proper control parameters given from the correlator control and operation computer, and then will dump the correlation results into the data archive system. The data archive system is also a kind of data server, which is used to capture the correlated data

output from the VCS, to save them in a structured file system. Finally there is also the correlator control and operation software for the overall system. KJJVC development is a joint project in close collaboration with KASI and NAOJ based on the MOU in 2005. NAOJ is responsible for the VERA2000 and other playback systems and RVDB development. KASI is responsible for the Mark 5B, VCS, and data archive system development. The control and operation software development is done jointly by KASI and NAOJ.

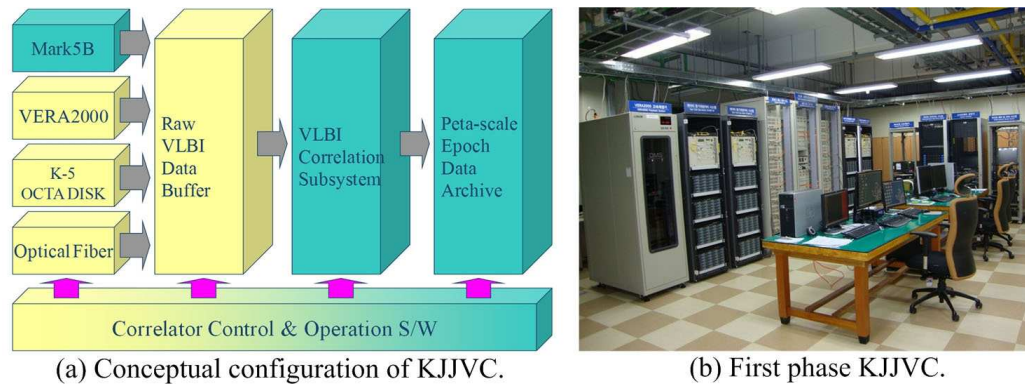


Figure 2. Conceptual configuration of KJJVC and the first phase implementation of KJJVC.

3.1. Playback System

KVN is now using the Mark 5B system [4] for recording and playing back the observed data. KASI participated in Mark 5B development with Haystack Observatory as a member of an international consortium. It can support the VSI compatible and RAID-based HDD storage system. Recording and playback speed is 1 Gbps. VERA is now extensively using the DIR2000 system for recording and playback with 1 Gbps. Recently the manufacturer of DIR2000 discontinued the production, so NAOJ developed a new playback system called VERA2000, which is a version of the DIR1000H system for playback only.

3.2. RVDB System

The RVDB system [5], which is developed by NAOJ, consists of a Data Input Output (DIO), a 10GbE switch, and a Disk Data Buffer (DDB). It is able to record the data with a maximum speed of 2 Gbps and to play back the data to the correlator with a nominal speed of 2 Gbps. So, RVDB has 2-Gbps recorder and playback functions. As shown in Figure 2 (a), KJJVC uses different types of playback systems. So, the purpose of the RVDB system is to adjust the data format, to easily synchronize the data during playback, and to maintain the buffering between recorder speed and correlation speed.

3.3. VLBI Correlation Subsystem

The main specifications of the VCS are described in Table 1. The VCS has the capability of processing a total of 120 cross-correlations and 16 auto-correlations intended for a maximum of 16 stations and 8 Gbps (4-streams \times 1 Gbps/2-bit/64 MHz clock) input data rate per station.

The correlation architecture is FX-based, and it will use the variable length of FFT (Fast Fourier Transform) to maintain the 0.05 km/sec velocity resolution at 22 GHz. The maximum delay rate (maximum baseline velocity) is 7.5 km/sec, and the maximum fringe tracking is 1.075 kHz. The number of frequency channels per correlation output is 8,192.

Table 1. Specifications of the VCS.

Items	Contents
# of stations	16
# of inputs/station	Max. 4 inputs
Max. # of correlations/Input	120 Cross + 16 Auto
Observation frequency	(VSOP-2) 45 GHz, 130/86/43/22 GHz
Largest baseline length	36,000 km(0.12 sec)
Max. data output rate	1.4 GBytes/sec
Digitization for each input	1 Gbps by 2-bit/sample
Quantization levels	4 levels as 00 01 10 11
Interface	VSI-H
Input data rate	2 Gbps/1 Gbps
Architecture	FX type, with FPGA and DSP chips
FFT points	256k/128k/64k/32k/16k/8k Adjustable
Word length in FFT	16 + 16-bit
Integration period	25.6 msec - 10.24 sec
Frequency binning	1-256 channels bin (powers of 2)
Correlation output data interface	10 Gbit Ethernet

3.4. Data Archive System

The basic architecture is infiniband. For KVN and KJJVN, the first phase of data archive system with about 100 TB capacity was implemented. It has four 10-Gbit-Ethernet input ports to connect with VCS output, and one 10-GbE-Ethernet port is connected to the data file system to share the disk. We plan to increase the system capacity corresponding to the EAVN including VSOP-2. The CODA file system [6] will be used in the data archive system, which is a modified Mitaka FX correlator file system. A new version of the CODA file system is expected to be completed in September 2010.

4. Current Progress and Future Plans

The first phase of the KJJVC hardware development has been completed, and all of the components were installed in October 2009. Field performance tests of the correlator hardware were successfully completed using VERA observation data which had already been verified with the Mitaka FX correlator. Then a test correlation experiment was conducted using KVN observation data at 22 GHz of the W49N spectral-line source between the KVN stations Yonsei and Ulsan. The correlation result is shown in Figure 3 as real and imaginary spectrum shape, phase, and

cross-spectrum. This result is just correlation spectrum without any other data processing such as global fringe search. The correlation post-processing software for KJJVC, including the CODA file system and the ability to perform a global fringe search, is now being developed jointly by KASI and NAOJ through 2010. After that we will employ the KJJVC operationally starting in 2011.

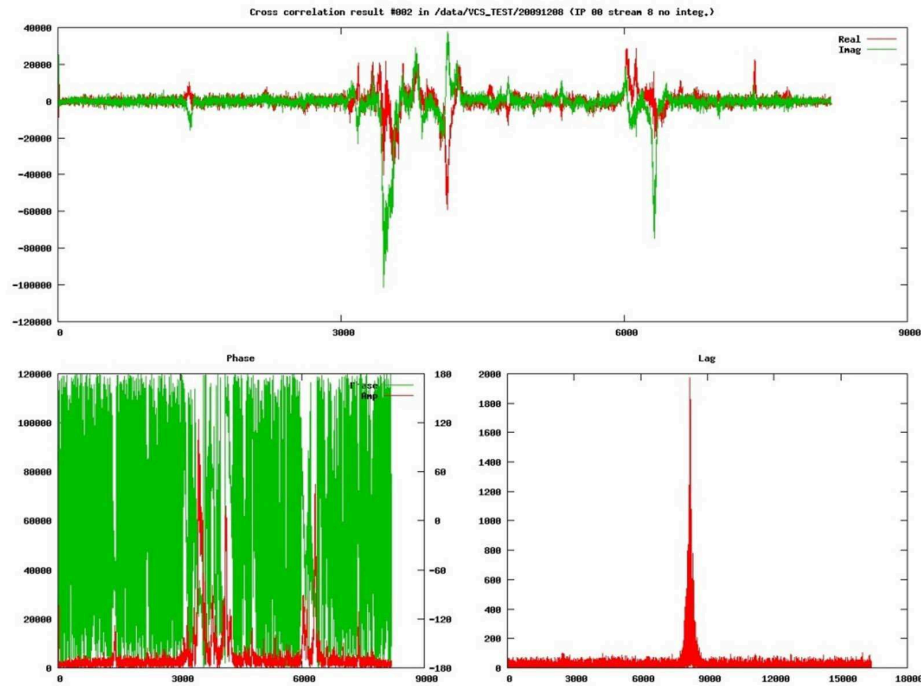


Figure 3. Spectral-line correlation result (cross spectrum, phase, lag) for W49N of a 22 GHz observation on the KVN baseline Yonsei to Ulsan.

References

- [1] Minh, Y. C., H. -G. Kim, S. -T. Han, D. -G. Roh, Present Status of the KVN Construction Project, In: International VLBI Service for Geodesy and Astrometry 2004 General Meeting Proceedings, NASA/CP-2004-212255, 156–160, 2004.
- [2] Kobayashi, H., Status and Future Plan of East Asia VLBI Network, In: 2010 East Asia VLBI Workshop Abstract Book, 1, 2009.
- [3] Roh, D. -G., K. -D. Kim, S. -J. Oh, H. -S. Chung, H. -K. Choi, A Design of Data Acquisition System for Korean VLBI Network, In: International VLBI Service for Geodesy and Astrometry 2004 General Meeting Proceedings, NASA/CP-2004-212255, 248–252, 2004.
- [4] Whitney, A. R., Mark 5 Disk-Based Gbps VLBI Data System, In: New Technologies in VLBI, ASP Conference Series, 306, Y. C. Minh (eds.) (San Francisco: ASP), 123–133, 2003.
- [5] Oyama, T., Y. Kono, T. Hara, N. Kawaguchi, The Development and Performance of a New 4 Gbps Disk Recorder and e-VLBI Systems Using a 10 GbE Network, In: International VLBI Service for Geodesy and Astrometry 2008 General Meeting Abstract Book, 68, 2008.
- [6] Kan-ya, Y., CODA I/O Library, Coda version 0.5 Manual, 2006.

Development of an e-VLBI Data Transport Software Suite with VDIF

Mamoru Sekido¹, Kazuhiro Takefuji¹, Moritaka Kimura¹, Thomas Hobiger¹,
Kensuke Kokado², Kentarou Nozawa³, Shinobu Kurihara², Takuya Shinno⁴,
Fujinobu Takahashi⁴

¹) *National Institute of Information and Communications Technology*

²) *Geospatial Information Authority of Japan*

³) *Advanced Engineering Services Co.,Ltd.*

⁴) *Electronic and Computer Engineering, Faculty of Engineering, Yokohama National University*

Contact author: Mamoru Sekido, e-mail: sekido@nict.go.jp

Abstract

We have developed a software library (KVTP-lib) for VLBI data transmission over the network with the VDIF (VLBI Data Interchange Format), which is the newly proposed standard VLBI data format designed for electronic data transfer over the network. The software package keeps the application layer (VDIF frame) and the transmission layer separate, so that each layer can be developed efficiently. The real-time VLBI data transmission tool ‘sudp-send’ is an application tool based on the KVTP-lib library. ‘sudp-send’ captures the VLBI data stream from the VSI-H interface with the K5/VSI PC-board and writes the data to file in standard Linux file format or transmits it to the network using the ‘simple-UDP’ (SUDP) protocol. Another tool, ‘sudp-recv’, receives the data stream from the network and writes the data to file in a specific VLBI format (K5/VSSP, VDIF, or Mark 5B). This software system has been implemented on the Wettzell–Tsukuba baseline; evaluation before operational employment is under way.

1. Introduction and Motivations

Progress in computer technology and high-speed networks have changed VLBI to so-called e-VLBI, which brings a number of advantages to the VLBI community. Remarkable benefits are not only quick transportation of VLBI data from observatory to data processing center via high-speed networks, but also the flexibility of data processing with software on off-the-shelf computers. One of the changes brought by e-VLBI is the software correlator, which is now being used in regular operation in place of traditional hardware correlators. Its advantages include easy maintenance and low cost for upgrading.

Another important benefit of e-VLBI is the relative ease of achieving compatibility between VLBI hardware developed by several leading institutes. The major VLBI recording and processing systems are the Mark III/IV/5 system (e.g., [1]) developed by MIT Haystack Observatory and NRAO in USA, the S2/LBA system (e.g., [2]) developed by Canadian and Australian institutes, and the K3/4/5 system (e.g., [3]) developed by NICT and NAOJ. Data compatibility and conversion issues have been drastically reduced because of the flexibility of the software-based recording system and data processing of e-VLBI.

The need for a standard data format for VLBI was discussed at the 7th International e-VLBI Workshop held in Shanghai in 2008. The VLBI Data Interchange Format (VDIF) [4] was ratified at the next international e-VLBI workshop held in Madrid in 2009. The VDIF is suitably designed

for network data transmission. We anticipate that VLBI data will be exchanged in VDIF form over the network and that differences of data interfaces and formats will be absorbed at either end (sender or receiver) of the data stream. For instance, Mark 5 data may be transferred in VDIF format over the network and will be saved or processed in K5 data format at the receiving end. Based on this notion, we have developed a software library (KVTP-lib) for data handling in the standard C++ language. This software package is designed as an object-oriented class library with an emphasis on separating the transmission and application layers. Details of the KVTP-lib will be discussed in Section 3. The software tools ‘sudp-send’ and ‘sudp-recv’ have been developed as application software with the KVTP-lib for capturing VSI-H data of a Mark 5 DAS, transferring it over the network, and saving it in K5/VSSP32 format. Some results of evaluating these tools with the Intensive UT1 measurement sessions are discussed in Section 4.

2. Brief Introduction of VLBI Data Interchange Format (VDIF)

The VDIF [4, 5], which is the new standard VLBI data format designed for exchanging data over computer-based media, has a frame structure with the minimum unit composed of a 32-byte header part and a flexible-length data part. Each frame is supposed to be conveyed via packets of network protocol.

The header contains information in order to uniquely identify the epoch of the data samples. Thus it is designed to be tolerant of missing or duplicate frames. The length of the data part is an adjustable parameter; thus the capacity ratio of header part to data part can be reduced when writing a file to recording media. The VDIF is designed to be independent of the lower level transport protocol. This is an important aspect of VDIF usage. Examples of VDIF are indicated in Figure 1. Please refer to VDIF specification [5] for more detail.

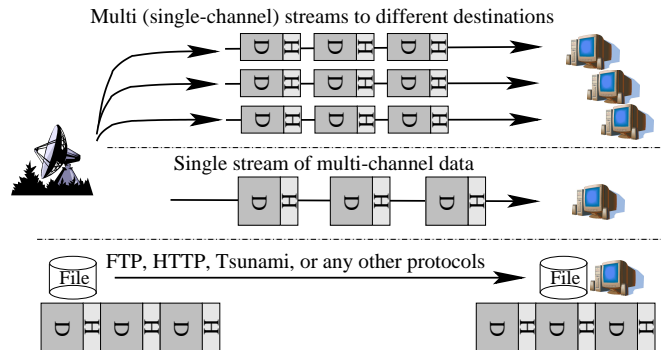


Figure 1. Examples of VDIF usage. ‘H’ and ‘D’ mean header and data parts, respectively. Data transport from data source to destination can be performed flexibly by real-time multiple single-channel streams, a single multiple-channel stream, or off-line using recording media.

3. VDIF/SUDP and C++ Class Library KVTP-lib

3.1. VDIF/SUDP

We have developed a software suite for VLBI data transport as an implementation of the VDIF. Lossless VLBI data transport via file on recording media or via TCP/IP over the network are included in the scope of VDIF; however, TCP/IP is not suitable for high data-rate transmission over long distance. Alternatively, we have introduced a simple transmission protocol, which we named SUDP, on top of the UDP/IP protocol stack. The format of the SUDP header of eight bytes size is indicated in the left panel of Figure 2. The idea of a sequential number has been used

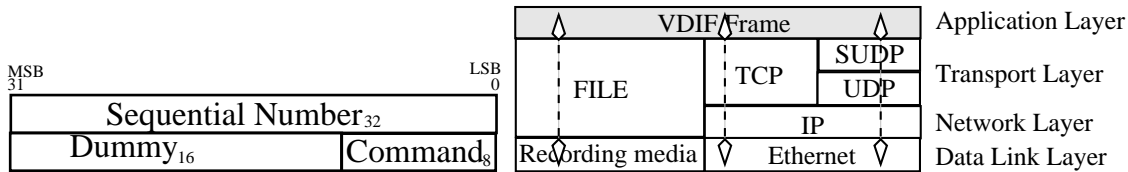


Figure 2. The left panel shows the header format of the simple-UDP (SUDP) protocol. ‘Sequential number’ is incremented for every packet. ‘Command’ may be used for ‘test packet’ or other functions for multi-streaming. The right panel shows the protocol stack model for VDIF and SUDP implemented in the KVTP-lib package.

in real-time VLBI experiments by JIVE/EVN. This header format was originally proposed by R. Hughes-Jones at the 8th International e-VLBI Workshop in 2009. The SUDP header belongs to the transport layer for monitoring the transmission rate, loss, and duplication of packets. Thus it is attached at the sender and stripped at the receiver. The SUDP does not include re-transmission mechanisms for lost packets. Since real-time VLBI data transfer is used and available only when the network has sufficient capacity for the VLBI observation data rate, this simple mechanism works fine for up to 512 Mbps when the network capacity is more than 600 Mbps. If a standard MTU (Maximum Transmission Unit) size of 1500 bytes and a packet size of 1464 bytes is used, the overhead cost including UDP/IP, SUDP, and VDIF header is 5.2%. For instance, a network capacity of 269.2 Mbps is needed for a data rate of 256 Mbps and a 538.5 Mbps capacity for a 512 Mbps rate. In our experience with international data transfers between European stations (Onsala, Metsähovi, Wettzell, and JIVE) and Japanese stations (Kashima and Tsukuba), sufficient network capacity was always available courtesy of the research networks (JGN2plus, SINET3, Internet2, and GEANT3) between these stations.

3.2. C++ Class Library KVTP-lib for Real-time Data Transmission/Conversion

The class library KVTP-lib (VTP library of Kashima) has been developed for a flexible coding of data conversion/transmission tools. It has been coded in C++ adhering to the object-oriented design features of ‘Encapsulation’, ‘Abstraction’, ‘Inheritance’, and ‘Polymorphism’. ‘Abstraction’ and ‘Polymorphism’ are techniques for reducing duplicated coding and providing common interfaces to the modules. Since any VLBI data formats (e.g., Mark 5B, K5, LBA) have essentially the same frame structure with repeating header and data parts, they are suitable for object-oriented coding via classes inherited from the same common class. By using these software features common interface functions are defined, and it is easy to switch between these different VLBI data formats. In the same way, data transport classes of TCP/IP, SUDP/UDP/IP, and FILE are easily exchanged using this library. The KVTP-lib uses a partly modified version of ‘vtp-1.0.H’ [6], which is a C++ class library originally developed by D. Lapsley at MIT Haystack Observatory. The application software ‘sudp-send’ and ‘sudp-recv’ have been developed for real-time VLBI data transfer over intercontinental baselines using KVTP-lib. ‘sudp-send’ captures the VLBI data stream from a VSI-H interface with a K5/VSI device and sends it to the network with VDIF/SUDP. ‘sudp-recv’ receives the data stream of VDIF/SUDP from the network and saves it in files in K5/VSSP32, Mark 5B, or VDIF format. Figure 3 gives an overview of the usage of KVTP-lib applications.

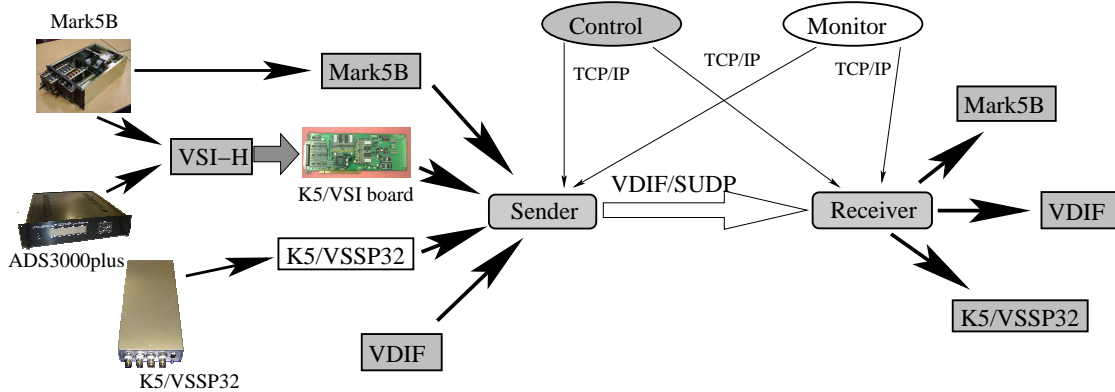


Figure 3. Overview of data transport tools ‘sudp-send’ and ‘sudp-recv’ based on the C++ class library KVTP-lib. The functions painted in gray are ready for use, whereas the ones in white are not yet implemented.

4. Application to Rapid UT1 Measurement

The real-time data transmission/conversion tools are being tested in the INT2 experiments on the Wettzell–Tsukuba baseline for rapid UT1 measurement. A Mark 5B DAS system with a VSI-H interface is continuously connected to a K5/VSI board of the server PC located at Wettzell station (Germany). During the VLBI observation, the VSI-H data stream of 16 channels at a total data rate of 256 Mbps is continuously transmitted to Tsukuba station (Japan) in VDIF format over the network in real-time. The receiver software at Tsukuba station captures the VDIF data stream from the network and saves it to four data files in K5/VSSP32 format on the fly.

Comparisons between the online data transmission and the conventional scheme, where locally recorded data in Mark IV format are transferred offline, have been performed using one month of Intensive-2 experiments. The comparison results of average SNR and residuals of the UT1 analysis by CALC/SOLVE are listed in Table 1. Online transmission does not show significant differences to transmission offline. In the online case, several seconds of longer recording duration is used at the receiver side of the transmission for safety reasons. This may be the reason for some better SNR and residual values than the offline case.

Table 1. Comparison between online and offline data transport of Intensive-2 (INT2) experiments on the Wettzell–Tsukuba baseline. ‘Online’ (On) means real-time data transmission, and ‘Offline’ (Off) means conventional sequence of local recording, offline transmission with Tsunami-UDP, and format conversion from Mark IV to K5/VSSP32.

Exp. Code	Avg. SNR _{on} /SNR _{off}		Residual On/Off (ps)
	X-band	S-band	
K10093	1.00	1.00	0.99
K10094	1.02	1.02	1.08
K10100	1.03	1.02	1.00
K10101	0.95	0.94	0.90
K10107	1.03	1.02	1.34
K10108	0.98	0.97	1.03
K10114	1.01	1.02	1.27
K10115	0.93	0.93	0.97
K10122	0.98	0.98	0.72

5. Summary and Prospects

The software suite of C++ class library ‘KVTP-lib’ has been developed as an implementation of VDIF. A simple-UDP protocol was introduced for real-time data transmission. The VLBI data formats of K5/VSSP32, Mark 5B, and VDIF are supported at present. Since the KVTP-lib is based on an object-oriented class design, it is useful for creating application software tools for data transmission and conversion. We have written tools for K5/VSI data capture, for real-time data transmission in VDIF/SUDP, and for writing K5/VSSP32 data for the rapid UT1 measurement on the Wettzell–Tsukuba baseline.

The SUDP protocol is our own version of VTP. An international standardization of VTP is currently under discussion. Even if a new protocol is defined as standard, it can be implemented in the KVTP-lib via small modifications. The source code package of KVTP-lib is available on the Web ¹ under the GPL license.

6. Acknowledgments

The authors thank Gerhard Kronschnabl for supporting our project by providing the Mark-5-VSI environment at Wettzell station. We appreciate Dan Smythe for kindly providing Mark 5/VSI board information. Finally we express special thanks to David Lapsley for his vtp-1.0.H software, which was the first proposal of a VLBI data transport protocol. His C++ class library was quite educative and useful for KVTP-lib. The current version of KVTP-lib works with our modified version vtp-1.0Hm.

References

- [1] Whitney, A. R., R. Cappallo, W. Aldrich, B. Anderson, A. Bos, J. Casse, J. Goodman, S. Parsley, S. Pogrebenko, R. Schilizzi, and S. Smythe, Mark IV VLBI correlator: Architecture and algorithms, *Radio Sci.*, 39, 1007W, 2004.
- [2] Carlson, B. R., P. E. Dewdney, T. A. Burgess, R. V. Casorso, W. T. Petrachenko, and W. H. Cannon, The S2 VLBI Correlator: A Correlator for Space VLBI and Geodetic Signal Processing, *Pub. Astr. Soc. Pacific*, 111, 1025-1047, 1999.
- [3] Kondo, T., Y. Koyama, J. Nakajima, M. Sekido, and H. Osaki, Internet VLBI system based on the PC-VSSP (IP-VLBI) board, *New Technologies in VLBI, ASP Conference Series*. 306, 205-216, 2003.
- [4] Whitney, A., VLBI Data Interchange Format (VDIF), *Proceedings of the 8th International e-VLBI Workshop, PoS(EXPReS09)042*, 2009.
- [5] Kettenis, M., C. Phillips, M. Sekido, and A. Whitney, VLBI Data Interchange Format (VDIF) Specification, <http://www.vlbi.org/vsi/index.html>, 2008.
- [6] Lapsley, D., and A. Whitney, VSI-E Software Suite, *Proceedings of 7th European VLBI Network Symposium on VLBI Scientific Research and Technology*, 291-292, 2004.

¹http://milkyway.sci.kagoshima-u.ac.jp/groups/vcon.lib/wiki/7cac1/Data_Transmission.html

Cryogenic Integration of the 2–14 GHz Eleven Feed in a Wideband Receiver for VLBI2010

Miroslav Pantaleev¹, Jian Jang², Yogesh Karadikar⁴, Leif Helldner¹, Benjamin Klein³,
Rüdiger Haas¹, Ashraf Zaman², Mojtaba Zamani², Per-Simon Kildal²

¹) *Onsala Space Observatory*

²) *Chalmers University of Technology, Dept. of Signals and Systems*

³) *Hartebeesthoek Radio Astronomy Observatory (HartRAO)*

⁴) *Chalmers University of Technology, Dept. of Microtechnology and Nanoscience*

Contact author: Miroslav Pantaleev, e-mail: miroslav.pantaleev@chalmers.se

Abstract

The next generation VLBI systems require the design of a wideband receiver covering the 2–14 GHz range, necessitating a wideband feed. Presented here are the 2009 development of a cryogenic 2–14 GHz Eleven feed for reflector radio telescope antennas, including its integration into a cryogenic receiver. The Eleven feed is designed for dual linear polarization and consists of four log-periodic folded dipole arrays. Each pair of arrays is fed by a differential two-wire transmission line connected either to balun or a differential LNA. The present configuration has been measured in many configurations, at various independent labs — corresponding simulations have been done. The results show (across the band) a high polarization efficiency for the feed, with a nearly constant beam width, a reflection coefficient below –10dB, and a constant phase center. Electrical parameters under cryogenic conditions and measured receiver noise temperatures are presented.

1. Introduction

New systems, such as the Square Kilometre Array (SKA) and VLBI2010, are planned to continuously cover a very wide frequency range, with very low noise performance and high receiving efficiency [1, 2, 3]. For example the SKA is planned to have anywhere between 1500 and 3000 reflectors, equipped with wideband, low-noise receivers (1–10 GHz, 35 K and an A/T of $5000 \text{ m}^2/\text{K}$ [4]).

The goal of VLBI2010 is highest-precision geodetic and astrometric results, defined as precision of 1 mm in the space domain, which corresponds to only 3 picoseconds in the time domain and can be achieved with extending the bandwidth to about 5:1. Furthermore, the technical realization of a VLBI observing system introduces another characterizing quantity: the signal-to-noise-ratio (SNR), which finally decides whether or not an observation is successful out of the correlation process. Therefore, the implementation of receivers with lower system noise temperature and feeds with higher efficiency is desirable—to allow shorter scans per unit time and better geometrical solutions. Current receivers for geodetic VLBI operate in an octave band, using optimized corrugated horn feeds, with cryo-cooled LNAs, covering a few hundred MHz in S and X band. In some cases, separate horns are used to switch between different bands, and a manual replacement of waveguides is required. Newly developed feeds like log-periodic antennas developed for the Alan Telescope Array (ATA) [5], the ETS Lindgren quadridge horn [6], and the Quasi-Self-Complimentary antenna [7], although covering enough broadband, do not meet all the required

specifications (e.g., polarization purity, beam width, and phase center location). In contrast to these, the Eleven feed shows good polarization characteristics and has a constant beam width and phase center and very wide frequency bandwidth [8]. All these characteristics are required for high performance radio astronomical applications. This view was supported by a recent international workshop on geodetic VLBI [9]. Experiments with the Eleven feed for single dish applications are taking place in America, India, China, and South Africa. Interest has been shown from Japan as well as from the international SKA office. The purpose of the present paper is to document the latest developments and present the recent measurement results of a coolable Eleven feed for VLBI2010 and SKA.

2. Feed Design

The Eleven feed is a decade-bandwidth log-periodic dual-dipole feed, developed at Chalmers University of Technology (Chalmers) beginning in 2005, originally proposed by P.-S. Kildal, and presented in [13]. The current realization operates across 2–14 GHz, within cryogenic systems. As seen in Figure 1, the feed is four petals above a ground plane, fed with four twin lead lines at each petal base. Depending on the application, it can be connected to the receiver backend in multiple ways, using either passive baluns and co-axial amplifiers or differential amplifiers. Five 2–14 GHz Eleven feeds based on the present design have been manufactured, and they either have been or will be tested at different places. The design is proven to have good features for the application in radio telescopes, such as nearly constant beamwidth with about 11 dBi directivity and fixed phase center location over the entire decade bandwidth (or more). It has also a low profile and simple geometry. Further details of the electrical design and measured results can be found in [8].

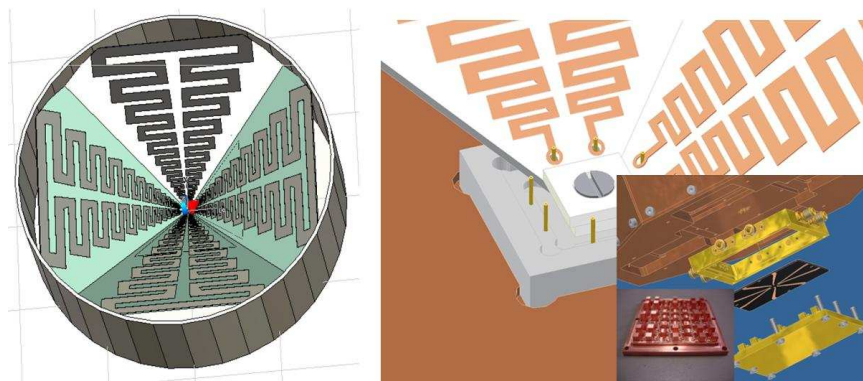


Figure 1. Front and back view of the Eleven feed. The picture on the left shows the front view of the Eleven Feed. The picture on the right shows the assembly of the center puck with the twin lead line. The insert shows a CAD-model of the descrambling board with four coaxial outputs per polarization.

3. Receiver Integration

Extremely low noise system performance requires cooling of both the cryogenic LNAs and the preceding lossy components. Even the feed has ohmic losses, and thus its integration into the cryostat improves system performance. An additional advantage of the feed integration is that we

can simplify the connection of the LNA and feeding network. Therefore, size and cryogenic coolability play important roles in the design of decade-bandwidth feeds for VLBI2010 and SKA radio telescopes. There are several issues that have to be considered in designing a feed for cryogenic integration: the microwave substrate should have well-matched thermal expansion coefficients for the copper and the dielectric; to follow the lob-periodic scaling, the dielectric thickness should change along the petal, and the petals should be well-attached thermally to the 20 K stage to allow effective cooling.

A very important component of the receiver chain is the LNA. The recent advance in GaAs and InP based low-noise cryogenic amplifiers allows the achievement of noise temperatures of less than 5 K for devices operated at 12 K physical temperature. Traditionally the ultra low-noise amplifiers were built using InP. The excellent low-noise characteristics are presented in a number of publications, for example [10] and [11]. Even though they demonstrate exceptional performance, the bandwidth of these amplifiers is usually limited to 2:1 since it is difficult to maintain optimal noise matching and stability over wider bandwidths. Recently the Caltech group led by Sander Weinreb has introduced several alternative designs of wideband LNAs with noise temperatures less than 5 K over 0.3–4 GHz and 1–10 GHz range [12]. Initial tests presented here used available LNAs with commercial GaAs transistors [14] — four such amplifiers were integrated with the feed for the first lab tests. The LNAs have 25 dB gain and noise temperature of 5K for the 4–8 GHz band. The amplifiers were connected directly to the descrambling board at the back side of the ground plane. The outputs were fed to the inputs of two 180 degree hybrids, and their differential outputs were combined in the power divider, all installed at the 70 K stage of the cryostat thus providing single polarization 50 ohm output.

The cryogenic integration takes advantage of the CTI 1020 cryogenic compressor and relatively large vacuum chamber available from an old receiver. The Eleven feed is installed on the 20K stage of the receiver. To decrease the infrared radiation, we have used Multi Insulation Layer (MIL) structure made of layers of Teflon separated by wedding veil [15]. Such MILs are installed in front of the antenna at 20 K and 70 K staged. The window on the cryostat is made from 0.35 mm thick Mylar and has diameter of 280 mm [15].

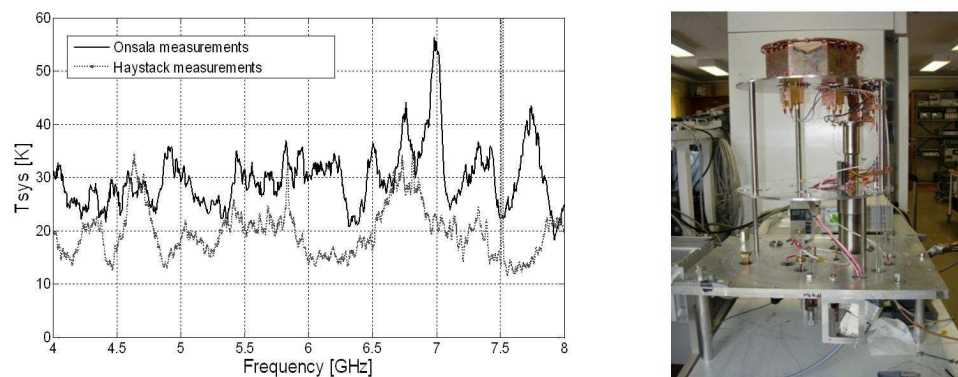


Figure 2. The measured reflection coefficient at room and cryogenic temperatures (left). The cryostat used for the measurements (right).

4. Measurement Results

The reflection coefficient of the Eleven feed was verified with numerous measurements. The results for room and cryogenic temperatures, along with simulations, are shown in Figure 3. The measurements were done using a 4-port Vector Network Analyser (VNA). The feeding network, hybrids, and power combiner were connected outside the cryostat. The small differences between the S11 at cryogenic and ambient temperatures confirms that neither the petals nor the twin lead line deform much, but rather the differences are due to changes in dielectrical permittivity.

The system noise temperature performance was measured using the common Y-factor approach. A microwave absorber was used for the hot load, and sky for the cold. The temperature of the hot load was measured using a temperature sensor, and the sky radiometric temperature was estimated using data available from the aeronomy station at Onsala Space Observatory (OSO).

The measured result is shown in Figure 3. The system noise temperature performance averaged across the band is 28 K. Plotted alongside are the corresponding results (for the 4-8 GHz band) from tests performed at the Haystack Observatory with the Eleven feed integrated into a cryostat with 2-12 GHz LNA from Caltech [16].

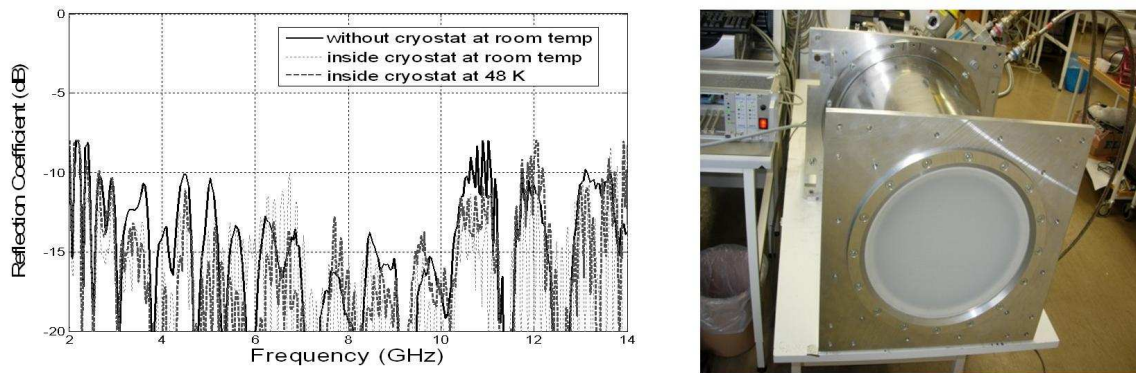


Figure 3. Preliminary results: measured system noise temperature of Eleven feed in cryostat at 28 K physical temperature (left picture) and Eleven feed prototype mounted in the test cryostat with 4-8 GHz cryogenic LNAs.

5. Conclusions and Future Work

This paper reports the first measurement results obtained with an Eleven feed integrated with LNAs and at cryogenic temperature. Even though the experiments at OSO were made with existing LNAs not optimal to achieve end-to-end optimal performance, we can claim that we have achieved good results in terms of low system noise temperature.

6. Acknowledgements

This work has been supported, in part, by The Swedish Foundation for Strategic Research (SSF) within the Strategic Research Center CHARMANT. The hardware development in this work was funded, partly, by The Swedish Governmental Agency for Innovation Systems (VINNOVA),

within a so-called VINN Verification project, and via hardware orders from Vertex Antennentechnik GmbH in Germany, the Norwegian Mapping Authority, and Haystack Observatory. Onsala Space Observatory has contributed in-kind with the cryogenic design, fabrication of the test cryostat, and cryogenic tests. There were also contributions to the evaluation of the electrical performance from Sander Weinreb at California Institute of Technology (Caltech) and from Christopher Beaudoin at MIT Haystack Observatory, who has also provided measurement data.

References

- [1] The Square Kilometer Array (SKA) At: <http://www.skatelescope.org/>
- [2] P.E. Dewdney, P.J. Hall, R.T. Schilizzi, T.J.L.W Lazio, The Square Kilometre Array, In: Proceedings of the IEEE, Vol. 97, Issue 8, p1482-1496, Aug 2009.
- [3] B. Petrachenko, IVS Memorandum 2008-015, In: IVS Memo series, 2008 <ftp://ivscc.gsfc.nasa.gov/pub/memos/>,
- [4] In: <http://www.aoc.nrao.edu/evla/>
- [5] D. Deboer et.al., The Allen Telescope Array, In: Experimental Astronomy, Volume 17, Numbers 1-3 / June, 2004.
- [6] W. A. Imbriale, S. Weinreb, and H. Mani, Design of a Wideband Radio Telescope, In: IPN Progress Report 42-168, February 2007.
- [7] G. Cortés-Medellín, Novel non-planar ultra wide band quasi self-complementary antenna, In: IEEE Trans. Antennas and Propag. Symposium, Hawaii, 2007.
- [8] J. Yang, M. Pantaleev, P.-S. Kildal, Y. Karandikar, L. Helldner, B. Klein, N. Wadefalk, Cryogenic 2-13 GHz Eleven feed for reflector antennas in future wideband radio telescopes, Submitted to: IEEE Trans. on Antennas Propag. Special Issue on Antennas for Next Generation Radio Telescopes, Dec 2009.
- [9] <http://www.fs.wetzell.de/veranstaltungen/vlbi/frff2009/frff2009.html>
- [10] M. W. Pospieszalski, W. J. Lakatos, R. Lai, K. L. Tan, D. C. Streit, P. H. Liu, R. M. Dia, and J. Velebir, Tuning Millimeter-wave, cryogenically cooled amplifiers using AlInAs/GaInAs/InP HEMTs, In: 1993 IEEE MTT-S Int. Microwave Symp. Dig., vol. 2, pp. 515-518, 1993.
- [11] J. J. Bautista, J. G. Bowen, N. E. Fernandez, Z. Fujiwara, J. Loreman, S. Petty, J. L. Pratar, R. Grunbacher, R. Lai, M. Nishimoto, M. R. Murti, and J. Lasker, Cryogenic, X-band and Ka-band InP HEMT based HEMT LNAs for the Deep Space Network, In: 2001 IEEE Aerospace Conference., vol. 2, pp. 829-842, 2001.
- [12] S. Weinreb, J. Bardin, H. Mani, G. Jones, Matched wideband low-noise amplifiers for radio astronomy, In: Review of Scientific Instruments, 80 (4). Art. No. 044702. ISSN 0034-6748, 2009.c
- [13] R. Olsson, P.-S. Kildal, S. Weinreb, The Eleven antenna: a compact low-profile decade bandwidth dual polarized feed for reflector antennas, In: IEEE Transactions on Antennas and Propagation, vol. 54, no. 2, pt. 1, pp. 368-375, Feb. 2006.
- [14] C. Riscaher, E. Sundin, V. Perez Robles, M. Pantaleev, V. Belitsky, Low noise and Low Power Consumption Cryogenic IF Amplifiers for Onsala and APEX telescopes, In: Proceedings of GaAs Conference, ISBN 1-58053-994-7, pp. 375-377, Amsterdam, The Netherlands, 11-12 October 2004.
- [15] S. Weinreb, private communications, 2009.
- [16] Christopher Beaudoin, Haystack Observatory, private communications.

Development of a Compact Eleven Feed Cryostat for the Patriot 12-m Antenna System

Christopher Beaudoin¹, Per-Simon Kildal², Jian Yang², Miroslav Pantaleev³

¹) MIT Haystack Observatory

²) Chalmers University of Technology

³) Onsala Space Observatory

Contact author: Christopher Beaudoin, e-mail: cbeaudoin@haystack.mit.edu

Abstract

The Eleven antenna has constant beam width, constant phase center location, and low spillover over a decade bandwidth. Therefore, it can feed a reflector for high aperture efficiency (also called feed efficiency). It is equally important that the feed efficiency and its subefficiencies not be degraded significantly by installing the feed in a cryostat. The MIT Haystack Observatory, with guidance from Onsala Space Observatory and Chalmers University, has been working to integrate the Eleven antenna into a compact cryostat suitable for the Patriot 12-m antenna. Since the analysis of the feed efficiencies in this presentation is purely computational, we first demonstrate the validity of the computed results by comparing them to measurements. Subsequently, we analyze the dependence of the cryostat size on the feed efficiencies, and, lastly, the Patriot 12-m subreflector is incorporated into the computational model to assess the overall broadband efficiency of the antenna system.

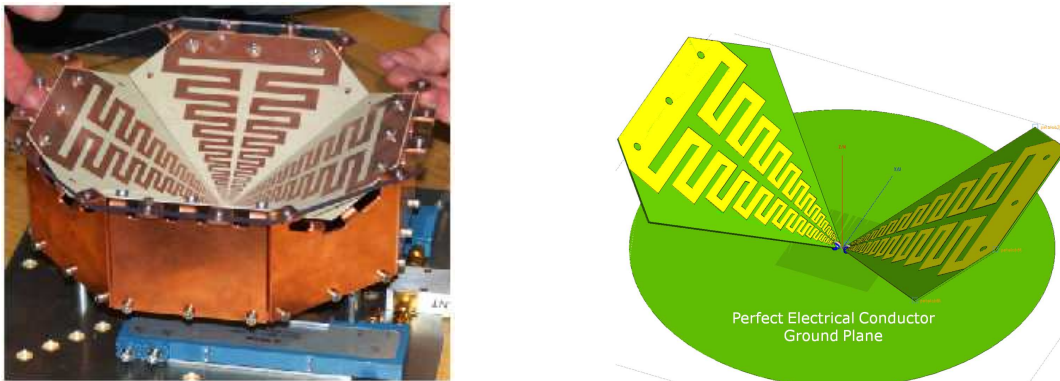


Figure 1. a) 2-14 GHz cryogenic Eleven antenna; b) geometric representation of the Eleven antenna used for computations.

1. Validation of Computational Results

Computational electromagnetic analysis of the Eleven antenna was performed using the commercial software suite FEKO. To give credence to the computations, a freespace model of the Eleven antenna was first constructed to compare the computational results against their measured counterparts. These results refer to the feed efficiencies, which are calculated from the antenna

radiation patterns as described in [1]. Figure 1a displays a photo image of the 2-14 GHz Eleven antenna, the radiation pattern of which was measured in an anechoic chamber at the Technical University of Denmark [2] [5]. Figure 1b displays the corresponding FEKO geometric representation used to model the electromagnetic behavior of the antenna in Figure 1a.

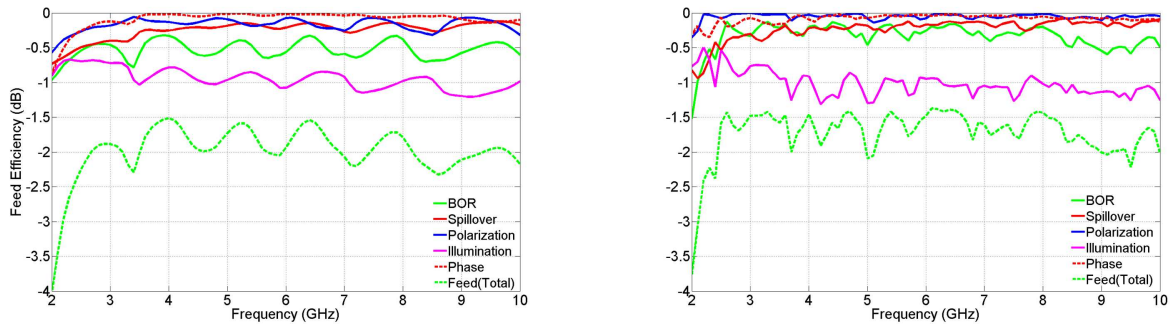


Figure 2. a) Eleven antenna feed efficiencies based on FEKO model; b) Eleven antenna feed efficiencies based on measurements.

In order to make the model computationally tractable, many of the components comprising the physical antenna were not modeled in FEKO as they do not contribute significantly to the feed efficiencies. Furthermore, we only model a single polarization (one pair of petals) as the two polarizations are rotationally symmetric. The feed efficiencies calculated from the measured and computed radiation patterns are shown in Figures 2a and 2b, respectively. These calculations were performed assuming a full-width primary reflector capture angle of 120 degrees. Comparison of these two plots provides faith in the computed radiation patterns which are used to calculate the feed efficiencies specific to the 12-m Patriot antenna system.

2. Feed Efficiency Dependence on Cryostat Size

In the interest of minimizing feed blockage and weight, it is desirable to make the cryostat as small as possible. However, if the cryostat is too small, the electromagnetic fields near the aperture of the antenna will be choked, and the feed efficiencies will be degraded. This trade-off has been analyzed by means of a computational model in FEKO. The feed model shown in Figure 1b was modified in order to study the dependence of the cryostat walls on the feed efficiencies; the modified geometric representation is shown in Figure 3.

Since the primary phenomenon expected to degrade the feed efficiencies is choking of the electromagnetic fields near the top of the feed, only the top most portion of the cryostat walls were modeled. Defining the problem in this way also has the advantage of minimizing the size of the computational problem to be solved. As indicated in Figure 3, the feed efficiencies were examined as a function of the cryostat wall length ‘L’ and the cryostat radius ‘R’. In this examination, the feed efficiencies were calculated from 2-10 GHz for each L,R pair and these quantities were subtracted from their corresponding freespace counterpart. The average of this difference over 2-10 GHz is referred to as the efficiency degradation and describes the feed efficiency losses relative to those shown in Figure 2a. The efficiency degradation data form a rectangular grid in L and R, and this data was interpolated to generate the efficiency degradation map shown in Figure 4.

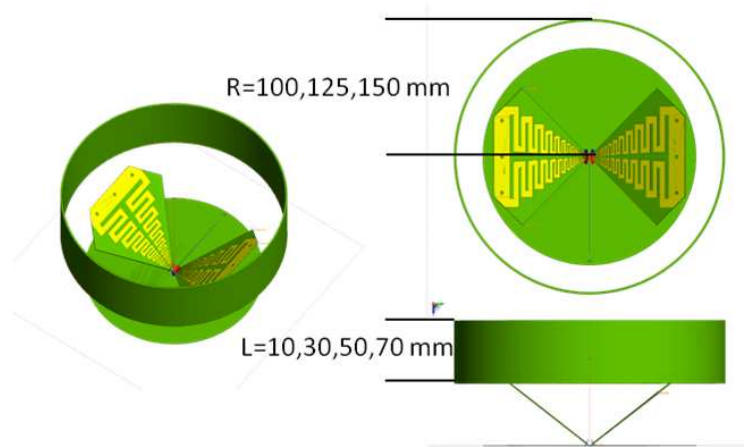


Figure 3. Geometric model used to study feed efficiency dependence on the cryostat size.

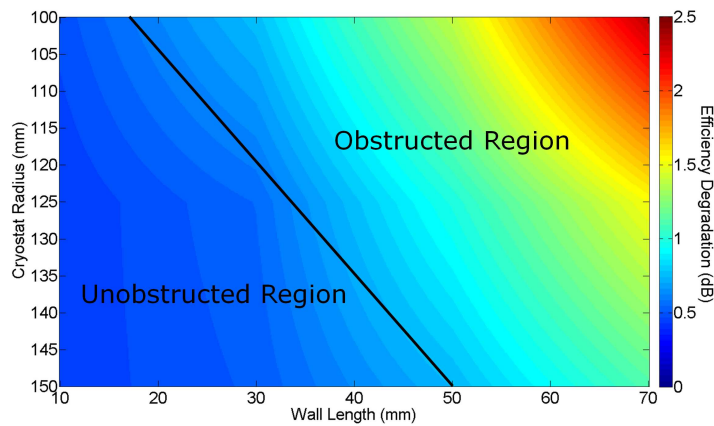


Figure 4. Feed efficiency dependence on cryostat size. The obstructed region is that in which the cylinder radius and length are such that the opening angle of the feed is obstructed by the cylinder in the geometrical optics sense. The efficiency degradation increases from bottom left to top right.

3. Feed Efficiencies on the Patriot 12-m Antenna

The Patriot 12-m antenna (Figure 6) is a dual-shaped reflector system which is one of the two new antenna systems being incorporated for use in the VLBI2010 network, the other being the VertexRSI design. Currently, a Patriot 12-m antenna is being installed at the Goddard Geophysical Astronomical Observatory (GGAO) in Greenbelt Maryland, USA. This antenna will be retrofit with an Eleven feed to provide broadband capability for VLBI2010 observations. As such, the feed efficiencies incorporating the 12-m subreflector have been calculated for future sensitivity estimates. The radiation pattern of the Patriot subreflector under illumination by the Eleven antenna was simulated in FEKO, and Figure 5 displays the feed efficiencies calculated from these patterns based on the 150 degree full-width capture angle of the primary reflector. Because the

subreflector is shaped, as a single reflector it does not possess a well-defined focal point. This being the case, the subreflector was assumed to not degrade the phase sub-efficiency of the feed pattern in order to avoid application of a phase correction needed to compensate for the surface shaping.

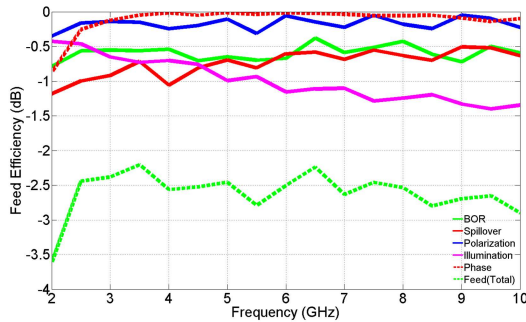


Figure 5. Feed efficiencies on the Patriot 12-m antenna system simulated with the Eleven antenna’s freespace radiation pattern.



Figure 6. Patriot 12-m antenna system (photo courtesy of Jim Lovell, University of Tasmania).

4. Conclusions

- The feed efficiencies based on the calculated radiation patterns computed from the FEKO Eleven antenna model (Figure 1b) demonstrate good agreement with the feed efficiencies obtained from measurements of the antenna’s (Figure 1a) radiation patterns.
- The feed efficiencies of the Eleven antenna are degraded when the Eleven antenna is placed in a cryostat that is too confining. Figure 4 exhibits the dependence between the cryostat size and the efficiency degradations.
- The frequency averaged efficiency is expected to be 55% when the Eleven antenna is used to feed the Patriot 12-m antenna system; this is 5% greater than the VLBI2010 specification [3].
- The feed efficiencies were derived assuming that the subreflector does not degrade the freespace phase sub-efficiency.
- The feed efficiencies were derived under the assumption of no blockage, but the subreflector shaping mitigates this efficiency loss.

References

- [1] P.-S. Kildal, “Factorization of the feed efficiency of paraboloids and Cassegrain antennas,” *IEEE Transactions on Antennas and Propagation*, vol. 33, no. 8, pp. 903–908, Aug. 1985.
- [2] P.-S. Kildal and J. Yang, Report with Measurements of a coolable 2-14 GHz Eleven feed for VLBI 2010 delivered to Vertex, June 2009.
- [3] B. Petrachenko, et. al., “Design Aspects of the VLBI2010 System,” *International VLBI Service for Geodesy and Astrometry Annual Report 2008*, NASA/TP-2009-214183, pp. 13–66, July 2009.

- [4] R. Olsson, P.-S. Kildal, S. Weinreb, "The Eleven antenna: a compact low-profile decade bandwidth dual polarized feed for reflector antenna", *IEEE Transactions on Antennas and Propagation*, vol. 54, no. 2, pt. 1, pp. 368–375, Feb. 2006.
- [5] J. Yang, X. Chen, N. Wadefalk, P.-S. Kildal, "Design and realization of a linearly polarized Eleven feed for 1-10 GHz", *IEEE Antennas and Wireless Propagation letters (AWPL)*, Vol. 8, pp. 64–68, 2009.

Radio Telescope Focal Container for the Russian VLBI Network of New Generation

Alexander Ipatov¹, Vyacheslav Mardyshkin¹, Andrey Cherepanov², Vitaly Chernov¹,
Dmitry Diky², Evgeny Khvostov¹, Alexander Yevstigneyev¹

¹) *Institute of Applied Astronomy of RAS*

²) *Saint Petersburg State Polytechnic University*

Contact author: Vyacheslav Mardyshkin, e-mail: mardyshkin@rambler.ru

Abstract

This article considers the development of the structure of receivers for Russian radio telescopes. The development of these radio telescopes is undertaken within the project for creating a Russian small-antenna-based radio interferometer of new generation. It is shown that for small antennas (10–12 meter) the principal unit, which provides the best SNR, is the so-called focal container placed at primary focus. It includes the primary feed, HEMT LNA, and cryogenic cooling system down to 20° K. A new multi-band feed based on traveling wave resonators is used. It has small dimensions, low weight, and allows working with circular polarizations. Thus it can be placed into focal container and cooled with the LNA. A sketch of the focal container, with traveling-wave-resonator feed, and calculations of the expected parameters of the multi-band receiver are presented.

1. Introduction

The so-called focal container (FC) is one of the key elements of the antenna of the radio telescope of the new generation Russian VLBI network. Located at the focal point of the antenna, the FC provides the required quality of the received signal. The FC contains the antenna feed, low-noise amplifiers, and microwave isolators, all cooled to cryogenic temperatures inside a dewar. As electromagnetic waves should freely get to the antenna feed within the dewar, the FC front wall should be transparent in all working frequencies of the radio telescope.

According to the requirements for the equipment of the above mentioned VLBI network, the reception path of a radio telescope should adhere to the recommendations of the IVS VLBI2010 Committee. That is, the FC should provide signal reception in several (from three to five) frequency bands (up to 1 GHz bandwidth, each situated within the range from 2 to 14 GHz). These requirements can be met when either a broadband antenna feed working in the full range (2–14 GHz) or a multiband feed accepting signals in several fixed frequency ranges lying in the specified limits are used. For the creation of the radio telescope, the second variant of construction of a feed was accepted: the multiband feed should contain five frequency channels and receive signals of two circular polarizations — left and right. The following borders of operational frequency bands were defined: 2.15–2.50 GHz (S-band), 3.3–4.3 GHz (C-low-band), 4.8–6.2 GHz (C-high-band), 7.5–9.7 GHz (X-band), and 11–14 GHz (Ku-band).

2. Focal Container Feed

The FC multiband feed is supposed to be built on the basis of traveling wave ring resonators (TWR). Such a feed consists of a set of cylindrical microwave units (the relevant frequency bands)

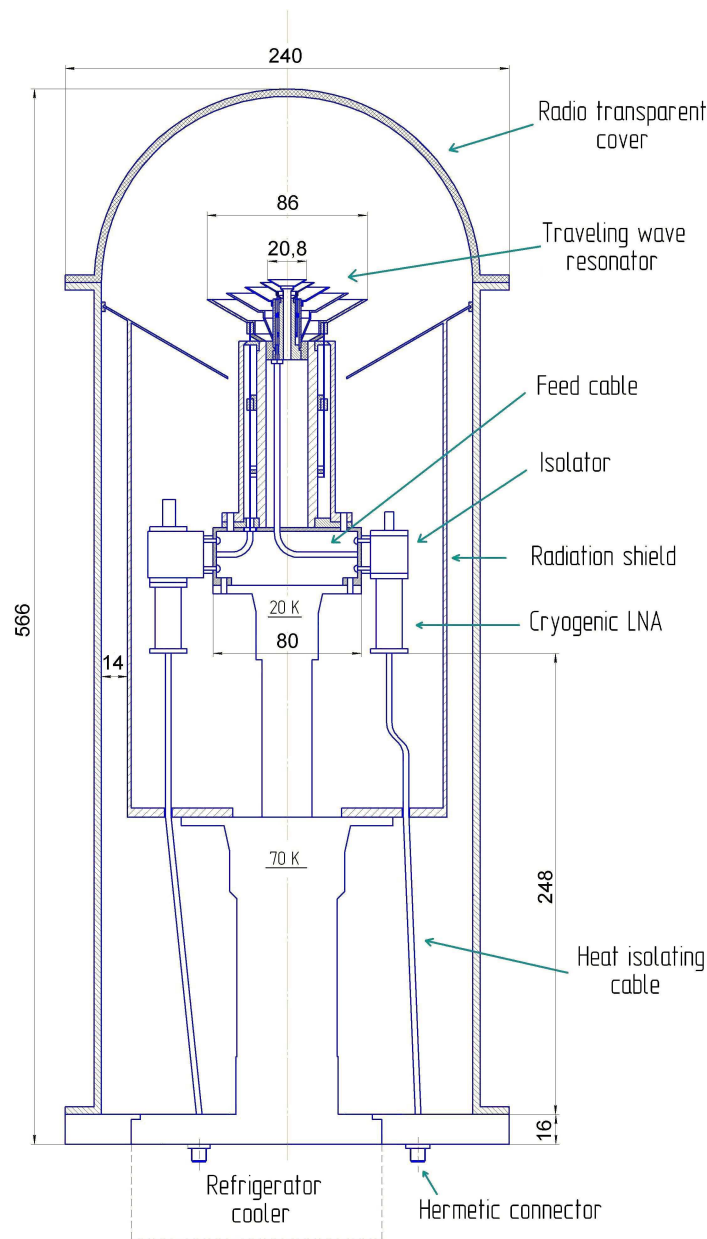


Figure 1. General view of the focal container with TWR feed.

placed coaxially — the C-low-band unit is placed inside the S-band unit, etc. (Figure 1).

TWR represents a stripline coiled into a ring [1]. Resonator excitation is carried out by means of a directional coupler. Two TWRs are cascaded to improve the feed gain-frequency characteristic. Only one of the TWRs (open TWR) radiates an electromagnetic wave of circular polarization. Both TWRs and the excitation line are connected by quarter-wavelength segments. The form of the gain-frequency characteristic of the TWR feed is defined by the link between the ring lines. Each of the coaxially placed frequency channels has two outputs of circular polarization—LCP and RCP. This TWR feed has a width of a far field pattern near $(120\text{--}130)^\circ$ on a level minus

(10–12) dB, and is intended for axial-symmetric parabolic antennas with an f/D ratio of about 0.3–0.4.

The reception path between the TWR feed and the low-noise amplifiers (LNA) contains ferrite isolators. They serve to eliminate the negative influence of a mismatch between feed outputs and LNA inputs. The isolators possess certain losses and, hence, raise noise temperature of the system a little. However, when using the TWR feed, utilization of the isolators is obligatory, as outputs of the right and left polarization channels of this feed are not completely isolated.

3. Low-noise Amplifiers

The input cascades of the low-noise amplifiers (LNA) define the key parameters of the radio astronomical receiver such as noise temperature and sensitivity. LNA noise temperature is largely dependent on the physical temperature of the amplifier. Therefore, input amplifiers need to be cooled to cryogenic temperatures. Among the manufacturers of cryogenic LNA, whose products basically correspond to the requirements, there are such companies as QuinStar Technology Inc. (USA), B&Z Technologies (USA), Low Noise Factory (Sweden), and SPE “Saturn” (Ukraine). Amplifier characteristics of these manufacturers are listed in Table 1.

Table 1. Characteristics of low-noise amplifiers

Manufacturer/model	Band, GHz	Noise figure, K	Gain, dB
Low Noise Factory/LNF-LNC1.8_2.8A	S: 1.8–2.8	3	43
SPE “Saturn”/13 cm	S: 2.3–2.64	3	35
QuinStar Technology Inc./C-4.0-30H	C-low: 3.5–4.5	8	30
SPE “Saturn”/7.6 cm	C-low: 3.7–4.2	4	30
QuinStar Technology Inc./C-5.0-30H	C-high: 4.8–5.1	3	28
SPE “Saturn”/5.8 cm	C-high: 4.8–5.5	4	30
Low Noise Factory/LNF-LNC7_10A	X: 7.0–10.0	6	35
SPE “Saturn”/3.5 cm	X: 8.0–9.2	5	30
B&Z Technologies/BZ0812CR1	Ku: 8.0–12.0	15	24
SPE “Saturn”/2.5 cm	Ku: 11.2–12.8	6	30

The most widespread cooling systems for input low-noise amplifiers of radio telescopes are two-stage systems, based on a cycle of Gifford-McMahon (GM). Such systems are currently used in the Russian VLBI network “Quasar” and will be introduced to the new VLBI network.

4. Radio Transparent Window

Electromagnetic waves, focused by the radio telescope antenna, should freely propagate to the cooled antenna feed, situated inside the cryogenic dewar. That is, the dewar should be equipped with a radio transparent (RT) window or cover. The following demands should be applied to the window:

- Active losses and reflections of electromagnetic waves from the material of the window in a range of frequencies from 2 to 14 GHz should not raise the noise temperature of the system

more than 1–3 K.

- The feed cover should prevent penetration of infrared radiation into the dewar.
- The cover should be strong enough to maintain external atmospheric pressure.
- The cover material should not pass or exhale gases into the dewar.

There is experience in the creation of a flat radio transparent dewar window. In [2], the design of a radio transparent window for X- and Ka-bands is described. This window is a three-layer structure, with a 0.08-mm Kapton layer for strength, backed by a 25-mm polystyrene layer for additional strength and thermal insulation, with a 0.38-mm Teflon over-layer to protect the Kapton, which will lose strength after long periods of exposure to the Sun. The window adds less than 1 K of noise temperature to the system in each band.

The width of pattern of the above mentioned multiband TWR feed is equal to $(120\text{--}130)^\circ$. To exclude the influence of the edges of the radio transparent window on the performance of such a feed, it is required that the cover should have a dome-shaped form. This complicates the problem of creating the cover and demands serious study.

5. Noise Temperature of the Receiver

We made a calculation of the noise temperature of the radio telescope receiver, considering losses in the radio transparent cover, TWR feed, internal and external cables, connectors, microwave isolators, and also the noise temperatures of the LNA and RF/IF convertor. The results are presented in Table 2. As real losses of RT cover and TWR feed have not been measured yet, expected values were used.

Table 2. Contribution of parts of the receiver to resulting noise temperature (K)

Part of the receiver	S-band	C-low-band	C-high-band	X-band	Ku-band
RT cover	3	3	3	3	3
TWR feed	3	3	3	3	3
Feed cable	0.11	0.37	0.55	0.85	1.04
Isolator	1.53	0.76	0.77	0.78	0.79
LNA	3.47	4.49	4.54	5.78	7.02
Heat isolating cable	0.01	0.01	0.01	0.01	0.02
Hermetic connector	0.01	0.01	0.01	0.01	0.01
External cable	0.01	0.02	0.03	0.04	0.04
RF/IF convertor	0.06	0.26	0.40	0.60	0.88
Total noise figure, K	11	12	13	14	16

References

- [1] Diki, D. V., Printed Antennas Based on Travelling Wave Resonators, Nice, France, November, JJINA-98.
- [2] Gatti, M., W. Imbriale, D. Hoppe, H. Reilly, J. Prater, M. Britcliffe, X/Ka-band feed for the DSN array, In: DSN Microwave Array Peer Review: Feeds/LNA/Crypto, Pasadena, CA, December 18, 2003.

Experiment of Injecting Phase Cal Ahead of the Feed: First Results

Dmitrij Ivanov, Anatolij Maslenikov, Alexander Vytnov

Institute of Applied Astronomy of RAS

Contact author: Dmitrij Ivanov, e-mail: ltf@ipa.rssi.ru

Abstract

For developing the Russian VLBI network of new generation, a few experiments of injecting the phase calibration signal ahead of the feed were carried out. In the experiments an external broadband phase calibration signal was emitted through a special feed to a receiver horn directly. Prototypes of the feed for a frequency range of 2–18 GHz were created. The first experiments on injection phase cal ahead of the feed were carried out at Svetloe Observatory of the QUASAR VLBI network. The phase cal signal was emitted by the broadband feed installed on the roof of a mirror cabin, reflected by the sub-reflector, and received by the horn of the receiving system. The results of these experiments are considered.

1. Phase Calibration System

The primary purpose of the phase calibration system is to monitor the instrumental phase delay. For most applications only temporal variations are of interest, but for a few critical applications, such as UT1 measurement and time transfer, knowledge of the absolute delays is also required. For VLBI2010, the specification on the instrumental delay measurement error has been set to < 1 ps, so that it is well below the single-observation stochastic error, which is targeted to be 4 ps [1].

In the current phase calibration system, a spectrally pure reference signal of 5 MHz is transmitted by cable to the mirror room of the radiotelescope, where it synchronizes a generator of very short impulses of about 45 ps duration. The impulses are injected through a direction couple into the input of receiver before the first LNA and passed, with the received signal, through receiver and data acquisition devices to digitization, after which the phases of the tones are extracted.

A similar system has been developed for the Russian VLBI network of new generation. One possible scheme under study is to radiate phase cal impulses from a special broadband feed located ahead of the receiving feed. The main advantage of injecting phase cal ahead of the receiving feed is in putting most of the VLBI signal path into the phase calibration loop; but multipath effects may be a problem.

The phase cal feed is supposed to be mounted on one of the legs supporting the focal box, in a distance from the mirror surface that satisfies the distant-zone condition for radiation. Then the surface will be radiated with a flat front, and radiation of the phase calibration will be focused on the receiving feed of the radiotelescope. Taking into consideration the geometrical sizes of a telescope and other common reasons the following rough characteristics of the phase cal feed are chosen:

Diameter	no more than 30 cm
Pattern width	no more than 40°
Level of side lobes	no more than -15 dB
Frequency band	2–14 GHz
VSWR	no more than 2.0

2. Experimental Research

The possible multipath in telescope has been investigated. The feed for 13 cm band with the demanded pattern width and a side lobe level has been produced. Spiral type of the feed is chosen because of simplicity of calculation and manufacturing. A photo of the manufactured feed is shown in Figure 1.

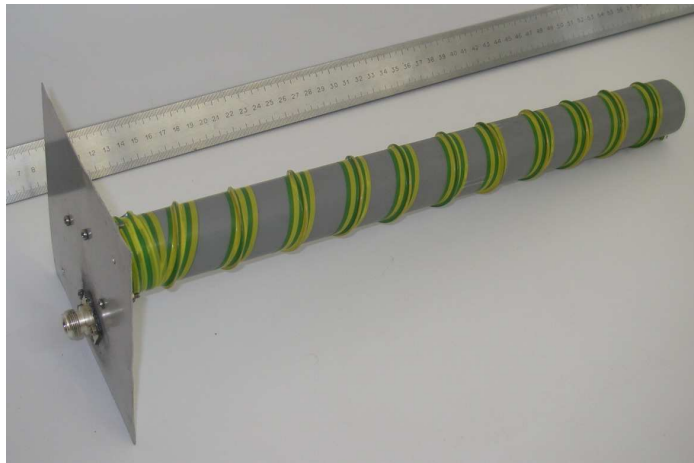


Figure 1. Photo of the manufactured spiral feed.

Measured characteristics of VSWR and radiation pattern of the feed (Figures 2 and 3) are matched with the requirements indicated above.

In mid-2009 a few experiments with the spiral feed were carried out at Svetloe Observatory of the Russian VLBI network Quasar. A feed connects to reserve generator which synchronizes by reference 5 MHz signal. In the output of the *S*-band receiver, impulses of the phase cal both from the regular generator and radiated from this spiral feed were observed by an oscillograph Agilent DSO 6102A. The output oscillograms are shown in Figures 4 and 5.

As no multipath effect was detected in the experiment, the phase calibration submission described above could be used in the system.

3. Wideband Feed

Transverse electromagnetic (TEM) horn antennas have been used as wideband antennas for various applications. This type of antenna has the advantages of being wideband, lacking dispersion, being unidirectional, and being easily constructed. An exponentially tapered TEM horn antenna with TEM double-ridged transition for the 2–14 GHz frequency band has been described in [2]. At IAA a similar TEM horn feed was built (Figure 6). This feed is now under testing. The

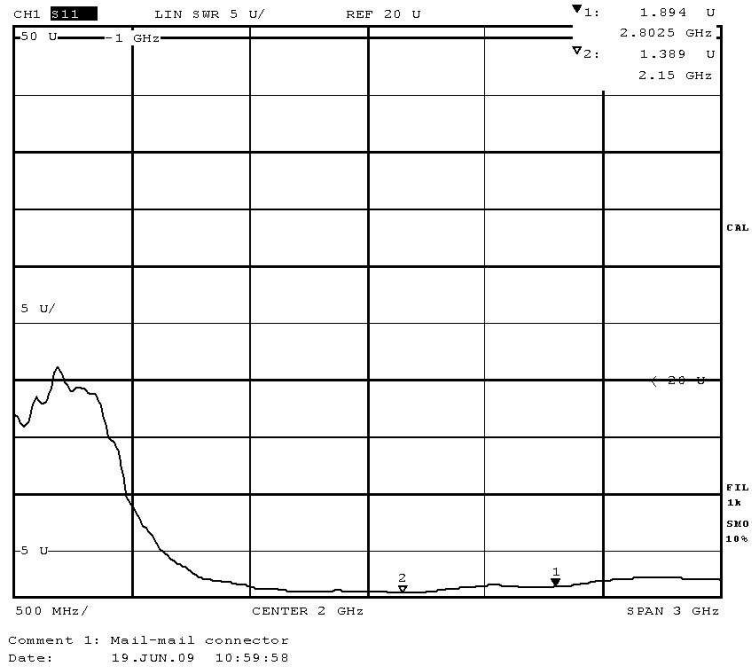


Figure 2. VSWR of spiral feed.

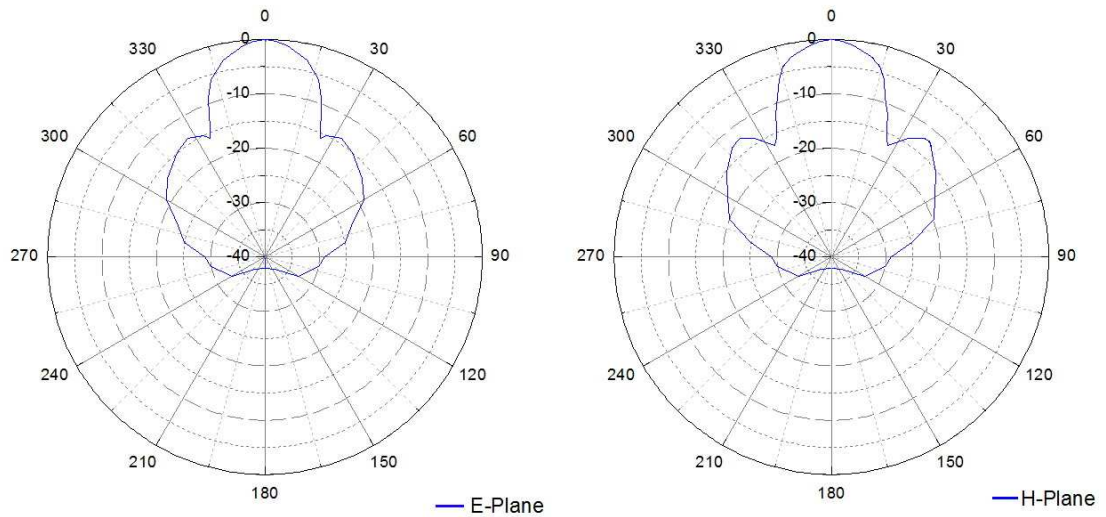


Figure 3. Radiation patterns of the spiral feed.

characteristics of the TEM horn feed indicate that it is feasible to use for emitting the phase cal signal.

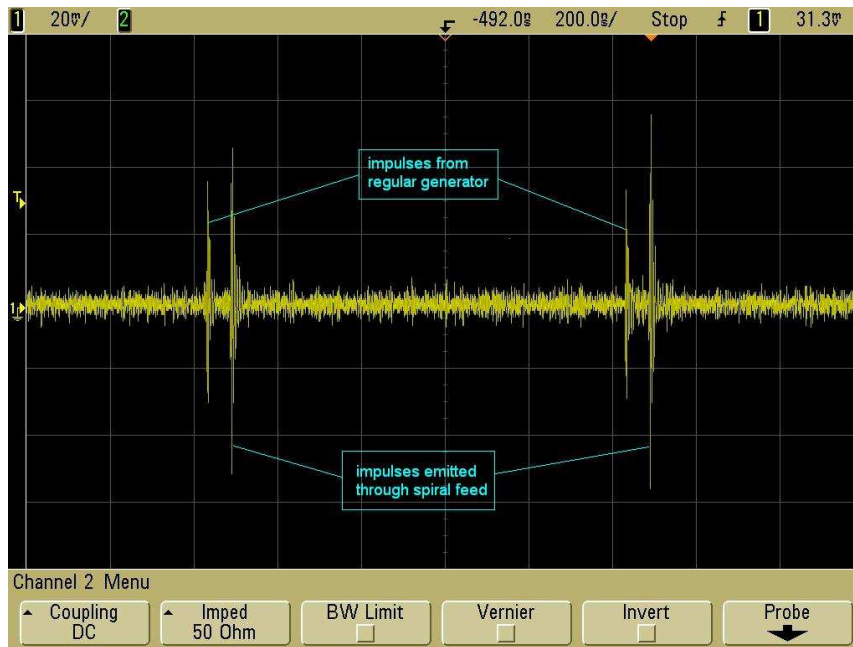


Figure 4. Oscillogram of the output signal from the S-band receiver.



Figure 5. Oscillogram of output signal for S-band receiver.

4. Conclusions

The research carried out showed the absence of multipath effects in the external radiation phase cal signal. A prototype broadband feed for emitting the phase cal signal was made and tested.

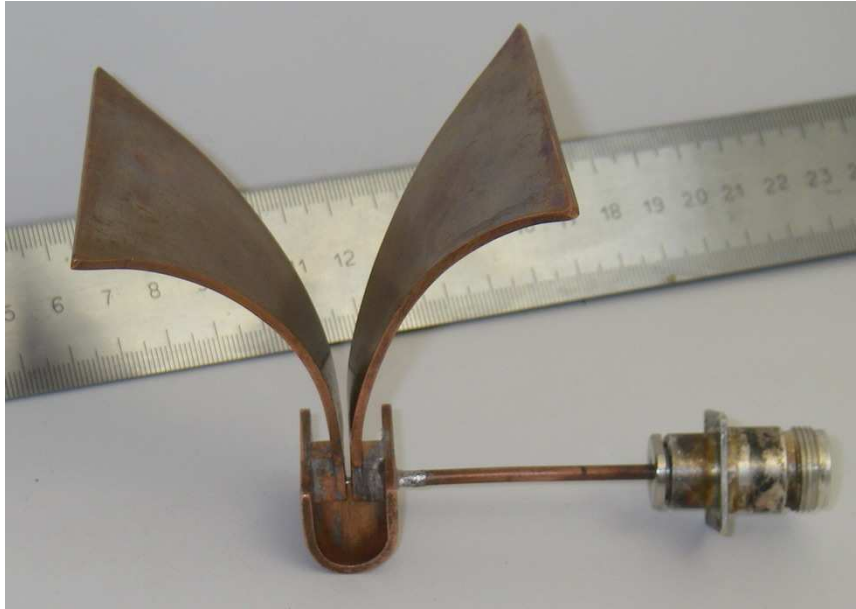


Figure 6. Photo of the manufactured TEM horn feed.

In the near future it is planned to produce a temperature controlled enclosure for the TEM horn feed. Mounting these devices permits us to investigate long-period phase stability and influence of weather conditions.

References

- [1] Petrachenko, B., A. Niell, D. Behrend, B. Corey, J. Böhm, P. Charlot, A. Collioud, J. Gipson, R. Haas, T. Hobiger, Y. Koyama, D. MacMillan, Z. Malkin, T. Nilsson, A. Pany, G. Tuccari, A. Whitney, and J. Wresnik, Design Aspects of the VLBI2010 System. Progress Report of the IVS VLBI2010 Committee. Goddard Space Flight Center Greenbelt, MD 20771, 2009.
- [2] Mallahzadeh, R., F. Karshenas, Modified TEM Horn Antenna for Broadband Applications. Progress In Electromagnetics Research, PIER 90, 105–119, 2009.

The Impact of Radio Frequency Interference (RFI) on VLBI2010

Bill Petrachenko

Natural Resources Canada (NRCan)

e-mail: `Bill.Petrachenko@nrcan.gc.ca`

Abstract

A significant motivation for the development of a next generation system for geodetic VLBI was to address growing problems related to RFI. In this regard, the broadband 2-14 GHz frequency range proposed for VLBI2010 has advantages and disadvantages. It has the advantage of flexible allocation of band frequencies and hence the ability to avoid areas of the spectrum where RFI is worst. However, the receiver is at the same time vulnerable to saturation from RFI anywhere in the full 2-14 GHz range. The impacts of RFI on the VLBI2010 analog signal path, the sampler, and the digital signal processing are discussed. In addition, a number of specific RFI examples in the 2-14 GHz range are presented.

1. Introduction

RFI is any man-made radio transmission inadvertently added to a signal of interest. It can originate from land, marine, aeronautical, or space-based transmitters and for purposes ranging from commercial broadcast to scientific and amateur. The entire VLBI2010 spectrum from 2-14 GHz is allocated to a myriad of applications through international, national, and regional agreements with only a tiny portion set aside for radio astronomy. Fortunately, interferometric techniques are comparatively robust against RFI. This is particularly true for VLBI where the antennas are typically so far apart that the sources of RFI at either end of a baseline are different and hence uncorrelated. Even when the RFI is correlated, as happens with geostationary satellites, the RFI output appears at a delay and fringe rate that are almost always significantly different from that of the astronomical signal.

2. The Impact of RFI on the VLBI2010 Analog Signal Path

In an idealized linear analog system, RFI can be analyzed simply as noise added to the astronomical signal. It has essentially the same impact as an increase in the system noise temperature (T_{sys}). If the RFI is band-limited, as is usually the case, the only region of the spectrum that is degraded is the region where the RFI actually exists. Provided that RFI is not too large, the VLBI2010 analog signal path can be analyzed under the linear assumption.

However, when RFI is larger, the situation is not so simple. The output of real analog devices cannot increase beyond a specific limiting voltage. As the input to the device increases, the output eventually hits this voltage, and it is said that the output is clipped or limited. The process is referred to as saturation. Under operational conditions, this occurs when RFI is much larger than the input astronomical signal. Since the small astronomical signal then rides almost unnoticed on top of the much larger RFI signal, it disappears entirely when the RFI is clipped. This obviously degrades the entire radio astronomical spectrum and not just the region of the spectrum where RFI occurs. To make matters worse, clipping generates harmonics and other intermodulation products

of the RFI, which spreads the RFI across the entire spectrum. In this way, even narrow band RFI, if large enough, can destroy an entire input band. This obviously has serious implications for the broadband 2-14 GHz input range of the VLBI2010 system where even a single source of strong RFI anywhere in the spectrum can bring down the entire system.

A proper analysis of saturation potential includes the entire analog signal chain. It is important to optimally adjust the gains of each stage in the chain to maximize the range of linear operation. If suitable devices are available and affordable, the range of operation can be increased by substituting higher dynamic range devices at critical points in the signal path. For VLBI2010, a dynamic range of 30 dB for the full analog signal path is a desirable and realistic target.

If the RFI level after optimal design of the analog signal path is still too large, another solution is to insert a filter to remove the region of the spectrum where the RFI occurs. To be effective, the filter must be inserted prior to the first point where saturation occurs. Under many circumstances this requires that the filter be inserted between the feed and front end Low Noise Amplifier (LNA). If this is the case, the filter must be cryogenically cooled to avoid unacceptable noise performance, and the front end must be mechanically and electrically designed to allow for the insertion of the filter.

Although not immediately obvious, the broadband frequency range of the VLBI2010 system also helps mitigate against saturation. This is particularly true for comparatively narrow band RFI. As an example consider RFI that has a spectral density as high as 70 dB above the noise floor but with a bandwidth of only 1 MHz. Since the 12 GHz LNA bandwidth is a factor of 12,000 greater than that of the RFI, the total RFI power ends up being only about 29 dB above the integrated noise power of the LNA. As a result, this apparently high level of RFI is easily within the dynamic range of a typical VLBI LNA.

Another RFI mitigating factor is the directionality of the parabolic antennas used in VLBI. The RFI power received through antenna sidelobes and backlobes is significantly attenuated relative to that of the astronomical signal of interest which is received along the axis of the antenna.

3. Impact of RFI on the VLBI2010 Sampler

In modern VLBI systems, most back-end receiver functions are now performed digitally. The device that converts the analog input signal into a time-tagged sequence of digital values is the sampler. To ensure adequate fidelity in the digital processing and enough dynamic range to handle RFI, a fairly high resolution 8- to 10-bit sampler is typically used.

In VLBI post-processing, the absolute scale of the input signal is of no consequence. Hence, its digital representation can vary within a settable constant factor. In practice, this variation is accomplished by either attenuating or amplifying the analog signal before it is sampled. The setting of this constant factor is, however, not arbitrary. If the attenuation is too high (resulting in a level that is too small), the signal is then very coarsely sampled. This transforms the smooth analog input into a *squared-up* signal with discrete steps that are large compared to its amplitude. On the other hand, if the input level is too large, the signal can exceed the maximum range of the sampler. This essentially saturates the sampler and clips the output. What is desired is a compromise that minimizes the net degradation.

Fortunately, correlation processing is not very sensitive to these sorts of signal distortions. Take as an example an 8-bit sampler which has a range of roughly ± 128 . If the attenuator setting results in an rms digital output anywhere in the surprisingly wide range of 1 to 128, the degradation in

correlated signal-to-noise ratio (SNR) is no more than about 10%; if it is set for an output anywhere in the range of 2 to 64, the SNR loss is never more than about 2%; and, if it is set in the output range of 4 to 32, the loss is never more than about 0.5%.

However, the situation becomes somewhat more complicated when RFI is present. The attenuator setting must then be adjusted to simultaneously satisfy restrictions imposed by both the RFI and the system noise. At the upper end, the RFI should never be allowed to saturate the sampler. In practical terms, this means that the rms RFI level should not be allowed to rise above about one quarter of the full range of the sampler. At the lower end, the digital value of the rms system noise should never be allowed to decrease below a value where the correlated SNR loss is more than a few percent. Thus, for an 8-bit sampler, the rms RFI level should be kept below about 32, and the rms system noise should be kept above about 2. This represents a dynamic range of $32/2 = 16$, which is equivalent to a power ratio of 24 dB. For a 9-bit sampler the dynamic range is about 30 dB; and for a 10-bit sampler it is about 36 db.

If the RFI is narrow band, a notch filter in cascade with the sampler antialias filter might be considered an acceptable solution to excise the RFI. However, this is not desirable for the VLBI2010 system where the individual bands are designed to be arbitrarily settable in the full 2.2-14 GHz range. In this case, the notch filter would be appropriate for one frequency setting of the band but not for others.

One simple scenario for setting the pre-sampler attenuator would be to continuously adjust its value to ensure that the rms digital value always stays as near as possible to one quarter of the full sampler range, i.e., 32 for an 8-bit sampler, 64 for a 9-bit sampler, or 128 for a 10-bit sampler. Another approach that is operationally even simpler would be to set the attenuator as high as possible before losses become unacceptable and then simply leave the attenuator fixed thereafter. Since this value of attenuation is already the largest tolerable, there is no need to consider increasing it as the RFI grows. Slow changes in the overall system gain may, however, require attenuator adjustments from time to time. In either operational scenario, there is still value in monitoring the digitized signal levels frequently to know if, when, how strong, and at what frequencies the RFI is occurring.

4. Impact of RFI on the VLBI2010 DBE/DBBC

The back-end digital processors in modern VLBI data acquisition systems serve many functions ranging from phase cal extraction and radiometry to requantization and formatting of data for recording. But their most fundamental function is the separation of the data into frequency channels. There are two conceptually different ways of doing this.

One is a straightforward digital implementation of the classical analog Baseband Converter (BBC). This implementation includes digital equivalents of the BBC local oscillator, single sideband mixer, and baseband filters. As a result, its functionality is essentially equivalent to that of the BBC including flexible setting of the center frequencies and bandwidths of the channels. If flexibility is an issue or if only a comparatively few channels are required, this approach is preferred.

The second method for channelization is conceptually a digital filter bank [3]. It involves the use of a Polyphase Filter (PPF) followed by a Fast Fourier Transform (FFT). Over the years, extremely efficient algorithms have been developed to carry out these functions. However, this method is considerably less flexible as it forces all channels to be contiguous and to have the same bandwidth. If flexibility is not an issue and a comparatively large number of channels is required,

this approach is preferred. It is the one selected for VLBI2010.

In order for the filter bank method to work effectively in the presence of RFI, it is necessary that there be adequate isolation between channels. In other words, if there is strong RFI in one channel, it is important that very little of the RFI leaks into its neighboring channels. This ensures that narrow band RFI will not degrade or destroy more than a single channel at a time. As it turns out, isolation as high as 60 dB between adjacent channels is routinely achieved with commonly used highly efficient PPF/FFT algorithms [3].

Another choice in the definition of the filter bank that is influenced by RFI is the channel bandwidth. If there is a lot of RFI in a given spectral region as happens for example in S-band, narrower bandwidth channels make it possible to acquire good data in the spaces between the RFI. Recall that any significant RFI in a given channel destroys the whole channel and not just the spectral region in which the RFI occurs. At the VLBI2010 Workshop on Future Radio Frequencies and Feeds (FRFF) in March 2009, Roberto Ambrosini presented a sample spectrum of RFI taken at the IVS Network Station Medicina [1]. Assuming a 1-GHz VLBI2010 band centered on 2.5 GHz, a simple analysis of this sample spectrum [2] found that the amount of usable spectrum increased by nearly a factor of two from just over 400 MHz to just under 800 MHz when the channel bandwidth was decreased from 32 to 2 MHz.

5. RFI in the 2-14 GHz Range

The entire radio spectrum from 2-14 GHz is allocated to one application or another. In the frequency range from 2.2-3.0 GHz, the U.S. regulations show over 70 separate allocations. Due to the distribution and operating modes of emitters, the RFI environment varies significantly from location to location and from time to time.

In many ways, urban areas, due to their greater population density, provide a more congested RFI environment. However, rural areas have their own challenges. In these areas, the laying of cables for communication and broadcast purposes is less cost effective and is often replaced by the use of airwaves. In addition, transportation routes through urban, rural, and remote areas, whether by land, sea, or air, all suffer from RFI related to the need for long-range mobile communications, radio-navigation, radiolocation, and weather surveillance. For the same reasons, airports, seaports, and military installations represent heavy concentrations of RFI emitters, both mobile and fixed.

It is recommended that site selection criterion for new VLBI2010 sites include a thorough RFI evaluation. It is further recommended that all VLBI sites make themselves and their spectrum needs known to local regulators so that appropriate considerations can be applied when applications for new emitters are processed.

There is one class of RFI emitters with nearly equal impact at all locations, those being space based emitters. Of particular concern are the emissions from geostationary Direct Broadcast Satellites (DBS) in the broad frequency ranges of 3.7–4.2 GHz (C-band) and 10.7–12.75 GHz (Ku-band). There are literally hundreds of DBSs (e.g., <http://www.geo-orbit.org>) in orbit, all at roughly 36,000 km altitude and directly above the equator. Signals are radiated into spot beams of varying sizes and the EIRP for the transmissions can range from below 40 dBW up to about 56 dBW. At these power levels, the DBS broadcasts cause no problems for VLBI2010 when received into the backlobes and far sidelobes of the VLBI antenna. However, when the VLBI antenna points within about 10 degrees of a satellite the received RFI begins to add noticeably to the system noise levels. Of course, the pointing distance from the satellite where this begins to be

a problem depends on the exact power of the transmitter and the orientation of the spot beam. Given the large number of DBS satellites this could in fact represent the loss of a significant area of sky at many locations. Fortunately, the VLBI2010 frequency sequences have significant resilience against a single weaker channel. When this is coupled with judicious scheduling enhancements, it is likely that the 10.7 to 12.75 GHz region of the spectrum will be usable by VLBI2010.

Two final RFI sources should at least be mentioned. These are directly related to space geodesy and are potentially an issue if VLBI is to operate optimally at multi-technique sites that are the foundation of the International Association of Geodesy's (IAG's) Global Geodetic Observing System (GGOS). They are the DORIS beacon and the Satellite Laser Ranging (SLR) aircraft avoidance radar. The DORIS frequency is at about 2 GHz with a transmit power of about 9.5 W into an omnidirectional antenna, and the SLR radar frequency is at about 9.3 GHz with a transmit power of about 1 KW into a parabolic antenna. These are both fairly powerful transmitters. If it is desired that all three techniques (DORIS, VLBI, and SLR) operate simultaneously in close proximity (i.e., within a few hundred meters of each other), preliminary calculations indicate that it would be prudent to erect simple signal deflectors or absorbers to attenuate the DORIS and SLR radar signals on the line-of-site to the VLBI2010 antenna.

6. Acknowledgements

Most results in this paper are based on an IVS memo currently in preparation [2].

References

- [1] Ambrosini, R., A spectral management view about VLBI2010: the CRAF experience, From: VLBI2010 Workshop on Future Radio Frequencies and Feeds (FRFF), Wetzell, Germany, March 18-21, 2009.
- [2] Petrachenko, B., Impact of radio frequency interference (RFI) on the VLBI2010 system, IVS memo in preparation, 2010.
- [3] Rogers, A.E.E., H.F. Hinteregger, Real to real polyphase filter bank, Mark 5 memo #18, 2004.

E-control: First Public Release of Remote Control Software for VLBI Telescopes

Alexander Neidhardt ¹, Martin Ettl ¹, Helge Rottmann ², Christian Plötz ³,
Matthias Mühlbauer ³, Hayo Hase ³, Walter Alef ², Sergio Sobarzo ⁴, Cristian Herrera ⁴,
Ed Himwich ⁵

¹) *Forschungseinrichtung Satellitengeodäsie, TU München, Geodätisches Observatorium Wettzell*

²) *Max-Planck-Institut für Radioastronomie*

³) *Bundesamt für Kartographie und Geodäsie, Geodätisches Observatorium Wettzell*

⁴) *Universidad de Concepción*

⁵) *NVI, Inc., National Aeronautics and Space Administration, Goddard Space Flight Center (NASA/GSFC)*

Contact author: Alexander Neidhardt, e-mail: neidhardt@fs.wettzell.de

Abstract

Automating and remotely controlling observations are important for future operations in a Global Geodetic Observing System (GGOS). At the Geodetic Observatory Wettzell, in cooperation with the Max-Planck-Institute for Radio Astronomy in Bonn, a software extension to the existing NASA Field System has been developed for remote control. It uses the principle of a remotely accessible, autonomous process cell as a server extension for the Field System. The communication is realized for low transfer rates using Remote Procedure Calls (RPC). It uses generative programming with the interface software generator “idl2rpc.pl” developed at Wettzell. The user interacts with this system over a modern graphical user interface created with wxWidgets. For security reasons the communication is automatically tunneled through a Secure Shell (SSH) session to the telescope. There are already successful test observations with the telescopes at O’Higgins, Concepción, and Wettzell. At Wettzell the software is already used routinely for weekend observations. Therefore the first public release of the software is now available, which will also be useful for other telescopes.

1. Introduction

The future Global Geodetic Observing System aims at 40 globally distributed VLBI sites in the station network with two telescopes at each site in the best case scenario. These new VLBI2010 antennas should be distributed more regularly over the surface of the earth [5]. Some of these telescopes may be in remote locations and have limited staff, such as the current O’Higgins station. Therefore a method for remote control of existing sites was developed as an extension to the NASA Field System, which is currently used to control the equipment. The already existing tools for forward mouse, keyboard, and video signals are suboptimal, because they do not allow monitoring of the Internet connection itself to facilitate safety actions. The new software offers this Ethernet-based, safe, and stable remote communication. Since most of the new devices controlled by the Field System are also connected via Ethernet, the new concept also includes ideas to standardize such individual communication needs. This combination offers the appropriate elements for remote control as a new VLBI observing mode, named “e-control”, which fits into the new observing strategies proposed in the VLBI2010 vision paper [3].

2. The Communication over Ethernet with Remote Procedure Calls

The communication in current communication systems over the Ethernet is usually a request and character-based (ASCII) client-server model. This means a service-requesting client starts the communication and sends an order request via message communication to a remote-service-offering server. On the server side the order is processed, and an answer message is returned to the client [6]. In classic communication networks each client-server-interaction is programmed individually during the software development process with the standard protocol stacks of either the Transmission Control Protocol over Internet Protocol (TCP/IP) or the User Datagram Protocol over Internet Protocol (UDP/IP). This proprietary approach makes it more difficult to set up a remote control and to include or adapt new properties of remotely usable devices.

A more modern attempt reduces the efforts of communication programming by defining a standardized way for the transmission of remote procedure calls (RPC). RPCs are comparable to local calls of procedures (functions) in a structured program, but are realized as standardized control and data flows over a communication network. The client calls a procedure or function without the concrete knowledge of the processing location. An additional RPC communication layer offers the transfer between the client and the remote processing server. The derived answer follows the same way but reversed to the client. This makes the procedure call seem local to the client. In the given context the Open Network Computing Remote Procedure Call (ONC RPC) is a preferred communication technique, because it is a standard part of each Linux Operating System and has been well tested since 1988. It also includes the platform-independent conversion of procedure parameter data using the External Data Representation (XDR) [8].

To reduce the programming effort, the communication layer can be created by using the generator utility “rpcgen”. This utility is available in each Linux system. It creates a low-level client-server communication based on ONC RPC. For sophisticated remote control implementations, higher level techniques are necessary, such as connection monitoring on client and server side and safety concepts. They realize stable states for the hardware even when the communication is broken. These higher level add-ons are used as middleware between the operating system and the application.

3. The Middleware Generator “Idl2rpc.Pl” and the Resulting e-control Stack

Common middleware systems extend the described communication with the needed higher level concepts and with advanced services. However these realizations are offered as huge, bulky, and abstract packages. The offered releases are correlated with operating system versions and are often commercial products. Additionally, they are not always flexible enough to be used in heterogeneous networks with different security guidelines and firewall implementations because of the additional proprietary protocol layers [1].

In order to deal with these issues a new middleware generator “idl2rpc.pl” was designed. This generator is just a single Perl script which uses only the ONC RPC realizations of standard Linux distributions. It extends “rpcgen” and reads a dedicated interface definition file to create several C++ adaptor classes for the C-coded RPC communication. They can directly be used in the application code. Dedicated modules offer threads to realize parallel tasks with semaphores to protect critical sections. A sophisticated communication control mechanism, such as a watchdog process, which always restarts the server after an unexpected crash, extends the stability. An Au-

automatic Safety Device (ASD) controls the existence of a responsible client and forces safety actions when the connection to the client breaks down. It is open source code, and no additional, external packages are needed [2]. The basic usage of TCP/IP and UDP/IP without additional, proprietary layers allows the generated communication to easily tunnel firewall barriers using a Secure Shell (SSH). Therefore an additional program, the “sshbroker”, is added to automatically control and monitor the SSH-connection to the VLBI systems or entire observatories. This helps to develop autonomous, distributed systems, consisting of several independent computers (processors), which are connected together to solve a collective task in a cooperative way [4].

Each hardware device can be represented as an individually programmed server which is autonomous in controlling the hardware and accessible via a generated idl2rpc communication. Higher level servers can contain several client modules to access and autonomously control different, subordinated device servers. The higher level combined servers themselves also offer services on a generated idl2rpc communication. The server accessing data on one platform can be found via registrations at a “portmapper”, where all services and their ports are registered. It is also possible to directly contact the servers on their dedicated communication ports. In summary, a hierarchical architecture is realized which establishes hierarchical and autonomous control zones. On the top level of this hierarchy a user interface allows human interaction.

For e-control the resulting communication stack is shown in Figure 1. One of the main drivers in the given design is a strict separation of control, communication, and presentation logic. The complete arithmetic and workflow control logic reside in the server, defined as device control code. It is an autonomous working process which interacts with the remote controlled device (in the case at hand, the FS). The communication code independently connects the server to the outer world for requesting clients which can also be realized over the mentioned SSH tunnels with the “sshbroker”. The clients are only used to realize a user interface with a presentation of the server-processed elements.

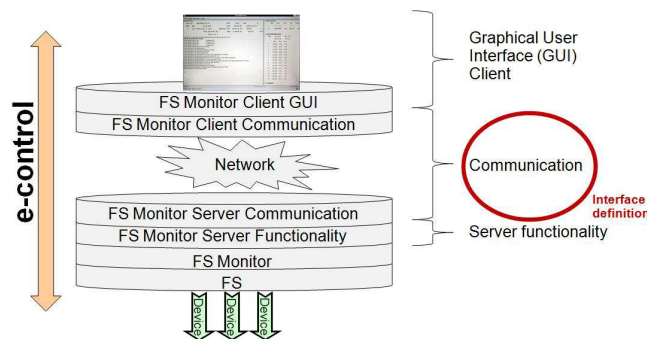


Figure 1. The communication stack of e-control.

4. The Features of the New Remote Control Software

It is helpful to provide a graphical user interface. For the described FS extension, wxWidgets is the preferred way to do this. It is a C++ based open source framework for platform-independent developments of graphical user interfaces [7]. Although the current RPC generator only supports Linux systems (32 and 64 Bit), the graphical user interface is modular enough to support different

platforms such as Windows, Linux, OSX, and others. In terms of the proposed FS extension a new graphical user interface was created using the wxWidgets framework for its realization (see Fig. 2). To keep usage similar, the display elements are organized to be like those of the current local interface for the FS. In addition a more graphical-oriented version can be chosen during runtime. The example in Figure 2 shows a realization with pie charts and line plots to present Mark 5 information and system temperatures over time.

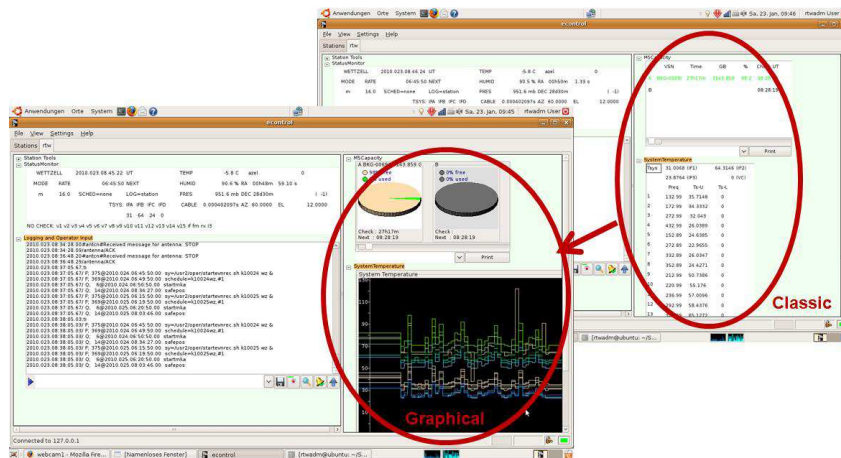


Figure 2. The new style of remote operator interaction with the NASA field system.

The entire interface is configurable during runtime, which allows switching between different telescope locations on-the-fly, just by reading a new configuration file. No additional software is needed, except the standard SSH client which is automatically controlled via different “sshbrokers”. The behavior of these “sshbrokers” can be set in the configuration mask, where also all of the other relevant configuration file parameters can be set. This is how the automated SSH-control and communication monitoring with re-establishment can be defined.

In addition to the standard behavior of the well-known FS windows, some additional features were added. This includes the implementation of a more sophisticated logging-command tool. With it, the operator can see the progress in the log-file and can enter FS commands. In addition, the user can also perform a search. This will open additional log tabs to present only lines where the defined search tag is found. It offers the ability to print only the error lines or especially interesting monitoring values such as the cryogenic parameters. The log output can be dumped into a local file copy. Furthermore it is also possible to generate acoustic “BEEP” signals for each error log via standard audio card.

To avoid a separate handling of the connection to a remote system, e.g., for additional software as terminals, it is possible to define hot keys in the configuration section. They are linked with remote programs and open them via separated and “sshbroker” controlled windows. These hot keys can also be defined during runtime. To complete the basic setup of tools, a direct output for the phase calibration monitor (MonPCal) and a chat tool for the inter-operator communication has been added.

5. Conclusion

The new software offers possibilities for new observing modes in line with the VLBI2010 project [3]. It should become an official part of the NASA Field System software. Additionally, a current version can be downloaded from the newly installed software servers at the Technische Universität München. As shown during the live demonstration at the 5th IVS General Meeting, it is easy to use the software. At the moment there are test sites in Hobart, Tasmania (both 26-m and 12-m antennas); in Wettzell, Germany; in Concepción, Chile; and in O'Higgins, Antarctica. It is planned to run shared shifts between these telescopes. Additional tests are planned at Westford and Kokee Park. For future developments to increase the security of access, the development team is participating in the NEXPRES project, funded by the European Union. Furthermore a corresponding software for controlling satellite laser ranging systems at Wettzell Observatory is in the final stage of development.

In summary, these new developments support the ability to check system states remotely, even for very remote sites. They allow shared observations and tele-working sessions and can facilitate remote specialists in assisting the local operators. They can form the new observing strategies. For the highest reliability, all telescopes need to support remote connections. A highly educated local staff will continue to be needed for maintenance and on-call service to react to critical situations.

References

- [1] Neidhardt, A.: Verbesserung des Datenmanagements in inhomogenen Rechnernetzen geodätischer Messstationen auf der Basis von Middleware und Dateisystemen am Beispiel der Fundamentalstation Wettzell, Dissertation, Mitteilungen des Bundesamtes für Kartographie und Geodäsie, 37, Bonifatius GmbH, 2006.
- [2] Neidhardt, A.: Manual for the remote procedure call generator "idl2rpc.pl", Geodetic Observatory Wettzell, 2009.
- [3] Niell, A., Whitney, A., Petrachenko, B., Schlüter, W., Vandenberg, N., Hase, H., Koyama, Y., Ma, C., Schuh, H., Tuccari, G., VLBI2010: Current and Future Requirements for Geodetic VLBI Systems, In: IVS Annual Report 2005, NASA, Behrend, D., Baver, K., 13–40, 2006.
- [4] Puder, A.; Römer, K.: Middleware für verteilte Systeme, dpunkt-Verlag GmbH, 2001.
- [5] Rothacher, M., Beutler, G., Bosch, W., Donnellan, A., Gross, R., Hinderer, J., Ma, C., Pearlman, M., Plag, H.-P., Richter, B., Ries, J., Schuh, H., Seitz, F., Shum, C.K., Smith, D.; Thomas, M., Velacogna, E., Wahr, J., Willis, P., Woodworth, P., The future Global Geodetic Observing System (GGOS), In: The Global Geodetic Observing System. Meeting the Requirements of a Global Society on a Changing Planet in 2020, Springer-Verlag, Plag, H.-P., Pearlman, M. (eds.), 2009.
- [6] Singhal, M., Shivaratri, N.G., Advanced Concepts in Operating Systems, McGraw-Hill, 1994.
- [7] Smart, J., Hock, K., Csomor, S., Cross-Platform GUI Programming with wxWidgets, Prentice Hall International, 2005.
- [8] Stevens, R.W., Programmieren von UNIX-Netzen. Grundlagen, Programmierung, Anwendung, Prentice-Hall International, 1992.

The Wettzell System Monitoring Concept and First Realizations

Martin Ettl¹, Alexander Neidhardt¹, Matthias Mühlbauer², Christian Plötz²,
Christopher Beaudoin³

¹) *Forschungseinrichtung Satellitengeodäsie, TU München, Geodätisches Observatorium Wettzell*

²) *Bundesamt für Kartographie und Geodäsie, Geodätisches Observatorium Wettzell*

³) *MIT Haystack Observatory*

Contact author: Martin Ettl, e-mail: ettl@fs.wettzell.de

Abstract

Automated monitoring of operational system parameters for the geodetic space techniques is becoming more important in order to improve the geodetic data and to ensure the safety and stability of automatic and remote-controlled observations. Therefore, the Wettzell group has developed the system monitoring software, “SysMon”, which is based on a reliable, remotely-controllable hardware/software realization. A multi-layered data logging system based on a fanless, robust industrial PC with an internal database system is used to collect data from several external, serial, bus, or PCI-based sensors. The internal communication is realized with Remote Procedure Calls (RPC) and uses generative programming with the interface software generator “idl2rpc.pl” developed at Wettzell. Each data monitoring stream can be configured individually via configuration files to define the logging rates or analog-digital-conversion parameters. First realizations are currently installed at the new laser ranging system at Wettzell to address safety issues and at the VLBI station O’Higgins as a meteorological data logger. The system monitoring concept should be realized for the Wettzell radio telescope in the near future.

1. Introduction

Current developments in the Global Geodetic Observing System (GGOS) indicate that permanent monitoring systems (e.g., for the determination of local ties with sub-millimeter accuracy) are needed to achieve the positioning precision goals [7]. The wide range of additional system parameters proposed for the GGOS (e.g., antenna survey, temperature sensors and strain meters in the monument, or radio frequency interference (RFI) monitoring) will further enhance the accuracy of the geodetic solutions computed during the analysis process. Other developments show an increased request for highly automated observations, not only for VLBI but also for Satellite and Lunar Laser Ranging (SLR/LLR). New observing strategies allow remote-controlled sessions from all over the world such that the responsible operator is not required to be within the local vicinity of the controlled system [5]. Therefore, highly sophisticated control systems are needed to provide additional capabilities in order to evaluate the state of devices on which the system depends (e.g., power distributions, servos, meteorology, or cabin and rack temperatures). In addition to these aspects of the monitoring system, security and safety mechanisms must be realized so that human beings on site are protected during automated telescope movements.

To achieve all of these data monitoring, analysis, environmental control, and safety requirements, a group at the Geodetic Observatory Wettzell has designed a dedicated system monitoring concept (SysMon). The main items of this system are (1) monitoring of key system-behavioral data, (2) archiving these data according to the observation epoch, (3) visualization of these data

for user interpretation, and (4) prompt operator intervention based on the state of the data. The main drivers behind the SysMon concept are to enhance the operator's knowledge of the system's state as well as to understand the system's behavior during an observation so that this information may be incorporated into post-processing analysis.

2. Basic Ideas and Concept Details

The basic ideas for technical requirements within SysMon are:

- All hardware components are based on standard equipment and robust hardware.
- The SysMon architecture is based on a multi-layer approach. It decomposes the whole system into modules that can be handled easily.
- The system is not limited in the number and type of sensors.
- The standard PC should be passively cooled (fanless) and can work without actuators.
- A Linux operating system with minimal installation overhead is used.
- The SysMon software is based on Open-Source software and is itself Open-Source. It has no dependencies on proprietary solutions (as far as possible).
- The programming language is C/C++.
- The communication part is based on the idl2rpc generator [6].
- The design is vendor independent.

2.1. The Used Hardware Concept

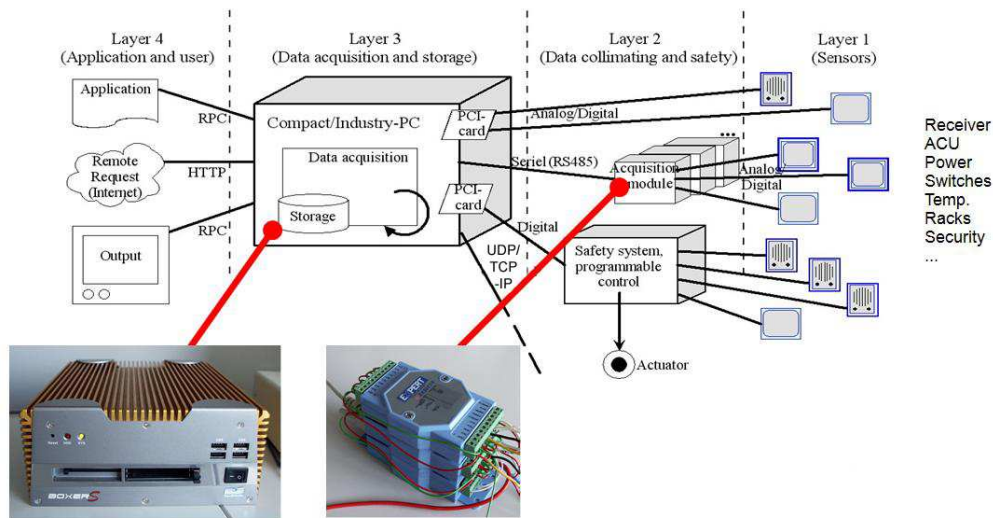


Figure 1. Basic concept with four layers and the according hardware components.

The whole system is decomposed into four layers for sensors, data collimating and safety, data acquisition and storage, and application and user interface (see Figure 1).

Layer one is responsible for the sensors, and only standard components are used. These sensors can be connected to an A/D-converter (analog-to-digital converter) card for a standard PC or via serial interface.

The second layer is optional and can be used to combine sensors with an additional micro-controller or a hardwired solution. Here fast logic decisions can be made in real-time, which are relevant for safety related activities, e.g., on critical interlock errors. Therefore programmable logic controllers or some low-level, proprietary systems can be implemented to protect humans.

The third layer is based on a standard fanless PC which incorporates a minimal (Debian) Linux-based operating system. These PCs are reliable and robust. In this layer, the data are recorded and high-level logic decisions can be made. Data collection from different devices is accomplished with “idl2rpc”-generated communications [6], which offers a low-level middleware based on Open Network Computing Remote Procedure Call (ONC RPC) [2]. The data recording itself is realized with SQLite¹ as a rudimentary database.

Layer four provides the data for visualization, user interaction, and higher-level automation logic. In order to visualize the data [4], a graphical user interface has been built upon the GUI-Framework wxWidgets² [8]. This layer can be designed individually and provides high flexibility for applications. Format converters can be realized as Web-based presentation applications for data recorded by the monitoring system. This layer can also be used for direct data requests made by analysts with remote access.

2.2. Software

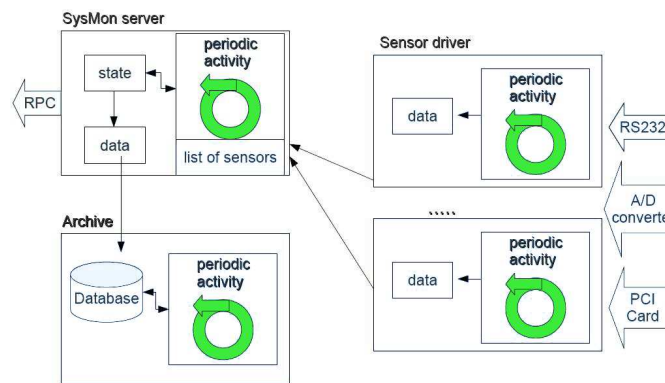


Figure 2. The processes of SysMon on the data acquisition PC.

The software architecture of SysMon (see Figure 2) is based on a client-server model and consists of two main layers. The first layer is built using servers as sensor drivers; these servers directly communicate with the sensor hardware. An internal independent thread reads data directly from the sensor hardware at regular intervals. If needed this layer can directly process low-level operations such as the inclusion of data time-stamps. A parallel thread within the sensor driver process is responsible for answering the asynchronous requests from external clients. The interaction of the external clients with the server is handled by a centralized main process, which

¹<http://www.sqlite.org/>

²<http://www.wxwidgets.org>

periodically requests data from each of the sensor servers. This process schedules the requests in an arrival-dependent fashion and transfers the received data in the order of their timestamps to a database server. This database is built on SQLite and stores the data values at time intervals which can be configured independently for each sensor.

The internal communication is generated with “idl2rpc” according to an interface description setup [6]. “idl2rpc” is a middleware generator developed at Wettzell on the basis of ONC RPC [2]. Using this generative programming technique with remote procedure calls, the software development process is simplified since the developers do not have to write their own communication software. Furthermore, a group of developers working on the same project can decompose the software into two units consisting of a client and a server part; the programming of these two modules can be done in parallel amongst the programmers.

All the software published by Wettzell is based on dedicated design rules, standardized by a committee of the observatory [1]. Static³ and dynamic⁴ code analysis tools are used to improve the reliability of the software.

3. First Realizations

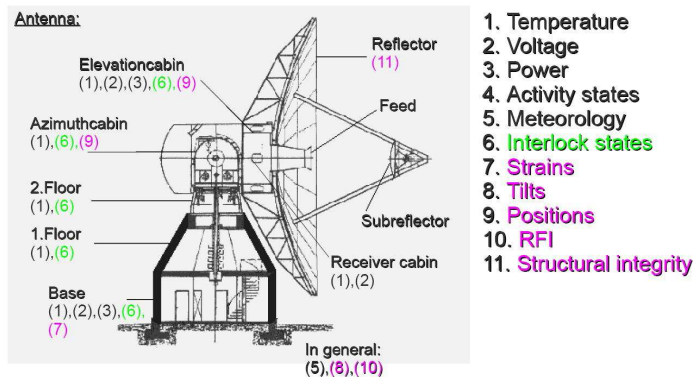


Figure 3. Possible sensor location and categories at the RTW.

As we have described, many of the observations at the radio telescope Wettzell are operated remotely or unattended. This capability has been made possible using a remote control extension to the NASA Field System. To improve safety and reliability during these observations, the first realization of the SysMon will incorporate additional sensors on the telescope (see Figure 3). In addition to these sensors, other analysis-type sensors will be incorporated in order to provide data to enhance the geodetic models. A case study about permanent measurement of the radio telescope’s reference point with an automated monitoring system was conducted by the University of Karlsruhe, Germany. It showed that changes in positions could be detected due to load changes or insolation (temperature changes). Therefore the reference point moves its position in both axes by about 0.2 mm over the period of one day [3]. In March 2010, a case study was initiated in which the sensor locations will be determined, e.g., according to useful support of geodetic and structural

³<http://sourceforge.net/apps/mediawiki/cppcheck>

⁴<http://valgrind.org/>

models and to acquire needed system parameters for automation. Constraints are the RFI behavior and keeping the sensor assembly minimally invasive. In this work, the first software and hardware components for the radio telescope will be developed based on the existing realizations.

Besides the developments and concepts for the RTW, SysMon is also implemented and installed at the new laser ranging system. At this site human safety is the main driver. Because the laser ranging system incorporates an active, non-eyesafe laser, special interlock detectors have been placed at the doors and windows. Additional sensors monitoring electrical power and temperatures in the hardware racks provide a better view of the system performance. A similar approach is under development for a meteorological system at the radio telescope O'Higgins, where the first sensors for wind parameters have already been realized.

4. Conclusion

The concept of SysMon is vendor and platform independent and very flexible and adaptable. It can be used for the different needs in VLBI and SLR as well as in other systems of the geodetic space techniques. Since standardized components (hardware/software) have been selected for the system, costs and development times are significantly reduced relative to those of a system comprised of custom-built hardware and non-standard software. Currently, there are several realizations at the Geodetic Observatory Wettzell and its affiliated sites. In addition to these sites, a cooperation for developing a monitoring standard was founded between the MIT Haystack Observatory and Wettzell during the IVS 2010 General Meeting. There is a close information exchange between these institutes and other related institutions within the VLBI2010 MCI Collaboration group.

References

- [1] Dassing, R., Lauber, P., Neidhardt, A., Design-Rules für die objektorientierte Programmierung in C++ und die strukturierte Programmierung in C, Fundamentalstation Wettzell, 2004.
- [2] Herlihy, M., The Art of Multiprocessor Programming, Morgan Kaufmann, 2008.
- [3] Loesler, M., Eschelbach, C., Schenk, A., Neidhardt, A., Permanentüberwachung des 20 m VLBI-Radioteleskops an der Fundamentalstation in Wettzell, ZfV, 1, 40–48, 2010.
- [4] Logan, S., Cross-Platform Development in C++-Building Mac OS-X, Linux and Windows Applications, Addison Wesley, 2008.
- [5] Neidhardt, A., Ettl, M., Zeitlhöfler, R., Plötz, C., Mühlbauer, M., Dassing, R., Hase, H., Sobarzo, S., Herrera, C., Alef, W., Rottmann, H., Himwich, E., A concept for remote control of VLBI-telescopes and first experiences at Wettzell, In: Proceedings of the 19th Working Meeting on European VLBI for Geodesy and Astrometry, Bourda, G., Charlot, P., Collioud, A. (eds.), 136–140, 2009.
- [6] Neidhardt, A.: Manual for the remote procedure call generator “idl2rpc.pl”, Geodetic Observatory Wettzell, 2009.
- [7] Rothacher, M., Beutler, G., Bosch, W., Donnellan, A., Gross, R., Hinderer, J., Ma, C., Pearlman, M., Plag, H.-P., Richter, B., Ries, J., Schuh, H., Seitz, F., Shum, C.K., Smith, D.; Thomas, M., Velocognia, E., Wahr, J., Willis, P., Woodworth, P., The future Global Geodetic Observing System (GGOS), In: The Global Geodetic Observing System. Meeting the Requirements of a Global Society on a Changing Planet in 2020, Springer-Verlag, Plag, H.-P., Pearlman, M. (eds.), 2009.
- [8] Smart, J., Cross-Platform GUI Programming with wxWidgets, Pearson Education, 2006.

Round-trip System Available to Measure Path Length Variation in Korea VLBI System for Geodesy

Hongjong Oh¹, Tetsuro Kondo², Jinoo Lee¹, Tuhwan Kim¹, Myungho Kim³,
Suchul Kim³, Jinsik Park³, Hyunhee Ju³

¹⁾ *Ajou University*

²⁾ *National Institute of Information and Communications Technology and Ajou University*

³⁾ *National Geographic Information Institute*

Contact author: Hongjong Oh, e-mail: stockoh@ajou.ac.kr

Abstract

The construction project of Korea Geodetic VLBI officially started in October 2008. The construction of all systems will be completed by the end of 2011. The project was named Korea VLBI system for Geodesy (KVG), and its main purpose is to maintain the Korea Geodetic Datum. In case of the KVG system, an observation room with an H-maser frequency standard is located in a building separated from the antenna by several tens of meters. Therefore KVG system will adopt a so-called round-trip system to transmit reference signals to the antenna with reduction of the effect of path length variations. KVG's round-trip system is designed not only to use either metal or optical fiber cables, but also to measure path length variations directly. We present this unique round trip system for KVG.

1. Introduction

The round-trip system used in the frequency distribution system is a system to transmit a reference frequency signal to a remote place separated by a few tens to hundreds of meters from a signal source such as an H-maser frequency standard while diminishing the effect caused by the change of transmission cable length. The reference frequency distribution system supplies reference frequency (10 MHz or 100 MHz) and timing signals (1 PPS) generated by the H-maser frequency standard to devices that require these reference signals. Such devices are located not only in the observation room close to the H-maser frequency standard, but also in the receiver cabin of the antenna separated from the observation building by several tens to hundreds of meters. Therefore, a system is needed to transmit reference signals to the receiver cabin in a stable manner. Buried cables or fibers at a depth of 1–2 m offer the greatest stability of the transmission path to the antenna. Path length variations are directly related to the accuracy of geodetic VLBI measurements, so they should be kept as small as possible. The effect of these path length variations can be diminished by using a round-trip system as a reference frequency transmitting system.

2. Principle of Round-trip System

Figure 1 shows a schematic block diagram of a round-trip system. The system consists of a reference signal generator, an oscillator, and transmission cables (metal co-axial cable).

A signal with a frequency of $f_0 (= f_1 + f_2)$ is generated by H-maser frequency standard and put into the system at A. The signal is mixed with signal f_2 transmitted from B to form signal

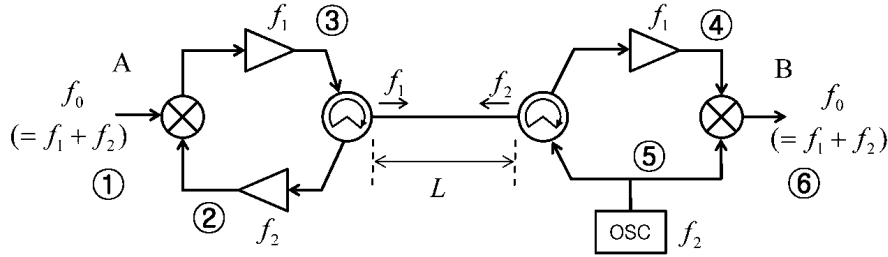


Figure 1. Schematic block diagram of a round-trip system.

f_1 . This signal is transmitted to B. At B, signal f_1 is mixed with signal f_2 , which is a locally generated signal, to form the sum frequency $f_1 + f_2 (= f_0)$. This is a reference signal transmitted to B. Signal f_2 is also transmitted to A.

The principle of operation can be expressed as follows. Signal at ① can be expressed as

$$S_1 = (\sin 2\pi(f_1 + f_2)t + \phi_0) \quad (1)$$

$$S_5 = \sin(2\pi f_2 t + \phi_{osc}) \quad (2)$$

therefore signal at ② is given by

$$S_2 = \sin\left(2\pi f_2\left(t - \frac{L}{v}\right) + \phi_{osc}\right) \quad (3)$$

where v is the velocity of signal transmission in a cable. Signal at ③ is a low-pass filtered signal of products of S_1 and S_2 , which is

$$S_1 \cdot S_2 = (\sin 2\pi(f_1 + f_2)t + \phi_0) \cdot \left(\sin\left(2\pi f_2\left(t - \frac{L}{v}\right) + \phi_{osc}\right)\right) \quad (4)$$

Hence

$$S_3 = \frac{1}{2} \cos\left(2\pi f_1 t + 2\pi f_2 \frac{L}{v} + \phi_0 - \phi_{osc}\right) \quad (5)$$

Therefore signal at ④, is given as

$$S_4 = \frac{1}{2} \cos\left(2\pi f_1\left(t - \frac{L}{v}\right) + 2\pi f_2 \frac{L}{v} + \phi_0 - \phi_{osc}\right) \quad (6)$$

Signal at ⑥ is a high-pass filtered signal of products of S_4 and S_5 .

$$S_4 \cdot S_5 = \frac{1}{2} \cos\left(2\pi f_1\left(t - \frac{L}{v}\right) + 2\pi f_2 \frac{L}{v} + \phi_0 - \phi_{osc}\right) \cdot \sin(2\pi f_2 t + \phi_{osc}) \quad (7)$$

$$S_6 = \frac{1}{4} \sin\left(2\pi(f_1 + f_2)t + \phi_0 - 2\pi(f_1 - f_2)\frac{L}{v}\right) \quad (8)$$

Note that the phase of an oscillator does not appear in the output. We focus on two components, which are frequency and length of cables. The phase difference between signals A and B is given by comparing Eq (1) and (9) as

$$\phi = 2\pi(f_1 - f_2)\frac{L}{v} \quad (9)$$

Hence the change of cable length from L to $L + \Delta L$ results in the change of phase as follows,

$$\Delta\phi = 2\pi(f_1 - f_2)\frac{\Delta L}{v} \quad (10)$$

When a signal is transmitted directly at $f_0 = f_1 + f_2$, the phase change due to cable length change is given by

$$\Delta\phi = 2\pi(f_1 + f_2)\frac{\Delta L}{v} \quad (11)$$

Therefore phase variation due to the cable length change can be suppressed to the level of $(f_1 - f_2)/(f_1 + f_2)$ compared with the case of that signal being directly transmitted at a frequency $f_0 (= f_1 + f_2)$. The round-trip system developed for the VERA project, which is the Japanese VLBI project dedicated to astrometry, adopts $f_1 = 690\text{MHz}$, $f_2 = 710\text{MHz}$ (i.e., f_0 is 1400 MHz). In this case the change of phase is suppressed by $|690 - 710|/1400 = 0.014$. Phase variation is suppressed about 1% level compared with the case of direct transmission.

3. Detection of Phase Variation

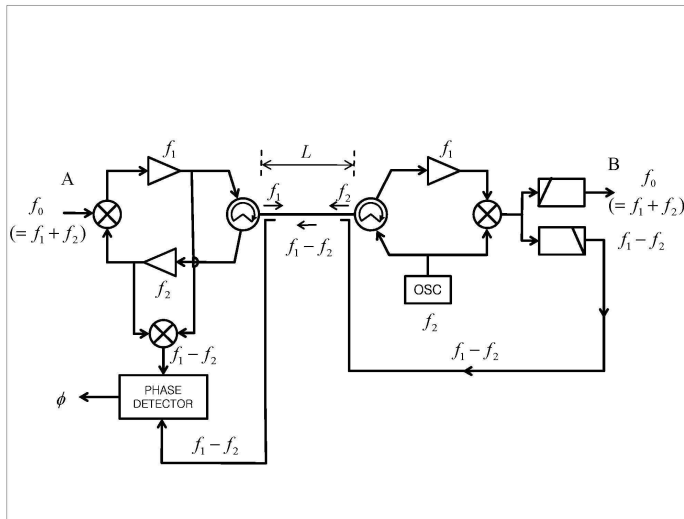


Figure 2. Schematic block diagram of round-trip system designed for measurement of phase variation.

A round-trip system as described in Section 2 is the system dedicated to suppress phase variation due to cable length change as much as possible. Therefore it does not intend to measure the phase variation itself.

In order to monitor phase change directly, we consider the system shown in Figure 2. At side B, signal $f_1 - f_2$ is generated. This signal is a low-pass filtered signal of products of S_4 and S_5 in the previous section (in this section written as S_{45L}).

$$S_{45L} = -\frac{1}{4}\sin(2\pi(f_1 - f_2)t - 2\pi(f_1 - f_2)\frac{L}{v} + \phi_0 - \phi_{osc}) \quad (12)$$

This signal is injected to a metal cable through a directional-coupler then transmitted to A. $S_{45L(A)}$ thus becomes

$$S_{45L(A)} = -\frac{1}{4}\sin(2\pi(f_1 - f_2)t - 2 \cdot 2\pi(f_1 - f_2)\frac{L}{v} + \phi_0 - 2\phi_{osc}) \quad (13)$$

At side A, the same frequency signal is generated independently of S_2 and S_3 in the previous section. The signal is a low-pass filtered signal of the product of S_2 and S_3 . Therefore it is expressed as follows,

$$S_{23L(A)} = -\frac{1}{4}\sin(2\pi f_1 - f_2 t + 2 \cdot 2\pi f_2 \frac{L}{v} + \phi_0 - 2\phi_{osc}) \quad (14)$$

Hence the phase difference between S_{23L} and $S_{45L(A)}$ is given by

$$\phi = 2 \cdot 2\pi f_1 \frac{L}{v} \quad (15)$$

Therefore the change of cable length from L to $L + \Delta L$ results in the change of phase as follows,

$$\Delta\phi = 2 \cdot 2\pi f_1 \frac{\Delta L}{v} \quad (16)$$

This corresponds to the double of phase change at frequency. In the case of VERA, the frequency was set to $f_1 = 690MHz$, $f_2 = 710MHz$, and $f_1 - f_2 = 20MHz$. In the case of KVG, it was set to $f_1 = 689.9MHz$, $f_2 = 710.1MHz$, and $f_1 - f_2 = 20.2MHz$. This frequency signal can be sampled by using the K5/VSSP32 VLBI sampler, which has a maximum sampling frequency of 64 MHz. We will reduce the sampling frequency; we can use 2 MHz, 1 MHz, and even 500 kHz as a sampling frequency. So that phase can be monitored digitally by using this sampler.

4. Application to KVG System

In the KVG system, we develop a round-trip system that can use both metal cable and optical fiber (not simultaneously but exclusively). Our plan is that the manufacturing will be finished in June 2010 and that we will proceed with testing in July. Figure 4 shows block diagrams of the transmitter and the receiver of the round-trip system under consideration.

References

- [1] Tetsuro Kondo, Conceptual Design of Backend System and Ground Surveying System for Korea VLBI System for Geodesy (KVG), Ajou University, 2009.
- [2] Tetsuro Kondo, Round trip system, KVG technical report, 2010.

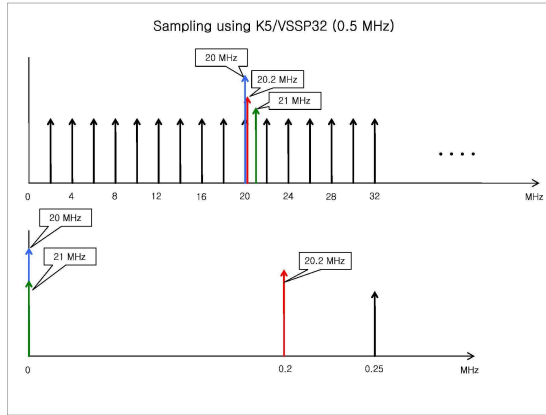


Figure 3. Sampling using K5/VSSP32(0.5 MHz).

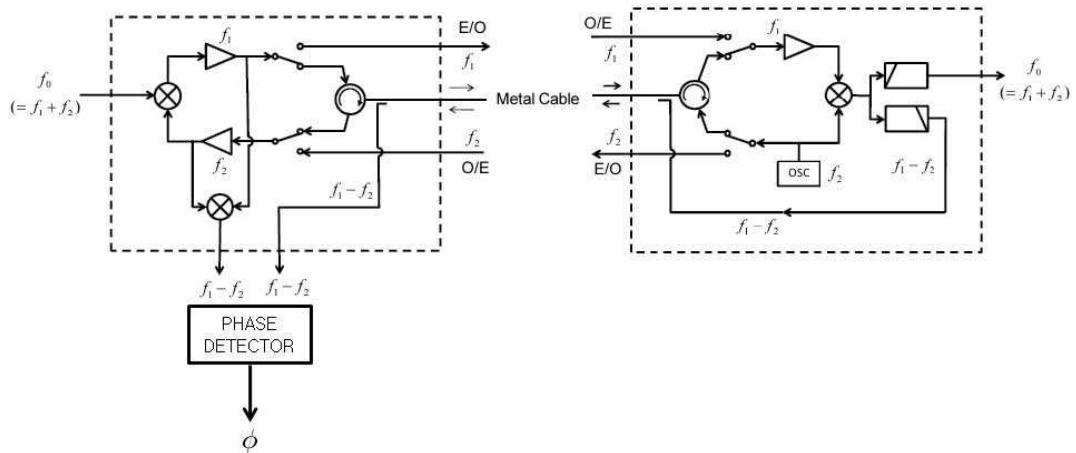


Figure 4. Round-trip system for KVG.



About the Meeting

Registered Participants

Name	Institution	Country	E-mail
Artz, Thomas	University of Bonn	Germany	thomas.artz@uni-bonn.de
Beaudoin, Christopher	MIT Haystack Observatory	USA	cbeaudoin@haystack.mit.edu
Behrend, Dirk	NVI, Inc./NASA GSFC	USA	Dirk.Behrend@nasa.gov
Bignall, Hayley	ICRAR/CIRA	Australia	hayley.bignall@icrar.org
Böckmann, Sarah	University of Bonn	Germany	boeckmann@uni-bonn.de
Böhm, Johannes	IGG Vienna	Austria	johannes.boehm@tuwien.ac.at
Bolotin, Sergei	NVI, Inc./NASA GSFC	USA	sergei.bolotin@nasa.gov
Botai, Ondego Joel	University of Pretoria	South Africa	joel.botai@up.ac.za
Bourda, Geraldine	Bordeaux Observatory	France	geraldine.bourda@obs.u-bordeaux1.fr
Cappallo, Roger	MIT Haystack Observatory	USA	rcappallo@haystack.mit.edu
Charlot, Patrick	Bordeaux Observatory	France	charlot@obs.u-bordeaux1.fr
Cho, Jungho	KASI	South Korea	jojh@kasi.re.kr
Collioud, Arnaud	Bordeaux Observatory	France	Arnaud.Collioud@obs.u-bordeaux1.fr
Colomer, Francisco	IGN Spain	Spain	f.colomer@oan.es
Colucci, Giuseppe	CGS/e-GEOS	Italy	giuseppe.colucci@e-geos.it
Corey, Brian	MIT Haystack Observatory	USA	bcorey@haystack.mit.edu
Curtis, Ron	Honeywell TSI	USA	Ronald.Curtis@Honeywell.com
Dickey, John	University of Tasmania	Australia	john.dickey@utas.edu.au
Dodson, Richard	ICRAR/UWA	Australia	richard.dodson@uwa.edu.au
Ellingsen, Simon	UTAS	Australia	Simon.Ellingsen@utas.edu.au
Engelhardt, Gerald	BKG Leipzig	Germany	gerald.engelhardt@bkg.bund.de
Ettl, Martin	FESG Wettzell	Germany	ettl@fs.wettzell.de
Fey, Alan	U.S. Naval Observatory	USA	afey@usno.navy.mil
Fomalont, Ed	NRAO	USA	efomalon@nrao.edu
García-Espada, Susana	IGN Spain	Spain	s.gespada@oan.es
Gaume, Ralph	U.S. Naval Observatory	USA	rgaume@usno.navy.mil
Gipson, John	NVI, Inc./NASA GSFC	USA	john.m.gipson@nasa.gov

Name	Institution	Country	E-mail
Gómez-González, Jesús	IGN Spain	Spain	jggonzalez@fomento.es
Gordon, David	NVI, Inc./NASA GSFC	USA	david.gordon-1@nasa.gov
Gulyaev, Sergei	AUT	New Zealand	sergei.gulyaev@aut.ac.nz
Guo, Li	SHAO	China	kent-gl@shao.ac.cn
Gurvits, Leonid	JIVE	The Netherlands	lgurvits@jive.nl
Haas, Rüdiger	Onsala Space Observatory	Sweden	rudiger.haas@chalmers.se
Hase, Hayo	BKG Concepción	Germany/Chile	hayo.hase@bkg.bund.de
Heinkelmann, Robert	DGFI	Germany	heinkelmann@dgfi.badw.de
Hoban, Timothy	UTAS	Australia	timothy.hoban@utas.edu.au
Hobiger, Thomas	NICT	Japan	hobiger@nict.go.jp
Horiuchi, Shinji	CDS/CC Canberra	Australia	shoriuchi@cdscc.nasa.gov
Ichikawa, Ryuichi	NICT	Japan	richi@nict.go.jp
Ipatov, Alexander	IAA RAS	Russia	ipatov@ipa.nw.ru
Ishii, Atsutoshi	NICT	Japan	ishii@nict.go.jp
Iwata, Takahiro	ISAS/JAXA	Japan	iwata.takahiro@jaxa.jp
Jacobs, Christopher	JPL	USA	christopher.s.jacobs@nasa.gov
Ju, Hyun-Hee	NGII Korea	South Korea	hee919@korea.kr
Kierulf, Halfdan Pascal	NMA	Norway	halfdan.kierulf@statkart.no
Kijima, Masachika	Sokendai Graduate University	Japan	masachika.kijima@nao.ac.jp
Kim, Myungho	NGII Korea	South Korea	myungho.kim@korea.kr
Kingham, Kerry	U.S. Naval Observatory	USA	kingham.kerry@usno.navy.mil
Kwak, Younghee	Ajou University/KASI	South Korea	bgirl02@kasi.re.kr
Langkaas, Line	NMA	Norway	Line.Langkaas@statkart.no
Le Bail, Karine	NVI, Inc./NASA GSFC	USA	karine.lebail@nasa.gov
Lee, Jinoo	Ajou University	South Korea	jinoolee@ajou.ac.kr
Liu, Li	SHAO	China	liuli@shao.ac.cn
Lovell, Jim	UTAS	Australia	jim.lovell@utas.edu.au
Ma, Chopo	NASA GSFC	USA	chopo.ma@nasa.gov

Name	Institution	Country	E-mail
MacMillan, Daniel	NVI, Inc./NASA GSFC	USA	daniel.s.macmillan@nasa.gov
Manabe, Seiji	NAOJ	Japan	manabe@miz.nao.ac.jp
Matsumoto, Koji	NAOJ	Japan	matsumoto@miz.nao.ac.jp
Matsuzaka, Shigeru	GSI	Japan	shigeru@gsi.go.jp
McCallum, Jamie	UTAS	Australia	Jamie.McCallum@utas.edu.au
McCulloch, Peter	UTAS	Australia	Peter.McCulloch@utas.edu.au
Natusch, Tim	AUT	New Zealand	tim.natusch@aut.ac.nz
Neidhardt, Alexander	FESG Wettzell	Germany	neidhardt@fs.wettzell.de
Niell, Arthur	MIT Haystack Observatory	USA	aniell@haystack.mit.edu
Nothnagel, Axel	University of Bonn	Germany	nothnagel@uni-bonn.de
Oh, Hongjong	Ajou University	South Korea	stockoh@ajou.ac.kr
Opseth, Per Erik	NMA	Norway	Per.Erik.Opseth@statkart.no
Petrachenko, Bill	NRCan	Canada	Bill.Petrachenko@nrc-cnrc.gc.ca
Phillips, Christopher	CSIRO-ATNF	Australia	Chris.Phillips@csiro.au
Plank, Lucia	IGG Vienna	Austria	lucia.plank@tuwien.ac.at
Poirier, Mike	MIT Haystack Observatory	USA	mpoirier@haystack.mit.edu
Porcas, Richard	MPIfR Bonn	Germany	porcas@mpifr-bonn.mpg.de
Poutanen, Markku	FGI	Finland	Markku.Poutanen@fgi.fi
Reid, Brett	UTAS	Australia	Brett.Reid@utas.edu.au
Reynolds, Cormac	ICRAR	Australia	c.reynolds@curtin.edu.au
Rioja, Maria	UWA Australia	Australia	maria.rioja@uwa.edu.au
Schuh, Harald	IGG Vienna	Austria	harald.schuh@tuwien.ac.at
Shield, Peter	Cobham InterTronic	Canada	pshield@intertronicsolutions.com
Shu, Fengchun	SHAO	China	sfc@shao.ac.cn
Spicakova, Hana	IGG Vienna	Austria	hana@mars.hg.tuwien.ac.at
Strand, Rich	NVI, Inc./NASA GSFC	USA	kl7ra@ptialaska.net
Takashima, Kazuhiro	GSI	Japan	takasima@gsi.go.jp
Takefuji, Kazuhiro	NICT	Japan	takefuji@nict.go.jp

Name	Institution	Country	E-mail
Thomas, Cynthia	NVI, Inc./NASA GSFC	USA	cynthia.c.thomas@nasa.gov
Thornton, Bruce	NVI, Inc./USNO	USA	thornton.bruce@usno.navy.mil
Tingay, Steven	ICRAR	Australia	Steven.Tingay@icrar.org
Titov, Oleg	Geoscience Australia	Australia	Oleg.Titov@ga.gov.au
Tornatore, Vincenza	Politecnico di Milano	Italy	vincenza.tornatore@polimi.it
Tzioumis, Tasso	CSIRO-ATNF	Australia	Tasso.Tzioumis@csiro.au
Wang, Guangli	SHAO	China	wgl@shao.ac.cn
Watson, Christopher	UTAS	Australia	Christopher.Watson@utas.edu.au
Whitney, Alan	MIT Haystack Observatory	USA	awhitney@haystack.mit.edu
Wright, Jill	InterTronic Solutions Inc.	Canada	jwright@intertronicsolutions.com
Xu, Zhijun	SHAO	China	xuthus@shao.ac.cn
Zhang, Xiuzhong	SHAO	China	xzhang@shao.ac.cn
Zharov, Vladimir	SAI MSU	Russia	zharov@sai.msu.ru
Zheng, Weimin	SHAO	China	zhwm@shao.ac.cn
Zhu, Renjie	SHAO	China	zhurj@shao.ac.cn

Sixth IVS General Meeting Hobart, Tasmania, Australia

PROGRAM

Sunday, February 7, 2010

14:00–18:00 Registration

Zero Penthouse at Zero Davey
(15 Hunter Street, Sullivans Cove, Hobart Waterfront)

16:00–18:00 Icebreaker Reception

Zero Penthouse at Zero Davey
(15 Hunter Street, Sullivans Cove, Hobart Waterfront)

Monday, February 8, 2010

Opening

08:30 Opening Ceremony

(1) Welcome by Prof. Margaret Britz, Dean of the Faculty of Science, Engineering and Technology
(2) Welcome by Harald Schuh, IVS Chair, and Chair's Report

Session 1: Realization and New Perspectives of VLBI2010

Chair: Bill Petrachenko

08:50 S1-T01 VLBI2010: An Overview

Bill Petrachenko (Natural Resources Canada)

09:05 S1-T02 VLBI2010: The Astro-Geo Connection (*invited*)

Richard Porcas (MPIfR Bonn)

09:30 S1-T03 Differences between VLBI2010 and S/X Hardware

Brian Corey (MIT Haystack Observatory)

09:45 S1-T04 The NASA VLBI2010 Proof-of-Concept Demonstration and Future Plans

Arthur Niell (MIT Haystack Observatory) and the Broadband Development Team

10:00 S1-T05 Differences between S/X and VLBI2010 Operations

Hayo Hase¹, Ed Himwich², Alexander Neidhardt³ (¹BKG, ²NVI, Inc./NASA GSFC, ³FESG Wetzell)

10:15 S1-T06 Post-Correlation Processing for the VLBI2010 Proof-of-Concept System

Christopher Beaudoin, Arthur Niell (MIT Haystack Observatory)

10:30 Coffee Break

Chair: Arthur Niell

11:00 S1-T07 GPU Based Software Correlators – Perspectives for VLBI2010

Thomas Hobiger¹, Moritaka Kimura¹, Kazuhiro Takefuji¹, Tomoaki Oyama², Yasuhiro Koyama¹, Tetsuro Kondo¹, Tadahiro Gotoh¹, Jun Amagai¹ (¹NICT Japan, ²NAOJ Japan)

11:15 S1-T08 VLBI2010 Imaging and Structure Corrections

Arnaud Collioud, Patrick Charlot (Laboratoire d'Astrophysique de Bordeaux)

11:30 S1-T09 The AuScope Project and Trans-Tasman VLBI

Jim Lovell¹, John Dickey¹, Sergei Gulyaev², Tim Natusch², Oleg Titov³, Steven Tingay⁴ (¹University of Tasmania, ²Auckland University of Technology, ³Geoscience Australia, ⁴Curtin University of Technology)

11:45 S1-T10 Current Status of the Development of a Transportable and Compact VLBI System by NICT and GSI

Atsutoshi Ishii^{1,2,4}, Ryuichi Ichikawa², Hiroshi Takiguchi², Kazuhiro Takefuji², Hideki Ujihara², Yasuhiro Koyama², Tetsuro Kondo^{2,3}, Shinobu Kurihara¹, Yuji Miura¹, Shigeru Matsuzaka¹, Daisuke Tanimoto^{1,4} (¹GSI Japan, ²NICT Japan, ³Ajou University, ⁴AES Co. Ltd.)

12:00 S1-T11 VLBI2020: From Reality to Vision

Oleg Titov (Geoscience Australia)

12:15 S1-T12 How and Why to Do VLBI on GNSS Spacecraft

John Dickey (University of Tasmania)

12:30 S1-T13 Planning of an Experiment for VLBI Tracking of GNSS Satellites

Vincenza Tornatore¹, Rüdiger Haas² (¹Politecnico di Milano, ²Chalmers University of Technology)

12:45 S1-T14 Multi-source Geodetic VLBI – A New Observing and Analysis Technique

Victus Uzodinma (University of Nigeria)

13:00 Lunch Break

Session 2: Network Stations, Operation Centers, Correlators

Chair: Kerry Kingham

14:00 S2-T01 An Introduction to SKED (*invited*)

John Gipson (NVI, Inc./NASA GSFC)

14:20 S2-T02 The State and Development Direction of the Geodetic VLBI Station in Korea (*invited*)

Hyunhee Ju¹, Myungho Kim¹, Suchul Kim¹, Jinsik Park¹, Tetsuro Kondo^{2,3}, Tuhwan Kim², Hongjong Oh², Sangoh Yi² (¹NGII Korea, ²Ajou University, ³NICT Japan)

14:45 S2-T03 RAEGE: An Atlantic Network of Geodynamical Fundamental Stations

Jesús Gómez-González¹, Francisco Colomer¹, José Antonio López-Fernández¹, Marlene Assis² (¹IGN Spain, ²SRCTE Portugal)

15:00 S2-T04 The New Generation Russian VLBI Network

Andrey Finkelstein, Alexander Ipatov, Sergey Smolentsev, Vyacheslav Mardyshkin, Leonid Fedotov, Igor Surkis, Dmitriy Ivanov, Iskandar Gayazov (Institute of Applied Astronomy)

15:15 S2-T05 Towards Establishing a Chinese Geodetic VLBI Observing System

Fengchun Shu¹, Weimin Zheng¹, Xiuzhong Zhang¹, Xiaoyu Hong¹, Aili Yusup², Ming Wang³ (¹Shanghai Astronomical Observatory, ²Urumqi Astronomical Observatory, ³Yunnan Astronomical Observatory)

15:30 S2-T06 Characterization and Calibration of the 12-m Antenna in Warkworth, New Zealand

Sergei Gulyaev, Tim Natusch (Auckland University of Technology)

15:45 S2-T07 COLD MAGICS – Continuous Local Deformation of an Arctic Geodetic Fundamental Station

Rüdiger Haas¹, Sten Bergstrand² (¹Chalmers University of Technology, ²SP Technical Research Institute)

Poster Session (Sessions 1–5) with coffee and refreshments

16:00-18:00 Core Poster Time for All Sessions

S1-P01...S1-P04, S2-P01...S2-P16, S3-P01...S3-P08, S4-P01...S4-P09, S5-P01...S5-P12

Tuesday, February 9, 2010

Session 2: Network Stations, Operation Centers, Correlators (cont'd)

Chair: Kazuhiro Takashima

08:30 S2-T08 Homologous Deformation of the Effelsberg 100-m Telescope Determined with a Total Station

Axel Nothnagel, Judith Pietzner, Christian Eling (University of Bonn)

08:45 S2-T09 Ultra-rapid dUT1 Experiments on Japan–Fennoscandian Baselines – Application to 24-hour Sessions

Shigeru Matsuzaka¹, Shinobu Kurihara¹, Mamoru Sekido², Thomas Hobiger², Rüdiger Haas³, Jouko Ritakari⁴, Jan Wagner⁴ (¹GSI Japan, ²NICT Japan, ³Chalmers University of Technology, ⁴Helsinki University of Technology)

09:00 S2-T10 MPIfR/BKG Correlator Report

Walter Alef¹, David Graham¹, Helge Rottmann¹, John Morgan¹, Richard Porcas¹, Arno Müskens², Alessandra Bertarini², Simone Bernhart² (¹MPIfR Bonn, ²University of Bonn)

09:15 S2-T11 Implementation and Testing of VLBI Software Correlation at USNO

Alan Fey¹, David Boboltz¹, Ralph Gaume¹, David Hall¹, Ken Johnston¹, Kerry Kingham¹, Roopesh Ojha² (¹U.S. Naval Observatory, ²NVI, Inc./USNO)

09:30 S2-T12 The Software Correlator of the Chinese VLBI Network

Weimin Zheng, Ying Quan, Fengchun Shu, Zhong Chen, Shanshan Chen, Weihua Wang (Shanghai Astronomical Observatory)

09:45 S2-T13 Zodiac Extragalactic Sources Densification Using Phase-Referencing Technology

Guangli Wang (Shanghai Astronomical Observatory)

Session 3: VLBI Data Structure, Analysis Strategies and Software

Chair: Thomas Hobiger

10:00 S3-T01 IVS Working Group 4: Proposed VLBI Data Format

John Gipson (NVI, Inc./NASA GSFC)

10:15 S3-T02 Development of a New VLBI Data Analysis Software

Sergei Bolotin, John Gipson, Dan MacMillan (NVI, Inc./NASA GSFC)

10:30 Coffee Break

11:00 S3-T03 Estimation of Geodetic and Geodynamical Parameters with VieVS

Hana Spicakova, Johannes Böhm, Sigrid Böhm, Tobias Nilsson, Andrea Pany, Lucia Plank, Kamil Teke, Harald Schuh (Vienna University of Technology)

11:15 S3-T04 VLBI Analysis with the Multi-technique Software GEOSAT

Halfdan Kierulf¹, Per-Helge Andersen², Sarah Böckmann³, Oddgeir Kristiansen¹ (¹Norwegian Mapping Authority, ²Norwegian Defence Research Establishment, ³University of Bonn)

11:30 S3-T05 Comparison Campaign of VLBI Data Analysis Software – First Results

Lucia Plank (Vienna University of Technology)

11:45 S3-T06 Consideration of Correlations between the Different Input Series in IVS Intra-technique Combination

Sarah Böckmann, Thomas Artz, Axel Nothnagel (University of Bonn)

Chair: John Gipson

12:00 S3-T07 VLBI–SLR Combination Solution Using GEODYN

Dan MacMillan¹, Frank Lemoine², Despina Pavlis³, Douglas Chinn³, David Rowlands² (NVI, Inc./NASA GSFC, ²NASA GSFC, ³SGT Inc./NASA GSFC)

12:15 S3-T08 Application of Ray-tracing through the High Resolution Numerical Weather Model HIRLAM for the Analysis of European VLBI

Susana García-Espada¹, Rüdiger Haas², Francisco Colomer¹ (¹IGN Spain, ²Chalmers University of Technology)

12:30 S3-T09 Atmospheric Delay Reduction Using KARAT for GPS Analysis and Implications for VLBI

Ryuichi Ichikawa¹, Thomas Hobiger¹, Yasuhiro Koyama¹, Tetsuro Kondo^{1,2} (¹NICT Japan, ²Ajou University)

12:45 Lunch Break

Visit of Mt. Pleasant Observatory and Dedication of AuScope Antenna

Master of Ceremonies: Jim Lovell

13:15 Bus departure from University of Tasmania

14:00-18:00 Excursion to Hobart Station and dedication of AuScope Antenna

18:00 Bus departure from Mt Pleasant Observatory

Wednesday, February 10, 2010

Session 3: VLBI Data Structure, Analysis Strategies and Software (cont'd)

Chair: John Gipson

08:30 S3-T10 Use of GPS TEC Ionosphere Maps for Calibrating Single Band VLBI Sessions

David Gordon (NVI, Inc./NASA GSFC)

08:45 S3-T11 Universal Time from VLBI Single Baseline Observations during CONT08

Johannes Böhm, Tobias Nilsson, Harald Schuh (Vienna University of Technology)

09:00 S3-T12 Application of Geodetic VLBI Data to Obtaining Long-term Light-curves for Astrophysics

Masachika Kijima (Sokendai Graduate University)

Session 4: Interpretation of VLBI Results in Geodesy, Astrometry and Geophysics

Chair: Rüdiger Haas

09:15 S4-T01 The Second International Celestial Reference Frame (ICRF2) (invited)

Chopo Ma (NASA GSFC)

09:35 S4-T02 Time-dependent Selection of an Optimal Set of Sources to Define a Stable Celestial Reference Frame

Karine Le Bail, David Gordon (NVI, Inc./NASA GSFC)

09:50 S4-T03 X/Ka-band Celestial Reference Frame Work: Recent Improvements

Chris Jacobs¹, Ojars Sovers (¹Jet Propulsion Laboratory, ²Remote Sensing Analysis Systems Inc.)

10:05 S4-T04 Effects of ICRF2 on Estimates of Earth Orientation Parameters and the Terrestrial Reference Frame

Robert Heinkelmann (DGFI Munich)

10:20 S4-T05 Long-term Variations of the EOP and ICRF2

Vladimir Zharov, Mikhail Sazhin, Valerian Sementsov (Sternberg State Astronomical Institute)

10:35 Coffee Break

11:05 S4-T06 Long-term Stability of Radio Sources in VLBI Analysis

Gerald Engelhardt, Volkmar Thorandt (BKG Leipzig)

11:20 S4-T07 The Position Stability of Four ICRF2 Radio Sources

Ed Fomalont¹, Ken Johnston², Alan Fey², David Boboltz², Tomoaki Oyama³, Mareki Honma³ (¹NRAO, ²U.S. Naval Observatory, ³NAOJ Japan)

11:35 S4-T08 Study of the Low Luminosity GPS Radio Source PKS B2254-367 (IC 1459) from VLBI Observations

Julia Sokolova, Steven Tingay (Curtin University of Technology)

Chair: Dan MacMillan

11:50 S4-T09 Global VLBI Observations of Weak Extragalactic Radio Sources: Imaging of Candidates to Align the ICRF and the Future GAIA Frame

Géraldine Bourda¹, Patrick Charlot¹, Arnaud Collioud¹, Richard Porcas², Simon Garrington³ (¹Laboratoire d'Astrophysique de Bordeaux, ²MPIfR Bonn, ³Jodrell Bank Observatory)

12:05 S4-T10 Enabling High Precision VLBI Relative Astrometry at the Highest Frequencies

Maria Rioja^{1,2}, Richard Dodson¹ (¹ICRAR/UWA, ²OAN Spain)

12:20 S4-T11 An Improved Lunar Gravity Field Model from SELENE and Historical Tracking Data (*invited*)

Koji Matsumoto¹, Sander Goossens¹, Yoshiaki Ishihara¹, Quinghui Liu², Fuyuhiko Kikuchi¹, Takahiro Iwata³, Noriyuki Namiki⁴, Hirotomo Noda¹, Hideo Hanada¹, Nobuyuki Kawano², and RSAT/VRAD Mission Team (¹NAOJ Japan, ²Shanghai Astronomical Observatory, ³JAXA, ⁴Chiba Institute of Technology)

12:45 S4-T12 Planetary Radio Interferometry and Doppler Experiment (PRIDE) in the IVS Context

Leonid Gurvits, Sergei Pogrebenko, Giuseppe Cimò (JIVE) and the PRIDE Team

13:00 Lunch Break

14:00 S4-T13 The First Experiment with VLBI–GPS Hybrid System

Younghee Kwak^{1,3}, Tetsuro Kondo^{1,2}, Tadahiro Gotoh², Jun Amagai², Hiroshi Takiguchi², Mamoru Sekido², Ryuichi Ichikawa², Tetsuo Sasao¹, Jungho Cho³, Tuhwan Kim¹ (¹Ajou University, ²NICT Japan, ³KASI Korea)

14:15 S4-T14 Ionospheric Response to the Total Solar Eclipse of July 22, 2009 as Deduced from VLBI and GPS Data

Li Guo¹, Fengchun Shu¹, Weimin Zheng¹, Tetsuro Kondo^{2,3}, Ryuichi Ichikawa², Shingo Hasegawa², Mamoru Sekido² (¹Shanghai Astronomical Observatory, ²NICT Japan, ³Ajou University)

14:30 S4-T15 Reliability and Stability of VLBI-derived Sub-daily EOP Models

Thomas Artz¹, Sarah Böckmann¹, Axel Nothnagel¹, Peter Steigenberger² (¹University of Bonn, ²TU Munich)

14:45 S4-T16 Extracting Independent Local Oscillatory Geophysical Signals in Geodetic Tropospheric Delay

Ondego Joel Botai¹, Ludwig Combrinck^{1,2}, Venkataraman Sivakumar^{1,3}, C.J. de W. Rautenbach¹, Harald Schuh⁴, Johannes Böhm⁴ (¹University of Pretoria, ²Hartebeesthoek RAO, ³South African National Laser Center, ⁴Vienna University of Technology)

Session 5: Progress in Technology Development

Chair: Alan Whitney

15:00 S5-T01 The Mark 5C VLBI Data System

Alan Whitney¹, Chester Ruszczyk¹, Jon Romney², Ken Owens³ (¹MIT Haystack Observatory, ²NRAO, ³Conduant Corp.)

15:15 S5-T02 Cryogenic Integration of 2-14 GHz Eleven Feed in Wideband Receiver for VLBI2010

Miroslav Pantaleev¹, Jian Yang¹, Yogesh Karadikar¹, Leif Helldner¹, Benjamin Klein², Rüdiger Haas¹, Ashraf Zaman¹, Mojtaba Zamani¹, Per-Simon Kildal¹ (¹Chalmers University of Technology, ²Hartebeesthoek Radio Astronomy Observatory)

15:30 S5-T03 Next Generation A/D Sampler ADS3000+ for VLBI2010

Kazuhiro Takefuji¹, Hiroshi Takeuchi², Masanori Tsutsumi¹, Yasuhiro Koyama¹ (¹NICT Japan, ²JAXA/ISAS)

15:45 S5-T04 e-control: First Public Release of Remote Control Software for VLBI Telescopes

Alexander Neidhardt¹, Martin Ettl¹, Helge Rottmann², Christian Plötz³, Matthias Mühlbauer³, Hayo Hase³, Walter Alef², Sergio Sobarzo⁴, Cristian Herrera⁴, Ed Himwich⁵ (¹FESG Wettzell, ²MPIfR Bonn, ³BKG Wettzell, ⁴Universidad de Concepción, ⁵NVI, Inc./NASA GSFC)

16:00 Coffee Break

16:30 S5-T05 The Wettzell System Monitoring Concept and First Realizations

Martin Ettl¹, Alexander Neidhardt¹, Matthias Mühlbauer², Christian Plötz² (¹FESG Wettzell, ²BKG Wettzell)

16:45 S5-T06 Lunar, Martian, and Jovian Geodesy and Science Mission Using VLBI and Astrometrical Technology

Takahiro Iwata¹, Hideo Hanada², Hiroto Noda², Fuyuhiko Kikuchi², Seiichi Tazawa², Hiroo Kunitani³, Koji Matsumoto², Kazumasa Imai⁴, Yoshiaki Ishihara², Yuji Harada², Sho Sasaki² (¹JAXA, ²NAOJ Japan, ³NICT Japan, ⁴Kochi National College of Technology)

17:00 S5-T07 The Development of VLBI Technologies at SHAO

Xiuzhong Zhang (Shanghai Astronomical Observatory)

17:15 S5-T08 The Progress of CDAS

Renjie Zhu, Ying Xiang, Yajun Wu (Shanghai Astronomical Observatory)

Closing

17:30 Closing Remarks

Harald Schuh, IVS Chair

17:45 Adjourn GM

General Meeting Banquet at Barilla Bay Restaurant

18:30 Bus departure from University of Tasmania

19:00-22:45 Banquet at Barilla Bay Restaurant

22:45 Bus departure from Barilla Bay Restaurant (back to accommodation)

Posters

Session 1: Realization and New Perspectives of VLBI2010

S1-P01 IVS Status Report 2008-2010

Dirk Behrend¹, Harald Schuh² (¹NVI, Inc./NASA GSFC, ²Vienna University of Technology)

S1-P02 Summary of the VLBI2010 Monte Carlo Simulations

Andrey Pany¹, Johannes Böhm¹, John Gipson², Rüdiger Haas³, Dan MacMillan², Arthur Niell⁴, Tobias Nilsson¹, Bill Petrachenko⁵, Harald Schuh¹, Anthony Searle⁵ (¹Vienna University of Technology, ²NVI, Inc./NASA GSFC, ³Chalmers University of Technology, ⁴MIT Haystack Observatory, ⁵Natural Resources Canada)

S1-P03 DBBC VLBI2010

Gino Tuccari¹, Walter Alef², Alessandra Bertarini³, Salvatore Buttaccio¹, Gianni Comoretto⁴, David Graham², Alexander Neidhardt⁵, Pier Raffaele Platania¹, Alan Roy², Michael Wunderlich², Reinhard Zeitlhöfler⁶ (¹Istituto di Radioastronomia/INAF, ²MPIfR Bonn, ³University of Bonn, ⁴Osservatorio Astrofisico di Arcetri/INAF, ⁵FESG Munich, ⁶BKG Wettzell)

S1-P04 VLBI2010 Related Research Activities at SHAO

Guangli Wang, Ming Zhao, Yong Zheng, Zhihan Qian (Shanghai Astronomical Observatory)

Session 2: Network Stations, Operation Centers, Correlators

S2-P01 The Composition of the Master Schedule

Cynthia Thomas, Dan MacMillan, Dirk Behrend (NVI, Inc./NASA GSFC)

S2-P02 Coordinating, Scheduling, Processing and Analyzing IYA2009

John Gipson¹, Dirk Behrend¹, Cynthia Thomas¹, David Gordon¹, Ed Himwich¹, Dan MacMillan¹, Mike Titus², Brian Corey² (¹NVI, Inc./NASA GSFC, ²MIT Haystack Observatory)

S2-P03 TIGO Station Report

Sergio Sobarzo (Universidad de Concepción)

S2-P04 Update on the TWIN Telescope Wettzell Project

Hayo Hase¹, Gerhard Kronschnabl¹, Reiner Dassing¹, Thomas Klügel², Christian Plötz¹, Ullrich Schreiber¹, Walter Schwarz¹, Alexander Neidhardt², Pierre Lauber² (¹BKG Wettzell, ²FESG Wettzell)

S2-P05 Update on the Fundamental Station Project in Ny-Ålesund

Per Erik Opseth, Line Langkaas, Terje Dahlen, Bjørn Engen, Frode Koppang (Norwegian Mapping Authority)

S2-P06 Reduction of GPS Observations in the Local Ties

Li Liu, Jinling Li, Zongyi Cheng (Shanghai Astronomical Observatory)

S2-P07 Permanent Monitoring of the Reference Point of the 20-m Radio Telescope Wettzell

Alexander Neidhardt¹, Michael Lösler², Cornelia Eschelbach², Andreas Schenk² (FESG Wettzell, University of Karlsruhe)

S2-P08 Proof-of-Concept Studies for a Local Tie Monitoring System

Benno Schmeing^{1,2}, Dirk Behrend², John Gipson², Axel Nothnagel¹ (¹University of Bonn, ²NVI, Inc./NASA GSFC)

S2-P09 The QUASAR Network Observations in e-VLBI Mode within Domestic VLBI Programs

Ilya Bezrukov, Andrey Finkelstein, Alexander Ipatov, Michael Kaidanovsky, Andrey Mikhailov, Alexander Salnikov, Elena Skurikhina, Igor Surkis (Institute of Applied Astronomy)

S2-P10 Implantation of Geodetic Networks of High Precision for the Monitoring of Deformations of the Crust at the Local Level

Niel Teixeira (State University of Santa Cruz)

S2-P11 Venus Express Spacecraft Observations with the Wettzell Radio Telescope – First Results

Alexander Neidhardt¹, Gerhard Kronschnabl², Jan Wagner³, Guifre Molera Calves³, Miguel Perez Ayucar⁴, Giuseppe Cimò⁵, Sergei Pogrebenko⁵ (¹FESG Wettzell, ²BKG Wettzell, ³HUT-MRO Metsahovi, ⁴ESA-ESAC Madrid, ⁵JIVE)

S2-P12 RDV77 VLBA Hardware/Software Correlator Comparison

David Gordon (NVI, Inc./NASA GSFC)

S2-P13 The JPL VLBI Correlator and SoftC

Stephen Rogstad, Stephen Lowe (Jet Propulsion Laboratory)

S2-P14 The IAA RAS Correlator Processing: First Results

Igor Surkis, Vladimir Zimovsky, Violetta Shantyr, Alexey Melnikov (Institute of Applied Astronomy)

S2-P15 CRF Network Simulations for the South

Oleg Titov¹, Dirk Behrend², Fengchun Shu³, Dan MacMillan², Alan Fey⁴ (¹Geoscience Australia, ²NVI, Inc./NASA GSFC, ³Shanghai Astronomical Observatory, ⁴U.S. Naval Observatory)

S2-P16 About the Compatibility of DORIS and VLBI Observations

Gennady Il'in, Sergey Smolentsev, Roman Sergeev (Institute of Applied Astronomy)

Session 3: VLBI Data Structure, Analysis Strategies and Software

S3-P01 VLBI Data Interchange Format

Alan Whitney¹, Mark Kettenis², Chris Phillips³, Mamoru Sekido⁴ (¹MIT Haystack Observatory, ²JIVE, ³CSIRO/ATNF, ⁴NICT Japan)

S3-P02 Combination Analysis at KASI

Younghee Kwak^{1,2}, Jungho Cho¹ (¹Korea Astronomy and Space Science Institute, ²Ajou University)

S3-P03 c5++ Multi-technique Analysis Software for Next Generation Geodetic Instruments

Thomas Hobiger¹, Toshimichi Otsubo², Tadahiro Gotoh¹, Toshihiro Kubooka¹, Mamoru Sekido¹, Hiroshi Takiguchi¹, Hiroshi Takeuchi³ (¹NICT Japan, ²Hitotsubashi University, ³JAXA)

S3-P04OCCAM-LSM for Linux: New Developments at DGFI

Robert Heinkelmann, Michael Gerstl (DGFI Munich)

S3-P05SAI Analysis Center Activity

Vladimir Zharov (Sternberg State Astronomical Institute)

S3-P06Antenna Axis Offset Estimation from VLBI

Sergey Kurdubov, Elena Skurikhina (Institute of Applied Astronomy)

S3-P07Strategies for Improving the IVS-INT01 UT1 Estimates: Results of RD0907–RD0910

John Gipson, Karen Baver, Dan MacMillan (NVI, Inc./NASA GSFC)

S3-P08CPO Prediction: Accuracy Assessment and Impact on UT1 Intensive Results

Zinovy Malkin (Pulkovo Observatory)

Session 4: Interpretation of VLBI Results in Geodesy, Astrometry and Geophysics

S4-P01Cartography in Space Geodesy

Hayo Hase (BKG Concepción) and the TANAMI Team

S4-P02Forthcoming Occultations of Astrometric Radio Sources by Planets

Victor L'vov, Zinovy Malkin, Svetlana Tsekmeister (Pulkovo Observatory)

S4-P03LBA Calibrator Survey of the Southern Sky

Leonid Petrov¹, Chris Phillips², Alessandra Bertarini³, Roy Booth⁴, Sarah Burke-Spolaor⁵, Ed Fomalont⁶, Ron Ekers², Kee-Tae Kim⁷, Tara Murphy⁸, Sergei Pogrebenko⁹, Elaine Sadler⁸, Tasso Tzioumis² (¹ADNET Systems, Inc./NASA GSFC, ²CSIRO/ATNF, ³University of Bonn, ⁴Hartebeesthoek Radio Astronomical Observatory, ⁵Swinburne University of Technology, ⁶NRAO, ⁷KASI, ⁸University of Sydney, ⁹JIVE)

S4-P04Finding Extremely Compact Sources using the ASKAP VAST Survey

Hayley Bignall¹, Cormac Reynolds¹, Roopesh Ojha², Jim Lovell³, Dave Jauncey⁴ (¹ICRAR/Curtin University, ²NVI, Inc./USNO, ³University of Tasmania, ⁴ATNF) and the ASKAP VAST Collaboration

S4-P05The Tropospheric Products of the International VLBI Service for Geodesy and Astrometry

Christian Schwatke, Robert Heinkelmann (DGFI Munich)

S4-P06Station Positions Intraday Variations

Elena Skurikhina (Institute of Applied Astronomy)

S4-P07Simulation of Local Tie Accuracy on VLBI Antennas

Ulla Kallio, Markku Poutanen (Finnish Geodetic Institute)

S4-P08Sub-diurnal EOP Variations from the Analysis of the CONT Campaigns

Rüdiger Haas (Chalmers University of Technology)

S4-P09 VLBI and GPS-based Time Transfer Using CONT08 Data

Carsten Rieck¹, Rüdiger Haas², Kenneth Jaldehag², Jan Johansson¹ (¹SP Technical Research Institute, ²Chalmers University of Technology)

Session 5: Progress in Technology Development

S5-P01 Development of a Compact Eleven Feed Cryostat for the Patriot 12-m Antenna

Christopher Beaudoin¹, Per-Simon Kildal², Jian Yang², Miroslav Pantaleev² (¹MIT Haystack Observatory, ²Chalmers University of Technology)

S5-P02 Radio Telescope Focal Container for the Russian VLBI Network of New Generation

Alexander Ipatov¹, Vyacheslav Mardyshev¹, Andrey Cherepanov² (¹Institute of Applied Astronomy, ²SPbSPU)

S5-P03 Digital Backend for JPL VLBI Data Acquisition Terminal

Robert Navarro (Jet Propulsion Laboratory)

S5-P04 DBBC2 Backend: Status and Development Plan

Gino Tuccari¹, Walter Alef², Alessandra Bertarini³, Salvatore Buttaccio¹, Gianni Comoretto⁴, David Graham², Alexander Neidhardt⁵, Pier Raffaele Platania¹, Alan Roy², Michael Wunderlich², Reinhard Zeitlhöfler⁶ (¹Istituto di Radioastronomia/INAF, ²MPIfR Bonn, ³University of Bonn, ⁴Osservatorio Astrofisico di Arcetri/INAF, ⁵FESG Munich, ⁶BKG Wettzell)

S5-P05 RDBE – A Second-Generation Digital Backend System

Alan Whitney¹, Shephard Doeleman¹, Alan Hinton¹, Russell McWhirter¹, Arthur Niell¹, Chester Ruszczyk¹, Michael Taveniku¹, Miguel Guerra², Matthew Luce² (¹MIT Haystack Observatory, ²NRAO)

S5-P06 The Digital Data Acquisition System for the Russian VLBI Network of New Generation

Leonid Fedotov, Eugene Nosov, Sergey Grenkov (Institute of Applied Astronomy)

S5-P07 Round Trip System Available to Measure Path Length Variation in Korean VLBI System for Geodesy

Hongjong Oh¹, Tetsuro Kondo^{1,2}, Tuhwan Kim¹, Sangoh Yi¹, Myungho Kim³, Suchul Kim³, Jinsik Park³, Hyunhee Ju³ (¹Ajou University, ²NICT Japan, ³NGII Korea)

S5-P08 Experiment of Injecting Phase Cal ahead of the Feed: First Results

Dmitrij Ivanov, Anatolij Maslenikov, Alexander Vytnov (Institute of Applied Astronomy)

S5-P09 First Phase Development of Korea-Japan Joint VLBI Correlator and its Current Progress

Se-Jin Oh¹, Duk-Gyoo Roh¹, Jae-Hwan Yeom¹, Hideyuki Kobayashi², Noriyuki Kawaguchi² (¹KASI, ²NAOJ Japan)

S5-P10 Development of an e-VLBI Data Transport Software Suite with VDIF

Mamoru Sekido¹, Kazuhiro Takefuji¹, Moritaka Kimura¹, Takuya Shinno², Fujinobu Takahashi² (¹NICT Japan, ²Yokohama University)

S5-P11 The Progress of the Hardware Correlator Development at SHAO

Zhijun Xu, Xiuzhong Zhang, Renjie Zhu, Ying Xiang, Yajun Wu (Shanghai Astronomical Observatory)

S5-P12 The Impact of Radio Frequency Interference (RFI) on VLBI2010

Bill Petrachenko (Natural Resources Canada)

Author Index

(First authors are designated by (1) at the end of the title.)

- Alef, Walter*: p. 28, **DBBC VLBI2010**
Alef, Walter: p. 392, **DBBC2 Backend: Status and Development Plan**
Alef, Walter: p. 439, **E-control: First Public Release of Remote Control Software for VLBI Telescopes**
Amagai, Jun: p. 40, **GPU Based Software Correlators - Perspectives for VLBI2010**
Amagai, Jun: p. 330, **The First Experiment with VLBI-GPS Hybrid System**
Andersen, Per-Helge: p. 207, **VLBI Analysis with the Multi-technique Software GEOSAT**
Artz, Thomas: p. 222, **Correlations Between the Contributions of Individual IVS Analysis Centers**
Artz, Thomas: p. 355, **Reliability and Stability of VLBI-derived Sub-daily EOP Models (1)**
Assis, Marlene C.S.: p. 101, **RAEGE: An Atlantic Network of Geodynamical Fundamental Stations**
Bagri, D. S.: p. 285, **X/Ka Celestial Frame Improvements: Vision to Reality**
Bark, M.: p. 396, **RDBE Development and Progress**
Baver, Karen: p. 256, **Strategies for Improving the IVS-INT01 UT1 Estimates (1)**
Beaudoin, Christopher: p. 35, **Post-correlation Processing for the VLBI2010 Proof-of-concept System (1)**
Beaudoin, C.: p. 396, **RDBE Development and Progress**
Beaudoin, Christopher: p. 420, **Development of a Compact Eleven Feed Cryostat for the Patriot 12-m Antenna System (1)**
Beaudoin, Christopher: p. 444, **The Wettzell System Monitoring Concept and First Realizations**
Behrend, Dirk: p. 85, **The Composition of the Master Schedule**
Behrend, Dirk: p. 90, **Coordinating, Scheduling, Processing and Analyzing IYA09**
Behrend, Dirk: p. 138, **Proof-of-Concept Studies for a Local Tie Monitoring System**
Behrend, Dirk: p. 176, **CRF Network Simulations for the South**
Ben Frej, H.: p. 396, **RDBE Development and Progress**
Bergstrand, Sten: p. 118, **COLD MAGICS – Continuous Local Deformation Monitoring of an Arctic Geodetic Fundamental Station**
Bertarini, Alessandra: p. 28, **DBBC VLBI2010**
Bertarini, Alessandra: p. 392, **DBBC2 Backend: Status and Development Plan**
Bezrukov, Ilya: p. 148, **The “Quasar” Network Observations in e-VLBI Mode Within the Russian Domestic VLBI Programs**
Bignall, Hayley E.: p. 325, **Finding Extremely Compact Sources Using the ASKAP VAST Survey (1)**
Boboltz, Dave: p. 153, **Implementation and Testing of VLBI Software Correlation at the USNO**
Boboltz, Dave: p. 300, **The Position/Structure Stability of Four ICRF2 Sources**
Böckmann, Sarah: p. 207, **VLBI Analysis with the Multi-technique Software GEOSAT**
Böckmann, Sarah: p. 222, **Correlations Between the Contributions of Individual IVS Analysis Centers (1)**
Böckmann, Sarah: p. 355, **Reliability and Stability of VLBI-derived Sub-daily EOP Models**
Böhm, Johannes: p. 202, **Estimation of Geodetic and Geodynamical Parameters with VieVS**
Böhm, Johannes: p. 217, **Comparison Campaign of VLBI Data Analysis Software - First Results**
Böhm, Johannes: p. 251, **Prospects for UT1 Measurements from VLBI Intensive Sessions (1)**
Böhm, J.: p. 345, **Extracting Independent Local Oscillatory Geophysical Signals by Geodetic Tropospheric Delay**
Böhm, Sigrid: p. 202, **Estimation of Geodetic and Geodynamical Parameters with VieVS**

- Bolotin, Sergei*: p. 197, **Development of a New VLBI Data Analysis Software (1)**
- Botai, O. J.*: p. 345, **Extracting Independent Local Oscillatory Geophysical Signals by Geodetic Tropospheric Delay (1)**
- Bourda, Géraldine*: p. 310, **Global VLBI Observations of Weak Extragalactic Radio Sources: Imaging Candidates to Align the VLBI and Gaia Frames (1)**
- Brisken, W.*: p. 396, **RDBE Development and Progress**
- Britcliffe, M. J.*: p. 285, **X/Ka Celestial Frame Improvements: Vision to Reality**
- Broadband Development Team*: p. 23, **The NASA VLBI2010 Proof-of-concept Demonstration and Future Plans**
- Buttaccio, Salvatore*: p. 28, **DBBC VLBI2010**
- Buttaccio, Salvatore*: p. 392, **DBBC2 Backend: Status and Development Plan**
- Charlot, Patrick*: p. 45, **VLBI2010 Imaging and Structure Corrections**
- Charlot, Patrick*: p. 310, **Global VLBI Observations of Weak Extragalactic Radio Sources: Imaging Candidates to Align the VLBI and Gaia Frames**
- Chen, Lan*: p. 388, **The Progress of CDAS**
- Chen, Shanshan*: p. 157, **The Software Correlator of the Chinese VLBI Network**
- Chen, Zhong*: p. 157, **The Software Correlator of the Chinese VLBI Network**
- Chen, Zhong*: p. 383, **VLBI Technology Development at SHAO**
- Cheng, Z. Y.*: p. 128, **Analysis of the GPS Observations of the Site Survey at Sheshan 25-m Radio Telescope in August 2008**
- Cherepanov, Andrey*: p. 425, **Radio Telescope Focal Container for the Russian VLBI Network of New Generation**
- Chernov, Vitaly*: p. 425, **Radio Telescope Focal Container for the Russian VLBI Network of New Generation**
- Chinn, Douglas*: p. 227, **VLBI-SLR Combination Solution Using GEODYN**
- Cho, Jungho*: p. 330, **The First Experiment with VLBI-GPS Hybrid System**
- Cimó, Giuseppe*: p. 171, **First Results of Venus Express Spacecraft Observations with Wettzell**
- Clark, J. E.*: p. 285, **X/Ka Celestial Frame Improvements: Vision to Reality**
- Collioud, Arnaud*: p. 45, **VLBI2010 Imaging and Structure Corrections (1)**
- Collioud, Arnaud*: p. 310, **Global VLBI Observations of Weak Extragalactic Radio Sources: Imaging Candidates to Align the VLBI and Gaia Frames**
- Colomer, Francisco*: p. 101, **RAEGE: An Atlantic Network of Geodynamical Fundamental Stations**
- Colomer, Francisco*: p. 232, **Application of Raytracing through the High Resolution Numerical Weather Model HIRLAM for the Analysis of European VLBI**
- Combrinck, L.*: p. 345, **Extracting Independent Local Oscillatory Geophysical Signals by Geodetic Tropospheric Delay**
- Comoretto, Giovanni*: p. 28, **DBBC VLBI2010**
- Comoretto, Giovanni*: p. 392, **DBBC2 Backend: Status and Development Plan**
- Corey, Brian*: p. 18, **Differences Between VLBI2010 and S/X Hardware (1)**
- Corey, Brian*: p. 90, **Coordinating, Scheduling, Processing and Analyzing IYA09**
- Dahlen, Terje*: p. 111, **New Fundamental Station in Ny-Ålesund**
- Dickey, John*: p. 50, **The AuScope Project and Trans-Tasman VLBI**
- Dickey, J. M.*: p. 65, **How and Why to Do VLBI on GPS (1)**
- Diky, Dmitry*: p. 425, **Radio Telescope Focal Container for the Russian VLBI Network of New Generation**
- Dodson, Richard*: p. 315, **Astrometric “Core-shifts” at the Highest Frequencies**
- Doeleman, S.*: p. 396, **RDBE Development and Progress**
- Durand, S.*: p. 396, **RDBE Development and Progress**
- Eling, Christian*: p. 123, **Homologous Deformation of the Effelsberg 100-m Telescope Determined with a Total Station**

- Engelhardt, Gerald*: p. 295, **Long-term Stability of Radio Sources in VLBI Analysis** (1)
- Eschelbach, Cornelia*: p. 133, **Permanent Monitoring of the Reference Point of the 20m Radio Telescope Wettzell**
- Ettl, Martin*: p. 439, **E-control: First Public Release of Remote Control Software for VLBI Telescopes**
- Ettl, Martin*: p. 444, **The Wettzell System Monitoring Concept and First Realizations** (1)
- Fedotov, Leonid*: p. 106, **The New Generation Russian VLBI Network**
- Fedotov, Leonid*: p. 400, **The Digital Data Acquisition System for the Russian VLBI Network of New Generation** (1)
- Fey, Alan*: p. 153, **Implementation and Testing of VLBI Software Correlation at the USNO** (1)
- Fey, Alan*: p. 176, **CRF Network Simulations for the South**
- Fey, Alan*: p. 300, **The Position/Structure Stability of Four ICRF2 Sources**
- Finkelstein, Andrey*: p. 106, **The New Generation Russian VLBI Network** (1)
- Finkelstein, Andrey*: p. 148, **The “Quasar” Network Observations in e-VLBI Mode Within the Russian Domestic VLBI Programs** (1)
- Fomalont, Ed*: p. 300, **The Position/Structure Stability of Four ICRF2 Sources** (1)
- Franco, M. M.*: p. 285, **X/Ka Celestial Frame Improvements: Vision to Reality**
- García-Espada, Susana*: p. 232, **Application of Raytracing through the High Resolution Numerical Weather Model HIRLAM for the Analysis of European VLBI** (1)
- Garcia-Miro, C.*: p. 285, **X/Ka Celestial Frame Improvements: Vision to Reality**
- Garrington, Simon*: p. 310, **Global VLBI Observations of Weak Extragalactic Radio Sources: Imaging Candidates to Align the VLBI and Gaia Frames**
- Gaume, Ralph*: p. 153, **Implementation and Testing of VLBI Software Correlation at the USNO**
- Gayazov, Iskander*: p. 106, **The New Generation Russian VLBI Network**
- Geiger, Nicole*: p. 153, **Implementation and Testing of VLBI Software Correlation at the USNO**
- Gipson, John*: p. 77, **An Introduction to Sked** (1)
- Gipson, John*: p. 90, **Coordinating, Scheduling, Processing and Analyzing IYA09** (1)
- Gipson, John*: p. 138, **Proof-of-Concept Studies for a Local Tie Monitoring System**
- Gipson, John*: p. 187, **IVS Working Group 4: VLBI Data Structures** (1)
- Gipson, John M.*: p. 197, **Development of a New VLBI Data Analysis Software**
- Gipson, John*: p. 256, **Strategies for Improving the IVS-INT01 UT1 Estimates**
- Gómez González, Jesús*: p. 101, **RAEGE: An Atlantic Network of Geodynamical Fundamental Stations** (1)
- Goodhart, C. E.*: p. 285, **X/Ka Celestial Frame Improvements: Vision to Reality**
- Gordon, David*: p. 90, **Coordinating, Scheduling, Processing and Analyzing IYA09**
- Gordon, David*: p. 162, **RDV77 VLBA Hardware/Software Correlator Comparisons** (1)
- Gordon, David*: p. 242, **Use of GPS TEC Maps for Calibrating Single Band VLBI Sessions** (1)
- Gordon, David*: p. 280, **Time-dependent Selection of an Optimal Set of Sources to Define a Stable Celestial Reference Frame**
- Gotoh, Tadahiro*: p. 40, **GPU Based Software Correlators - Perspectives for VLBI2010**
- Gotoh, Tadahiro*: p. 212, **c5++ - Multi-technique Analysis Software for Next Generation Geodetic Instruments**
- Gotoh, Tadahiro*: p. 330, **The First Experiment with VLBI-GPS Hybrid System**
- Graham, Dave*: p. 28, **DBBC VLBI2010**
- Graham, Dave*: p. 392, **DBBC2 Backend: Status and Development Plan**
- Grenkov, Sergey*: p. 400, **The Digital Data Acquisition System for the Russian VLBI Network of New Generation**
- Guerra, M.*: p. 396, **RDBE Development and Progress**
- Gulyaev, Sergei*: p. 50, **The AuScope Project and Trans-Tasman VLBI**
- Gulyaev, Sergei*: p. 113, **Characterization and Calibration of the 12-m Antenna in Warkworth, New Zealand** (1)

- Guo, L.:* p. 335, **Ionospheric Response to the Total Solar Eclipse of 22 July 2009 as Deduced from VLBI and GPS Data (1)**
- Haas, Rüdiger:* p. 70, **Planning of an Experiment for VLBI Tracking of GNSS Satellites**
- Haas, Rüdiger:* p. 118, **COLD MAGICS – Continuous Local Deformation Monitoring of an Arctic Geodetic Fundamental Station (1)**
- Haas, Rüdiger:* p. 143, **Ultra-rapid dUT1 Measurements on Japan-Fennoscandian Baselines – Application to 24-hour Sessions**
- Haas, Rüdiger:* p. 232, **Application of Raytracing through the High Resolution Numerical Weather Model HIRLAM for the Analysis of European VLBI**
- Haas, Rüdiger:* p. 365, **VLBI and GPS-based Time-transfer Using CONT08 Data**
- Haas, Rüdiger:* p. 415, **Cryogenic Integration of the 2–14 GHz Eleven Feed in a Wideband Receiver for VLBI2010**
- Hall, David:* p. 153, **Implementation and Testing of VLBI Software Correlation at the USNO**
- Hase, Hayo:* p. 31, **Differences Between S/X and VLBI2010 Operation (1)**
- Hase, Hayo:* p. 439, **E-control: First Public Release of Remote Control Software for VLBI Telescopes**
- Hasegawa, S.:* p. 335, **Ionospheric Response to the Total Solar Eclipse of 22 July 2009 as Deduced from VLBI and GPS Data**
- Heflin, M. B.:* p. 305, **Rotational Alignment Altered by Source Position Correlations**
- Heinkelmann, Robert:* p. 340, **The Tropospheric Products of the International VLBI Service for Geodesy and Astrometry (1)**
- Helldner, Leif:* p. 415, **Cryogenic Integration of the 2–14 GHz Eleven Feed in a Wideband Receiver for VLBI2010**
- Hering, Claudia:* p. 123, **Homologous Deformation of the Effelsberg 100-m Telescope Determined with a Total Station**
- Herrea, Cristian:* p. 439, **E-control: First Public Release of Remote Control Software for VLBI Telescopes**
- Himwich, Ed:* p. 31, **Differences Between S/X and VLBI2010 Operation**
- Himwich, Ed:* p. 90, **Coordinating, Scheduling, Processing and Analyzing IYA09**
- Himwich, Ed:* p. 439, **E-control: First Public Release of Remote Control Software for VLBI Telescopes**
- Hinton, A.:* p. 396, **RDBE Development and Progress**
- Hobiger, Thomas:* p. 40, **GPU Based Software Correlators - Perspectives for VLBI2010 (1)**
- Hobiger, Thomas:* p. 143, **Ultra-rapid dUT1 Measurements on Japan-Fennoscandian Baselines – Application to 24-hour Sessions**
- Hobiger, Thomas:* p. 212, **c5++ - Multi-technique Analysis Software for Next Generation Geodetic Instruments (1)**
- Hobiger, Thomas:* p. 237, **Atmospheric Delay Reduction Using KARAT for GPS Analysis and Implications for VLBI**
- Hobiger, Thomas:* p. 410, **Development of an e-VLBI Data Transport Software Suite with VDIF**
- Honma, Mareki:* p. 300, **The Position/Structure Stability of Four ICRF2 Sources**
- Horiuchi, S.:* p. 285, **X/Ka Celestial Frame Improvements: Vision to Reality**
- Ichikawa, Ryuichi:* p. 55, **Current Status of the Development of a Transportable and Compact VLBI System by NICT and GSI**
- Ichikawa, Ryuichi:* p. 237, **Atmospheric Delay Reduction Using KARAT for GPS Analysis and Implications for VLBI (1)**
- Ichikawa, Ryuichi:* p. 330, **The First Experiment with VLBI-GPS Hybrid System**
- Ichikawa, R.:* p. 335, **Ionospheric Response to the Total Solar Eclipse of 22 July 2009 as Deduced from VLBI and GPS Data**
- Ivin, Gennady:* p. 180, **About the Compatibility of DORIS and VLBI Observations (1)**
- Ipatov, Alexander:* p. 106, **The New Generation Russian VLBI Network**

- Ipatov, Alexander*: p. 148, **The “Quasar” Network Observations in e-VLBI Mode Within the Russian Domestic VLBI Programs**
- Ipatov, Alexander*: p. 425, **Radio Telescope Focal Container for the Russian VLBI Network of New Generation (1)**
- Ishii, Atsutoshi*: p. 55, **Current Status of the Development of a Transportable and Compact VLBI System by NICT and GSI (1)**
- Ivanov, Dmitriy*: p. 106, **The New Generation Russian VLBI Network**
- Ivanov, Dmitriy*: p. 429, **Experiment of Injecting Phase Cal Ahead of the Feed: First Results (1)**
- Jacobs, C. S.*: p. 285, **X/Ka Celestial Frame Improvements: Vision to Reality (1)**
- Jacobs, C. S.*: p. 305, **Rotational Alignment Altered by Source Position Correlations (1)**
- Jaldehyag, Kenneth*: p. 365, **VLBI and GPS-based Time-transfer Using CONT08 Data**
- Jang, Jian*: p. 415, **Cryogenic Integration of the 2–14 GHz Eleven Feed in a Wideband Receiver for VLBI2010**
- Jauncey, David L.*: p. 325, **Finding Extremely Compact Sources Using the ASKAP VAST Survey**
- Jensen, Laura*: p. 355, **Reliability and Stability of VLBI-derived Sub-daily EOP Models**
- Johansson, Jan*: p. 365, **VLBI and GPS-based Time-transfer Using CONT08 Data**
- Johnston, Ken*: p. 153, **Implementation and Testing of VLBI Software Correlation at the USNO**
- Johnston, Kenneth*: p. 300, **The Position/Structure Stability of Four ICRF2 Sources**
- Ju, Hyunhee*: p. 95, **The State and Development Direction of the Geodetic VLBI Station in Korea (1)**
- Ju, Hyunhee*: p. 449, **Round-trip System Available to Measure Path Length Variation in Korea VLBI System for Geodesy**
- Kaidanovsky, Michael*: p. 148, **The “Quasar” Network Observations in e-VLBI Mode Within the Russian Domestic VLBI Programs**
- Kallio, Ulla*: p. 360, **Simulation of Local Tie Accuracy on VLBI Antennas (1)**
- Karadikar, Yogesh*: p. 415, **Cryogenic Integration of the 2–14 GHz Eleven Feed in a Wideband Receiver for VLBI2010**
- Kawaguchi, Noriyuki*: p. 405, **First Phase Development of Korea-Japan Joint VLBI Correlator and Its Current Progress**
- Kettenis, Mark*: p. 192, **VLBI Data Interchange Format (VDIF)**
- Khvostov, Evgeny*: p. 425, **Radio Telescope Focal Container for the Russian VLBI Network of New Generation**
- Kierulf, Halfdan Pascal*: p. 207, **VLBI Analysis with the Multi-technique Software GEOSAT (1)**
- Kijima, Masachika A.*: p. 266, **Application of Geodetic VLBI Data to Obtaining Long-term Light Curves for Astrophysics (1)**
- Kildal, Per-Simon*: p. 415, **Cryogenic Integration of the 2–14 GHz Eleven Feed in a Wideband Receiver for VLBI2010**
- Kildal, Per-Simon*: p. 420, **Development of a Compact Eleven Feed Cryostat for the Patriot 12-m Antenna System**
- Kim, Myungho*: p. 95, **The State and Development Direction of the Geodetic VLBI Station in Korea**
- Kim, Myungho*: p. 449, **Round-trip System Available to Measure Path Length Variation in Korea VLBI System for Geodesy**
- Kim, Suchul*: p. 95, **The State and Development Direction of the Geodetic VLBI Station in Korea**
- Kim, Suchul*: p. 449, **Round-trip System Available to Measure Path Length Variation in Korea VLBI System for Geodesy**
- Kim, Tuhwan*: p. 95, **The State and Development Direction of the Geodetic VLBI Station in Korea**
- Kim, Tuhwan*: p. 330, **The First Experiment with VLBI-GPS Hybrid System**
- Kim, Tuhwan*: p. 449, **Round-trip System Available to Measure Path Length Variation in Korea**

VLBI System for Geodesy

- Kimura, Moritaka*: p. 40, **GPU Based Software Correlators - Perspectives for VLBI2010**
- Kimura, Moritaka*: p. 410, **Development of an e-VLBI Data Transport Software Suite with VDIF**
- Kingham, Kerry*: p. 153, **Implementation and Testing of VLBI Software Correlation at the USNO**
- Klein, Benjamin*: p. 415, **Cryogenic Integration of the 2–14 GHz Eleven Feed in a Wideband Receiver for VLBI2010**
- Kobayashi, Hideyuki*: p. 405, **First Phase Development of Korea-Japan Joint VLBI Correlator and Its Current Progress**
- Kokado, Kensuke*: p. 410, **Development of an e-VLBI Data Transport Software Suite with VDIF**
- Kondo, Tetsuro*: p. 40, **GPU Based Software Correlators - Perspectives for VLBI2010**
- Kondo, Tetsuro*: p. 55, **Current Status of the Development of a Transportable and Compact VLBI System by NICT and GSI**
- Kondo, Tetsuro*: p. 95, **The State and Development Direction of the Geodetic VLBI Station in Korea**
- Kondo, Tetsuro*: p. 237, **Atmospheric Delay Reduction Using KARAT for GPS Analysis and Implications for VLBI**
- Kondo, Tetsuro*: p. 330, **The First Experiment with VLBI-GPS Hybrid System**
- Kondo, T.*: p. 335, **Ionospheric Response to the Total Solar Eclipse of 22 July 2009 as Deduced from VLBI and GPS Data**
- Kondo, Tetsuro*: p. 449, **Round-trip System Available to Measure Path Length Variation in Korea VLBI System for Geodesy**
- Koyama, Yasuhiro*: p. 40, **GPU Based Software Correlators - Perspectives for VLBI2010**
- Koyama, Yasuhiro*: p. 55, **Current Status of the Development of a Transportable and Compact VLBI System by NICT and GSI**
- Koyama, Yasuhiro*: p. 237, **Atmospheric Delay Reduction Using KARAT for GPS Analysis and Implications for VLBI**
- Koyama, Yasuhiro*: p. 378, **Next-generation A/D Sampler ADS3000+ for VLBI2010**
- Kristiansen, Oddgeir*: p. 207, **VLBI Analysis with the Multi-technique Software GEOSAT**
- Kronschnabl, Gerhard*: p. 171, **First Results of Venus Express Spacecraft Observations with Wettzell**
- Kubooka, Toshihiro*: p. 212, **c5++ - Multi-technique Analysis Software for Next Generation Geodetic Instruments**
- Kurdubov, Sergey*: p. 247, **Antenna Axis Offset Estimation from VLBI (1)**
- Kurihara, Shinobu*: p. 55, **Current Status of the Development of a Transportable and Compact VLBI System by NICT and GSI**
- Kurihara, Shinobu*: p. 143, **Ultra-rapid dUT1 Measurements on Japan-Fennoscandian Baselines – Application to 24-hour Sessions**
- Kurihara, Shinobu*: p. 410, **Development of an e-VLBI Data Transport Software Suite with VDIF**
- Kwak, Younghee*: p. 330, **The First Experiment with VLBI-GPS Hybrid System (1)**
- Langkaas, Line*: p. 111, **New Fundamental Station in Ny-Ålesund (1)**
- Lanyi, G.E.*: p. 305, **Rotational Alignment Altered by Source Position Correlations**
- Le Bail, Karine*: p. 280, **Time-dependent Selection of an Optimal Set of Sources to Define a Stable Celestial Reference Frame (1)**
- Lee, Jinoo*: p. 449, **Round-trip System Available to Measure Path Length Variation in Korea VLBI System for Geodesy**
- Lemoine, Frank*: p. 227, **VLBI-SLR Combination Solution Using GEODYN**
- Li, Bin*: p. 388, **The Progress of CDAS**
- Li, J. L.*: p. 128, **Analysis of the GPS Observations of the Site Survey at Sheshan 25-m Radio Telescope in August 2008**
- Liu, L.*: p. 128, **Analysis of the GPS Observations of the Site Survey at Sheshan 25-m Radio**

Telescope in August 2008 (1)

- López Fernández, José Antonio:* p. 101, **RAEGE: An Atlantic Network of Geodynamical Fundamental Stations**
- Lösler, Michael:* p. 133, **Permanent Monitoring of the Reference Point of the 20m Radio Telescope Wettzell**
- Lovell, Jim:* p. 50, **The AuScope Project and Trans-Tasman VLBI (1)**
- Lovell, James E. J.:* p. 325, **Finding Extremely Compact Sources Using the ASKAP VAST Survey**
- Lowe, S. T.:* p. 285, **X/Ka Celestial Frame Improvements: Vision to Reality**
- Luce, M.:* p. 396, **RDBE Development and Progress**
- Luo, Jintao:* p. 383, **VLBI Technology Development at SHAO**
- Luo, Jintao:* p. 388, **The Progress of CDAS**
- L'vov, Victor:* p. 320, **Forthcoming Occultations of Astrometric Radio Sources by Planets (1)**
- Ma, Chopo:* p. 273, **The Second International Celestial Reference Frame (ICRF2) (1)**
- MacMillan, Daniel S.:* p. 85, **The Composition of the Master Schedule**
- MacMillan, Dan:* p. 90, **Coordinating, Scheduling, Processing and Analyzing IYA09**
- MacMillan, Dan:* p. 176, **CRF Network Simulations for the South**
- MacMillan, Daniel S.:* p. 197, **Development of a New VLBI Data Analysis Software**
- MacMillan, Dan:* p. 227, **VLBI-SLR Combination Solution Using GEODYN (1)**
- Malkin, Zinovy:* p. 261, **CPO Prediction: Accuracy Assessment and Impact on UT1 Intensive Results (1)**
- Malkin, Zinovy:* p. 320, **Forthcoming Occultations of Astrometric Radio Sources by Planets**
- Mardyshkin, Vyacheslav:* p. 106, **The New Generation Russian VLBI Network**
- Mardyshkin, Vyacheslav:* p. 425, **Radio Telescope Focal Container for the Russian VLBI Network of New Generation**
- Marshalov, Dmitry:* p. 400, **The Digital Data Acquisition System for the Russian VLBI Network of New Generation**
- Maslenikov, Anatolij:* p. 429, **Experiment of Injecting Phase Cal Ahead of the Feed: First Results**
- Matsuzaka, Shigeru:* p. 55, **Current Status of the Development of a Transportable and Compact VLBI System by NICT and GSI**
- Matsuzaka, Shigeru:* p. 143, **Ultra-rapid dUT1 Measurements on Japan-Fennoscandian Baselines – Application to 24-hour Sessions (1)**
- McWhirter, R.:* p. 396, **RDBE Development and Progress**
- Melnikov, Alexey:* p. 167, **The IAA RAS Correlator First Results**
- Mikhailov, Andrey:* p. 148, **The “Quasar” Network Observations in e-VLBI Mode Within the Russian Domestic VLBI Programs**
- Miura, Yuji:* p. 55, **Current Status of the Development of a Transportable and Compact VLBI System by NICT and GSI**
- Molera, Guifré:* p. 70, **Planning of an Experiment for VLBI Tracking of GNSS Satellites**
- Molera Calvés, Guifré:* p. 171, **First Results of Venus Express Spacecraft Observations with Wettzell (1)**
- Moll, V. E.:* p. 285, **X/Ka Celestial Frame Improvements: Vision to Reality**
- Morris, K.:* p. 396, **RDBE Development and Progress**
- Mühlbauer, Matthias:* p. 439, **E-control: First Public Release of Remote Control Software for VLBI Telescopes**
- Mühlbauer, Matthias:* p. 444, **The Wettzell System Monitoring Concept and First Realizations**
- Natusch, Tim:* p. 50, **The AuScope Project and Trans-Tasman VLBI**
- Natusch, Tim:* p. 113, **Characterization and Calibration of the 12-m Antenna in Warkworth, New Zealand**
- Navarro, R.:* p. 285, **X/Ka Celestial Frame Improvements: Vision to Reality**
- Neidhardt, Alexander:* p. 28, **DBBC VLBI2010**

- Neidhardt, Alexander*: p. 31, **Differences Between S/X and VLBI2010 Operation**
- Neidhardt, Alexander*: p. 133, **Permanent Monitoring of the Reference Point of the 20m Radio Telescope Wettzell (1)**
- Neidhardt, Alexander*: p. 171, **First Results of Venus Express Spacecraft Observations with Wettzell**
- Neidhardt, Alexander*: p. 392, **DBBC2 Backend: Status and Development Plan**
- Neidhardt, Alexander*: p. 439, **E-control: First Public Release of Remote Control Software for VLBI Telescopes (1)**
- Neidhardt, Alexander*: p. 444, **The Wettzell System Monitoring Concept and First Realizations**
- Niell, Arthur*: p. 23, **The NASA VLBI2010 Proof-of-concept Demonstration and Future Plans (1)**
- Niell, Arthur*: p. 35, **Post-correlation Processing for the VLBI2010 Proof-of-concept System**
- Niell, A.:* p. 396, **RDBE Development and Progress (1)**
- Nilsson, Tobias*: p. 202, **Estimation of Geodetic and Geodynamical Parameters with VieVS**
- Nilsson, Tobias*: p. 251, **Prospects for UT1 Measurements from VLBI Intensive Sessions**
- Nosov, Eugeny*: p. 400, **The Digital Data Acquisition System for the Russian VLBI Network of New Generation**
- Nothnagel, Axel*: p. 123, **Homologous Deformation of the Effelsberg 100-m Telescope Determined with a Total Station (1)**
- Nothnagel, Axel*: p. 138, **Proof-of-Concept Studies for a Local Tie Monitoring System**
- Nothnagel, Axel*: p. 222, **Correlations Between the Contributions of Individual IVS Analysis Centers**
- Nothnagel, Axel*: p. 355, **Reliability and Stability of VLBI-derived Sub-daily EOP Models**
- Nozawa, Kentarou*: p. 410, **Development of an e-VLBI Data Transport Software Suite with VDIF**
- Oh, Hongjong*: p. 95, **The State and Development Direction of the Geodetic VLBI Station in Korea**
- Oh, Hongjong*: p. 449, **Round-trip System Available to Measure Path Length Variation in Korea VLBI System for Geodesy (1)**
- Oh, Se-Jin*: p. 405, **First Phase Development of Korea-Japan Joint VLBI Correlator and Its Current Progress (1)**
- Ojha, Roopesh*: p. 153, **Implementation and Testing of VLBI Software Correlation at the USNO**
- Ojha, Roopesh*: p. 325, **Finding Extremely Compact Sources Using the ASKAP VAST Survey**
- Opseth, Per Erik*: p. 111, **New Fundamental Station in Ny-Ålesund**
- Otsubo, Toshimichi*: p. 212, **c5++ - Multi-technique Analysis Software for Next Generation Geodetic Instruments**
- Owens, Ken*: p. 373, **The Mark 5C VLBI Data System**
- Oyama, Tomoaki*: p. 40, **GPU Based Software Correlators - Perspectives for VLBI2010**
- Oyama, Tomoaki*: p. 300, **The Position/Structure Stability of Four ICRF2 Sources**
- Pantaleev, Miroslav*: p. 415, **Cryogenic Integration of the 2–14 GHz Eleven Feed in a Wideband Receiver for VLBI2010 (1)**
- Pantaleev, Miroslav*: p. 420, **Development of a Compact Eleven Feed Cryostat for the Patriot 12-m Antenna System**
- Pany, Andrea*: p. 202, **Estimation of Geodetic and Geodynamical Parameters with VieVS**
- Park, Jinsik*: p. 95, **The State and Development Direction of the Geodetic VLBI Station in Korea**
- Park, Jinsik*: p. 449, **Round-trip System Available to Measure Path Length Variation in Korea VLBI System for Geodesy**
- Pavlis, Despina*: p. 227, **VLBI-SLR Combination Solution Using GEODYN**
- Peck, G.:* p. 396, **RDBE Development and Progress**
- Peréz Ayúcar, Miguel*: p. 171, **First Results of Venus Express Spacecraft Observations with Wettzell**

- Petrachenko, Bill*: p. 3, **VLBI2010: An Overview** (1)
- Petrachenko, Bill*: p. 434, **The Impact of Radio Frequency Interference (RFI) on VLBI2010** (1)
- Phillips, Chris*: p. 192, **VLBI Data Interchange Format (VDIF)**
- Pietzner, Judith*: p. 123, **Homologous Deformation of the Effelsberg 100-m Telescope Determined with a Total Station**
- Plank, Lucia*: p. 202, **Estimation of Geodetic and Geodynamical Parameters with VieVS**
- Plank, Lucia*: p. 217, **Comparison Campaign of VLBI Data Analysis Software - First Results** (1)
- Platania, Pier Raffaele*: p. 28, **DBBC VLBI2010**
- Platania, Pier Raffaele*: p. 392, **DBBC2 Backend: Status and Development Plan**
- Plötz, Christian*: p. 439, **E-control: First Public Release of Remote Control Software for VLBI Telescopes**
- Plötz, Christian*: p. 444, **The Wettzell System Monitoring Concept and First Realizations**
- Pogrebenko, Sergei*: p. 70, **Planning of an Experiment for VLBI Tracking of GNSS Satellites**
- Pogrebenko, Sergei*: p. 171, **First Results of Venus Express Spacecraft Observations with Wettzell**
- Porcas, Richard*: p. 8, **VLBI2010: The Astro-Geo Connection** (1)
- Porcas, Richard*: p. 310, **Global VLBI Observations of Weak Extragalactic Radio Sources: Imaging Candidates to Align the VLBI and Gaia Frames**
- Poutanen, Markku*: p. 360, **Simulation of Local Tie Accuracy on VLBI Antennas**
- Proctor, R. C.*: p. 285, **X/Ka Celestial Frame Improvements: Vision to Reality**
- Quan, Ying*: p. 157, **The Software Correlator of the Chinese VLBI Network**
- Revnell, M.*: p. 396, **RDBE Development and Progress**
- Reynolds, Cormac*: p. 325, **Finding Extremely Compact Sources Using the ASKAP VAST Survey**
- Rieck, Carsten*: p. 365, **VLBI and GPS-based Time-transfer Using CONT08 Data** (1)
- Rioja, María*: p. 315, **Astrometric “Core-shifts” at the Highest Frequencies** (1)
- Ritakari, Jouko*: p. 143, **Ultra-rapid dUT1 Measurements on Japan-Fennoscandian Baselines – Application to 24-hour Sessions**
- Rogers, A.*: p. 396, **RDBE Development and Progress**
- Rogstad, S. P.*: p. 285, **X/Ka Celestial Frame Improvements: Vision to Reality**
- Roh, Duk-Gyoo*: p. 405, **First Phase Development of Korea-Japan Joint VLBI Correlator and Its Current Progress**
- Romney, Jon*: p. 373, **The Mark 5C VLBI Data System**
- Romney, J.*: p. 396, **RDBE Development and Progress**
- Rottmann, Helge*: p. 439, **E-control: First Public Release of Remote Control Software for VLBI Telescopes**
- Rowlands, David*: p. 227, **VLBI-SLR Combination Solution Using GEODYN**
- Roy, Alan*: p. 28, **DBBC VLBI2010**
- Roy, Alan*: p. 392, **DBBC2 Backend: Status and Development Plan**
- Russo, Antonietta*: p. 28, **DBBC VLBI2010**
- Russo, Antonietta*: p. 392, **DBBC2 Backend: Status and Development Plan**
- Ruszczyk, Chester*: p. 373, **The Mark 5C VLBI Data System**
- Ruszczyk, C.*: p. 396, **RDBE Development and Progress**
- Salnikov, Alexander*: p. 148, **The “Quasar” Network Observations in e-VLBI Mode Within the Russian Domestic VLBI Programs**
- Sasao, Tetsuo*: p. 330, **The First Experiment with VLBI-GPS Hybrid System**
- Sazhin, Mikhail*: p. 290, **Long-term Variations of the EOP and ICRF2**
- Sazhina, Olga*: p. 290, **Long-term Variations of the EOP and ICRF2**
- Schenk, Andreas*: p. 133, **Permanent Monitoring of the Reference Point of the 20m Radio Telescope Wettzell**
- Schmeing, Benno*: p. 138, **Proof-of-Concept Studies for a Local Tie Monitoring System** (1)
- Schuh, Harald*: p. 202, **Estimation of Geodetic and Geodynamical Parameters with VieVS**
- Schuh, Harald*: p. 217, **Comparison Campaign of VLBI Data Analysis Software - First Results**

- Schuh, Harald*: p. 251, **Prospects for UT1 Measurements from VLBI Intensive Sessions**
- Schuh, H.*: p. 345, **Extracting Independent Local Oscillatory Geophysical Signals by Geodetic Tropospheric Delay**
- Schwatke, Christian*: p. 340, **The Tropospheric Products of the International VLBI Service for Geodesy and Astrometry**
- Sekido, Mamoru*: p. 143, **Ultra-rapid dUT1 Measurements on Japan-Fennoscandian Baselines – Application to 24-hour Sessions**
- Sekido, Mamoru*: p. 192, **VLBI Data Interchange Format (VDIF)**
- Sekido, Mamoru*: p. 212, **c5++ - Multi-technique Analysis Software for Next Generation Geodetic Instruments**
- Sekido, Mamoru*: p. 330, **The First Experiment with VLBI-GPS Hybrid System**
- Sekido, M.*: p. 335, **Ionospheric Response to the Total Solar Eclipse of 22 July 2009 as Deduced from VLBI and GPS Data**
- Sekido, Mamoru*: p. 410, **Development of an e-VLBI Data Transport Software Suite with VDIF (1)**
- Sementsov, Valerian*: p. 290, **Long-term Variations of the EOP and ICRF2**
- Sergeev, Roman*: p. 180, **About the Compatibility of DORIS and VLBI Observations**
- Shantyr, Violet*: p. 167, **The IAA RAS Correlator First Results**
- Shinno, Takuya*: p. 410, **Development of an e-VLBI Data Transport Software Suite with VDIF**
- Shu, Fengchun*: p. 157, **The Software Correlator of the Chinese VLBI Network**
- Shu, Fengchun*: p. 176, **CRF Network Simulations for the South**
- Shu, F.C.*: p. 335, **Ionospheric Response to the Total Solar Eclipse of 22 July 2009 as Deduced from VLBI and GPS Data**
- Shu, Fengchun*: p. 383, **VLBI Technology Development at SHAO**
- Shu, Fengchun*: p. 388, **The Progress of CDAS**
- Sigman, E. H.*: p. 285, **X/Ka Celestial Frame Improvements: Vision to Reality**
- Sivakumar, V.*: p. 345, **Extracting Independent Local Oscillatory Geophysical Signals by Geodetic Tropospheric Delay**
- Skjerve, L. J.*: p. 285, **X/Ka Celestial Frame Improvements: Vision to Reality**
- Skurikhina, Elena*: p. 148, **The “Quasar” Network Observations in e-VLBI Mode Within the Russian Domestic VLBI Programs**
- Skurikhina, Elena*: p. 247, **Antenna Axis Offset Estimation from VLBI**
- Smolentsev, Sergey*: p. 106, **The New Generation Russian VLBI Network**
- Smolentsev, Sergey*: p. 180, **About the Compatibility of DORIS and VLBI Observations**
- Sobarzo, Sergio*: p. 439, **E-control: First Public Release of Remote Control Software for VLBI Telescopes**
- Soriano, M. A.*: p. 285, **X/Ka Celestial Frame Improvements: Vision to Reality**
- Sovers, O. J.*: p. 285, **X/Ka Celestial Frame Improvements: Vision to Reality**
- Sovers, O. J.*: p. 305, **Rotational Alignment Altered by Source Position Correlations**
- Spicakova, Hana*: p. 202, **Estimation of Geodetic and Geodynamical Parameters with VieVS (1)**
- Steigenberger, Peter*: p. 355, **Reliability and Stability of VLBI-derived Sub-daily EOP Models**
- Steppe, J. A.*: p. 305, **Rotational Alignment Altered by Source Position Correlations**
- Surkis, Igor*: p. 106, **The New Generation Russian VLBI Network**
- Surkis, Igor*: p. 148, **The “Quasar” Network Observations in e-VLBI Mode Within the Russian Domestic VLBI Programs**
- Surkis, Igor*: p. 167, **The IAA RAS Correlator First Results (1)**
- Takahashi, Fujinobu*: p. 410, **Development of an e-VLBI Data Transport Software Suite with VDIF**
- Takefuji, Kazuhiro*: p. 40, **GPU Based Software Correlators - Perspectives for VLBI2010**
- Takefuji, Kazuhiro*: p. 55, **Current Status of the Development of a Transportable and Compact VLBI System by NICT and GSI**

- Takefuji, Kazuhiro*: p. 378, Next-generation A/D Sampler ADS3000+ for VLBI2010 (1)
- Takefuji, Kazuhiro*: p. 410, Development of an e-VLBI Data Transport Software Suite with VDIF
- Takeuchi, Hiroshi*: p. 212, c5++ - Multi-technique Analysis Software for Next Generation Geodetic Instruments
- Takeuchi, Hiroshi*: p. 378, Next-generation A/D Sampler ADS3000+ for VLBI2010
- Takiguchi, Hiroshi*: p. 55, Current Status of the Development of a Transportable and Compact VLBI System by NICT and GSI
- Takiguchi, Hiroshi*: p. 212, c5++ - Multi-technique Analysis Software for Next Generation Geodetic Instruments
- Takiguchi, Hiroshi*: p. 330, The First Experiment with VLBI-GPS Hybrid System
- Tanimoto, Daisuke*: p. 55, Current Status of the Development of a Transportable and Compact VLBI System by NICT and GSI
- Taveniku, M.*: p. 396, RDBE Development and Progress
- Teke, Kamil*: p. 202, Estimation of Geodetic and Geodynamical Parameters with VieVS
- Thomas, Cynthia C.*: p. 85, The Composition of the Master Schedule (1)
- Thorandt, Volkmar*: p. 295, Long-term Stability of Radio Sources in VLBI Analysis
- Tingay, Steven*: p. 50, The AuScope Project and Trans-Tasman VLBI
- Titov, Oleg*: p. 50, The AuScope Project and Trans-Tasman VLBI
- Titov, Oleg*: p. 60, VLBI2020: From Reality to Vision (1)
- Titov, Oleg*: p. 176, CRF Network Simulations for the South (1)
- Titus, Mike*: p. 90, Coordinating, Scheduling, Processing and Analyzing IYA09
- Tornatore, Vincenza*: p. 70, Planning of an Experiment for VLBI Tracking of GNSS Satellites (1)
- Tsekmeister, Svetlana*: p. 320, Forthcoming Occultations of Astrometric Radio Sources by Planets
- Tsutsumi, Masanori*: p. 378, Next-generation A/D Sampler ADS3000+ for VLBI2010
- Tuccari, Gino*: p. 28, DBBC VLBI2010 (1)
- Tuccari, Gino*: p. 392, DBBC2 Backend: Status and Development Plan (1)
- Tucker, B. C.*: p. 285, X/Ka Celestial Frame Improvements: Vision to Reality
- Ujihara, Hideki*: p. 55, Current Status of the Development of a Transportable and Compact VLBI System by NICT and GSI
- Vytnov, Alexander*: p. 429, Experiment of Injecting Phase Cal Ahead of the Feed: First Results
- Wagner, Jan*: p. 143, Ultra-rapid dUT1 Measurements on Japan-Fennoscandian Baselines – Application to 24-hour Sessions
- Wagner, Jan*: p. 171, First Results of Venus Express Spacecraft Observations with Wettzell
- Walker, R.*: p. 396, RDBE Development and Progress
- Wang, D.*: p. 285, X/Ka Celestial Frame Improvements: Vision to Reality
- Wang, Guangli*: p. 157, The Software Correlator of the Chinese VLBI Network
- Wang, Jinqing*: p. 388, The Progress of CDAS
- Wang, Weihua*: p. 157, The Software Correlator of the Chinese VLBI Network
- Wei, Wenren*: p. 388, The Progress of CDAS
- White, L. A.*: p. 285, X/Ka Celestial Frame Improvements: Vision to Reality
- Whitney, Alan*: p. 192, VLBI Data Interchange Format (VDIF) (1)
- Whitney, Alan*: p. 373, The Mark 5C VLBI Data System (1)
- Whitney, A.*: p. 396, RDBE Development and Progress
- Wilson, David*: p. 113, Characterization and Calibration of the 12-m Antenna in Warkworth, New Zealand
- Wu, Yajun*: p. 383, VLBI Technology Development at SHAO
- Wu, Yajun*: p. 388, The Progress of CDAS
- Wunderlich, Michael*: p. 28, DBBC VLBI2010
- Wunderlich, Michael*: p. 392, DBBC2 Backend: Status and Development Plan

- Xiang, Ying*: p. 28, **DBBC VLBI2010**
- Xiang, Ying*: p. 383, **VLBI Technology Development at SHAO**
- Xiang, Ying*: p. 388, **The Progress of CDAS**
- Xiang, Ying*: p. 392, **DBBC2 Backend: Status and Development Plan**
- Xu, Zhijun*: p. 383, **VLBI Technology Development at SHAO**
- Xue, Zhuhe*: p. 388, **The Progress of CDAS**
- Yang, Jian*: p. 420, **Development of a Compact Eleven Feed Cryostat for the Patriot 12-m Antenna System**
- Yeom, Jae-Hwan*: p. 405, **First Phase Development of Korea-Japan Joint VLBI Correlator and Its Current Progress**
- Yevstigneyev, Alexander*: p. 425, **Radio Telescope Focal Container for the Russian VLBI Network of New Generation**
- Yi, Sangoh*: p. 95, **The State and Development Direction of the Geodetic VLBI Station in Korea**
- Zaman, Ashraf*: p. 415, **Cryogenic Integration of the 2–14 GHz Eleven Feed in a Wideband Receiver for VLBI2010**
- Zamani, Mojtaba*: p. 415, **Cryogenic Integration of the 2–14 GHz Eleven Feed in a Wideband Receiver for VLBI2010**
- Zeitlhöfler, Reinhard*: p. 28, **DBBC VLBI2010**
- Zeitlhöfler, Reinhard*: p. 392, **DBBC2 Backend: Status and Development Plan**
- Zhang, Xiuzhong*: p. 383, **VLBI Technology Development at SHAO (1)**
- Zhang, Xiuzhong*: p. 388, **The Progress of CDAS**
- Zhao, Rongbin*: p. 388, **The Progress of CDAS**
- Zharov, Vladimir*: p. 290, **Long-term Variations of the EOP and ICRF2 (1)**
- Zheng, Weimin*: p. 157, **The Software Correlator of the Chinese VLBI Network (1)**
- Zheng, W.M.*: p. 335, **Ionospheric Response to the Total Solar Eclipse of 22 July 2009 as Deduced from VLBI and GPS Data**
- Zheng, Weimin*: p. 383, **VLBI Technology Development at SHAO**
- Zhu, Renjie*: p. 383, **VLBI Technology Development at SHAO**
- Zhu, Renjie*: p. 388, **The Progress of CDAS (1)**
- Zimovsky, Vladimir*: p. 167, **The IAA RAS Correlator First Results**

REPORT DOCUMENTATION PAGE				Form Approved OMB No. 0704-0188	
<p>The public reporting burden for this collection of information is estimated to average 1 hour per response, including the time for reviewing instructions, searching existing data sources, gathering and maintaining the data needed, and completing and reviewing the collection of information. Send comments regarding this burden estimate or any other aspect of this collection of information, including suggestions for reducing this burden, to Department of Defense, Washington Headquarters Services, Directorate for Information Operations and Reports (0704-0188), 1215 Jefferson Davis Highway, Suite 1204, Arlington, VA 22202-4302. Respondents should be aware that notwithstanding any other provision of law, no person shall be subject to any penalty for failing to comply with a collection of information if it does not display a currently valid OMB control number.</p> <p>PLEASE DO NOT RETURN YOUR FORM TO THE ABOVE ADDRESS.</p>					
1. REPORT DATE (DD-MM-YYYY) 20-12-2010		2. REPORT TYPE Conference Publication		3. DATES COVERED (From - To)	
4. TITLE AND SUBTITLE International VLBI Service for Geodesy and Astrometry 2010 General Meeting Proceedings				5a. CONTRACT NUMBER	
				5b. GRANT NUMBER	
				5c. PROGRAM ELEMENT NUMBER	
6. AUTHOR(S) Dirk Behrend and Karen D. Baver, Editors				5d. PROJECT NUMBER	
				5e. TASK NUMBER	
				5f. WORK UNIT NUMBER	
7. PERFORMING ORGANIZATION NAME(S) AND ADDRESS(ES) Goddard Space Flight Center Greenbelt, MD 20771				8. PERFORMING ORGANIZATION REPORT NUMBER	
9. SPONSORING/MONITORING AGENCY NAME(S) AND ADDRESS(ES) National Aeronautics and Space Administration Washington, DC 20546-0001				10. SPONSORING/MONITOR'S ACRONYM(S)	
				11. SPONSORING/MONITORING REPORT NUMBER NASA/CP-2010-215864	
12. DISTRIBUTION/AVAILABILITY STATEMENT Unclassified-Unlimited, Subject Category: 46 Report available from the NASA Center for Aerospace Information, 7121 Standard Drive, Hanover, MD 21076. (301)621-0390					
13. SUPPLEMENTARY NOTES Dirk Behrend, NVI, Inc.; Karen D. Baver, NVI, Inc.					
14. ABSTRACT This volume is the proceedings of the sixth General Meeting of the International VLBI Service for Geodesy and Astrometry (IVS), held in Hobart, Tasmania, Australia, February 7-13, 2010. The contents of this volume also appear on the IVS Web site at http://ivscc.gsfc.nasa.gov/publications/gm2010 . The keynote of the sixth GM was the new perspectives of the next generation VLBI system under the theme "VLBI2010: From Vision to Reality". The goal of the meeting was to provide an interesting and informative program for a wide cross-section of IVS members, including station operators, program managers, and analysts. This volume contains 88 papers. All papers were edited by the editors for usage of the English language, form, and minor content-related issues.					
15. SUBJECT TERMS Geodesy, astrometry, VLBI, geophysics, Earth orientation, very long baseline interferometry, interferometry, radioastronomy, geodynamics, reference frames, terrestrial reference frame, celestial reference frame, length of day, Earth system science, Earth rotation.					
16. SECURITY CLASSIFICATION OF:			17. LIMITATION OF ABSTRACT	18. NUMBER OF PAGES	19b. NAME OF RESPONSIBLE PERSON
a. REPORT	b. ABSTRACT	c. THIS PAGE			Dirk Behrend
Unclassified	Unclassified	Unclassified	Unclassified	486	19b. TELEPHONE NUMBER (Include area code) 301-614-5939

